2006

Foraminiferal and stable isotope investigation of the Cenomanian-Turonian extinction and oceanic anoxic event

Fisher, Jodie Katherine

A foraminiferal and stable isotope investigation of the Cenomanian-Turonian extinction and oceanic anoxic event

by

Jodie Katherine Fisher

A thesis submitted to the University of Plymouth
in partial fulfilment for the degree of

DOCTOR OF PHILOSOPHY

School of Earth Ocean and Environmental Sciences
Faculty of Science

September 2006

Abstract

Jodie Katherine Fisher

A foraminiferal and stable isotope investigation of the Cenomanian-Turonian extinction and oceanic anoxic event

The Cretaceous was a time of significant global change, particularly around the Cenomanian-Turonian Boundary (CTB) (93.5 Ma). The mid-Cretaceous is considered to mark a period of intense global warming related to widespread tectonic activity, leading to periods of high sea level and no polar ice. This had great effects on the ocean's structure, chemistry and circulation, and led to both extinction and diversification of biota.

At the time of the CTB a number of events occurred. Particularly well researched is the oceanic anoxic event (OAE 2) and the organic-rich black shales deposited during this interval. Associated with these organic-rich sediments is a positive carbon isotope anomaly. This excursion has a distinct profile and has hence been used for global correlation. There was also a significant extinction event, 26% of all genera disappeared making it one on the five largest extinction events to have occurred in the last 100 my.

This study looks at a number of sites (ODP Sites 762, & 766 (Exmouth Plateau), Aksudere (in the Crimea), Flaine (French Alps) and Rio Mondego (Portugal)), at a range of palaeodepths from epicontinental seas to abyssal plains. These sites were chosen from both the northern and southern hemispheres, giving a range of sites spanning all faunal realms. Each site was analysed at a high resolution for foraminiferal and isotopic analysis, along with TOC, trace element and Rock Eval analysis where necessary, in order to understand the events surrounding the CTB, their effects, and the timings of them at each location to ultimately produce a global palaeodepth model of the CTB. It is clear that a record of OAE 2 is seen in all locations examined, both with or without organic rich sediments being recorded.

At all locations a characteristic increase in $\delta^{13}C$ values is seen at the CTB, from ~2 to 4‰. The start of the $\delta^{13}C$ excursion is in the upper part of the Cenomanian *R. cushmani* Zone. This is particularly well seen in the Crimea, a site on the northeastern Tethys margin at a palaeodepth of ~500m. Data from ODP Sites 762 and 766 also show similar carbon isotope trends in both bulk and foraminiferal samples. These data do, however, also indicate a degree of diagenetic alteration. Trace elements and SEM analysis of the foraminifera enable a better understanding of the diagenesis at these sites and demonstrate the importance of understanding diagenetic effects when looking at these materials. Taking this into account, all sites studied show more negative values of $\delta^{18}O$ over the CTB, possibly indicating warming over this period.

Foraminiferal analysis of the localities has enabled correlation and timing of the isotopic and depositional events globally, as well as giving further insight into the extinction and diversification events seen. Increased productivity is evidenced at all sites and explains the deposition of both the organic-rich sediments and the associated sediments. A stepwise extinction and diversification of species is recorded as well as a progression from oligotrophic competitive species opportunistic eutrophic species as the marine environments changed and the oxygen minimum zone expanded. This is observed in regions of organic rich sediment deposition and also settings where no organic matter was deposited, such as Flaine and Portugal, indicating the global effect of changes in the ocean structure, chemistry and circulation in all marine environments.

Contents

List of Figures

Chapter 5

Chapter 6

Chapter 7

Acknowledgements

I would like to thank my supervisors Professor Malcolm Hart and Dr. Gregory Price, for selecting me for this project and all their help and support over the last few years. Thanks also to Prof. Melanie Leng who supported my work at the NERC Isotope Laboratories and helped greatly with the analysis of materials, and Dr Philipp Steinmann who ran my RockEval samples.

Thanks to all the technicians who have also helped so much, particularly Maggie Grimbly, Roger Bowers, Marilyn Tucker and Kevin Solman, who without, my thin sections, photography, and numerous carbon analysed samples would certainly not be to the standard they are.

Thanks also to all at the SEM unit for their patience and fantastic help in photographing my numerous foraminifera.

I would also like to thank the support of the Geology and Geography postgrads, particularly Claire, Ben, Jenny, Liz, Becky and Katie, who with numerous cups of tea, a few pints of beer and chats over work have made my time during my PhD study such a great experience.

To my friends Debbie and Belinda, and my brother James, who have been a fantastic support over the last few years, thank you.

To Gregory who never stopped believing I could do it and helping me through.

And most importantly my Parents, for their support, encouragement and help over the years, without which I would not have been able to achieve all that I have.

Thank you.

AUTHOR'S DECLARATION

At no time during the registration for the degree of Doctor of Philosophy has the author been registered for any other University award without prior agreement of the Graduate Committee.

This study was financed with the aid of a studentship from the University of Plymouth.

A programme of advanced study was undertaken, which included training in micropalaeontological, isotopic and geochemical analytical techniques. At both the University of Plymouth and the NERC Isotope Geosciences Laboratory.

Relevant scientific seminars and conferences, both national and international were regularly attended at which work was often presented; external institutions were visited for consultation purposes and several papers prepared for publication.

Publications (or presentation of other forms of creative and performing work):

Papers:-

- **Fisher J.K.**, Price, G.D., Hart, M.B. and Leng, M.J. Stable isotope analysis of the Cenomanian-Turonian (Late Cretaceous) oceanic anoxic event of the Crimea. Cretaceous Research, 26, 853-863.
- Hart, M.B., Callapez, P., **Fisher, J.K.**, Hannant, K., Monteiro, J.F., Price, G.D. and Watkinson, M.W. 2005. Micropalaeontology and stratigraphy of the Cenomanian-Turonian boundary in the Lusitanian Basin, Portugal. Journal of Iberian Geology. 31, 295-310.

Conference and Meeting Abstracts:-

- **Fisher, J.K.**, Hart, M.B. and Price, G.D., 2001. The distribution of agglutinated foraminifera across the Late Cenomanian "anoxic event". Sixth International Workshop on Agglutinated Foraminifera, 2001. Prague, Czech Republic.1st – 7th September.
- **Fisher, J.K.** 2002. The distribution of foraminifera across the Cenomanian - Turonian
  Boundary Event. Progressive Palaeontology 2002, Leicester 12-13th June.
- **Fisher, J.K.**, Price, G.D., Hart, M.B. and Leng, M.J., 2003. Isotopic analysis of the Middle Cretaceous of the Southwest Crimea. BSRG Annual Meeting 2003, University of Leeds 20-22nd December, 2003.
- **Fisher, J.K.**, Price, G.D., Hart, M.B. and Leng, M. J., 2004. Isotopic and foraminiferal analysis of the Cenomanian-Turonian boundary event in the Crimea. A workshop on: Isotope studies of Palaeoclimate (IsoPal-2) – through geological time 23rd November 2004.
- **Fisher, J.K.**, Price, G.D., Hart, M.B. and Leng, M.J., 2004. Isotopic and foraminiferal analysis of the Middle Cretaceous of the Southwest Crimea. BSRG Annual Meeting 2004, Manchester Metropolitan, December 19-21st 2004.

- **Fisher, J.K.**, Hart, M.B, Price, G.D. and Leng, M.J., 2005. Foraminiferal and isotopic evidence for palaeoceanographic and palaeoclimatic change during the mid-Cretaceous. 7th International Symposium on the Cretaceous, University of Neûchatel, Switzerland, 5th – 9th September, 2005.

Published abstracts:-

- **Fisher, J.K.**, Hart, M.B. and Price, G.D., 2001. New data on the distribution of foraminifera across the Late Cenomanian "anoxic event". Bulletin de la Société d'etude des Sciences Naturelles d'elbeuf – Colloquium on the Cenomanian Stage 2001 Communication Volume 46-49.
- **Fisher J.K.**, Price, G.D., Hart, M.B. and Leng, M.J. Isotopic and foraminiferal analysis of the Cenomanian-Turonian boundary event of the Indian Ocean. Geophysical Research Abstracts, 5, EGS-AGU-EUG Joint Assembly, Nice, France. Abstract number EAE03-A-09131.
- Price, G.D., **Fisher, J.K.** and Hart, M.B., 2004. New constraints upon carbon isotopic variation of early-middle Cretaceous marine successions. 32nd International Geological Congress, Florence, Italy.

External Contacts: Melanie J. Leng, NERC Isotope Geosciences Laboratory

Philipp Steinmann, University of Neuchâtel

Word count of main body of thesis: 73,965

Signed .....

Date 15/09/06

Chapter 1: Introduction

1.1 Introduction

The mid-Cretaceous (informally defined by some as the Aptian to Turonian) was a time of great environmental change, within both the marine and terrestrial realms. A timescale for the mid-Cretaceous is shown in Figure 1.1. It was characterised by high atmospheric CO_2 concentrations (Berner and Kothavala, 2001), a low latitudinal temperature gradient (Barron, 1983) and unusually high temperatures in the global ocean (Norris and Wilson, 1998; Fassell and Bralower, 1999; Huber et al., 1999). The mid-Cretaceous, therefore, represents one of the best examples of "greenhouse" climate conditions in the geological record. A global eustatic high, as sea levels increased rapidly (Hallam, 1992; Haq *et al.,* 1987), is also reported. This is linked with an increase in global ocean crustal production, with both enhanced tectonic movements as South America began to separate from Africa and the North, and later, the South Atlantic Ocean began to open (Schlanger *et al.,* 1981; Larson, 1991; Kaiho and Saito, 1994), and the emplacement of Large Igneous Provinces (LIPs) (Larson, 1991: Kerr, 1998). The increased production of oceanic crust, combined lack of polar ice during the mid-Cretaceou (e.g., Huber, 1998), may have led to the global eustatic highs reported for this time interval.

This increase in global sea level and temperature, affected the oceans greatly with major changes in circulation and productivity. This, in turn, led to widespread faunal diversification and extinction (e.g., Hart, 1996), and the deposition of globally extensive organic-rich black shales (Schlanger and Jenkyns, 1976; Jenkyns, 1980; Hart and Bigg, 1981; Arthur *et al.,* 1987; Schlanger *et al.,* 1987; Jarvis *et al.,* 1988; Paul *et al.,* 1999; Keller *et al.,* 2001). The deposition of these black shales is generally thought to represent widespread anoxia in the oceans, and these events have become known as 'oceanic anoxic events' (Schlanger and Jenkyns, 1976; Jenkyns, 1980).

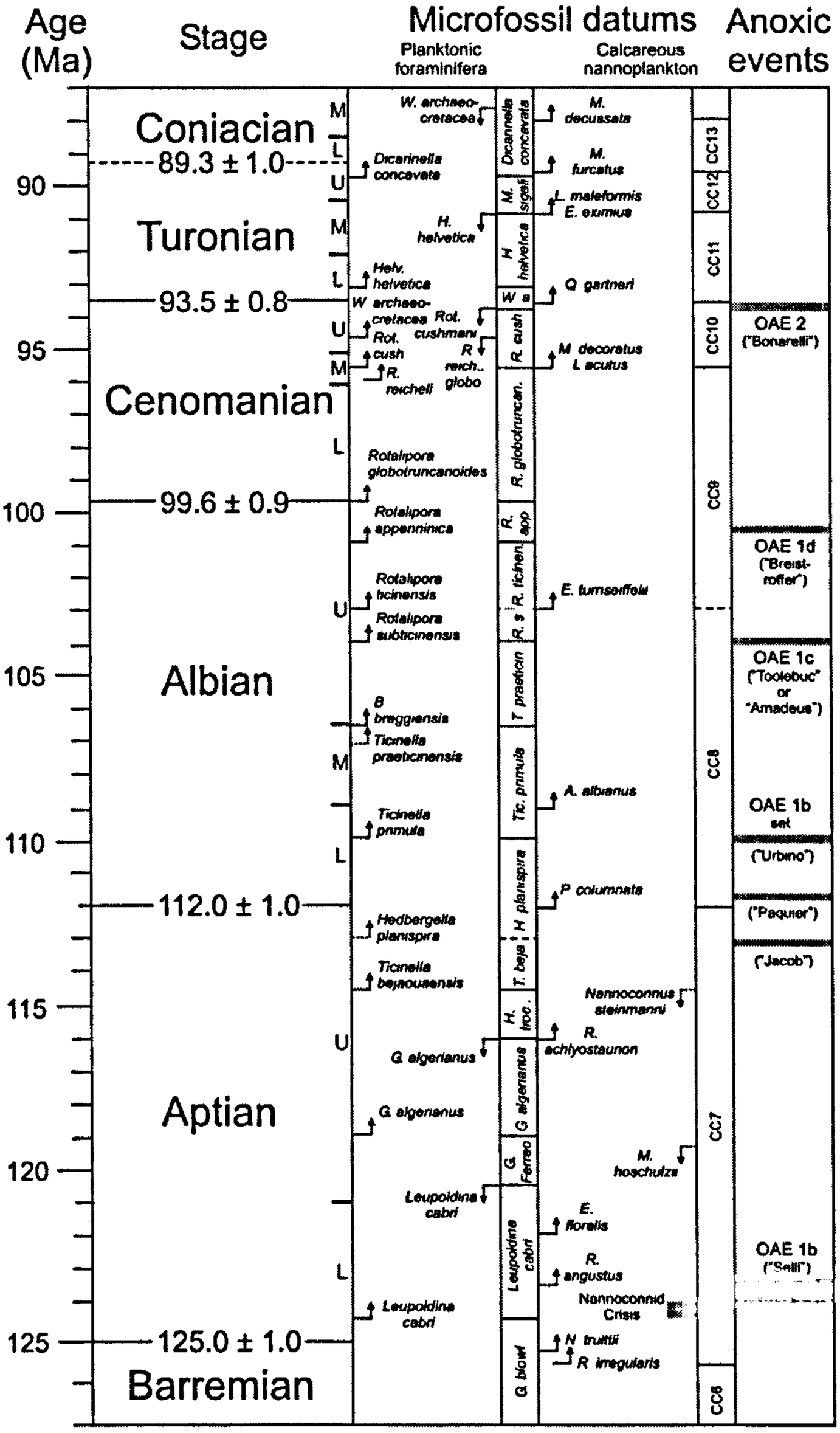

Figure 1.1: Geological timescale for the mid-Cretaceous, showing planktonic foraminiferal and calcareous nannofossil datums used in this study, and illustrating the anoxic events that occurred during this time period (modified from Gradstein *et al.*, 2004).

There are a number of oceanic anoxic events (OAEs) throughout the Cretaceous Period, from the early Aptian (OAE 1) to the Campanian (OAE 3), and these are shown in Figure 1.1. Particularly well researched is OAE 2 and the organic-rich black shales deposited during this interval close to the Cenomanian-Turonian boundary (CTB) (Schlanger and Jenkyns, 1976; Jenkyns, 1980; Hart and Bigg, 1981; Arthur *et al.*, 1987; Schlanger *et al.*, 1987; Jarvis *et al.*, 1988; Paul *et al.*, 1999; Keller *et al.*, 2001) at 93.5 (±0.8) Ma (Gradstein *et al.*, 2004).

Two main models exist for black shale deposition: (1) increased productivity, the increased flux of organic matter to the sea floor exceeding the rate of oxidation (e.g., Parrish, 1995); and (2) enhanced preservation of organic matter on the sea floor (e.g., Tyson, 1995), formed due to the expansion of the oxygen minimum zone (OMZ). Precise mechanisms are, however, still controversial. The dominant mechanism may be related to the palaeoceanographical setting in which deposition occurred (Kuhnt and Wiedmann, 1995).

Associated with these organic-rich sediments is a global positive carbon isotope anomaly (Scholle and Arthur, 1980; Pratt and Threlkeld, 1984; Arthur *et al.*, 1988; Hart *et al.*, 1993; Gale *et al.*, 1993; Jenkyns *et al.*, 1994; Voigt and Hilbrecht, 1997). This excursion has a distinctive profile and has been used for global correlation. In addition to marine carbonates, a carbon isotope excursion has also been identified in marine organic carbon and terrestrial organic carbon (e.g., Hasegawa, 1997), indicating the linkage between the ocean-atmosphere CO_2 reservoir.

Using high-resolution carbon and oxygen isotope analyses of marine carbonates from the mid-Cretaceous, and more specifically the Cenomanian-Turonian boundary, together with measurements of total organic carbon (TOC), Rock-Eval pyrolysis and petrographic analysis, fluctuations in the global carbon reservoir can be studied, and the environment of deposition assessed. This study, alongside high resolution analysis of foraminiferal diversification and extinction events during the mid-Cretaceous, can further determine the

condition of the water column and the relative timing of these events, enabling correlation across broadly diverse palaeodepths and palaeolocations.

1.2 Environmental change in the mid-Cretaceous

1.2.1 Palaeoceanography

The mid-Cretaceous oceans were very different from today, with higher sea levels, higher global temperatures and ocean circulation may have been driven by warm, saline bottom waters (e.g., Brass *et al.,* 1982; Barron and Peterson 1990). More recently, GCM simulations of the Cretaceous ocean predict deep water formation in higher latitudes (e.g., Brady *et al.,* 1998; Poulsen *et al.,* 2001). The mid-Cretaceous is thought to encompass one of the warmest climate intervals of the Phanerozoic (Frakes *et al.*, 1992; Barron *et al.*, 1995) Enhanced atmospheric CO_2 (estimated to be 3-12 times greater than today, Berner and Kothavala, 2001) led to warm global temperatures, with a low pole to equator gradient. Figure 1.2 shows this change in gradient and the temperature, compared to the present day.

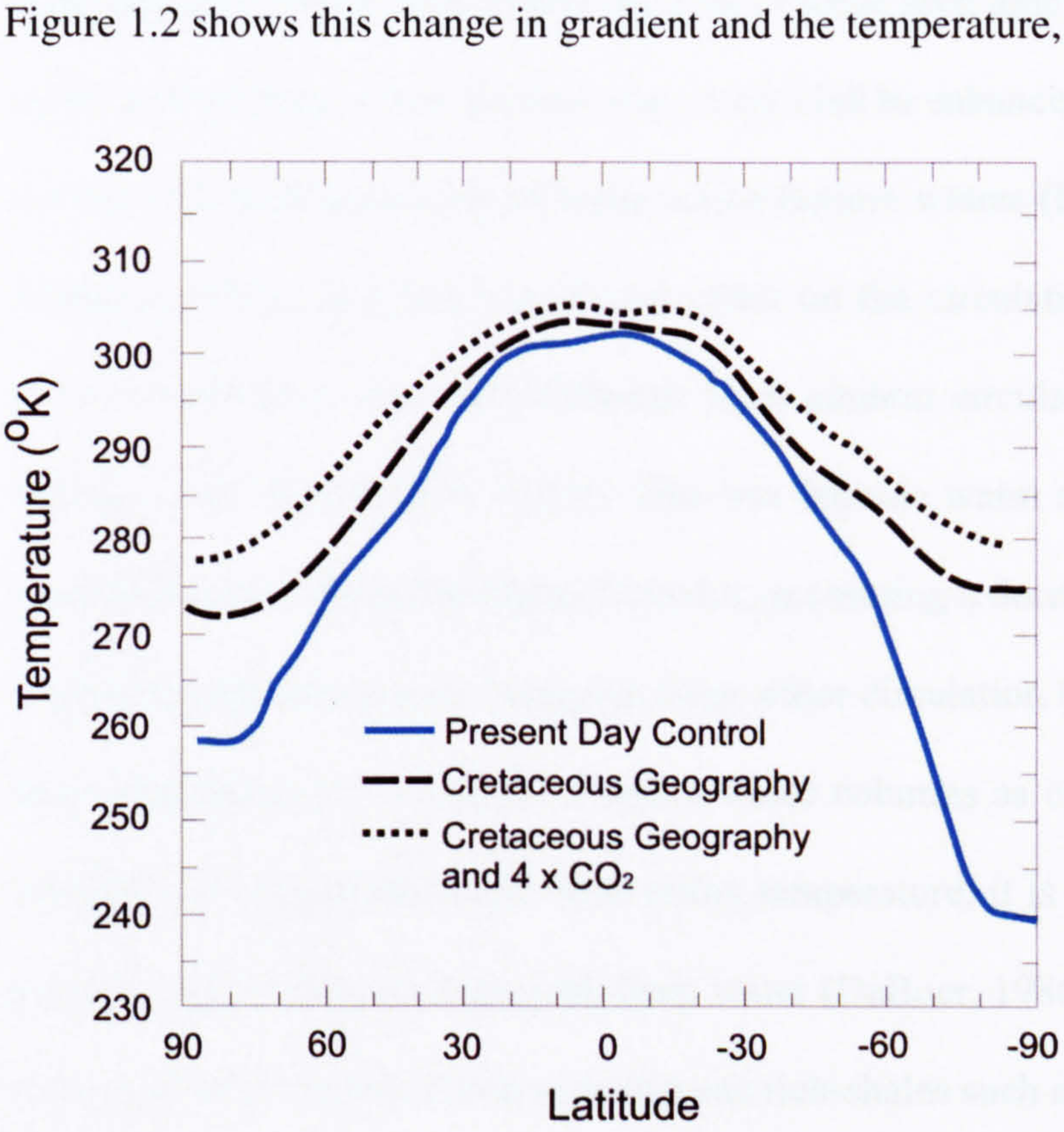

Figure 1.2: Model for mid-Cretaceous temperature gradients related to increased atmospheric CO_2 and Cretaceous palaeogeography (from Barron, 1983).

This led to increased ocean temperatures in both surface and bottom waters. Palaeotemperatures determined from oxygen isotopes, indicate that globally-averaged surface temperatures may have been 10°C higher than today. Measurements from pristine ('glassy') foraminifera may indicate sea surface temperatures as high as 35°C in tropical regions (Norris *et al.*, 2002; Wilson *et al.*, 2002), 22-28°C at southern high latitude sites (Huber *et al.*, 1995), and bathyal temperatures between 11°C and 19°C (Huber *et al.*, 1999, 2002).

It is thought that the increase in carbon dioxide required to produce the observed temperature changes over the CTB may have been sourced from enhanced tectonic activity (Larson, 1991). This tectonic activity also led to a eustatic sea level rise of ~130-350 m from the early Aptian to the Cenomanian (Larson, 1991). This rise in sea level led to the formation of widespread epicontinental seas particularly over much of northern Europe (forming the shallow chalk seas) and in America (forming the Western Interior Seaway). Shelf areas may have been double the area of those seen today (Tyson, 1995). The increase in the area of these warm shallow seas in turn led to enhanced evaporation at low latitudes and the increased formation of warm saline bottom waters (Brass *et al.*, 1982; Barron and Peterson, 1990). This had a profound effect on the circulation of the Cretaceous oceans, which would have been very different from modern circulation which is driven by high latitude, cold, deep bottom waters. This low latitude warm saline bottom water (WSBW) would transport heat to the higher latitudes, promoting a decrease in vertical and latitudinal temperature gradients and a sluggish deep water circulation (Brass *et al.*, 1982). This may have promoted more stratified, stagnant water columns as circulation slowed, and, as the solubility of oxygen decreases with rising temperature, it is likely that WSBW was more prone to anoxia than modern cold, deep water (DeBoer, 1986). This may have contributed to the formation of mid-Cretaceous organic rich-shales such as those seen at the CTB.

1.2.2 Oceanic anoxic events

Oceanic Anoxic Events (OAE's) were defined by Schanger and Jenkyns (1976) to explain the widespread, seemingly global, distribution of organic carbon-rich sediments (>1 wt% TOC) during the Cretaceous. These events are characterised by the widespread accumulation of organic-rich sediments in a variety of palaeo-bathymetric settings including deep ocean plateaus and basins, continental margins and epicontinental seas, over a relatively short period of geological time. Six events have been highlighted from the Aptian to Coniacian and the causes of each remains uncertain. Each event is very different in geographical extent, although all record rapid changes in the carbon cycle, and/or major changes in the marine biota was recorded (Bralower *et al.*, 2002).

The most extensive of these events is OAE2, characterised by a large positive global carbon-isotope excursion in both carbonate and organic matter, caused by a major perturbation of the global carbon budget that was, probably due to the extensive burial of organic matter in black shales (Schlanger and Jenkyns, 1976; Arthur and Schlanger, 1979; Jenkyns, 1980; Scholle and Arthur, 1980; Arthur *et al.*, 1988; Jenkyns *et al.*, 1994). Figure 1.3 shows the generalised distribution of organic rich shales at the CTB.

The duration of OAE2 was originally estimated on the basis biostratigraphical evidence and interpolation of geological timescale data points as being between 0.5 and 0.8 my (Arthur *et al.*, 1988) and 0.4 my (Caron *et al.*, 1999). Recently, orbital cyclicity has been used to estimate the duration of the event. These estimates range from 720 ky in Colorado (Meyers *et al.*, 2001), approx. 400 ky (Kuhnt *et al.*, 1997) in the Tarfaya Basin (Morocco) to 320 ky in western Canada (Prokoph *et al.*, 2001).

Although the carbon isotope excursion is now the most widely accepted means of discriminating the event, as opposed the spatially variable organic enrichment, this excursion does change in response to local and/or diagenetic influences (Hasegawa *et al.*, 2002; Tsikos *et al.* 2004; Kolonic *et al.*, 2005).

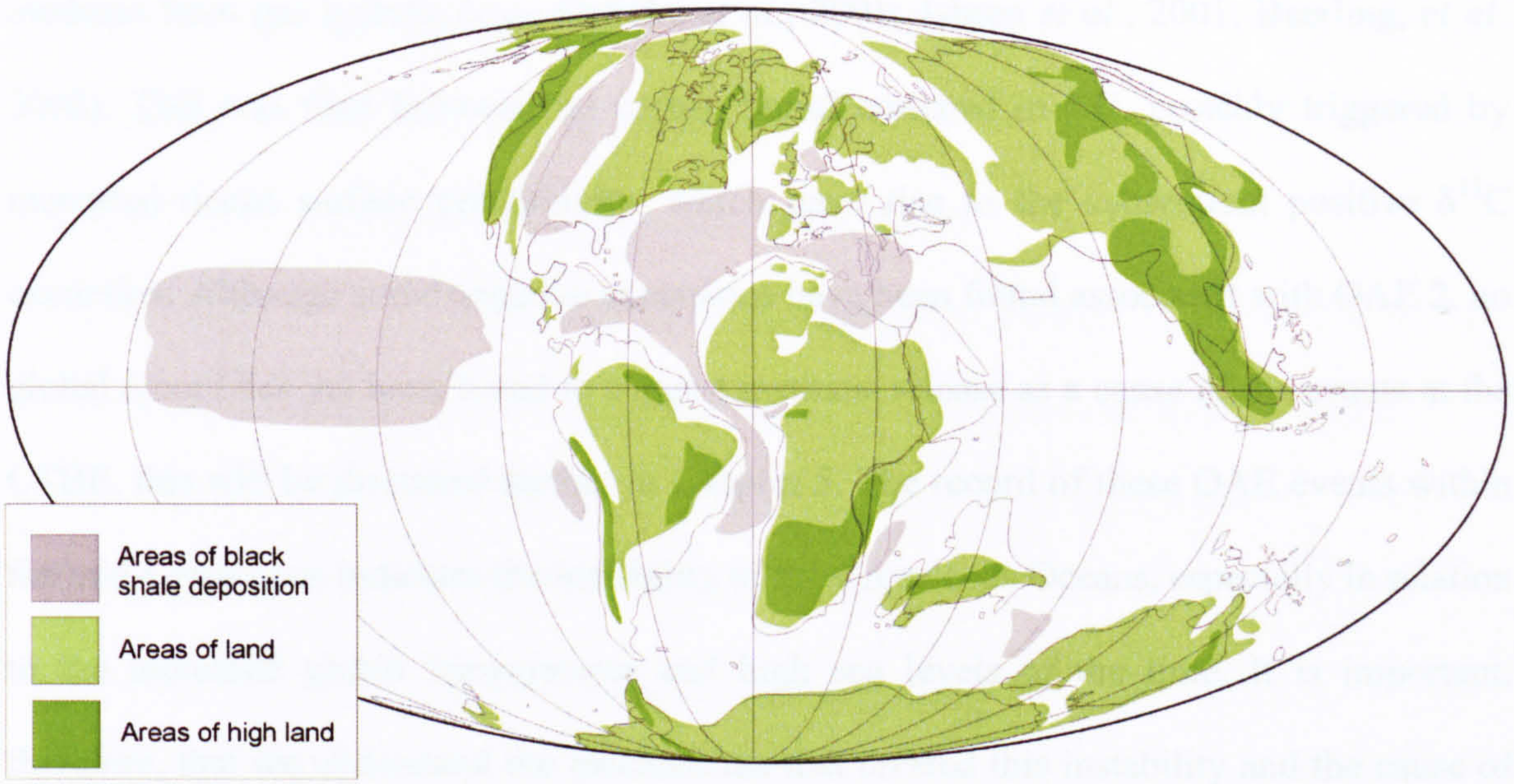

Figure 1.3: Geographical distribution of oxygen restricted deposition during the Cenomanian-Turonian boundary interval (modified from Wignall, 1994)

Additional disparity of these values arise from concerns over the radiometric data and assumptions and/or methods used in the development of orbital time-scales (Sageman *et al.*, 2006). Most recently Sageman *et al.* (2006) have presented a new orbital time-scale for the Cenomanian-Turonian GSSP at Pueblo, Colorado. Although the onset of the event is well defined by an abrupt enrichment in $\delta^{13}C$, the end point, like other sites, is more difficult to define. A duration from the onset of the carbon isotope excursion, to the end of the $\delta^{13}C$ curve represents 847 to 885 kyr, whilst a more conservative estimate to the end of the 'plateau' phase (used in Tsikos *et al.*, 2004; and this study) represents 847 to 885 kyr.

As mentioned above the cause of these anoxic events is widely debated. The carbon isotope curve provides crucial information for understanding the origin of these anoxic events. Of note, at OAE 1a in the early Aptian a negative carbon isotope excursion is seen within both organic carbon (e.g., Gröcke *et al.,* 1999; Jahren *et al.*, 2001) and carbonate (e.g., Menegatti *et al.,* 1998; Jenkyns and Wilson, 1999) prior to the characteristic positive excursion. This has been accounted for by an extremely voluminous rapid release of

methane from gas hydrate (e.g., Opdyke *et al.*, 2001; Jahren *et al.*, 2001; Beerling, *et al.* 2002). This was then followed by carbon burial enriched in ^{12}C, possibly triggered by increased ocean surface productivity, which gave rise to the subsequent positive $\delta^{13}C$ excursion. Although some negative excursions have been found associated with OAE 2, no global record has yet been found to suggest methane release as a cause of the events at the CTBE, this will be discussed further in Chapter 5. The record of these OAE events within the mid-Cretaceous indicates the instability of the Cretaceous Oceans, especially in relation to the increased global temperatures and high sea levels of the time. It is important, therefore, that we understand the mechanisms that created this instability and the cause of all the biotic and palaeoceanographic changes.

1.2.3 Extinction events

The mid-Cretaceous was also a time of rapid diversification and turnover of biota, particularly at the CTB. Recognised by Raup and Sepkoski (1982) in their study of periodic extinctions, the CTB, although not one of the 'big five', does represent a time of significant change, with 7% of marine families and 26% of marine genera eliminated (Harries, 1993). Figure 1.4 shows the extinctions of the various groups of marine organisms at the CTB, based on data in Sepkoski (1986, 1990) and Kerr (1998).

The composition of planktonic foraminiferal assemblages were particularly affected, with 20% of surface dwelling species becoming extinct compared to 50% of deeper water species (Kaiho, 1994). This predominance of deeper water species extinction may provide clues as to the cause of the faunal change, for which many suggestions have been advanced. A review of these causes and the evidence for them has been presented in Hart *et al.* (2002) and are listed as follows:

a) expansion of the oxygen minimum zone within the water column, leading to development of an oceanic anoxic event (see above) (Schlanger and Jenkyns, 1976; Jarvis *et al.*, 1988; Kaiho and Hasegawa, 1994; Hart, 1996);

b) Oceanographic changes (Gale *et al.*, 2000);

c) Bolide impact (Monteiro *et al.*, 1998a, b);

d) Multiple bolide/meteorite impact (Hut *et al.*, 1987)

e) Changes in the food chain (Paul and Mitchell, 1994; Paul *et al.*, 1999; Hart, 1996)

f) Sea level changes (Hancock and Kaufman, 1979; Hallam and Wignall, 1999)

g) Global cooling with an associated fall in sea level (Jeans *et al.*, 1991)

h) Major volcanism (Courtillot, 1992; Kerr, 1998)

i) Changes in carbonate production (Caus *et al.*, 1997)

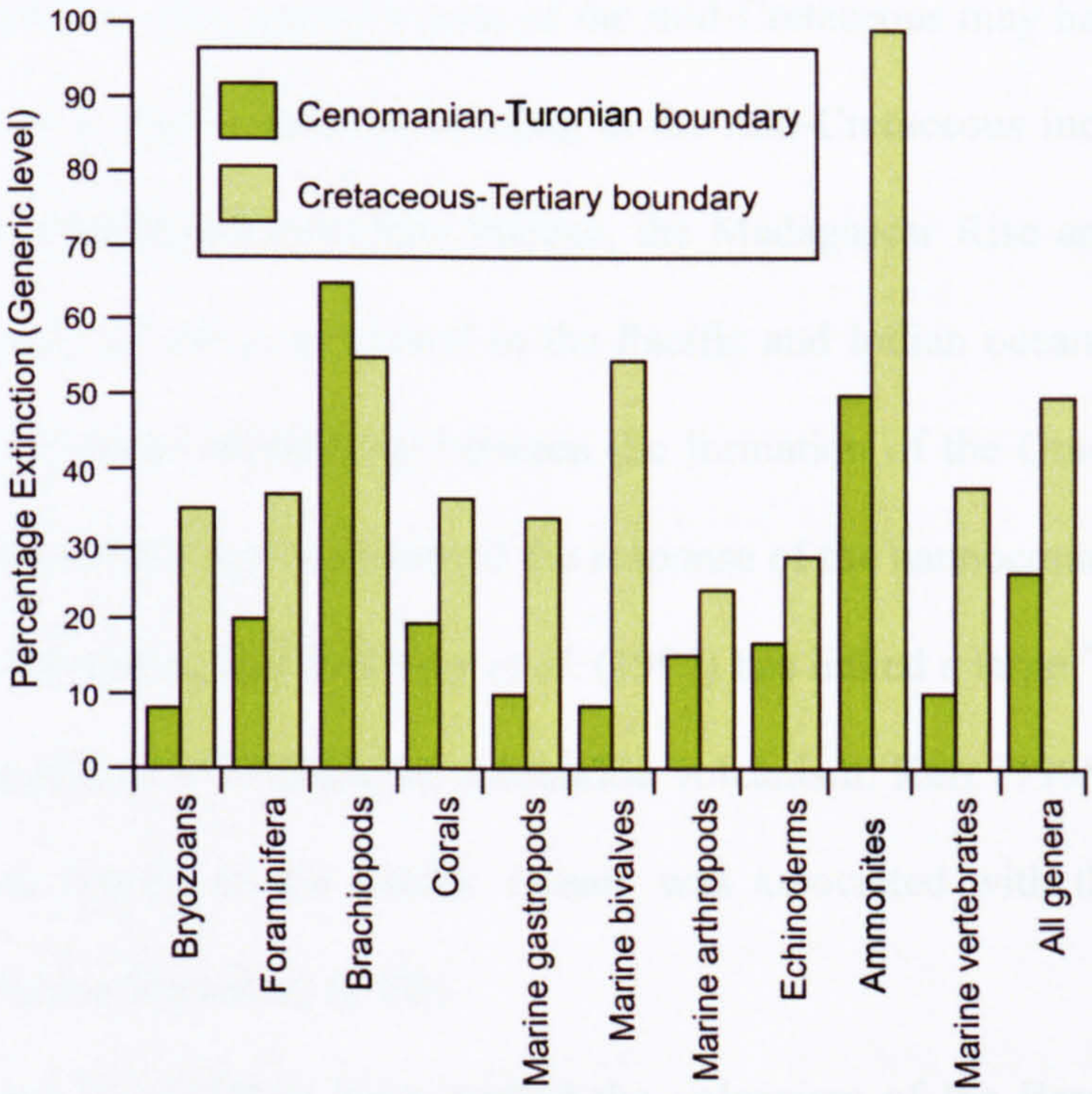

Figure 1.4: Bar graph comparing the pattern of extinction at the Cenomanian-Turonian boundary with that of the Cretaceous-Tertiary boundary (data from Sepkoski, 1986, 1990) for various taxonomic groups of marine organisms (modified from Kerr, 1998).

It is clear that the environmental changes in the ocean system at the time of the CTB are substantial. The development of anoxia in many of the ocean basins and shelf seas causing a very significant environmental stress for the biota and especially the foraminifera.

The analysis of foraminifera in this project aims to assess the effect of anoxia on the benthonic and planktonic populations, and assess the extinction potential of these events, both locally and globally.

1.2.4 Igneous activity

Unusually high rates of production of oceanic crust both at spreading centres and through the eruption of Large Igneous Provinces (LIPs) (e.g., Larson 1991; Larson and Erba, 1999; Kerr, 1998) has been observed in the mid-Cretaceous, with production peaking at the CTB. Larson (1991) documented widespread oceanic volcanism between ~85-125 Ma, and suggested that other global events of the mid-Cretaceous may have resulted from this volcanic activity. Those dated as forming in the mid-Cretaceous include the Ontong Java Plateau, the Caribbean/Columbian Plateau, the Madagascar Rise and the Kerguelen Plateau, the majority of which are found in the Pacific and Indian oceans. Tarduno *et al.* (1991) suggested a direct relationship between the formation of the Ontong Java Plateau and OAE 1A. Erba (1994) has documented the response of the nannoconids to the onset of mid-Cretaceous volcanism, and Bralower *et al.* (1997) has linked a large $^{87}Sr/^{86}Sr$ anomaly in the Barremian-Albian to widespread submarine volcanism. Kerr (1998) also suggested excess volcanism, largely in the Pacific Ocean, was associated with the events of the Cenomanian-Turonian Boundary (CTB).

Larson and Erba (1999) have studied the volcanism of the Barremian-Aptian in more detail. This time period signals the initiation of mid-Cretaceous volcanism and also the largest pulse of the entire mid-Cretaceous episode. Despite much speculation on the timing of these events and the linkages between volcanism and the events recorded in the sediments, it is likely that this pulse of activity led to a global response in the Earth's biotic, sedimentary, and geochemical systems which led, in turn, to the mid-Cretaceous greenhouse environment (Larson and Erba, 1999). Figure 1.5 shows some of cause and effect relationships that may be seen as a result of excess igneous activity. The rise in sea

level associated with tectonic and igneous activity would also have had an effect on ocean circulation and productivity as discussed above.

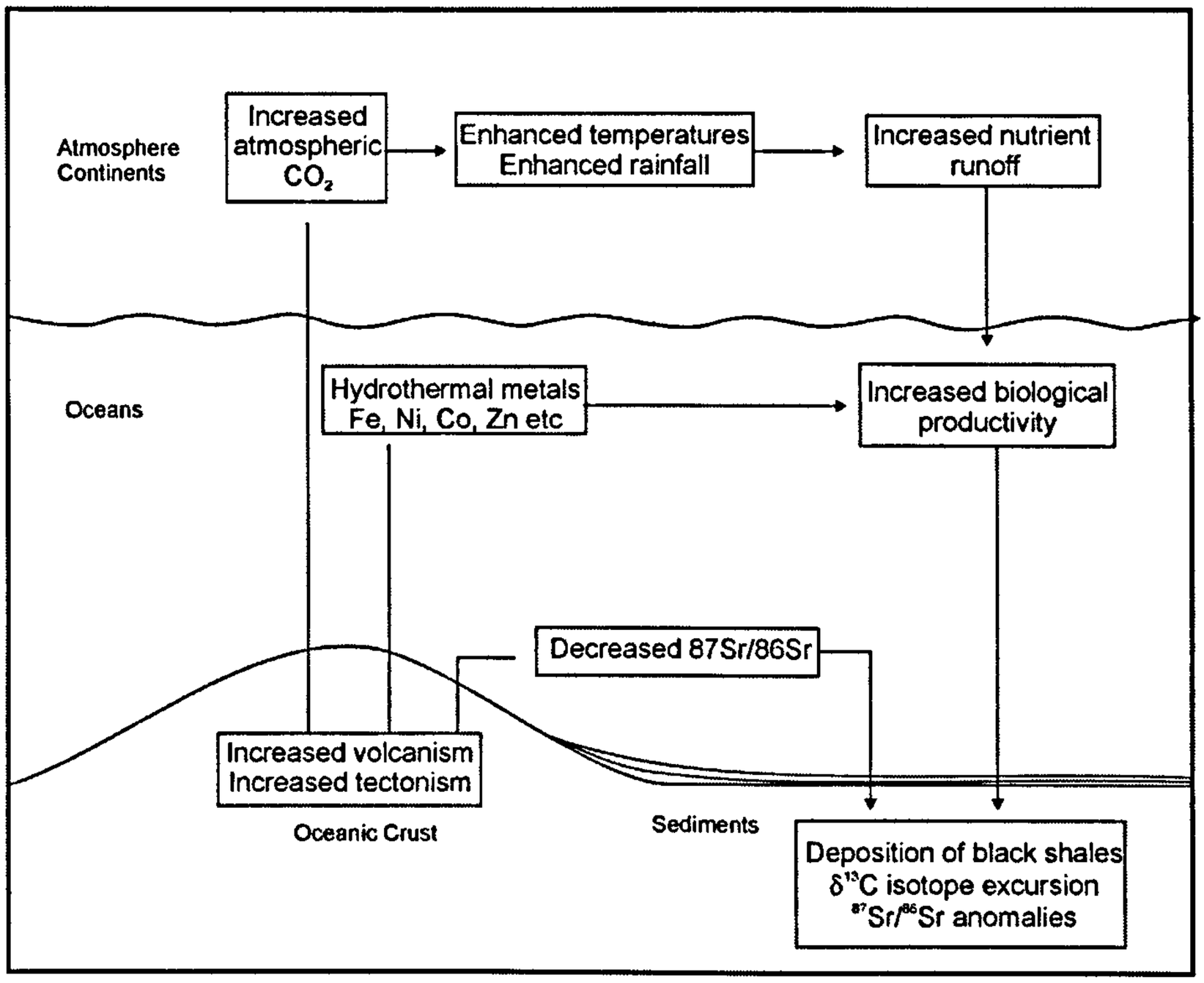

Figure 1.5: Summary of processes that might relate oceanic igneous events to geological responses (modified from Larson and Erba, 1999).

At the time of the Cenomanian-Turonian boundary, Kerr (1998) suggested that around 8-10 x 10^6 km^3 of lava was erupted onto the ocean floor from a series of plateau that are predominantly in the Pacific area. It is possible, therefore, that as well as the rise in sea level this volcanism may have contributed to many of the environmental perturbations seen at the CTB.

1.3 This study

Aim

The aim of this research project is to assess the palaeoceanographic and palaeoenvironmental changes across the mid-Cretaceous, and particularly the Cenomanian – Turonian boundary. The distribution of foraminifera and stable isotope stratigraphy are the principal proxies used in this investigation.

Objectives

- To provide a foraminiferal and geochemical analysis of the Cenomanian-Turonian boundary at a number of sites located at different palaeodepths during the mid-Cretaceous.
- To provide a foraminiferal and geochemical analysis of a series of sites located in both the northern and southern hemispheres, from Tethyan, Boreal and Austral realms.
- To provide a taxonomic analysis of planktonic and benthonic foraminiferal species from all the selected sites.
- To provide a biostratigraphical analysis of the previously unzoned Albian to Turonian succession of the eastern Indian Ocean.
- To provide a critical analysis of the palaeoenvironmental changes of the mid-Cretaceous and the Cenomanian-Turonian boundary.
- To evaluate the potential effect of diagenesis on palaeoenvironmental analysis and the importance of interpreting this diagenesis at each site.
- To provide a palaeoenvironmental model of the palaeoceanographical changes at the Cenomanian-Turonian boundary.

Locations

In order to undertake this study a number of sites were chosen in order to fully assess the Cenomanian–Turonian boundary at a range of palaeodepths and globally diverse locations. Although focussed around the Tethyan Ocean, sites were located on the southern margin off the northwest coast of Australia, the north-east Peri-Tethys and in north-west Europe's epicontinental seas and continental margins. Figures 1.6 and 1.7 show the location of these sites on a palaeogeographic a map of the Cenomanian-Turonian and on a palaeodepth model. Further information on each location is given in the respective chapters.

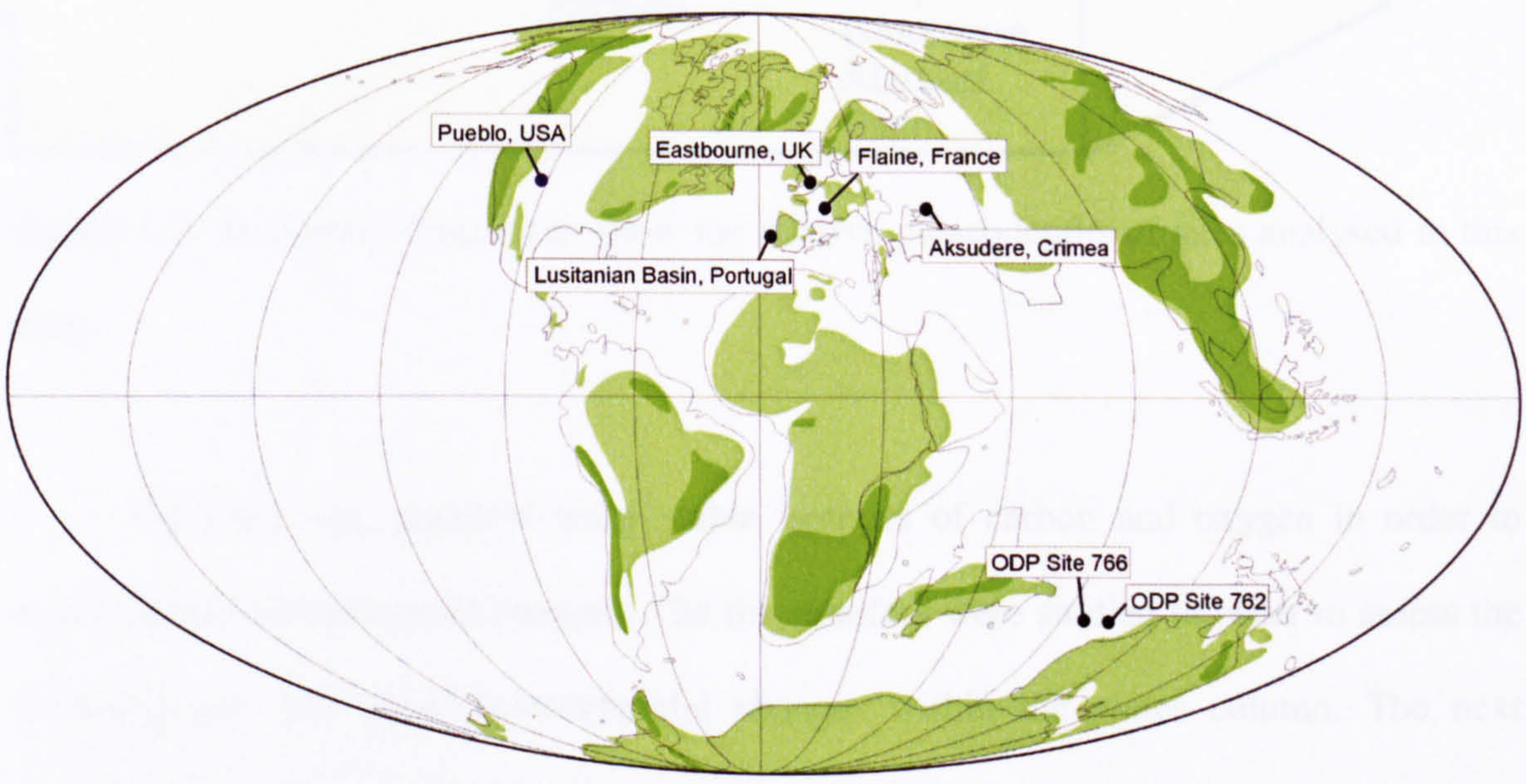

Figure 1.6: Palaeogeographical map showing the position of the locations analysed in this study at the Cenomanian-Turonian boundary. The Cenomanian-Turonian boundary GSSP at Pueblo, Colorado, is indicated on the map for reference only. No samples were studied, as this is the subject of on-going doctoral research by Delphine Desmares at the University of Strasbourg. Map modified from Smith *et al.* (1994).

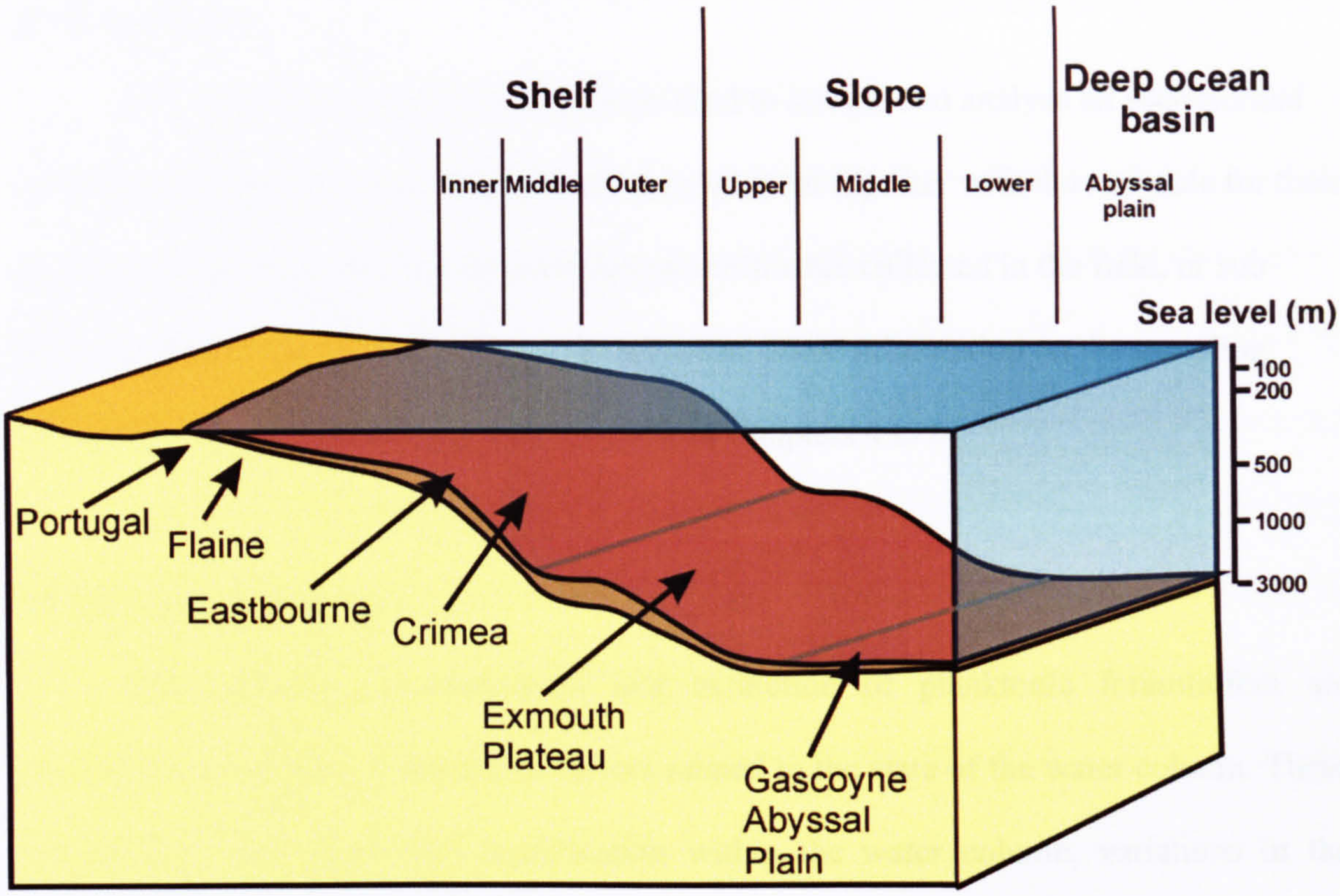

Figure 1.7: Schematic diagram to show the relative palaeodepths of sites analysed in this study.

Each site was analysed using stable isotopes of carbon and oxygen in order to assess palaeoceanographical changes. The foraminifera were studied in order to assess the biostratigraphy and palaeoenvironmental changes within the water column. The next chapters outline the methods, results and synthesis of this research.

Chapter 2 Methodology

2.1 Introduction

This chapter will outline the methods used to sample and analyse all sections and cores used in this study. Each method will be explained together with the rationale for their use in this study. The samples used for this research were collected in the field, or sub-sampled from Ocean Drilling Project (ODP) cores. More information on the sampling rationale of each section or core will be given in Chapters 4 to 6.

2.2 Foraminiferal analysis

The evolution, diversification and extinction of planktonic foraminifera are generally controlled by a number of factors related to the state of the water column. These are primarily associated with stratification within the water column, variations in the trophic structure and vertical temperature and density gradients (Leckie *et al.*, 1998; Price and Hart, 2002; Keller, 2002; Keller and Pardo 2004; Coccioni and Luciani, 2004). In modern oceans high diversity assemblages are typically seen within a well stratified water column, with normal salinity and nutrient content (Coccioni and Luciana, 2004), as depth stratification provides distinct biotic and physical environments in which stable ecological niches can be filled, and potentially competing species are separated (Lipps, 1979; Hemleben *et al.*, 1989). If nutrient conditions change, the structure of foraminiferal assemblages in the water column will also. Increased nutrient influx will lead to unstable eutrophic conditions favouring opportunistic (r-selected) species. These species, typically small in size, e.g., hedbergellids, heterohelicids and schackoinids, are characterised by fast reproduction, rapidly increasing their population densities. A reduction in nutrient influx however will lead to more stable, oligotrophic conditions, favouring more specialised (K-selected) species. These species, larger in size (e.g., rotaliporids), have much lower reproductive potential and longer life spans (MacArthur and Wilson, 1967). Between these two extremes are r/K intermediates. These species, adapted to mesotrophic environments,

have a range of trophic strategies (Coccioni and Luciani, 2004). By looking at the abundance, diversity and morphology of Cretaceous planktonic and benthonic foraminifera information on the state of the water column and ecological niches filled can be obtained.

In order to analyse the samples for foraminifera, each sample was processed according to the rock type to liberate the foraminifera and differentiate the species. Where it was not possible to break down the sediments, thin sections were made in order to determine foraminifera and relative abundances of biota in the samples. Thin sections were also made of the different sediments throughout each section and core, to support the foraminiferal counts, and provide sedimentological information. Liberated foraminifera were determined to the species level (where this was possible) and utilised for the determination of both biostratigraphy and palaeoceanographic change, as well as for isotopic analysis as will be discussed below.

2.2.1 Processing methods and preparation of samples

Where possible, and sample size allowed, around 50g of sample was processed for foraminiferal analysis, leaving a portion of sediment available for further analysis or repeats if required. This sample size was impossible for the ODP cores, where only limited sample size was provided by the ODP Core Repository. 10cc of sediment was provided for each sample, and around half was processed, again leaving enough material for further or repeat analysis. Around 15g of sample was, therefore, processed.

2.2.1.1 Clay rich and soft sediments

Samples rich in clay, and soft in nature, were processed in a 10% sodium hexametaphosphate (Calgon) solution, made up in deionised water, to prevent any dissolution of foraminiferal tests in impure or slightly acidic water.

The sediments were broken into small pieces of less than 1 cm^3 to increase their surface area during processing, and the samples were weighed. They were then dried

overnight in an oven to eliminate any residual and interstitial water, cooled and weighed again. Samples were then placed into a 100ml glass beaker. The beakers were filled to 100 ml with the sodium hexametaphosphate solution, agitated and left for 24 hours to allow the sediments to break down. Once thoroughly soaked the samples were washed over a 63μm sieve with deionised water. Whilst sieving a portion of the <63μm fraction was retained and dried for geochemical and isotopic analysis (see below). Once the samples had been washed thoroughly, ensuring all the clays had been washed through the sieve, the samples were dried in an oven at 40°C overnight. Once dry the sediments were dry sieved over a 63μm sieve. The >63μm fraction retained on the sieve was then weighed, in order to determine the amount of sediment processed, and stored in a specimen tube container ready for analysis.

2.2.1.2 Limestones and highly lithified chalks

Samples with harder lithologies, such as encountered in the Crimea or in the upper portion of ODP Site 762C, were processed with white spirit. If the samples failed to disaggregate in the white spirit, they were processed again in acetic acid. The methods for both these processes are outlined below.

White spirit

This process was carried out using the solvent method of Brasier (1980). Samples were broken into small <1 cm^3 fragments, dried in an oven overnight at 40°C, cooled and weighed. The samples were placed in beakers in a fume cupboard and white spirit was poured onto each. The samples were then left until the samples were saturated, which can take from 30 minutes to 8 hours (depending on lithology). The samples were, therefore, left for 8 hours in order to ensure full absorption. Once saturated the excess white spirit was poured off, and hot water was poured onto the samples until covered. The samples were then left to break down until the reaction had completed, gently agitating the samples

throughout the process. Once the reaction was complete the samples were thoroughly washed over a 63 μm sieve to remove any residue of the white spirit and wash out the finer clays and sediments. Collecting a portion of the < 63 μm sample for geochemical analysis, the > 63 μm portion was washed, collected, dried and weighed as before. The residue was then placed in sample tubes prior to analysis.

Acetic Acid

Acetic acid was used on samples that were very lithified and showed no breakdown using either calgon or white spirit, and follows the methodology of Lirer (2000). This method is a cold digestion using highly concentrated acetic acid similar to techniques commonly used in conodont studies (Graves and Ellison, 1941; Stouge and Boyce, 1983). Samples were broken down to small fragments around 5 mm in diameter, allowing sufficient surface area for the reaction, dried and weighed, and placed into a glass beaker. Glacial acetic acid was then used to make up a solution of ethenoic acid (CH_3COOOH) (80% acetic acid and 20% H_2O). The acetic acid causes a very slow reaction, disaggregating the rocks without destroying and corroding the fossil content (Lirer, 2000).

The samples were covered by the acetic acid solution to a level 2 cm above the fragment level. On addition of the solution to the sample a vigorous, but slow reaction is seen, the sediment absorbing the acetic acid which then breaks the links between particles. The process could be seen to be taking place with the deposition of fine residue on the bottom of the beaker, and the swelling of some of the rock fragments. As the process continued the solvent could be seen to foam and thicken as the sediment absorbed the acid and continued to break down. The samples were left for 2 hours, checking the samples at regular intervals, in order to remove the sediment from the acid as soon as the process was complete.

Within 2 hours most of the sediments had broken down sufficiently. Those that had not completely broken down at this point were left in the acid for longer, regular checks being made until the disaggregation was complete.

As soon as the reaction had completed the samples were immediately removed from the acid in order to prevent any etching of the liberated foraminifera from prolonged contact with the acid. The samples were then washed over a 63 μm sieve with abundant deionised water to collect the >63 μm residue and eliminate any remaining acid from the sediments. Again a portion of the <63 μm fraction was collected for geochemical and isotopic analysis as before. Once washed thoroughly the samples were dried overnight at 40°C, cooled and dry sieved over a 63 μm sieve. Samples were then weighed, and placed in specimen tubes to await analysis.

Using this technique, foraminifera are disaggregated extremely well, producing clean and clear specimens, this can be seen in Figure 2.1, where the sample processed in acetic acid can be seen compared with the same sample processed in white spirit. However the process did appear to make some of the specimens quite fragile. For example, some specimens showed chambers to pull apart from the tests during the picking of the dry sediment. Great care was taken with these samples so as not to bias the picking regime. Once processed each sample was split into two portions. The first to be picked for species analysis, the second to be picked for isotopic analysis of the foraminifera. It was important to separate the samples into these two portions in order to avoid a bias of species in species analysis following the preferential removal of specimens for isotopic analysis.

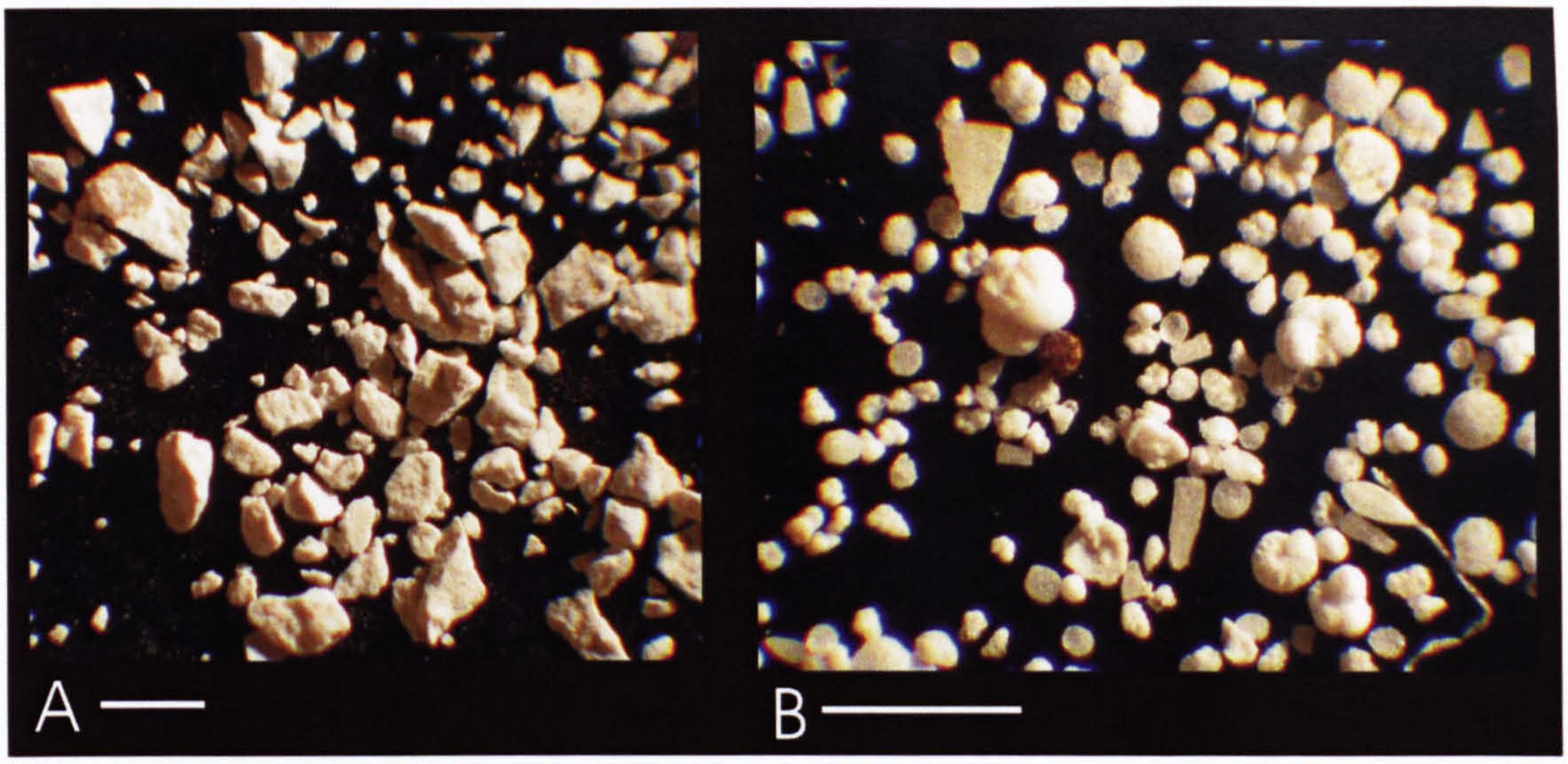

Figure 2.1: Results of processing techniques for the liberation of foraminifera from limestone sediments of the Crimea, using white spirit (A) and acetic acid (B). Scale bars = 500 μm.

Thin Sections

Sediments that were particularly lithified or phosphatised, such as those from Flaine, were unable to be processed using the techniques above. Thin sections were, therefore, made of these samples in order to analyse the foraminiferal components. Thin sections were also made of sediments from each core and section to analyse the sedimentological nature of the sediments further, and provide information on any diagenesis affecting the sediments and foraminifera.

2.2.2 Picking rationale

In order to analyse the foraminifera liberated from the sediments a picking rationale was devised to enable unbiased analysis of all samples, at all sites, in order to make comparative analysis through sections and cores, and cross site analysis viable.

Little consensus exists in the literature to determine a valid methodology for gaining a representative measure of the fauna in any one sample. To do so a numbers of variables must be decided upon:

- What sieve size to use
- Whether to split the sample into fractions
- How many individuals to pick per sample

Many workers sieve the samples on 63 μm, 125 μm, 250 μm and 500 μm sieves, undertaking full quantitative analysis on different size fractions depending on the nature of sediment, foraminiferal assemblages and type of study i.e. biostratigraphic or palaeoenvironmental.

In this study it was decided to sieve and pick the > 63 μm sediment. This was decided for two main reasons. Firstly, this size fraction provides a better spectrum of potential indicator species, and produces larger assemblages (over 300 specimens) giving a more reliable statistical spread of species in each sample. Secondly, the sieve size allows clays and silts to be removed from the sediment samples whilst retaining the foraminifera. A larger sieve size, whilst still eliminating the finer particles, will also cause the loss of small potentially important environmental indicator species, and may create artificial barren intervals in samples dominated by small sized species. This was particularly important in those clay rich sediments where foraminifera were rare and commonly small in size. A number of samples in ODP Core 766A were sieved over the different sieves to analyse the numbers of species and individuals retained on each sieve. It was immediately apparent that a great number of foraminifera, less than 125 μm in size, were present on the 63 μm sieve, and in not including this fraction in analysis would limit to species to only those larger and less abundant producing very different assemblages from those actually present. Further discussion on the size of foraminifera throughout the sections and cores is discussed later.

Each sample was examined on a gridded tray and greater than 300 specimens were picked to obtain a representative assemblage of the species present. For most samples between 300-400 specimens were picked.

Generally a sample contains between 200 and 1000 specimens, although 300 specimens are typically picked by workers. This is based on the work of Phelger (1960) who using his experience and an equation determined by Dryden (1931) for counting heavy mineral grains, suggested that 301 specimens provided sufficient accuracy for most quantitative studies. Counting more than 300 specimens would provide no more information on the foraminiferal assemblage and no more new species.

2.2.3 Methods of analysis

The picked specimens were mounted on gridded (plummer) slides for full identification and counts to be undertaken. The foraminifera were identified both by their species and by their morphotype. The morphotypes used in this study were determined based on work by Koutsoukos and Hart (1990) and Jones and Charnock (1985), the morphotypes used and each genus type can be seen in Table 2.1. Morphotype analysis has been used by a number of workers, particularly in Quaternary and Recent sediments (e.g. Corliss, 1985; Jones, 1986; Severin, 1983). However a number of other workers have applied the techniques developed in the analysis of modern species, and the form and function of their test structure, to fossil sediments and foraminiferal assemblages (e.g. Chamney, 1976; Bernhard, 1986; Koutsoukos and Hart, 1990). Koutsoukos and Hart present a full analysis of this technique in their 1990 paper on foraminiferal morphogroup distribution patterns, palaeocommunities and trophic strunctures, and it is not in the scope of this study to repeat this work, however, the main findings are used to define the morphotype groups in this study. In using morphotype analysis the limitations to the technique must be acknowledged. It would be near impossible to detail the complete behavioural structure of fossil foraminifera, instead the probable main environmental and physiological driving forces behind their distribution is attempted to be discerned.

	General morphotype	Inferred microhabitat	Inferred trophic group	Taxa groups	
Planktonic	biserial and triserial	shallow planktonic	suspension feeder	*Guembelitria*, *Heterohelix*	P1
	unkeeled planispiral	shallow planktonic	suspension feeder	*Globigerinelloides*	P2
	unkeeled trochospiral	shallow planktonic	suspension feeder	*Hedbergella*, *Whiteinella*	P3
	keeled planispiral/trochospiral	deep planktonic	suspension feeder	*Rotalipora*, *Praeglobotruncana*, *Dicarinella*, *Marginotruncana*	P4
Benthic agglutinated	tubular or branching	epifaunal	suspension feeder	*Rhizzammina*, *Hippocrepina*	BA1
	Globular	epifaunal/shallow infaunal	deposit feeder	*Psammosphaera*	BA2
	planispiral/streptospiral subspherical/flattened	epifaunal/shallow infaunal	deposit feeder	*Ammodiscus*, *Glomospira*, *Glomospira*	BA3
	low trochospire/streptospiral spherical/subspherical	epifaunal/shallow infaunal	deposit feeder	*Ammosphaeroidina*	BA4
	elongate, variably coiled uni and multiserial	infaunal	deposit feeder	*Reophax*, *Dorothia*, *Marssonella*, *Tritaxia*, *Gaudryina*, *Spiroplectinella*, *Spiroplectammina*, *Vernuilina*, *Textularia*, *Arenobulimina*	BA5
Benthic calcareous hyaline	plano/concavoconvex, low trochospiral	epifaunal/shallow infaunal	deposit feeder	*Gavelinella*, *Berthelina*, *Lingulogavelinella*, *Anomalina*	BC2
	inflated, biconvex, periphery rounded	epifaunal/shallow infaunal	deposit feeder	*Gyroidinoides*, *Pullenia*, *Valvulineria*	BC4
	biconvex lenticular, trochospiral	epifaunal	deposit feeder	*Osangularia*, *Conorotalites*, *Charltonina*, *Schiebnerova*	BC1
	biconvex lenticular, planispiral	epifaunal/shallow infaunal	deposit feeder	*Lenticulina*, *Saracenaria*,	BC5
	Conical, low trochospiral	epifaunal	deposit feeder and passive herbivore	*Eurycheilostoma*, *Iulisina*, *Quadromorphina*, *Gubkinella*	BC3
	globular/ovate to elongate/fusiform	epifaunal/infaunal	deposit feeder	*Globulina*, *Pyrulina*, *Ellipsoglandulina*, *Lagena*, *Fissurina*, *Oolina*	BC6
	elongate broad to palmate uniserial	epifaunal/infaunal	deposit feeder	*Citharina*, *Vaginulina*, *Psilocitharella*, *Frondicularia*, *Vaginulinosis*, *Hemirobulina*	BC7
	elongate straight to arcuate uniserial/planispiral to uniserial	epifaunal/infaunal	deposit feeder	*Dentalina*, *Laevidentalina*, *Nodosaria*, *Tricarinella*, *Pseudonodosaria*, *Marginulina*, *Marginulinopsis*, *Vaginulina*, *Nodosarela*, *Pleurostomella*, *Astacolus*, *Planularia*, *Ellipsodimorphina*	
	tapered rounded, elongate tri-bi-uniserial	infaunal	deposit feeder	*Neobulimina*, *Praebulimina*, *Cassidella*, *Cuneus*, *Turrilina*, *Bulimina*	BC8
	tapered flattened elongate biserial	infaunal	deposit feeder	*Bolivina*, *Coryphostoma*, *Bolivinoides*, *Tappanina*, *Spirobolivina*	BC9
	irregular, meadrine	epifaunal	deposit feeder	*Ramulina*	BC10
Benthic calcareous porcelanous	elongate to ovate, quinquloculine	epifaunal/shallow infaunal	deposit feeder	*Quinqueloculina*	BP1

Table 2.1: Table of Morphotypes used in this study, with life mode, trophic type and typical genus types for each category (Based on work by Koutsoukos and Hart, 1990).

Similarly many modern (and fossil) foraminifera can live in a variety of habits directly related to changes in the sediment/water interface, distribution of food, and environmental stress. It must be stressed therefore that the inferred life positions (infaunal, epifaunal and epifaunal/infaunal) represent only preferential habits (Koutsoukos and Hart, 1990). Distinct microhabitat differences have been shown to exist between benthonic foraminiferal species of the same genus and this must be taken into account when assessing the life mode of certain species. More recent work on the isotopic composition of foraminiferal species has led to further understanding of depth habitats (planktonic) and microhabitats (benthonic), and it is hoped this may help in the future to further understand the life habits of specific fossil foraminiferal species.

Species identification was undertaken as far as possible with those not identifiable to the species level were placed in open nomenclature. This is discussed further in Chapter 3. The presence of other sedimentary components such as glauconite and pyrite, and other biological components such as fish scales and teeth, shell fragments and other microfossils (ostracods, radiolaria and calcispheres) was also noted, and examples were picked for further analysis.

Counts of each species were recorded (see Appendix 2) and key species, genus' and morphotypes were calculated as percentages for full comparative analysis throughout the cores and sections, and across all sites. These are presented as tables and graphs in the results sections of Chapters 4 and 5.

Analysis was also carried out on abundance, species richness and diversity, using the fisher alpha index (see Murray, 1991). All foraminiferal slides have been kept and our housed as part of the School of Earth, Ocean and Environmental Sciences micropalaeontological collection.

Analysis of the thin sections was undertaken using qualitative analysis. Each species seen was noted and photographed using a Nikon Coolpix 4500 on an Olympus Vanox microscope. Scanning electron microscopy was undertaken in the Electron

Microscopy Centre at the University of Plymouth. Selected specimens were mounted onto stubs and coated with approximately 10Å of gold. Analysis of the foraminifera was carried out on a JEOL 5600 scanning electron microscope. Photomicrographs of the scanned specimens were taken digitally and used to make up plates seen in Appendix 1.

2.3 Carbon and oxygen stable isotopic analysis

Isotope analyses were carried out on both bulk (whole rock fine fraction, < 63 μm) samples and monospecific foraminiferal samples, in order to gain isotopic information on the whole water column at different oceanographic settings.

Carbon isotopes relate to the amount of dissolved inorganic carbon (DIC) in seawater, which is maintained relatively near to zero (relative to the PDB international standard), balanced by the influx of carbon from terrestrial weathering, volcanic sources, oxidation of organic matter, and the output through the production of marine carbonates and burial of organic matter. Typically there is not a large amount of variation in the amount of DIC in the ocean. A gradient of $\delta^{13}C$ values is, however, seen through the water column (Berger and Vincent, 1986; Marshall, 1992). This is related to ocean productivity. Organic matter is predominantly composed of light carbon, and, therefore, has very negative $\delta^{13}C$ values. Removal of organic carbon from the oceanic reservoir therefore renders surface waters relatively enriched in ^{13}C (Berger & Vincent 1986; Marshall 1992). As the organic matter moves down through the water column to the sea floor, it begins to breakdown and be oxidised, returning the light carbon back into ocean waters. The surface waters, therefore, often show more positive $\delta^{13}C$ values than deeper in the water column and at the sea floor, and the more enhanced productivity is, the more pronounced this difference in surface and deep water $\delta^{13}C$ values becomes. Organisms, such as foraminifera, are considered to precipitate their tests in equilibrium with the isotopic composition of the water (e.g., Fairbanks *et al.,* 1980; Savin *et al.,* 1985). Hence, assuming little or no 'vital effects', those organisms living in the surface waters (e.g., planktonic

foraminifera and nannofossils) record the isotopic composition of the surface waters, whilst those origin living on the seafloor (e.g., benthonic foraminifera and molluscs) will record the isotopic composition at the bottom of the water column. Comparison of these values enable the cycling of carbon through the water column to be determined, and productivity or stratification of the water column at that time to be determined.

Oxygen isotopes are similarly related to the oxygen isotope composition of the water (related to salinity), and importantly temperature of the water mass. Globally, the oxygen isotope value of seawater is predominantly controlled by the amount of polar ice. Polar ice preferentially takes up the lighter ^{16}O, leaving global waters enriched in the heavier ^{18}O and more positive $\delta^{18}O$ values. At times such as the mid-Cretaceous when it is believed there is no polar ice (e.g., Huber, 1998) the ocean waters were enriched with lighter ^{16}O and more negative oxygen isotope values are seen. Similar to the carbon isotopes, the calcium carbonate tests of foraminifera and nannofossils will precipitate in equilibrium with the oxygen isotope value of the seawater. In nearshore settings in particular, variation in the isotopic composition of water can be caused variations in evaporation and precipitation and/or freshwater runoff.

Diagenesis can cause large changes in the primary isotopic signal, the original isotope values of the carbonate becoming overprinted by recrystalisation of the sediment and its components, in an environment different from that in which it originally formed. The amount of diagenesis depends on the type of sediment, and its diagenetic history, related for instance to burial depth and rate. Diagenesis can occur early on (e.g., on the sea floor), or in shallow burial, or much later at depth. These both have a differing effect on the isotope signals, but both will overprint any original isotope signal. All samples were assessed for diagenesis using scanning electron microscopy, thin section analysis, and trace element analyses to determine the validity to isotope results and interpretation.

Assuming that the isotopic compositions of the foraminifera do represent primary marine values, a number of assumptions regarding the temperature of the oceans during the

mid-Cretaceous may be made. Calcite palaeotemperatures have been calculated using the equation of Anderson & Arthur (1983). This expresses the oxygen isotopic composition of the water, δw directly relative to the (Standard Mean Ocean Water) SMOW standard:

$$T(^{\circ}C) = 16.0 - 4.14\,(\delta c - \delta w) + 0.13\,(\delta c - \delta w)^2$$

where δc equals the oxygen isotopic composition of the calcite with respect to the PDB international standard and δw equals the oxygen isotopic composition of the water from which the calcite was precipitated with respect to the SMOW standard. A δw of -1.0‰ SMOW is thought to be appropriate for an ice free world (Shackleton & Kennett, 1975). Zachos *et al.* (1994) used a $\delta^{18}O$ adjustment factor which compensates for possible changes in surface waters (due to evaporation and precipitation) at different latitudes based on modern latitudinal changes in δw related latitudinal salinity gradients in the modern ocean system. Given the palaeolatitude of, for example, Sites 766 and 762, such an adjustment would have a negligible effect on calculated temperatures.

2.3.1 Processing methods and preparation of samples

2.3.1.1 Bulk isotope analysis

For samples that had been processed for foraminiferal analysis bulk isotope analysis was carried out on the fine (<63 μm) fraction of the sediment samples. This fraction was chosen over ground homogenised whole rock samples in order to control the source of the carbonate in the sediment being analysed and, therefore, the part of the water column that the isotope results represent. The < 63 μm fraction was collected during the processing of the samples for foraminiferal analysis. Following the breakdown of sediments as outlined above, a portion of the < 63 μm fraction can be collected as the samples are washed over a 63 μm sieve to collect the coarser foraminiferal portion. At less than 63 μm the majority of the calcium carbonate in this fraction will be coccolithic in

origin, and contamination of the sample by secondary cements, or other carbonate allochems such as shell fragments and foraminifera found in the coarser fractions, can be kept to a minimum. Coccoliths inhabited the surface waters of the oceans, and by controlling the source of the calcium carbonate as much as possible, we should find the results from the fine fraction to represent the isotopic composition of these surface waters. The fine fraction samples were collected from the wash of the 63 μm sieve, in a large beaker. As a lot of water was also collected the samples were left to stand until the sediment had settled on the base of the beaker. The water was then pipetted off as much as possible and the samples were placed in an oven at 40°C for 24 hours until dry. Once dried the samples were removed from the beakers and ground in an agate pestle and mortar to powder the sediment for analysis. The samples were then weighed and placed in small sample bags to await analysis. These samples were also used for trace element analysis, Rock Eval and total organic carbon (TOC) measurements. These methods will be discussed below.

For samples rich in TOC a portion of the fine fraction sediment was treated with sodium hypochlorite, in order to remove any organics from the samples and rule out contamination of the isotopic analysis by the presence of organic matter. Samples were soaked overnight in a solution of 5% sodium hypochlorite. Once soaked the samples were washed and filtered 3 times with deionised water in order to remove all traces of the sodium hypochlorite. Once washed the samples were dried in an oven at 40°C, and placed in sample bags ready for analysis. A sample of both treated and untreated sediment from these samples were analysed for isotopes, in order to compare the results and assess the influence of organic matter in these sediments.

For those sediment samples, that were too hard to be broken down and the <63 μm collected, specific sub-samples of the rock specimens were removed and crushed to a powder in an agate pestle and mortar. In doing this we are not constraining the source of the carbonate as well. Careful subsampling, however, allows the bulk carbonate of the rock

sample to be analysed. Careful thin section analysis is, therefore, required for these samples when interpreting the isotopic results.

2.3.1.2 Foraminiferal isotope analysis

Samples picked for isotope analysis were processed as outlined above for foraminiferal analysis. Once processed the samples were split into two portions, and specimens were picked from the fraction chosen for isotope analysis. To avoid ontogenetic effects each foraminiferal species used for analysis should be of a similar size. Samples were, therefore, dry sieved over 125, 250 and 500 μm sieves and specimens were picked where possible from single size fractions for each species.

For the isotope analysis of foraminifera, particular species were chosen to represent specific parts of the water column, depending on their life mode and depth of habitat. Species to represent benthic, deep dwelling planktonic and shallow planktonic environments were chosen, that were abundant and relatively well preserved. Preservation of the foraminifera will be discussed in more detail in Chapters 4 and 5.

Planktonic foraminiferal species

Where possible monospecific planktonic foraminifera were picked from each sample. Where specimens were rare monogeneric assemblages were picked. To represent surface waters species of the planktonic genus *Hedbergella*, thought to have grown in near surface waters (Caron and Homewood, 1982; Leckie, 1987), were used. To minimise ontogenetic effects specimens were picked where possible, from one size fraction. For *Hedbergella* the 125-250 μm size fraction was used primarily, where specimens were rare in this size fraction the 63-125 μm was used. In order to undertake the isotopic analysis 60-80 μg of foraminifera was required. Between 20 and 30 specimens of *Hedbergella* were, therefore, picked from the 125-250 μm size fraction, and as many as 60 specimens from the 63-125 μm fraction. The keeled planktonic foraminifera, *Rotalipora,* was chosen to represent

deeper dwelling planktonics (e.g., Hart and Bailey, 1979; Caron and Homewood, 1982; Leckie, 1987). Other keeled foraminifera such as *Planomalina, Dicarinella, Marginotruncana* and *Praglobotruncana* were also analysed alongside *Rotalipora* to look at variations in the isotopic composition of these species, and to provide isotopic information in parts of the core where *Rotalipora* are not found. Between 10-15 specimens of these larger planktonic foraminifera were picked from the >250 μm fraction.

Benthic foraminiferal species

Due to the lower abundance of benthonic foraminifera, monogeneric assemblages of benthonic foraminifera were picked. The genus *Berthelina* was primarily used for benthonic analyses. Characterised by Koutsoukos and Hart (1990) as epifaunal to shallow infaunal, measurements of *Berthelina* provide us with isotopic information of conditions at the seafloor. Analyses were also carried out on *Gyroidinoides*, again to provide a comparison with *Berthelina* and provide information on the benthonic environment where *Berthelina* was absent. Around 15 – 20 benthonic specimens were picked from the >250 μm fraction. Where larger specimens were rare, greater numbers were picked from the smaller 125-250 μm and 63-125 μm fractions.

In choosing foraminiferal specimens for analysis it was important that those showing the least amount of diagenetic alteration were chosen. Thin section and SEM analysis was used to provide a general view on the diagenetic state of the foraminifera in different portions of the cores and sections analysed. However, in picking individual specimens, optical analysis was used, choosing those specimens that appeared to have glassy and transparent tests, retaining original features and showing no evidence of recrystalisation. Some specimens were broken open to analyse any infilling by secondary calcite and again, where possible specimens showing signs of secondary calcite overgrowths and infilling were not chosen for analysis. Unfortunately a large proportion of specimens from the upper part of ODP Core 762C were infilled to some extent. Analysis

was continued on these specimens, those least effected were picked preferentially where possible, and the results will be discussed later. Specimens of foraminifera were also chosen that were clean from adhering clay or grains. Any remaining clays were removed as much as possible and the specimens were cleaned in ethanol before analysis. Once picked, the specimens were placed in small sample tubes ready for analysis.

2.3.2 Instrumentation

In order to analyse the isotopic composition of bulk and foraminiferal sediments a number of different mass spectrometer equipment was used. A brief outline of the instruments used in this study is given below.

Bulk isotope methods

Oxygen and carbon isotope analyses on the fine fraction carbonate from the Crimea and ODP Sites 762C and 766A were undertaken the NERC Isotope Geosciences Laboratory at the British Geological Survey in Keyworth, UK. 10 mg of each sample was analysed using standard offline vacuum methods (McCrea, 1950) on a dual inlet stable isotope mass spectrometer.

Foraminiferal isotope methods

All foraminiferal isotope analyses were carried out at the NERC Isotope Geosciences Laboratory at the British Geological Survey in Keyworth, UK, on a VG Optima Gas Source Mass Spectrometer attached to an Isocarb online preparation system. Each sample of foraminifera was homogenised in a pestle and mortar and between 60–80 µg of the sample was weighed into small sample boats to be placed directly into the Isocarb. As the samples are smaller contamination is more significant, and sample homogeneity is also an issue. A larger spread of data can, therefore, be expected with this method.

Analysis of results

The resultant gas values of all results were corrected using the Craig Correction to adjust for small levels of ^{17}O isotopes, and a fractionation factor. Further normalisation through the primary standard was also applied. Analytical precision, based on duplicate samples was typically <0.1‰ for both oxygen and carbon isotope ratios. Consistency of results was achieved by comparison of laboratory standards against NBS-19. The ratios obtained are presented in relation to the heavier isotope using the δ notation and the VPDB scale.

2.4 Geochemical analysis

A number of geochemical analyses were undertaken on the samples to obtain further information on the sediments and diagenesis. This included measurement of total organic carbon (TOC), determination of the source of organic carbon (RockEval) and trace element analysis.

2.4.1 Instrumentation

All analyses were carried out on the fine fraction sediments collected from the previous processing of sediments for foraminifera as outlined above. The methods of analysis for each process will be discussed below.

2.4.1.1 Total organic carbon

TOC analysis was carried out at the University of Plymouth. Initially samples were analysed for TOC using the loss on ignition (LOI) method. This method is commonly used to estimate the organic and carbon content of sediments (e.g., Dean, 1974; Bengtsson and Enell, 1986). Around 200-500 mg of sediment was placed in weighed crucibles. The sediment was then weighed and dried in an oven overnight at 105°C. Once dried and cooled they were weighed again to determine the dry weight and not bias the results to

include water content in the measurements. Samples were then placed in a muffle furnace at a temperature of 550°C for two hours. At this temperature any organic matter in the sediments will become oxidized to carbon dioxide and ash. The samples were then removed from the furnace and cooled, before being weighed again. The amount of organic matter can then be calculated as a weight percent using the weight loss measured. The samples were then returned to the furnace at a temperature of 950°C for four hours to determine the weight percent of carbonate in the sample. At 950°C the carbonate in the samples will evolve carbon dioxide. Once removed from the furnace the samples were again cooled and weighed to determine the weight loss and weight percent of carbonate in the samples. Dean (1974) evaluated the method and concluded it was a fast and effective, inexpensive method of determining carbonate and organic contents of sediments. However, Dean (1974) indicates that the method to be good for clay poor sediments and notes various losses of salts, structural water and inorganic carbon can occur. Bengtsson and Enell (1986) warn that clay may lose structural water during LOI, and according to Ball (1964) this can occur at temperatures as low as 500°C, causing a weight loss of up to 20% in clay minerals. Once the analysis was completed the values for organic carbon appeared very high compared to the available published data. On comparison with alternative results for the measurement of organic carbon on a carbon analyser (see below), it was clear the weight percentages of organic carbon were much higher in the LOI method. This was thought to be due to the high clay content of the sediments and the presence of interstitial waters. It was concluded, therefore, that LOI was unsuitable as a method for determining TOC in the sediments encountered in this study.

As an alternative to LOI weight percentage of both organic and inorganic carbon can be determined using a carbon analyzer. A small amount of sample (40-50 mg) was crushed and homogenised in an agate pestle and mortar, and analysed in a solid sample module 55M-5000A. Samples were duplicated where possible and reproducibility was generally better than 0.1%. All results are given as wt. % TOC.

2.4.1.2 Rock-Eval analysis

Samples containing organic matter (as determined by the TOC measurements) were analysed with a Rock-Eval 6 at the University of Neuchâtel, to determine the source of organic matter.

Rock-Eval pyrolysis is a widely used method for characterizing organic matter first described by Espilalié *et al.* (1977). A 60 mg sample of sediment is heated in an inert helium atmosphere in a number of stages, pyrolysis occurs and hydrocarbons, other organic compounds and carbon dioxide are generated. Measurements of these fractions determine the Hydrogen Index (HI) and Oxygen Index (OI) values, which are then used to characterize the kerogen type.

Pyrolysis was carried out on all samples with TOC values >0.5 wt.%. Samples with <0.5 wt. % were eliminated from analysis because of mineral matrix effects, giving erroneous oxygen indices, especially in samples containing appreciable calcium carbonate (Katz, 1983; Peters, 1986). Once the HI and OI were determined the values were plotted on a Van Krevelen diagram to classify the type of Kerogen and determine the source of organic carbon.

2.4.1.3 Trace element analysis

Trace element analysis was carried out on sediment samples from ODP Core 762C and 766A. Trace element analysis can be measured using either flame atomic absorption (AA) or inductively coupled plasma - atomic emission spectrometry (ICP-AES), chosen depending on the elements to be analysed and expected concentrations of them. For this study the atomic absorption was chosen, and samples were run on the Spectra 220 Atomic Absorption Spectrometer at the University of Plymouth.

In order to measure the trace elements in the sediments, samples are dissolved in acid to produce a solution which can be analysed by the AA. In order to determine the best

methodology to dissolve the carbonate in the samples a number of factors were taken into consideration.

This analysis is carried out on the calcium carbonate component of the sediments. Care must be taken to dissolve only the calcium carbonate. This is particularly important in samples such as those from the ODP cores being analysed, which are clay rich. Clays often contain high concentrations of iron and increased levels of magnesium. Dissolving any of the clays may, therefore, cause increases in these elements and lead to an incorrect interpretation of results. The amount and concentration of acid used in the digestion must be enough to digest the calcium carbonate in all of the samples, but not too much so as to etch and dissolve the clays. The amount of carbonate in the samples must, therefore, be determined.

Sample no.	TC (%)	IC (%)	TOC (%)	CaCO3 (%)	% digested	% undigested
123-766C-15R-1 80-82	6.61	6.04	0.57	50.31	71.95	28.05
123-766C-15R-1 105-107	6.22	5.80	0.42	48.32	66.08	33.92
123-766C-15R-1 130-132	1.81	1.71	0.10	14.25	23.05	76.95
123-766C-15R-2 1-3	5.72	4.95	0.78	41.20	59.25	40.75
123-766C-15R-2 10-12	3.45	2.96	0.50	24.62	43.15	56.85
123-766C-15R-2 20-22	4.11	3.70	0.41	30.78	41.88	58.12
123-766C-15R-2 30-32	5.11	4.45	0.66	37.08	45.92	54.08
123-766C-15R-2 40-42	2.29	1.76	0.53	14.65	23.39	76.61
123-766C-15R-2 50-52	0.99	1.10	0.00	9.17	8.63	91.37
123-766C-15R-2 60-62	1.21	0.91	0.30	7.56	8.46	91.54
123-766C-15R-2 70-72	1.00	0.91	0.09	7.56	7.78	92.22
123-766C-15R-2 80-82	1.10	1.01	0.10	8.38	6.39	93.61
123-766C-15R-2 90-92	1.09	1.21	0.00	10.09	7.17	92.83
123-766C-15R-2 100-102	1.06	1.01	0.05	8.40	6.55	93.45
123-766C-15R-2 110-112	1.28	1.27	0.01	10.55	7.25	92.75
123-766C-15R-2 120-122	1.03	0.97	0.06	8.09	8.06	91.94
123-766C-15R-2 130-132	1.36	1.40	0.00	11.68	13.14	86.86
123-766C-15R-2 140-142	1.45	0.91	0.54	7.56	10.85	89.15

Table 2.2: This table shows a selection of data from ODP Core 766A. Percent digested can be seen to show slightly greater value than the percentage of calcium carbonate.

Total carbon (TC) was measured in a number of samples on the carbon analyser in order to calculate the amount of inorganic carbon (IC). These results were then used to calculate the amount of calcium carbonate (% weight of inorganic carbon x 8.33). Concentrations of calcium carbonate were seen to fluctuate greatly from concentrations <10 to 70 wt. % (see Table 2.2). Based on this information it was decided to use 20 ml of 50% hydrochloric acid to dissolve between 300-500 mg of sediment. The sediment was weighed into volumetric flasks to which the acid was added. The flasks were then topped up to 100 ml with 2% nitric acid. As the acid only digested the calcium carbonate, the solutions were filtered to remove the clay residue. This residue could then be retained and dried to calculate the actual weight of sediment digested to provide more accurate results, and to determine if any of the clays had been digested. This could be carried out by a comparison of the percentage of sediment digested with the calcium carbonate wt. % values. This comparison showed the percent digested to generally be slightly more than the percent of calcium carbonate in the sample, a sample of this data is seen in Table 2.2. This implies that some of the clay had been digested. In order to determine the full effect of this a complete digestion of the sample, with hydrofluoric acid, would need to be carried out. Unfortunately, this was beyond the timescale and scope of this project. It must, therefore, be taken into account on analysis of the trace element results that values of iron and to a lesser extent magnesium may be enhanced by the concentration of them in the clays. The general trends of the trace elements used to determine diagenesis with in the cores, should however remain unaffected.

Chapter 3 Taxonomy

3.1 Introduction

This chapter presents a systematic record of the planktonic and benthonic foraminifera from the Albian – Turonian of the Tethyan and Indian Oceans. 194 species belonging to 84 genera are recognised.

Where possible the taxa are illustrated by scanning electron microphotographs presented in Plates 1 to 15 in Appendix 1 of this study.

3.1.1 Classification

The classification followed in this study is that of Loeblich and Tappan (1987, 1992). The classification above the family level follows Loeblich and Tappan (1992), whist the generic definitions used for benthonic foraminifera are according to Loeblich and Tappan (1987), and for the planktonic foraminifera by Robaszynski and Caron (1979) and Caron (1985). Where exceptions to this classification exist, a short description following the taxonomic unit is given to discuss the differences, with references if possible, to other classifications and usage. An example of such a change includes the generic revision of five rotaliine genera proposed by Revets (1996).

A full monographic description of each genus and species is not undertaken in this study. Remarks will follow the genus where necessary to describe the author's concept of that particular genus, including any notable variation. For each species the taxonomic description has been kept brief, with only diagnosis being given. More extensive morphological descriptions are made where the species is new or poorly described in the literature, or significant variation is observed.

A full synonymy and reference list is not presented. The references have, therefore, been restricted to the original description of the species, and subsequent references that show taxonomic change, or show superior descriptions or illustrations particularly

resembling the current diagnosis of the taxon. A recent reference has also being included where possible.

Open nomenclature has been used for taxa that do not closely match published descriptions, and the following abbreviations have been used:

cf.	for taxa similar to a known species but different in some detail.
aff.	for taxa showing close affinity to a well defined taxonomic group.
sp. 1, 2...	for potentially new species which do not match published descriptions.
spp.	for taxa not determinable at the specific level.
ex. gr.	for species thought to belong to a specific group, often where a complex lineage exists.

Following the diagnosis of the taxa the stratigraphical range of the species is given, followed by the life mode and morphotype. As previously discussed in Chapter 2 the morphological analysis of foraminiferal species can provide important information on the palaeoenvironmental and on population dynamics not seen in analysis at the specific level. Morphotypes used were defined by Koutsoukos and Hart (1990) with additional information from Charnock and Jones (1985). A table of morphotypes and corresponding genera is also found in Chapter 2.

3.1.2 Taxonomic problems

Taxonomic confusion can also exist in the variation of species. Species such as the planktonic taxon *Globigerinelloides bentonensis* have a number of synonyms arising from size and slight morphological differences. Carter and Hart (1977) determined that size alone was not a criteria for separating these species and upheld *G. bentonensis* as the valid name encompassing the small variations seen in the synonyms *G. caseyi* and *G. eaglefordensis*. Similarly, on a larger scale, the suprageneric classification within the

family Nodosariacea is also controversial, and taxonomic confusion exists at the species and generic levels because of the considerable variation seen within the group. Numerous transitional forms exist between species, leading to subjective and arbitrary classification.

These problems have been taken into account during the determination of foraminiferal species in this study, and an effort has been made to relate some of the more 'provincial' studies to a more global classification. References have been included to support assumptions made on the determination of certain species and their global distribution.

3.2 Systematic descriptions

Class FORAMINIFEREA Lee, 1990

Order ASTORHIZIDA Lankester, 1885

Superfamily ASTRORHIZACEA Brady, 1881

Family RHABDAMMINIDAE Brady, 1884

Subfamily RHABDAMMININAE Brady, 1884

Genus ***Rhabdammina*** Sars, 1869

Type species: *Rhabdammina abyssorum* Sars, 1869

***Rhabdammina* spp.**

Plate 1, Fig. 1

Diagnosis: Short, unbranched, compressed tubular fragments of *Rhabdammina*. Coarsely agglutinated with a terminal aperture.

Age range: Upper Cenomanian to Lower Turonian

Genus ***Rhizammina*** Brady, 1879

Type species *Rhizammina algaeformis* Brady, 1879

***Rhizammina* spp.**

Plate 1, Figs 2-3

Diagnosis: Finely-medium agglutinated, branched, or unbranched tubes of *Rhizammina*.

Remarks: In the Upper Albian at Site 766 specimens are very fine grained, agglutinated with short spines, unflattened tubes.

Age range: Upper Albian to Lower Turonian

Family PSAMMOSPHAERIDAE Haeckel, 1894

Genus ***Psammosphaera*** Schulze, 1875

Type species: *Psammosphaera fusca* Schulze, 1875

Psammosphaera fusca Schulze, 1875

Plate 1, Fig. 4

1875 *Psammosphaera fusca* Schulze, p.113, pl. 2, fig. 8a-f.

1997 *Psammosphaera fusca* Schulze: Holbourn & Kaminski, p. 32, pl. 2, figs 4-5.

Diagnosis: *Psammosphaera* with a spherical to subspherical test. Coarsely agglutinated.

The aperture is a small, single hole, but is indistinct.

Age range: Upper Albian to Lower Cenomanian

Superfamily HIPPOCREPINACEA Rhumbler, 1895

Family HIPPOCREPINIDAE Rhumbler, 1895

Subfamily HYPERAMMININAE Eimer & Frickert, 1899

Genus ***Hippocrepina*** Parker, 1870

Type species: *Hippocrepina indivisa* Parker, 1870

Hippocrepina gracilis Holbourn & Kaminski, 1995

Plate 1, Figs 5, 10

1995 *Hippocrepina gracilis* Holbourn & Kaminski, p. 34, pl. 1, figs 15-16.

1997 *Hippocrepina gracilis* Holbourn & Kaminski: Holbourn & Kaminski, p. 34, pl. 4, figs 3-5.

Diagnosis: *Hippocrepina* with a narrow, elongated, gently compressed tube that tapers towards the base. Finely agglutinated wall. Aperture is the open end of the tube.

Age range: Upper Albian to Lower Turonain

Order LITUOLIDA Lankaster, 1885

Superfamily AMMODISCACEA Reuss, 1862

Family AMMODISCIDAE Reuss, 1862

Subfamily AMMODISCINAE Reuss, 1862

Genus ***Ammodiscus*** Reuss, 1862

Type species: *Ammodiscus infimus* Bornemann, 1874

Ammodiscus cretaceus (Reuss, 1845)

Plate 1, Fig. 6

1845 *Operculina cretacea* Reuss, 1845, p. 35, figs 64-65.

1946 *Ammodiscus cretaceus* (Reuss): Cushman, pl. 1, fig. 35.

1997 *Ammodiscus cretaceus* (Reuss): Holbourn & Kaminski, p. 35, pl. 4, figs 7-8.

Diagnosis: A species of *Ammodiscus* with a finely agglutinated tube. The test slowly increases in diameter, each new whorl slightly overlapping the last.

Age range: Upper Cenomanian

Subfamily AMMOVERTELLININAE Suleymanov, 1959

Genus ***Glomospira*** Rzehak, 1885

Type species: *Trochammina squamata* Jones and Parker var. *gordialis* Jones and Parker, 1860

Glomospira charoides (Jones & Parker, 1860)

Plate 1, Fig. 7

1860 *Trochammina squamata* var. *charoides* Jones & Parker, p. 304.

1997 *Glomospira charoides* (Jones & Parker): Holbourn & Kaminski, p. 36, pl. 5, figs 7-11.

Diagnosis: *Glomospira* with a tubular test, coiling about a vertical axis, with four to five whorls in the outermost layer of coils. Coiling may be variable, and the tubular chamber may become irregular in the later part of the test

Remarks: The "*Glomospira* biofacies" is often found in association with siliceous and organic rich sediments and may reflect higher surface water productivity. In modern environments large numbers of *Glomospira charoides* have been recorded in organic rich substrates, indicating that the species is tolerant of dysoxic conditions.

Age range: Upper Albian to Lower Turonian

Glomospira irregularis (Grzybowski, 1896)

Plate 1, Fig. 8

1896 *Ammodiscus irregularis* Grzybowski, p. 285, pl. 11, figs 2-3.

1997 *Glomospira irregularis* (Grzybowski): Holbourn & Kaminski, pp. 36-37, pl. 6, figs 1-2.

Diagnosis: A tubular, streptospirally enrolled species of *Glomospira* with a coarse wall. The tube remains a constant thickness throughout.

Age range: Uppr Albian

Genus ***Glomospirella*** Plummer, 1945

Type species: *Glomospira umbilicata* Cushman &Waters, 1927

Glomospirella gaultina (Berthelin, 1880)

Plate 1, Fig. 9

1880 *Ammodiscus gaultinus* Berthelin, p. 19, pl. 1, fig. 13.

1973 *Ammodiscus gaultinus* Berthelin: Maync, p. 1081, pl.1, figs 4-5.

1997 *Glomospirella gaultina* (Berthelin): Holbourn & Kaminski, 1997, pp. 36-37, pl. 6, figs 4-6.

Diagnosis: Finely agglutinated species of *Glomospirella* that is initially streptospiral or irregular coiling, becoming planispiral in later stages. Aperture at open end of tube.

Age range: Upper Albian

Superfamily HORMOSINACEA Haeckel, 1894

Family HORMOSINIDAE Haeckel, 1894

Subfamily REOPHACINAE Cushman, 1910

Genus ***Reophax***, de Montfort, 1808

Type species: *Reophax scorpiurus* de Montfort, 1808

Reophax sp. 1

Plate 1, Fig. 11

Diagnosis: A species of *Reophax* with a compressed test formed of 3-4 chambers that gradually increase in size. Aperture terminal.

Age range: Upper Cenomanian

Reophax sp. 2

Plate 1, Fig. 12

Diagnosis: A species of *Reophax* comprised of 3-4 chambers rapidly increasing in size. The final chamber makes up nearly half of the test and is bent at an angle to the initial part of the test. The sutures are slightly depressed and indistinct, and the aperture is terminal and round.

Remarks: It is difficult to differentiate this species from *Uvigerammina* due to the indistinctness of the initial part of the test. As none of the species present show an initial trochospiral portion or overlapping chambers, specimens are determined to be species of *Reophax.*

Age range: Upper Albian

Superfamily HAPLOPHRAGMIACEA Eimer & Fickert, 1899

Family AMMOSPHAEROIDINIDAE Cushman, 1927

Subfamily AMMOSPHAEROIDININAE Cushman, 1927

Genus ***Ammosphaeroidina*** Cushman, 1910

Type species: *Haplophragmium sphaeroidiniforme* Brady, 1884

Ammosphaeroidina **sp. 1**

Plate 1, Fig. 13

1997 *Ammosphaeroidina* sp. Holbourn and Kaminski, p. 40, pl. 12, figs 5-6.

Diagnosis: *Ammosphaeroidina* with a subsphaerical test, slightly streptospiral coiling and only four chambers visible from the exterior. The aperture is interiomarginal, but indistinct.

Age range: Upper Albian to Upper Cenomanian

Superfamily SPIROPLECTAMMINACEA Cushman, 1927

Family SPIROPLECTAMMINIDAE Cushman, 1927

Subfamily SPIROPLECTAMMININAE Cushman, 1927

Genus ***Spiroplectinella*** Kisel'man, 1972

Type species: *Spiroplecta wrightii* Silvestri, 1903

Spiroplectinella gandolfi (Carbonnier, 1952)

Plate 1, Fig. 14

1952 *Spiroplectammina gandolfi* Carbonnier, p. 112, pl. 5, fig. 2.

1992 *Spiroplectinella gandolfi* (Carbonnier): Haig, p. 287, pl. 1, fig. 7.

1997 *Spiroplectinella gandolfi* (Carbonnier): Holbourn & Kaminski, p. 46, pl. 16, figs 3, 5.

Diagnosis: *Spiroplectinella* with an elongate and flattened test. Initially planispiral, it becomes biserial, flaring rapidly. Chambers low and broad, separated by depressed sutures.

The wall is agglutinated, smoothly cemented with calcareous cement. The aperture is a low arch at the base of the last chamber.

Age range: Upper Albian to Lower Cenomanian

Spiroplectinella sp. 1

Plate 1, Figs 15, 20

1997 *Spiroplectinella* sp. Holbourn & Kaminski, p. 46, pl. 16, fig. 4 a-b.

Diagnosis: A broad species of *Spiroplectinella* with short planispiral phase becoming biserial and flaring rapidly. Chambers low and broad, separated by depressed sutures. Wall finely agglutinated. Aperture a low arch at the base of the last chamber.

Remarks: This species can be seen to make its test from coccoliths, found cemented in a preferred orientation, the convex, distal side of the coccolith facing outwards from the test. This was also seen at ODP Site 766 by Holbourn and Kaminski (1997), who determined the coccoliths to be *Watznaueria barnesae*. This use of coccoliths in test formation was also seen in the species *Gaudryina cribrosphaerellifera* from the Upper Cretaceous of the Central Pacific Ocean, by Widmark and Henriksson (1995) and in *Gaudryina pulvina* in Sikora and Olsson (1991). It was suggested by Widmark and Henriksson (1995) that the central areas of the coccoliths may have acted as sieve-plates, to protect the pore entrances of the test.

Age range: Upper Albian to Lower Turonian

Superfamily VERNEUILINACEA Cushman, 1911

Family VERNEUILINIDAE Cushman, 1911

Subfamily VERNEUILINOIDINAE Suleymanov, 1973

Genus ***Eggerellina*** Marie, 1941

Type species: *Bulimina brevis* d'Orbigny, 1840

Eggerellina brevis Marie, 1941

Plate 1, Fig. 16

1840 *Bulimina brevis* d'Orbigny, p. 41, pl. 4, figs 13-14.

1988 *Eggerellina brevis* Marie: Jarvis *et al.*, figs 10f, 11d.

Diagnosis: *Eggerellina* with an elongate, triserial test. Chambers are inflated and globular, separated by depressed sutures and increase rapidly in size. Wall smoothly agglutinated. Aperture an interiomarginal slit.

Age range: Upper Cenomanian to Lower Turonian

Eggerellina mariae ten Dam, 1950

Plate 1, Figs 17-18

1950 *Eggerellina mariae* ten Dam, pp. 15-16, pl. 1, fig. 17.

1972 *Eggerellina mariae* ten Dam: Gawor-Biedowa, pp. 33-34, pl. 3, figs 1a-b, 2a-b.

1977 *Eggerellina mariae* ten Dam: Carter & Hart, p. 1, pl. 2, fig. 17.

Diagnosis: *Eggerellina* with a triserial test and inflated subglobular chambers, rapidly increasing in size. Wall smoothly agglutinated. Aperture an interiomarginal slit, occasionally arch-like.

Remarks: The outline of this test is very variable as noted by Carter & Hart (1977), the different species actually being intergrading variants of a single plexus which begins with *E. mariae* in the Albian and leads to *E. intermedia* in the Turonian. However, *E. mariae*

has been separated from *E. brevis* in this study by the more defined chambers in *E brevis* and more elongate test.

Age range: Upper Albian to Lower Turonian

Subfamily SPIROPLECTINATINAE Cushman, 1928

Genus *Spiroplectinata* Cushman, 1927

Type species: *Textularia annectens* Parker & Jones, 1865

Spiroplectinata annectens (Parker & Jones, 1865)

Plate 1, Fig. 19

1865 *Textularia annectens* Parker & Jones, p. 92, pl. 1, fig. 1.

1972 *Spiroplectinata annectans* Parker & Jones: Gawor-Bedowa, p. 23, pl. 1, fig. 8.

2000 *Spiroplectinata annectens* (Parker & Jones): Howe, Haig & Apthorpe, fig. 8, no. 25.

Diagnosis: An elongate species of *Spiroplectinata* with large subsphaerical chambers. Wall is finely agglutinated. Aperture terminal and rounded.

Age range: Lower Turonian

Spiroplectinata bettenstaedti Grabert, 1959

Plate 1, Figs 21-22

1959 *Spiroplectinata bettenstaedti* Grabert, p. 15, pl. 1, fig. 14 a-c; pl. 2, figs 42-45; pl. 3, figs 53-59.

2000 *Spiroplectinata bettenstaedti* Grabert: Howe, Haig & Apthorpe, fig.9, no. 1.

Diagnosis: A species of *Spiroplectinata* with short initial triserial portion, becoming flattened and biserial. Numerous low pairs of chambers, finally becoming irregularly uniserial. Aperture terminal and round.

Remarks: Most of the specimens in this study have not preserved the uniserial portion of the test at ODP Site 766. ODP Site 762 however preserves the whole test more readily.

Age range: Lower Turonian

Spiroplectinata complanata (Reuss, 1860)

Plate 1, Fig. 23

1860 *Proroporous complanatus* Reuss, p. 231, pl. 12, fig. 5a-b.

1972 *Spiroplectinata complanata* (Reuss): Gawor-Biedowa, p. 24, pl. 1, fig. 9.

2000 *Spiroplectinata complanata* (Reuss): Howe, Haig & Apthorpe, fig.8, no. 26.

Diagnosis: A species of *Spiroplectinata* with an elongate test that has a very short initial triserial portion, becoming flattened and biserial. Chambers low and broad increasing slowly in size, the final pair increasing more rapidly and becoming more globular.

Age range: Lower Turonian

Subfamily VERNEUILININA Cushman, 1911

Genus ***Gaudryina*** d'Orbigny, 1839

Type species: *Gaudryina rugosa* d'Orbigny, 1840

Gaudryina ex gr. *dividens* Grabert, 1959

Plate 1, Figs 24-25; Plate 2, Figs 1-6

1959 *Gaudryina dividens* Grabert, p. 9, pl. 1, figs 3-5; pl. 2, figs 16-30; pl. 3, figs 53-59.

1992 *Pseudogaudryinella* sp. A: Haig, p. 287, pl. 1, figs 10-11.

1992 *Pseudogaudryinella* sp. B: Haig, p. 287, pl. 1, fig. 12.

1992 *Pseudogaudryinella* sp. C: Haig, p. 287, pl. 1, figs 13-14.

1997 *Gaudryina ex gr. dividens* Grabert: Holbourn & Kaminski, p. 54, pl. 23, figs 1-13; pl. 24, figs 1.

Diagnosis: An elongate species of *Gaudryina* with sharp to rounded corners. The test may becomes biserial or biserial to uniserial with a variable number of chambers separated by distinct, depressed sutures. The wall is thick and smoothly cemented with calcareous cement. The aperture is an interiomarginal arch at the base of the last chamber in triserial tests, and in biserial and uniserial tests it tends to become circular and terminal.

Remarks: This species shows quite a lot of variation, at all stages of test growth, unabling a more specific classification of species to be given. Some specimens are triserial before beginning the biserial phase, others showing the different stages of the biserial and uniserial phases. The figured specimens show a cross section of these varying stages. Morphological differences are also seen. Haig (1992) appears to have separated these different morphotypes as *Pseudogaudryina* A, B and C. However, they are considered here to represent different morphotypes of the same species

Age range: Upper Albian to Lower Turonian

Gaudryina pyramidata Cushman, 1926

Plate 2, Figs 7-8

1926 *Gaudryina laevigata* Franke var. *pyramidata* Cushman, p. 587, pl. 16, fig. 8a-b.

1968 *Gaudryina pyramidata* Cushman: Sliter, p. 48, pl. 3, fig. 9.

1990 *Gaudryina pyramidata* Cushman: Kuhnt & Kaminski, p. 467, pl. 5, figs c-e, j.

1996 *Gaudryina pyramidata* Cushman: Tewari, p. 110, pl. 4, figs 11-12

Diagnosis: *Gaudryina* with a conical trochoid to pyramidal test. Initially triserial with slightly concave sides and acute edges, becoming biserial in the later stages. Chambers increase slowly in the triserial stage, increasing more rapidly as the test becomes biserial. Aperture a low interiomarginal arch.

Remarks: Similar to *Spiroplectinella* sp. 1 this species appears to make its test from coccoliths cemented in a preferred orientation. Although the wall structure appears very similar to *Spiroplectinella* sp. 1 the species of coccolith that is being used cannot be determined without further investigation.

Age range: Upper Albian to Lower Turonian

Genus *Verneuilina* d'Orbigny, 1839

Type species: *Verneuilina tricarinata* d'Orbigny

Verneuilina cretacea Karrer, 1870

Pl. 2, Figs 9-11

1870 *Verneuilina cretacea* Karrer, p. 164, pl. 1, fig. 1

1974 *Verneuilina cretacea* Karrer: Krasheninnikov, p. 643, pl. 7, fig. 1a-c.

Diagnosis: A species of *Verneuilina* with an elongate test that is pyramidal in shape, with concave sides, and rounded sub-acute edges. The chambers increase rapidly in width and slowly in height. Wall smoothly agglutinated. Aperture a high arch at the base of the last chamber

Age range: Upper Albian to Lower Turonian

Family TRITAXIIDAE Plotnikova, 1979

Genus ***Tritaxia*** Reuss, 1860

Type species: *Textularia tricarinata* Reuss, 1844

Tritaxia gaultina (Morozova, 1948)

Plate 2, Fig. 12

1948 *Clavulina gaultina* Morozova, p. 36, pl. 1, fig, 4.

1974 *Clavulina gabonica* Le Calvez de Kalsz & Brun: Schiebnerová, p. 711, pl. 2, figs 5-9.

1992 *Tritaxia gaultina* (Morozova): Haig, p. 287, pl. 1, fig. 15.

1997 *Tritaxia gaultina* (Morozova): Holbourn & Kuhnt, pp. 54-55, pl. 25, figs 1-5.

Diagnosis: *Tritaxia* with an elongate test, initially triserial and triangular in shape with sharp carinate angles, becoming uniserial in adult tests. The low chambers in the uniserial portion are inflated and separated by distinct, depressed sutures. The aperture is round.

Age range: Upper Albian to Upper Cenomanian

Tritaxia **sp. cf.** ***T. gaultina***

Pl. 2, Fig. 13

Diagnosis: A species of *Tritaxia* with an elongate initial triserial portion, becoming irregularly uniserial, with poorly defined sutures. Aperture round and terminal.

Remarks: This species differs from *Tritaxia gaultina* in its more elongate triserial portion and more irregular uniserial part. The chambers are not as regular nor as defined. This variation on *Tritaxia gaultina* becomes more abundant in the Turonian of ODP cores 766A and 762C.

Age range: Lower Turonian

Superfamily ATAXOPHRAGMIACEA Schwager, 1877

Family ATAXOPHRAGMIIDAE Schwager, 1877

Subfamily ATAXOPHRAGMIINAE Schwager, 1877

Genus ***Arenobulimina*** Cushman, 1927

Type species: *Bulimina preslii* Reuss, 1845

Arenobulimina anglica Cushman, 1936

Plate 2, Fig. 14

1936 *Arenobulimina anglica* Cushman, p. 27, pl. 4, fig. 8a-b.

1977 *Arenobulimina anglica* Cushman: Carter & Hart, p. 14, pl. 2, fig. 3.

Diagnosis: A species of *Arenobulimina* with coarse, sugary texture to the agglutinated test. The last whorl occupies over half the test and chambers are rounded and slightly inflated, with distinct, depressed sutures. Aperture interiomarginal loop.

Age range: Mid-Cenomanian

Arenobulimina cf. *frankei* Cushman, 1936

Plate 2, Fig. 15

1936 *Arenobulimina frankei* Cushman, p. 27, pl. 4, fig. 5a-b.

1969 *Arenobulimina frankei* Cushman: Gawor-Biedowa, pp. 84-86, pl. 5, figs 4-5; pl. 7, figs 6, 7a-b, 8a-b; text-figs 5-6

Diagnosis: A triangular species of *Arenobulimina*. The last three chambers occupying almost half the test. Chambers are inflated with distinct sutures. Aperture interiomarginal loop in the hollow in the face of the last chamber.

Remarks: This species is less elongate than typical species of *A. frankei*. Similar in shape to *Arenobulimina advena*, the specimens show no sign of the complex internal partitions that would be expected in this species.

Age range: Upper Albian to Upper Cenomanian

Family GLOBOTEXTULARIIDAE Cushman, 1927

Subfamily LIEBUSELLINAE Saidova, 1981

Genus ***Remesella*** Vašiček, 1947

Type species: *Remesella mariae* Vašiček, 1947

Remesella sp. 1

Plate 2, Figs 16-18

1992 *Remesella* sp. Haig, p. 287, pl. 2, figs 1-2.

1997 *Remesella* sp. 2 Holbourn & Kaminski, p. 55, pl. 25, figs 9, 13.

Description: Species of *Remesella* with an elongate, subconical, trochospirally coiled test. Initially increasing rapidly in width, becoming biserial later. Chambers are inflated and separated by depressed sutures. Wall thin, finely agglutinated, smoothly finished, with calcareous cement. The aperture is an interiomarginal arch.

Age range: Upper Albian to Mid-Cenomanian

Order TEXTULARIDDA Lankester, 1885

Superfamily TEXTULARIACEA Ehrenberg, 1838

Family EGGERELLIDAE Cushman, 1927

Subfamily DOROTHINAE Balakhmatova, 1972

Genus ***Dorothia*** Plummer, 1931

Type species: *Gaudryina bulletta* Carsey, 1926

Dorothia filiformis (Berthelin, 1880)

Plate 2, Fig. 19

1880 *Gaudryina filiformis* Berthelin, p. 25 pl. 1, fig. 8 a-d.

1977 *Dorothia filliformis* (Berthelin): Carter & Hart, p. 7, pl. 1, fig. 3

Diagnosis: A species of *Dorothia* with a slender, elongate test with almost parallel sides, initially triserial, followed by a long biserial stage of inflated chambers. Moderately to coarsely agglutinated. The aperture is interiomarginal.

Age range: Lower to Mid-Cenomanian

Dorothia gradata (Berthelin, 1880)

Plate 2, Figs 20-21

1880 *Gaudryina gradata* Berthelin, p. 24, pl. 1, fig. 6.

1983 *Dorothia gradata* (Berthelin): Basov & Krasheninnikov, p. 761, pl.1, figs 4-6.

1992 *Dorothia* sp.: Haig, p. 288, pl. 2, fig. 3.

Diagnosis: A species of *Dorothia* with distinct initial trochospiral portion later becoming biserial. Chambers globular and rounded. Aperture arch at the base of the last chamber.

Age range: Mid-Cenomanian

Dorothia* cf. *gradata (Berthelin, 1880)

Plate 2, Fig. 22

1880 *Gaudryina gradate* Berthelin, p. 24, pl. 1, fig. 6 a-b.

1997 *Kadryina gradata* (Berthelin): Holbourn & Kaminski, pp. 51-52, pl. 21, figs 2, 4.

Diagnosis: A species of *Dorothia* with a gently flaring test that has a very short initial trochospiral or triserial portion, then becoming biserial. The last two chambers of the test increasing rapidly in size, becoming larger and markedly inflated. The wall is smoothly agglutinated. The aperture is an arch at the base of the last chamber.

Remarks: This species is very short and not typical of the elongate form descried by Berthelin which often has 6-10 pairs of biserial chambers. Holbourn and Kaminski (1997) called this shorter more inflated species *Kadryina gradata*, based on the analysis of sectioned specimens. On analysis these specimens reveal a solid non-canaliculate wall, it can not, therefore, be placed in *Dorothia*. Without being able to section the specimens in this study the name *Dorothia gradata* has been retained, until further study of the species

can resolve the generic position of the species.

Age range: Upper Albian

Genus ***Marssonella*** Cushman, 1933

Type species: *Gaudryina oxycona* Reuss, 1860

Marssonella oxycona (Reuss, 1860)

Plate 2, Figs 23-25

1860 *Gaudryina oxycona* Reuss, p. 229, pl. 12, fig. 3a-c.

1992 *Marssonella oxycona* (Reuss): Haig, p. 288, pl. 2, fig. 4.

Diagnosis: Species of *Marssonella* with conical, broadly flaring test. Initially trochospiral becoming biserial, with an oval cross section. Aperture interiomaginal and slightly arched.

Remarks: Considerable confusion exists in this group, with respect to the identification of the *Marssonella* species *M. trochus* (d'Orbigny, 1840), *M. turris* (d'Orbigny, 1840) and *M. oxycona* (Reuss, 1860). It is thought that d'Orbigny erected his two species on specimens representing end members of one highly variable species, from the rapidly flaring (*trochus*) to the gradually flaring (*turris*) (Swiecicki, unpub. thesis). Reuss (1860) then erected *Gaudryina oxycona* for more typical, moderately flaring members of this same species. In this study *M. oxycona* is by far the most abundant of the species, whilst the more extreme *M. trochus* and *M. turris* are relatively rare. The name *M. oxycona* has, therefore, been retained in this study, and includes the extreme end members of this species.

Age range: Lower Cenomanin to Lower Turonian

Family TEXTULARIIDAE Ehrenberg, 1838

Subfamily TEXTULARIINAE Ehrenberg, 1838

Genus ***Textularia*** Defrance, 1824

Type species: *Textularia sagittula* Defrance in de Blainville, 1824

Textularia chapmani Lalicker, 1935

Plate 3, Fig. 1

1935 *Textularia chapmani* Lalicker, p. 13, pl. 2, figs 8a-c, 9.

1972 *Textularia chapmani* Laliker: Gawor-Biedowa, p. 19, pl. 1, fig. 2a-b.

1995 *Textularia chapmani* Lalicker: Lamolda & Peryt, pl. 1, fig. 26.

Diagnosis: A biserial, slightly compressed species of *Textularia* with 8-10 chambers, widening rapidly. Sutures indistinct and depressed. Aperture a low arch at base of last chamber.

Age range: Mid-Cenomanian to Upper Cenomanian

Order MILIOLIDA Lankester, 1885

Suborder MILIOLINA Delage & Hérouard, 1896

Superfamily MILIOLACEA Ehrenberg, 1839

Family HAUERINIDAE Schwager, 1876

Subfamily HAUERININAE Schwager, 1876

Genus ***Quinqueloculina*** d'Orbigny, 1826.

Type species: *Serpula seminulum* Linné, 1758

Quinqueloculina antiqua (Franke, 1928)

Plate 3, Fig. 2

1928 *Miliolina* (*Quinqueloculina*) *antiqua* Franke, p. 126, pl. 11, fig. 26.

1950 *Quinqueloculina aniqua* (Franke): ten Dam, p. 17, pl. 1, fig. 18.

1972 *Quinqueloculina aniqua* (Franke): Gawor-Biedowa, pp. 35-36, pl. 3, fig. 6a-c.

1977 *Quinqueloculina aniqua* (Franke): Carter & Hart, p. 25, pl. 1, figs 7-8.

Diagnosis: *Quinqueloculina* with an ovate, flattened test. Aperture terminal on short neck, tooth not normally visible.

Age range: Upper Albian

Order LAGENIDA Lankester, 1885

Superfamily NODOSARIACEA Ehrenberg, 1836

Family NODOSARIIDAE Ehrenberg, 1838

Subfamily NODOSARIINAE Ehrenberg, 1838

Genus *Dentalina* Risso, 1826

Type species: *Nodosaria* (les Dentalines) *cuvieri* d'Orbigny, 1826

Remarks: This genus is restricted to those species with a longitudinally costate ornament. (Loeblich & Tappan, 1987). Those species lacking costae are included in the genus *Laevidentalina.*

Dentalina delicatula Cushman, 1938

Plate 3, Fig. 3

1938 *Dentalina delicatula* Cushman, pp. 40-41, pl. 6, figs 19-20.

2000 *Dentalina delicatula* Cushman: Howe *et al.*, p. 550, fig. 8, no. 11.

Diagnosis: A species of *Dentalina* with cylindrical chambers that increase slowly in size. Test characterised by 14-16 strong longitudinal costae and short spike on the proloculus.

Remarks: An elongate species only the first chamber with proloculus has been found preserved in the Indian Ocean in this study.

Age range: Lower Cenomanian

Genus ***Laevidentalina*** Loeblich and Tappan, 1986

Type species: *Laevidentalina aphelis* Loeblich & Tappan, 1986

Laevidentalina basiplanata (Cushman, 1938)

Plate 3, Fig. 4

1938 *Dentalina basiplanata* Cushman, p. 38, pl. 6, figs 6-8.

1970 *Dentalina basiplanata* Cushman: Eicher & Worstell, p. 284, pl. 2, fig. 22.

2000 *Laevidentalina basiplanata* (Cushman): Howe *et al.*, p. 550, fig. 9, no. 19.

Diagnosis: An elongate species of *Laevidentalina* that is slightly arcuate. Chambers are indistinct and increase in size slowly, the test becoming broader in shape towards the terminal, radiate aperture.

Age range: Upper Albian to mid-Cenomanian

Laevidentalina catenula Reuss, 1860

Plate 3, Fig. 5

1860 *Dentalina catenula* Reuss, p. 185, pl. 3, fig. 6.

1983 *Dentalina catenula* Reuss: Basov & Krasheninnikov, p. 762, pl. 6, fig. 8.

Diagnosis: An elongate, tapered species of *Laevidentalina*. Usually two chambered, the first has a short spine. A well defined depressed suture separates the chambers.

Age range: Upper Cenomanian

Laevidentalina communis (d'Orbigny, 1826)

Plate 3, Fig. 6

1826 *Nodosaria communis* d'Orbigny, p. 254, fig. 35.

1997 *Laevidentalina communis* (d'Orbigny) Holbourn & Kaminski, pp. 58-59, pl. 28, figs 4-5.

Diagnosis: An elongate species of *Laevidentalina* with an elliptical cross-section and slightly curved axis. Variable number of chambers, increasing slowly in size and separated by inclined, slightly depressed sutures.

Age range: Upper Albian to Lower Turonian

Laevidentalina cylindroides (Reuss, 1863)

Plate 3, Fig. 7

1863 *Dentalina cylindroides* Reuss, p. 185, pl. 2, fig. 16.

1980 *Dentalina cylindroides* Reuss: Sliter, pl. 6, figs 21-22.

1996 *Dentalina cylindroides* Reuss: Tewari, p. 123, pl. 6, figs 3-4.

Diagnosis: A species of *Laevidentalina* that is oblong to tear drop in shape. Composed of

only two chambers. Aperture terminal and radiate.

Age range: Lower Turonian

Laevidentalina gracilis (d'Orbigny, 1840)

Plate 3, Fig. 8

1840 *Nodosaria gracilis* d'Orbigny, p. 14, pl.1, fig. 5.

1980 *Dentalina gracilis* (d'Orbigny): Sliter, pl. 7, fig. 1.

1996 *Dentalina gracilis* (d'Orbigny): Tewari, p. 123, pl. 6, fig. 7.

Diagnosis: A slender species of *Laevidentalina*, with a rectilinear to slightly arcuate test. Numerous inflated chambers, increase slowly in size and are separated by distinct, depressed sutures.

Age range: Upper Albian to Lower Turonian

Laevidentalina nana (Reuss, 1863)

Plate 3, Figs 9-10

1863 *Dentalina nana* Reuss, p. 39, pl. 2, figs 10, 18.

1984 *Dentalina nana* Reuss: Moullade, p. 446, pl. 2, fig. 15.

1997 *Laevidentalina nana* (Reuss): Holbourn & Kaminski, p. 59, pl. 28, fig. 9.

Diagnosis: A species of *Laevidentalina* with straight to slightly curved test. Made up of few chambers, with indistinct sutures. The firs chamber is markedly rounded and the last chamber tapers towards a terminal, radiate aperture.

Age range: Upper Albian to Lower Turonian

Laevidentalina oligostega (Reuss, 1845)

Plate 3, Figs 11-12

1845 *Nodosaria oligostega* Reuss, p. 27, pl. 3, figs 19-20.

1984 *Dentalina oligostega* (Reuss): Moullade, p. 446, pl. 2, fig. 16.

1997 *Laevidentalina oligostega* (Reuss): Holbourn & Kaminski, p. 59, pl. 28, fig. 10; pl. 29, fig. 3.

Diagnosis: A species of *Laevidentalina* that consists of two globular, elongate, and ovate chambers, separated by distinct and depressed sutures. Last chamber is elongated towards a terminal, radiate aperture.

Age range: Upper Albian to Lower Turonian

Laevidentalina **sp. cf.** ***L. sororia*** (Reuss, 1863)

Plate 3, Fig. 13

1863 *Nodosaria (Dentalina) sororia* Reuss, p. 42

2000 *Laevidentalina* cf. *soria* (Reuss): Howe, Haig & Apthorpe, fig. 9, no. 21.

Diagnosis: A species of *Laevidentalina* with a narrow elongate test. Chambers elongate, separated by distinct depressed sutures. Initial chamber shows pointed proloculus.

Age range: Upper Turonian

Genus *Nodosaria* Lamarck, 1812

Type species: *Nautilus radicula* Linné

Nodosaria aspera Reuss, 1845

Plate 3, Fig. 14

1845 *Nodosaria aspera* Reuss, p. 26, pl.13, figs 14-15.

1983 *Nodosaria aspera* Reuss: Basov & Krasheninnikov, p. 761, pl. 6, fig. 1.

Diagnosis: A species of *Nodosaria* with distinct, inflated, sub-globular chambers enlarging uniformly and with distinct, horizontal, depressed sutures. Aperture terminal, at the end of slender, elongate, cylindrical neck.

Age range: Upper Albian

Nodosaria soluta (Reuss, 1851)

Plate 3, Figs 15, 20

1851 *Dentalina soluta* Reuss, p. 60, pl. 3, fig. 4a-b.

1984 *Nodosaria soluta* (Reuss): Moullade, p. 446, pl. 2, fig. 10.

Diagnosis: An elongate species of *Nodosaria* with three or four chambers that increase moderately in size, separated by distinct depressed sutures.

Age range: Mid-Cenomanian to Lower Turonian

***Nodosaria* sp. 1**

Plate 3, Fig. 16

Diagnosis: An elongate species of *Nodosaria* with three chambers that increase rapidly in size, the last making up over half the test. Depressed sutures separate the chambers.

Age range: Upper Albian to Upper Cenomanian

Nodosaria **sp. 2**

Plate 3, Fig. 17

Diagnosis: An elongate, slightly arcuate species of *Nodosaria* with four or five chambers that increase moderately in size, separated by distinct sutures.

Age range: Upper Albian to Lower Turonian

Genus ***Pseudonodosaria*** Boomgart, 1949

Type species: *Glandulina discreta* Reuss, 1850

Pseudonodosaria humilis (Roemer, 1841)

Plate 3, Fig. 18.

1841 *Nodosaria humilis* Roemer p. 95, pl. 15, fig. 6.

1997 *Pseudonodosaria humilis* (Roemer): Holbourn & Kaminski, p. 60, pl. 29, figs 6-7.

1998 *Pseudonodosaria humilis* (Roemer): Mitchell & Carr, p. 112, pl. 2, fig. 13.

Diagnosis: A species of *Pseudonodosaria* with a rectilinear test that is cylindrical in cross-section. Broad inflated chambers are separated by straight flush sutures, which become markedly depressed in the younger part of the test.

Age range: Upper Albian to Lower Turonian

Genus ***Pyramidulina*** Fornasini, 1894

Type species: *Pyramidulina eptagona* Fornasini, 1894

Pyramidulina sceptrum (Reuss, 1863)

Plate 3, Fig. 19

1863 *Nodosaria sceptrum* Reuss, p. 37, pl. 2, fig. 3.

1997 *Pyramidulina sceptrum* (Reuss): Holbourn & Kaminski, p. 60, pl. 29, figs 11-12.

2005 *Pyramidulina sceptrum* (Reuss): Haig, p. 63, pl. 2, fig. 29.

Diagnosis: An elongate species of *Pyramidulina* with chambers that increase moderately in size. The test is ornamented by thick costae. Aperture terminal, at the end of slender, elongate, cylindrical neck.

Age range: Upper Cenomanian

Pyramidulina zippei (Reuss, 1845)

Plate 3, Fig. 21

1845 *Nodosaria zippei* Reuss, p. 25, pl. 8, figs 1-3.

1997 *Pyramidulina zippei* (Reuss): Holbourn & Kaminski, p. 61, pl. 30, fig. 6.

Diagnosis: A species of *Pyramidulina* with a rectilinear test, the sides of which are nearly parallel becoming slightly wider towards the top. The first chamber is spherical and slightly pointed, the last one is flattened with a small apertural neck. Nine prominent costae ornament the test.

Age range: Upper Albian

Subfamily FRONDICULARIINAE Reuss, 1860

Genus ***Frondicularia*** Defrance, 1826

Type species: *Renulina complanata* Defrance, in de Blainville, 1824

Frondicularia archiaciana d'Orbigny, 1840

Plate 3, Figs 22-23

1840 *Frondicularia archiaciana* d'Orbigny, p. 20, pl. 1, figs 34-36.

1996 *Frondicularia archiaciana* d'Orbigny: Tewari, p. 117, pl. 7, fig. 15.

Diagnosis: A flattened species of *Frondicularia* with broad chambers and arched sutures angled to a mid-line of the test. The sides gently flare, tapering at the top to a terminal, central aperture.

Age range: Middle Cenomanin to Lower Turonian

Family VAGINULINIDAE Reuss, 1860

Subfamily LENTICULININAE Chapman, Parr & Collins, 1934

Genus ***Lenticulina*** Lamarck, 1804

Type species: *Lenticulites rotulatus* Lamarck, 1804

Lenticulina circumcidanea (Berthelin, 1880)

Plate 3, Fig. 24

1880 *Cristellaria circumcidanea* Berthelin, p. 52, pl. 3, fig. 1.

1997 *Lenticulina circumcidanea* (Berthelin): Holbourn & Kaminski, p. 62, pl. 31, fig. 8.

Diagnosis: A species of *Lenticulina* with subcircular outline, and usually seven to eight chambers in the last whorl. The periphery is acute with a narrow keel. Sutures are flush becoming slightly depressed in the final part of the test.

Age range: Upper Albian to Lower Turonian

Lenticulina gaultina (Berthelin, 1880)

Plate 3, Fig. 25

1880 *Cristellaria gaultina* Berthelin, p. 49, pl. 3, figs 15-19.

1940 *Lenticulina gaultina* (Berthelin): Tappan, p. 101, pl. 15, fig. 11.

1970 *Lenticulina gaultina* (Berthelin): Eicher & Worstell, p 286, pl. 2, figs 14-15, 19.

Diagnosis: A species of *Lenticulina* oval in outline with sub acute periphery, sometimes slightly angular. Usually with 8-10 chambers, and straight to curved sutures

Age range: Upper Albian to Lower Turonian

Lenticulina muensteri (Roemer, 1841)

Plate 4, Figs 1-3

1841 *Robulina muensteri* Roemer, p. 98, pl. 15, fig. 30.

1997 *Lenticulina muensteri* (Roemer): Holbourn & Kaminski, p. 63, pl. 33, figs 1-2.

Diagnosis: A species of *Lenticulina* with a smooth test. Sutures are flush and curved coalescing into a slightly projecting umbonal disc. The periphery is sharp with a radiate aperture at the peripheral angle.

Remarks: The number of chambers and prominence of the umbonal disc varies in this species. This has led to confusion and difficulty in dividing this species from similar

lenticuline species such as *L. rotulata* (Lamarck) and *L. macrodisca* (Reuss) (Bartenstein and Bolli, 1986). Meyn and Vespermann (1994) consider *L. macrodisca* to be a subjective synonym of *L. muensteri*. In this study *L. muensteri* is separated from *L. rotulata* by the formers slightly sharper periphery and more elongate and pointed last chamber with more acute apertural angle.

Age range: Lower Cenomanian to Mid-Cenomanian

Lenticulina pulchella (Reuss, 1863)

Plate 4, Figs 4-5.

1863 *Cristellaria pulchella* Reuss, p. 71, pl. 8, fig. 1.

1997 *Lenticulina pulchella* (Reuss): Holbourn & Kaminski, p. 64, pl. 33, figs 1-2.

Diagnosis: A species of *Lenticulina* with around eight chambers in the last whorl increasing rapidly in size. Sutures are fine and curved, flush and indistinct in the early part of the test becoming slightly depressed in later parts. With a small, depressed umbilicus, the test has an acute periphery and oval to polygonal outline. The last chamber is pointed towards a terminal, radiate aperture.

Age range: Upper Albian to Mid-Cenomanian

Lenticulina rotulata Lamarck, 1804

Plate 4, Figs 6-7.

1804 *Lenticulina rotulata* Lamarck, p. 188.

1991 *Lenticulina rotulata* Lamarck: Leary and Peryt, p. 133, fig. 7, nos. 6, 8.

Diagnosis: A species of *Lenticulina* circular in outline, with rounded to sub-acute

periphery. 8-10 chambers with flush and indeterminate sutures.

Age range: Upper Albian to Lower Turonian

Lenticulina saxocretacea Bartenstein, 1954

Plate 4, Figs 8-10.

1863 *Cristellaria saxocretacea* Reuss, p. 76, pl. 8, fig. 10; pl. 9, fig. 1.

1954 *Lenticulina saxocretacea* Bartenstein, p. 45-46.

1997 *Lenticulina saxocretacea* Bartenstein: Holbourn & Kaminski, p. 64, pl. 33, fig. 3.

Diagnosis: An oval shaped species of *Lenticulina*, with 7-10 chambers in the final whorl, becoming more elongate and less arcuate in shape to give the characteristic shape of this species. The periphery is sharp and the sutures limbate, raised and curved. The aperture is radiate near to the dorsal margin.

Age range: Upper Albian to Lower Turonian

Lenticulina subangulata (Reuss, 1863)

1863 *Cristellaria subangulata* Reuss, p. 74, pl. 8, fig. 7.

1984 *Lenticulina subangulata* (Reuss): Moullade, pl. 3, fig. 3.

1997 *Lenticulina subangulata* (Reuss): Holbourn & Kaminski, pp. 64-65, pl. 33, fig. 5.

Diagnosis: A species of *Lenticulina* with fine, slightly raised sutures, inclined backwards. The last two chambers become elongate and sharply angled, giving the test a distinctive angular outline.

Age range: Upper Cenomanian

Lenticulina **sp. 1**

Plate 4, Figs 11-12

Diagnosis: A species of *Lenticulina* that is rounded and oval in shape with flush indistinct sutures.

Age range: Upper Albian to Lower Turonian

Genus ***Marginulinopsis*** Silvestri, 1904

Type species: *Cristellaria bradyi* Goës, 1894

***Marginulinopsis* sp. 1**

Plate 4, Fig. 13

Diagnosis: An elongate species of *Marginulinopsis*, comprised of three globular chambers, the final chamber becoming more elongate and pointed towards the terminal aperture. The test has sharp edges giving the chambers a near an angular cross section. The surface of the test shows faint costate striations, more prominent on the first chamber, becoming fainter on the earlier chambers.

Age range: Lower Turonian

Genus ***Saracenaria*** Defrance, 1824

Type species: *Saracenaria italica* Defrance, 1824

Saracenaria erlita Ludbrook, 1966

1966 *Saracenaria erlita* Ludbrook, pl. 8, fig. 10.

1974 *Saracenaria erlita* Ludbrook: Scheibnerová, p. 711, pl. 2, figs 25-26.

1997 *Saracenaria erlita* Ludbrook: Holbourn & Kaminski, p. 66, pl. 34, fig. 8.

Diagnosis: Elongate and triangular species of *Saracenaria* with rounded edges on the ventral side and sharper edges on the dorsal, although no keel is present. Initially planispirally coiled the final chamber becoming markedly inflated ventrally. Sutures curved and slightly depressed.

Age range: Mid-Cenomanian

Saracenaria triangularis (d'Orbigny, 1840)

Plate 4, Fig. 15

1840 *Cristellaria triangularis* d'Orbigny, p. 27, pl. 2, figs 21-22.

1984 *Saracenaria triangularis* (d'Orbigny): Moullade, pl. 3, fig. 11.

1997 *Saracenaria trianguaris* (d'Orbigny): Holbourn & Kaminski, p. 67, pl. 36, fig. 1.

2000 *Saracenaria triangularis* (d'Orbigny): Howe *et al.*, p.534, fig. 10, no. 11

Diagnosis: Triangular shaped species of *Saracenaria* with thin keel and sharp edges. The chambers are low and broad the last chamber becoming more inflated and flaring broadly.

Age range: Mid-Cenomanian

Saracenaria sp. 1

Plate 4, Fig. 16

Diagnosis: Triangular shaped species of *Saracenaria*, almost spherical in outline with very broad, flat apertural face. The edges of the test are sharp and the aperture terminal and radiate.

Remarks: This species is very similar to *S. triangularis*, however is less elongate and

more evolute.

Age range: Upper Albian

Subfamily MARGINULININAE Wedekind, 1937

Genus *Astacolus* de Montfort, 1808

Type species: *Astocolus crepidulatus* de Montfort, 1808

Astacolus calliopsis (Reuss, 1863)

Plate 4, Fig. 17

1863 *Marginulina linearis* Reuss, p. 60, pl. 5, fig. 6.

1997 *Astacolus calliopsis* (Reuss): Holbourn & Kaminski, p. 68, pl. 36, figs 8-9;

pl. 37, fig. 1.

Diagnosis: Elongate species of *Astacolus* with short enrolled initial portion, becoming uniserial along a curved axis. Chambers are slightly compressed and separated by depressed, strongly inclined sutures. The final chamber becomes more inflated and tapers towards the radial and terminal aperture.

Age range: Lower Turonian

Genus *Hemirobulina* Stache, 1864

Type species: *Cristellaria (Hemirobulina) arcuatula* Stache, 1864

Hemirobulina bullata (Reuss, 1860)

Plate 4, Fig. 18

1860 *Marginulina (Marginulina) bullata* Reuss, p. 29, pl. 6, figs 4-6.

1976 *Marginulina bullata* Reuss: Scheibnerová, pl. 29, fig. 1.

1997 *Hemirobulina bullata* (Reuss): Holbourn & Kaminski, pp. 68-69, pl. 37, fig. 5.

Diagnosis: A short species of *Hemirobulina* with a robust test and broad chambers. The last chamber is very inflated, bearing a radiate, terminal aperture at the dorsal edge. Sutures are oblique and slightly depressed.

Age range: Upper Albian

Hemirobulina hamulus (Chapman, 1894)

Plate 4, Fig. 19

1894 *Marginulina hamulus*, Chapman, p. 75, pl. 4, fig. 13 a-b.

2005 *Hemirobulina hamulus* (Chapman): Haig, p. 61, pl. 1, fig. 30.

Diagnosis: An elongate species of *Hemirobulina*, comprised of three inflated chambers, separated by inclined depressed sutures, along a curved axis. The first chamber has a slightly pointed proloculus, whilst the final chamber becomes larger and more inflated than those preceding.

Age range: Upper Cenomanian

Hemirobulina inaequalis (Reuss, 1860)

Plate 4, Fig. 20

1860 *Marginulina inaequalis* Reuss p. 59, pl. 7, fig. 3.

1997 *Hemirobulina inaequalis* (Reuss): Holbourn & Kaminski, p. 69, pl. 37, fig. 6.

Diagnosis: An elongate species of *Hemirobulina* with circular cross section. The first

chamber is very rounded and can be slightly pointed. The final chamber becoming slightly inflated and drawn out to a radial and terminal aperture. Sutures are oblique and slightly depressed.

Age range: Upper Albian

Genus ***Vaginulinopsis*** Silvestri, 1904

Type species: *Vaginulina soluta* Silvestri var. *carinata* Silvestri, 1898

Vaginulinopsis harpa (Reuss, 1860)

Plate 4, Fig. 21

1860 *Cristellaria harpa* Reuss, p. 211, pl. 10, figs 1-2.

1997 *Vaginulinopsis harpa* (Reuss): Holbourn & Kaminski, p. 69, pl. 38, fig. 7.

Diagnosis: An elongate, flattened species of *Vaginulinopsis* with elliptical cross section and curved axis. Sutures are inclined and slightly depressed.

Age range: Upper Albian to Lower Turonian

Subfamily VAGINULININAE Reuss, 1860

Genus ***Planularia*** Defance, 1826

Type species: *Peneropilis auris* Defrance, in de Blainville, 1824

Planularia bradyana (Chapman 1894)

Plate 4, Figs 22-23

1894 *Cristellaria bradyana* Chapman, p. 654, pl. 10, fig. 13.

1972 *Planularia bradyana* (Chapman): Gawor-Biedowa, p. 40, pl. 3, fig. 11.

2000 *Planularia bradyana* (Chapman): Howe, Haig & Apthorpe, fig. 9, no. 26.

Diagnosis: A flattened, sub-oval species of *Planularia*, composed of 10 to 12 low, arcuate chambers in the uncoiled portion of the test, inclined towards the proloculus.

Age range: Upper Albian to Lower Turonian

Genus ***Psilocitharella*** Loeblich & Tappan, 1986

Type species: *Vaginulina leptoteicha* Loeblich & Tappan

Psilocitharella arguta (Reuss, 1860)

Plate 4, Fig. 24

1860 *Vaginulina arguta* Reuss, p. 202, pl. 8, fig. 4

1972 *Vaginulina arguta* Reuss: Gawor-Biedowa, p. 46, pl. 4, fig. 14.

1997 *Psilocitharella arguta* (Reuss): Holbourn & Kaminski, p. 71, pl. 40, fig. 8;
pl. 41, fig. 1

Diagnosis: Elongate, narrow species of *Psilocitharella* with a flattened test. The first chamber is slightly inflated, whilst the final chamber is elongate towards the terminal, radiate aperture. Sutures are raised and inclined and lateral carinae are present.

Age range: Upper Albian to mid-Cenomanian

Psilocitharella paucistriata (Reuss, 1862)

Plate 4, Fig. 25

1862 *Vaginulina paucistriata* Reuss, p. 48, pl. 3, fig. 16a-b.

1972 *Vaginulina* aff. *paucistriata* Reuss: Gawor-Biedowa, p. 48, pl. 4, fig. 15.

1997 *Psilocitharella paucistriata* (Reuss): Holbourn & Kaminski, pp. 71-72, pl. 41, figs 4, 8-9.

Diagnosis: Elongate, flattened species of *Psilocitharella* with gently flaring sides. The test is sharply carinate, with oblique, limbate sutures. The test is ornamented with longitudinal ribs, more prominent in the early portion of the test.

Age range: Upper Albian

Genus *Vaginulina* d'Orbigny, 1826

Type species: *Nautilus legumen* Linné, 1758

Vaginulina cretacea Plummer 1927

Plate 5, Fig. 1

1927 *Vaginulina gracilis* Plummer var. *cretacea* Plummer, p. 172, pl. 2, fig. 8.

1936 *Vaginulina cretacea* Plummer: Cushman, p. 417, pl. 1, fig. 5.

1970 *Vaginulina cretacea* Plummer: Eicher & Worstell, p. 288, pl. 3, figs 5-6.

Diagnosis: A species of *Vaginulina* with near parallel sides. The test is flattened and chambers low and broad, increasing slowly in size, the first chamber is slightly inflated and more rounded. Sutures are oblique and gently curved.

Age range: Upper Albian

Vaginulina recta (Reuss, 1863)

Plate 5, Fig. 2

1863 *Vaginulina recta* Reuss, p. 48, pl. 3, figs 14-15.

1972 *Vaginulina recta* Reuss: Gawor-Biedowa, p. 4, pl. 4, fig. 11.

1984 *Lenticulina (Vaginulina) recta* (Reuss): Moullade, p. 449, pl. 3, fig 16.

Diagnosis: A species of *Vaginulina* with a prominent rounded and inflated first chamber. Later chambers are flattened and oblique, increasing slowly in size, the final chamber extending slightly to a terminal aperture. Sutures inclined and depressed.

Age range: Upper Albian

Family LAGENIDAE Reuss, 1862

Genus ***Lagena*** Walker and Jacob, 1798

Type species: *Serpula (Lagena) sulcata* Walker and Jacob, in Kanmacher, 1798

Lagena globulosa (Montagu, 1803)

Plate 5, Fig. 3

1803 *Vermiculum globosum* Montagu, p. 523

1984 *Lagena globulosa* (Montagu): Moullade, p. 449, pl. 3, fig. 17

Diagnosis: A globular species of *Lagena*, slightly elongate with a flattened bottom giving a droplet shape. It has a smooth test surface and terminal round aperture on very short produced neck.

Age range: Upper Albian

Superfamily POLYMORPHINACEA d'Orbigny, 1839 (nom. Transl. Grigelis, 1980)

Family POLYMORPHINIDAE d'Orbigny, 1839

Subfamily POLYMORPHININAE d'Orbigny, 1839

Genus ***Globulina*** d'Orbigny, 1839

Type species: *Polymorphina* (les Globulines) *gibba* d'Orbigny, 1826

Globulina lacrima (Reuss 1845)

Plate 5, Fig. 4

1845 *Polymorphina lacrima* Reuss, pp. 40, 110, pl. 12, fig. 6a-c; pl. 13, fig. 83 a-c

1997 *Globulina lacrima* (Reuss): Holbourn & Kaminski, p. 73, pl. 42, figs 2-3.

Diagnosis: A subglobular and drop-like shaped species of *Globulina*. It has few chambers and the sutures are indistinct and flush. The base of the test is rounded, but tapers very slightly and is characterised by a very short point.

Age range: Lower Cenomanian

Globulina prisca Reuss, 1863

Plate 5, Fig. 5

1862 *Polymorphina prisca* Reuss, p. 79, pl. 9, fig. 8 a-b.

1951 *Globulina prisca* (Reuss): Bartenstein & Brand, pl. 10, fig. 286.

1997 *Globulina prisca* (Reuss): Holbourn & Kaminski, p. 73, pl. 42, figs 5-7.

Diagnosis: Elongate species of *Globulina,* ovate in shape with slightly pointed proximal end, sutures indistinct, aperture radiate and terminal.

Remarks: Similar to *G. lacrima*, this species differs in its more elongate shaped test.

Age range: Mid-Cenomanian to Lower Turonian

Genus ***Pyrulina*** d'Orbigny, 1839

Type species: *Polymorphina* (les Pyrulines) *gutta* d'Orbigny, 1826

Pyrulina cylindroides (Roemer, 1838)

Plate 5, Fig. 6

1838 *Polymorphina cylindroides* Roemer, pl. 3, fig. 26 a-b.

1946 *Pyrulina cylindroides* (Roemer): Cushman, p. 97, pl. 40, figs 18-19.

1983 *Pyrulina cylindroides* (Roemer): Basov & Krasheninnikov, p. 763, pl. 7, fig. 1.

1998 *Pyrulina cylindroides* (Roemer): Holbourn & Kaminski, p. 384, pl. 1, fig. 10.

Diagnosis: An elongate species of *Pyrulina*, tapering towards both ends. Chambers are elongate with oblique indistinct sutures, invisible in most specimens. Aperture terminal and radiate.

Age range: Lower Turonian

Subfamily RAMULININAE Brady, 1884

Genus ***Ramulina*** Jones, 1875

Type species: *Ramulina laevis* Jones, in Wright, 1875

Remarks: Individuals within this genus are very rarely complete, and are commonly found in the samples as fragments of the complete specimen, usually as single chambers with tubular projections. This makes identification and absolute counts of the species

impossible. In this work each fragment has been counted as one specimen.

Ramulina aculeata Wright, 1886

Plate 5, Fig. 7

1840 *Dentalina aculeata* d'Orbigny, p. 13, pl. 1, figs 2-3.

1886 *Ramulina aculeata* Wright, p. 31, pl. 27, fig. 11.

1996 *Ramulina aculeata* Wright: Tewari, p. 166, pl. 10, fig, 17.

1998 *Ramulina aculaeta* Wright: Mitchell & Carr, pl. I, fig. 9.

Diagnosis: A globular species of *Ramulina* usually comprised of single, elongate chambers with stolon-like necks at both ends. Surface hispid.

Age range: Lower Cenomanian to Lower Turonian

Ramulina spandeli Paalzow, 1917

Plate 5, Fig. 8

1917 *Ramulina spandeli* Paalzow, p. 246, pl. 47, fig. 15

1974 *Ramulina spandeli* Kuznetsova, pl. 2, fig. 20

Diagnosis: A large and globular species of *Ramulina*, comprised of single chambers with 2 short open stolons located on one side of the test.

Age range: Upper Albian

***Ramulina* sp. 3**

Plate 5, Figs 9-10

Diagnosis: A fragment of *Ramulina* comprised of a globular chamber ornamented in short,

thick spines.

Remarks: This species is only seen as fragments in this study, however the globular chamber does not appear to show affinities to any of the other *Ramulina* species. It is therefore left as open nomenclature.

Age range: Lower Cenomanian

Family ELLIPSOLAGENIDAE Silvestri, 1923

Subfamily OOLININAE Loeblich & Tappan, 1961

Genus ***Oolina*** d'Orbigny, 1839

Type species: *Oolina laevigata* d'Orbigny, 1839

Oolina globosa (Montagu, 1803)

Plate 5, Fig. 11

1803 *Vermiculum globosum* Montagu, p. 523

1997 *Oolina globosa* (Montagu): Holbourn & Kaminski, pp. 74-75, pl. 44, fig. 10.

1998 *Oolina globosa* Montagu: Mitchell & Carr, pl. 1, fig. 13.

Diagnosis: A globular, ovate species of *Oolina*. Inflated, narrowing at the base and top of the test. The aperture is produced on a short neck surrounded by radial grooves.

Age range: Lower Turonian

Genus ***Fissurina*** Reuss, 1850

Type species: *Fissurina laevigata* Reuss, 1850

Fissurina **sp. 1**

Plate 5, Fig. 12

Diagnosis: A spherical species of *Fissurina*, with smooth test and terminal oval to slit like aperture.

Age range: Upper Cenomanian

Subfamily ELLIPSOLAGENINAE Silvestri, 1923

Genus ***Tricarinella*** ten Dam & Schiijfsma, 1945

Type species: *Rhabdogonium excavatum* Reuss, 1863

Remarks: *Tricarinella* was previously regarded as a synonym of *Tristix*, however the latter has a radiate rather than tri-radiate aperture, and the lacks the entosolenian tube of *Tricarinella* (Loeblich and Tappan, 1987).

Tricarinella excavata (Reuss, 1863)

Plate 5, Fig. 13.

1863 *Rhabdogonium excavata* (Reuss), pl. 12, fig 8a-c.

1978 *Tribrachia australiana* Ludbrook: Scheibnerová, p. 712, pl. 2, fig. 16.

1996 *Tristix excavata* (Reuss): Tewari, pp. 139-140 pl. 7, fig. 17.

2000 *Tricarinella excavata* (Reuss): Howe *et al.*, fig. 10, no. 12.

Diagnosis: An elongate species of *Tricarinella*, rectilinear and triangular in cross section throughout. Sides deeply convex, and chambers low and broad, strongly arching upwards.

The sutures are arched, deep and distinct.

Age range: Lower Cenomanian to Lower Turonian

Order GLOBIGERINIDA Lankester, 1885 (as Globigerinidea; nom. Corr. Calkins, 1909)

Superfamily HETEROHELICACEA Cushman, 1927

Family GUEMBELITRIIDAE Montanaro Gallitelli, 1957

Genus ***Guembelitria*** Cushman, 1933

Type species: *Guembelitria cretacea* Cushman, 1933

Guembelitria cenomana (Keller, 1935)

Plate 5, Figs 14-15

1935 *Guembelitria cenomana* Keller, p. 547, pl. 3, figs 13-14.

1985 *Guembelitria cenomana* (Keller): Caron, p. 57, figs 24 (3-4).

1996 *Guembelitria cenomana* (Keller): Tewari, p. 174, pl. 12, fig. 1.

Diagnosis: A small species of *Guembelitria*. The initial chambers increase in size slowly, whilst the last chambers flare greatly, becoming large and globular, giving this species its distinctive test shape.

Age range: Upper Cenomanian to Lower Turonian

Family HETEROHELICIDAE Cushman, 1927

Subfamily HETEROHELICINAE Cushman, 1927

Genus ***Heterohelix*** Ehrenberg, 1843

Type species: *Textularia americana* Ehrenberg, 1843

Heterohelix globulosa (Ehrenberg, 1840)

Plate 5, Fig. 16

1840 *Textularia globulosa* Ehrenberg, p. 135, pl. 4, figs 2, 4-5, 7-8.

1899 *Guembelina globulosa* (Ehrenberg): Egger, p. 32, fig. 43.

1967 *Heterohelix globulosa* (Ehrenberg): Pessagno, p. 260, pl. 87, figs 5-9, 11-13.

1985 *Heterohelix globulosa* (Ehrenberg): Caron, p. 60, pl. 24, fig 5.

1996 *Heterohelix globosa* (Ehrenberg): Tewari, p. 175, pl. 12, fig. 2.

Diagnosis: A small species of *Heterohelix*. The chambers initially increase slowly in size, later increasing more rapidly and becoming more globular. Faint costae are present on all chambers, although more marked in the later ones.

Age range: Lower Turonian

Heterohelix moremani (Cushman, 1938)

Plate 5, Fig. 17

1938 *Guembelina moremani* Cushman, p. 10, pl. 2, figs 1-3.

1967 *Heterohelix moremani* (Cushman): Pessagno, p. 11, pl. 48, figs 10-11.

1985 *Heterohelix moremani* (Cushman): Caron, p. 60, fig. 24 (6-7).

1996 *Heterohelix moremani* (Cushman): Tewari, p. 175, pl. 12, fig. 3.

Diagnosis: Small slender species of *Heterohelix*, made up of 6 – 9 pairs of chambers increasing slowly and regularly in size, the final chambers often becoming slightly more globular. Test surface smooth.

Age range: Upper Cenomanian to Lower Turonian

Heterohelix reussi (Cushman, 1938)

Plate 5, Fig. 18

1938 *Güembelina reussi* Cushman, p. 11, pl. 2, fig. 6a-b.

1985 *Heterohelix reussi* (Cushman): Caron, p. 60, figs 24 (10-11).

Diagnosis: Small species of *Heterohelix*. The chambers initially increase slowly in size, later becoming more rapid and globular. Distinct depressions are seen where the sutures join.

Remarks: Differs from *H. globulosa* in having slightly more compressed chambers, and lacking surface costae of *H. globulosa.*

Age range: Lower Turonian

Superfamily PLANOMALINACEA Bolli, Loeblich & Tappan, 1957

Family GLOBIGERINELLOIDEDAE Longoria, 1974

Subfamily GLOBIGERINELLOIDINAE Longoria, 1974

Genus ***Globigerinelloides*** Longoria, 1974

Type species: *Globigerinelloides algeriana* Longoria, 1974

Globigerinelloides bentonensis (Morrow, 1934)

Plate 5, Figs 19-20

1934 *Anomalina bentonensis* Morrow, p. 201, pl. 30, fig. 4.

1957 *Planomalina caseyi* Bolli, Loeblich & Tappan, p. 2, pl. 1, figs 4-5.

1970 *Globigerinelloides bentonensis* (Morrow): Eicher & Worstell, p. 297, pl. 8, figs 17-19; pl. 9, fig. 3.

1970 *Globigerinelloides caseyi* (Bolli, Loeblich and Tappan): Eicher & Worstell,

pp. 297-298, pl. 8, figs 11, 15a-b, 16.

1977 *Globigerinelloides bentonensis* (Morrow): Carter & Hart, p. 27, pl. 1, fig. 11; pl. 2, figs 19-20.

1989 *Globigerinelloides bentonensis* (Morrow): Hart *et al.*, pl. 7.13, figs 7-9.

Diagnosis: A small species of *Globigerinelloides* with 6-7 globular chambers in the last whorl. Each chamber is slightly longer than high, and residual apertures are clearly visible.

Remarks: Species of G*lobigerinelloides* have caused confusion with regards to the differentiation of *G. bentonensis, G. caseyi* and *G. eaglefordensis.* This has been looked at in detail by Carter and Hart (1977). *P caseyi* was regarded by Loeblich & Tappan (1961) to be a junior synonym of *G. eaglefordensis*, and the similarity between *G. caseyi* and *G. bentonensis* was also noted by a number of authors. Low (1961) regarded them to be separate species with respect to the difference in overall size, tightness of coiling and in the number of chambers in the final whorl, whilst Eicher (1965) considered them almost inseparable. Therefore, as suggested by Carter & Hart (1977) forms that may have been considered as *G. caseyi* and *G. eaglefordensis* by other authors are considered, in this study, to be *G. bentonensis*. Carter & Hart (1977) based these views on the re-sampling of the Arlesey succession the type locality of *G. caseyi* as well as the topotype specimen of *G. bentonensis* provided to them by Don Eicher.

Age range: Upper Albian to Lower Turonian

Family PLANOLAMINIDAE Bolli, Loeblich & Tappan, 1957

Genus ***Planomalina*** Loeblich & Tappan, 1946

Type species: *Planomalina apsidostroba* Loeblich & Tappan

Planomalina buxtorfi (Gandolfi, 1942)

Plate 5, Figs 23-24

1942 *Planulina buxtorfi* Gandolfi, p. 103, pl. 3, fig. 7a-c.

1979 *Planomalina buxtorfi* (Gandolfi): Robaszynski & Caron, pp. 45-46, pl. 1, figs 2-4.

1985 *Planomalina buxtorfi* (Gandolfi): Caron, p. 65, figs 29 (1-2).

1992 *Planomalina buxtorfi* (Gandolfi): Haig, p. 290, pl. 5, figs. 6-7.

Diagnosis: A symmetrical species of *Planomalina,* laterally compressed with a single keel. Sutures are raised and curved backwards. The final whorl is made up of 7-9 chambers.

Age range: Upper Albian

Family SCHACKOINIDAE Pokorný, 1958

Genus ***Schackoina*** Thalmann, 1932

Type species: *Siderolina cenomana* Schacko, 1897

Schackoina cenomana (Schacko, 1897)

Plate 5 Fig. 25; Plate 6, Figs 1-3

1897 *Siderolina cenomana* Schacko, p. 166, pl. 4, figs 3-5.

1928 *Hantkenina cenomana* (Schacko): Cushman & Wickenden, p. 4, pl. 6, figs 4-6.

1970 *Schackoina cenomana* (Schacko): Eicher & Worstell, p. 298, pl. 9, figs 1, 2, 4.

Diagnosis: A species of *Schackoina* characterised by 3-5 inflated chambers, rapidly increasing in size, with one tubulospine extending from the mid-line of each chamber.

Remarks: This species appears with three, four and five chambers in the last whorl. Four

is most abundant in all sections studied. The length of tubulospines can be seen to change throughout all sections, and is considered to be an environmental adaptation to changing oxygen levels.

Herb (1972) found small isolated species of *Schackoina*, indistinguishable from typical *Schackoina cenomana* in the Upper Albian. This species can therefore be defined as extending slightly below the Albian-Cenomanian Boundary.

Age range: Upper Albian to Lower Turonian

Schackoina multispinata (Cushman & Wickenden, 1930)

Plate 6, Fig. 4

1930 *Hantkenina multispinata* Cushman & Wickenden, p. 40, pl. 6, figs 4-6.

1983 *Schackoina multispinata* (Cushman & Wickenden): Krasheninnikov & Basov, p. 803, pl. 1, figs 4-7

Diagnosis: A species of *Schackoina* with 4 chambers in the last whorl, increasing moderately in size. Each chamber has one tubulospine extending from it, apart from the last chamber, which has two.

Age range: Lower Turonian

Schackoina sp. 1

Plate 6, Fig. 5

Diagnosis: A species of *Schackoina* with 4 chambers in the last whorl and characterised by its bent, and off centre, tubules.

Age range: Lower Turonian

Superfamily ROTALIPORACEA Sigal, 1958

Family HEDBERGELLIDAE Loeblich & Tappan, 1961

Subfamily HEDBERGELLINAE Loeblich & Tappan, 1961

Genus *Hedbergella* Bronnimann & Brown, 1958

Type species: *Anomalina lorneiana* d'Orbigny var. *trochoidea* Gandolfi, 1942

Hedbergella brittonensis Loeblich & Tappan, 1961

Plate 6, Figs 6-8

1934 *Globigerina cretacea* d'Orbigny: Morrow, p. 198, pl. 30, figs 7, 8, 10a-b.

1961 *Hedbergella brittonensis* Loeblich & Tappan, pp. 274-275, pl. 4, fig. 1a-c.

1970 *Hedbergella portdownensis* (Williams-Mitchell): Eicher & Worstell, p. 304, pl. 10, figs 1a-c, 2a-b.

1972 *Hedbergella brittonensis* Loeblich & Tappan: Gawor-Biedowa, pp. 67-68, pl. 8, figs 1a-c, 2a-c.

1977 *Hedbergella brittonensis* Loeblich & Tappan: Carter & Hart, p. 31, pl. 4, figs 13-15.

Diagnosis: A species of *Hedbergella* characterised by its high spire, and strongly convex spiral side. The last whorl contains six chambers gradually increasing in size, and the wall is distinctly spinose.

Age range: Upper Albian to Mid-Cenomanian

Hedbergella delrioensis (Carsey, 1926)

Plate 6, Figs 9-10, 14-15, 20-22

1926 *Globigerina cretacea* d'Orbigny var. *delrioensis* Carsey, p. 43.

1977 *Hedbergella delrioensis* (Carsey): Carter & Hart, p. 35, pl. 4, figs 1-3.

1979 *Hedbergella delrioensis* (Carsey): Robaszynski & Caron, pp 123,128, pl. 22, figs 1-2; pl. 23, figs 1-3.

Diagnosis: A species of *Hedbergella* with low to moderate spire, lobate periphery and 5-6 chambers in final whorl. Test visibly hispid.

Remarks: Variations exist in this species, which encompasses all individuals from the Albian to Turonian possessing a low to moderate spire. A range of morphologies exist from the almost flat *H. planispira* to the high spired *H. brittonensis*, this is thought to be continuous (Carter & Hart, 1977), and although separate specific names have been proposed for many of the intermediate forms *Hedbergella delrioensis* is retained in this work for the range between the two end members.

Age range: Upper Albian to Lower Turonian

Hedbergella planispira (Tappan)

Plate 6, Figs 11-13, 16-19

1940 *Globigerina planispira* Tappan, p. 122, pl. 19, fig. 12.

1961 *Hedbergella planispira* (Tappan): Loeblich & Tappan, pp. 276-277, pl. 5, figs 4-11.

1970 *Hedbergella planispira* (Tappan): Eicher & Worstell, p. 302, 304, pl. 9, figs 12, 13 a-c.

1985 *Hedbergella planispira* (Tappan): Caron, p. 59, figs 25 (23-24).

Diagnosis: A species of *Hedbergella* characterised by its small size, low to flat trochospire and circular shape. It has globular, smooth chambers increasing in size gradually throughout.

Remarks: The number of chambers in the final whorl is often greater than seen in other hedbergellids.

Age range: Upper Albian to Lower Turonian

Hedbergella simplex (Morrow, 1934)

Plate 6, Figs 23-25; Plate 7, Fig. 1

1934 *Hastigerinella simplex* Morrow, p. 198, pl. 30, fig. 6.

1961 *Hedbergella amabilis* Loeblich & Tappan, p. 274, pl. 3, figs 1-10.

1977 *Hedbergella amablis* Loeblich & Tappan: Carter & Hart, pp. 29, 31, pl. 3, figs 22-23.

Diagnosis: A small species of *Hedbergella* with a low trochospire. Characterised by its 4 sub-clavate, often rapidly increasing in size, chambers in the last whorl.

Age range: Upper Albian to Lower Turonian

Genus ***Whiteinella*** Pessagno, 1967

Type species: *Whiteinella archaeocretacea* Pessagno, 1967

Whiteinella aprica (Loeblich & Tappan, 1961)

1961 *Ticinella aprica* Loeblich & Tappan, p. 292, pl. 4, figs 14-16.

1970 *Whiteinella aprica* (Loeblich & Tappan): Eicher & Worstell, p. 314, pl. 11, fig. 7a-c; pl. 12, fig. 1a-c.

1979 *Whiteinella aprica* (Loeblich & Tappan): Robaszynski & Caron, pp. 157-160, pl. 32, figs 1-2.

Diagnosis: A species of *Whiteinella* with low trochospire and rounded periphery. Chambers inflated, increasing slowly in size, with typically 5 chambers in the final whorl. Sutures are deep and radial. Umbilicus is shallow and wide, making up around one-forth of the maximum diameter.

Remarks: This species differs from *W. archaeocretacea* in having radial sutures, and no

imperforate band on the rounded periphery.

Age range: Lower Turonian

Whiteinella archaeocretacea Pessagno, 1967

Plate 7, Figs 3-4

1967 *Whiteinella archaeocretacea* Pessagno, pp. 288-289, pl. 51, figs 2-4; pl. 54, figs 19-25; pl. 100, fig. 8.

1985 *Whiteinella archaeocretacea* Pessagno: Caron, p. 79, figs 37 (4-5)

Diagnosis: A species of *Whiteinella* with low trochospire and flattened biconvex test, and imperforate peripheral border. The final whorl is made up of five chambers increasing fairly rapidly in size and becoming more elongate in the direction of coiling. The umbilicus is wide, a quarter to a third of the test diameter, and the aperture is almost umbilical. Sutures are deep throughout the test, becoming more curved in later chambers.

Remarks: This species differs from other *Whiteinella* in having an imperforate periphery.

Age range: Lower Turonian

Whiteinella baltica Douglas & Rankin, 1969

Plate 7, Figs 6-7, 11-12

1969 *Whiteinella baltica* Douglas & Rankin, p. 198, text-fig. 9a-c.

1985 *Whiteinella baltica* Douglas & Rankin,: Caron, p. 79, pl. 37, figs 1-3.

Diagnosis: A species of *Whiteinella* with low trochospire, and characterised by 4 globose chambers in the final whorl. Sutures are deep and radial and umbilicus is narrow, making up less than one forth of the maximum diameter.

Remarks: This species from *W. archaeocretacea* in having 4 chambers instead of 5 in the

final whorl, these chambers are more globular than seen in *W. archaeocretacea.*

Age range: Upper Cenomanian to Lower Turonian

Whiteinella brittonensis (Loeblich & Tappan, 1961)

Plate 7, Fig. 5, 9-10

1961 *Hedbergella brittonensis* Loeblich & Tappan, pp. 274-275, pl. 4, fig. 1a-c.

1979 *Whiteinella brittonensis* (Loeblich & Tappan): Robaszynski & Caron, pp. 175-180, pl. 37, figs 1-2; pl. 38, figs 1-2.

Diagnosis: A species of *Whiteinella* with a moderately high trochospire and rounded periphery. The final whorl is made up of 5 globular chambers increasing slowly in size. Sutures are deep and radial.

Age range: Lower Turonian

Subfamily ROTUNDININAE Bellier & Salaj, 1977

Genus *Praeglobotruncana* Bermúdez, 1952

Type species: *Globorotalia delrioensis* Plummer, 1931

Praeglobotruncana aumalensis (Sigal, 1952)

Plate 7, Figs 16-19

1952 *Praeglobotruncana aumalensis* Sigal (*fide* Robaszynski & Caron, 1979)

1979 *Praeglobotruncana aumalensis* (Sigal): Robaszynski & Caron, pp. 25-28, pl. 42, fig. 1.

Diagnosis: An asymmetrical biconvex species of *Praeglobotruncana* with a moderately high trochospire. Chambers are gently compressed to subangular and frequently marked by a concentration of pustules, at least in the first chamber of the whorl. Umbilicus is about one forth of the maximum diameter and final whorl is made up of 5-6 inflated petaloid chambers. Sutures deep and radial in early part, becoming curved. Surface often pustulose in texture.

Remarks: This species differs from *W. archaeocretacea* in its high trochospire, and differs from *P. stephani* in not having raised sutures.

Age range: Upper Cenomanian to Lower Turonian

Praeglobotruncana delrioensis (Plummer, 1931)

Plate 7, Figs 20, 24-25

1931 *Globorotalia delrioensis* Plummer, p. 199, p. 13, fig. 2a-c.

1979 *Praeglobotruncana delrioensis* (Plummer): Robaszynski & Caron, pp. 29-31, pl. 43, figs 1-2.

1985 *Praeglobotruncana delrioensis* (Plummer): Caron, p. 65, figs 30 (1-2)

Diagnosis: A species of *Praeglobotruncana* with a flat to low trochospire. Periphery lobate with an imperforate peripheral band lined by a faint row of pustules. 5-6 chambers in the final whorl, increasing slowly in size. Sutures are deep and radial, and the surface is pustulose.

Remarks: This species differs from *P. stephani* by having a lower trochospire.

Age range: Upper Albian to Upper Cenomanian

Praeglobotruncana gibba Klaus, 1960

Plate 7, Figs 21-23

1960 *Praeglobotruncana stephani* Gandolfi var. *gibba* Klaus, pp. 304-305; holotype designated in Reichel, 1950, pl. 16, fig. 6, pl. 17, fig. 6.

Diagnosis: This species of *Praeglobotruncana* is characterised by its high trochospire and 2 to 3 row of pustules on the periphery. It is made up of 2 ½ to 3 whorls, the final whorl with 5-6 chambers which are petaloid to triangular in shape, and flat to slightly inflated. The spiral sutures are curved and beaded, whereas umbilical sutures are radial and deep. Surface is slightly pustulose.

Remarks: *P. gibba* differs from *P.stephani* in its higher spire and well developed and distinct 2 ½ to 3 whorls. Specimens in the both the Indian Ocean and Crimea show a range of spire heights, but a general trend of increasing spire up through the sections from Cenomanian to Turonian is apparent.

Age range: Upper Cenomanian to Lower Turonian

Praeglobotruncana inornata (Bolli, 1957)

Plate 8, Figs 3-4

2004 *Praeglobotruncana inornata* (Bolli): Keller & Pardo, p. 5, pl. 3, figs 5-7

Diagnosis: A species of *Praeglobotruncana* with a moderate to high trochospire and characterised by 4 chambers in last whorl. Spiral side is very convex with flat to slightly globular chambers with depressed spiral sutures.

Age range: Mid-Cenomanian to Lower Turonian

Praeglobotruncana oraviensis Schiebnerová, 1960

Plate 8, Figs 1-2, 6

1960 *Praeglobotruncana oraviensis* Scheibnerová, pp. 85-86, text-fig. 4a-c.

1972 *Praeglobotruncana oraviensis* Scheibnerová: Gawor-Biedowa, pp. 75-76, pl. 8, fig. 5a-c.

Diagnosis: A biconvex species of *Praeglobotruncana* with a convex spiral side and row of pustules on the periphery. There are 6-7 chambers in the final whorl, showing an imbricate arrangement in the last whorl. The final chamber is radially stretched and appears slightly flattened.

Remarks: This species can be compared to *P. stephani*. It can be distinguished however by its greater number of chambers in the last whorl, more incised periphery and the imbricate arrangements of the chambers.

Age range: Lower Turonian

Praeglobotruncana stephani (Gandolfi, 1942)

Plate 8, Figs 7-9

1942 *Globotruncana stephani* Gandolphi, p. 130, pl. 3, figs 4, 5; pl. 4, figs 36, 37, 41-45; pl. 6, figs 4, 6; pl. 9, figs 5, 8; pl. 13, fig. 5; pl. 14, fig. 2.

1957 *Praeglobotruncana stephani* (Gandolfi): Bolli, Loeblich & Tappan, p. 39, pl. 9, fig. 2

1970 *Praeglobotruncana stephani* (Gandolfi): Eicher & Worstell, p. 308, pl. 10, fig. 9; pl. 11, figs 2a-c, 3.

1977 *Praeglobotruncana stephani* (Gandolfi): Carter & Hart, pp. 40-41, pl. 4, figs 16-21.

1985 *Praeglobotruncana stephani* (Gandolfi): Caron, p. 65, figs 30 (3-4).

Diagnosis: A species of *Praeglobotruncana* with low to moderately high trochospire. The periphery in marked by 2 to 3 rows of pustules which become fainter in the final chambers. Spiral side shows petaloid chambers which are flat to slightly inflated, increasing moderately in size. The spiral sutures are curved and beaded.

Remarks: This species differs from *P. aumalensis* in having beaded spiral sutures and well developed row of pustules, and from *P. gibba* in having a low to moderate trochospire.

Age range: Mid Cretaceous to Lower Turonian

Subfamily HELVETOGLOBOTRUNCANINAE Lamolda, 1976

Genus ***Helvetoglobotruncana*** Reiss, 1957

Type species: *Globotruncana helvetica* Bolli, 1945

Helvetoglobotruncana praehelvetica (Trujillo, 1960)

Plate 8, Figs 5, 10, 15

1960 *Rugoglobigerina praehelvetica* Trujillo, p. 340, pl. 49, fig. 6.

1985 *Helvetoglobotruncana praehelvetica* (Trujillo), Caron, p. 60, figs 30.7-8; 10, 12, 15

Diagnosis: A species of *Helvetoglobotruncana* characterised by a strongly asymmetrical, plano-convex test, with nearly flat spiral side with depressed sutures. 4-5 petaloid chambers make up the final whorl. A slight keel is developed on the earlier chambers with a sharp line of pustules.

Remarks: This species differs from *H. helvetoglobotruncana* by the absence of a true keel and depressed sutures on the spiral side. It can be determined from species of *Whiteinella* by it plano-convex test and flattened spiral side.

Age range: Mid-Cenomanian to Lower Turonian

Helvetoglobotruncana helvetica (Bolli, 1945)

1945 *Globotruncana helvetica* Bolli, p. 226, pl. 9, fig. 6

1963 *Globotruncana carpathica* Scheibnerova, p. 140, fig. 2 a-c

1985 *Heveltoglobotruncana helvetica* (Bolli), Caron, p. 60, figs 30.9-10; 10, 12, 15

Diagnosis: Species of *Helvetoglobotruncana* characterised by a strongly asymmetrical, plano-convex test, with nearly flat spiral side and raised sutures. Typically comprised of 4-6 chambers in the final whorl, this species has a wide umbilicus (1/3 of the test diameter) and a single keel.

Remarks: This species was only observed rarely in Crimean sections, and predominantly in thin sections of the sediments. Analysis of these specimens in thin section show possible indications of a slight double keel in earlier chambers, possibly indicating a similarity to *Dicarinella elata* as opposed to *H. helvetica*. In further comparison of these specimens with the holotype of *Dicarinella elata*, illustrated and described by Lamolda (1977), it was decided to retain *H. helvetica* as the species name for these specimens. This was decided upon due to the degree of convexity of the umbilical side when compared to the less convex holotype, and the distinct dorsal keel observed in specimens, typical of *H. helvetica* compared to the marginal keel of *D. elata*.

Age range: Lower Turonian

Family ROTALIPORIDAE Sigal, 1958

Subfamily ROTALIPORINAE Sigal, 1958

Genus ***Rotalipora*** Brotzen, 1942

Type species: *Rotalipora turonica* Brotzen, 1942 = *Globorotalia cushmani* Morrow, 1934

Rotalipora appenninica (Renz, 1936)

Plate 8, Figs 11-13

1936 *Globotruncana appenninica* Renz, pp. 20, 135, text-fig. 2, 7a; p. 14, text-fig. 7a; p. 71, pl. 6, figs 1-11; pl. 7, fig. 1; pl. 8, fig. 4.

1979 *Rotalipora appenninica* (Renz): Robaszynski & Caron, pp. 59-64, pl. 4, figs. 1-3; pl. 5, figs 1-3.

1985 *Rotalipora appenninica* (Renz): Caron, p. 67, figs 31 (1-4).

Diagnosis: A symmetrical biconvex species of *Rotalipora* with a low trochospiral test, and a marked single keel. The spiral side has 6 petaloid chambers in the final whorl, increasing rapidly in size, the final chamber is often relatively large. It has raised spiral sutures, each joining the last at an angle of 90°. The umbilical side has deep and radial sutures and a narrow umbilicus 1/4 to 1/5 of the maximum diameter.

Age range: Upper Albian to Upper Cenomanian

Rotalipora brotzeni (Sigal, 1948)

Plate 8, Figs 14, 18-19

1948 *Thalmanninella brotzeni* Sigal, p. 102, pl. 1, figs. 5a-c.

1985 *Rotalipora brotzeni* (Sigal): Robaszynski & Caron, pp. 65-68, pl. 6, figs 1-2.

1985 *Rotalipora brotzeni* (Sigal): Caron, p. 67, figs 31 (5-7).

Diagnosis: An asymmetrical species of *Rotalipora* with 5-7 chambers in the final whorl that are trapezoidal in shape and increase moderately in size. The spiral sutures are curved and raised, but not as prominently in the latest chambers.

Age range: Lower to mid-Cenomanian

Rotalipora cushmani (Morrow, 1934)

Plate 8, Figs 16-17

1934 *Globorotalia cushmani* Morrow, p. 199, pl. 31, figs 2, 4.

1948 *Rotalipora cushmani* (Morrow): Sigal, p. 96, pl. 1, fig. 2; pl. 2, fig. 1.

1970 *Rotalipora cushmani* (Morrow): Eicher & Worstell, pp. 310, 312, pl. 12, figs 3a-c, 4a-c; pl. 13, fig. 1a-b.

1977 *Rotalipora cushmani* (Morrow): Carter & Hart, p. 41, pl. 2, fig. 18; pl. 4, figs 7-9.

1985 *Rotalipora cushmani* (Morrow): Caron, p. 69, figs 31 (8-11).

Diagnosis: An equally biconvex species of *Rotalipora* with a moderate to high trochospire. There are 4 ½ to 5 inflated semicircular chambers in the last whorl that increase rapidly in size. The spiral sutures are raised and curved, whilst the umbilical sutures are depressed.

Remarks: This species varies from *R. montsalvensis* in having a high trochospire and a raised spiral suture.

Age range: Mid- to Upper Cenomanian

Rotalipora deecki (Franke, 1925)

Plate 8, Figs 20, 24-25

1925 *Rotalia deecki* Franke, pp. 90-91, pl. 8, fig. 7a-c.

1972 *Rotalipora deecki* (Franke): Gawor-Biedowa, pp. 82-83, pl. 11, figs 2a-c, 3a-c.

1979 *Rotalipora deecki* (Franke): Robaszynski & Caron, pp. 75-80, pl. 9, figs 1-2; pl. 10, figs 1-2.

Diagnosis: An asymmetrical species of *Rotalipora* with strongly convex umbilical side, the spiral side often becoming slightly concave. 7-9 elongate, crescent shaped chambers make up the final whorl, increasing slowly in size. The spiral suture are raised, each

meeting very obliquely with the preceding one.

Remarks: This species if very similar to *R. reicheli*, other than stratigraphical range it can be differentiated by the occurrence of sutural ridges extended by periumbilical ridges on most of the chambers.

Age range: Upper Cenomanian

Rotalipora globotruncanoides (Sigal, 1948)

Plate 8, Fig. 22

1948 *Thalmanninella globotruncanoides* Sigalm p. 102, pl. 1, fig. 5a-c.

1979 *Rotalipora brotzeni* Sigal: Robasynski and Caron, pp. 65-68, pl. 6, figs 1-2.

1985 *Rotalipora brotzeni* Sigal: Caron, pp. 67, 70, pl. 31, figs 5-7.

Diagnosis: An unequally biconvex species of *Rotalipora*. The spiral side is slightly convex, and comprised of 2 ½ to 3 whorls of chambers. There are 5-7 chambers in the last wall and the sutures on the spiral and umbilical side are raised (on early chambers on the umbilical side). The periphery is lobulate.

Remarks: This species differ from *R. gandolfi* in having raised umbilical sutures, and from *R.greenhornensis* in having a more lobulate periphers and in lacking raised umbilical sutures between the latest chambers.

Age range: Lower to Upper Cenomanian

Rotalipora greenhornensis Morrow, 1934

Plate 8, Fig. 21

1934 *Globorotalia greenhornensis* Morrow, p. 199, pl. 39, fig. 1.

1948 *Rotalipora greenhornensis* (Morrow): Sigal, p. 100, pl. 1, fig. 4; pl. 2, figs 3-5.

1970 *Rotalipora greenhornensis* (Morrow): Eicher & Worstell, p. 312, pl. 12, fig. 2a-c; pl. 13, fig. 3a-b.

1977 *Rotalipora greenhornensis* (Morrow): Carter & Hart, pp. 44-45, pl. 4, figs 10-12.

Diagnosis: A large biconvex species of *Rotalipora* characterised by its beaded sutures on both umbilical and spiral sides, and large number of chambers in the final whorl, which can reach up to 10 in advanced forms. Chambers are crescent shaped to semi-circular, increasing slowly in size.

Remarks: This species differs from *R. brotzeni* in its greater number of chambers and more asymmetrical test.

Age range: Upper Cenomanian

Rotalipora micheli (Sacal & Debourle, 1957)

1979 *Rotalipora micheli* (Sacal & Debourle): Robaszynski & Caron, pp. 91-94, pl. 14, figs 1-3.

Diagnosis: An asymmetrical species of *Rotalipora* with slightly convex spiral side and inflated umbilical side. It has 5-6 triangular inflated chambers in the final whorl. Spiral sutures are raised and each obliquely joins the preceding ones.

Remarks: *R. micheli* are considered to be a transitional form between *R. appenninica* and *R. reicheli* (Robaszynski & Caron, 1979).

Age range: Upper Cenomanian

Rotalipora montsalvensis Mornod, 1950

Plate 8, Fig. 23

1950 *Globotruncana (Rotalipora) reicheli* Mornod, pp. 583-584, text-fig. 5 (IV a-c)

1979 *Rotalipora montsalvensis* Mornod: Robaszynski & Caron, pp. 99, 106, pl. 16, fig. 1; pl. 17, fig. 1; pl. 18, figs 1-2.

1985 *Rotalipora montsalvensis* Mornod: Caron, p. 69, figs 32 (3-4).

Diagnosis: A biconvex species of *Rotalipora,* with 4 ½ to 5 elongate chambers in the last whorl. The chambers increase rapidly in size and sutures are strongly depressed.

Remarks: This species is differentiated from *R. cushmani* by its more elongate chambers and depressed sutures.

Age range: Upper Cenomanian

Rotalipora reicheli Mornod, 1949

Plate 9, Figs 1-3

1942 *Globotruncana appenninica* Renz var. *gamma* Gandolfi: Gandolfi, p. 119, text-figs 41-42; p. 122, pl. 6, fig. 6; pl. 14, fig. 6.

1949 *Globotruncana (Rotalipora) reicheli* Mornod, pp. 583-584, text-fig. 5; p. 581, text-fig. 6; p. 583, pl. 15, figs 2a-p, 3-8.

1972 *Rotalipora reicheli* Mornod: Gawor-Biedowa, pp. 84-85, pl. 11, fig. 1a-c.

1985 *Rotalipora reicheli* Mornod: Caron, p. 69, figs 32 (5-6).

Diagnosis: A strongly asymmetrical species of *Rotalipora*, with characteristic plano-convex shape. The spiral side is flat to slightly concave with raised spiral sutures, whilst the umbilical side is high with inflated final chambers. The chambers are crescent shaped, 6-8 making up the final whorl

Remarks: This species is very similar to *R. deecki* although the range of the two species is very different. *R. reicheli* can be differentiated by its lower number of chambers in the last whorl and wider chambers on the umbilical side.

Age range: Lower to mid-Cenomanian

Rotalipora ticinensis (Gandolfi, 1942)

Plate 9, Figs 4-5, 10

1942 *Globotruncana ticinensis* Gandolfi, pp. 113-135, pl. 2, figs 3-4; pl. 4, figs 8-11, 21-23; pl. 5, figs 2-4; pl. 8, figs 3-7; pl. 11, fig. 5; pl. 12, fig. 1; pl. 13, figs 9-12, 14.

1979 *Rotalipora ticinensis* (Gandolfi): Robaszynski & Caron, 1979, pp. 111, 114, pl. 20, figs 1-2.

1985 *Rotalipora ticinensis* (Gandolfi): Caron, p. 72, figs 33 (3-4).

Diagnosis: A biconvex species of *Rotalipora* with moderate to high trochospire. The final whorl has 6-9 petaloid chambers increasing gradually in size. The spiral sutures are raised and oblique to gently curved.

Remarks: This species varies from *R. appenninica* in its greater number of chambers and by the chambers increasing slowly in size.

Age range: Upper Albian

Superfamily GLOBOTRUNCANACEA Brotzen, 1942

Family GLOBOTRUNCANIDAE Brotzen, 1942

Subfamily GLOBOTRUNCANINAE Brotzen, 1942

Genus ***Dicarinella*** Porthault, 1970

Type species: *Globotruncana indica* Jacob & Sastry, 1950

Dicarinella algeriana (Caron, 1966)

Plate 9, Figs 6-7

1966 *Praeglobotruncana algeriana* Caron, pp. 74-75.

1979 *Dicarinella algeriana* Caron: Robaszynski & Caron, pp. 57, 60, pl. 49, fig. 2; pl. 50, figs 1-2

1985 *Dicarinella algeriana* Caron: Caron p. 43, figs 17 (1-2)

Diagnosis: A species of *Dicarinella* with a low to moderately high trochospire. The periphery is lobate and shows two bands of pustules separated by a narrow imperforate band. These become less distinct in the final chambers. There are 5-6 petaloid chambers in the final whorl, increasing slowly in size. The sutures are curved and depressed on the spiral side.

Remarks: This species is the most primitive of the genus *Dicarinella*. It is a transitional form between *P. stephani* and *Dicarinella hagni*. Differing from *P. stephani* due to the presence of the two rows of pustules, and *D. hagni* due to the absence of a true double keel.

Age range: Upper Cenomanian to Lower Turonian

Dicarinella biconvexiformis Maslakova, 1978

1978 *Dicarinella biconvexiformis*, Maslakova (*fide* Kopaevich & Kuzmicheva, 2002)

2002 *Dicarinella biconvexiformis* Maslakova: Kopaevich & Kuzmicheva, p. 148, pl. 3, fig. 5 a-c.

Diagnosis: A biconvex form of *Dicarinella* with high trochospire. 6-7 chambers in the final whorl, increase slowly in size. Spiral sutures are raised and a double keel is present on the earlier chambers.

Remarks: This species is only seen in the Crimean sections and is similar to *P. gibba* but with a double keel as opposed to a single keel.

Age range: Lower Turonian

Dicarinella canaliculata (Reuss, 1854)

Plate 9, Fig. 8

1854 *Rosalina canaliculata* Reuss, p. 70, pl. 26, fig. 4a-b.

1967 *Marginotruncana canaliculata* (Reuss): Pessagno, p. 303, pl. 74, figs 5-8.

1979 *Dicarinella canaliculata* (Reuss): Robaszynski & Caron, pp. 67, 70, pl. 53, figs 1-3.

Diagnosis: A flattened form of *Dicarinella,* this species is characterised by two widely spaced parallel keels, continuing to the last chamber giving a sub-rectangular profile. The spiral side is flat to slightly convex with 5 to 6 petaloid chambers increasing slowly in the final whorl. Sutures are raised and curved.

Age range: Lower Turonian

Dicarinella elata Lamolda, 1977

Plate 9, Fig. 9

1977 *Dicarinella elata* Lamolda p. 471, pl. 1 (1). , fig 3-4

2002 *Dicarinella elata* Lamolda: Kopaevich and Kuzmicheva, pl. 3, fig 4a-c.

Diagnosis: A species of *Dicarinella* with a single keel, and depressed sutures on the umbilical side. The chambers are conical, and specimens are seen to have a low trochospire.

Remarks: *Dicarinella elata* Lamolda can be differentiated from *D. indica* by possession of a single keel instead of a double keel on the outer whorl, from *M. marianosi* by depressed sutures on the umbilical side and from *Helvetoglobotruncana helvetica* by

conical rather than hemispherical chambers, and by a strong, marginal (never dorsal) keel on all chambers.

Age range: Lower Turonian

Dicarinella hagni (Schiebnerová, 1962)

Plate 9, Figs 11-13

1962 *Praeglobotruncana hagni* Scheibnerová, p. 219, fig 6a-c.

1979 *Dicarinella hagni* (Scheibnerová): Robaszynski & Caron, pp. 79, 84-86, pl. 56, figs 102; pl. 57, figs 1-2.

1985 *Dicarinella hagni* (Scheibnerová): Caron, p. 45, figs 18 (1-3)

Diagnosis: An asymmetrically biconvex to planoconvex species of *Dicarinella* with a low to moderate trochospire. There are 5-8 (most typically 6) petaloid, and sometimes slightly convex, chambers in the final whorl. These increase slowly in size. The periphery is lobate with two keels which are close together and parallel, often disappearing on the final chamber, which often shows no keel. Chambers on the spiral side are raised, oblique and curved forwards.

Remarks: Sutures on the umbilical side can appear to be slightly raised in early chambers of some specimens. This is due to calcitic overgrowths, the later chambers showing distinctly depressed sutures, typical of *Dicarinella hagni.*

Age range: Lower Turonian

Dicarinella imbricata (Mornod, 1950)

Plate 9, Figs 14-15, 19-20

1950 *Globotruncana (Globotruncana) imbricata* Mornod, pp. 589-590, fig. 5 (III a-d)

1979 *Dicarinella imbricata* (Mornod): Robaszynski & Caron, pp. 87, 92, pl. 58, figs 1-2; pl. 59, figs 1-2

1985 *Dicarinella imbricata* (Mornod): Caron, p. 45, figs 18 (4-5)

Diagnosis: A convexo-concave test with a low to moderate trochospire. The periphery has 2 keels separated by a wide, imperforate band, not seen in the final 2 chambers. The keels diverge obliquely from one chamber to the next, forming an imbricated sequence, that characterises the test. 5-6 chambers form the last whorl, with curved and raised spiral sutures.

Age range: Upper Cenomanian to Lower Turonian

Dicarinella* cf. *imbricata

Plate 9, Fig. 16

1950 *Globotruncana (Globotruncana) imbricata* Mornod, pp. 589-590, fig. 5 (III a-d)

1979 *Dicarinella imbricata* (Mornod): Robaszynski & Caron, pp. 87, 92, pl. 58, figs 1-2; pl. 59, figs 1-2

1985 *Dicarinella imbricata* (Mornod): Caron, p. 45, figs 18 (4-5)

Remarks: This species has the same imbricated keel as *D. imbricata* although the final wall is made up of only 4 – 4 ½ chambers. This species is seen in the Upper Cenomanian of the Crimea as a precursor to *D. imbricata.*

Age range: Upper Cenomanian

Genus ***Marginotruncana*** Hofker, 1956

Type species: *Rosalina marginata* Reuss, 1846

Marginotruncana cf. *marianosa* (Douglas, 1969)

Plate 9, Fig. 17

1969 *Globotruncana marianosi* Douglas, p. 183, text figs 5a-c.

2000 *Marginotruncana* cf. *marianosa* (Douglas): Howe *et al.*, fig. 12 (15-17)

Diagnosis: An asymmetrical planoconvex species of *Marginotruncana* with 7-8 chambers in the final whorl. This species has only a single keel and is characterised by the depth of the chambers on the umbilical side. Sutures are raised and curved and oblique in shape.

Remarks: This species can often be mistaken for *R. reicheli* in its lateral view, however it can be distinguished from this species by the presence/absence of supplementary apertures. The species found in ODP Site 762 show slightly more elongate chambers than is typically seen for this species and is identical to species illustrated by Howe *et al.* (2000).

Age range: Lower Turonian

Marginotruncana sigali (Reichel, 1950)

Plate 9, Fig. 18

1950 *Globotruncana (Globotruncana)sigali* Reichel, p. 610, figs 5a-c

1979 *Marginotruncana sigali* (Reichel), Robaszynski & Caron, p. 146, pl. 72, figs 1-2; pl. 73, fig. 1

1985 *Marginotruncana sigali* (Reichel), Caron, p. 61, figs 27.7-8; 11, 12, 15

Diagnosis: A species of *Marginotruncana* with 5 to 7 chambers in the final whorl. It is charaterised by by its U-shaped sutures on the umbilical side and flattened, sub-trapezoidal chamber on the spiral side. This species has a single keel formed by a close double row of pustules.

Remarks: This species is seen only at Site 762. Preservation at this site is poor, the U-shaped sutures being seen only rarely on the calcified tests.

Age range: Lower Turonian

Suborder ROTALIINA Delage & Hérouard, 1896

Superfamily BOLIVINACEA Glaessner, 1937

Family BOLIVINIDAE Glaessner, 1937

Genus ***Bolivina*** d'Orbigny, 1839

Type species: *Bolivina plicata* d'Orbigny, 1839

Bolivina sp. 1

Plate 9, Fig. 21

Diagnosis: A small elongate species of *Bolivina* with tapering sides, and 4-5 pairs of chambers.

Age range: Upper Albian to Lower Turonian

Bolivina sp. 2

Plate 9, Figs 22-23

Diagnosis: A small species of *Bolivina* with slightly tapering sides, and 4-5 pairs of elongate chambers. The chambers increase slowly in size, the last pair becoming larger and more inflated than the other chambers

Remarks: This species differs from *Bolivina* sp. 1 in its less elongate and more rounded shape, with more inflated final chambers.

Age range: Upper Albian to Lower Turonian

Genus ***Bolivinoides*** Cushman, 1927

Type species: *Bolivina draco* Marsson, 1878

***Bolivinoides* sp. 1**

Plate 9, Fig. 24

Diagnosis: A small flattened species of *Bolivinoides*. Chambers broad and low and irregular in shape.

Age range: Lower Turonian

Genus ***Tappanina*** Montanaro Gallitelli, 1955

Type species: *Bolivinita selmensis* Cushman, 1933

Tappanina* cf. *lacinosa Eicher & Worstell, 1970

Plate 9, Figs 25-26

1970 *Tappanina lacinosa* Eicher & Worstell, p. 291, pl. 4, figs 6-7, 11-12.

Diagnosis: A small, flaring species of *Tappanina* showing an irregular periphery. Chambers begin subglobular, becoming cuneiform and increasing more in width than height as the test develops. Irregular skirt like flanges extend brokenly from one side to the other and around the periphery. Aperture an arch in one side of the apertural face, bordered by a lip.

Remarks: Not all specimens develop the skirt like flanges, although it is seen in most of the specimens.

Age range: Lower Cenomanian to Upper Turonian

Superfamily EOUVIGERINACEA Cushman, 1927

Family LACOSTEINIDAE Sigal, 1952

Genus ***Spirobolivina*** Hofker 1956

Type species: *Bolivinopsis pulchella* Cushman & Stainforth, 1947

Spirobolivina australis Scheibnerová 1974

Plate 10, Fig. 1

1974 *Spirobolivina australis* Scheibnerová, p. 713, pl. 4, fig. 4; pl. 10, fig. 14.

1983 *Spirobolivina australis* Scheibnerová: Basov & Krasheninikov, p. 768, pl. 4, fig. 7.

Diagnosis: A species of *Spirobolivina* with flat parallel sides. The chambers of the biserial portion are low and broad with straight sutures. The periphery is broad and flat with sharp angled edges. The aperture is loop shaped and situated at the base of the apertural face of the last chamber.

Age range: Upper Albian

Superfamily TURRILINACEA Cushman, 1927

Family TURRILINIDAE Cushman, 1927

Genus ***Cuneus*** Voloshina, 1974

Type species: *Tritaxia minuta* Marsson, 1878

Cuneus **cf.** ***ludbrookae*** (Haig, 1982)

Plate 10, Fig. 2

1982 *Neobulimina ludbrookae* Haig, pp. 50-52, pl. 10, figs 1-7; pl. 16, fig, 4.

1992 *Cuneus* cf. *ludbrookae* (Haig): p. 289, pl. 2, fig. 15.

Diagnosis: A species of *Cuneus* showing slightly twisted pyramidal form and concave sides. The periphery is angular but rounded and the test wall smooth

Age range: Mid-Cenomanian

Genus ***Neobulimina*** Cushman and Wickenden, 1928

Type species: *Neobulimina Canadensis* Cushman and Wickenden, 1928

Neobulimina australiana Ludbrook, 1966

Plate 10, Figs 3-4

1966 *Neobulimina australiana* Ludbrook, p. 132, pl. 10, fig 20.

1972 *Neobulimina australiana* Ludbrook: Scheibnerová, p. 712, pl. 4, figs 1-2; pl. 10, fig. 20.

2000 *Neobulimina australiana* Ludbrook: Howe, Haig & Apthorpe, p. 551, fig. 10, no. 14.

Diagnosis: An elongate species of *Neobulimina*. Very tiny, the test is triserial, becoming loosely triserial or biserial. The chambers are inflated, increasing slowly in size. Sutures are distinct and moderately depressed. Aperture an asymmetrical arch, on one side of a depression in the apertural face.

Remarks: This species typically occurs in sediments characterised by a relatively deep-

water (outer shelf) assemblage with planktonic foraminifera (*Hedbergella*) present.

Age range: Upper Albian to Upper Cenomanian

Genus ***Praebulimina*** Hofker, 1953

Type species: *Bulimina ovulum* Reuss, 1844

Praebulimina nannina (Tappan, 1940)

Plate 10, Figs 5-7

1940 *Bulimina nannina* Tappan, p. 116, pl. 19, fig. 4.

1984 *Praebulimina nannina* (Tappan): Moullade, pl. 3, figs 25-26.

1992 *Praebulimina* cf. *nannina* (Tappan); Haig, p. 289, pl. 2, fig. 17.

Diagnosis: A small species of *Praebulimina* with a flaring, triserial test. Chambers inflated and separated by distinct sutures. Aperture at base of last chamber, with simple internal toothplate.

Age range: Upper Albian to Lower Turonian

Praebulimina reussi (Morrow, 1934)

Plate 10, Figs 8-9

1934 *Bulimina reussi* Morrow, p. 195, [new name for *Bulimina ovulum* Reuss, 1845, p. 37, pl. 8, fig. 57; pl. 13, fig. 73]

2000 *Praebulimina reussi* (Morrow): Howe, Haig & Apthorpe, fig. 10, no. 19-20.

Diagnosis: An elongate species of *Praebulimina*. The test has a rounded base and chambers are elongate increasing slowly in size

Age range: Upper Albian to Lower Turonian

Praebulimina cf. *reussi* (Morrow, 1934)

Plate 10, Figs 10-11

1934 *Bulimina reussi* Morrow, p. 195, [new name for *Bulimina ovulum* Reuss, 1845, p. 37, pl. 8, fig. 57; pl. 13, fig. 73]

2000 *Praebulimina reussi* (Morrow): Howe, Haig & Apthorpe, fig. 10, no. 19-20.

Remarks: Similar to *Praebulimina reussi,* this variation is smaller with more globular chambers, the last chambers making up over half of the test.

Age range: Upper Albian to Lower Turonian

Praebulimina robusta (Klasz, Magné & Rérat)

Plate 10, Fig. 12

1963 *Bulimina (Praebulimina?) exigua robusta* de Klasz, Magné, & Rérat, pl. 1, fig. 5; pl. 2, figs. 7-8.

1998 *Praebulimina robusta* (Klasz, Magné & Rérat): Holbourn & Kuhnt, p. 383, pl. 3, fig. 7.

Diagnosis: A large species of *Praebulimina* characterised by large globular chambers, the species appears irregular and angular in shape.

Age range: Lower Turonian

Praebulimina sp. 1

Plate 10, Figs 13-14

Diagnosis: A very small, triserial, smooth species of *Praebulimina* with inflated chambers.

Aperture loop shaped, with simple tooth plate.

Age range: Mid- Cenomanian to Lower Turonian

Genus ***Turrilina*** Andreae, 1884

Type species: *Turrilina alsatica* Andreae, 1884

Turrilina evexa (Loeblich & Tappan, 1949)

Plate 10, Figs 16-19

1949 *Bulimina evexa* Loeblich & Tappan, p. 263, pl. 52, fig. 5a-b.

1972 *Praebulimina evexa* (Loeblich & Tappan): Gawor-Biedowa, p. 55, pl. 5, fig. 1.

2000 *Turrilina evexa* (Loeblich & Tappan): Howe, Haig & Apthorpe, p. 534, fig 10 (23).

Diagnosis: A very small and short species of *Turrilina,* with 3 to 3 ½ chambers making up the final whorl. Test is smooth and a lip can be observed near the aperture.

Age range: Upper Albian to Lower Turonian

Superfamily BULIMINACEA Jones, 1875

Family BULIMINELLIDAE Hofker, 1951

Genus ***Buliminella*** Cushman, 1911

Type species: *Bulimina elegantissima* d'Orbigny, 1839

Buliminella fabilis Cushman & Parker, 1936

Plate 10, Fig. 20

1936 *Buliminella fabilis* Cushman & Parker, p. 7, pl. 2, fig. 5.

1970 *Buliminella fabilis* Cushman & Parker: Eicher & Worstell, p. 290, pl. 3, figs 13-14.

Diagnosis: An elongate, small species of *Buliminella*. The test is smooth and sutures flush. 3 to 3 ½ chambers make up the final whorl.

Age range: Lower Turonian

Superfamily FURSENKOINACEA Loeblich & Tappan, 1961

Family FURSENKOINIDAE Loeblich & Tappan, 1961

Genus ***Cassidella*** Hofker, 1951

Type species: *Virgulina tegulata* Reuss, 1846

***Cassidella* sp. 1**

Plate 10, Fig. 21

Diagnosis: An elongate, tapered, species of *Cassidella*. The test is flattened and slightly twisted. Chambers increase in size slowly in the early portion of the test, chambers enlarging more rapidly in the latter stages.

Age range: Upper Cenomanian to Lower Turonian

Genus ***Coryphostoma*** Loeblich & Tappan, 1962

Type species: *Bolivina plaitum* Carsey, 1926

***Coryphostoma* sp. 1**

Plate 10, Fig. 22

1973 *Coryphostoma* sp. Scheibnerová, p. 714, pl. 4, figs 13-26; pl. 11, fig. 3.

1982 *Corophostoma* sp. A Haig, pp. 62-62, pl. 12, figs 19-22.

1992 *Corophostoma* sp. Haig, p. 289, pl. 2, fig. 18.

1997 *Corophostoma* sp. Holbourn & Kaminski, p. 76, pl. 45, figs 5-6.

Diagnosis: An elongate, flattened species of *Coryphostoma* with sub-parallel sides. The last few chambers become more elongated and can become uniserial. Sutures are distinct and slightly depressed. Aperture terminal.

Age range: Upper Albian

Superfamily PLEUROSTOMELLACEA Reuss, 1860

Family PLEUROSTOMELLIDAE Reuss, 1860

Subfamily PLEUROSTOMELLINAEA Reuss, 1860

Genus ***Ellipsodimorphina*** Silvestri, 1901

Type species: *Ellipsodimorphina subcompacta* Liebus, 1922

Ellisodimorphina sp. 1

Plate 10, Fig 23

Diagnosis: An elongate species of *Ellipsodimorphina*. The test is initially biserial and flattened, the chambers increasing rapidly in size and becoming more globular and cuneate. The last chamber makes up more than a third of the test and shows a prominent aperture.

Age range: Upper Albian to Mid-Cenomanian

Genus ***Ellipsoglandulina*** Silvestri, 1900

Type species: *Ellipsoglandulina laevigata* Silvestri, 1900

Ellipsoglandulina **sp. 1**

Plate 10, Fig. 24

Diagnosis: A short and very globular species of *Ellipsoglandulina*. Chambers are strongly overlapping. The final chamber is very large making up nearly the whole test. Aperture terminal.

Age range: Upper Albian

Genus **Nodosarella** Rzehak, 1895

Type species: *Lingulina tuberose* Gümbel, 1870

Nodosarella **sp. 1**

Plate 10, Fig. 25

Diagnosis: An elongate species of *Nodosarella*. Circular in cross section and made up of 4 chambers separated by straight, depressed sutures.

Age range: Lower Turonian

Genus ***Pleurostomella***, Reuss, 1860

Type species: *Dentalina subnodosa* Reuss, 1851

Pleurostomella nitida Morrow, 1934

Plate 11, Fig. 1

1934 *Pleurostomella nitida* Morrow, p. 4, pl. 30, fig. 22.

1970 *Pleurostomella nitida* Morrow: Eicher & Worstell, p. 291, pl. 4, figs 5, 8-10.

Diagnosis: A species of *Pleurostomella* with slightly inflated chambers, increasing regularly in size. Aperture on most specimens is terminal on a short extension of the final chamber.

Age range: Lower Turonian

Pleurostomella reussi Berthelin, 1880

Plate 11, Figs 2-5

1880 *Pleurostomella reussi* Berthelin, p. 28, pl. 1, figs 10-12.

1997 *Pleurostomella reussi* Berthelin: Holbourn & Kaminski, 1997, p. 78, pl. 45, figs 8-13.

Diagnosis: An elongate species of *Pleurostomella*, initially biserial becoming loosely uniserial with alternating chambers. The chambers are inflated and separated by oblique, depressed sutures. The aperture is terminal with a pair of triangular teeth and is partially covered by a hood.

Age range: Upper Albian to Lower Turonian

Pleurostomella subnodosa Reuss, 1860

Plate 11, Figs 6-8

1860 *Pleurostomella subnodosa* Reuss, p. 204, pl. 8, fig. 2.

1983 *Pleurostomella subnodosa* Reuss: Basov & Krasheninnikov, p. 767, pl. 11, fig. 8.

Diagnosis: An elongate species of *Pleurostomella*. Initially biserial the chambers are inflated and loosely alternating. Sutures are straight or slightly inclined and depressed

Remarks: This species differs from *P. reussi* by the slightly longer biserial phase.

Age range: Lower Turonian

Pleurostomella sp. 1

Plate 11, Fig. 1

Diagnosis: A thin species of *Pleurostomella*, initially biserial the test is narrow and straight. The last two chambers increasing in size and becoming more globular.

Age range: Upper Cenomanian to Lower Turonian

Superfamily DISCORBACEA Ehrenberg, 1838

Family CONORBINIDAE Reiss, 1963

Genus *Eurycheilostoma* Loeblich & Tappan, 1957

Type species: *Eurycheilostoma altispira* Loeblich & Tappan, 1957.

Eurycheilostoma? hettgottensis (Ludbrook, 1966)

Plate 11, Fig. 10

1999 *Eurycheilostoma? hettgottensis* (Ludbrook): Campbell & Haig, p. 411, figs 5 (38-39)

Diagnosis: An elongate species of *Eurycheilostoma.* Trochospiral, the chambers increase slowly, becoming more inflated. 3-4 chambers are found in the last whorl.

Age range: Lower Cenomanian to Upper Cenomanian

Eurycheilostoma? moorei, Haig

Plate 11, Fig. 11

Diagnosis: A small species of *Eurycheilostoma.* Trochospiral and very globular, the

chambers increase rapidly in size. The last whorl is made up of 3 very globular chambers, with slightly depressed chambers making up most of the test.

Age range: Lower Cenomanian

Genus ***Iuliusina*** Fuchs, 1971

Type species: *Iuliusina grata* Fuchs, 1971

Iuliusina grata Fuchs, 1971

Plate 11, Figs 12-17

1971 *Iuliusina grata* Fuchs, p. 34.

1995 *Iuliusina grata* Fuchs: Lamolda & Peryt, p. 114, pl. 3, figs 11-12.

Diagnosis: A species of *Iuliusina.* Small and trochospiral the species is composed of 2.5-3 whorls and the periphery is rounded. Chambers increase slowly in size initially, becoming rapid in the last whorl, chambers becoming more globular and oval in shape.

Age range: Upper Cenomanian to Lower Turonian

Superfamily CHILOSTOMELLACEA Brady, 1881

Family CHILOSTOMELLIDAE Brady, 1881

Subfamily PALLAIMORPHININAE Loeblich & Tappan, 1987

Genus ***Gubkinella*** Suleymanov, 1955

Type species: *Gubkinella asiatica* Suleymanov, 1955

Gubkinella sp. 1

Plate 11, Figs 18-20, 25

1978 *Gubkinella californica* Church: Schiebnerová, p. 141, pl. 8, figs 1-3.

Diagnosis: Small species of *Gubkinella* with a high trochospire. Made up of 2-2 ½ whorls the chambers initially increase slowly in size, the final whorl becoming largely inflated. Sutures are depressed and wall appears to be sparsely perforate.

Remarks: Originally classed as a planktonic taxon, a study of the wall structure of *G. asiatica* by Gorbachik and Suleymanov (1985) showed *Gubkinella* to be a benthonic genus related to *Quadrimorphina*. The species found in this study shows close affinities to Schiebnerová's small, high trochospiral species of *Gubkinella californica* Scheibnerová (1978). However, these specimens show 4-6 chambers in the final whorl, not 4 as illustrated by Scheibnerová. They cannot, therefore, be classed *G. californica*.

Age range: Lower Turonian

Family QUADRIMORPHINIDAE Saidova, 1981

Genus ***Quadrimorphina*** Finlay, 1939

Type species: *Valvulina allomorphinoides* Reuss, 1860

Quadrimorphina allomorphinoides (Reuss, 1860)

Plate 11, Figs 21-22

1860 *Valvulina allomorphinoides* Reuss, p. 223, pl. 10, fig. 20.

1978 *?Discorbis* sp. Scheibnerová, p. 713, pl. 2, fig. 14; pl. 3, figs 1-3.

1984 *Quadrimorphina allomorphinoides* (Reuss): Moullade, pl. 4, figs. 15-16.

1992 *Quadrimorphina allomorphinoides* (Reuss): Haig, p. 290, pl. 3, fig. 6.

1997 *Quadrimorphina allomorphinoides* (Reuss): Holbourn & Kaminski, p. 77

pl. 46, figs 1-2.

Diagnosis: A biconvex species of *Quadrimorphina* with four inflated, broad chambers in the last whorl and a lobulate periphery. The sutures are depressed and nearly radial on the umbilical side and curving back on the spiral side. The aperture is an interiomarginal slit, which extends from the umbilicus to the periphery and is covered by a lip.

Age range: Mid-Cenomanian

Family ALABAMINIDAE Hofker, 1951

Remarks: Revets (1996) transferred the genera *Charltonina, Conorotalites* and *Osangularia* to the Alabaminidae, based on the presence of a supplementary areal aperture or areal extension. Loeblich and Tappan originally assigned these genera to the Globorotalitidae, based on the presence of a deep indentation at the base of the apertural face which was not a true aperture. Holbourn and Kaminski (1997) used this new definition of the genus in there study of Lower Cretaceous benthonic species of the Indian Ocean and it has been retained here for use in this study.

Genus *Charltonina* Bermúdez, 1952

Type species: *Pseudoparrela madrugaensis* Cushman and Bermúdez, 1948

Charltonina australis Scheibnerová, 1978

Plate 11, Figs 23-24

1978 *Charltonina australis* Scheibnerová, p. 140, pl. 5, figs 2-5.

1997 *Charltonina australis* Scheibnerová: Holbourn & Kaminski, p. 77, pl. 46, fig. 5;

pl. 47, figs 1-7.

Diagnosis: A species of *Charltonina* with a biconvex to planoconvex test. The periphery is carinate and lobulate in shape. Usually five or six moderately inflated chambers in the last whorl are separated by slightly depressed sutures, which are straight or gently curved on the umbilical face and oblique on the spiral side. The aperture is an interiomarginal slit, which extends from the umbilicus to the periphery and is bordered by a lip.

Remarks: Tests vary in convexity, ranging from nearly biconvex to planoconvex with a flattened dorsal side. Albian tests have five to six chambers unlike Upper Aptian forms which have four to five

Age range: Upper Albian to Lower Turonian

Charltonina* cf. *australis (Scheibnerová, 1978)

Plate 12, Fig. 1

1978 *Charltonina australis* Scheibnerová, p. 140, pl. 5, figs 2-5.

1992 *Charltonina* cf. *australis* Scheibnerová, p. 290, pl. 3, figs 12-13.

Diagnosis: A species of *Charltonina* characterised by 4 elongate chambers in the last whorl.

Age range: Upper Albian

***Charltonina* sp. 1**

Plate 12, Fig. 2

1978 *Rotaliatina asiatica* Bykova: Scheibnerová, p. 140, pl. 4, figs 8-12; pl. 5, fig. 1.

2000 *Charltonina* sp. Howe *et al.*, 2000, fig. 11 (13-15).

Diagnosis: A species of *Charltonina* with a slightly concave spiral side with raised central part, sometimes becoming slightly conical. Five to six chambers are present in the last whorl, and the aperture is short and interiomarginal.

Remarks: Although this species resembles specimens of *Rotaliatina asiatica* found by Scheibnerová (1978), the name here is left open as a species of *Charltonina* the author believing the specimens seen in this study to show closer affinities to *Charltonina* than the high trochospiral species *Rotaliatina*.

Age range: Upper Albian

Genus ***Conorotalites*** Kaever, 1959

Type species: *Globorotalites bartensteini* Bettenstaedt subsp. *aptiensis* Bettenstaedt, 1952

Conorotalites aptiensis (Bettenstaedt, 1952)

Plate 12, Figs 3-5

1952 *Globorotalites bartensteini aptiensis* Bettenstaedt, p. 282, pl. 3, fig. 32;
pl. 4, figs 59-72.

1996 *Conorotalites aptiensis* (Bettenstaedt): Revets, p. 70, pl. 5, figs 9-12.

1997 *Conorotalites aptiensis* (Bettenstaedt): Holbourn and Kaminski, p. 78, pl. 46, figs 3-4.

Diagnosis: A planoconvex species of *Conorotalites* with flattened dorsal side and sharp periphery. Six to seven chambers in the last whorl gradually increase in size and are moderately inflated. Chambers are separated by raised sutures, which gently curved and . Large, irregular pores are present on the umbilical side. The aperture is a wide interio-

marginal slit, which extends to a distinctive sulcus bordered by a thin lip.

Age range: Upper Albian to Lower Turonian

Genus ***Osangularia*** Brotzen, 1940

Type species: *Cribroparrella regadana* ten Dam, 1948

Osangularia schloenbachi (Reuss, 1863)

Plate 12, Figs 6-7

1863 *Rotalia schloenbachi* Reuss, p. 84, pl. 10, fig. 5 a-b.

1978 *Osangularia utaturensis* (Sastry & Sastri): Scheibnerová, p. 714, pl. 4, figs 27-28; pl. 5, figs 1-9; pl. 11, figs 4a-c, 5a-c.

1997 *Osangularia schloenbachi* (Reuss): Holbourn & Kaminski, p. 78 pl. 47, fig. 8; pl. 48, figs 1-7.

Diagnosis: Trochospiral, biconvex species of *Osangularia* with a flattened ventral side and a sharp, carinate periphery. The chambers increase gradually in size and are slightly inflated, except for the last chamber which is generally larger and more inflated than the previous ones. The sutures are thick, strongly curved backwards on the spiral side, but slightly depressed and gently curved on the umbilical side. The aperture is an interiomarginal slit, which extends from the umbilicus to the periphery.

Age range: Upper Albian to Upper Cenomanian

Family GAVELINELLIDAE Hofker, 1956

Genus ***Berthelina*** Malapris, 1965

Type species: *Anomalina intermedia* Berthelin, 1880

Remarks: Revets (1996) *Berthelina* are distinguished from *Gavelinella* by the absence of a clear, depressed umbilicus and the presence of a wide apertural slit, extending from the periphery to the umbilicus, in contrast to the narrow interiomarginal slit observed in *Gavelinella.* This differentiation of these two genera is retained for this study.

Berthelina berthelini (Keller, 1935)

Plate 12, Figs 8-10

1935 *Anomalina berthelini* Keller, pp. 552-553, pl. 3, figs 25-27.

1982 *Anomalinoides berthelini* (Keller): Haig, p. 27, pl. 13, figs 6-8.

1962 *Gavelinella intermedia* (Berthelin): Tappan, p. 197, pl. 58, fig. 1.

1997 *Berthelina berthelini* (Keller): Holbourn & Kaminski, p. 78, pl. 48, fig. 10.

2001 *Berthelina berthelini* (Keller): Revets, pp. 20-22.

Diagnosis: A species of *Berthelina* that is asymmetrically involute with a rounded or slightly angled periphery. There are approximately 10-12 chambers in the last whorl, each moderately inflated and separated by slightly depressed gently arched sutures. Relict apertural flaps coalesce to form a large, elevated umbonal boss on the spiral side, giving the test an unequally biconvex appearance. The aperture is interiomarginal with a lip, which extends from the periphery to the umbilicus.

Remarks: Revets (2001) reviewed the descriptions given by Holbourn & Kaminski (1997) for *Berthelina intermedia* and *Berthelina berthelini*, concluding them to be the same

species, with *B. intermedia* appearing to be absent from the Austral realm. Although *B. intermedia* and *B. berthelini* have some similarities, *B. Berthelini* differs in its constantly higher number of chambers in the final whorl, the wider umbilicus, and the umbilical sutures which are less raised.

Age range: Upper Albian to Lower Turonian

Berthelina cf. *berthelini*

Plate 12, Figs 11-12, 16-17

1997 *Berthelina intermedia* (Berthelin): Holbourn & Kaminski, p. 78, pl. 48, fig. 8.

Diagnosis: A large, planoconvex species of *Berthelina,* some species with a slight umbilical boss. 10-12 slightly inflated chambers make up the final whorl, separated by slightly depressed, oblique sutures on the spiral side, whilst on the convex umbilical side sutures are perpendicular.

Age range: Upper Albian to Lower Turonian

Berthelina cenomanica (Brotzen, 1945)

Plate 12, Figs 13-18

1945 *Cibicides (Cibicidoides) cenomanica* Brotzen, p. 54, pl. 2, fig. 2.

1977 *Gavelinella cenomanica* (Brotzen): Carter & Hart, pl. 1, figs 1-3.

1993 *Berthelina cenomanica* (Brotzen): Haig & Lynch, p. 349, pl. 5, figs 1-3.

1997 *Berthelina cenomanica* (Brotzen): Holbourn & Kaminski, p. 79, pl. 48, fig. 9; pl. 49, figs 1, 3; pl. 50, fig. 3.

Description: A biconvex and asymmetrically involute species of *Berthelina*, with an acute

periphery. Approximately 10-12 chambers in the last whorl are separated by raised, limbate sutures, curving backwards. Both umbilical and dorsal sides may appear slightly depressed in the centre. The chambers are extended by relic apertural flaps, partially covering the umbilicus. The aperture is interiomarginal with a lip, extending from the periphery to the umbilicus.

Age range: Upper Albian to Lower Turonian

Berthelina* cf. *daktoensis (Fox, 1954)

Plate 12, Figs 14-15, 19

1954 *Planulina daktoensis* Fox, p. 119, pl. 26, figs 19-21.

1970 *Gavelinella daktoensis* (Fox): Eicher & Worstell, p. 293, pl. 5, figs 5-6.

2001 *Berthelina daktoensis* (Fox): p. 22, pl. 7, figs 1-3.

Diagnosis: A compressed species of *Berthelina*, with low trochospire. Periphery is rounded and loblate. 10-12 chambers are seen in the final whorl, and the chambers are slightly inflated the final few chambers increasing in size rapidly. Sutures on the spiral side are slightly arcuate and depressed becoming raised.

Remarks: These species differ from the typical *G. daktoensis* in the grater number of chambers in the last whorl. Typically only 8-9 chambers are seen.

Age range: Upper Albian to Lower Turonian

Berthelina* cf. *tenuis (Bukalova, 1958)

Plate 12, Figs 20, 25

2000 *Berthelina* cf. *tenuis* (Bukalova): Howe *et al.*, fig. 9 (7-12)

Diagnosis: A compressed species of *Berthelina,* slightly biconvex in shape, with 8-10 chambers in the final whorl. Sutures on both umbilical and spiral side are depressed. This is more pronounced in the later chambers.

Age range: Upper Albian to Lower Turonian

Berthelina cf. *tenuissima* (Gawor-Biedowa, 1992)

Plate 12, Figs 21-22

1992 *Gavelinella tenuissima*, Gawor-Biedowa, p. 87, pl. 3, figs 5-6.

2000 *Berthelina* cf. *tenuissima* (Gawor-Biedowa): Howe *et al,* fig 11 (1-3).

2001 *Berthelina tenuissima* (Gawor-Biedowa): Revets, pp. 27-28, pl. 10, figs 1-3.

Diagnosis: A planoconvex species of *Berthelina*. The spiral side is evolute and slightly convex, the umbilical side is flattened and the umbilicus is of average width and about half a chamber deep. Sutures are arcuate and slightly depressed, and 8-10 chambers make up the final whorl.

Remarks: This species differs from that of Revets (2001) in the lower number of chambers and absence of a defined spiral boss.

Age range: Lower Turonian

Berthelina sp. 2

Plate 12, Figs 23-24; Plate 13, Fig. 1

Diagnosis: A planoconvex species of *Berthelina* with moderate trochospire and rounded periphery. The chambers initially increase slowly in size, the last 2 chambers becoming larger and more inflated. Sutures are arcuate and depressed, becoming straighter on the last few chambers. There are about 8 chambers in the final whorl. On the umbilical side

chambers are separated by lightly depressed sutures and the umbilicus is normal width and depressed.

Age range: Upper Albian to Lower Turonian

Berthelina sp. 3

Plate 13, Figs 2-4

Diagnosis: A small species of *Berthelina* showing a high trochospire that almost forms a point. The periphery is rounded to sub-acute, and the umbilical side flattened. The spiral sutures are oblique and flush, becoming raised in the later part of the test.

Remarks: Many of the species of *Berthelina* from the Indian Ocean are characterised by a high trochospire, making them different from many of the published species. A full taxonomic analysis of the *Berthelina* and *Gavelinella* needs to be carried out in order to look at the affinities of the species with those published.

Age range: Upper Albian to Lower Turonian

Genus *Gavelinella* Brotzen, 1942

Type species: *Discorbina pertusa* Marsson, 1878

Gavelinella cf. *plummerae* (Tappan, 1940)

Plate 13, Figs 5-9, 10

1940 *Anomalina plummerae* Tappan, p. 124, pl. 18, figs 15-16.

1970 *Gavelinella plummerae* (Tappan): Eicher and Worstell, p. 293, pl. 6, figs 4a-b, 5a-c.

Diagnosis: A species of *Gavelinella* characterised by its high trochospire. It has a sharply rounded periphery, and flattened umbilical side. It has 6-7 chambers in the final whorl,

gradually increasing in size, and with a lobulate outline. Spiral sutures are oblique and depressed, umbilical sutures begin straight and raised to flush in early chambers, becoming more depressed.

Age range: Lower Turonian

Gavelinella tormarpensis Brotzen, 1942

Plate 13, Figs 6-7

1942 *Gavelinella tormarpensis* Brotzen, p. 52, pl. 1, fig. 6.

1977 *Gavelinella tormarpensis* Brotzen: Carter & Hart, p. 48, pl. 1, figs 32-33.

2001 *Gavelinella tormarpensis* Brotzen: Revets, p. 15, pl. 4, figs 4-9.

Diagnosis: A species of *Gavelinella* with a low trochospire. The spiral side is evolute and slightly convex with a central depression. The sutures are slightly curved and lightly depressed in the later chambers. The umbilical side also shows a depression, and straight to slightly curved lightly depressed sutures.

Age range: Lower Turonian

Gavelinella sp. 1

Plate 13, Figs 8, 13

Diagnosis: A biconvex species of *Gavelinella* characterised by a sharp periphery and angular outline. The test is elongate towards the final chamber, and shows raised sutures particularly apparent on the umbilical side.

Age range: Lower Turonian

Gavelinella sp. 2

Plate 13, Figs 11-12

Diagnosis: A species of *Gavelinella* with a low trochospire. This species has a slightly convex umbilicus, spiralling inwards with the proloculus covered. The periphery is angular and lobulate in outline. The spiral side shows up to 12 chambers in the final whorl and very distinctive raised arcuate sutures.

Remarks: This species shows great affinity with *Berthelina pluriocostata* of Reuss (2001) found in Albian sediments of the Exmouth Plateau. Specimens from this study are found in the Upper Albian of the Crimea, without full analysis at this time the species is left as open nomenclature.

Age range: Upper Cenomanian to Lower Turonian

Gavelinella sp. 3

Plate 13, Figs 14-15

Diagnosis: A flattened specimen of *Gavelinella*. Both umbilical and spiral side show straight, raised sutures, more pronounced on the later chambers.

Remarks: The preservation of this species was generally poor and further analysis of specimens is necessary to determine this species further.

Age range: Upper Albian

Gavelinella sp. 4

Plate 13, Fig. 16

Diagnosis: A very small species of *Gavelinella*. It is biconvex and shows a very characteristic angular outline, as each new chamber slightly overlaps the preceding one.

Sutures are slightly depressed. Chambers are inflated, only 6-8 found in the last whorl.

Remarks: Similar to *Gavelinella* sp. 3, this species is rare and specimens fond are very poorly preserved and a full description is unable to be determined.

Age range: Upper Albian

Gavelinella sp. 5

Plate 13, Figs 17-18

Diagnosis: A planoconvex species of *Gavelinella.* With moderate trochospire and rounded periphery. Sutures are flush to slightly depressed.

Age range: Upper Cenomanian to Lower Turonian

Gavelinella sp. 6

Plate 13, Fig. 19

Diagnosis: A planoconvex species of *Gavelinella*. The spiral side is convex and shows a low to moderate trochospire. 8-10 chambers are seen in the final whorl separated by depressed sutures.

Age range: Upper Albian

Genus *Lingulogavelinella* Malapris, 1965

Type species: *Lingulogavelinella albiensis* Malapris, 1965

Lingulogavelinella albiensis Malapris, 1965

Plate 13, Fig. 20

1965 *Lingulogavelinella albiensis* Malapris, 1965, pl. 10, figs 10-12.

2001 *Lingulogavelinella albiensis* Malapris: Revets, p. 29, pl. 10, figs 10-12.

Diagnosis: A planoconvex species of *Lingulogavelinella* with a low trochospire. The spiral side is evolute, and moderately convex, with a central depression. Umbilical side is flattened, with a wide umbilicus, partially covered. 8 chambers can be seen in the final whorl. Sutures on the spiral side are slightly depressed becoming flush.

Age range: Lower Cenomanian

Lingulogavelinella indica (Scheibnerová, 1974)

Plate 13, Fig. 21

1974 *Orithostella indica* Scheibnerová, pl. 7, figs 4, 8-13; pl. 8, figs 1-9.

1982 *Lingulogavelinella indica* (Scheibnerová): Haig, p. 74, pl. 13, figs 18-20.

1993 *Lingulogavelinella indica* (Scheibnerová); Haig & Lynch, p. 355, pl. 5, figs. 7-9.

Diagnosis: A biconvex to planoconvex species of *Lingulogavelinella*, slightly evolute on spiral side. The periphery is rounded and faintly lobulate. 6-8 chambers in the last whorl are separated by slightly depressed radial or gently curved sutures. The umbilicus is completely masked by overlapping umbilical flaps forming distinctive stellate pattern, Aperture interiomarginal arch, bordered by narrow lip, from the periphery to the umbilicus, extending underneath the apertural flap of the last chamber.

Age range: Upper Albian to Lower Turonian

Lingulogavelinella newtoni Eicher & Worstell, 1970

Plate 13, Figs 22-23

1970 *Lingulogavelinella newtoni* Eicher & Worstell, p. 294, pl. 5, figs 2a-c, 3, 4a-c.

2001 *Lingulogavelinella newtoni* Eicher & Worstell: Revets, pp. 33-34

Diagnosis: A small species of *Lingulogavelinella,* biconvex in shape. The periphery is rounded and smooth in shape becoming more lobulate in later chambers. There are seven to nine chambers in the final whorl. Umbilical sutures are radial, curving slightly and slightly depressed, more so in the later chambers. The umbilicus is narrow and deep, and the aperture is a low slit extending from the periphery to the umbilicus, bordered by a flap.

Age range: Upper Albian to Lower Turonian

Family CANCRISIDAE Chapman, Parr & Collins, 1934

Remarks: Cancrisidae was separated from the Bagginidae by Haynes (1981). This was followed by Revets (1996), and is followed in this study. This family is characterised by the interiomarginal aperture partially hidden under a flap, the open umbilicus, secondarily obstructed by umbilical flaps or an umbilical plug, and the presence of open relict apertures (Holbourn & Kaminski, 1997).

Genus *Gyroidinoides* Brotzen, 1942

Type species: *Rotalina nitida* Reuss, 1844

Remarks: This genus encompasses a range of morphotypes, which vary in size, degree of inflation and extent of apertural flap. The different morphotypes may be stratigraphically useful within geographical areas, and important in palaeoenvironmental changes. Open nomenclature has therefore been used for species showing large variations from the typical morphotype and to distinguish them through the sections and determine if any stratigraphical or environmental change exists within the morphotypes. A full account of this genus and *Valvulineria* was written by Magniez-Jannin (1975, pp. 239-246).

Gyroidinoides infracretacea Morozova, 1948

Plate 14, Figs 1-13

1948 *Gyroidina nitida Reuss* var. *infracretacea* Morozova, pl. 2, figs 12-14.

1972 *Gyroidinoides infracretacea* (Morozova): Gawor-Biedowa, p. 98, pl. 13, fig. 8a-c.

1974 *Gyroidinoides* cf. *primitive* Hofker: Scheibnerová, p. 715, pl. 5, figs 10-12; pl. 11, fig. 6.

1992 *Serovaina infracretacea* (Morozova): Haig, p. 289, pl. 3, figs 8-9.

1993 *Gyroidinoides infracretaceus* (Morozova): Haig & Lynch, p. 353, pl. 4, figs 16-18.

1997 *Gyroidinoides infracretaceus* (Morozova): Holbourn & Kaminski, p. 81, pl. 52, figs 3-6.

Diagnosis: A species of *Gyroidinoides* with a flattened to slightly convex spiral side and involute, strongly convex umbilical side. It has a rounded periphery and rounded outline, six to seven inflated chambers in the last whorl separated by depressed sutures and the last chamber is generally larger and more inflated than the previous ones. Aperture is an interomarginal slit, extending from the periphery, with a flap obscuring the umbilicus.

Remarks: Problems have arisen with the study of this species, with many forms of this "plexus" existing. Morozova created *G. infracretacea* from *G. nitida* (Upper Cretaceous form) to define a Lower Cretaceous form, and others have arisen since. In this study *G. infracretacea* was used for all specimens, as described above, in order to retain some consistency at each site, any variation to this 'norm' has been given a different species number to differentiate any changes in morphotype.

Age range: Upper Albian to Lower Turonian

Gyroidinoides sp. 1

Plate 14, Figs 14-15, 20

Diagnosis: A biconvex species of *Gyroidinoides* showing slight spire on spiral side. 8-10 chambers are seen in the final whorl, the chambers increase slowly in size, and showing a moderate apertural flap.

Age range: Upper Albian to Lower Turonian

Gyroidinoides sp. 2

Plate 14, Figs 16-17

Diagnosis: A very rounded species of *Gyroidinoides* with a very broad and wide apertural flap and rounded periphery.

Age range: Upper Albian to Upper Cenomanian

Gyroidinoides sp. 3

Plate 14, Figs 18-19

Diagnosis: A very large plano-convex species of *Gyroidinoides*. 6 chambers make up the final whorl. The chambers are inflated and globular, giving the species a slightly globular outline. The periphery is rounded.

Age range: Upper Albian to Lower Turonian

Gyroidinoides sp. 4

Plate 14, Fig. 21

Diagnosis: A very globular, biconvex species of *Gyroidinoides*. 5-6 chambers make up the

final whorl, each separated by faint, depressed sutures.

Age range: Upper Albian

Genus ***Valvulineria*** Cushman, 1926

Type species: *Valvulineria californica* Cushman, 1926

Valvulineria gracillima ten Dam, 1947

Plate 14, Figs 22-23, 24-25

1947 *Valvulineraia gracillima* ten Dam, p. 26, fig. 4a-c.

1972 *Valvulineria gracillima* ten Dam: Gawor-Biedowa, p. 59, pl. 6, fig. 5a-c.

1997 *Valvulineria gracillima* ten Dam: Holbourn & Kaminski, p. 82, pl. 52, figs 1-2.

Diagnosis: A planoconvex species of *Valvulineria*. The spiral side is flattened, the umbilical side involute and convex, with a faintly lobulate, rounded periphery. There are 6-8 chambers in the last whorl, the chambers are moderately inflated and separated by radial, slightly depressed sutures. The last chamber is usually higher then the previous ones, making the test slightly longer than broad. The umbilicus is obscured by flaps extending from the successive chambers.

Age range: Upper Albian to Lower Turonian

Valvulineria lenticula (Reuss, 1845)

Plate 15, Fig. 1

1845 *Rotalina lenticula* Reuss, p. 35, pl. 12, fig. 17a-c.

1972 *Valvulineria lenticula* (Reuss): Gawor-Biedowa, p. 59-60, pl.6, fig. 6a-c.

1996 *Gyroidinoides lenticulus* (Reuss): Revets, p. 78, pl. 11, figs 9-12.

Diagnosis: A biconvex species of *Valvulineria*. The spiral side is evolute and slightly to moderately convex, the umbilical side involute and convex, with a faintly lobulate, rounded periphery. There are 6-8 chambers in the last whorl, the chambers are moderately inflated and separated by radial, slightly depressed sutures. The chambers increase slowly in size giving the test a very round outline. The umbilicus is obscured by flaps extending from the successive chambers.

Remarks: Similar to *Valvulineria gracillima* this species varies in the convexity of the spiral side of the test, the depression of sutures on the umbilical side and the number of chambers in the last whorl. Sometimes difficult to differentiate from *V. gracillima*, *V. lenticula* is seen to have a more oval outline, a narrower periphery and a more strongly elongate last chamber.

Age range: Lower Turonian

Valvulineria sp. 1

Plate 15, Fig. 2

Diagnosis: A biconvex species of *Valvulineria*. The chambers increase slowly in size, the last 2 increasing rapidly, to give an irregular, globular outline to the test. 6 chambers make up the final whorl. They are globular and separated by slightly depressed sutures; see most clearly on the latest chambers.

Age range: Upper Cenomanian

Genus *Scheibnerova* Quilty, 1984

Type species: *Scheibnerova proindica* Quilty, 1984

Scheibnerova proindica Quilty, 1984

Plate 15, Figs 3-5

1984 *Scheibnerova proindica* Quilty, p. 234, fig. 5A-K.

1992 *Scheibnerova proindica* Quilty: Haig, p. 290, pl. 4, figs 5, 9-10.

1997 *Scheibnerova proindica* Quilty: Holbourn & Kaminski, p. 82, pl. 53, figs 6-7.

Diagnosis: A species of *Scheibnerova* with a gently curved ventral face, strongly convex spiral side, deep umbilicus and lobulate periphery. Five to six chambers in the last whorl are separated by depressed sutures, which are slightly arched ventrally but curve strongly backwards on the dorsal side. The chambers are extended by umbilical flaps and bear some large, irregular pores on the ventral side. The spiral face is ornamented by dense, short, blunt spines and a hispid peripheral band may also surround the test. The aperture is an interiomarginal slit extending approximately halfway from the umbilicus to the periphery.

Age range: Upper Albian to Lower Turonian

Chapter 4: Palaeoceanography of the Eastern Indian Ocean during the mid-Cretaceous

4.1 Introduction

This chapter discusses the palaeoceanographical changes seen during the mid-Cretaceous in the eastern Indian Ocean. Samples were analysed from two ODP sites located at different palaeodepths off the northwest coast of Australia. These sites were located on the Exmouth Plateau (Site 762) and the lowest western flank of the Exmouth Plateau adjacent to the Gascoyne Abyssal Plain (Site 766).

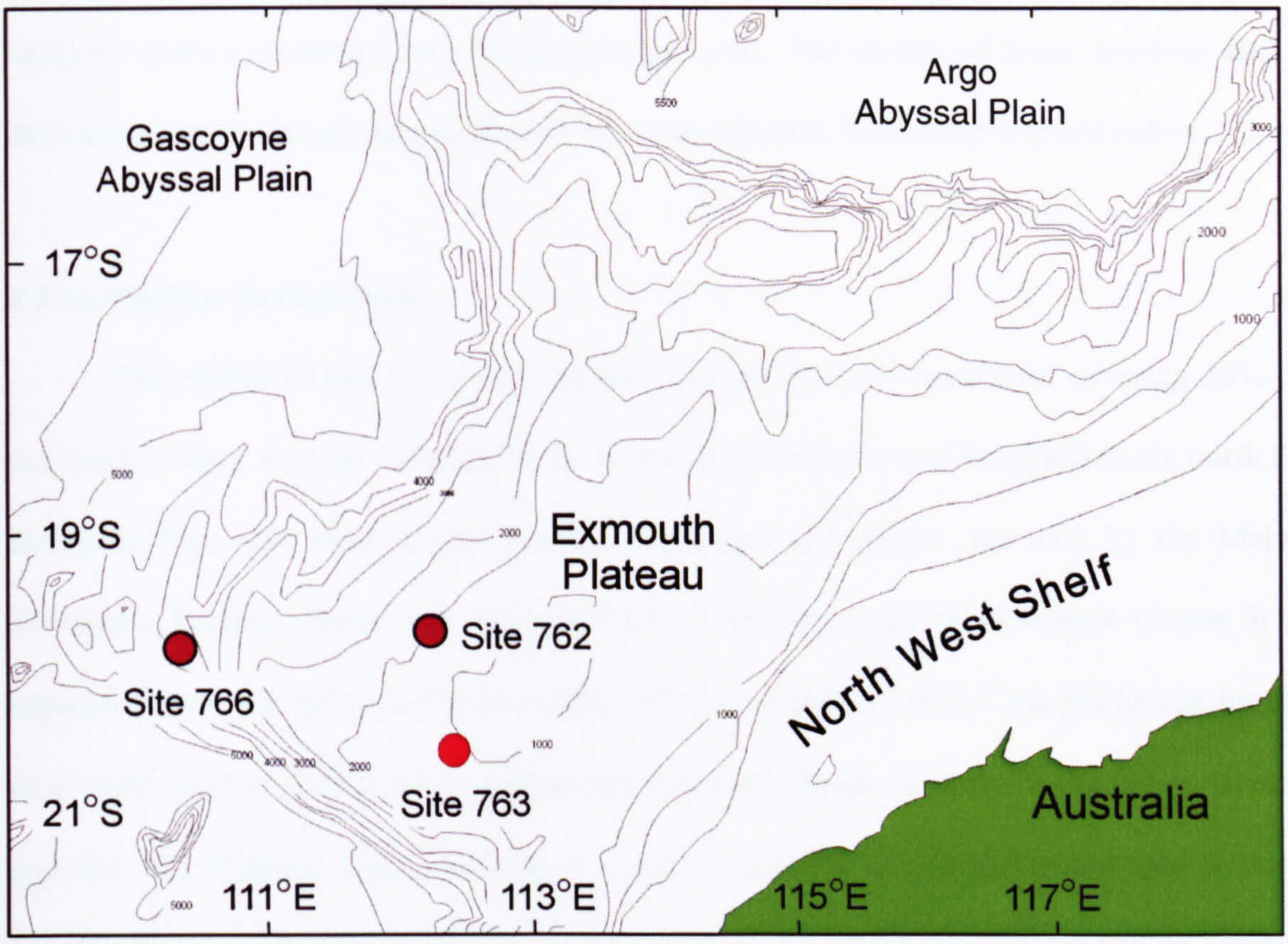

Figure 4.1: Location of ODP Sites analysed in this study. Site 762 on the Exmouth Plateau, and Site 766 on the western slope of the Exmouth Plateau adjacent to the Gascoyne Abyssal Plain. Site 763 is also shown on the map. Although not analysed in this study, it is important when considering any palaeoceanographic model of the Indian Ocean.

During the Cretaceous the sites would have lain on the southern margin of the Tethys Ocean. The locations today can be seen in Figure 4.1.

Samples were investigated using a range of techniques. Foraminiferal analysis was used to determine the biostratigraphy and relative timing of events at the sites, and establish palaeoceanographic changes, using analysis of the foraminiferal species and assemblages present in the sediments. Isotopic analysis of both bulk sediments and foraminiferal species were used to determine changes in the water column, both spatially and temporally, with regards to temperature and carbon cycling. Geochemical analysis was carried out to determine the amount and source of organic carbon in the samples. Trace element analysis was also used to investigate the diagenesis within the samples, along with analysis of thin sections taken throughout the core. The results of these analyses and a discussion of the palaeoceanography of the eastern Indian Ocean is presented below.

4.2 Geological Background

The Indian Ocean is the third largest body of water in the world, covering 20% of the Earth's water surface. Situated in the southern hemisphere it is bordered to the north by Southern Asia, the west by the Arabian Peninsula and Africa, the east by the Malay Peninsula, Sundra islands and Australia and, in the south, by the Southern Ocean. It is separated from the Atlantic Ocean by the 20° east meridian and the Pacific Ocean by the 147° east meridian. The African, Indian and Antarctic plates converge in the Indian Ocean, and the Mid-Oceanic Ridge formed at these boundaries divide the ocean into 3 large basins, which are in turn subdivided into smaller basins. The Indian Ocean has an average depth of 3890 m, and 86% of the main basin is covered by pelagic sediments, more than 50% of which is "Foraminiferal Ooze". The remaining 14% being formed of layered terriginous sediments. The ocean's continental shelves are generally narrow, averaging 200 km in width. On the west coast of Australia however shelf widths exceed 1000 km. It is in this region that the sediment cores analysed in this study were taken.

The Indian Ocean began to form in mid-Jurassic times. The supercontinent Gondwana had begun to break apart in the late Permian, with further rifting in the Permo-Triassic forming marine basins in northern India-Nepal and in northwest Australia (Holmes and Watkins, 1992). It was not until a second major rifting event in the mid-Jurassic, however, that the earliest northeast Indian Ocean began to form, with the rapid formation of an abyssal oceanic graben, north of the Exmouth and Wombat Plateaus, in the present Argo Abyssal Plain. Rifting continued through the Jurassic and early Cretaceous along what is now the west coast of Australia, and around 130 Ma India began to separate from western Australia (Powell *et al.*, 1988) when seafloor spreading was initiated in the present Gascoyne and Cuvier abyssal plains (Von Rad *et al.*, 1992; Haq *et al.*, 1992; Exon and Buffler, 1992).

By the mid-Cretaceous the Exmouth Plateau, Gascoyne Abyssal Plain and Argo Abyssal Plain had all formed, and pelagic sedimentation was widespread in these areas. However, the region was still tectonically active as India began to move more rapidly northwards towards Asia, and Antarctica and Australia began to separate.

4.2.1 Geology of the Exmouth Plateau

The Exmouth Plateau is a rifted and deeply subsided fragment of continental crust, covered by more than 8 km of sediments. During the Palaeozoic the Exmouth Plateau was part of Gondwana, surrounded by continental crust. As the Tethys Ocean began to form to the north of the plateau during the Permian, the crust of the Exmouth Plateau became considerably stretched and thinned. This led to the rapid subsidence of the plateau and subsequent deposition of Mesozoic sediments (Mutter *et al.*, 1988; Williamson *et al.*, 1990; Von Rad *et al.*, 1992).

The sediments of the Exmouth Plateau were deposited in an extension of the Carnarvon and Canning basins that formed a Tethyan embayment in Gondwana opening to the north. This embayment received detrital material from the south and east until the Early

Cretaceous. In the deeper central part of the plateau around 3000 m of shallow marine detrital material was deposited during from the Permian to the mid-Jurassic. Following this rifting activity, which continued into the Triassic, 1000m of deltaic sediments derived from the south and east were deposited, covering the Upper Jurassic and Lower Cretaceous block-faulted surface. The mid-Cretaceous records 200 m of hemipelagic shallow marine sediments, followed by 500-1000m of Upper Cretaceous to Cenozoic pelagic carbonate sediment. As Greater India migrated northwards the southern supply of eroded rocks was cut off and cyclic deposition of deep-water claystones during the mid-late Aptian marks the onset of hemipelagic deposition. This was followed by a period of stagnation producing black shales at the CTB and the post-Cenomanian deposition of pelagic carbonate. By the Miocene the Exmouth Plateau had developed into its present form, having subsided to bathyal depths (Von Rad *et al.*, 1992; Gradstein *et al.*, 1990). Located today at 19°53.23'S and 112°15.24'E, Site 762 was located close to 50°S at the southernmost margin of Tethys during the Late Cretaceous, moving from ~40°S in the Aptian to ~55°S in the Campanian (Ogg *et al.*, 1992; Petrizzo, 2002).

4.2.2 Geology of the western flank of the Exmouth Plateau and Gascoyne Abyssal Plain

The breakup of western Australia and Greater India led to the formation of the Gascoyne Abyssal Plain around 134 Ma (Fullerton *et al.*, 1989). The basement is observed to be formed of transitional crust, Valanginian in age, and made up of alternating volcanic flows and sills extruded and intruded during the breakup (Mutter *et al.* 1988). Overlying sediments (466.7 m thick) range from uppermost Valanginian sandstones, siltstones and altered volcaniclastics, to lower Pleistocene nannofossil ooze. During the early Cretaceous at least 300m of sediment accumulated, although, sedimentation rates slowed markedly in the late Cretaceous with less than 150m of sediment being deposited.

Hauterivian to Barremian sands, silts and clays are interpreted as the distal part of a submarine fan, thickening towards the continental margin. The Barremian-Aptian boundary represents a marked change in sedimentation, from hemipelagic deposition of terriginous and shallow-marine sediments with abundant plant spores, to pelagic and hemipelagic deposition of calcareous sediment. This change in sedimentation, and resultant decrease in sedimentation rates, is thought to mark the transition from juvenile to mature oceanic conditions (Von Rad *et al.*, 1992). This is most likely to be related to a rise in sea level. A similar reduction in sedimentation rates is seen on the Argo Abyssal Plain and abyssal areas of the Atlantic Ocean. This appears to indicate a eustatic global sea level event (Gradstein *et al.*, 1990). Pelagic carbonate sedimentation continued through the Upper Cretaceous and Cenozoic.

Subsidence and sedimentation analysis indicate that Site 766 originated at a depth of 800m. Following an initial rapid subsidence rate of 20 cm/ky this had declined to 4 cm/ky by the early Cretaceous, and continued to slow into the Cenozoic eventually reaching its present water depth just below 4000 m. Despite its depth however, Site 766 is thought to have remained above or near the CCD throughout its history. Today lying at 19°55.925'S and 110°27.243'E, Site 766 would also have been located near to 50°S in he Late Cretaceous.

4.3 Sediment description

4.3.1 Site 766

Site 766 lies at 19°55.925'S, 110°27.243'E at the foot of the western escarpment of the Exmouth Plateau, facing the Gascoyne Abyssal Plain, in a water depth of 3997.5 m. The site was drilled to a depth of 527.2 mbsf, penetrating rocks of Valanginian to Pleistocene age.

The mid-Cretaceous sediments from this core are comprised of pelagic clay-rich nannofossil chalks and oozes with zeolites, indicating open ocean conditions (Gradstein *et al.*, 1990).

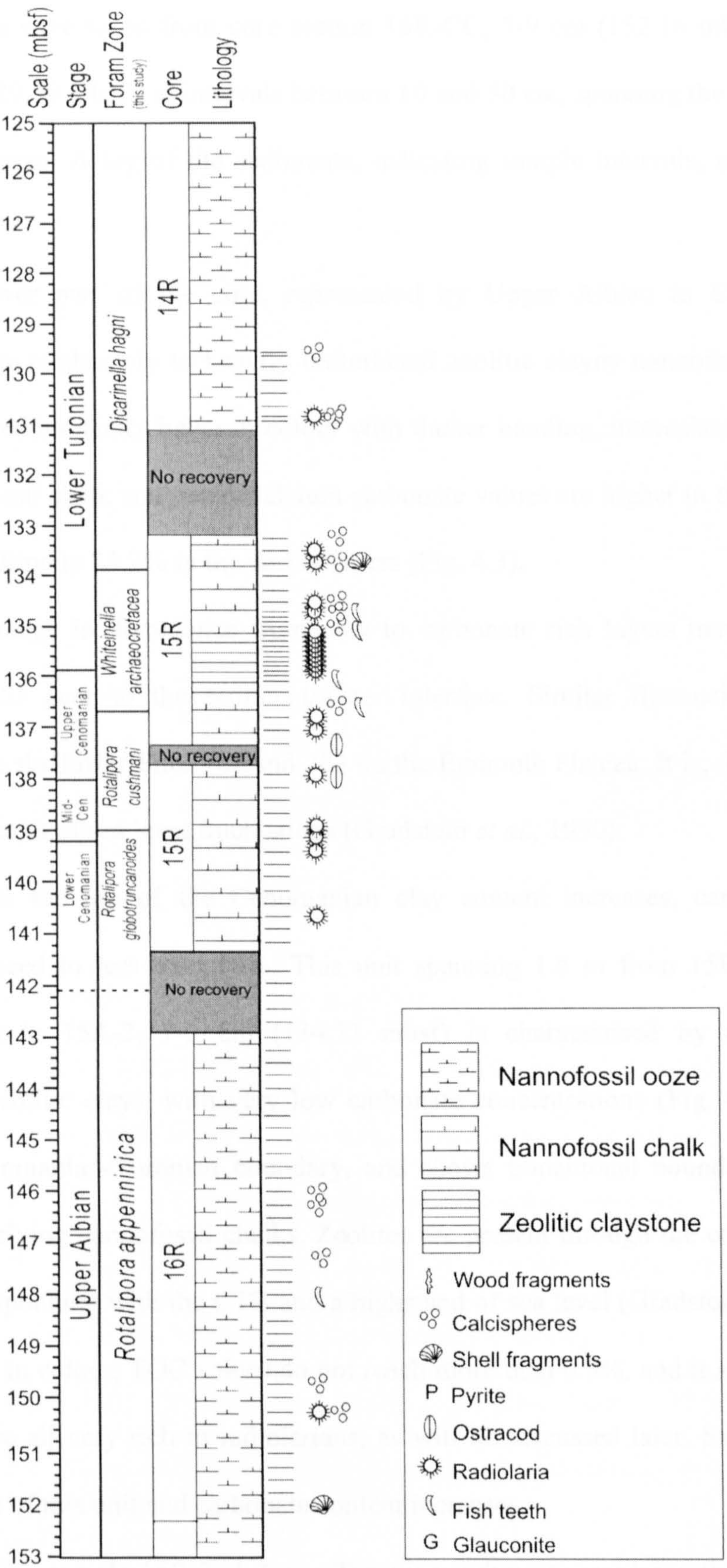

Figure 4.2: Log of sediments analysed from Site 766. Biostratigraphic zonation is from this study. Lines adjacent to the stratigraphic column indicate sampled levels. The presence of other biota, and other sedimentary components, is also indicated.

Samples were taken from core section 16R-CC, 7-9 cm (152.16 mbsf) to 14R-4, 149-151 cm (129.59 mbsf), at intervals between 10 and 50 cm, spanning the Upper Albian to Lower Turonian. A log of the sediments, indicating sample intervals, can be seen in Figure 4.2.

The lower part of the core, represented by Upper Albian to Cenomanian is characterised by moderately to heavily bioturbated zeolitic clayey nannofossil chalk and ooze, this is predominantly beige in colour with darker banding, intercalated with lighter brown nannofossil chalk and ooze. Calcium carbonate values are higher in the paler layers (up to 60%), falling to 23.2% in the darker layers (Fig. 4.3).

This change in dominance from clay to carbonate rich layers may be due to a fluctuating CCD near to the sediment/water interface. Similar fluctuations are seen, however, at the shallower Sites 762 and 763 on the Exmouth Plateau. It is, therefore, more likely to be a result of sea level fluctuations (Gradstein *et al.*, 1990).

Towards the top of the Cenomanian clay content increases, carbonate values becoming reduced to less than 10%. This unit spanning 1.6 m from 15R-3, 10-12 cm (136.30 mbsf) to 15R-2, 1-3 cm (134.71 mbsf) is characterised by dark black to green/brown zeolitic clays, with very low carbonate concentrations (Fig. 4.3). This unit spans the Cenomanian-Turonian boundary, and shows transitional boundaries from the under-and overlying nannofossil chalks. Zeolites are present through the core but peak in this unit corresponding with the CTB and a highstand of sea level (Gradstein *et al.*, 1990). Although dark in colour, TOC values do not reach more than 0.5%, and it should be noted the samples are all very rich in radiolarians, as will be discussed later. Samples become paler at the top of this unit and carbonate content increases.

Following sample 15R-2, 1-3 cm, Turonian sediments overlying the zeolitic clays are characterised by alternating calcareous oozes and dark laminated clays. A distinct colour banding is seen, distinguishing this unit from the underlying Cenomanian and Albian chalks, along with a decrease in bioturbation (Fig. 4.3).

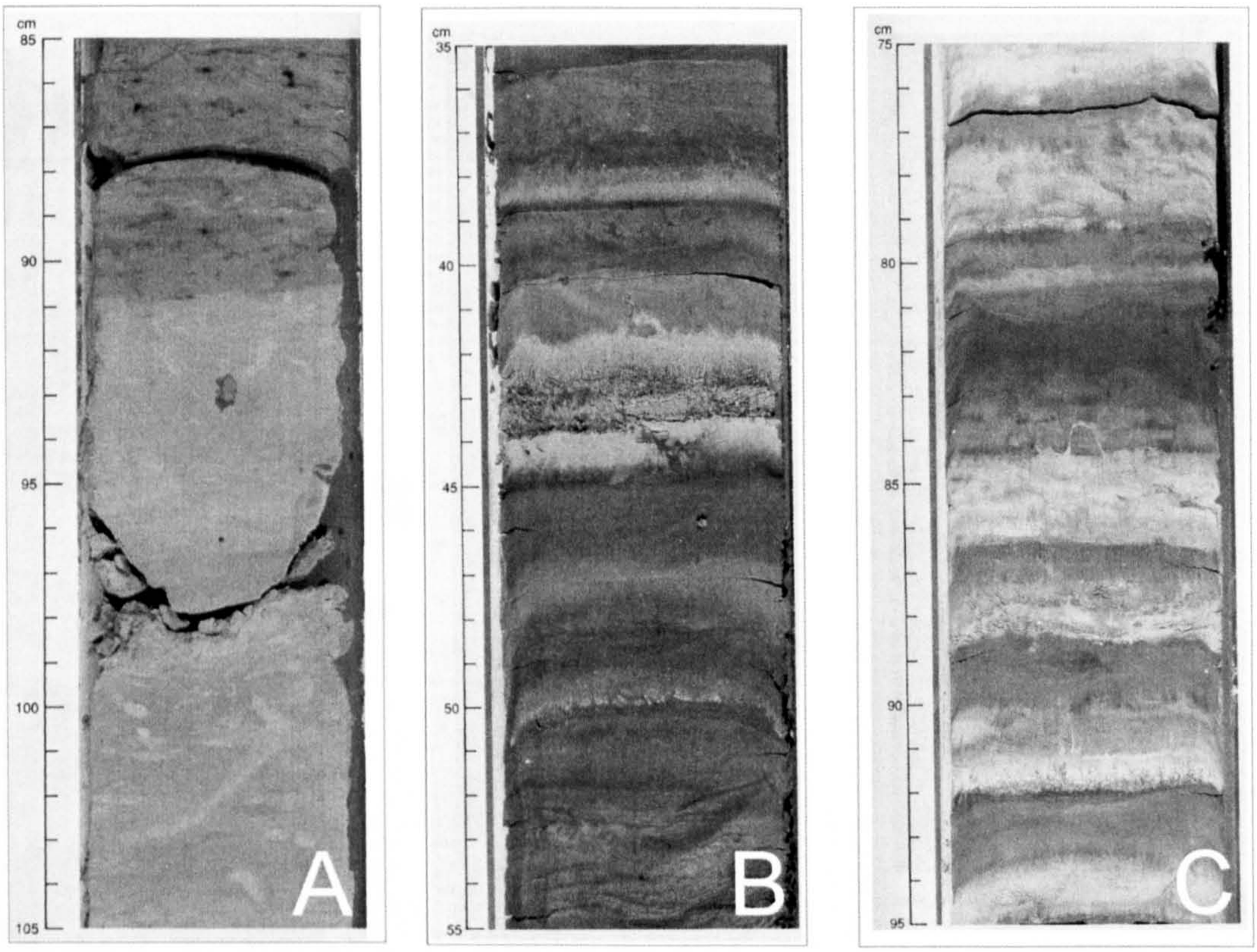

Figure 4.3: Core photographs of sediments found at Site 766.

A) Albian sediments from 18R-3, 85-105 cm (165.95–165.15 mbsf). Pale coloured bioturbated zeolitic nannofossil ooze, similar to that seen in the Albian - Cenomanian sediments analysed in this study.

B) Lower Turonian, CTB boundary sediments from 15R-2, 35-55 cm (135.05–135.25). Dark, colour banded zeolitic clays.

C) Lower Turonian nannofossil ooze from 14R-3, 75-95 cm (127.35-127.55 mbsf). Distinctly colour banded, bioturbation is largely absent in these sediments.

4.3.2 Site 762

Site 762 lies on the Western Central part of the Exmouth Plateau at 19°53.23'S, 112°15.24'E (Figure 4.1), at a water depth of 1360 m.

The site was drilled to a depth of 940 metres below sea floor (mbsf), recovering rocks from the Berriasian to the Quaternary.

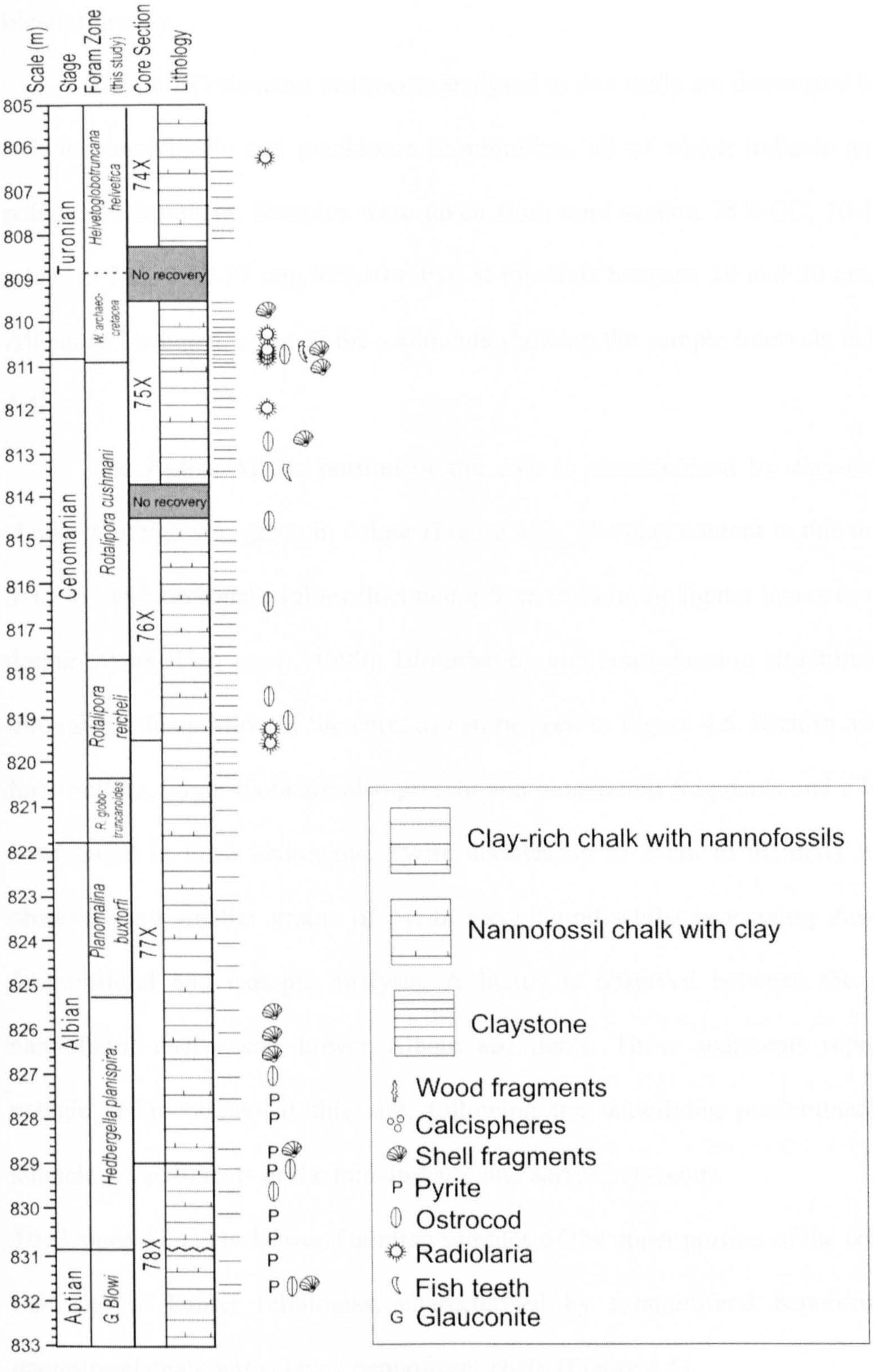

Figure 4.4: Log of sediments analysed from Site 762. Biostratigraphic zonation is from this study. Lines adjacent to the stratigraphic column indicate sampled levels. The presence of other biota, and other sedimentary components, is also indicated.

The mid-Cretaceous to Palaeogene is essentially complete and well preserved, making this site ideal for studying Cretaceous and Tertiary depositional sequences and biostratigraphy.

The mid-Cretaceous sediments analysed in this study are dominated by chalk that is rich in nannofossils and planktonic foraminifera, all of which indicate an open marine pelagic environment. Samples were taken from core section 78X-CC, 10-12 cm, 831.81 mbsf, to 74X-2 19-22 cm, 806.19 mbsf, at intervals between 10 and 50 cm, spanning the Albian to Turonian, a log of the sediments showing the sample intervals is seen in Figure 4.4.

The Aptian-Albian portion of the core is characterised by clay-rich nannofossil chalks white/grey to green in colour (Figure 4.5). The clay content in this unit varies from 3-15 %, with carbonate values fluctuating from 90% in the lighter layers to 61.64 % in the darker layers (Haq *et al.*, 1990). Bioturbation and anastomosing structures are abundant throughout this portion of the core, as can be seen in Figure 4.5. Rich in nannofossils and foraminifera, larger biota are also present and inoceramid fragments and a belemnite have been found in these sediments. Pyrite nodules up to 2 cm in diameter have also been observed and smaller grains of pyrite were found whilst processing these samples for foraminiferal and isotopic analysis. A hiatus is observed between the Lower Aptian nannofossil chalks and Lower Albian sediments. These sediments represent the first pelagic sedimentation at this site, following the underlying predominantly terriginous siliciclastic sediments of the mid-Jurassic and early Cretaceous.

The Upper Albian to Lower Turonian samples of the upper portion of the core are less clay rich and of harder lithologies, characterised by foraminiferal nannofossil chalk and nannofossil chalk with clayey nannofossil chalk (Figure 4.5).

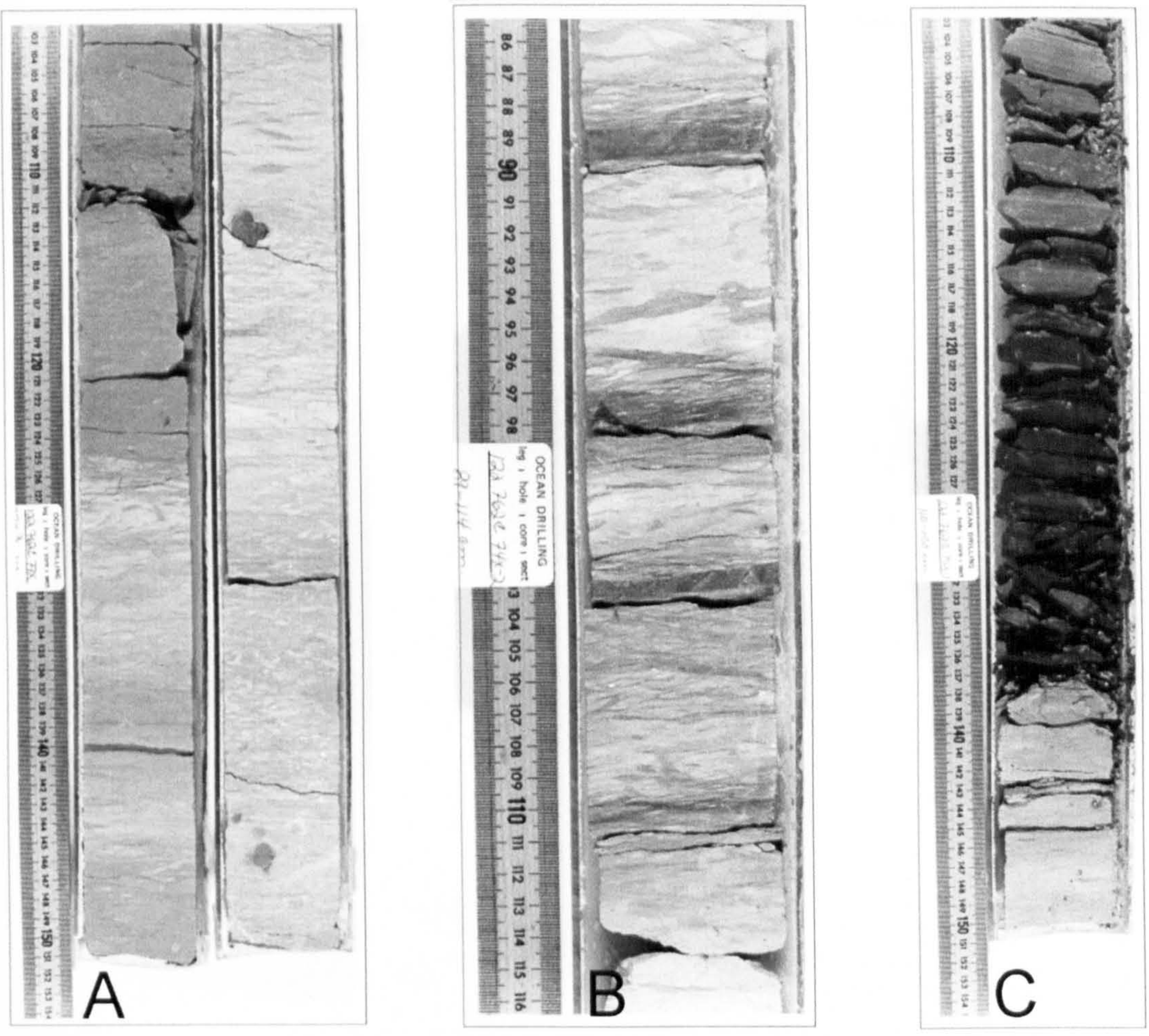

Figure 4.5: Core photographs of sediments found at Site 762.

A) Albian sediments from interval 77X-2, 110-150 cm (left hand side) and 77X-3, 110-150 cm (right hand side). Alternating dark and light green/grey nannofossil chalks with varying amounts of clay can be seen. Bioturbation is strongly evident throughout the core and pyrite nodules can be seen, up to 2 cm in diameter, scattered throughout.

B) Turonian sediments from interval 74X-2, 89-114 cm. Darker in colour, cyclic colour changes can still be seen, with moderate bioturbation and anatomising seams.

C) Dark brown fissile claystone from interval 75X-1, 110-150 cm, thought to represent the Cenomanian-Turonian boundary, the sediments show fine laminations devoid of bioturbation and carbonate.

Cyclic colour changes are seen from brown to grey/white to green to pale pink. Lighter beds are again more rich in carbonate (92-93%) and richer in foraminifera (up to 24%). The darker beds have a higher clay content and carbonate values of 51-64% (Haq *et al.*, 1990). Bioturbation is moderate throughout the core with *Planolites, Teichichnus, Zoophycos* and *Chondrites* being identified (Haq *et al.*, 1990). Anatomising seams are again abundant cross cutting the trace fossils. These are defined as microstylolites.

In addition to these nannofossil chalks an interval of dark brown fissile claystone is present in core 75X-1, 115-138 cm (Figure 4.4). With gradational upper and lower boundaries this unit is thought to represent the Cenomanian-Turonian boundary (Haq *et al.*, 1990).

4.4 Methodology

The techniques to be used in this study have been described in Chapter 2, however not all methods have been used at each locality. The ODP cores from the Indian Ocean were processed for foraminiferal, isotopic and geochemical analysis. Foraminiferal biostratigraphy and palaeoenvironmental analysis was carried out on the foraminifera, along with isotopic analysis of planktonic and benthonic species. Isotope analysis was also carried on the fine fraction samples along with trace element, carbon and Rock Eval analysis. The results of each of these analyses are described and discussed below.

4.5. Biostratigraphy of the Indian Ocean

4.5.1 Introduction to biostratigraphy of the Indian Ocean

Biostratigraphical analysis was carried out on the core samples in order to determine the relative age of the sediments. Planktonic foraminifera were used primarily, in conjunction with benthonic foraminifera, and evidence from the distribution of nannofossils and radiolaria carried out by other workers through the core. Much of the previous biostratigraphical analysis of Cretaceous sediments in the Indian Ocean has

focused around the Lower Cretaceous (e.g., planktonic biostratigraphy by Haig (1992) and benthonic stratigraphy by Holbourn and Kaminski (1997)). Planktonic biostratigraphy has been tentative due to the lack of the typical zonal species used in more Tethyan environments, morphological similarities between key species of keeled rotaliporids, and dominance of long-ranging hedbergellid species. Wonders (1992) produced a zonation for the Exmouth Plateau from the Albian to Maastrictian, but was unable to define the typical rotaliporid zones of the Cenomanian further than *Rotalipora* spp. A more detailed late Cretaceous zonation was produced by Petrizzo (2000) for the Turonian to Lower Campanian of the Exmouth Plateau, but the Cenomanian and Lower Turonian were not addressed.

Previous investigations of benthonic have also focused on Tethyan and Boreal regions (e.g., Bartenstein, 1979; Moullade, 1984; Riegraf and Luterbacher, 1989) and the zonal markers defined by these studies are either absent or extremely rare in the Indian Ocean. Holbourn and Kaminski (1997) addressed this partially with their early Cretaceous benthonic foraminiferal zonation for the Indian Ocean, but the late Cretaceous remains unzoned.

Using data from this study, along with that of previous studies, and using additional information from other microfossil groups, a more detailed stratigraphy has been determined for the mid-Cretaceous of the Indian Ocean in the cores analysed here. This zonation is based where possible on the stratigraphy determined by Robaszynski and Caron (1995). The zonations defined in this study are described below.

4.5.2 Biostratigraphy of Site 766

The biostratigraphic zonation defined for Site 766 is shown in Figure 4.6, corresponding range charts can be seen in Figure 4.7 and the count sheets can be seen in Appendix 2.

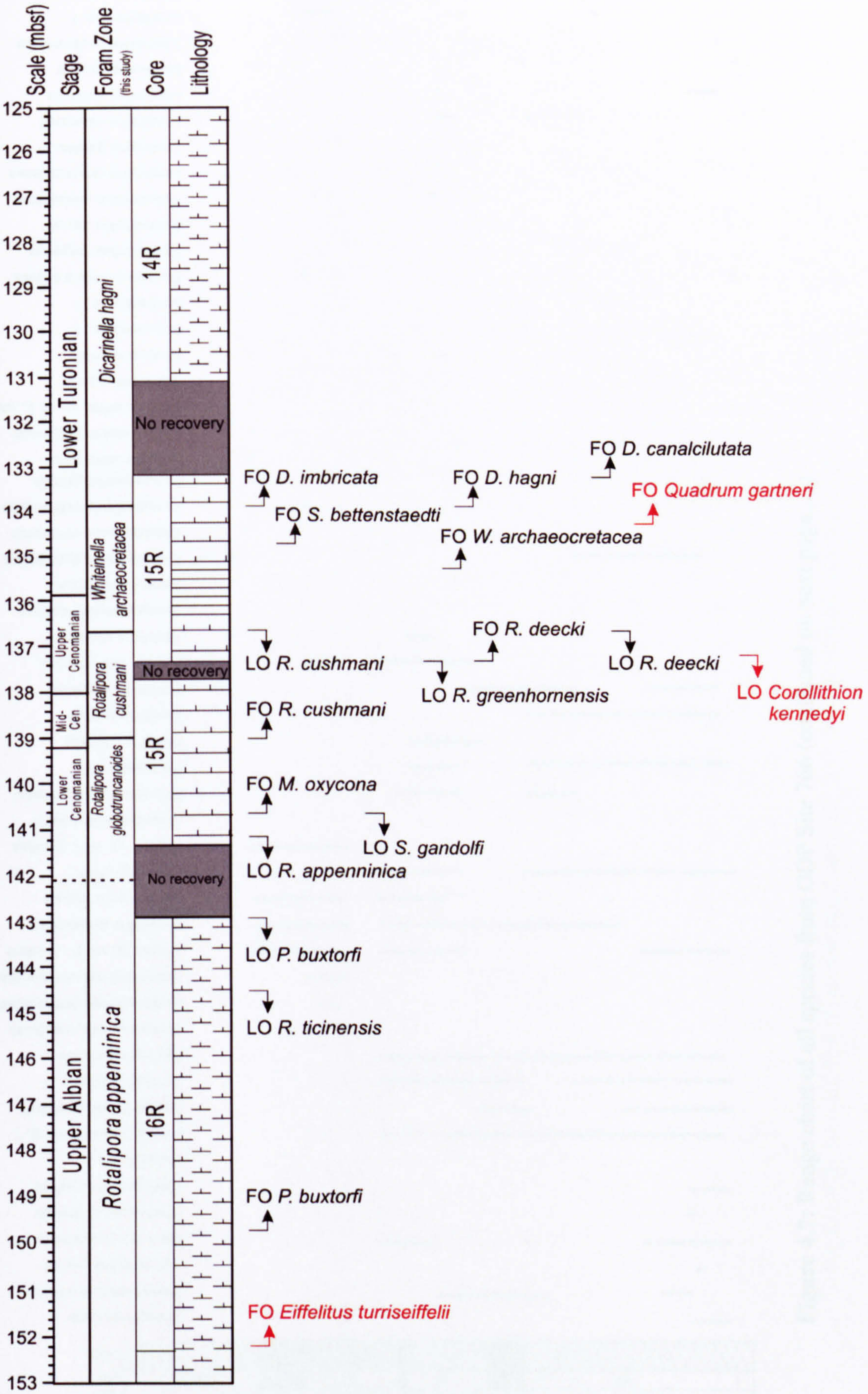

Figure 4.6: Biostratigraphy defined in this study for Site 766, showing first (FO) and last (LO) occurrences of important biostratigraphic markers.

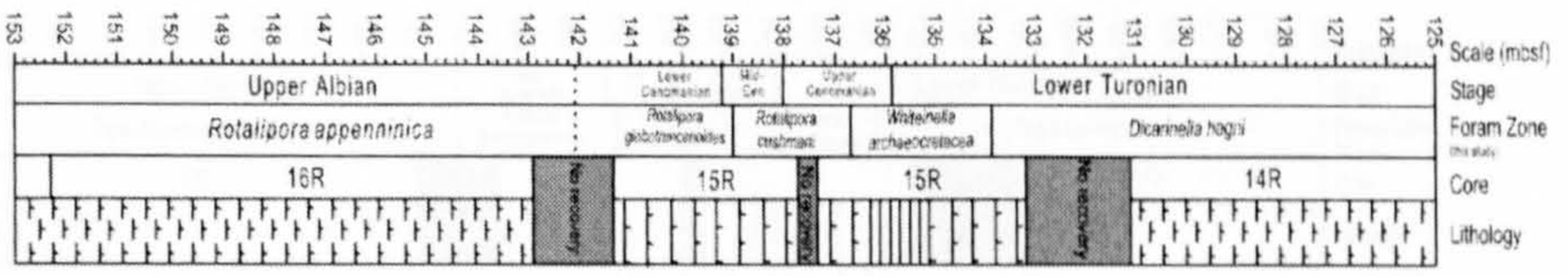

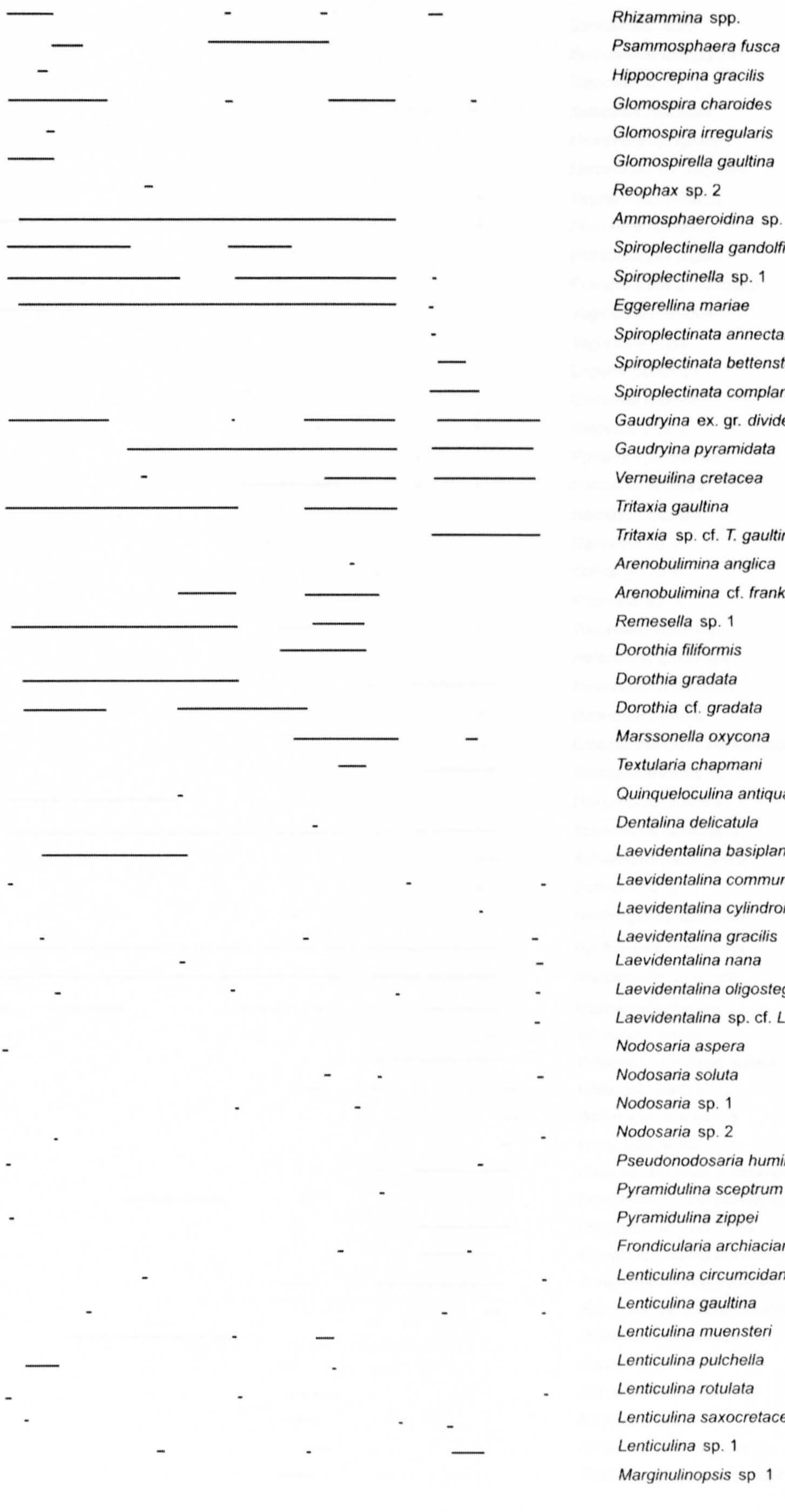

Figure 4.7: Range chart of all species from ODP Site 766 (continued on next page.....)

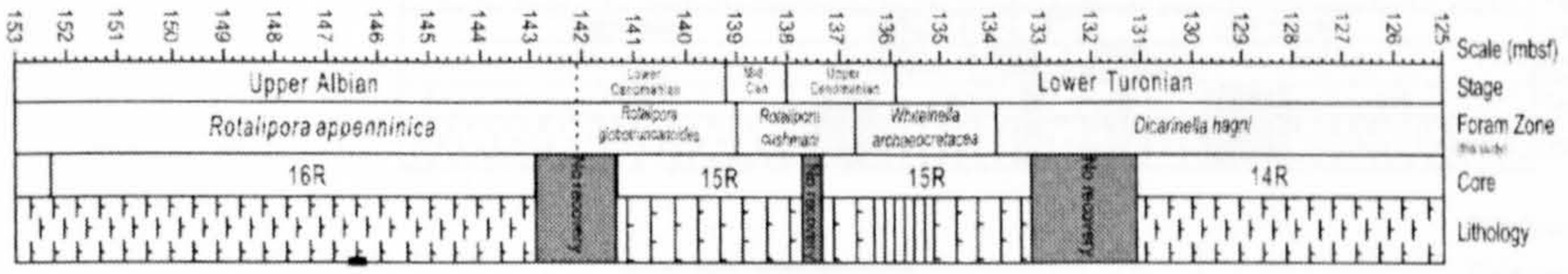

Saracenaria erlita
Saracenaria triangularis
Saracenaria sp. 1
Astacolus calliopsis
Hemirobulina bullata
Hemirobulina inaequalis
Vaginulinopsis harpa
Planularia bradyana
Psilocitharella arguta
Psilocitharella paucistriata
Vaginulina cretacea
Vaginulina recta
Lagena globulosa
Globulina lacrima
Globulina prisca
Pyrulina cylindroides
Ramulina aculeata
Ramulina spandeli
Ramulina sp. 3
Oolina globosa
Fissurina sp. 1
Tricarinella excavata
Heterohelix globulosa
Heterohelix moremani
Heterohelix reussi
Globigerinelloides bentonensis
Globigerinelloides sp. 2
Planomalina buxtorfi
Schackoina cenomana
Schackoina multispinata
Schackoina sp. 1
Hedbergella brittonensis
Hedbergella delrioensis
Hedbergella planispira
Hedbergella simplex
Whiteinella aprica
Whiteinella archaeocretacea
Whiteinella baltica
Whiteinella brittonensis
Whiteinella hessi
Praeglobotruncana aumalensis
Praeglobotruncana delrioensis
Praeglobutruncana gibba
Praeglobotruncana inornata
Praeglobotruncana stephani
Helvetoglobotruncana praehelvetica
Rotalipora appenninica
Rotalipora brotzeni
Rotalipora cushmani
Rotalipora deecki
Rotalipora greenhornensis
Rotalipora globotruncanoides

Figure 4.7: Range chart of all species from ODP Site 766 (continued on next page....)

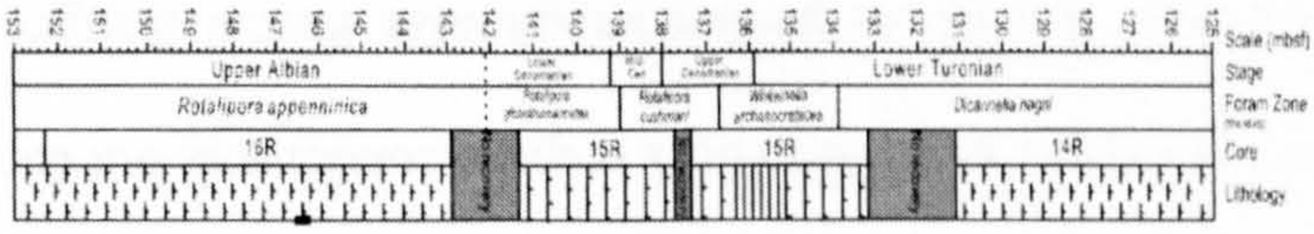

Figure 4.7: (...continued from last page) Range chart of all species from ODP Site 766

Rotalipora montsalvensis
Rotalipora ticinensis
Dicarinella canaliculata
Dicarinella hagni
Dicarinella imbricata
Marginotruncana cf. *marianosa*
Bolivina sp. 1
Bolivina sp. 2
Bolivinoides sp. 1
Tappanina cf. *lacinosa*
Spirobolivina australis
Cuneus cf. *ludbrookae*
Neobulimina australiana
Praebulimina nannina
Praebulimina reussi
Praebulimina cf. *reussi*
Praebulimina robusta
Praebulimina sp. 1
Praebulimina sp. 2
Turrilina evexa
Bulimina fabilis
Cassidella sp. 1
Coryphostoma sp. 1
Ellipsodimorphina sp. 1
Ellipsoglandulina sp. 1
Nodosarella sp. 1
Pleurostomella nitida
Pleurostomella reussi
Pleurostomella subnodosa
Pleurostomella sp. 1
Eurycheilostoma? hettgottensis
Eurycheilostoma? moorei
Iuliusina grata
Quadromorphina allomorphinoides
Gubkinella sp. 1
Charltonina australis
Charltonina cf. *australis*
Charltonina sp. 1
Conorotalites aptiensis
Osangularia schloenbachi
Berthelina bethelini
Berthelina cf. *bethelini*
Berthelina cenomanica
Berthelina cf. *daktoensis*
Berthelina tenuis
Berthelina tennuissima
Berthelina sp. 2
Berthelina sp. 3
Gavelinella cf. *plummerae*
Gavelinella tormarpensis
Gavelinella sp. 1
Gavelinella sp. 3
Gavelinella sp. 4
Gavelinella sp. 6
Lingulogavelinella albiensis
Lingulogavelinella globulosa
Lingulogavelinella indica
Lingulogavelinella newtoni
Lingulogavelinella sp. 1
Anomalina? Santoodnae
Gyroidinoides infracretacea
Gyroidinoides sp. 1
Gyroidinoides sp. 2
Gyroidinoides sp. 3
Gyroidinoides sp. 4
Valvulineria gracillima
Valvulineria lenticula
Valvulineria sp. 1
Schiebnerova proindica

Site 766A can be seen to include the Upper Albian to the Lower Turonian. The latest Albian can be defined by the partial range zone of *Rotalipora appenninica*. This is recorded at Site 766A from sample 16R-CC, 7-9 cm (152.16 mbsf) to sample 16R-1, 8-10 cm (142.98 mbsf). Accompanied by *Planomalina buxtorfi, Rotalipora ticinensis*, abundant *Hedbergella* (predominantly *H. planispira* and *H. delrioensis* with some *H. simplex* and *H. brittonensis*) and a few primitive *Praeglobotruncana*, the assemblages are typically latest Albian in age throughout this portion of the core. It is important to note both *R. appenninica* and *R. ticinensis* are present in forms, at Site 766, that are more umbilico-convex than their typical biconvex forms. Benthonic species are predominantly calcareous with species of *Gyroidinoides* and *Berthelina* (particularly *B. cenomana* and *B. berthelini*, again typical of latest Albian to early Cenomanian in age), along with relatively high numbers of *Osangularia schloenbachi, Pleurostomella reussi, Scheibnerova proindica, Valvulineria gracillima* and *Charltonina australis*. Species of *Bolivina, Lenticulina, Laevidentalina, Praebulimina, Coryphostoma,* and *Spirobolivina australis* and *Quadromorphina allomorphinoides* are also present in lower abundances.

Agglutinated species are much less abundant. The fauna is dominated by *Gaudryina* ex. gr. *dividens* and *Tritaxia gaultina* with species of *Dorothia, Eggerellina, Glomospira, Psammosphaera, Remessella* and *Spiropectinella* also present. *Spiroplectinella gandolfi* was used as a zonal marker by Holbourn and Kaminski (1997) in their early Cretaceous benthonic foraminiferal zonation for the Indian Ocean. They defined an interval zone of *Spiroplectinella gandolfi* spanning the late Albian to the early Cenomanian, parallel to the *R. appenninica* Zone and the lower part of the *R. globotruncanoides* Zone. Using the planktonic zonation defined in this study, *S. gandolfi* can be seen to show a similar range at Site 766 and therefore aids the correlation of the uppermost Albian – lowermost Cenomanian sediments.

The Cenomanian of Site 766A is quite condensed, but can be divided into the early-mid Cenomanian *Rotalipora globotruncanoides* Partial Range Zone (PRZ), the mid-late

Cenomanian *Rotalipora cushmani* Total Range Zone (TRZ), and the *Whiteinella archaeocretacea* Partial Range Zone (PRZ), spanning the Cenomanian-Turonian boundary and into the Turonian, with no *Rotalipora reicheli* present at Site 766, the mid-Cenomanian *R. reicheli* Zone is not defined.

The lower part of the Cenomanian lacks many of the zonal species, the only keeled foraminifera present being extremely poorly preserved and possibly reworked *Planomalina buxtorfi* and *Rotalipora ticinensis*, and the early-middle Cenomanian species *Rotalipora montsalvensis*. However, advanced *R. appenninica,* at the top of the *R. appenninica* Zone (16R-1), tending towards *R. globotruncanoides* are seen, indicating the proximity of these samples to the Albian-Cenomanian boundary (Wonders, 1980). *R. globotruncanoides* is not seen in this study until the *R. cushmani* Zone, although it has been recorded by Haig (1992) as being present in this portion of the core. The *R. globotruncanoides* PRZ is defined by the last occurrence (LO) of un-reworked *Planomalina buxtorfi* at 16R-1, 8-10 cm (142.98 mbsf) and the first occurrence (FO) of *R. cushmani* at 15R-4, 120-122 cm (138.90 mbsf). It must be noted the LO of *P. buxtorfi* at this level is located at the base of an interval of no recovery, and the actual LO of *P. buxtorfi* and the Albian-Cenomanian boundary may lie in this interval. With no samples from this interval the boundary can therefore only be defined as lying within this interval and not at a distinct level.

Assemblages in the *R. globotruncanoides* zone are again dominated by species of *Hedbergella,* with *Shackoina* and rare *Praeglobotruncana*. Benthonic foraminifera are dominated by calcareous species of typical Cenomanian age *Osangularia, Berthelina, Praebulimina, Gyroidinoides* and *Scheibnerova*. The presence of agglutinated species of *Gaudryina* and *Tritaxia*, and especially early Cenomanian *Remessella, Dorothia* and *Spiroplectinella*, support the early Cenomanian age of these samples. This zone also contains the FO of *Massonella oxycona* at 15R-5, 145-147 cm (140.65 mbsf).

The first occurrence of *Rotalipora cushmani* in sample 15R-4, 120-122 cm (139.90 mbsf) indicates the base of the *R. cushmani* TRZ. The absence of *Rotalipora reicheli* at

this site means that the *R. reicheli* Total Range Zone and, therefore, the boundary between the lower and middle Cenomanian cannot be fully defined. Analysis of the core sediments does not indicate any break in sedimentation and it is likely, therefore, that the *R. reicheli* Zone lies within the top of the *R. globotruncanoides* Zone that has been defined in this study. Middle Cenomanian sedimentation at Site 766, therefore, begins at the top of the *R. globotruncanoides* Zone.

The *R. cushmani* Zone spans the middle to late Cenomanian until the LO of *R. cushmani* in sample 15R-3, 58-60 cm (136.78 mbsf). The presence of *Rotalipora deeckei* in samples 15R-4, 20-22 cm (137.90 mbsf) to 15R-3, 58-60 cm (136.78 mbsf) determines the late Cenomanian age of the upper part of this zone. The samples continue to be dominated by small hedbergellids, however, other Cenomanian planktonic species *R. greenhornensis, R. brotzeni, Praeglobotruncana stephani* and *Whiteinella baltica* are recorded.

Species of *Gaudryina, Tritaxia* and *Eggerellina* still dominate the agglutinated fauna with increased numbers of *Massonella oxycona*. The calcareous benthonic fauna continues to be dominated by species of *Charltonina, Berthelina, Osangularia, Scheibnerova* and *Gyroidinoides*, with increased numbers of *Praebulimina* spp. and *Tricarinella* spp. and rare specimens of *Lenticulina, Nodosaria, Saracenaria* and polymorphinids. *Laevidentalina* spp. are not recorded in this zone.

The *Whiteinella archaeocretacea* Partial Range Zone straddles the Cenomanian-Turonian boundary and extends from the last occurrence of *Rotalipora cushmani* (15R-3, 58-60 cm (136.78 mbsf) in Core 766A) to the first occurrence of *Helvetoglobotruncana helvetica*.

H. helvetica is absent in the samples studied from Site 766, so this zone is not defined. Instead the FO of *Dicarinella hagni* at 15R-1, 55-57 cm (133.75 mbsf) is used in this study to define the base of the zone preceeding the *W. archaeocretacea* Zone in this core. The FO of *Dicarinella hagni* has been used in previous studies to represent the

Cenomanian-Turonian boundary and as an index species of the upper subzone of the *W. archaeocretacea* Zone (see, for example, Salaj, 1996; Tur *et al.*, 2001; Kopaevich and Kuzmicheva, 2002). In this core *Dicarinella hagni* appears around 2 m above the defined CTB (see below), well into the Lower Turonian, and marks a defined change in the foraminiferal assemblage, from an impoverished *W. archaeocretacea* Zone assemblage to a more diverse typical Lower Turonian assemblage. *D. hagni* is the dominant species of these Lower Turonian samples and with the absence of *Helvetoglobotruncana helvetica, Dicarinella hagni* is used as a zonal species defining the Lower Turonian following the *W. archaeocretacea* Zone. It must be noted that elsewhere *Dicarinella hagni* has been used as a subzone of the *W. archaeocretacea* zone (e.g., Keller and Pardo, 2004). The *D. hagni* Zone used in this study could therefore be placed in the *Whiteinella archaeocretacea* Zone, however with the lack of typical zonal species and the distinctive change in assemblage seen with the FO of *D. hagni* at Site 766, the *D. hagni* Zone is determined as a separate zone correlative with the top part of the *W. archaeocretacea* Zone and lower part of the *H. helvetica* Zone.

The diversity of species is much lower in the *W. archaeocretacea* Zone. Planktonic species are limited to *Hedbergella, Whiteinella* and *Schackoina*. Agglutinated species of *Gaudryina, Tritaxia* and *Verneuilina* are present in the upper part of the zone, and the FO of *Spiroplectinata annectans, S. bettenstaedti and S. complanata* is also recorded, just after the CTB barren zone. Calcareous benthonic species are largely absent from the lower part of this zone. However, the upper part of the zone records species of *Bolivina, Praebulimina, Pleurostomella, and Iuliusina* in moderate numbers, with much higher abundances of *Berthelina* spp. and *Gyroidinoides* spp..

The Cenomanian-Turonian boundary is placed within the *W. archaecretacea* Zone at 135.95 mbsf, between samples 15R-2, 130-132 cm (136 mbsf) and 15R-2, 120-122 cm (135.90 mbsf). Previous studies have found it difficult to determine the CTB due to widely spaced sampling of the core and a lack of microfossils in the clay-rich sediments.

Shipboard nannofossil workers placed the boundary between 15R-1, 100-101 cm (the FO of *Quadrum gartneri*) and 15R-3, 100-101 cm (the LO of *Corollithion kennedyi*) (~ 137.2 and 134.4 mbsf respectively). Sedimentologists place the boundary in 15R-3, at 26 cm (136.5 mbsf), the boundary being defined by a thin conglomerate with clasts of glauconitic sandstone and acidic volcanic rocks in a matrix of zeolitic clay. All of 15R-2, however, contains dark carbonate poor zeolitic claystones, typical of boundary sediments of Cenomanian-Turonian age. The boundary is able to be constrained further by the presence of Lower Turonian assemblages from 15R-2, 60-62 cm (135.30 mbsf), and Upper Cenomanian assemblages below 15R-2, 130-132 cm (136 mbsf). Unfortunately the sediments between these samples are barren of foraminifera, although they are very abundant in radiolaria. Although the abundance of radiolarian may be due to condensation of the sediments, an increase in abundance has been recorded at a number of CTB sites globally (Thurow *et al.*, 1992). Further analysis of the radiolaria species may additionally enable further correlation of the boundary. For this study the boundary is placed after the last Cenomanian species of foraminifera are observed prior to the barren zone, at 135.95 mbsf.

The *Dicarinella hagni* Zone is characterised by Lower Turonian species of *Praeglobotruncana* and *Whiteinella*, with the continued dominance of long ranging *Hedbergella*, with *Schackoina* and *Heterohelix*. Calcareous species of *Berthelina, Gavelinella, Pleurostomella, Iuliusina,* with rarer species of *Laevidentalina, Nodosaria* and *Lenticulina* are also present. Species of *Gaudryina* still dominate the agglutinated benthonic species, with *Massonella, Verneuilina* and *Spiroplectinata* also present.

Further discussion on the abundance of species within these zones can be seen below.

4.5.3 Biostratigraphy of Site 762

Samples taken from Site 762 span the Lower Aptian to mid-Turonian. Although detailed foraminiferal analysis was only undertaken on the Cenomanian and Turonian

samples. Specimens from the Lower Aptian and Albian were studied and picked for isotopic analysis. The key zonal fossils were therefore recorded in this lower part of the core. The biostratigraphic zonation for Site 762 and first and last occurrences of zonal and key foraminiferal species is shown in Figure 4.8 and corresponding range charts can be seen in Figure 4.9.

The lowest samples of the core (78X-CC, 10-12 cm to 78X-2, 60-62 cm) are dominated by small planktonic species, particularly hedbergellids. Wonders (1992) defined these sediments as early Aptian in age as determined by the presence of *Globigerinelloides blowi,* which defines the *G. blowi* Zone, and by the presence of *Gavelinella barremiana* which has its LO in the Lower Aptian. Other benthonic species present in this zone are large *Lenticulina* spp. and large agglutinated forms including *Tritaxia* spp.

Following this Lower Aptian zone, the assemblages continue to be dominated by the long ranging *Hedbergella* spp., particularly *H. planispira.* This, along with the absence of any of the typical Tethyan foraminiferal zonal markers, makes it difficult to date this portion of the core. The FO of nannofossil *Prediscosphaera cretacea* in 78X-4 at 830.65 mbsf however defines these sediments as early Albian in age (Brawlower and Siesser, 1992), indicating the presence of a hiatus, corresponding to the Lower Aptian to Lower Albian. The dominance of *Hedbergella planispira* in this zone led to Wonders (1992) to define this zone between the LO of *G. blowi* and FO of Upper Albian marker *Planomalina buxtorfi* as the *H. planispira* Zone. With the lack of any other zonal species, this definition is retained in this study, defining an age of early to mid-Albian. Species of *Berthelina, Tritaxia, Gaudryina* and *Dorothia*, continue to be present in the assemblages along with rarer *Arenobulimina* and *Ammosphaeroidina* spp., branching agglutinated species of *Rhizzammina*, and the irregular calcareous *Ramulina* spp. Samples continue to be dominated by small hedbergellids up through the core with assemblages similar to those seen at Site 766, however, large keeled forms become more abundant, enabling a more detailed zonation through the Upper Albian and Cenomanian to be defined.

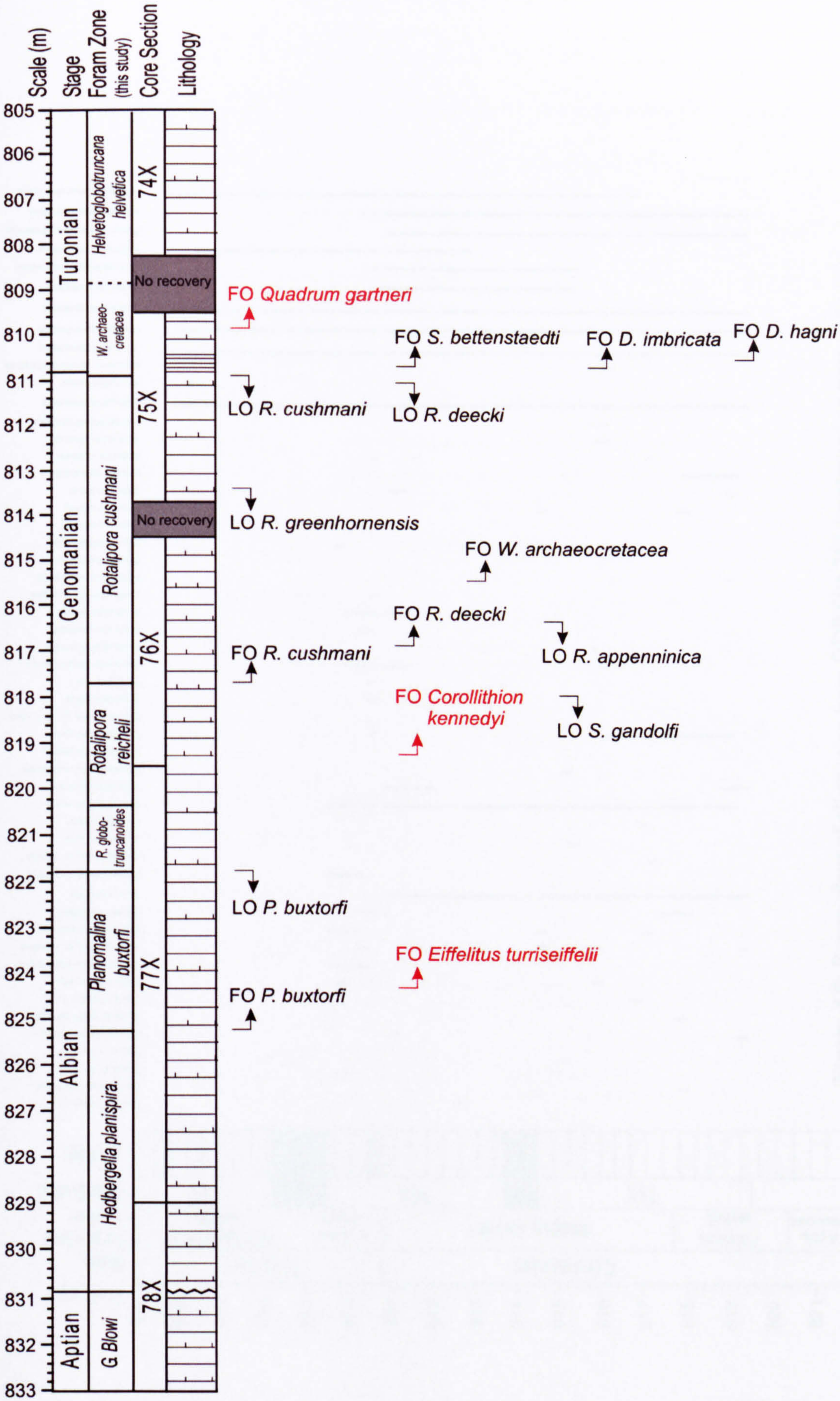

Figure 4.8: Diagram showing the first and last occurrences of zonal and key species at Site 762

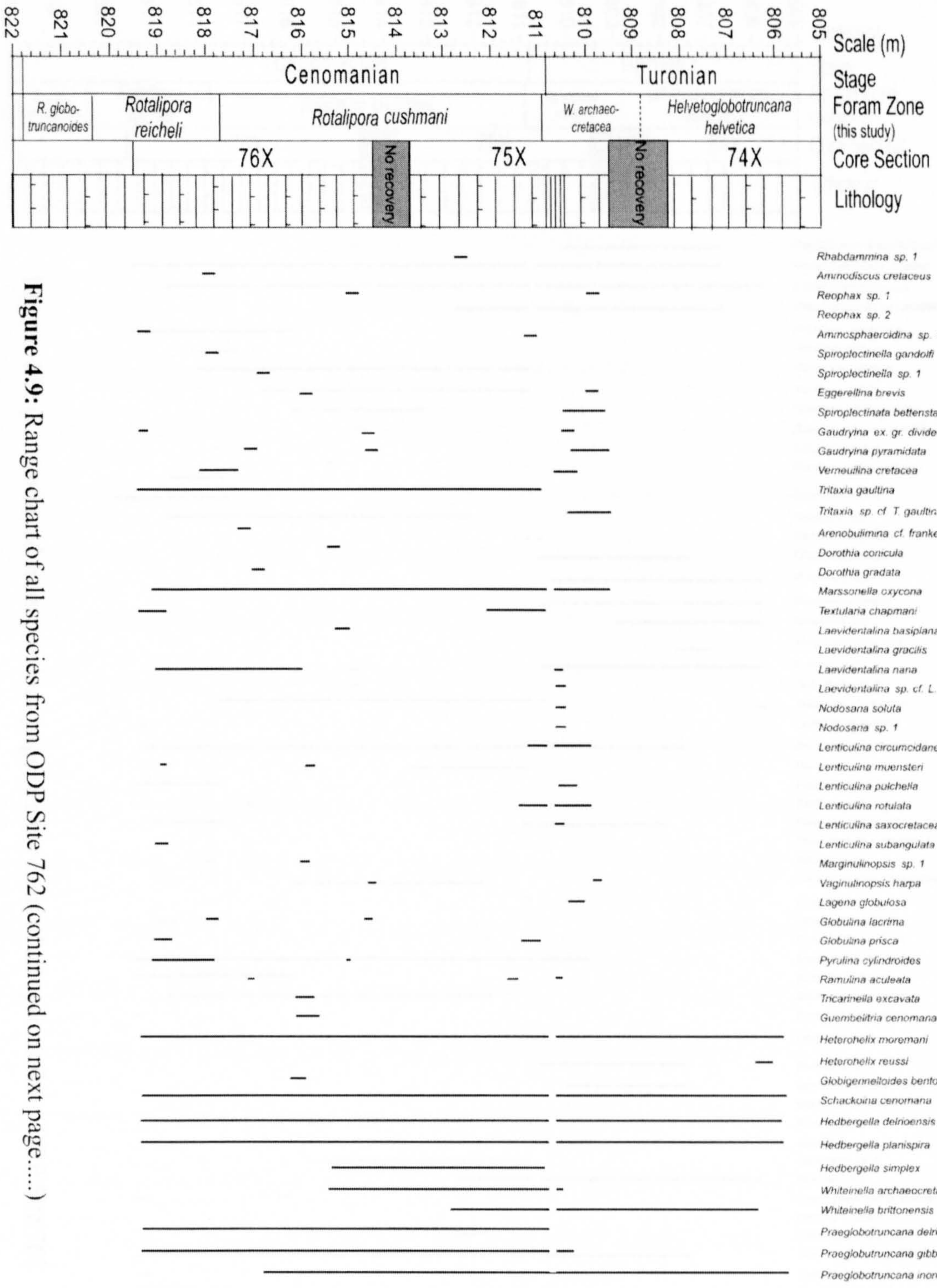

Figure 4.9: Range chart of all species from ODP Site 762 (continued on next page.....)

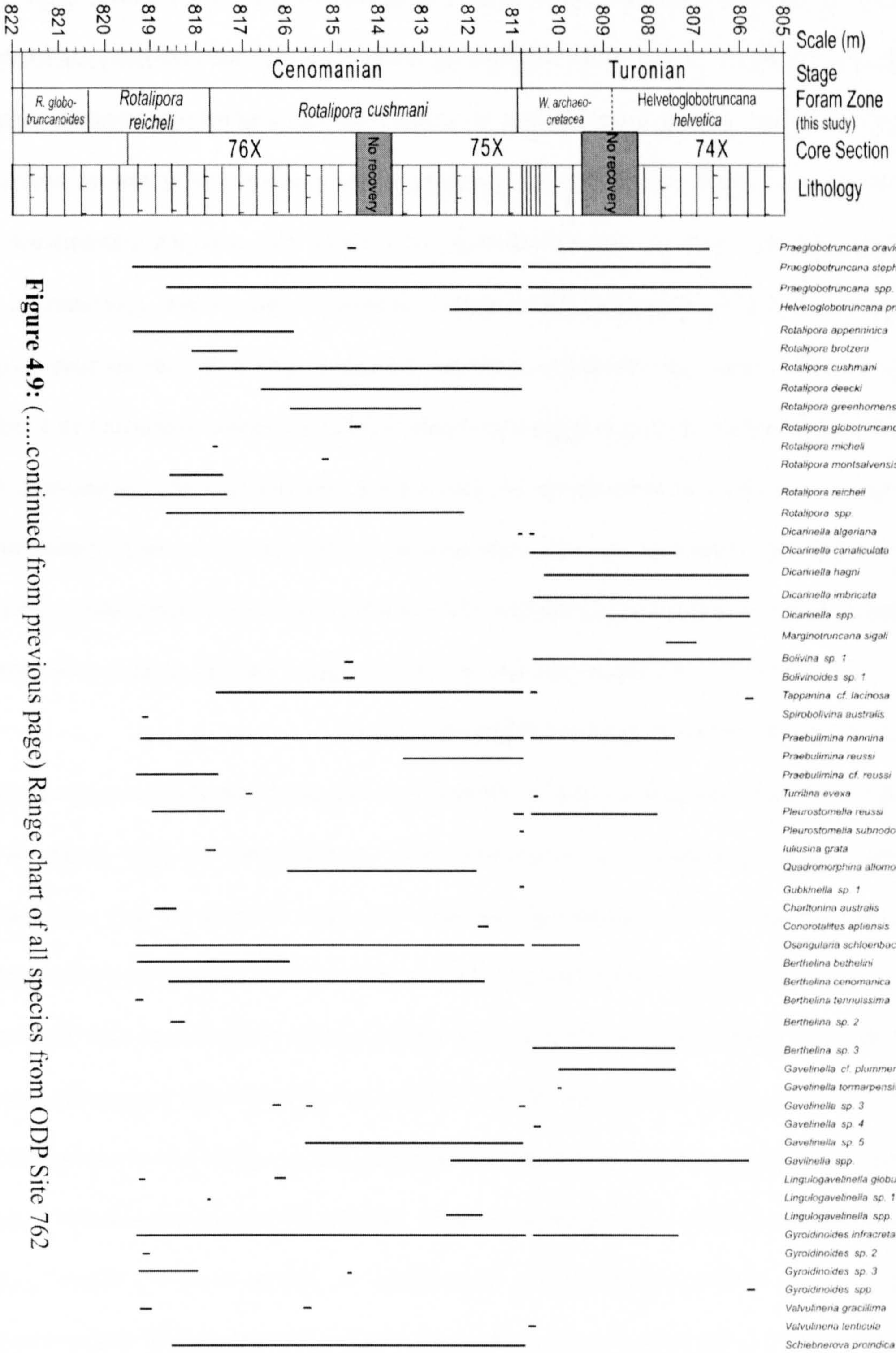

Figure 4.9: (.....continued from previous page) Range chart of all species from ODP Site 762

Sample 77X-4, 100-102 cm (825.00 mbsf) contains the FO of *Planomalina buxtorfi*, the first keeled species of core 762, and the first real Tethyan zonal foraminifera. This presence of *P. buxtorfi* in these samples indicates a Late Albian age, further verified by the FO of nannofossil *Eiffellithus turriseiffelii* at 824.30 mbsf in section 77X-4 (Brawlower and Siesser, 1992). Specimens of *P. buxtorfi* are present until sample 77X-2, 100-102 cm (822.00 mbsf), marking the top of the Albian. *P. buxtorfi* is found within the Upper Albian Tethyan zone of *Rotalipora appenninica* (Robaszynski and Caron, 1995). With the lack of abundant *Rotalipora* in these Upper Albian samples, very few specimens of *R. appenninica* being present, the *Planomalina buxtorfi* Zone defined for Upper Albian sediments on the Exmouth Plateau by Wonders (1992) is retained for this study. With continued high abundances of *Hedbergella* spp., assemblages are also made up of *Praeglobotruncana delrioensis*, few *R. appenninica* and benthonic species of *Berthelina*, *Tritaxia* and other primitive elongate agglutinated forms.

The LO of *P. buxtorfi* marks the top of the Albian and the Albian-Cenomanian boundary, with the presence of *Rotalipora globotruncanoides* in the upper part of section 77X defining the sediments as early Cenomanian in age. The FO of early Cenomanian nannofossil *Corollithion kennedyi* in section 76X-CC verifies this age (Brawlower and Siesser, 1992). Wonders (1992) defines the proceeding Cenomanian sediments as a single *Rotalipora* spp. zone. The increased sampling interval in this study has enabled further definition of the Cenomanian foraminiferal biozones. The Lower Cenomanian *R. globotruncanoides*, low to mid-Cenomanian *R. reicheli* and mid-late Cenomanian *R. cushmani* Zones being easily defined. Throughout the Cenomanian it can be seen that strongly umbilico-convex morphotypes of rotaliporids are particularly common, and a continuous lineage is seen from *R. reicheli* to *R. deeckei* through the mid-late Cenomanian. This, along with the condensed nature of the Cenomanian at Site 762, makes it difficult to separate the two species morphologically. Although with *R. reicheli* commonly showing a flatter spiral side and depressed sutures in the later chambers of the umbilical side

(Robaszynski and Caron, 1979), and the species having very distinct ranges, the top of the mid-Cenomanian *R. reicheli* Zone can be marked by the FO of *Rotalipora cushmani*, umbilico-convex morphotypes above this level being included as the Upper Cenomanian *Rotalipora deeckei*.

The Lower Cenomanian *R. globotruncanoides* partial range zone is relatively thin (~1.5 m) and defined by the LO of *P. buxtorfi* (822.00 mbsf) and FO of *R. reicheli* (820.05 mbsf). Assemblages continue to be rich in *Hedbergella* spp. with specimens of *R. appenninica* and *Praeglobotruncana* spp. also present. Some species of *Berthelina*, *Osangularia* and *Tritaxia* are rare but also present.

The *R. reicheli* interval zone encompasses the part of the core from the FO of *R. reicheli* to the FO of *R. cushmani*, from 820.05 to 817.78 mbsf, spanning the lower-mid Cenomanian boundary. Accompanied by a more diverse planktonic assemblage, and increasing numbers of *Rotalipora* spp., the *R. reicheli* zone is much more Tethyan than the underlying assemblages. Specimens of *R. appenninica* and *R. brotzeni* are present with *Praeglobotruncana delrioensis, Praeglobotruncana gibba* and *Praeglobotruncana stephani*, and the FO of *Schackoina cenomana* and *Heterohelix moremani* are seen. Species of *Hedbergella* still dominate the assemblage. Less abundant specimens of *Berthelina* spp., *Gyroidinoides* spp., *Osangularia* spp. and *Tritaxia* spp. are observed with rare elongate calcareous species, including *Laevidentalina* spp., *Pyrulina* spp. and *Praebulimina* spp.

The *R. cushmani* Total Range Zone (TRZ), from the first to last occurrence of *R. cushmani* (817.59-810.90 mbsf) spans the mid- to upper Cenomanian. The diversity of the planktonic assemblage continues to diversify through the Cenomanian, *H. planispira* and *H. delrioensis* still dominating the assemblage, with numbers of *Praeglobotruncana* spp. greatly increasing, especially with the introduction of *Praeglobotruncana inornata*. The FO of *Whiteinella archaeocretacea* is seen in sample 76X-1, 97-99 cm (815.47 mbsf).The abundance of *Heterohelix moremani* also increases greatly up through this zone. Benthonic

numbers remain low and continue to be dominated by *Berthelina* spp., *Gavelinella* spp., *Gyroidinoides* spp. and *Praebulimina* spp, and are joined by increased numbers of *Tappannina* spp. Agglutinated *Tritaxia* spp. is also still consistently present in each sample, with rare *Massonella* spp., *Laevidentalina* spp. and *Lenticulina.*

The last occurrence of *R. cushmani* is seen in sample 75X-1, 140-142 cm (810.90 mbsf) just 2 cm below the dark claystone horizon seen at 75X-1, 115-138 cm, and coinciding with the LO of nannofossil *Microstaurus chiastius* at 810.91 mbsf marking the top of the Cenomanian (Bralower and Siesser, 1992). It should be noted the FO of lower Turonian nannofossil *Eiffellithus eximus* is seen just above the claystone horizon at 810.63 mbsf, indicating how condensed the CTB interval is at Site 762 (Bralower and Siesser, 1992). The claystone unit lies in the *W. archaeocretacea* Zone, defined by the LO of *R. cushmani* and FO of *Helvetoglobotruncana helvetica.* With the absence of *H. helvetica* until section 73X-CC (Haq *et al.*, 1990) the presence of *Marginotruncana sigali* from section 74X-CC can be used to determine the base of the *H. Helvetica* Zone. The *W. archaeocretacea* Zone therefore extends from sample 75X-1, 129-131 cm (810.79 mbsf) to sample 75X-1, 5-6 cm (809.55 mbsf) making the zone less than 1.5 m in length. Spanning the CTB, the boundary can be constrained by the LO of nannofossil *M. chiastus* and FO of *E. eximus* as described above, and therefore lies within the claystone layer. The boundary can be further constrained by the FO of Turonian *Dicarinella hagni* in sample 75X-1, 99-100 cm (810.49 mbsf). The boundary is, therefore, placed in this core at the base of the claystone unit corresponding to the barren zone and highest TOC values, in sample 75X-1, 129-131 cm.

The assemblages seen in the *W. archaeocretacea* Partial Range Zone (PRZ) are much lower in diversity than those seen above and below, and planktonic species of *Hedbergella* and *Praeglobotruncana* although present show much lower numbers. An increase is seen however in the diversity of agglutinated benthonic specimens, with an increase in abundance of more primitive species such as *Reophax* spp. and other

agglutinated species of *Eggerellina, Gaudryina* and *Marssonella*. It should be noted that the first occurrence of *Tritaxia* cf. *gaultina* and *Spiroplectinata bettenstaedti* are seen in sample 75X-1, 120-121 cm (810.70 mbsf), this can be correlated with the FO of these species in core 766. Similarly a large rise in calcareous benthonic foraminifera was seen with increases in species of *Berthelina, Gubkinella, Osangularia, Gyroidinoides, Pleurostomella, Praeglobotruncana* and *Bolivina,* directly after the barren zone. By the top of the *W. archaeocretacea* PRZ diversity has decreased to pre-boundary levels and planktonics dominate assemblages again. Early Turonian marker, nannofossil *Quadrum gartneri*, is also seen in this zone at 809.93 mbsf.

The *H. Helvetica* Total Range Zone is defined in this core by the FO of *Marginotruncana sigali* in sample 74X-CC, 14-16 cm (808.05 mbsf), it defines a mid-Turonian age and makes up the upper portion of the core analysed in this study. The exact boundary between the *W. archaeocretacea* PRZ and *H. Helvetica* TRZ cannot be defined due to a lack of recovery between sections 74X and 75X of nearly 1.25 m. Samples are dominated again by planktonics *Hedbergella* spp. and *Heterohelix* spp., with species of *Praeglobotruncana, Marginotruncana* and *Dicarinella,* replacing the extinct *Rotalipora* spp. Species of *Guembelitria, Whiteinella* and *Schackoina* are also present. Agglutinated benthonic foraminiferal species are completely absent from this zone, and calcareous forms are present only in very low numbers and low diversities; species of *Berthelina, Gavelinella, Gyroidinoides* and *Bolivina* being present.

Further discussion on the abundance of species within these zones can be seen below.

4.6 Results Site 766

4.6.1 Foraminiferal results

The results of the foraminiferal distribution of species, genera and morphotypes are shown in Figures 4.10- 4.14. The main features of these distributions are discussed below.

4.6.1.1 Specimen and species distribution

Abundance

Abundance of foraminifera is presented as numbers per gram and as accumulation rates (number of foraminifera per cm^3 per kyr), these are illustrated in Figure 4.10B and 4.10C. As can been seen both graphs show identical changes in abundance. As abundances are typically expressed as specimens per gram (SPG) in palaeoenvironmental analyses all data below will be discussed as such.

The number, or abundance, of specimens fluctuates rapidly throughout the core. Through the Upper Albian *Rotalipora appenninica* Zone, abundance is around 65000 SPG, however fluctuations are seen from 4000 SPG to 185000 SPG, in very rapid shifts of specimen numbers. In the Lower Cenomanian abundances can be seen to increase rapidly to peak values of ~277000 SPG. Large fluctuations of abundance are still seen through this portion of the core, however peak values remain high through the Cenomanian into the Lower Turonian of the *Whiteinella archaeocretacea* Zone. Following the final peak in the *W. archaeocretacea* PRZ at 135.1 mbsf, abundance numbers fall rapidly to a low of 6280 SPG at the *W. archaeocretacea – Dicarinella hagni* PRZ boundary. Values remain low through the Lower Turonian, increasing to ~95000 SPG in the upper part of the core.

Diversity

Species richness (number of species) and the Fisher alpha index were used to determine diversity throughout the core. Although the Fisher alpha index takes into account the sample size as well as the number of species picked, the results show nearly identical traces. These results can be seen in Figure 4.10 D-E.

Diversity remains relatively constant throughout the Upper Albian with averages of around 28 species, showing lows of 25 and highs of 34. The Fisher alpha index similarly shows values of 6.5 to 9.5 with averages of 7.5. A sharp decrease in diversity is seen at 147.75 mbsf, the number of species decreasing to 11, with Fisher alpha index values

falling to 2.22. However values rapidly return to more typical Upper Albian values, of 25 species per sample (Fisher alpha values of 7.5). A second marked decrease in diversity is seen in the Lower Cenomanian, immediately following the Albian-Cenomanian Boundary at 141.15 mbsf. Species numbers again decrease to 12, with Fisher alpha index values of 2.44.

Through the Cenomanian values increase rapidly reaching a peak in the mid-Cenomanian at 138.90 mbsf, specimen numbers reaching 40, with Fisher alpha index values peaking at 12.14. Diversity can then be seen to decrease very slowly through the Upper Cenomanian until the Cenomanian-Turonian Boundary where values fall to zero in the barren claystones. Following this barren zone, diversity slowly increases in the Turonian to species numbers of 34, and Fisher alpha index values of 9.31. Diversity remains around these values through the Turonian.

Planktonic/Benthonic Ratio

The planktonic/benthonic ratio (Figure 4.10F) fluctuates greatly through the core, planktonic abundance varying from near 100% dominance to near zero. The Albian, and Turonian, portions of the core are generally dominated by planktonic assemblages, although a few samples in the Upper Albian show benthonic dominance (~90%) at 149 and 148 mbsf, and most significantly at the very top of the Upper Albian, at 143 mbsf, where planktonic species make up only 0.7% of the assemblage.

Through the Cenomanian and lowest Turonian *W. archaeocretacea* Zone benthonic species predominantly dominate the foraminiferal assemblages making up 50-90% of the specimens. This is seen particularly around the CTB, assemblages of 100% benthonic species being seen at 134.71 mbsf. Following this low, planktonic species increase rapidly through the *Dicarinella hagni* Zone and clearly dominate the Turonian samples in this zone.

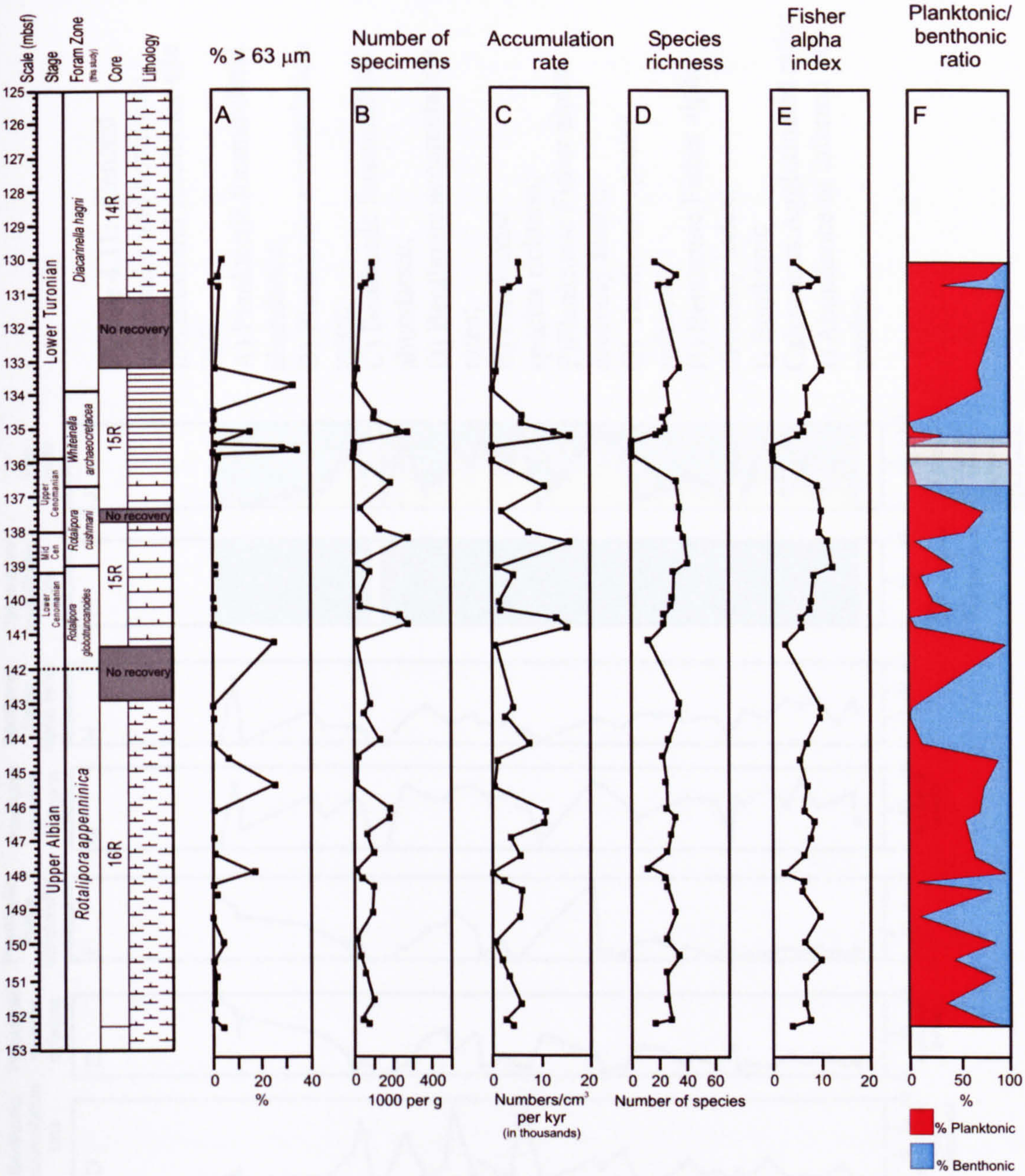

Figure 4.10: General foraminiferal results for Site 766. A) % of sample greater than 63µm; B) Foraminiferal abundance; C) Accumulation rate; D) Species richness; E) Fisher alpha diversity index; E) Planktonic:Benthonic ratio

4.6.1.2 Planktonic foraminiferal distribution

As discussed above, the abundance and diversity of planktonic specimens varies throughout the core. These variations in diversity and abundance are shown in Figure 4.11, where 10 genera and 36 species of planktonic foraminifera are seen.

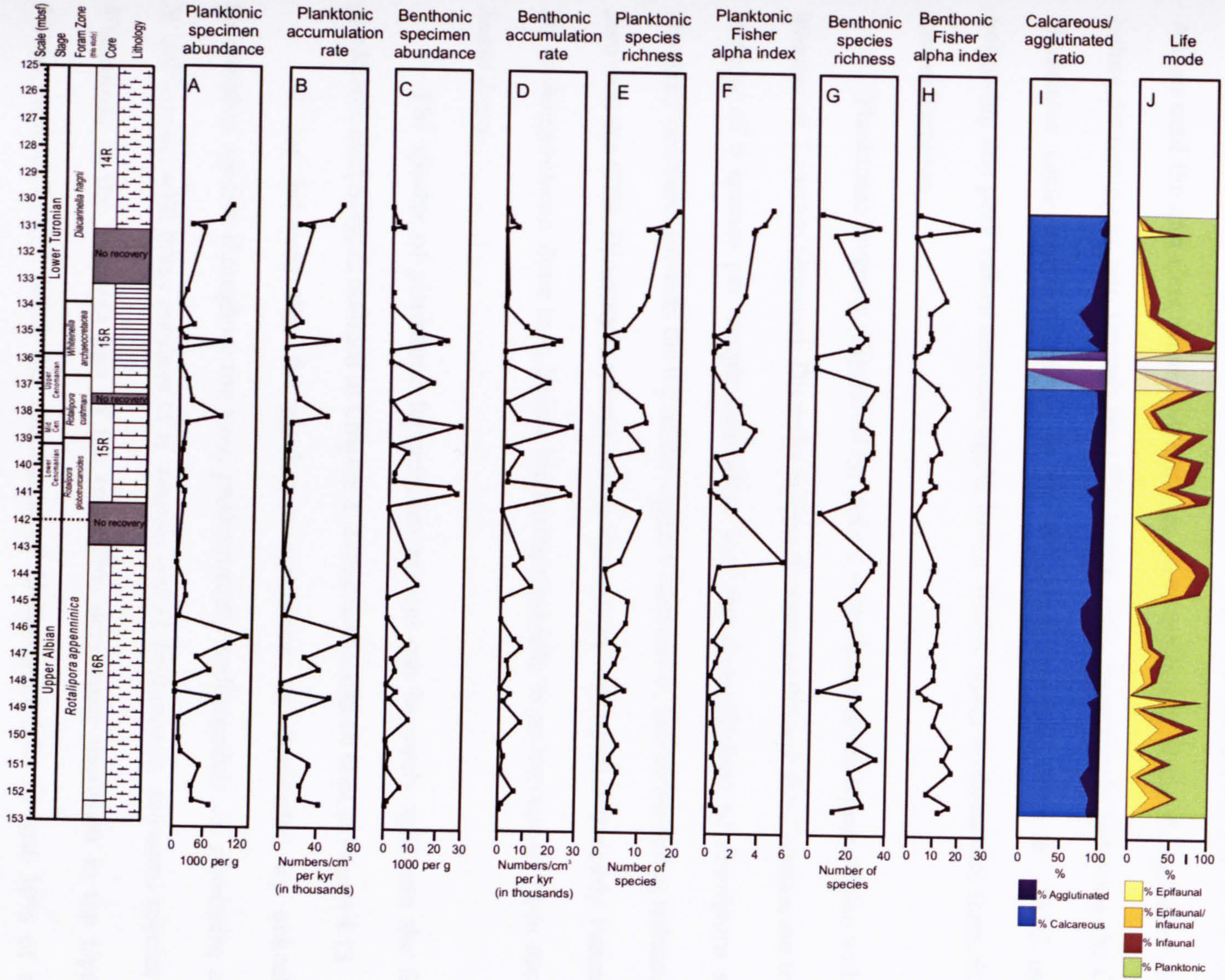

Figure 4.11: General planktonic and benthonic foraminiferal results for site 766.
A) Planktonic foraminiferal abundance;
B) Planktonic accumulation rates;
C) Benthonic foraminiferal abundance;
D) Benthonic accumulation rates;
E) Planktonic species richness;
F)Planktonic Fisher alpha diversity index;
G) Benthonic species richness;
H) Benthonic Fisher alpha diversity index;
I) Benthonic Calcareous:Agglutinated ratio;
J) Abundance of inferred life modes.

As above the planktonic abundance is expressed as SPG and as accumulation rates of number of specimens per cm^3 per kyr (Figures 4.10A and B). Although the values of SPG are greater than the accumulation rates identical trends are observed in both, and it is these trends that will be described below.

Although abundance fluctuates through the core, a general trend is seen. Relatively high values are observed through the Upper Albian until a maximum abundance of 130769 SPG and 78670 species per cm^3 per kyr is observed in the *R. appenninica* zone ~146 mbsf. Following these peak values low abundances are observed through the rest of the Upper Albian until the mid-Cenomanian. Abundance increases briefly in the *R. cushmani* Zone, before decreasing to zero through the CTB barren zone. Immediately following the CTB abundance again increases sharply in the *W. archaeocretacea* Zone at ~135.5 mbsf. Following this peak values decrease again, before slowly rising in abundance through the Lower Turonian

Planktonic diversity (Figure 4.11E and G) is moderate in the Upper Albian with an average of 7 species observed. Diversity is seen to increase through the Cenomanian to an average of 8 species per sample coincident with the diversification of *Rotalipora* spp. Diversity decreases towards the top of the Upper Cenomanian, before becoming reduced to zero over the CTB. Diversity increases slowly through the lower part of the early Turonian *W. archaeocretacea* Zone to 4, before increasing markedly to an average of 14 in the *D. hagni* Zone.

The species of planktonic foraminifera present can be easily split into the four planktonic morphotypes outlined in Chapter 2. These results can be seen in Figure 4.13.

It can be seen that the planktonic specimens are dominated by unkeeled trochospiral species throughout the core, predominantly hedbergellids, *H. planispira* and *H. delrioensis*, with fewer numbers of *H. simplex and H. brittonensis,* and some species of *Whiteinella* in the Turonian part of the core. This dominance decreases in the Upper Albian, and at 145.25 mbsf, the abundance of *Hedbergella* falls to just 30% of the

planktonic assemblage, keeled forms of *Rotalipora* spp. dominating this portion of the core. Following this numbers of *Hedbergella* spp. increase and the genus returns to dominance by 144.50 mbsf. Through the top part of the Albian and Cenomanian abundance of the hedbergellids fluctuates between 70-100%, as species of *Rotalipora* become more abundant in the latest Albian and Cenomanian, before becoming extinct just below the CTB at 136.55 mbsf. It is interesting to observe through this portion of the core that *Rotalipora* spp. show a marked decrease in size, the number of *Rotalipora* spp. seen in the greater than 500μm peaking in the *R. appenninica* Zone at sample 16R-2, 85-87 cm (145.25 mbsf) with 29 individuals. Similarly in the less than 500μm size fractions the average size can also be seen to decrease, this will be discussed further in section 4.8.

Proportions of unkeeled trochospiral specimens decline again around the CTB along with all planktonic groups, leading to several parts of the core barren of planktonic foraminifera at 135.80-135.50 and 134.71 mbsf. Following the CTB unkeeled trochospiral specimens of *Hedbergella* and *Whiteinella* increase in numbers and again dominate the planktonic assemblages, however at lower proportions as numbers of keeled *Dicarinella* spp. and *Praeglobotruncana* spp., and species of unkeeled planispiral and elongate bi-triserial morphotypes increase through the Turonian, and more diverse planktonic assemblages are seen. Particular increases are seen in species of *Heterohelix,* and *Schackoina* and *Globigerinelloides,* which although present through the core show a marked increase in abundance at the base of the Lower Turonian *Dicarinella hagni* Zone.

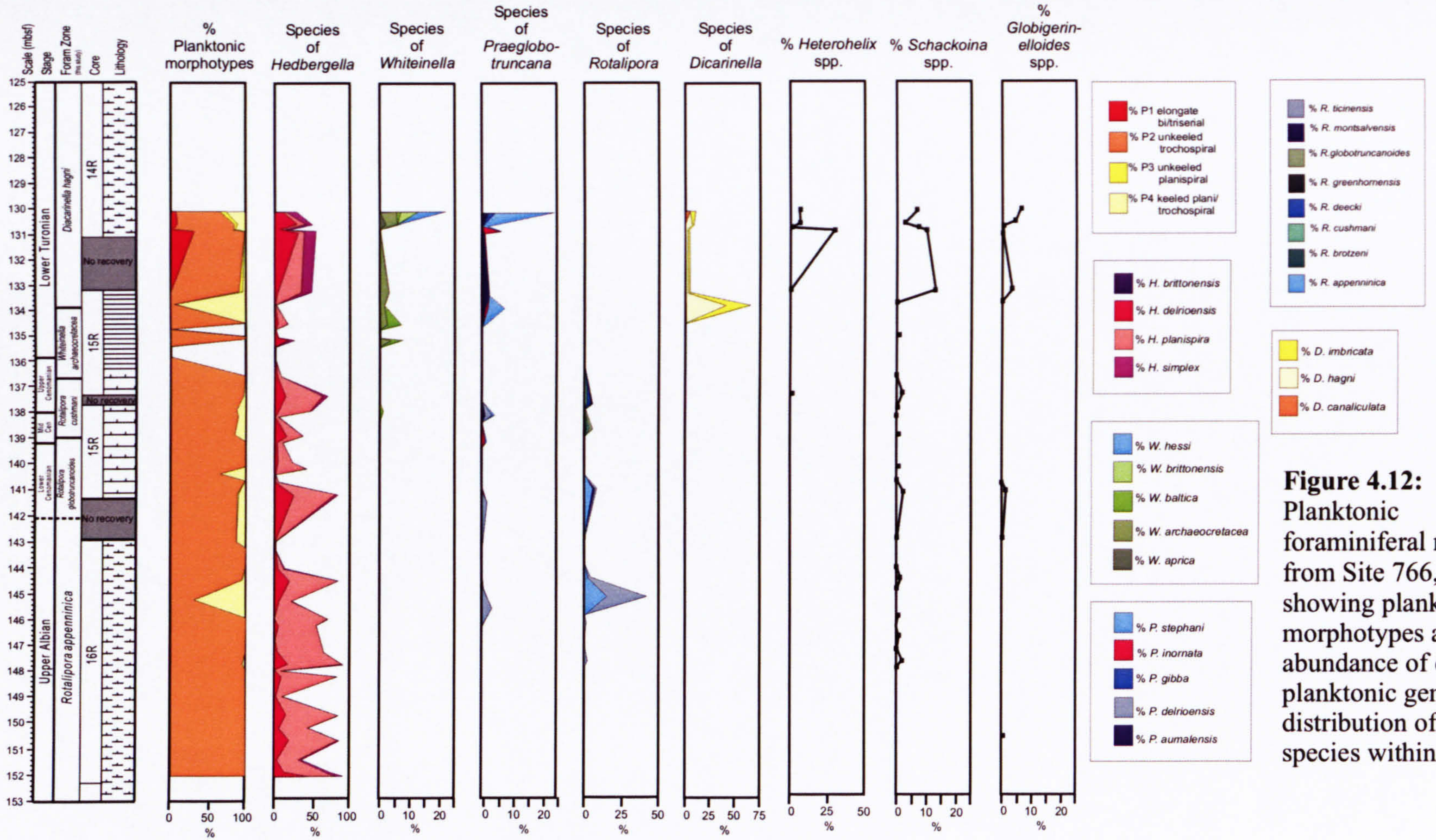

Figure 4.12: Planktonic foraminiferal results from Site 766, showing planktonic morphotypes and the abundance of each planktonic genus and distribution of species within each

4.6.1.3 Benthonic foraminiferal distribution

The abundance of benthonic foraminifera is shown in Figure 4.11 C and D. Although present in much lower numbers than the planktonic specimens, distinct trends in abundance can be observed. As before the results are illustrated as both SPG and accumulation rates, similar trends being observed in both. Although fluctuating through the core, abundance remains relatively low through the Upper Albian. Into the Cenomanian abundances increase markedly, peaks reaching values 3 times greater than those observed through the Upper Albian. Fluctuating greatly peaks are seen in the *R. globotruncanoides* Zone at 140.65 mbsf, in the *R. cushmani* Zone at 138.15 mbsf, and in the *W. archaeocretacea* Zone just before and after the CTB barren zone at 136.55 and 135.00 mbsf. Following this final peak values decrease markedly and remain low through the Lower Turonian.

The diversity of all benthonic foraminiferal specimens is also illustrated in Figure 4.11 G and H. Species richness (Figure 4.11 G) shows similar trends to the Fisher alpha index (Figure 4.11 H), however the Fisher alpha index takes into account the number of specimens as well as the number of species and shows a much smoother graph with less fluctuations than are observed in species richness. Generally diversity can be seen to decrease through the Upper Albian, increasing slightly in the Cenomanian before declining at the top of the Cenomanian just prior to the CTB. Following the barren zone diversity increases into the Lower Turonian.

These benthonic specimens can be simply divided into those with a calcareous test, and those with an agglutinated test. Figure 4.11 I shows the ratio of calcareous to agglutinated individuals within the benthonic assemblages. Calcareous species can be seen to dominate throughout the core, making up 80-90% of the benthonic specimens present. Following the extinction event of all foraminiferal species at the CTB, numbers of agglutinated specimens increase slightly, reaching a peak of 35% of the benthonic foraminifera at 133.75 mbsf, before returning to pre-extinction values of ~5 %.

Agglutinated benthonic specimens

Eighteen genera and 27 species of agglutinated foraminifera are seen at Site 766. Diversity is relatively constant throughout the Upper Albian and Cenomanian with around 7 species present, with a short increase to 11 species just below the Albian-Cenomanian boundary. Diversity declines rapidly to zero in sample 15R-2, 110-112 cm, and remains at zero through the CTB barren Zone. Species numbers begin to increase in the Lower Turonian, but not to pre-extinction levels reaching an average of 4.

Similar to the planktonic species, the benthonic foraminifera have been grouped according to their morphotype, as well as looking at the relative abundance of common species and genera. Most of the species of agglutinated foraminifera in this core occur sporadically and in low numbers. Looking at the species in terms of their morphotype and life mode, therefore, allows us to compare the main trends of foraminiferal change within the core. A number of specimens however, do occur in larger numbers dominating the benthonic agglutinated assemblages, these are *Gaudryina* ex. gr. *dividens*, *Gaudryina pyramidata*, and *Tritaxia gaultina* and *Tritaxia* cf. *gaultina*. These results can be seen in Figure 4.13.

Gaudryina ex. gr. *dividens* shows a bimodal abundance through the core. Present in the Upper Albian at abundances up to 5.98% it becomes absent, or present in only very small numbers, until the *W. archaeocretacea* Zone where abundances increase to 10.16% at the base of the Lower Turonian. It is interesting to note the morphology within this species varies throughout the core, those in the upper parts of the core showing a longer biserial to uniserial phase than those in the Upper Albian.

Gaudryina pyramidata ranges from the Upper Albian (147.75 mbsf) to the Lower Turonian (130.60 mbsf). Over this range specimen numbers increase gradually in abundance to a peak of 7.28% at 140.65 mbsf, in the middle of the *R. globotruncanoides* Zone. Abundance then decreases gradually until specimens of *G. pyramidata* dissappear in the Lower Turonian.

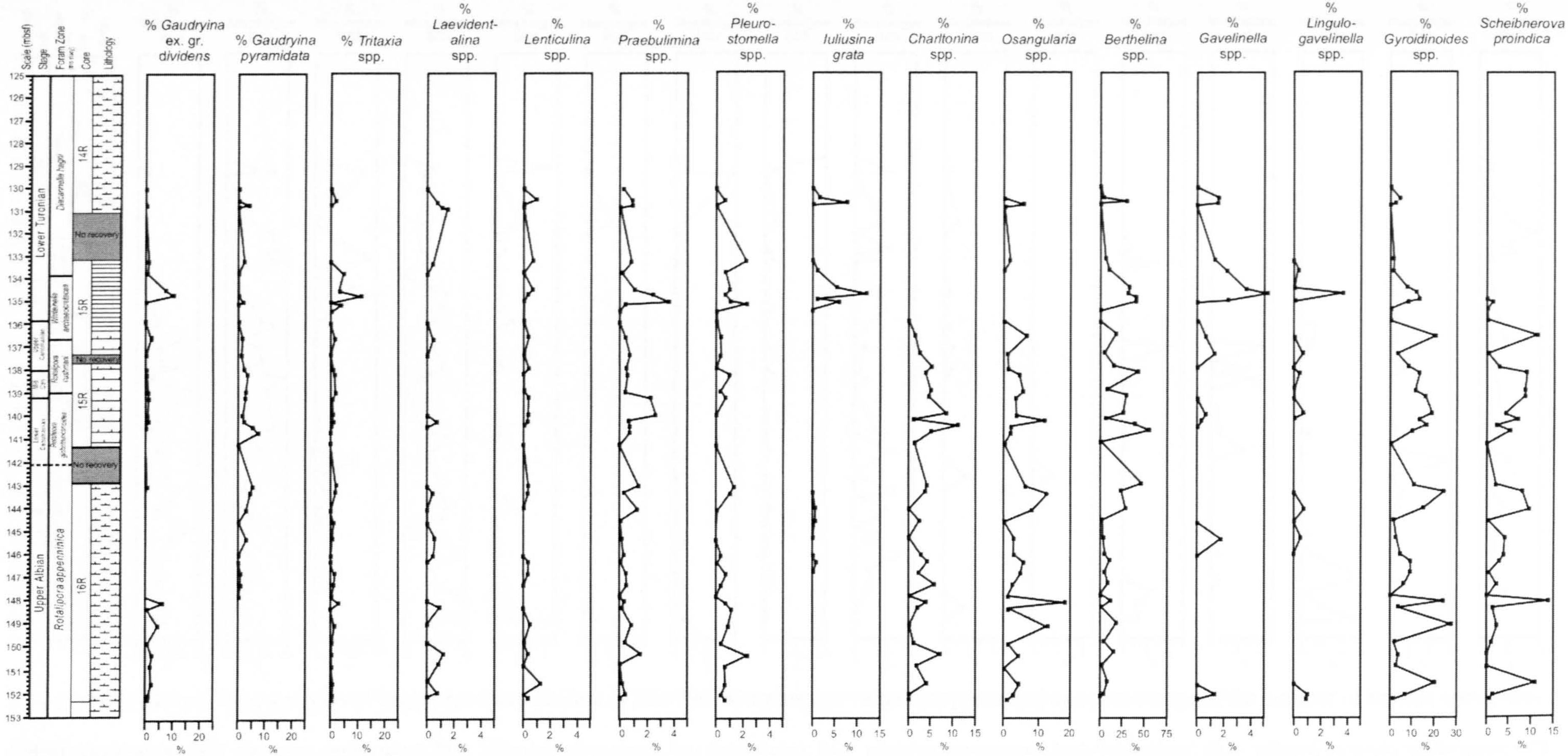

Figure 4.13: Benthonic foraminiferal results from Site 766.

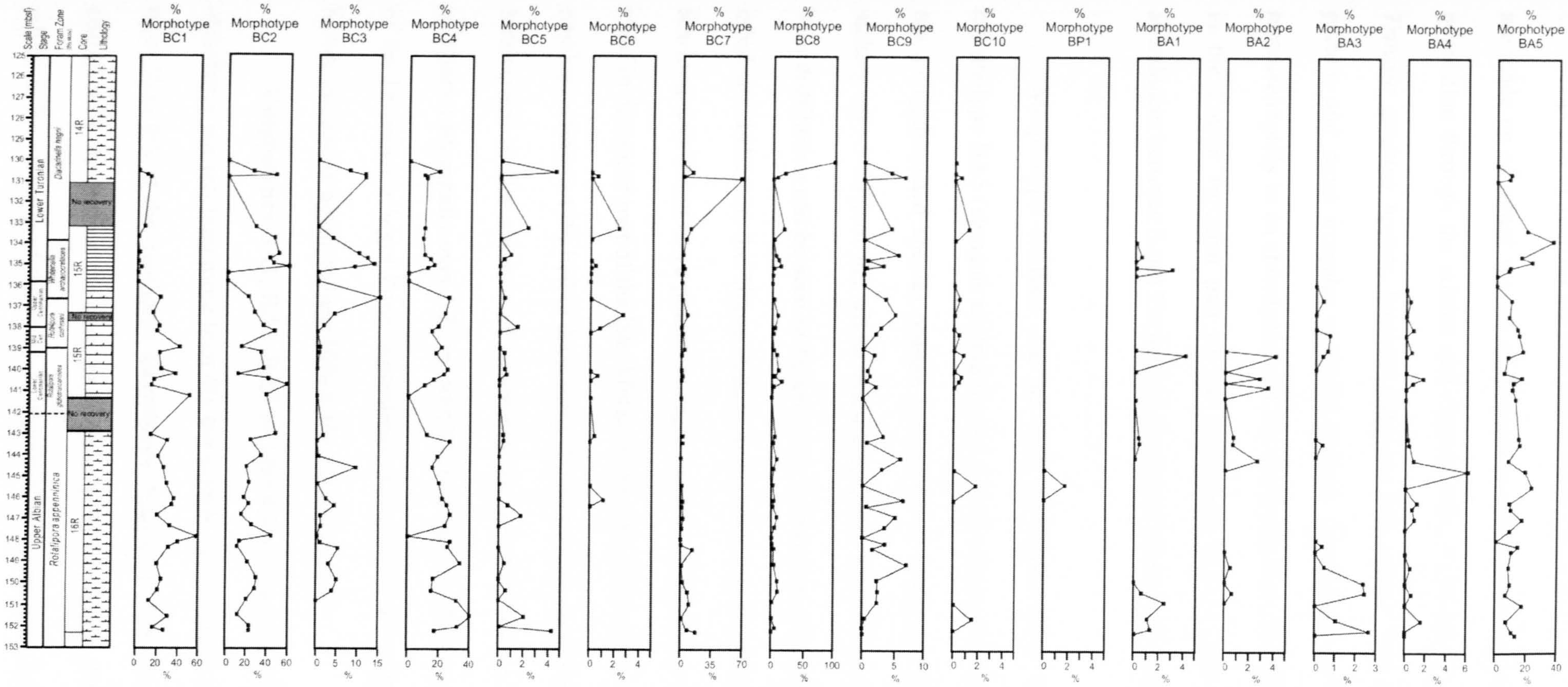

Figure 4.14: Morphotype analysis of benthonic foraminifera at Site 766. Morphotype values are presented as a percentage of the number of benthic specimens.

Calcareous hyaline: BC1 biconvex, trochospiral; BC2 plano/concavoconvex, low trochospiral; BC3 plano/concavoconvex, high trochospiral; BC4 inflated, biconvex trochospiral; BC5 biconvex, lenticularm planispiral; BC6 Globular/ovate; BC7 elongate, straight to arcuate, broad to narrow, uniserial; BC8 tapered rounded, elongate tri-bi-uniserial; BC9 tapered flattened, elongate, biserial; **Porcellaneous:** BP1 elongate to ovate quinqueloculine; **Agglutinated:** BA1 tubular or branching; BA2 globular; BA3 planispiral/streptospiral, subsphaerical/flattened; BA4 low trochospire/streptospiral, sphaerical/subsphaerical; BA5 elongate, variably coiled, uni-multiserial.

Species of *Tritaxia* are also present throughout the core. Up to the CTB specimens are made up of robust species of *Tritaxia gaultina* a making up to 3% of the benthonic population through the Albian and Cenomanian. Following the CTB species similar to *Tritaxia gaultina* appear, however they are less robust, with a more elongate triserial portion and more irregular uniserial portion. Specimens of this *Tritaxia* cf. *gaultina* increase rapidly to an abundance of 11%, following the CTB barren zone, at 134.71 mbsf in the Lower Turonian part of the *W.archaeocretacea* Zone. They then decrease to abundances between 0 and 2% through the rest of the Lower Turonian.

Morphotype analysis can be seen in Figure 4.14. At Site 766 agglutinated morphotype BA5 (elongate uni/multiserial forms) is the most abundant, made up of 20 of the 27 agglutinated species present in Site766. It is present throughout the entire core making up ~5-10% of the whole assemblage, and 10-20% of the benthonic assemblage. This distribution can be seen in Figure 4.14. A decrease in numbers is observed at 147.45 mbsf and 141.15 in the Upper Albian and Lower Cenomanian respectively, abundance reaching near 0% at these points. A slight increase in abundance is seen to 23% at 145.25 mbsf in the upper part of the late Albian. Following the decline in the Lower Cenomanian numbers return to 17% before decreasing slowly towards the CTB.

Subsequent to the absence of specimens in the CTB barren Zone, diversity of BA5 increases very rapidly over 1.75 m from 0% to a high of 35.29% at 133.75 mbsf at the base of the *Dicarinella hagni* Zone. Abundance then decreases rapidly to 0% at 130.88 mbsf, before increasing again, to near 10% at the top of the core.

Morphotypes BA1, BA2, BA3 and BA4 are seen in much lower proportions, their abundance not reaching more than 4% per sample of the whole assemblage, or making up more than 6% of the benthonic assemblage. Species of BA1 (tubular forms) are present sporadically throughout the core, peaking at 4.1% in sample 15R-4, 145-147 cm (139.15 mbsf) at the very top of the *R. globotruncanoides* Zone. BA2 (globular) morphotypes are

only present from the Upper Albian to the Lower Cenomanian, becoming extinct at the top of the *R. globotruncanoides* Zone, present in only small numbers at the base of the core (~0.5%) numbers increase at the top of the Albian and peak in *R. globotruncanoides* Zone with a maximum abundance of 4% at the very top of this zone. BA3 (strepto/planispiral, subsphaerical to flattened) morphotypes, similar to BA1 are sporadic through the core, reaching abundances of no more than 3% within the benthonic population. BA3 species are however generally more abundant in the lowest part of the core in the Upper Albian. BA4 (rounded streptospiral/low trochospiral) morphotypes are made up of only one species in this core, *Ammosphaeroidina* sp. 1. This species is most abundant in the Upper Albian, reaching a peak abundance of 6.25% at 144.50 mbsf, before becoming extinct at the CTB,

Calcareous benthonic specimens

Fifty two genus and 110 species of calcareous benthonic foraminifera are seen at Site 766, dominating the benthonic assemblages. Diversity is quite high throughout the core with around 20 species present in each sample. However, short decreases in diversity are seen, with species numbers becoming reduced to less than 5 species in the Upper Albian, at 147.74 mbsf, and Lower Cenomanian, at 141.15 mbsf. Diversity decreases to zero in the CTB barren zone.

The calcareous assemblages are dominated by epifaunal trochospiral species, particularly species of *Berthelina, Gyroidinoides* and *Osangularia*. Species of *Praebulimina, Iuliusina, Charltonina* and *Schiebnerova* are also prominent in the assemblages, with lower values of *Laevidentalina, Lenticulina, Pleurostomella, Lingulogavelinella, Gavelinella* and *Valvulineria*. Other species present are low in number and sporadic throughout the core. All results can be seen in the range chart (Figure 4.9) and as abundance graphs in Figure 4.13.

Species of *Berthelina* are by far the dominant genus, making up to 55% of the foraminiferal assemblages in the Lower Cenomanian. The abundance of *Berthelina*

increases through the core. However this does fluctuate and values of only ~7% are seen in the lower part of the Upper Albian. At 144 mbsf, at the top of the Albian, abundance increases markedly to 28.4%. Although the abundance continues to fluctuate (related to the P:B ratio) values generally remain high, gradually increasing to a peak of 54.6% at 140.65 mbsf in the early Cenomanian. Abundance then decreases slowly to zero at the CTB. Following the CTB barren zone values increase instantly to 39.3% before decreasing again through the rest of the Turonian. Species of *Praebulimina, Pleurostomella, Iuliusina, Gavelinella, Lingulogavelinella* and *Gyroidinoides* also show this sudden short-lived increase following the CTB barren zone. Similarly species of *Charltonina, Osangularia, Gyroidinoides* and *Schiebnerova* show the same increase and decrease in abundance as *Berthelina* spp. through the Cenomanian, and species of *Pleurostomella, Osangularia, Gyroidinoides* and *Schiebnerova*, along with *Berthelina* show a peak in abundance at the top of the Upper Albian around 144 mbsf.

Species of *Gyroidinoides, Osangularia* and *Schiebnerova* show a slightly different trend to *Berthelina* and show their peak abundances at the base of the core in the Lower Albian. Although abundance decreases through the upper part of the Upper Albian, abundances generally remain high through the Cenomanian before becoming extinct or reduced to very low numbers after the CTB.

As before the calcareous foraminifera were grouped as morphotypes and the results are shown in Figure 4.14.

The calcareous benthonic assemblages are dominated by BC1 (bi/planoconvex trochospiral), BC2 (plano/concavoconvex low trochospiral) and to a lesser extent BC4 (inflated bi/planoconvex). Both BC1 and BC2 have maximum benthonic abundances of near 60% and are present throughout the core. However, whilst BC1 has its highest numbers in the Albian, BC2 peaks in the Lower Turonian.

BC4 is present in lower abundances but dominates the lower part of the upper Albian with a peak abundance of 40% at 151.5 mbsf. Abundance of this group fluctuates

through the rest of the core, with a general decrease in values from 40 to 20%.

The remaining morphotypes, although present at much lower abundances, still show defined changes through the core. BC3 (plano/concavo convex, high trochospire), BC5 (lenticular planispiral), BC7 (elongate, uniserial or planispiral to unsiserial) and BC8 (tapered elongate rounded) all show initial increases in abundance in the lower part of the Albian, followed by a decrease in abundance through the upper part of the Albian and lower to mid-Cenomanian. A slight increase in numbers is seen prior to the CTB barren zone, followed by a large increase in the Lower Turonian following the CTB. BC 6 (globular, ovate) shows the same increase before and after the CTB, but is present only in very low numbers (<0.5%) through the Cenomanian and absent completely from the lower part of the Upper Albian sediments. BC9 (tapered, flattened) shows highly variable abundances through the core, however peak values remain relatively constant around 6.5% from the Albian to Turonian, with just a small decrease in values to 1-2%, from the top of the upper Albian (142.98 mbsf) to the top of the mid-Cenomanian (137.90 mbsf). BC10 (irregular meandrine) are low in number and sporadic through the core.

One final morphogroup not yet mentioned is BP1 which includes those porcelaneous species that are elongate to ovate quinqueloculine in shape. Only one specimen of *Quinqueloculina antiqua* was seen at site 766, in sample 16R-2, 85-87 cm (145.25 mbsf) from the upper part of the Upper Albian.

4.6.1.4 Life mode

Analysis of morphotypes also enables the inferred life mode of each group to be determined, whether epifaunal, infaunal or a species which can live both infaunally and epifaunally. Although determining the life mode of fossil species can be difficult, the use of morphotype analysis and comparison to similar species present in the oceans today can be of use (Koutsoukos and Hart, 1990). The life mode of each group can also be

determined by isotope results which can be used to establish the life habitat depending on the isotope values seen (Wilson *et al.*, 2002). This is discussed further in Section 4.8.

Results from the life mode analysis can be seen in Figure 4.11. It can be seen that epifaunal species dominate through the core particularly in the Albian and Cenomanian, averaging ~55% and reaching peak dominances of 100% and 87.5% in the Upper Albian (147.75 mbsf) and Lower Cenomanian (141.15 mbsf) respectively. Following the CTB barren zone however, epifaunal abundance is reduced from 75% to 22% with an increase in infaunal and shallow infaunal species.

4.6.1.5 Other biota found at Site 766

Figure 4.2 shows the presence of other components within Core 766. Radiolaria, ostrocods and calcispheres are seen through the core, however a large increase is seen, particularly in radiolaria, but also in calcispheres. Fish teeth and shell fragments are also seen throughout the core.

4.6.2 Isotope results

Isotopic analysis was carried out on both fine fraction and foraminiferal samples. The results of both are outlined below. The raw data can be seen in Appendix 3, and analytical data is presented in Figures 4.15.

4.6.2.1 Fine fraction samples

Ninety six samples were measured for fine fraction isotope analysis over 25 m of Albian to Turonian sediments.

Carbon isotope results

$\delta^{13}C$ values at Site 766 show fluctuations throughout, general trends however can be seen, and an overall increase in $\delta^{13}C$ values through the core to a peak at the CTB,

followed by a decrease in values through the Turonian is evident. Carbon isotope values are at 3.1‰, 152 mbsf, at the base of the *R. appenninica* Zone. Through the *R. appenninica* Zone values reach a maximum 3.79‰ at 149.25 mbsf, but generally remain around 3.2‰, with a slight increase to 3.5‰ at the top of the Upper Albian.

Values continue to increase gradually through the Cenomanian until a peak of 4.1‰ in sample 15R-3, 35-37 cm (136.55 mbsf) at the base of the *Whiteinella archaeocretacea* Zone. A lack of carbonate over the CTB barren Zone prevents analysis of this section of the core and following this zone $\delta^{13}C$ values have decreased slightly to 3.6‰. Values continue to decrease to 3.4‰ at the base of the *Dicarinella hagni* Zone, sample 15R-1, 5-7 cm (133.25 mbsf). A gap in the core following these values creates a 2.5 m interruption in the isotope data. Following this gap values increase rapidly to 4.0‰ at 130.79 mbsf. However, in this final part of the core $\delta^{13}C$ values fluctuate much more than in the earlier sediments. Despite these fluctuations the values show a general decrease to ~3.2‰ at the top of the core, similar to pre-excursion values.

Oxygen isotope values

Similar to the $\delta^{13}C$ results the oxygen isotope values fluctuate throughout the core, but generally show less variation than seen in the carbon isotopes. Generally the values are relatively constant through the Albian and Cenomanian, decreasing rapidly through the Upper Cenomanian to the CTB, followed by a gradual increase through the Lower Turonian.

The Upper Albian $\delta^{18}O$ values show nearly constant values ~-1.9‰, with some slight fluctuations between -1.7 and -2.2 ‰. Values increase slightly at the top of the Lower Cenomanian *R. globotruncanoides* Zone to -1.4 but are seen to decrease again to a constant value of ~-1.7‰ through the Cenomanian, until the top of the *Rotalipora cushmani* Zone.

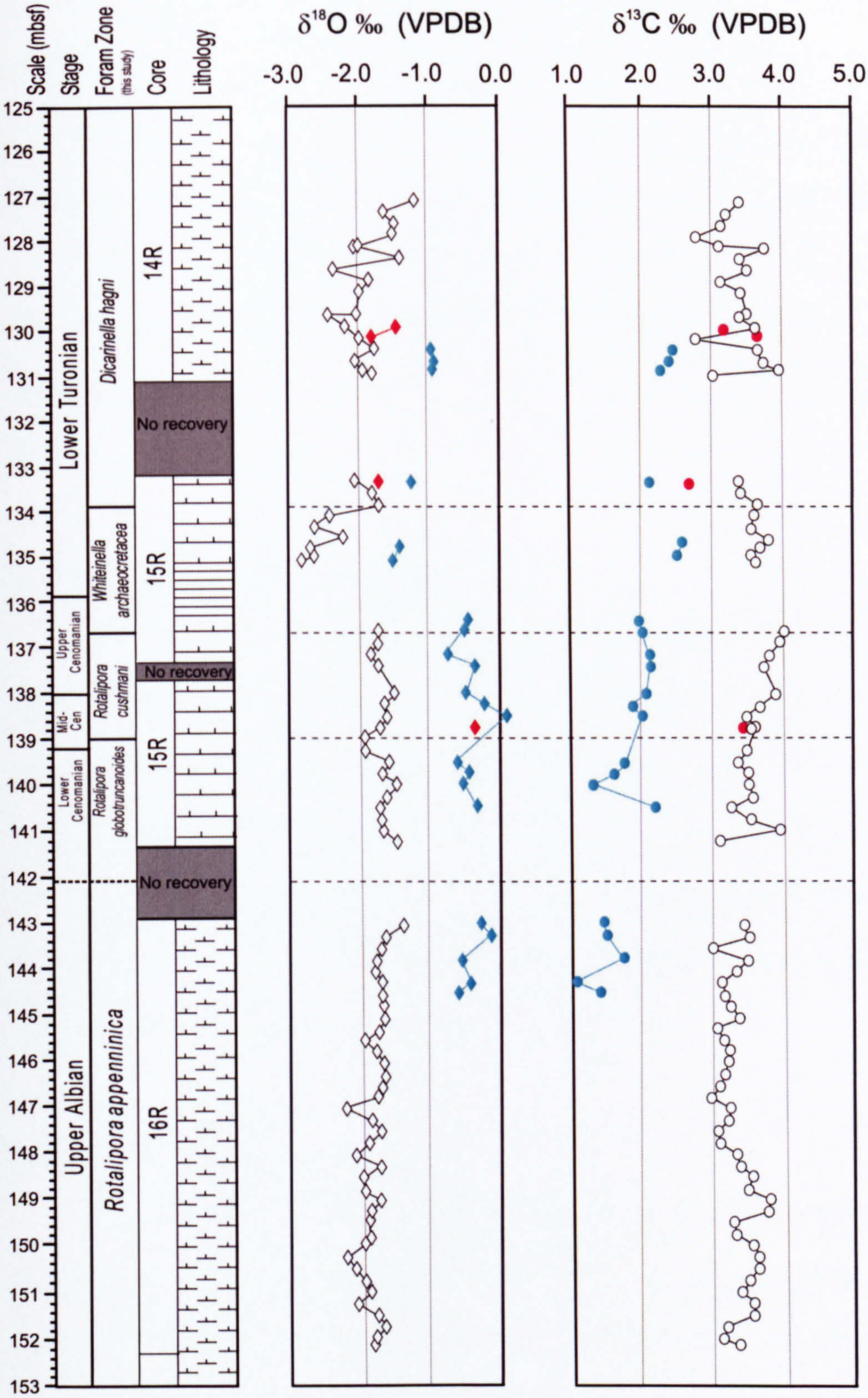

Figure 4.15: Isotopic results from Site 766. Fine fraction isotope results are shown in white. Benthonic foraminiferal results from the genus *Berthelina* are shown in blue, and planktonic foraminiferal results from species of *Hedbergella* are shown in red. Dashed lines indicate the Biozone boundaries.

Following the CTB barren zone, values can be seen to have decreased markedly to -2.8‰ in sample 15R-2, 30-32 cm (135.00 mbsf). Values then increase more gradually to -1.72‰ at the very top of the *W. archaeocretacea* Zone, before levelling out to ~-2.0‰ through the *D. hagni* Zone, and increasing gradually to -1.2‰ at the top of the core.

Similar to the $\delta^{13}C$ results, $\delta^{18}O$ values also fluctuate greatly in the *D. hagni* Zone. This may be due to the rapidly fluctuating lithology in this part of the core and reflect changes in the carbonate values of the sediments, this will be discussed further in Section 4.8.

4.6.2.2 Foraminiferal isotope results

The dominance of small planktonic foraminifera through Core 766A and lack of the larger sized foraminifera limited the isotopic foraminiferal analysis in this core. Keeled foraminifera were unfortunately not abundant enough in the core samples to enable analysis, and the small size of trochospiral hedbergellid species meant it was difficult to pick enough sample for analysis of many of the samples. Benthonic planoconvex, trochospiral species of *Berthelina* were, however, abundant and of an appropriate size to allow analysis of this genus through portions of the core.

Benthonic foraminiferal results

The benthonic foraminiferal genus *Berthelina* shows $\delta^{13}C$ values of 1.4‰ in the upper part of the *R. appenninica* Zone. Values increase slowly through the Cenomanian to a peak of 2.6‰ at the *W. archaeocretacea-D. hagni* boundary. Values can then be seen to remain ~2.5‰ through the Lower Turonian.

In comparison with the $\delta^{13}C$ values of the fine fraction analyses, *Berthelina* spp. show consistently lower values. In the uppermost Albian a difference of ~2.0‰ is seen. This difference deceases slowly through the Cenomanian and by the top of the *W. archaeocretacea* Zone there is only a 1‰ difference in values. This difference remains

through the Turonian, becoming slightly more reduced in the middle of the *D. hagni* Zone around 130 mbsf.

Values of $\delta^{18}O$ are consistently higher than the fine fraction samples. *Berthelina* spp. show values between 0 and -0.5‰ through the Albian and Cenomanian. These values can then be seen to decrease slightly to -1.5‰ at the top of the *W. archaeocretacea* Zone, before increasing to -0.9‰ in the *D. hagni* Zone around 130.5 mbsf.

Similar to $\delta^{13}C$ values, the $\delta^{18}O$ values show a comparable difference between benthonic and fine fraction samples. This offset is large in the Albian with an difference of ~1.5‰. This remains constant until the top of the *W. archaeocretacea* Zone where only a difference of 0.4‰ is seen. By the *D. hagni* Zone the offset has increased again, and is seen to be 1.1‰ in the middle of the zone at 130.6 mbsf.

Planktonic foraminiferal results

Planktonic isotope analyses are very few at Site 766. However the few that have been obtained show an affinity with the both $\delta^{13}C$ and $\delta^{18}O$ values obtained from the fine fraction analyses. This can be seen in Figure 4.15. Two anomalous values exist, however, the first in sample 15R-1, 5-7cm (133.25 mbsf) the $\delta^{13}C$ value lying between that of the benthonic foraminifera and fine fraction result, at 2.7‰. The second at 15R-4, 95-97cm (138.65 mbsf) the $\delta^{18}O$ value nearly identical to that of the *Berthelina* spp. at -0.3. These anomalous values are thought to be due to sampling bias or diagenesis and are therefore not considered in the analysis of these results.

4.6.3 Geochemical results

4.6.3.1 TOC analysis

TOC values were measured throughout the core with all samples within the CTB claystone being analysed. Values were seen to not reach more than 0.1 % in any sample and RockEval was not able to determine any results from these samples.

4.6.3.2 Trace element analysis

Each of the 96 samples analysed for isotopes were also analysed for trace elements, iron, magnesium, manganese, strontium and calcium. The raw data are shown in Appendix 3, and the analytical data are presented in Figures 4.16 - 4.18. Results are shown as both ppm/kg and as calcium ratios, in order to look at the effect of lithology on the elemental values through the core.

Manganese, iron and magnesium all show relatively low background levels through the Albian and Cenomanian of Site 766, with a short, yet sharp increase seen at 145.00 mbsf in the Upper Albian. At the CTB all three again show an increase in values, reaching a high at 136.10 mbsf. However, whereas manganese returns to background levels very quickly, both iron and magnesium show a slight decrease, before peaking again near 133.50 mbsf in the lower part of the *D. hagni* Zone. Following this second peak values are reduced slightly but do not return to background levels, instead showing fluctuations of around 500 ppm in both curves, and a slight increase at the top of the core. Manganese values also show greater fluctuation in this upper part of the core, but at a much lower magnitude of ~150 ppm.

Strontium and calcium show very different traces to manganese, iron and magnesium, although calcium shows much higher concentrations. Generally their values show a much greater fluctuation through the core than the first three elements. However, a distinct trend in values can be seen. Values begin relatively constant at the base of the core, but decrease through the upper part of the Upper Albian into the Lower Cenomanian, reaching a low at 140.90 mbsf. A gentle increase is then seen to a peak at the top of the mid-Cenomanian followed by a decrease to very low concentrations over the CTB barren zone. Following this low, values increase again over the Turonian to a high at 130.88 mbsf in the middle of the *D. hagni* Zone before decreasing again over the upper portion of the core. Similar to manganese, iron and magnesium the fluctuation in values reaches a high in this upper portion of the core.

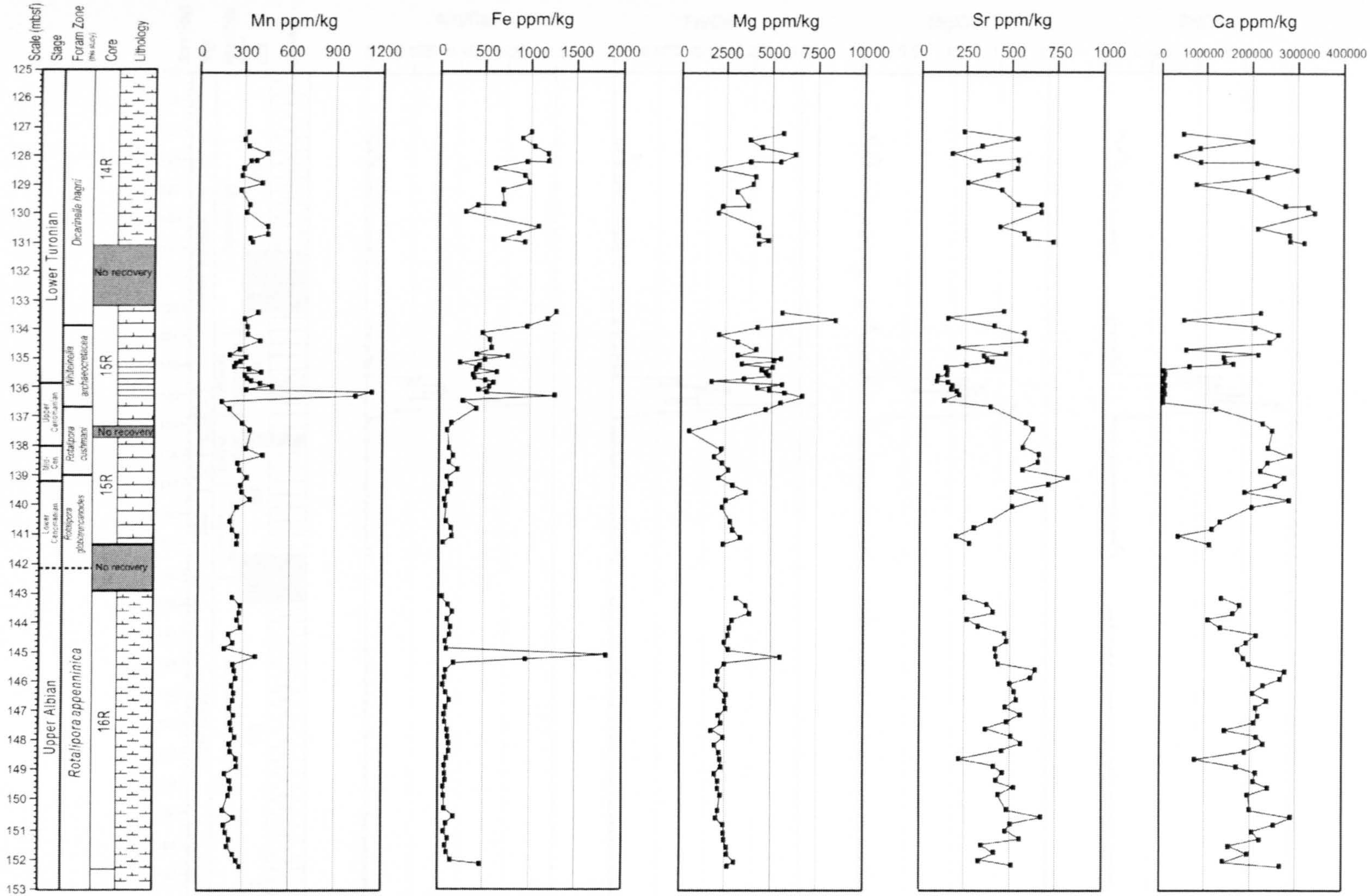

Figure 4.16: Results of geochemical analysis at Site 766 shown as ppm/kg

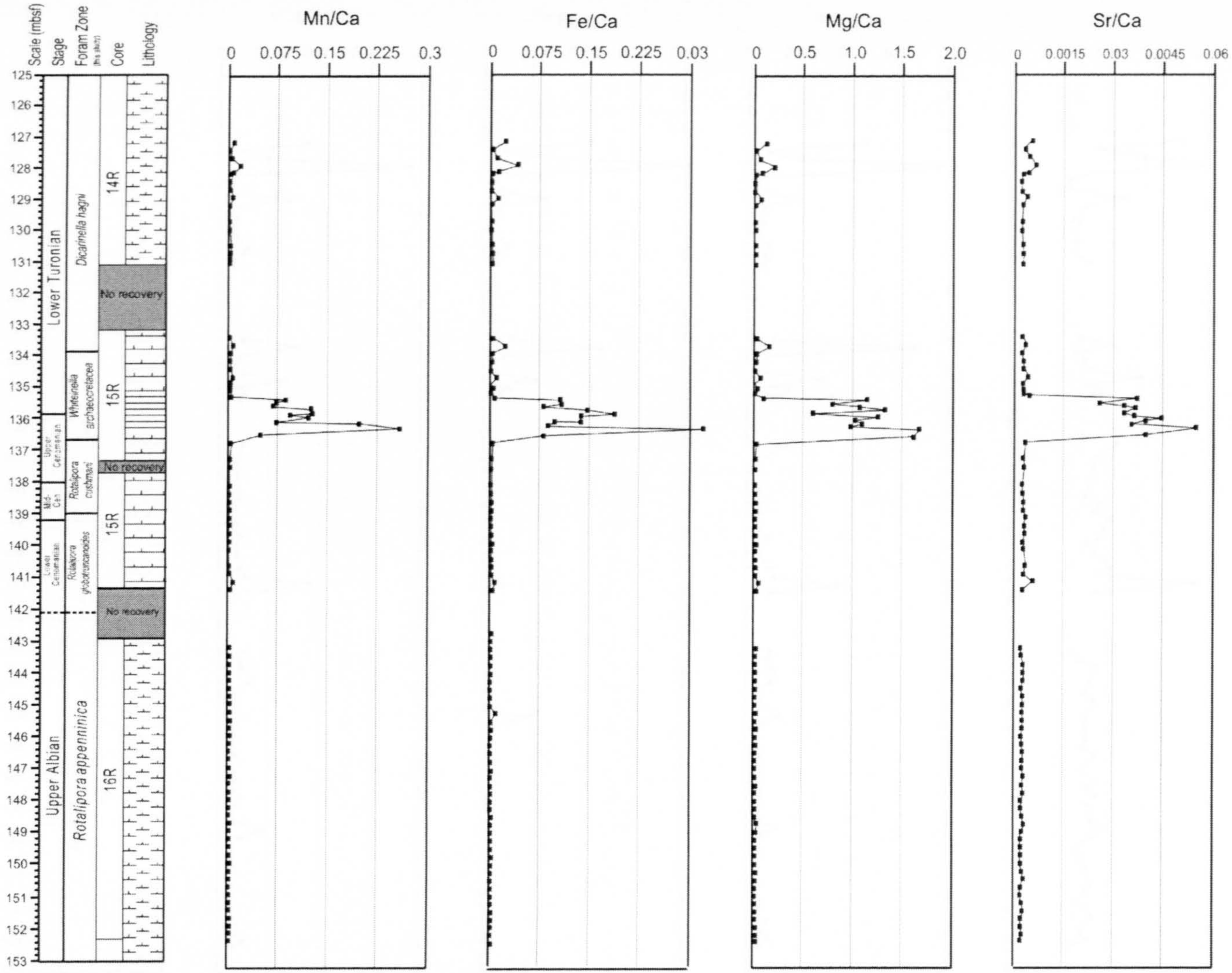

Figure 4.17: Results of geochemical analysis at Site 766 shown as a ratio against Calcium.

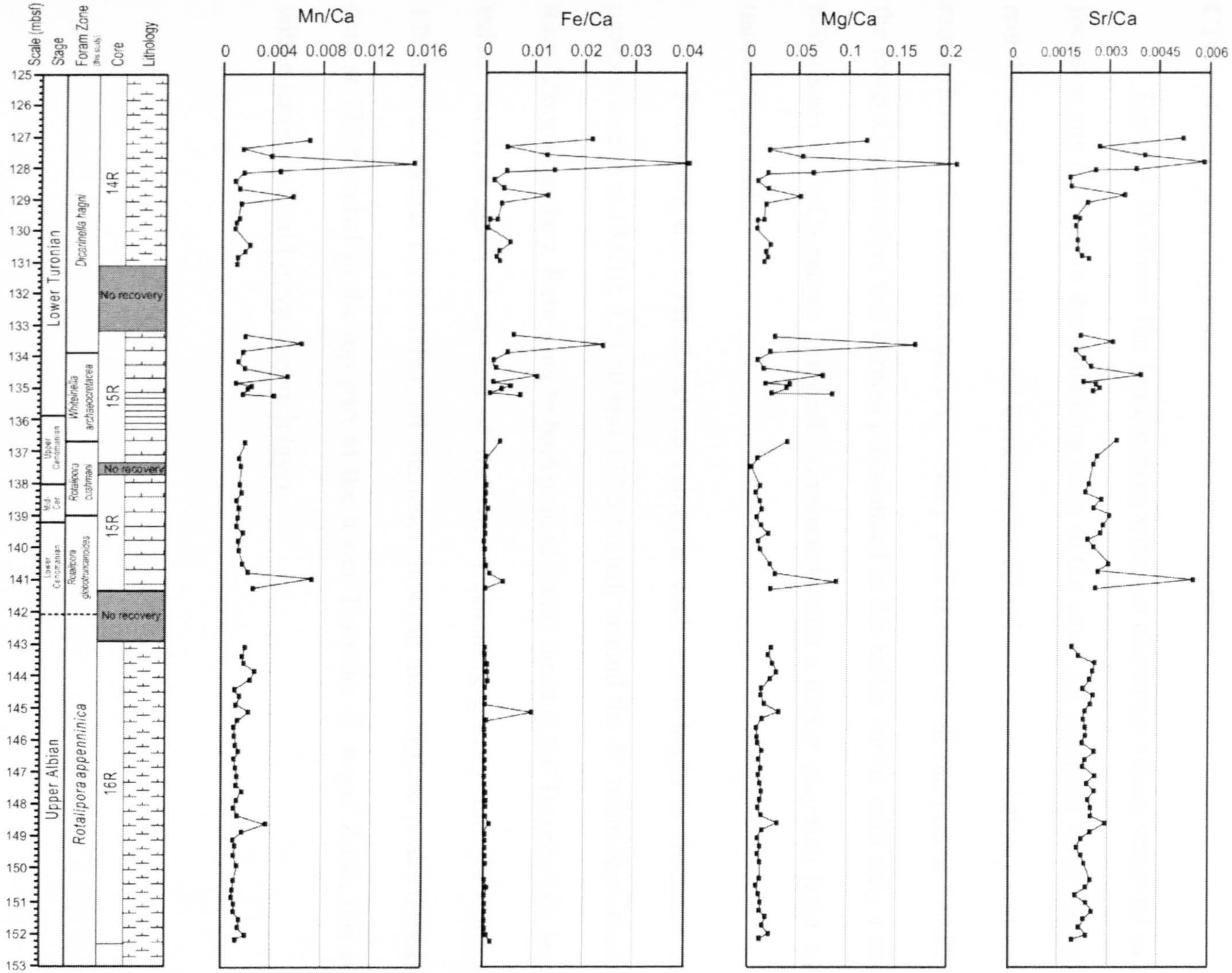

Figure 4.18: Results of geochemical analysis from Site 766. Results are shown as a ratio against calcium and the very high values have been removed in order to show the smaller scale fluctuation with the core

In order to eliminate bias in the results from changes in lithology, each trace element was also plotted as a ratio with calcium. These results are seen in Figure 4.17 and 4.18. In Figure 4.17 it can be seen all elements show a very distinctive curve, values remaining extremely low throughout the core, with increased values being seen over the CTB carbonate poor claystone.

Figure 4.18 shows the same curves with the claystone values removed in order to focus on any changes in the remaining parts of the core. All elements show the same trend and through the upper Albian and Cenomanian all values remain relatively constant, Sr/Ca ratios showing the most fluctuation. A sharp peak is seen in all samples at 140.90 mbsf in the lower Cenomanian, this is most pronounced in the Sr/Ca curve, with only a small peak being seen in Fe/Ca ratios, this peak corresponds with a darker clay rich layer within the nannofossil chalks.

Following the CTB claystone values in each curve begin to fluctuate more and peaks are seen at 135.10, 134.50 and 133.50 mbsf, around the *W. archaeocretacea* and *D. hagni* Zone boundary. Returning to background levels through the Turonian *D. hagni* Zone values increase again at the top of the core fluctuating greatly and showing peaks at 128.85, 127.85 and 127.10 mbsf, all elements showing there highest peaks throughout the core at 127.85 mbsf in the top part of the lower Turonian *D. hagni* Zone, this coincides with a laminated red/brown clay rich layer.

4.7 Site 762

4.7.1 Foraminiferal results

The results of the foraminiferal distribution of species, genera and morphotypes are shown in Figures 4.19- 4.23. The main features of these distributions are discussed below.

4.7.1.1 Specimen and species distribution

Abundance

The abundance of specimens fluctuates throughout the core, this can be seen in Figure 4.19B and C, illustrated as both SPG and accumulation rate (number of specimens per cm^3 per kyr. Both show identical trends and are discussed below as SPG.

Starting at values of 20200 SPG, in the *R. reicheli* Zone, numbers remain between 15 and 20 thousand SPG through the *R. cushmani* Zone. A decrease to less than 650 SPG is seen at the very top of the *R. reicheli* Zone, however numbers quickly recover.

At the CTB numbers increase suddenly to 26500 SPG just before the claystone unit before plummeting to zero in sample 75X-1, 129-131 cm (810.79 mbsf). Foraminifera are present through the rest of the claystone unit but abundances remain low, reaching no more than 400 SPG. As samples become more carbonate rich through the lower Turonian abundance slowly increases, reaching pre extinction levels by sample 74X-2, 111-113 cm (807.11 mbsf).

Diversity

Species richness and the Fisher Alpha index both show similar trends representing diversity at site 762 (Figure 4.19 D-E).

Numbers are generally constant through the Cenomanian, species numbers fluctuating around 25 species per sample, whilst fisher alpha values are ~6.5. An increase to 29 species and a fisher alpha value to 8.73 is seen at 815.59 mbsf, at the top of the *R. reicheli* Zone coinciding with the low abundance numbers. At the CTB numbers begin to decrease

at the top of the *R. cushmani* Zone falling rapidly to zero in the barren zone.

Immediately following this low, diversity increases rapidly in the upper part of the claystone to a maximum of 30 species, coinciding with the low specimen numbers of these early Turonian samples. Diversity decreases again to 9 species in the lowermost Turonian, before quickly returning to relatively constant values between 15 and 20 species (fisher values of 3.5-5.5) in the rest of the Turonian of this core.

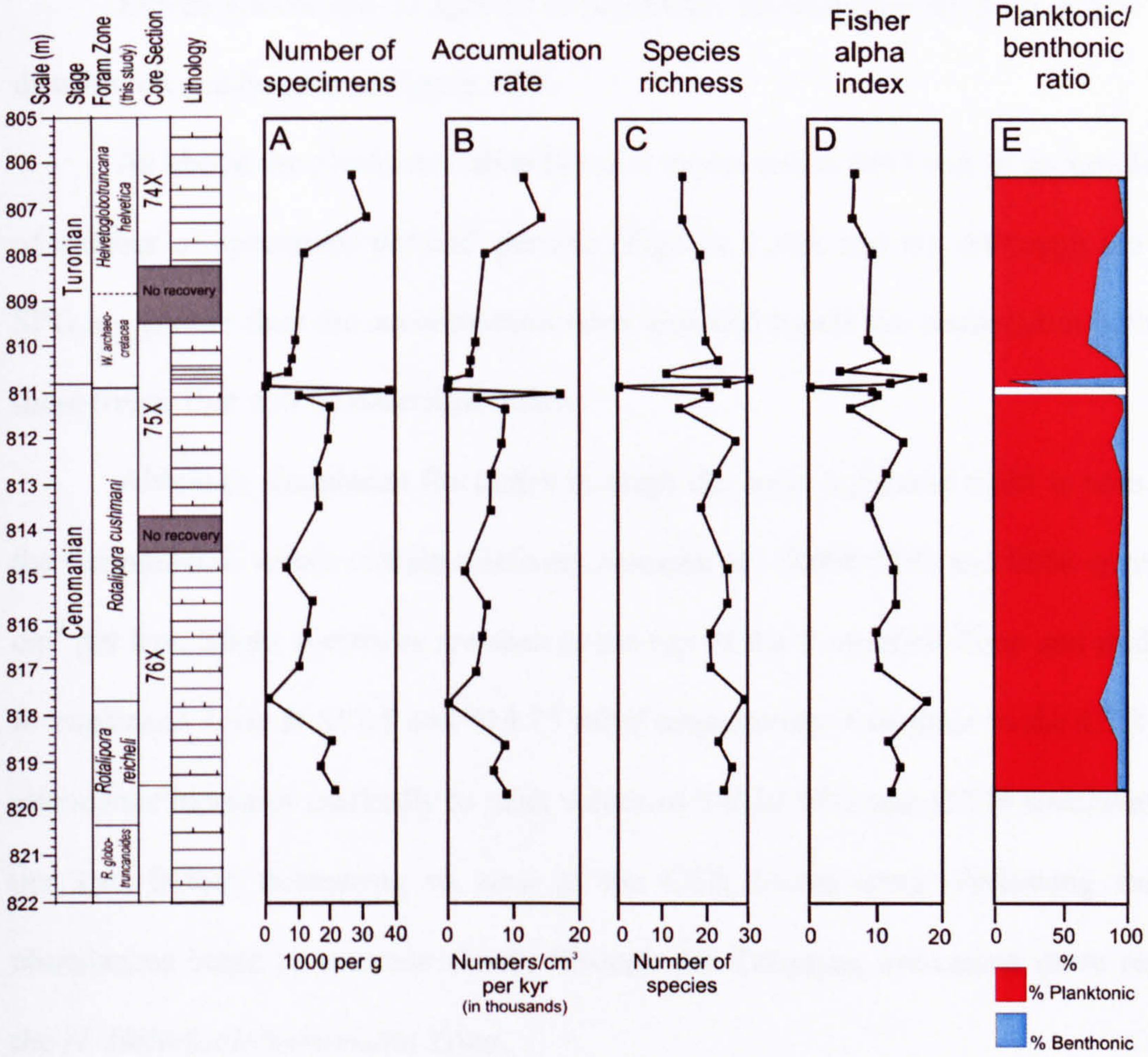

Figure 4.19: General foraminiferal results from Site 766.

Planktonic/benthonic ratio

Planktonic specimens dominate Site 766, generally making up over 90% of the assemblage, this can be seen in Figure 4.19 F. However the abundance of benthonic specimens does increase over a few portions of the core. Coinciding with the low abundance and maximum diversity values benthonic numbers increase to 20% at 815.59 mbsf. Similarly the abundance of benthonic specimens increases around the CTB,

increasing to 10% just prior to the barren zone and increasing to 90% in the claystone following the barren Zone. Although planktonic specimens regain dominance through the lower Turonian 20-30% of benthonic specimens are seen over this period. By the top of the core, however, planktonic species have returned to dominate 95% of the assemblage.

4.7.1.2 Planktonic foraminiferal distribution

Eleven genera and 33 species of planktonic foraminifera are seen at Site 762; their distribution can be seen in Figure 4.20.

As above the planktonic abundance is expressed as SPG and as accumulation rates of number of specimens per cm^3 per kyr (Figures 4.20A and B). Although the values of SPG are greater than the accumulation rates identical trends are observed in both, and it is these trends that will be described below.

Although abundance fluctuates through the core, a general trend is seen. Through the Cenomanian values remain relatively constant at ~20000 SPG and 8000 specimens per cm^3 per kyr. Slight decreases are seen at the top of the *R. reicheli* Zone and middle of the *R. cushmani* Zone at 817.5 and 814.75 mbsf respectively. Just prior to the CTB however, abundance increases markedly to peak values of 34810 SPG and 15734 specimens per cm^3 per kyr, before decreasing to zero in the CTB barren zone. Following this decline abundances begin to increase slowly through the Turonian, increasing more rapidly into the *H. Helvetoglobotruncana* Zone.

Diversity of planktonic species (Figure 4.20 E and F) remains relatively constant through the core with an average of around 11 species. A slight increase to 17 species is seen in the mid-Cenomanian at 815.47 mbsf, values return to background levels through the upper Cenomanian. Following the CTB barren zone diversity plummets to 8 species recovering to background levels in the upper part of the *W. archaeocretacea* zone 50 cm above the barren zone. Diversity remains constant throughout the remainder of the Turonian.

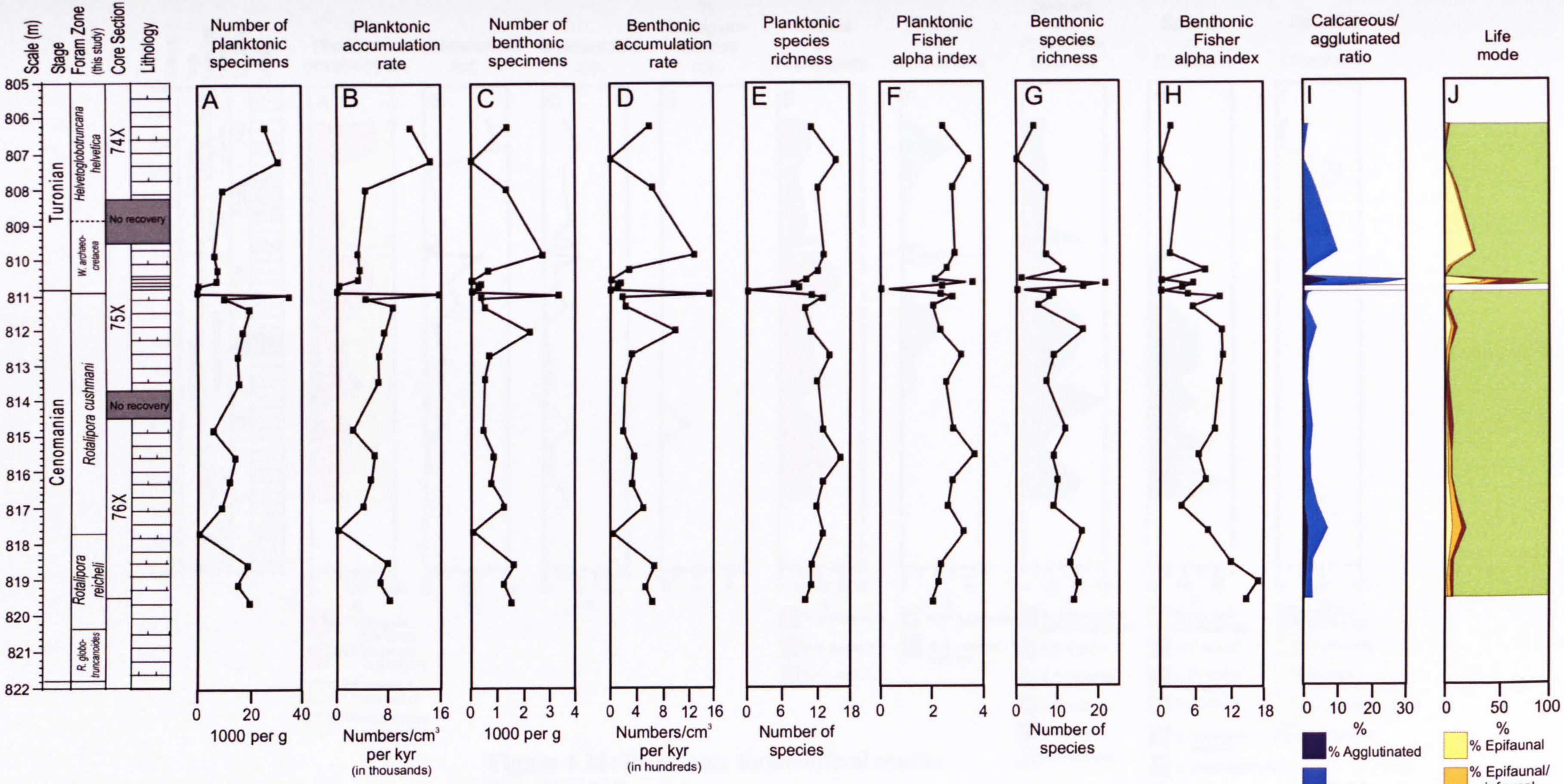

Figure 4.20: General planktonic and benthonic foraminiferal results for Site 762. A) Planktonic foraminiferal abundance; B) Planktonic accumulation rates; C) Benthonic foraminiferal abundance; D) Benthonic accumulation rates; E) Planktonic species richness; F)Planktonic Fisher alpha diversity index; G) Benthonic species richness; H) Benthonic Fisher alpha diversity index; I) Benthonic Calcareous:Agglutinated ratio; J) Abundance of inferred life modes.

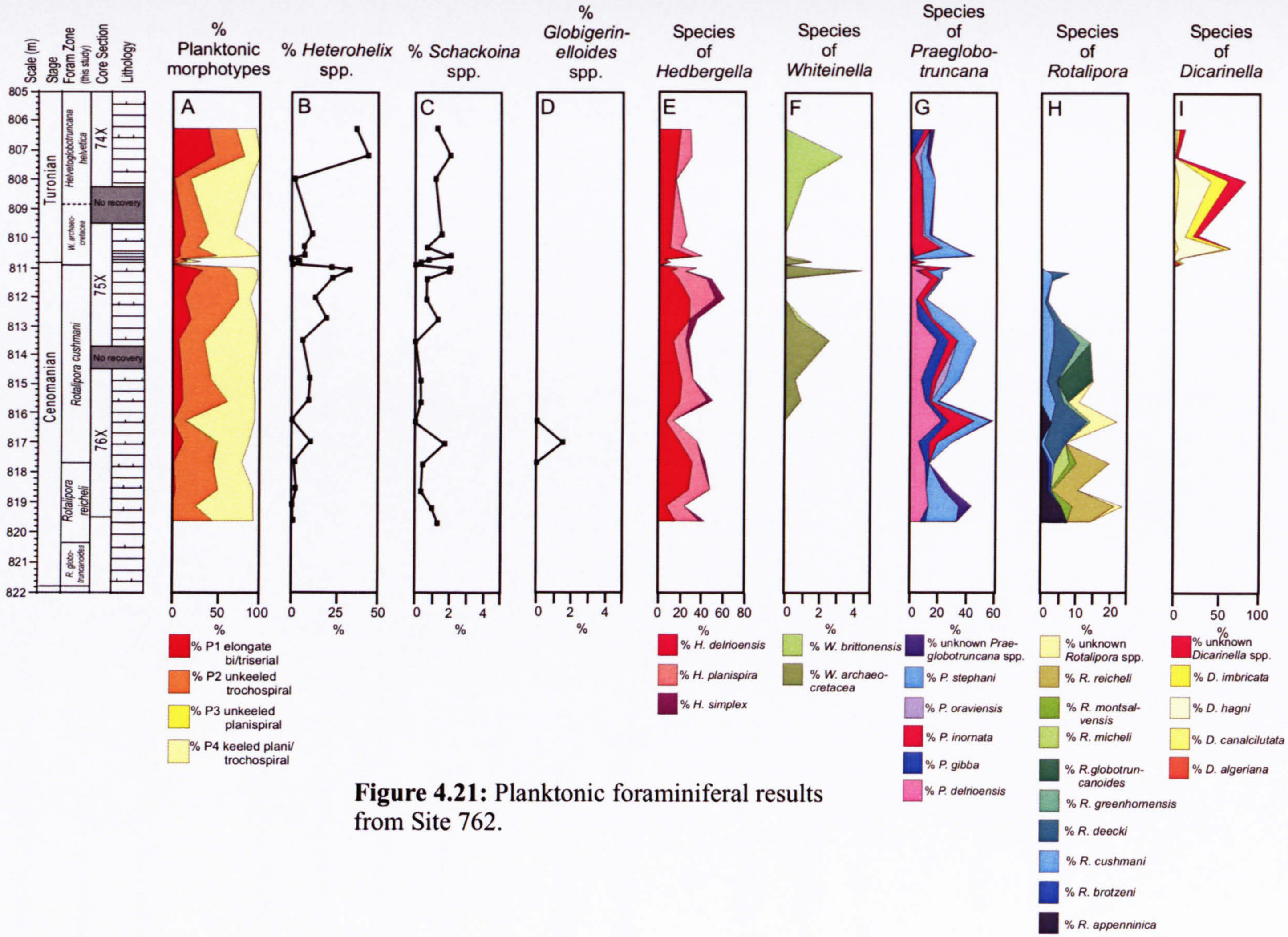

Figure 4.21: Planktonic foraminiferal results from Site 762.

The distribution of planktonic morphotypes, as used above, can be seen in Figure 4.19. Unlike Site 766 a more even distribution is seen between plani/trochospiral keeled (P4) and unkeeled trochospiral (P2) forms. Keeled trochospiral morphotypes dominating the assemblages in the parts of the core, particularly in lower part of the *R. cushmani* Zone, and through the *W. archaeocretacea* Zone into the lower part of the *H. helvetica* Zone. Trochospiral unkeeled forms show a relatively steady distribution in assemblages through the Cenomanian, typically making up around 40% of assemblages, with a brief reduction in the mid-Cenomanian, at 816.15 mbsf, to 14%. This coincides with the mid-Cenomanian increase of keeled forms. Following the CTB barren zone numbers are reduced again, only making up ~25% of the Turonian assemblages.

Elongate bi/triserial (P1) forms increase in numbers up through the core, rising from less than 1% to 33.5% just before the CTB. Following the CTB numbers remain low (~7%) through the *W. archaeocretacea* Zone, before increasing to dominate the assemblages at the top of the core, making up 46% of the assemblage.

The distribution of species' within each genus is also shown in Figure 4.19. *Hedbergella* spp., which dominate morphotype P2, are dominated by *Hedbergella delrioensis*, which replaces from *Hedbergella planispira* which dominated the Aptian and Albian sediments. *H. planispira* still makes up a large proportion of the hedbergellids but to a much smaller extent. *Hedbergella simplex* is also present making up a small part of the hedbergellid population through the Cenomanian. This decrease in dominance of *H. planispira* coincides with the increase in keeled morphotypes through the late Albian and into the Cenomanian.

Praeglobotruncana spp. dominates the keeled population of the Cenomanian, averaging abundances of ~30%, and making up to as much as 60% of the assemblage. *Praeglobotruncana delrioensis* dominates, along with *P. stephani,* and some *P. gibba, P. inornata* and *P. oraviensis*. *Rotalipora* spp. make up the remaining keeled morphotypes in the Cenomanian, dominated by deep umbilico-convex species *R. reicheli* and *R. deeckei*,

other flatter species, including key zonal species, are present in lower numbers. The abundance of *Rotalipora* spp. fluctuates throughout the Cenomanian, but peak abundances generally decrease showing a decline in the genus numbers to its extinction at the CTB. Into the Turonian *Praeglobotruncana* spp. are still present but at much lower numbers (~15%), instead the assemblages becomes dominated by double keeled species of *Dicarinella,* predominantly *Dicarinella hagni.*

Other species, such as *Schackoina cenomana* and *Heterohelix moremani,* are present throughout the Cenomanian and Turonian, generally increasing in abundance up through the core, and showing the highest abundances following the CTB barren zone. A slight increase in numbers is seen at 816.89 mbsf in the mid-Cenomanian and this coincides with the only occurrence of *Globigerinelloides* spp. at Site 762.

4.7.1.3 Benthonic foraminiferal distribution

The abundance of benthonic foraminifera is shown in Figure 4.20 C and D. Although present in much lower numbers than the planktonic specimens, distinct trends in abundance can be observed. As before the results are illustrated as both SPG and accumulation rates, similar trends being observed in both.

Similar to the abundance of the planktonics the abundance of benthonic foraminifera is relatively stable through the Cenomanian at ~1500 SPG and 600 specimens per cm^3 per kyr, decreasing slightly through the *R. cushmani* Zone, and showing a brief decline at the top of the *R. reicheli* Zone at 817.5 mbsf, coincident with a decline in planktonic abundance. Just prior to the CTB a sharp increase is seen in abundance, this is again coincident with planktonic abundance changes, abundances reaching maximum values of 3291 SPG and 1487 specimens per cm^3 per kyr. This increase is followed by a decline to zero in the CTB barren zone. Following the barren zone abundances increase markedly through the Lower Turonian before returning to values similar to those observed through the Cenomanian in the *H. helvetica* Zone.

The diversity of all benthonic foraminiferal specimens is also illustrated in Figure 4.20 G and H. Species richness (Figure 4.20 G) shows similar trends to the Fisher alpha index (Figure 4.20 H), however the Fisher alpha index takes into account the number of specimens as well as the number of species and shows a much smoother graph with less fluctuations than are observed in species richness. Generally diversity can be seen to decrease slightly through the Lower Cenomanian , becoming more stable through the *R. cushmani* Zone with fisher alpha index values of ~8. Showing slight increases in diversity before and after the CTB barren zone (where diversity is zero), diversity decreases further in the *W. archaeocretacea* Zone of the Lower Turonian and values remain low (~3) through the *H. helvetica* Zone.

Calcareous foraminifera dominate the benthonic assemblages at Site 762 (Figure 4.20 I), generally making up 80-90% of the species. Agglutinated forms do increase at levels within the core, particularly at the top of the *R. reicheli* Zone, where agglutinated species make up ~30% of the benthonic assemblage, and just after the CTB barren zone. There are no agglutinated forms seen in the *H. helvetica* Zone. The results of the benthonic distribution are shown in Figures 4.22 and 4.23.

<u>Agglutinated benthonic distribution</u>

There are 14 genera and 19 species of agglutinated foraminifera at Site 762. As described above the abundance of benthonic foraminiferal species is low throughout the core, with only a few species being present throughout, or in comparably large numbers. Diversity begins at around 5 species per sample in the lower to mid-Cenomanian, numbers decrease to only 2 of 3 species per sample though the upper Cenomanian, and remain low until just after the CTB where numbers increase briefly to 5 species again. This peak after the CTB also coincides with the peak abundance in agglutinated forms in sample 75X-1, 120-121 cm (810.60 mbsf).

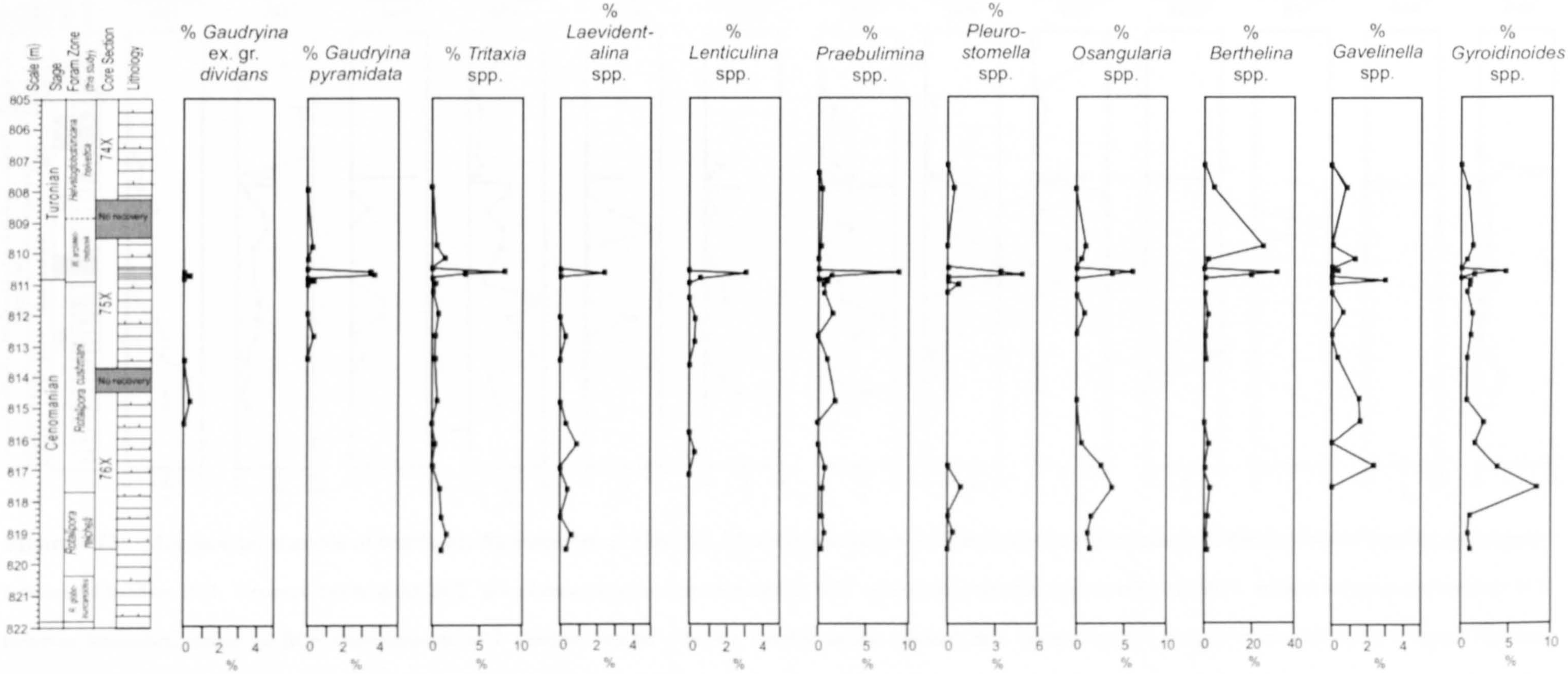

Figure 4.22: Benthonic foraminiferal results from Site 762

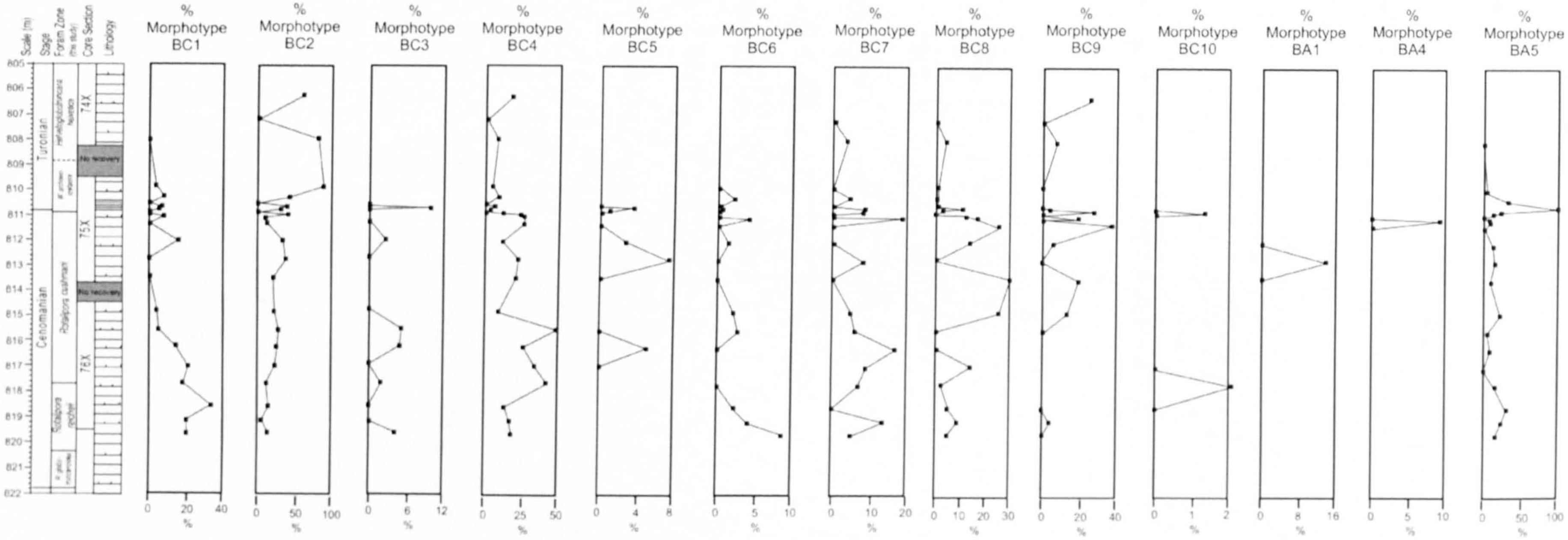

Figure 4.23: Morphotype analysis of benthonic foraminifera at Site 762. Morphotype values are presented as a percentage of the number of benthic specimens. **Calcareous hyaline:** BC1 biconvex, trochospiral; BC2 plano/concavoconvex, low trochospiral; BC3 plano/concavoconvex, high trochospiral; BC4 inflated, biconvex trochospiral; BC5 biconvex, lenticularm planispiral; BC6 Globular/ovate; BC7 elongate, straight to arcuate, broad to narrow, uniserial; BC8 tapered rounded, elongate tri-bi-uniserial; BC9 tapered flattened, elongate, biserial; **Porcellaneous:** BP1 elongate to ovate quinqueloculine; **Agglutinated:** BA1 tubular or branching; BA2 globular; BA3 planispiral/streptospiral, subsphaerical/flattened; BA4 low trochospire/streptospiral, sphaerical/subsphaerical; BA5 elongate, variably coiled, uni-multiserial.

Tritaxia is the only genus present throughout the core. Values generally reach no more than 2% abundance, however following the CTB barren zone values increase rapidly to 6%. A similar peak is seen in *Gaudryina* spp., *Eggerllina brevis*, *Reophax* sp. 1 and *Spiroplectinata bettenstaedti*, this distribution can be seen in Figure 4.22 and the count sheets in Appendix 2.

Only morphotypes BA1 (branching), BA4 (rounded/streptospiral) and BA5 (elongate) are seen at Site 762. BA5 is by far the most abundant making up 2-20% of the whole assemblage and 5-100% of the benthonic assemblage. This can be seen in Figure 4.23.

Calcareous benthonic distribution

Twenty-nine genera and 57 species of calcareous benthonic forms are seen at Site 762. The diversity varies through the core, averaging ~8 species per sample and showing peaks at the base of the *R. reicheli* Zone, the top of the *R. cushmani* Zone (811.95 mbsf) and just after the CTB in the *W. archaeocretacea* Zone in sample 75X-1, 110-111 cm (810.60 mbsf) where 17 species are observed. This early Turonian peak in diversity, within the *W. archaeocretacea* Zone, coincides with peak abundances of the dominant calcareous species *Bolivina* sp. 1, *Praebulimina nannina*, *Pleurostomella reussi*, *Osangularia schloenbachi*, *Berthelina* sp. 3, *Gyroidinoides infracretacea* and *Gubkinella* sp. 1, as well as peaks in the abundance of *Lenticulina* spp., *Laevidentalina* spp. and *Nodosaria* spp. Following this peak, abundance and diversity decrease again, into the *H. helvetica* Zone.

Only a few of the species show significant range and abundance within the core, except of course from those with biostratigraphical significance which have been highlighted above.

Berthelina spp. are present in the largest abundance, making up to 30% of the assemblage in the Turonian, following the CTB barren zone. However, species of *Berthelina* are only present at very low abundances through the Cenomanian.

Gyroidinoides spp. can be seen to dominate the calcareous assemblages in the lower part of the *R. cushmani* Zone, making up to 8.5% of the assemblage, along with *Gavelinella* spp., *Osangularia* spp. and *Pleurostomella* spp. at lower values. As numbers of *Gyroidinoides* spp. decrease through the Cenomanian, *Gavelinella* spp. and *Praebulimina* spp. begin to dominate the calcareous benthonic assemblages, with some *Gyroidinoides* spp. and *Osangularia* spp. All main calcareous benthonic foraminiferal genera seen at Site 762, and illustrated in Figure 4.20, show an increase in numbers directly following the CTB barren zone, except for *Gavelinella* spp. which show a peak abundance directly below the CTB barren zone. This distribution can be seen in Figure 4.22.

As before each species can be placed in a morphotype according to the shape of its test. These results are shown in Figure 4.23 and described below. At the base of the core, within the *R. reicheli* Zone, assemblages are initially dominated by bi-planoconvex trochospiral (BC1) morphotypes, with some elongate (BC7) and globular-ovate (BC6) forms. As the numbers of BC1 decline up through the core, inflated bi-planoconvex (BC4) forms begin to dominate through the lower part of the *R. cushmani* Zone making up nearly as much as 50% of the benthonic assemblage. BC7 continues to be present at relatively high abundances (15%), and BC3 (plano-concavo convex, high trochospire) reaches its highest abundances within the core with peak values of 5.3%.

In the upper part of the *R. cushmani* Zone (section 75X-1) tapered and elongate species (BC8 and BC9) dominate up to 50% of the benthonic assemblage. Just prior to the CTB BC1, BC2, BC4, BC7, BC8 and BC9 all show a slight increase in numbers, before all morphotypes decline to zero over the barren zone. Following the CTB BC3, BC5 and BC10 all show a sharp increase before disappearing through the Turonian. BC6 also disappears soon after the CTB.

BC1, BC7 and BC8 show substantial declines in numbers following the CTB, and although present through the *H. helvetica* Zone remain at low abundances. Similarly BC4

and BC9 also show a large decline following the CTB, however, an increase in numbers is seen at through the *H. helvetica* Zone at the top of the core.

Only BC2 (plano-concavo convex, low trochospiral) shows a large increase following the CTB, remaining generally high through the Turonian. BC2 was present through the Cenomanian at a relatively high abundance, increasing from ~10-40% just before the CTB. Following the barren zone BC2 make up as much as 90% of the benthonic assemblage through the Turonian, only one sample showing none of these forms in the *H. helvetica* Zone at 807.11 mbsf.

4.7.1.4 Life mode

Life modes derived from morphotype and isotopic information are shown in Figure 4.18. Initially epifaunal, epifaunal/infaunal and infaunal species show an even distribution. A decrease in numbers in the middle of the *R. cushmani* zone shows a dominance of infaunal species through this portion of the core. Prior to the CTB epifaunal species begin to dominate, and this continues, following the CTB, into the Turonian. Infaunal species decrease to low abundances through the Turonian, following a peak in numbers directly after the CTB coinciding with the peak abundance in benthonic foraminifera.

4.7.1.5 Other biota found at Site 766

Figure 4.4 shows the presence of other components within Core 762. Similar to Site 766 radiolaria, ostrocods and calcispheres are seen through the core, however a large increase is seen, particularly in radiolaria, but also in calcispheres. Fish teeth and shell fragments are also seen throughout the core.

4.7.2 Isotope results

Isotopic analysis was carried out on both fine fraction and foraminiferal samples. The results of both are outlined below. The raw data can be seen in Appendix.3, and analytical data are presented in Figures 4.24.

4.7.2.1 Fine fraction samples

82 samples were measured for fine fraction isotope analysis over 25.62 m of Aptian to Turonian sediments.

Carbon isotope results

Carbon isotope results at Site 762 show a general trend of increasing $\delta^{13}C$ values from the Aptian to Turonian; values are observed to increase from ~0‰ to 3‰. However, a few fluctuations on this general trend are seen, including a peak in values at the CTB. The results are outlined below.

The lower part of the core, corresponding to the clay rich sediments, generally show greater fluctuations than the Cenomanian and Turonian chalky sediments. The lowermost Aptian samples from the core show an initial decrease in $\delta^{13}C$ values from 0.7 to 0.1 ‰. This is followed by a rapid increase through the lower part of the *H. planispira* Zone to 1.4‰ at 830.10 mbsf. Values continue to fluctuate (up to 1‰) and increase through the Albian, reaching 2‰ in the *P. buxtorfi* Zone at sample 77X-4, 5-7 cm (824.05 mbsf). After this point values fluctuate much less and generally remain at ~2‰ though the upper part of the Albian and lower part of the Cenomanian. A couple of small fluctuations are observed with a slight decrease to 1.5‰ at 819.57 mbsf, and a slight increase at 817.59 mbsf. Although only small, both fluctuations correspond to larger changes seen in the $\delta^{18}O$ curve which shall be discussed below.

From sample 76X-1, 145-147 cm (815.95 mbsf) in the lower part of the *R. cushmani* Zone values begin to increase again reaching 3‰ 1m below the CTB. At this

point $\delta^{13}C$ fluctuates rapidly over this CTB zone. Initially decreasing to 2‰ at 811.51 mbsf and 71 cm below the CTB, values then increase rapidly to 3.7‰ at 810.60 mbsf, in the upper part of the CTB claystone, 20 cm above the barren zone. Values rapidly return to 3‰ through the top part of the *W. archaeocretacea* Zone, and although showing a slight increase in the *H. helvetica* Zone to 3.2‰, remain relatively constant through the top part of the core.

Oxygen isotope results

The oxygen isotopes show similar trends to those seen in the carbon isotope curve, and an overall decrease in values is seen up through the core. However larger perturbations are seen, particularly in the upper portion.

Like the carbon isotopes the lower clay rich samples show a greater fluctuation in values and although a general decrease in values is seen, from -0.5 to -2‰, at 824.05 mbsf in the *P. buxtorfi* Zone, fluctuations of up to 0.5‰ are observed through this zone.

After this initial decrease, values through the upper part of the *P. buxtorfi* Zone and into the Cenomanian and Turonian show less fluctuation and generally remain between -2.0 and -3.0‰. A few peaks and troughs are seen, however, which are described below.

Values remain at ~-2‰ through the Upper Albian and into the Lower Cenomanian *R. globotruncanoides* Zone, with a short increase is seen in sample 77X-2, 100-102 cm (822 mbsf) just below the Albian-Cenomanian boundary, to -1.2‰. Following this increase values are seen to gradually decrease to the lowest values observed at Site 762 of -3.1‰, 819.57 mbsf, in the mid Cenomanian *R. reicheli* Zone. This is followed by a gradual increase to -1.6‰ at *R. reicheli* - *R. cushmani* boundary, 817.59 mbsf, and subsequent decrease to -2.5‰, where values remain stable through the lower part of the *R. cushmani* Zone. At 813.12 mbsf, following a slight increase to -2‰, $\delta^{18}O$ values decrease again to a second low peak at the CTB. Values reach -3.0‰ at 810.99 mbsf, at the base of the *W. archaeocretacea* Zone, just below the CTB, and remain at this level until 810.10 mbsf.

Values are then seen to increase slowly to -2‰ at the top of the *W. archaeocretacea* Zone, before returning to steady levels of -2.5‰ through the Turonian *H. helvetica* Zone.

4.7.2.2 Foraminiferal isotope results

The abundance of both keeled and unkeeled planktonic foraminifera at Site 762, and the presence of species of *Berthelina*, enabled measurements of shallow and deep dwelling planktonics and epifaunal benthonic foraminifera to be undertaken. All foraminiferal results are shown along with fine fraction results, to enable a visible correlation of the values, in Figure 4.24. An analysis of any diagenetic alteration that has occurred is undertaken in section 4.8.

Carbon isotope results

The foraminiferal carbon isotope results are markedly different from those obtained from the fine fraction analysis. Foraminiferal results showing a constant offset to more negative values.

In the lower, Aptian-Albian part of the core, the shallow dwelling hedbergellids generally show more negative values than the benthonic taxa. Both showing more negative values than the fine fraction results, at a maximum offset of ~3‰ from the shallow dwelling planktonic taxa, and ~2‰ from the benthonic values. The amount of offset in values does however change through the core, reaching a maximum offset in the upper part of the Albian *P. buxtorfi* Zone, the difference becomes reduced to around 1-1.5‰, through the Cenomanian and Turonian

By the top of the *P. buxtorfi* Zone the foraminiferal values are fluctuating less, and are starting to show a convergence, the offset between planktonic and benthonic species becoming reduced to just 0.3‰. Keeled planktonics are also present in the *P. buxtorfi* Zone and the $\delta^{13}C$ values, although also having lower values than the fine fraction samples, are

consistently more positive than both benthonic and shallow planktonic results. An offset, to more positive values, of ~0.2‰ being maintained throughout the core.

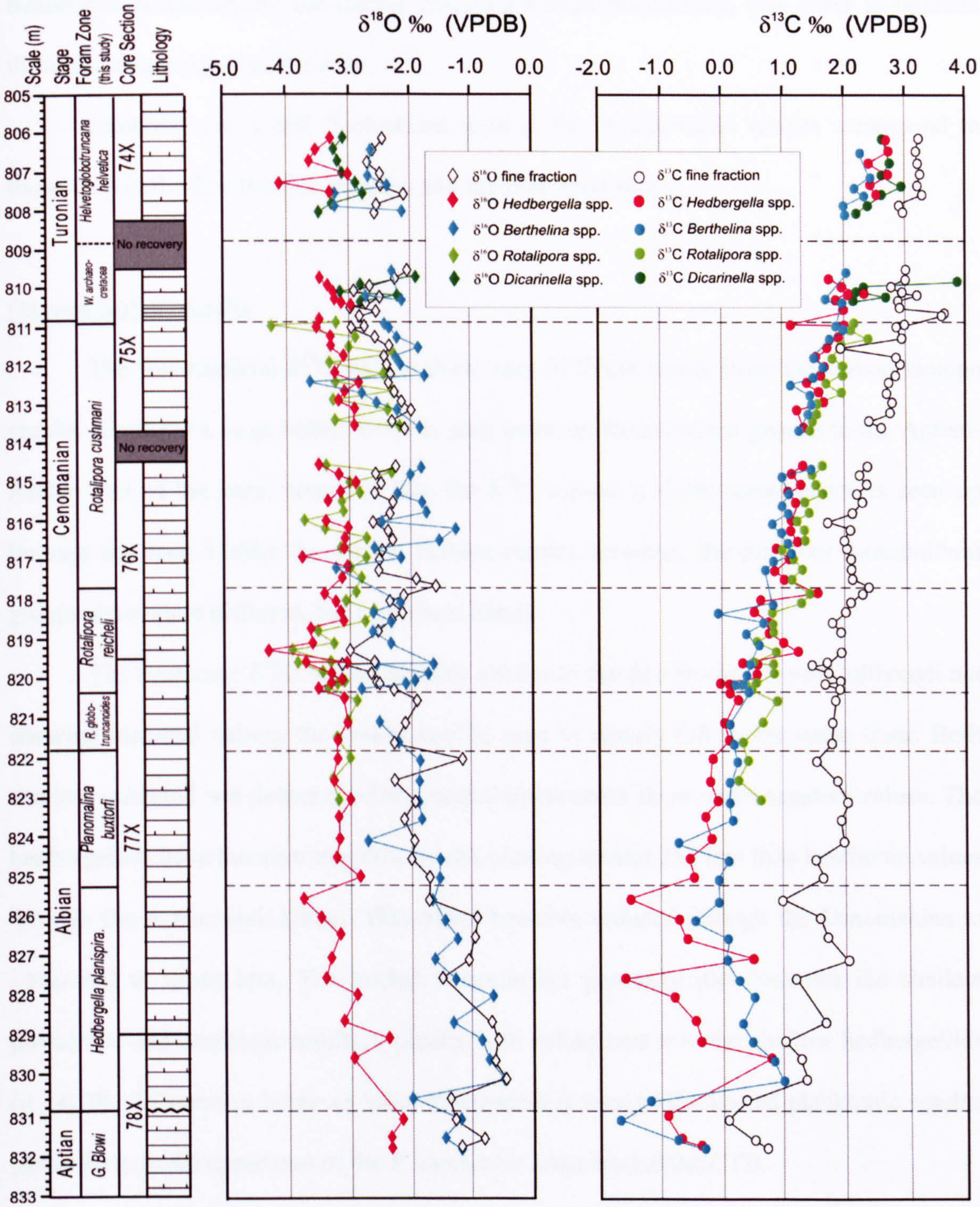

Figure 4.24: Foraminiferal and fine fraction isotope results from Site 762. Dashed lines indicate the Biozone boundaries.

Continuing into the Cenomanian further convergence is seen between the foraminiferal groups, however a defined offset can still be observed and a difference of ~0.2‰ is seen between each group. Interestingly at the base of the Cenomanian the benthonic values start to show the most negative values, followed by the shallow hedbergellids and finally the deeper dwelling keeled planktonics, this order is retained through the upper part of the core.

Generally any small fluctuations seen in the foraminiferal results correspond to those seen in the fine fraction samples and are described above.

Oxygen isotope results

The foraminiferal $\delta^{18}O$ values show very different trends from the carbon isotope results. Similarly a large initial offset is seen between foraminiferal groups in the Aptian-Albian part of the core, however, like the $\delta^{13}C$ values, a slight convergence is seen up through the core. Unlike the carbon isotope results, however, the different foraminiferal groups show quite different, but consistent trends.

The benthonic $\delta^{18}O$ values are very similar to the fine fraction results, although not showing identical values, the results can be seen to closely follow the same trace. Both shallow unkeeled and deeper dwelling keeled planktonics show more negative values. The hedbergellids have the most negative results plotting around 2‰ less than benthonic values through the Aptian and Albian. This offset becomes reduced through the Cenomanian to ~1‰ and at times less. The keeled foraminifera generally plot between the shallow planktonic and benthonic results, typically with values nearer to the shallow hedbergellids (0.1-0.2‰ difference), however much fluctuation is seen in the keeled planktonic results, particularly in the upper part of the *R. cushmani* Zone around the CTB.

As mentioned above the foraminiferal results do show a marked convergence at times through the core, most significantly in the mid-Cenomanian at the base of the *R. cushmani* Zone, and at the CTB.

4.7.3 Geochemical analysis

4.7.3.1 TOC analysis

TOC values were measured throughout the core with all samples within the CTB claystone being analysed. Values were seen to reach no more than 0.5 % in any of the samples analysed in this study. RockEval was not able to be determined therefore on any results from this study. TOC values of up to 2% have been found, however, in the black shale bed, with values of up to 2 wt% (Haq *et al.* 1992).

4.7.3.2 Trace element analysis

Each of the 82 samples analysed for isotopes were also analysed for trace elements, iron, magnesium, manganese, strontium and calcium. The raw data is shown in Appendix 3, and the analytical data is presented in Figures 4.25-4.26. Results are shown as both ppm/kg and as calcium ratios, in order to look at the effect of lithology on the elemental values through the core.

Manganese, magnesium and iron all show there highest concentrations in the lower part of the core, peaking in the Albian *Hedbergella planispira* Zone. Following these maxima both magnesium and iron return background levels through the rest of the core, however manganese shows much greater fluctuation. Reaching a minimum at the top of the *H. planispira* Zone, values can be seen to increase slowly through the upper Albian and lower Cenomanian plateauing at ~600 ppm/kg in the lower part of the *R. cushmani* Zone. Values then decrease gradually through the upper Cenomanian and Turonian, a short, rapid decrease in values being seen at the CTB.

Strontium and carbon show very different trends from the above 3. Values generally remaining constant trough the core. Showing a slight increase through the Cenomanian both strontium and calcium show a peak in values in the mid-Cenomanian, at 814.99 mbsf, and at the CTB.

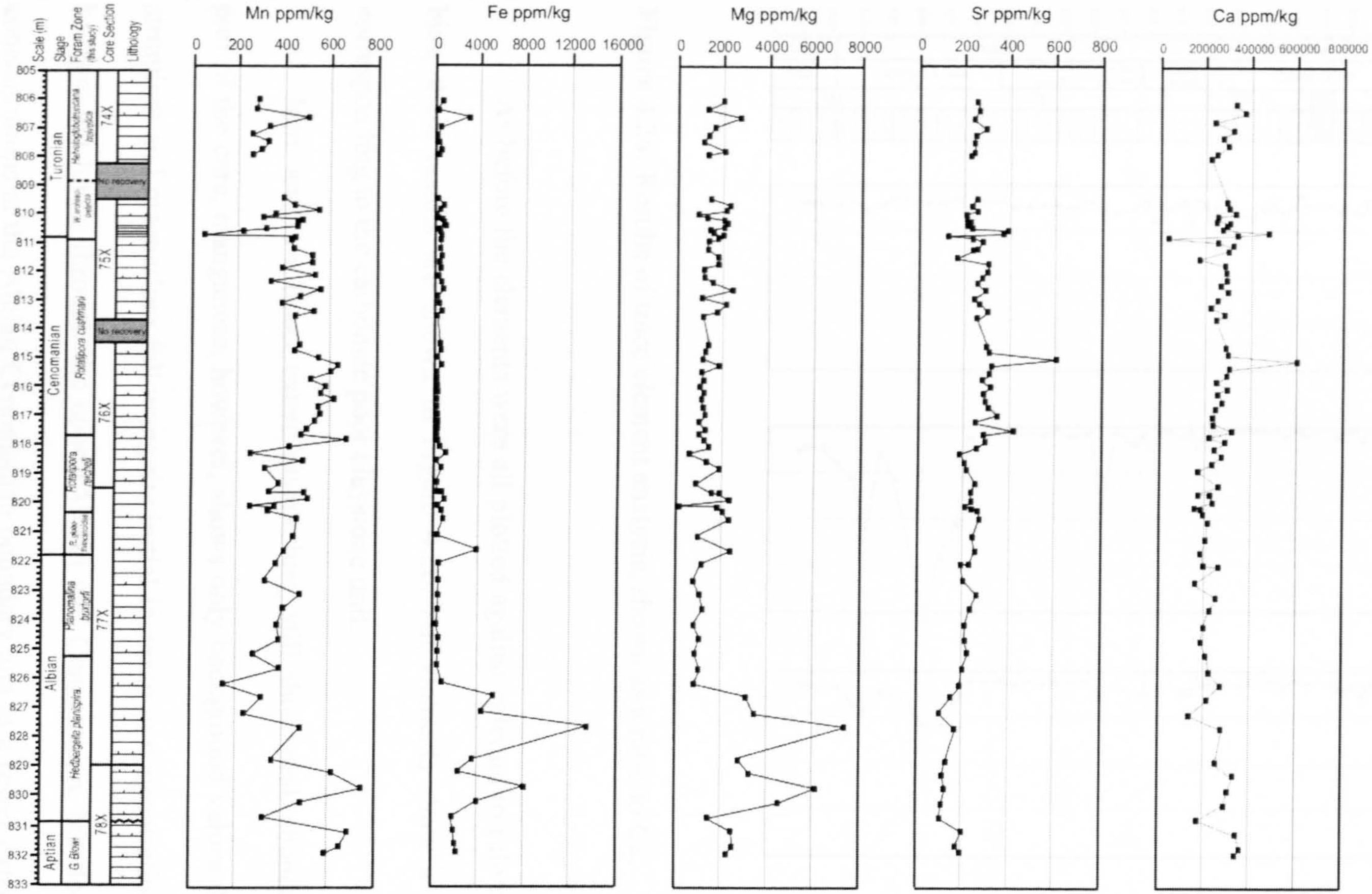

Figure 4.25: Results of trace element analysis from Site 762 shown as ppm/kg

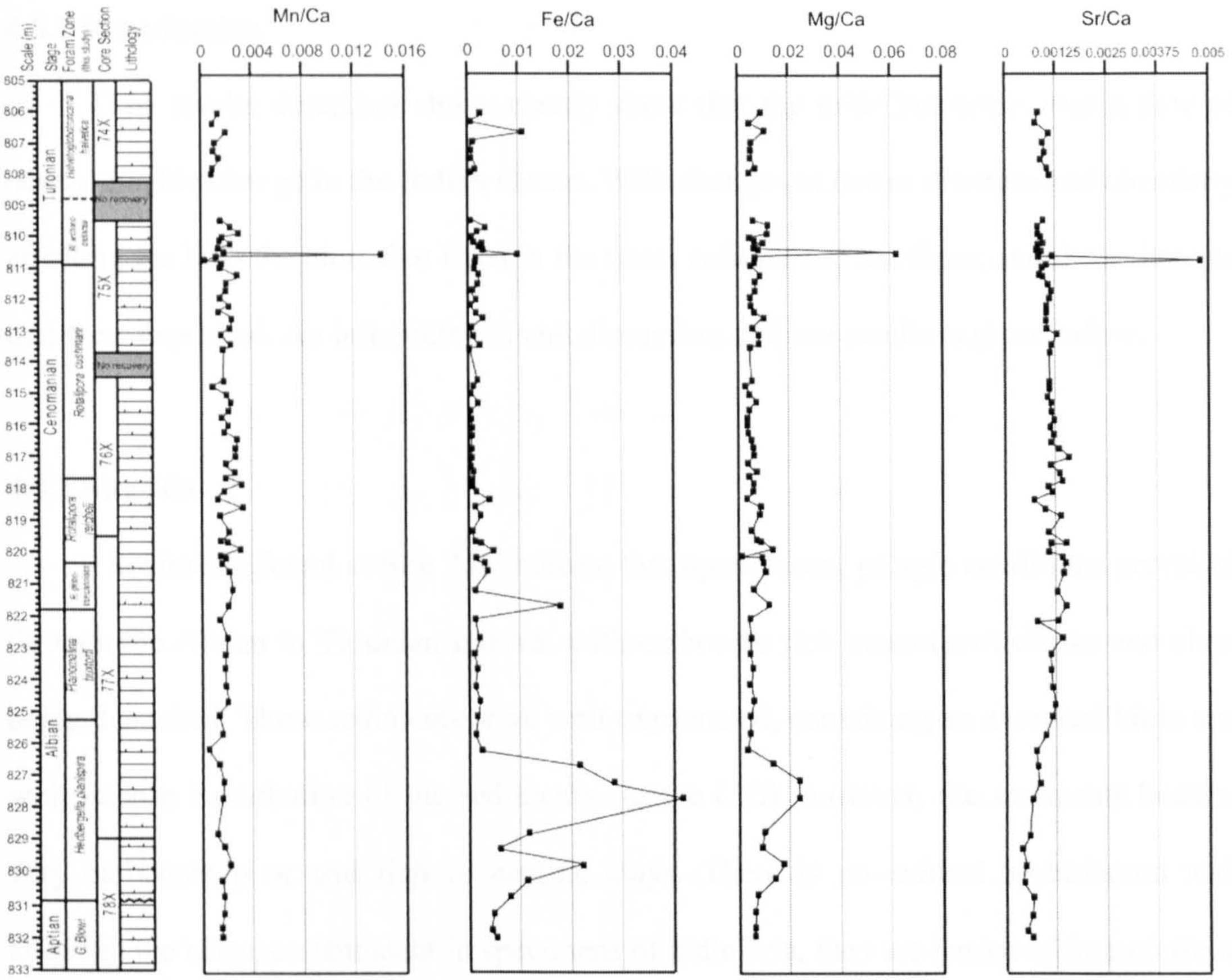

Figure 4.26: Results of trace element analysis, shown as a ratio to Ca.

As before the elements were all plotted against calcium to rule out any lithological bias, these results are shown in Figure 4.26. All elements show a spike at the CTB corresponding to the carbonate poor claystone unit.

Iron, and to a lesser extent magnesium, still show peak abundances in the lower part of the core, manganese, however, shows only background values throughout, as does strontium and magnesium following the initial increase in concentration. Iron also shows background levels through the upper Albian and Cenomanian, but does show increased concentrations at the Albian-Cenomanian boundary and to a lesser extent a slight increase at the top of the core in the *H. helvetica* Zone.

4.8 Palaeoceanographic change in the Indian Ocean

4.8.1 Introduction

The results described above clearly show that the mid-Cretaceous was a time of oceanographic change in the Indian Ocean. With changes in ocean structure and chemistry affecting the both the biota that lived in the water column and sea floor, and the sediments that were deposited. An interpretation and discussion of these results is given below.

4.8.2 Site 766

Sediments found at Site 766 indicate that open-ocean, pelagic conditions prevailed through the Albian to Turonian interval with carbonate rich nannofossil chalks and clays being deposited. These sediments were well oxygenated, containing an abundant biota and with intense bioturbation of the sediments. At the CTB, however, the sediments became very carbonate poor and rich in zeolitic clays. There is no evident bioturbation and, although the clays are abundant in specimens of radiolaria, they are barren of foraminiferal species.

The isotope data provides some information on the chemistry and temperature of the water column, and therefore the depositional conditions in which these sediments were formed. However, in order to fully analyse the data the diagenetic potential of the sediments must assessed and any evidence of diagenesis analysed. This was done at Site 766 by analysing thin sections of the sediments, looking at the preservation of the foraminifera using thin sections and scanning electron imagery, and from trace element analysis.

4.8.2.1 Diagenetic potential at Site 766

Although the sediments analysed in this study were deposited at a palaeodepths of around 3000m, they were only buried to 125-155 mbsf. This relatively shallow burial, especially when compared to Site 762 (buried to over 800 mbsf), will lower the diagenetic

potential of the sediments. Similarly, the clay rich sediments also have low diagenetic potential, clays sediments are less porous than carbonates and therefore limit the fluid flow through the sediments, and with lower amounts of calcium carbonate in the matrix there is less chance of re-precipitation and incorporation of new and isotopically different carbonate into the original calcium carbonate of the foraminifera or coccoliths. Trace element analysis additionally shows no increase in manganese or iron, typically indicative of diagenetic environments, through the core. An increase in manganese, iron, magnesium and strontium is, however, seen at the CTB and this corresponds to the deposition of a zeolitic clay, this will be discussed further in 4.8.2.3.

Thin sections were taken at intervals through the core to analyse any secondary calcite in the sediments or associated with the foraminiferal test. The sections show the samples to consist predominantly of micritic packstones and wackestones, with intercalations of clay rich layers showing faint laminations. Examples of these sediments and this can be seen in Figure 4.27.

From the thin section analysis it can be shown that there is little secondary calcite cement lithifying the soft clays and oozes found in the core, and the foraminifera are largely unfilled and show good to moderate preservation of the test wall. The preservation of the foraminifera can further be examined using the scanning electron microscope, this can be seen in Figure 4.28.

The foraminifera generally show good preservation with little infilling of the test. Some overgrowth of the test wall is present and infilling of some of the original test porosity by secondary calcite can be seen in some of the specimens. It was important the specimens were, therefore, carefully chosen for isotopic analysis, breaking the specimens if necessary to make sure only the most pristine were measured. This was required in order that a diagenetic overprint would be avoided as much as possible in the results. Preservation of the foraminifera varies slightly throughout the core, with the more clay rich sediments typically yielding better preserved specimens.

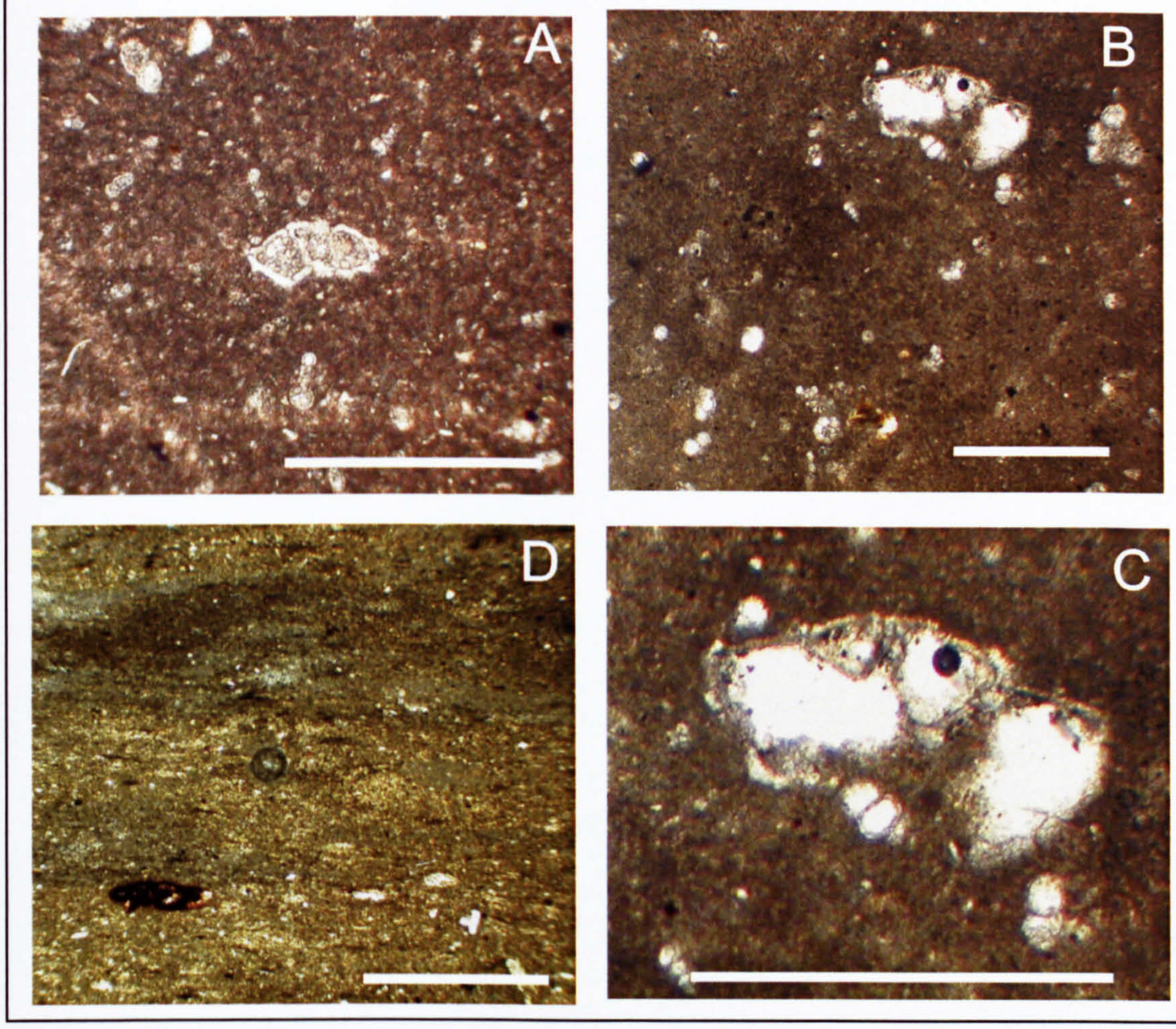

Figure 4.27: Photomicrographs of thin-sections taken of sediments from Site 766. All scale bars 200 μm.

A) Packstone from the nannofossil chalk of the Lower Cenomanian *Rotalipora globotruncanoides* Zone (sample 15R-5, 96-97 cm, 140.15 mbsf). Abundant small *Hedbergella* spp. can be seen with a larger *Rotalipora globotruncanoides*, in a micritic matrix. The rotaliporid shows some evidence of infilling in the test, although the test wall appears well preserved with no recrystallisation present. Smaller hedbergellid foraminifera show predominantly unfilled tests.

B) Wackestone from the nannofossil ooze of the Upper Aptian *Rotalipora appenninica* Zone (sample 16R-3, 60-62 cm, 146.50). A large *R. appenninica* is seen with smaller species of *H. delrioensis* and *H. planispira*. The rotaliporid shows a completely unfilled test and relatively little recrystallisation of the test

wall. Smaller specimens similarly show unfilled tests and low recrystallisation.

C) Close up of *Rotalipora appenninica* shown in photomicrograph B. The test can be seen to be completely absent of any secondary calcite.

D) Laminated claystone from within the nannofossil ooze of the Upper Albian *R. appenninica* Zone (sample 16R-5, 110-112 cm, 150.00 mbsf). Appearing largely devoid of foraminifera a distinct lamination in the sample can be seen.

Foraminifera derived from clay-rich sediments have commonly been found to yield the most pristine preservation (Pearson *et al.*, 2001), due to low fluid flow and low amounts of calcium carbonate giving clay sediments a low diagenetic potential. Specimens 1-6 in Figure 4.28 are from the upper Albian *R. appenninica* Zone and show no infilling of the test. There is some partial secondary calcite infilling of pores and a slight overgrowth of the test wall is apparent in some specimens (1 and 2). Specimens 3, 5 and 6 are calcareous benthonic foraminifera and again, no infilling is seen. The wall structures are largely free of secondary calcite overgrowths, with the specimens retaining much of the original external features. Specimen 4 is an agglutinated specimen, and while not measured for isotopic analysis, has been included here to show the preservation of the test wall made up of aligned coccoliths. The coccoliths can be seen to show no secondary calcite on the test wall and near pristine preservation.

These foraminifera from the Albian can be considered to show good to excellent preservation. Specimens 7-12 show species from the Cenomanian and again records excellent preservation in the hedbergellids (8-9) and good preservation in the rotaliporids and praeglobotruncanids (10-12) which show no infilling and little secondary calcite overgrowth, or infilling of the pores. It should be noted that these specimens show signs of dissolution. Although dissolution was unable to be quantified in the cores and sediments sampled in this study, due to the lack of fragmented specimens, the effects of the dissolution will be discussed below.

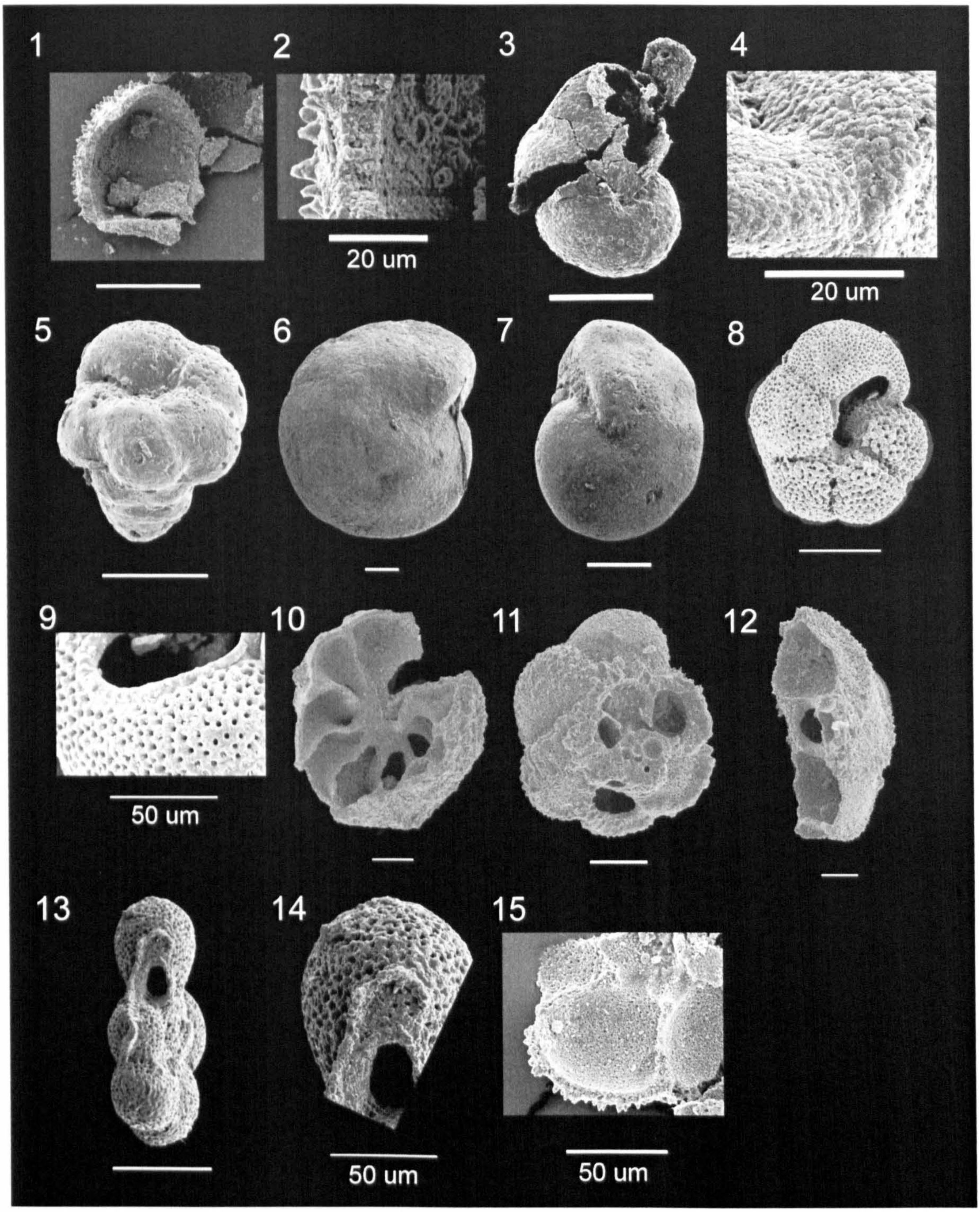

Figure 4.28: Photomicrographs illustrating the preservation of foraminiferal tests at Site 766. All scale bars are 100 μm unless otherwise stated.

1) *Hedbergella delrioensis* 16R-CC, 7-9 cm Upper Albian

2) *Hedbergella delrioensis* 16R-CC, 7-9 cm Upper Albian

3) *Valvulineria gracillima* 16R-7, 10-12 cm Upper Albian

4) *Spiroplectinella* sp. 1 16R-7, 10-12 cm Upper Albian

5) *Gubkinella* sp. 1 16R-5, 135-137 cm Upper Albian

6) *Berthelina* cf. *berthelini* 16R-4, 60-62 Upper Albian

7) *Lingulogavelinella albiensis* 15R-5, 70-72 cm Lower Cenomanian

8) *Hedbergella delrioensis* 15R-4, 20-22 cm Upper Cenomanian

9) *Hedbergella delrioensis* 15R-4, 20-22 cm Upper Cenomanian

10) *Rotalipora deeckei* 15R-3, 110-112 cm Upper Cenomanian

11) *Praeglobotruncana stephani* 15R-3, 110-112 cm Upper Cenomanian

12) *Rotalipora deeckei* 15R-3, 110-112 cm Upper Cenomanian

13) *Hedbergella planispira* 15R-1, 5-7 cm Lower Turonian

14) *Hedbergella planispira* 15R-1 5-7 cm Lower Turonian

15) *Hedbergella delrioensis* 14R-CC, 3-5 cm Lower Turonian

Specimens 13-15 show specimens from the Lower Turonian and, again, excellent preservation is observed in the hedbergellids. Specimen 15 does show some recrystallisation of the internal test wall as can be observed by the granular texture. However the tests are not infilled and the pores show no signs of secondary calcite infilling.

Additional to the SEM analysis, preservation can also be analysed using a light microscope. Many of the specimens of Site 766, particularly specimens of *Valvulineria* (specimen 3), show translucent and glassy tests when looked at with a light microscope. Following diagenesis, calcareous foraminifera typically change from glassy, translucent and reflective textures, to chalky and opaque (Pearson *et al.*, 2001; Wilson *et al.*, 2002). The "glassiness" or hyaline nature of *Valvulineria* specimens and other species at Site 766 give further evidence of the excellent preservation of the foraminifera and absence of widespread diagenesis at Site 766.

From the preservation analysis of the foraminifera and the selective picking of specimens for isotope analysis, as well as using the fine (coccolithic) fraction of sediment for bulk analyses the measurement of diagenetic material has been limited as much as possible.

Further analysis of potential diagenesis within the sediments can be determined by plotting the fine fraction carbon and oxygen isotope results against each other in a cross plot. This can be seen in Figure 4.29. With diagenesis a covariance of oxygen and carbon results will occur as values of both carbon and oxygen shift towards those in equilibrium with the diagenetic conditions. In meteoric and burial environments carbon and oxygen values typically become more negative (Brand and Veizer, 1980; Marshall, 1992), whilst during early diagenesis occurring on or near the sea floor at the sediment water interface, oxygen values will increase in the cold bottom waters, carbon values becoming more negative (Schrag, 1999; Pearson *et al.*, 2001). Results at Site 766 show there is no positive correlation of values in the fine fraction samples, carbon values showing no covariance with oxygen. Values measured in *Berthelina* spp., however, show a slight correlation, higher, more positive, oxygen values typically correlating with lower more negative $\delta^{13}C$ values. This is consistent with early diagenesis and the diagenetic textures seen in some of the benthonic species in Figure 4.28.

Overall the isotopic values at Site 766 can be determined as largely free of diagenetic effects, particularly in the bulk samples. Foraminiferal values do show signs of some diagenesis, particularly in the benthonic specimens and interpretation of these results is done so with care.

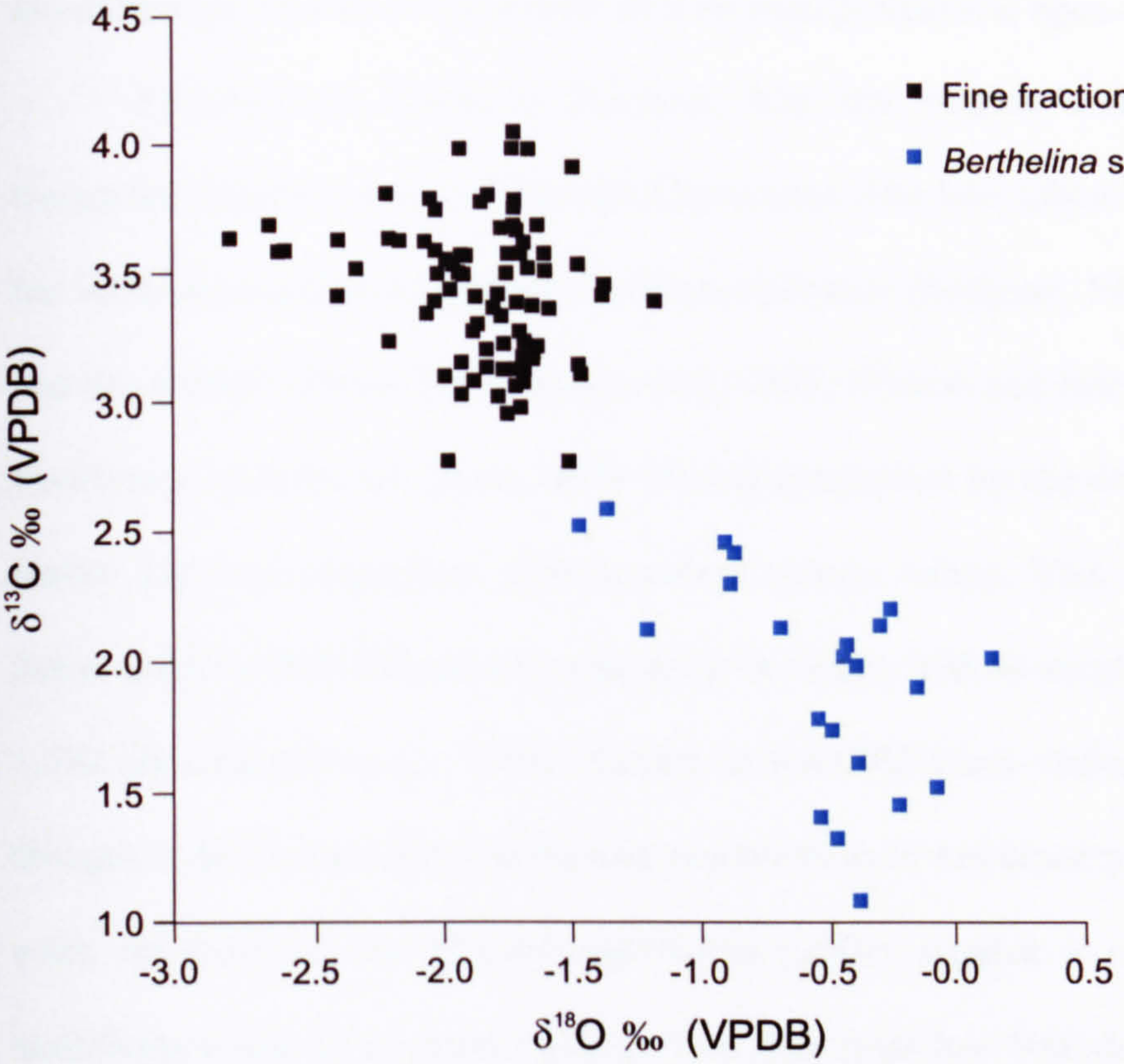

Figure 4.29: Cross-plot of oxygen and carbon isotope values from fine-fraction and *Berthelina* spp. samples of Site 766.

4.8.2.2 Upper Albian palaeoenvironmental change

Carbon isotopes of the fine fraction samples at Site 766 show background values ~3-3.5 ‰. With similar values being observed in the surface dwelling planktonic foraminiferal analyses, the fine fraction results can therefore be confirmed as recording surface water isotopic values. These results are slightly higher than typical mid-Cretaceous background values where fine-fraction results are often ~2-3 ‰ (e.g., Eastbourne – Tsikos *et al.*, 2004; Pueblo – Keller *et al.*, 2004; North Atlantic – Huber *et al.,* 1999). The higher values at Site 766 may be due to enhanced preservation of sediments at this site, diagenesis typically lowering $\delta^{13}C$ values. Benthonic foraminiferal $\delta^{13}C$ values are consistently lower than the fine fraction values by ~1.5-2‰. This may indicate a stratification in the water column, with a gradient typical of a productive open ocean environment, lighter carbon

being removed from surface waters, and organic matter being oxidised and light carbon recycled back into the water column at depth. These background values seen at Site 766 are consistent with those associated with normal, productive, open ocean conditions.

Spanning the Albian to Turonian, Site 766 extends over a number of globally recognised oceanic events of the mid-Cretaceous. The late Albian anoxic event (OAE 1d) has been described by a number of authors in France (Bréhéret, 1994; Giraud *et al.*, 2003), and the Atlantic Ocean (Nederbragt *et al.*, 2001; Wilson and Norris, 2001). Spanning the *Rotalipora appenninica* Zone, OAE 1d is characterised by the deposition of organic rich shales, and a corresponding shift in carbon isotope values. This isotope signal shows an initial negative shift followed by a positive excursion with an amplitude between 0.5‰ and 1.5‰ (Bornemann *et al.*, 2005). Similar to the CTB black shales, those of OAE 1d are thought to be formed due to enhanced preservation or increased productivity. Most recent work on OAE 1d by Wilson and Norris (2001) suggest a collapse in upper-ocean stratification due to increased mixing from data from low latitude ODP Site 1052, Blake nose in the western Atlantic. This was proposed to cause the deposition of black shales due to enhanced productivity, related to the mixing and upwelling. Bornemann *et al.* (2005), however, suggest that in more epicontinental regions, such as the Vocontian Basin, increased humidity led to increased surface water stratification and a decrease in deep water formation. This led to increased oxygen consumption in the bottom water and enhanced preservation potential of organic matter. It is likely that the very different palaeoceanographic settings would lead to different mechanisms of black shale deposition, as is also proposed for black shale deposition at the CTB. However, at all sites the same $\delta^{13}C$ trends are observed, coincident with increased sea surface temperatures, indicating the global nature of the event.

Although OAE 1d has mainly been reported from the North Atlantic and the western Tethys, occurrences have been seen in the South Atlantic, Pacific Ocean, southern high-latitude sites and the Western Interior Seaway (Wilson and Norris, 2001). Site 766,

however, although spanning the Upper Albian, has been described as showing no obvious lithological expression of OAE 1d (Wilson and Norris, 2001), with no organic rich sediments being present. Isotope results from this study do however show similar trends to those reported for the event, particularly comparable with those described by Wilson and Norris (2001) for Blake Nose, and the Niveau Breistroffer event in Col de Palluel (SE France) (Bornemann *et al.*, 2005).

Carbon isotope values, shown in more detail in Figure 4.28, clearly show an initial increase in values at the base of the core followed by a negative shift of nearly 1‰, and successive positive shift of at least 0.5‰ in line with the amplitude seen at other Upper Albian sites. Unfortunately boundary samples from Site 766 are missing and it is not possible to see the isotope record over the Albian-Cenomanian boundary. Smaller scale changes in the isotope record of Site 766 can also be correlated with those of the Col de Palluel (Bornemann *et al.*, 2005), although higher resolution isotope measurements would need to be taken at Site 766 in order to fully verify and correlate these small scale changes.

In line with other studied sections, fine fraction oxygen isotope results also show a slight decrease in values, possibly indicative of a rise in sea surface temperatures at the end of the Albian. Measurements of benthonic foraminifera show a consistent offset with these surface values, represented by the fine fraction (coccolithic) samples. Indicating a thermal gradient to exist from the sea surface to sea floor.

This data indicates a stratified ocean existed through the upper part of the Albian at Site 766 and no stratification collapse, as postulated for the Atlantic Ocean by Wilson and Norris (2001), occurred.

Palaeontological evidence can provide further information on the state of the water column. However, care must be taken at Site 766 due to potential dissolution of specimens and bias within samples, as species with thinner, less robust tests have been preferentially removed from the assemblages.

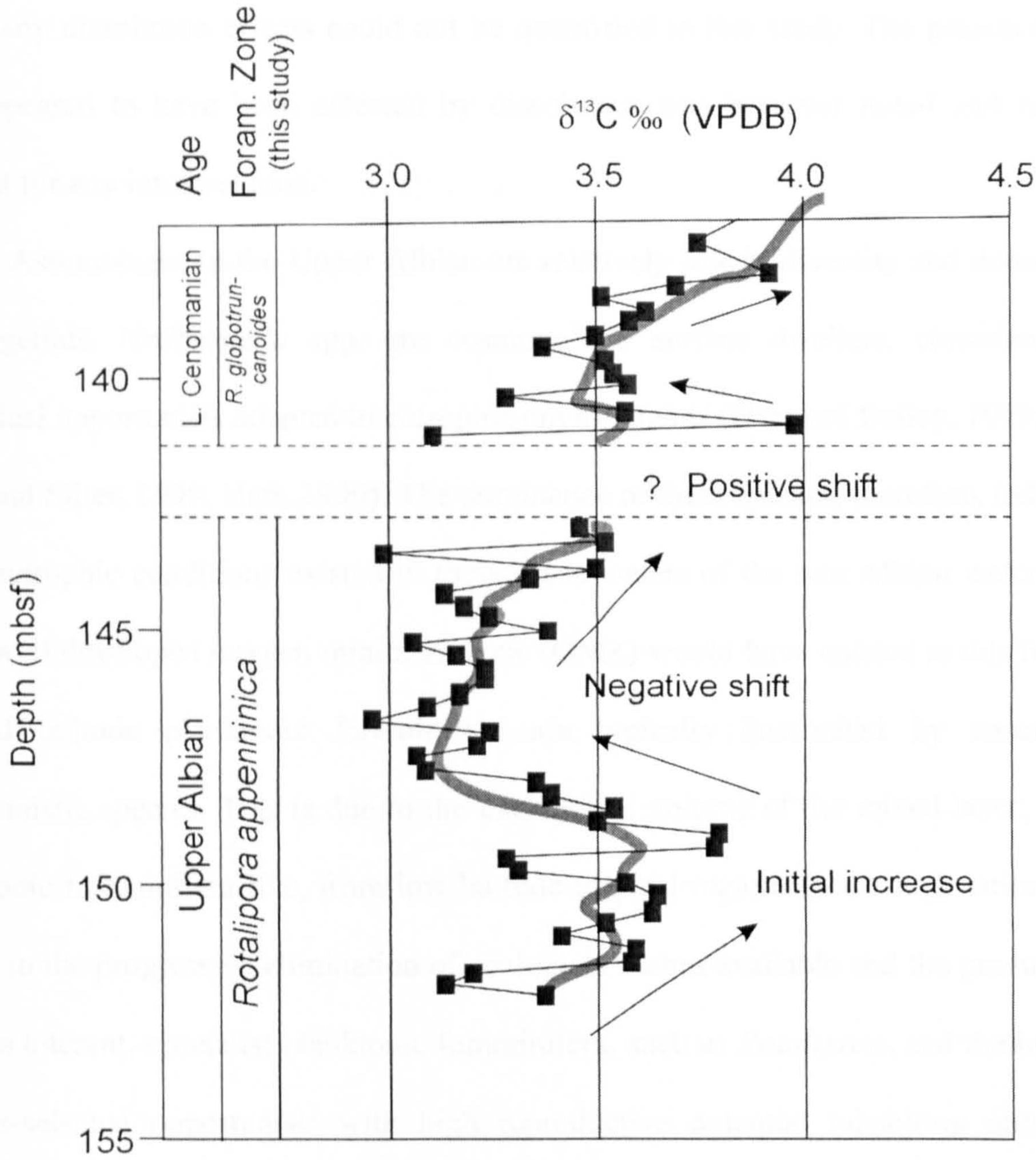

Figure 4.30: Close up of fine fraction carbon isotope data from Site 766 over the Upper Albian OAE 1d. The bold line shows a five point moving average of the values and the general trends in the isotope values. Similar trends are seen to those observed at Blake Nose and in the SE France; these trends are marked by black arrows.

Site 766 is thought to have remained above the CCD for the duration of its history (Gradstein *et al.*, 1990). However, as evidence of dissolution can be seen in specimens 10-12 of Figure 4.26 some dissolution may have occurred as the position of the CCD fluctuated. Interestingly, although dissolution is seen in these specimens, sample 15R-3,

110-112 cm in which they were found, is still dominated by the more fragile *Hedbergella planispira*. As mentioned above the lack of fragments in many of the core samples studied meant any dissolution effects could not be quantified in this study. The presence of tests that appeared to have been affected by dissolution was however noted and taken into account for any interpretation.

Assemblages in the Upper Albian are relatively low in diversity and dominated by hedbergellids. *Hedbergella* spp. are cosmopolitan surface dwellers, considered to be ecological opportunists adapted to eutrophic environments (Hart and Bailey, 1979; Premoli Silva and Sliter, 1999; Hart, 1999). The dominance of these species, therefore, indicate that meso-eutrophic conditions existed in the surface waters of the late Albian water column, and a well developed oxygen minimum zone (OMZ) would have existed at this time. Low to mid latitude planktonic foraminifera are typically dominated by cosmopolitan, opportunistic species. This is due to the decrease in volume of the mixed layer, in which planktonic foraminifera live, from low latitude tropical regions to the high latitudes. This results in the progressive elimination of ecological niches available and the gradual loss of the less tolerant, specialist planktonic foraminifera, such as *Rotalipora*, and the increase in these r-selected opportunists with high reproductive potential inhabiting nutrient rich waters close to eutrophic parts of the resource spectrum. They are therefore considered indicators of cooler/or unstable environments (Petrizzo, 2002).

Rotalipora species are present however at Site 766, although in low numbers. These are large, complex, keeled and flattened species, occupying deeper oligotrophic habitats at, or below, the thermocline (Corfield *et al.*, 1990; Price and Hart, 2002) and indicate a stratified water column in the Albian of Site 766. Prior to the Upper Albian planktonic assemblages lack Tethyan planktonic forms, such as age diagnostic *Ticinella* and *Biticinella*, this is probably due to cool high-latitude water masses being present at this time (Haig, 1992; Haig and Lynch, 1993). The presence of these species at lower latitudes in the Upper Albian therefore indicates the influx of warm waters and introduction of

Tethyan species to the region, most likely a result of eustatic sea level rise, and a significant shift southwards (of ~10° of latitude) of warm water surface-masses carrying Tethyan planktonic fauna along the northern and western margins of the Australian continent (Haig and Lynch, 1993).

The low numbers of *Rotalipora* support the presence of a well developed OMZ, limiting the growth and numbers of the species, and possibly some mixing of the upper part of the water column. An increase in numbers is seen however at the top of the Upper Albian, coincident with a reduction in the numbers of *Hedbergella*, this is likely to indicate a reduction in surface productivity and more oligotrophic conditions to prevail at this time. Although it must be noted that dissolution may be responsible for the low numbers of thin walled hedbergellids in this part of the core.

This distribution of planktonic species at higher latitude is similar to patterns seen today and to that postulated for the mid-Cretaceous. In modern oceans planktonic foraminifera inhabiting the mixed layer characteristically decrease in number from the tropics towards the higher latitudes (Silva and Sliter, 1999). This decrease is due to the progressive loss of less tolerant (K-selected) species, as the assemblages become dominated by the most tolerant cosmopolitan and opportunistic forms, typically of small sized, simple morphologies. A similar pattern is observed at intense upwelling zones, diversity decreasing with less stable conditions in the upper water column, this leads to the loss of stratification and decrease in ecological niches.

Benthonic foraminifera can additionally be used to assess the condition of the sea floor. At Site 766 a high diversity mix of both epifaunal and infaunal species of calcareous and agglutinated species are seen indicating oxic conditions. Species of *Gyroidinoides* and *Berthelina* dominate the fauna indicating meso- to eutrophic conditions at the sea floor, and increased organic flux (Erbacher *et al.*, 1999). *Gyroidinoides* has little tolerance of oxygen poor environments, its dominance indicating the oxic nature of the sediment-water interface. The abundance of *Gyroidinoides* does fluctuate however, and drops in

abundance can be observed to coincide with an overall decrease in benthonic diversity and an increase in morphotype BC1. BC1, defined by biconvex and trochospiral epifaunal specimens, is predominantly made up of species such as *Osangularia* which are tolerant of dysoxic, but not eutrophic, environments (Erbacher *et al.*, 1999). This distribution and change in dominance patterns indicates a generally mesotrophic to eutrophic, oxic sea floor. At times the sea floor became dysoxic, causing both the diversity and abundance of foraminifera to fall and giving rise to more low oxygen tolerant species.

Overall a relatively stable water column existed at Site 766 throughout the late Albian. Surface waters were productive and well stratified, with a well developed oxygen minimum zone. At times of enhanced productivity the OMZ expanded which led to fluctuations in the abundance of deeper dwelling planktonic foraminiferal species such as *Rotalipora*. Carbon and oxygen isotope data show stratification of the water column from sea surface to sea floor, with a marked difference between surface water and benthonic isotope values. The $\delta^{13}C$ gradient indicates productive surface waters and recycling of light carbon back into the water column, as organic matter is oxidised in the oxygenated bottom waters of the sea floor. The $\delta^{18}O$ values indicate a temperature gradient through the water column, and using the modified version of Craig's palaeotemperature equation (as given in Anderson and Arthur, 1983), estimates of sea surface and bottom water temperatures can be made. Using an isotope value of -1‰ for seawater, which is the $\delta^{18}O$ (SMOW) for ice-free conditions in polar-regions during the middle-Late Cretaceous (Shackleton and Kennett, 1975), all temperature estimates can be seen in Table 4.3. Sea surface temperatures through the Albian are estimated to be around 19-20°C. This is around 4-6°C cooler than current sea surface temperatures at Site 766, but 10-15°C warmer than current sea surface temperatures at a latitude of 50°S; the position Site 766 would have been in the mid-Cretaceous. These warm surface temperatures are consistent with those seen in other studies low latitude sites such as Site 511 on the Falkland Plateau (Huber *et al.*, 1995), and those proposed in models of the Cretaceous world (e.g., Barron, 1983). Bottom water

temperatures from benthonic isotope values are markedly lower giving palaeotemperature estimates of ~13-14°C, around 4-6°C less than the sea surface temperatures. Although this indicates a stratification and temperature gradient in the water column, it is much lower than is seen in modern oceans today (Huber *et al.*, 2002, fig. 3) Temperature gradients are typically lower at high latitudes than seen in equatorial and tropical regions which leads to a lower difference in temperatures from surface to bottom waters. Additionally ocean circulation in the Cretaceous was thought be dominated by warm saline bottom waters formed at low latitudes (e.g., Brass *et al.*, 1982), rather than the cold dense waters formed at high latitude polar regions today. This influx of warm water into the lower part of the water column would have also lowered the thermal gradient, and promoted more sluggish circulation in these regions. However although these warm sluggish waters promoted stagnant or dysoxic conditions, the sea floor remained largely oxygenated, with slight fluctuations to dysoxic conditions related to increased organic flux as the OMZ higher in the water column expanded.

This evidence, along with the lack of any organic rich sediments at Site 766 indicate that the water column remained generally oxic during the Upper Albian, with no encroachment of anoxic waters onto the sea floor. The isotopes shifts observed are therefore recording a global signal of enhanced organic deposition not seen at Site 766.

4.8.2.3 Cenomanian palaeoenvironmental change

The Cenomanian at Site 766 is very condensed. Small scale palaeoenvironmental changes defined in other studies are not well represented, therefore, and the typical isotope signature observed at other CTB sites is not seen in detail.

Globally the Cenomanian is a time of sea level and temperature rise, and this is represented at Site 766 by the diverse foraminiferal assemblages and influx of more Tethyan forms into the Austral realm. Planktonic foraminifera are abundant, in what would have been a well stratified water column with all niches of shallow to deep dwelling forms

present. *Rotalipora* and intermediate dwellers *Praeglobotruncana* and *Heterohelix* are still low in numbers, which again may be due to a well developed OMZ and meso- to eutrophic conditions in the upper part of the water column. Isotope results also indicate a stratified water column with a vertical temperature gradient of ~4-6°C, and a $\delta^{13}C$ gradient of 1.5-2‰, similar to that seen through the late Albian, indicating no collapse of stratification within the water column due to mixing over this time period. This gradient is also consistent with a number of other studies (e.g. Huber *et al.*, 1995; Price and Hart, 2002).

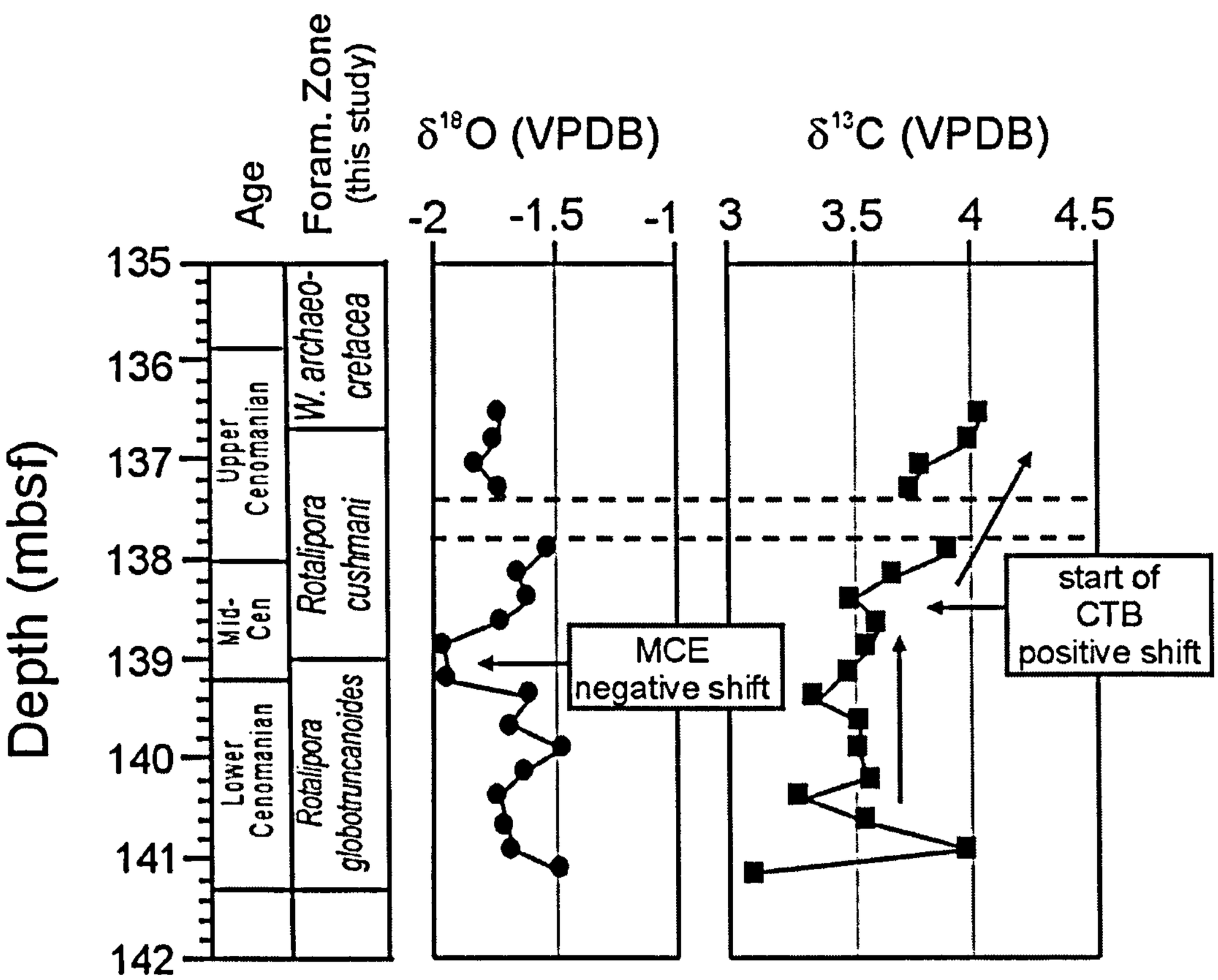

Figure 4.31: Close up of carbon and oxygen isotope fine fraction data from Site 766 over the Cenomanian. Main trends are shown related to the MCE and start of the CTBE. Dotted lines border interval of no core recovery.

Coccioni and Galeotti (2003) have presented data from the Umbria-Marche Basin in Italy, indicating a mid-Cenomanian event occurring in the *Rotalipora cushmani* Zone

which is associated with several changes associated with biotic and abiotic events. In particular an organisation of planktonic foraminiferal assemblages, a major change in benthonic foraminifera, a positive shift (0.7‰) in carbon isotope values and positive shift of Sr/Ca ratio. The event is preceded (~400Ky) by a short term negative (0.5‰) excursion in the oxygen isotope record (Jenkyns *et al.*, 1994; Coccioni and Galeotti, 2003). Although this event has only previously been identified in the northern hemisphere, some evidence of this event at Site 766 may be observed and is shown in Figure 4.31.

A 0.5‰ negative excursion is observed in the oxygen isotope record during the mid-Cenomanian (*R. cushmani* Zone), however no proceeding $\delta^{13}C$ shift, or Sr/Ca shift is observed. An increase in $\delta^{13}C$ values is seen in the mid-Cenomanian, however with the condensed nature of the Cenomanian at Site 766 it is impossible to differentiate any MCE positive shift from the general increase in $\delta^{13}C$ values through the upper part of the Cenomanian to the CTB.

Foraminiferal diversity remains high until the top of the *Rotalipora cushmani* Zone. Benthonic species are seen to dominate through the Cenomanian and this may be interpreted as related to palaeoenvironmental factors, although dissolution cannot be ruled out. The high abundance and diversity of benthonic specimens does however, indicate oxic conditions existed on the sea floor during the Cenomanian. Calcareous trochospiral species of *Gyroidinoides, Charltonina, Schiebnerova, Osangularia* and *Berthelina* again dominate the assemblages indicating meso-eutrophic conditions. However *Charltonina* and *Osangularia,* and to a leser extent *Berthelina,* do show a decrease over the Cenomanian possibly indicating increasingly more eutrophic conditions to which they are not tolerant, towards the CTB (Erbacher *et al.*, 1999). More changes occur as the CTB is approached and this is discussed below.

4.8.2.4 Cenomanian-Turonian palaeoenvironmental change

At the end of the Cenomanian a number of changes are seen within the water column and this is reflected in the isotope record and foraminiferal population, and are comparable with those seen at other CTB sites (e.g. Jarvis *et* al, 1988; Hart, 1996, 1999; Keller *et al.*, 2001; Coccioni and Luciana, 2004).

Sedimentologically a large change is seen from the pale clay rich Cenomanian nannofossil chalk and ooze to dark zeolite rich clays. These clays are extremely carbonate poor and barren of foraminifera so that it is impossible to obtain isotopic data for this part of the core. However, the presence of radiolarians and geochemical analysis can provide some information on the depositional environment of these clays. The clays are zeolitic, and represent a peak in the occurrence of zeolites at Site 766, coinciding with a high-stand in sea level (Gradstein *et al.*, 1990). Although deposited at the same time as the organic rich sediments on the Exmouth Plateau, the claystone of Site 766 does not contain any organic matter. This may have been due to a negligible flux of organic material to the sea floor, but evidence of productive surface waters imply that some organic matter would have fallen through the water column. It can therefore be inferred the clays were not deposited in anoxic conditions. The clays are rich, however, in trace elements such as manganese, iron, magnesium and strontium. The concentration of these elements in the CTB clays indicates the presence of an expanded OMZ in the water column. Manganese, for example, becomes mobilised in the anoxic waters, and is transported through the OMZ to deeper parts of the water column where it is oxidised and finely accumulated in the deep sea clays (Klinkhammer and Bender, 1980; Martin and Knauer, 1984; Thurow *et al.*, 1992). The presence of abundant, diverse and well preserved radiolarian specimens, which are considered eutrophic indicators (Hallock, 1987), indicates high surface productivity at Site 766 over the CTB interval. Similar radiations in radiolaria are seen in many CTB sediments globally and may indicate a global biosiliceous event (Thurow *et al.*, 1992). It can be postulated, therefore, that the clays were deposited beneath extremely productive

and eutrophic surface waters, which led to a highly expanded oxygen minimum zone in the water column. The lack of bioturbation and foraminiferal evidence in the CTB clays may be due to the temporary rise of the CCD coincident with the sea level rise and increase in productivity. It must be noted the presence of radiolaria may also be a product of condensation of the sediments at this level.

Although isotopic data was not obtainable from the carbonate poor CTB clays, changes in the environment leading up to, and following the deposition of the clay layer are evident, with an increase in carbon isotope, and decrease in oxygen isotope values apparent, along with rapid changes in both planktonic and benthonic foraminiferal assemblages.

The initial increase in $\delta^{13}C$ values by 1.2‰ (see Figure 4.32) through the mid-Upper Cenomanian at Site 766 indicates the removal of light carbon from the ocean carbon reservoir through enhanced burial of organic matter. However, as mentioned above, the clays at Site 766 show no organic carbon to be present, indicating either recycling of, or no enhanced delivery of, organic matter to the sea floor. With the absence of organic rich clays, the increase in carbon isotope values can be seen therefore to represent a global signal of enhanced burial of organic matter, both marine and terrestrial in origin (Hasegawa *et al.*, 2003). Although the isotope curve may represent local changes in surface and deep waters, a global drawdown of light carbon would be required to produce the magnitude of shift seen at a Site such as 766 with no organic rich sediments present. Although it must be noted that organic sediments are observed on the nearby shallower Exmouth Plateau, this will be discussed further below.

The carbon isotope profile observed at the CTB has been analysed at high resolution at a number of sites to provide an isotope stratigraphy of this global event (Pratt & Threlkeld 1984; Watkins, 1985; Gale et al. 1993; Pratt et al. 1993; Kennedy et al. 2000; Tsikos *et al.*, 2004; Gale *et al.*, 2005). Significant correlation has been seen between sites particularly in the northern hemisphere at the type section of Pueblo (USA) and the

expanded section of Eastbourne (UK), along with further correlation at sites such as El Kef in Tunisia and Gubbio in Italy. The typical CTB carbon isotope excursion has been described as showing a rapid build up and increase of $\delta^{13}C$ values to an initial peak. This is followed by a slight trough and a second peak and plateau, before a gradual decrease to background levels. Although condensed and parts of the core are missing at Site 766, a similar pattern to this is observed, further verifying the global nature of this event. These trends can be seen highlighted on Figure 4.32.

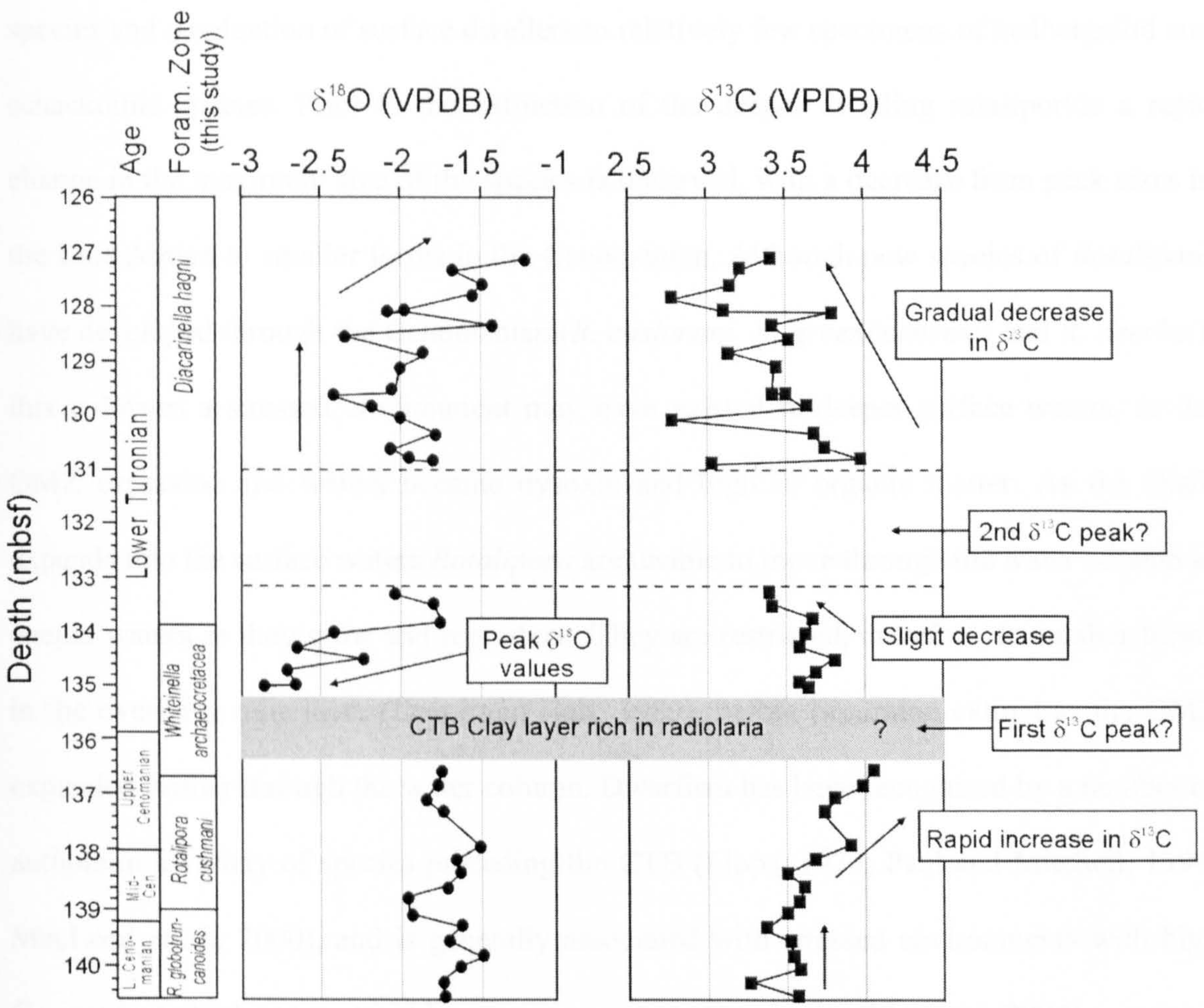

Figure 4.32: Close up of carbon and oxygen isotope data from Site 766 over the Cenomanian-Turonian Boundary. Main trends associated with the CTBE are indicated. Dashed lines indicate the portion of the core with no recovery.

This initial increase of $\delta^{13}C$ values over the Late Cenomanian, indicates the initial build up of the CTBE, and although bottom waters appear to have remained oxic, this global event did affect the water column and this is reflected by the changes observed in the biota at Site 766.

Cenomanian planktonic foraminiferal assemblages, still dominated by hedbergellids, with some deeper dwelling praeglobotruncanids and rotaliporids, indicate surface waters continued to be mesotrophic up to the CTB. Just prior to the, boundary, however the planktonic fauna underwent a large change with the extinction of rotaliporid species and a reduction of surface dwellers to relatively few specimens of hedbergellid and schackoinid species. Prior to the extinction of the deeper dwelling rotaliporids a rapid change in the maximum size of the species is observed, with a decrease from peak sizes in the Late Albian to smaller forms in the Cenomanian. Although new species of *Rotalipora* have developed through the Cenomanian (*R. cushmani, R. greenhornensis* and *R. deeckei*), this indicates a stressed environment may have existed in deeper surface waters, as the OMZ expanded and waters became dysoxic and high in organic matter. As the OMZ expands into the surface waters *Rotalipora* are unable to move through the water column to deeper waters as they grow and reproduce. They are restricted, therefore, to smaller forms in the overlying oxic layer (Leary and Hart, 1989), before becoming extinct as the OMZ expanded further through the water column. Dwarfism has been recognised by a number of authors in a variety of species preceding the CTB (Lipps, 1979; Paul and Mitchell, 1994; MacLeod *et al.*, 2000), and is generally associated with stressed environments with high C_{org} content, high nutrient and low oxygen waters (Coccioni and Luciani, 2004).

An abundant and diverse benthonic fauna, however, indicates oxygenated bottom waters continued up to the CTB, and although the clays are barren of foraminifera, the lack of organic matter indicates relatively oxic bottom waters continued to persist through the event. Some change in the benthos is seen, prior to the disappearance of foraminifera in the barren clays, with a decrease in epifaunal, trochospiral, biconvex and

plano/concavoconvex morphotypes (BC1 and BC2) and dominance of eutrophic tolerant shallow infaunal species such as *Gyroidinoides*. This may have been due to enhanced organic detritus from higher in the water column causing eutrophic conditions. The following barren conditions in the CTB clays are thought to be due to a rise in the CCD and not anoxic bottom waters at Site 766. However, calcareous, benthonic foraminifera would not have been able to live in such an environment, and the subsequent inferred fall in the CCD in the Early Turonian would have may have led to the recolonisation of habitats by the benthonic fauna. Similarly, if the sea floor was located below the CCD over the CTB, planktonic foraminifera would also be absent from the sediments. No assumption can be made, therefore, with regards to the planktonic assemblages over the CTB, other than the observed extinction of *Rotalipora,* and the decline in surface dwellers as seen in samples on either side of the barren Zone, although this decline may also be as a result of dissolution.

Following the deposition of the CTB clays oxygen isotope values show a marked decrease peaking just after the deposition of the CTB clay layer, at the very start of the earliest Turonian. Interestingly although the carbon isotope values are seen to increase over the Cenomanian at Site 766, oxygen values remain at background levels decreasing rapidly by 1.1‰ over the CTB to reach a value of -2.84‰, indicating a lag between draw down of light carbon and increase in temperature. This decrease in $\delta^{18}O$ corresponds to the highest temperatures observed in this study of Site 766, with a calculated palaeotemperature of 24.1°C, showing an increase of 5°C over the CTB. Corresponding to the rise in sea surface temperatures, bottom waters also increase by a similar amount to 18°C. These values for isotopic palaeotemperature estimates are comparable to other studies of mid-Cretaceous temperatures in southern high latitudes such as at DSDP Site 511 on the Falkland Plateau located at a palaeolatitude of 59°S (Huber *et al.*, 1995). These isotopically light benthonic values are not thought to be an artefact of diagenesis, for reasons outlined above and that the observed shift does not correspond with the negative shift of surface water values from

fine fraction and planktonic foraminiferal measurements. Additionally the diagenesis in pelagic chalk settings with shallow burial depths normally drives $\delta^{18}O$ values in the more positive direction (Schrag *et al.*, 1995; Huber *et al.*, 1999, Pearson *et al.*, 2001). This decline in $\delta^{18}O$ therefore indicates rapid warming of the whole water column in the Early Turonian and no breakdown of the thermal gradient at Site 766.

In parallel with the thermal gradient, the $\delta^{13}C$ gradient also remains through the Cenomanian and Turonian, however, it is reduced from a peak difference of ~2‰ before the CTB, to just 1‰ proceeding the clay deposition. This may indicate a less stratified water column. This is due to a reduction in the contrast of light carbon removal between the sea surface and sea floor, and a possible reduction in productivity at the sea surface, as fine fraction $\delta^{13}C$ values are seen to decrease at the top of the *Whiteinella archaeocretacea* Zone.

The decrease in oxygen isotope values is also brief, and values rapidly return to ~2‰ at the top of the *W. archaeocretacea* Zone, indicating surface temperatures of ~19-20°C. Interestingly bottom water temperatures decrease much more slowly and are estimated still to be ~17°C at the top of the *W. archaeocretacea* Zone. The thermal gradient was decreased from 1.5 to 1‰ (equivalent to 3°C). This may be due to an increase in bottom water circulation and influx of warm saline bottom waters at this time, and enhanced mixing of the water column.

Concurrently with this postulated palaeotemperature high and subsequent decrease in temperatures, and inferred decrease in productivity in this early part of the Turonian, foraminifera also return to the sea floor and water column. Initially planktonic shallow and intermediate dwellers (*Hedbergella* and *Whiteinella*) are present but not in high numbers. This may be due to the effect of dissolution, however with the absence of the thicker more robust tests of deeper dwelling planktonics (*Praeglobotruncana* and *Rotalipora*) and the abundance of benthonic foraminifera on, and within the sea floor, it can be inferred that this assemblage represents the actual planktonic distribution of the early Turonian,

signifying oxic surface waters. Radiolaria are also present but in fewer numbers than previously recorded, possibly indicating a reduction in productivity, in line with the decrease in $\delta^{13}C$ values as discussed above. Also present in the surface waters are calcispheres. Previously described as *Pithonella* spp., these small calcite "balls" are thought to represent calcified dinoflagellate cysts (Hart, 1992), and have been found in abundance in Early Turonian sections such as those seen in the UK (Jarvis *et al.* 1988; Hart, 1991), the Alps (this study; Hart, *pers. comm.*) and Spain (Caus *et al.*, 1997). Used as an indicator of the CTB extinction event these cysts are thought to represent times of environmental stress, the dinoflagellates producing cysts as a mechanism for survival (Hart, 1991), calcispheres increasing greatly in numbers just as organic-walled dinocysts become reduced (Jarvis *et al.*, 1988). Although not present in high numbers at Site 766 it is important to note their presence.

By the start of the *Dicarinella hagni* Zone waters have become markedly more stable, hedbergellids are still present in low numbers but a dominance is now seen in keeled foraminifera, particularly *Dicarinella*, indicating normally stratified, oligotrophic surface waters, to exist at this time. Coincident with a second increase in $\delta^{13}C$ values, *Hedbergella* rapidly increase in numbers, however, as mesotrophic conditions appear to dominate the rest of the *Dicarinella hagni* Zone. Diverse assemblages are seen with low numbers of deep to intermediate dwellers (*Dicarinella, Helvetoglobotruncana* and *Praeglobotruncana*), shallow water species of *Whiteinella,* and high numbers of opportunistic species of *Hedbergella, Heterohelix* and *Schackoina*. Present in low number throughout the core, *Heterohelix* and *Schackoina* show a huge increase in numbers in the Lower Turonian. Often regarded as indicators of stressful surface water conditions, large increases, particularly in *Heterohelix*, have been seen associated with the CTB (Leckie *et al.*, 1998; Nederbracht *et al.*, 1998; Keller *et al.*, 2001; Keller and Pardo, 2004). This '*Heterohelix* shift' has been used as a global biomarker reflecting the expansion of the oxygen minimum zone, after the major sea level transgression and $\delta^{13}C$ excursion in the

Late Cenomanian. Occurring higher in the section observed here, the shift is coincident with the latter part of the $\delta^{13}C$ excursion and has also been observed at other sections occurring in the Lower Turonian (e.g. Huber *et al.*, 1999). Typically this shift is accompanied by low diversities. The Lower Turonian samples at Site 766 show, however, high diversities and species representing a variety of depth habitats. The increase in *Heterohelix*, may reflect therefore eutrophic to mesotrophic conditions in the surface waters and normal ocean stratification, as both oxygen and carbon isotope values return to background levels. Sea surface palaeotemperatures at the top of the core are estimated as having been ~17°C. Interestingly both carbon and oxygen profiles show much higher fluctuation in values than in earlier parts of the core. This may be a diagenetic effect with carbonate to clay alternations occurring regularly through the *Dicarinella hagni* Zone. Additionally bioturbation is much less prominent in this portion of the core, which when present can cause small scale mixing of sediment and less fluctuation in the isotope values seen.

On the sea floor following the deposition of CTB clays, the recolonisation of the benthonic fauna is similar to that seen elsewhere following environmental stress, and a clear pattern is seen with the introduction of more opportunistic (r-selected) forms. An initial increase in the infaunal agglutinated forms (*Tritaxia* and *Gaudryina*) and infaunal calcareous forms including *Praebulimina* and *Pleurostomella*, and epifaunal species of *Berthelina, Lingulogavelinella* and *Iuliusina*, are represented by morphotypes BC2, BC3 and BA5. One form of *Berthelina* is particularly abundant along with eutrophic species of *Gyroidinoides*. This species, *Berthelina.* sp. 2 is a plano-convex species with moderate to low trochospire and rounded periphery. It is present throughout the core in moderate abundance, however, it shows a high increase in abundance at the CTB. Koutsoukos and Hart (1990) indicate species such as this are r-selected opportunists able to live in aerobic to dysaerobic, meso- to eutrophic conditions. Coincident with the decrease in $\delta^{18}O$ values and postulated increase in bottom water temperatures, this increase in diversity and

abundance of benthonic foraminifera may also have been due to an influx of warmer nutrient rich waters. This would have led to the rapid proliferation of species and subsequent decline as competition increased.

The top of the core sees a typical open ocean assemblage of foraminifera of a predominantly planktonic fauna associated with a variety of epi- and infaunal benthonic species.

4.8.3 Site 762

Sediments found at Site 762 indicate that open-ocean pelagic conditions prevailed throughout the Aptian to Turonian interval, with carbonate rich nannofossil chalks and clays being deposited. These sediments were generally well oxygenated containing an abundant biota and evident bioturbation of the sediments. At the CTB, however, a 23 cm dark brown fissile clay was deposited. Carbonate poor and barren of foraminifera at the base, it appears that the clay was deposited in dysoxic or anoxic conditions. The clay has a gradational boundary upwards into nannofossil chalks and the depositional environment will discussed further below.

The isotope data give us some information on the chemistry and temperature of the water column and, therefore, the depositional conditions in which these sediments formed. However, in order to fully analyse the data, the diagenetic potential of the sediments must assessed and any evidence of diagenesis analysed. This was done at Site 762 by analysing thin sections of the sediments, looking at the preservation of foraminifera using thin sections and scanning electron imagery, and from trace element analysis.

4.8.3.1 Diagenetic potential at Site 762

Sediments at Site 762 were deposited at water depths of around 1350m. They were subsequently buried and the sediments analysed in this study at depths of 830 mbsf. Burial

to such depths increases the diagenetic potential greatly, sediments becoming exposed to high temperatures and fluids different from those in which the carbonate was deposited.

Similar to Site 766 the clay rich sediments were less prone to diagenetic alteration than the carbonate chalks and foraminifera are likely to be better preserved in the clay matrix.

Trace element analysis of the sediments show no coeval increases in manganese and iron as would be expected in diagenetic environments. However a marked increase in Fe/Ca and Mg/Ca ratios is seen in the clay rich Albian sediments. The increase of these elements in the sediments could have been partially related to increased levels of dissolved Mg2+ in pore-fluids, a likely consequence of the decomposition of volcaniclastic materials to Mg-rich clays [e.g., smectite, $(Al, Mg)(OH)_2Si_4O_{10}Na(H_2O)_4$] during burial (Lawrence *et al.*, 1979, Whittaker *et al.*, 1987, Pirrie & Marshall, 1990). No evidence of diagenesis is otherwise seen in the presence of trace elements. Similar to Site 766 an increase in trace elements is also seen within the claystone at the CTB. This is, however, again due to the composition of the clay as opposed to any diagenetic signal.

Thin sections were taken at intervals through the core to analyse any secondary calcite in the sediments or associated with the foraminiferal test. The sections show the samples to consist predominantly of micritic packstones and wackestones. Examples of these sediments can be seen in Figure 4.33. From the thin section analysis it can be shown that there is little secondary calcite cement lithifying the chalks found in the core. However, the foraminifera are nearly all infilled with abundant secondary calcite, seen in the thin sections as large calcite crystals. Test walls, although initially appearing well preserved and at times retaining the original wall structure (Figure 4.33E) and original surface textures, also show evidence of recrystallisation. The preservation of the foraminifera can further be examined using the scanning electron microscope; this can be seen in Figure 4.34.

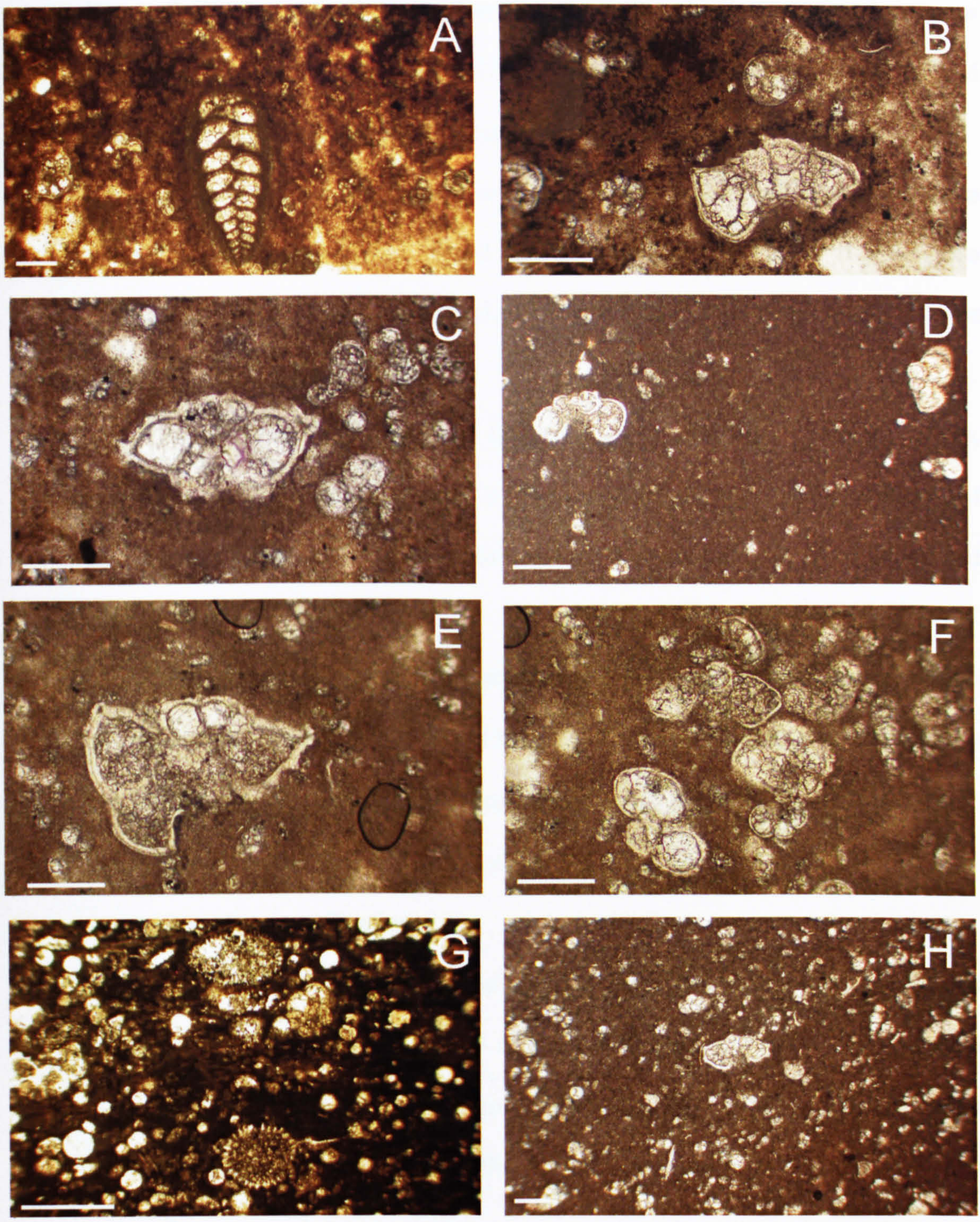

Figure 4.33: Photomicrographs of thin-sections taken of sediments from Site 762. All scale bars 200 μm.

A) Packstone from the nannofossil chalk of the Lower Cenomanian *Rotalipora reicheli* Zone (sample 77X-1, 98-100 cm, 820.40 mbsf). A large agglutinated benthonic, *Dorothia* spp. is present with abundant small *Hedbergella* spp. in a micritic matrix. Each foraminifera shows infilling with sparry calcite, and recrystallisation of the test walls of the smaller calcareous foraminifera.

B) Packstone from the nannofossil chalk of the mid-Cenomanian *Rotalipora reicheli* Zone (sample 77X-1, 98-100 cm, 820.40 mbsf), showing largely infilled *Rotalipora reicheli* and hedbergellid specimens.

C) Packstone from the nannofosssil chalk of the mid-Cenomanian *Rotalipora reicheli* Zone (sample 76X-3, 50-52 cm, 818 mbsf). A specimen of *Rotalipora brotzeni* and some small hedbergellids are seen. Again all show infilling and some recrystallisation of the test wall.

D) Wackestone from upper Cenomanian *Rotalipora cushmani* Zone, nannofossil chalks (sample 76X-2, 40-42 cm, 816.40 mbsf). Species of *Hedbergella, Whiteinella* and *Praeglobotruncana* are present showing infilling and recrystallisation.

E) Packstone from the nannofossil chalk of the Upper Cenomanian *Rotalipora cushmani* Zone (sample 75X-1, 149-150 cm, 810.99 mbsf). Specimen of *Rotalipora deeckei* showing large crystals of calcite infilling test. The wall structure appears to be quite well preserved showing a double layered structure, although there are some signs of recrystallisation.

F) Packstone from the nannofossil chalk of the Upper Cenomanian *Rotalipora cushmani* Zone (sample 75X-1, 149-150 cm, 810.99 mbsf). *Rotalipora cushmani* and *Whiteinella archaeocretacea* are present together with the some smaller hedbergellids present. Abundant infilling is again seen, with recrystallisation of the test walls.

G) Clay rich nannofossil chalk from just above the Cenomanian-Turonian Boundary claystone. Abundant radiolaria and silicified calcispheres are present.

H) Packstone from the nannofossil chalk of the Lower Turonian *Helvetoglobotruncana helvetica* Zone. A specimen of *Dicarinella hagni* is shown with prominent double keel in micritic matrix and abundance of small unkeeled hedbergellids. Secondary calcite infilling present.

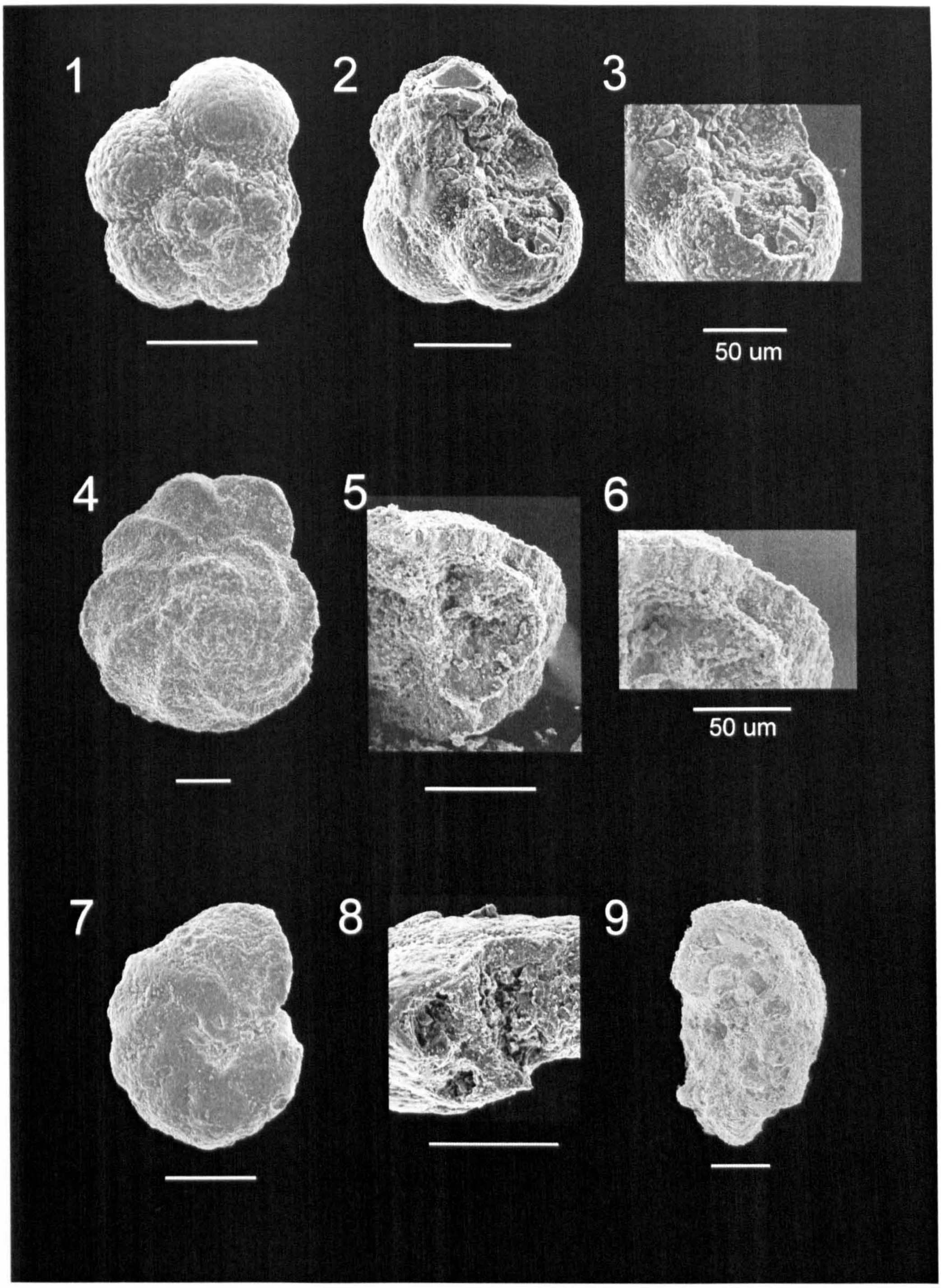

Figure 4.34: Photomicrographs illustrating the preservation of foraminiferal tests at Site 762. All scale bars are 100 μm unless otherwise stated.

1) *Hedbergella delrioensis* 78X-2, 10-12 cm Upper Albian

2) *Hedbergella delrioensis* 78X-2, 10-12 cm Upper Albian

3) *Hedbergella delrioensis* 78X-2, 10-12 cm Upper Albian

4) *Rotalipora globotruncanoides* 77X-3, 5-7 cm Lower Cenomanian

5) *Berthelina* sp. 2 76X-1, 121-123 cm Upper Cenomanian

6) *Berthelina* sp. 2 76X-1, 121-123 cm Upper Cenomanian

7) *Berthelina* sp. 78X-2, 10-12 cm Upper Albian

8) *Berthelina* sp. 3 74X-3, 10-13 cm Lower Turonian

9) *Dicarinella hagni*, 74X-3, 10-13 cm Lower Turonian

The foraminifera predominantly show poor to moderate preservation. The majority of the tests are infilled, and show overgrowths of secondary calcite on the test walls. Many of the tests also show evidence of recrystallisation.

It was decided to measure the isotopic composition of species of foraminifera from Site 762, although it was understood that the absolute values of the isotope measurements would probably be pushed towards more negative values (from burial diagenesis) it was hoped that the relative values would provide some information on the condition of the water column and that some of the diagenetic processes affecting calcareous foraminifera buried to deep levels could be understood. Presuming diagenesis occurred at burial depths beneath the sea floor, it is thought that due to temperature fractionation in oxygen isotopes, this burial will lead to more negative values in the reprecipitating carbonates, as temperatures increase with depth below the seafloor (Marshall, 1992). Carbon isotopes, however, are not as affected by temperature and in a calcium carbonate environment it is thought that diagenesis occurs in a relatively closed system. Secondary calcites forming from solutions of the original calcite, and therefore precipitating out at a similar composition. The porosity of the carbonate will affect this, however, and the more porous the rock the more externally sourced pore waters may affect the composition of the secondary calcite. It is thought, therefore, that the lower more clay rich sediments will yield better preservation of the foraminifera.

Although it is recognised that many of the specimens are infilled, care was taken in picking the specimens for analysis to limit the diagenetic alteration as much as possible,

only choosing those with the least amount of external alteration.

As with the results of Site 766, the carbon and oxygen values of Site 762 were also plotted against each other in order to understand any diagenetic processes that may have occurred further. Cross plots of oxygen and carbon isotope results from fine fraction and foraminiferal results are shown in Figure 4.35.

Initial analysis of the results in Figure 4.35 show that each species of foraminifera, and the fine fraction results, plot at a distinct position on the cross plot diagram. With regards to oxygen isotopes each species plot relative to each other as would be expected with respect to temperature. Benthonic species *Berthelina* spp. exhibiting the most positive isotope values, indicative of cooler bottom waters. Shallow dwelling planktonic *Hedbergella* spp. show the most negative values indicating warm surface waters, and the keeled deeper dwelling planktonics show intermediate values, between the inferred shallow and benthonic organisms. However, this pattern may also be indicative of diagenesis, and a diagenetic signal as opposed to a primary signal may exist in the isotopic measurements of Site 762.

As discussed in Section 4.8.2.1 a covariance of carbon and oxygen isotope values indicate diagenesis may have occurred. At site 762 fine fraction, and to a lesser extent *Berthelina*, measurements both show a similar trend, with a coincident shift of oxygen to more positive values and carbon to more negative. A linear regression was applied to this data and the trend lines and r^2 values can be seen on Figure 4.35.

This covariance (although not statistically significant) is suggestive of early seafloor diagenesis, carbonates reprecipitating out in equilibrium with the colder bottom waters that are rich in heavier oxygen, and lighter carbon as organic matter is oxidised. The light carbon is returned to the water column (Marshall, 1992). Interestingly it is the deepest buried Albian sediments which show the strongest covariance, possibly due to reduced sedimentation rates at this time, and, therefore, slower burial. The sediments are therefore exposed potentially to seafloor diagenesis.

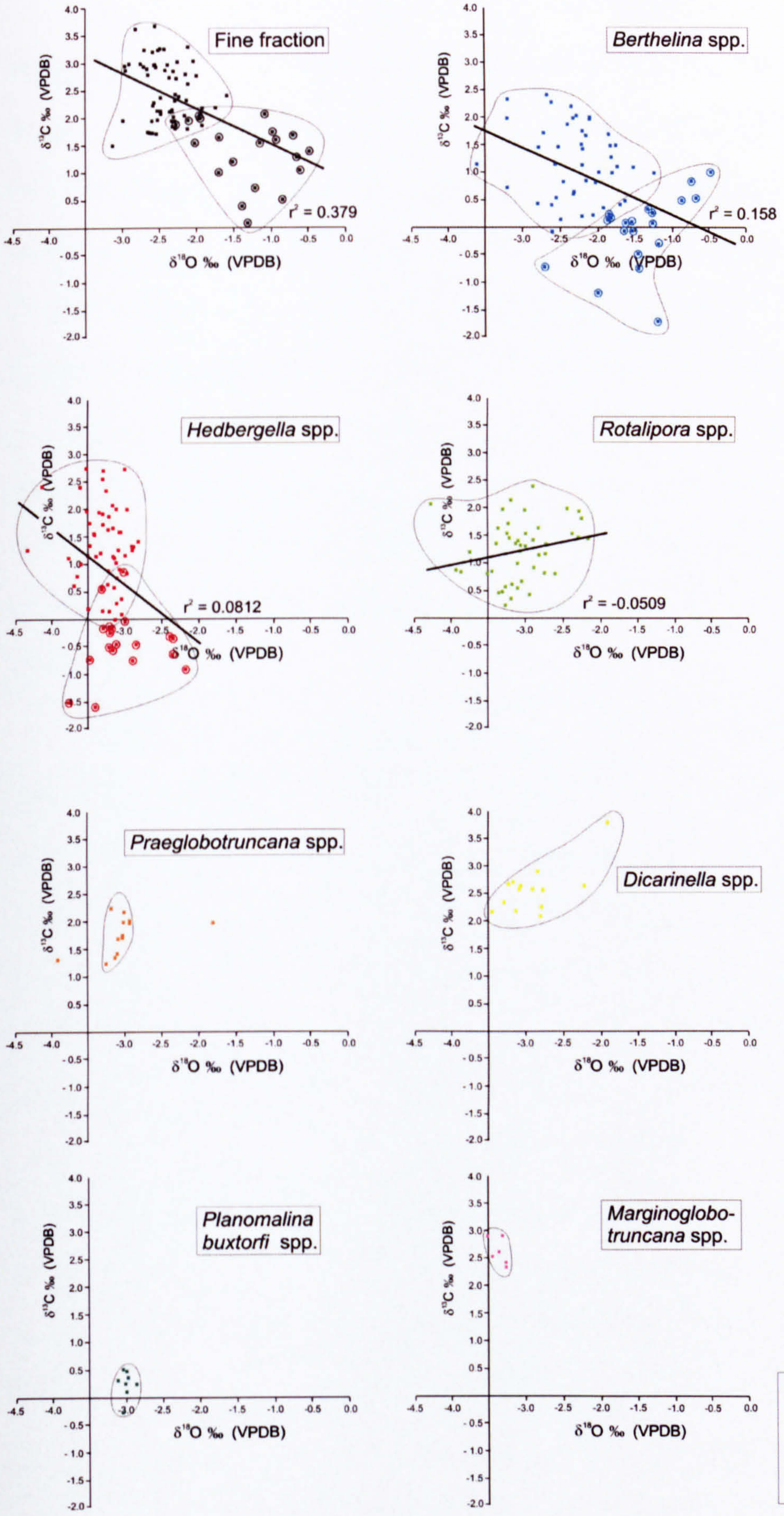

Figure 4.35 Cross-plot of oxygen and carbon isotope values from fine-fraction and all foraminiferal samples of Site 762. r^2 values are given to show the amount of covariance.

The effect of sea floor diagenesis is seen most markedly in the less robust oxygen isotope system. In unaltered sediments one would expect to see a difference in fine fraction (reflecting sea surface conditions) and benthonic measurements, similar to that seen at Site 766. This is reflecting a temperature gradient in the water column. At Site 762, however, benthonic and fine fraction results show near identical profiles in both value and variation. A weak gradient may exist in upwelling or intensely mixed waters, but with other diagenetic evidence presented here, and very different planktonic isotope values, there is no evidence to suggest well mixed waters at this time. Samples of *Hedbergella* spp., also show a similar trend in these lowermost samples from the Upper Albian (Figure 4.35), with the specimens demonstrating the most positive oxygen isotope values, also recording the most negative carbon values. This indicates these samples may also have been affected by sea floor diagenesis.

Through the Cenomanian and Turonian samples show quite different trends. Both fine fraction and *Berthelina* samples show a more general spread of values on the cross plots, with no or very weak covariance of oxygen and carbon isotope values. *Rotalipora* results also show a spread of values, with no distinct covariance. The $\delta^{18}O$ values, however, are not as widespread as those observed from the fine fraction and benthic foraminiferal samples, generally ranging from -2 to -4 ‰. *Hedbergella* spp., and to a lesser extent the other planktonics, however, show an even more distinct trend in values. A spread of $\delta^{13}C$ values is observed, but only a very narrow range of $\delta^{18}O$ values is seen, with measurements generally ranging around 3 to 3.5 ‰. Only a few Cenomanian and Turonian measurements lying outside this range. The palaeotemperature estimate obtained from 3‰ is 24.8°C, similar to what would be expected for sea surface temperatures around the CTB. However it is generally accepted that the Cenomanian-Turonian was a time of global warming and in comparison with other results from southern latitudes (this study; Huber *et al.* 1995; Clarke and Jenkyns, 1999) a decrease in surface water $\delta^{18}O$ values to more negative values would expected to be seen. Such a narrow spread of oxygen values

through the Cenomanian and Turonian, indicate that the $\delta^{18}O$ values are more likely to be a result of late stage burial diagenesis. With burial depth temperatures increase at a rate of ~27°C/km (Hunt, 1979). At a burial depth of ~800 m at Site 762, a temperature of ~22.5°C would be expected. This is similar to the palaeotemperature obtained from the *Hedbergella* spp. of 24.8°C. It is therefore likely the planktonic specimens analysed at Site 762 are largely affected by burial diagenesis. Calcite infilling the foraminiferal test reprecipitating out of the pore waters in equilibrium with the higher temperatures. Carbon is much more robust and is not affected by temperature to the same extent as oxygen, as discussed above. The carbon isotope values may, therefore, preserve some original signal, or at least relative changes through the core, if not absolute values.

All samples were buried to depths ~800 mbsf, so it is interesting that *Berthelina* spp., fine fraction samples, and to a lesser extent species of *Rotalipora* show little covariance of isotopic values. Benthonic foraminifera have been noted previously as being less prone to diagenesis in earlier studies (e.g., Pearson *et al.,* 2001; Gustafsson, *et al.*, 2003) and deep water palaeotemperature estimates are often found to be more reliable from these species. *Hedbergella,* in contrast, shows the most distinct vertical trend in carbon and oxygen isotope values. This may be due to the thin walled nature of the test of *Hedbergella*, making it more susceptible to dissolution and diagenesis than the thicker test of *Rotalipora* and *Berthelina.* Additionally these small tests would be more sensitive to a small amount of diagenetic $\delta^{13}C$ or $\delta^{18}O$ being incorporated into the test. This could cause a quite large effect, compared to a similar amount in the larger and thicker walled test where it would make little difference to the overall composition of the test.

The analysis of the carbon isotope profile of foraminiferal values, both benthonic and planktonic results show a convergence through the core. The fine fraction samples, however, plot at markedly more positive values. The convergence of the foraminiferal isotope profiles is consistent with either breakdown in water stratification, or diagenesis, which can typically lead to the convergence of $\delta^{13}C$ and $\delta^{18}O$ to equilibrium values

depending on the environment of diagenesis. In this case values become more negative, indicative of burial. The thin walled *Hedbergella* showing the greatest shift to more negative values.

It is difficult to determine the full diagenetic history of Site 762 which is complex and not within the scope of this project. However, a number of assumptions can be made. The sediments of Site 762 underwent both early seafloor diagenesis, and subsequent late diagenesis at depth. Early diagenesis is most prominent in the Upper Albian samples where a covariance is seen; oxygen isotopes becoming more positive as carbon isotopes became more negative. These sediments are the most clay rich of the core and the subsequent overprinting of the isotope signal by burial diagenesis may not have affected these sediments due to the nature of the clay as discussed above. Burial diagenesis is then thought to have occurred at depth, normalising all values to ~3‰ (±1‰ depending on species). Carbon isotope values are not as affected by this diagenesis. Although $\delta^{13}C$ values are thought to typically become more negative with depth, which may account for the convergence of species data on the $\delta^{13}C$ isotope curve. Following the early diagenesis of Albian fine fraction samples, the 'bulk' samples do not appear to have subsequently been as affected as the foraminiferal species, and a general shift from 2 to 4‰ is seen through the Cenomanian to the CTB. This is in line with other analyses of the CTB (Tsikos *et al.*, 2004; Paul, *et al.*, 1999) and therefore implies some primary signal has been retained in this core.

The oxygen isotope profile of the fine fraction samples also shows some trends which could be interpreted as primary palaeoenvironmental change, especially related to the expected negative shift of $\delta^{18}O$ values at the CTB. These trends can be seen in Figure 4.36. Values of the same magnitude from this core are used by Clarke and Jenkyns (1999) in their study of long term Cretaceous climate change in the Southern Hemisphere (discussed further in Chapter 7).

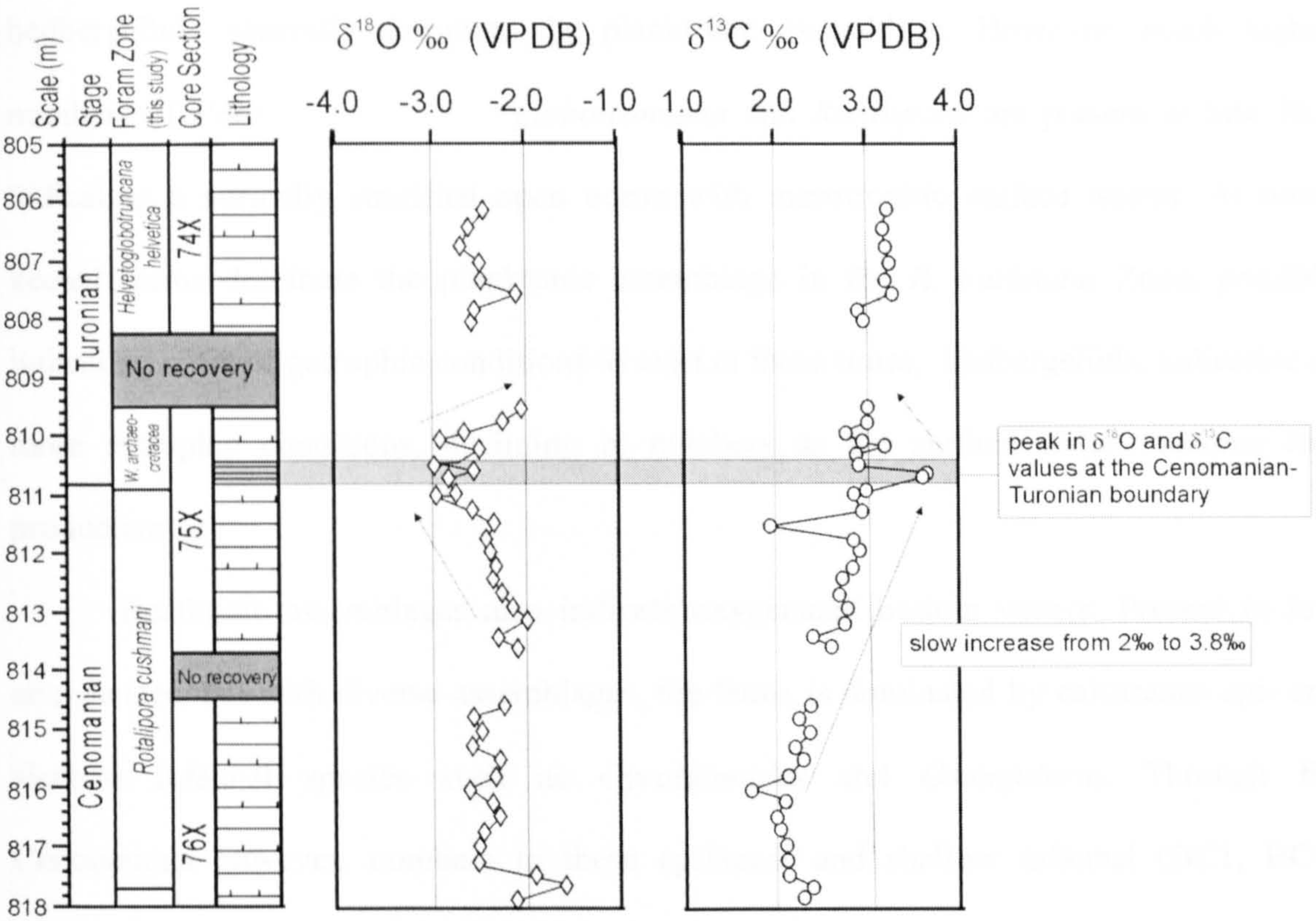

Figure 4.36: Close up of oxygen and carbon isotope profiles from fine fraction samples across the Cenomanian- Turonian boundary.

It is apparent, therefore, that Site 762 is highly affected by diagenesis and alteration of the carbonates. As has been discussed above some information can be gained on the palaeoenvironment of the core, these will be discussed further in conjunction with foraminiferal palaeoenvironmental evidence to fully analyse the core in section 4.8.3.2. Due to the diagenesis of the oxygen isotope signal, palaeotemperatures have not been calculated for the foraminiferal analyses and fine fraction palaeotemperature estimates will be referred to where necessary in the text.

4.8.3.2 Cenomanian palaeoenvironmental change

On the shallower Exmouth Plateau, Site 762 shows a fully Tethyan assemblage of planktonic foraminifera through the Cenomanian. Abundance and diversity are high and there is no evidence of dissolution. Planktonics dominate the samples and, as at Site 766

hedbergellids generally dominate the planktonic assemblage. However, much higher numbers of *Prae* *globotruncana* and *Rotalipora* are present at Site 762, indicating a normally stratified open ocean with mesotrophic surface waters. At times keeled forms dominate the planktonic assemblage in the *R. cushmani* Zone, possibly indicating more oligotrophic conditions to exist at these times, hedbergellids, indicative of more eutrophic conditions, declining in numbers as the surface waters become less productive.

Benthonic assemblages also indicate oxygenated bottom waters. Present in low abundances, but with diverse assemblages, the fauna is dominated by calcareous epi- and shallow infaunal species such as *Gyroidinoides* and *Osangularia*. Through the Cenomanian however, numbers in these epifaunal and shallow infaunal (BC1, BC4) species decrease and infaunal morphotypes BC7, BC8 and BC9 begin to dominate, as abundance declines. This possibly indicates more stressful and dysoxic conditions on the sea floor leading up to the CTB. This is coincident with a postulated increase in carbon isotope values, and warming of the surface waters in the upper half of the *Rotalipora cushmani* Zone.

Planktonic taxa in the upper portion of the *R. cushmani* Zone also show a change in dominance and assemblage. Unkeeled trochospiral morphotypes still dominate but a marked increase in *Heterohelix* is recorded. As discussed above, *Heterohelix* is considered as an opportunistic, low oxygen tolerant genus, and has been seen to thrive in low-middle latitudes in well stratified open marine settings with a well developed oxygen minimum zone (Keller *et al.*, 2001) and abundance of this genus, therefore, often reflects the expansion of the oxygen minimum zone. This increase is coincident with an increase in the intermediate water dwellers *Praeglobotruncana* and *Whiteinella,* considered to be r/k selected species, and a decrease in oligotrophic, K-selected *Rotalipora*. Premoli Silva and Sliter (1999) suggest this change in foraminiferal assemblage indicates the onset of less stable, eutrophic conditions, culminating in the events seen at the CTB.

4.8.3.3 Cenomanian-Turonian palaeoenvironmental change

The Cenomanian-Turonian boundary at Site 762 is represented by a dark claystone. Nearly black and clay rich at the bottom, this layer has a gradational boundary with the overlying chalks, slowly becoming more carbonate rich. Although adjacent to organic rich (up to 15% TOC) shales found at the CTB of Site 763 (located on the Exmouth Plateau 84 km to the south of Site 762) only low amounts of organic carbon are found at Site 762, with no more than 2% TOC being recorded (Haq *et al.*, 1990). Located at similar depths, Site 762 lies slightly more oceanwards than Site 763, which is also situated on a topographic high. Which may explain the lack of organic rich shales at Site 762. This will be discussed further in Chapter 7. However, the small amount of TOC and nature of the boundary sediments may indicate dysoxic conditions to have prevailed at the CTB.

Just prior to the CTB foraminiferal assemblages underwent further modification and change. The number of *Heterohelix* increased even more as *Hedbergella* numbers decreased, indicating further expansion of the OMZ. Supporting this expansion are a number of other changes in the foraminiferal assemblage. Increases are seen in the numbers of *Schackoina,* another low oxygen tolerant species (Coccioni and Luciana, 2004), and the extinction of *Rotalipora*. Declining in numbers through the upper part of the *Rotalipora cushmani* Zone, the last species (*R. deeckei* and *R. cushmani*) becomes extinct just before claystone deposition. Jarvis *et al.* (1988) suggest this extinction is due to the expansion and intensification of the OMZ into shallower waters. Initially this would cause the progressive decline of the genus, as the individuals were unable to reproduce as the deeper waters became oxygen deficient, as this effect increased and became prolonged the subsequent extinction of the deep water species occurred. Species of intermediate water dwellers (*Whiteinella* and *Praeglobotruncana*), also decrease in number, but remain present in the water column until the onset of clay deposition indicating the anoxic waters did not reach these intermediate levels at this time. Although the decline in numbers may be due to anoxic waters expanding to levels at which these species descend during there

reproduction cycle (Jarvis *et al.* 1988; Hart, 1996). It is likely the *Rotalipora* were already under stress with increased competition from the rise of *Dicarinella* and *Praeglobotruncana* species, although *Dicarinella* are not see in the Cenomanian at Site 762, this genus is often found in uppermost Cenomanian sediments coincident with the decline in rotaliporid numbers (Keller and Pardo, 2004).

Coincident with these major changes in the shallower planktonic environment, the abundance and diversity of benthonic foraminifera remains low, assemblages being represented by only a few infaunal agglutinated and calcareous specimens such as *Tritaxia, Gaudryina, Textularia, Praebulimina* and *Tappannina*. A slight increase in the number of *Gavelinella* spp. is typical of low oxygen conditions.

In the black clay boundary layer no foraminifera are recorded, although radiolaria are present, having increased in abundance over the CTB and indicating highly intensified productive surface waters. Very little organic matter is deposited within the black clays but the lamination and lack of benthos and bioturbation indicates that dysoxic waters may have prevailed at this time. An absence of planktonic foraminifera also indicates a largely anoxic or dysoxic water column. However, dissolution induced by the strong oxidation of organic matter can occur (Coccioni and Luciana, 2004) and very high fertility may have prevented even the most eutrophic of forms from surviving. It is difficult therefore to presume the existence of completely anoxic shallow waters at the CTB. However, the OMZ was clearly extremely expanded at this time, and productivity in the oxic surface waters high.

Only the base of the clay layer is barren of foraminifera and within 10 cm an extremely diverse and abundant benthos is observed indicating more oxygenated conditions had returned to the bottom waters.

Benthonic species meanwhile show a huge increase in diversity and abundance, dominating the assemblages in the upper part of the clay layer. Dominated by infaunal species a range of agglutinated and calcareous forms are seen with particularly high

numbers of *Bolivina*, accompanied by *Praebulimina, Pleurostomella, Tritaxia, Gaudryina* and *Eggerellina*. The dominant species is *Berthelina* sp. 3, a planoconvex morphotype, with rounded periphery and moderate spire. This species shows similarities to *Gavelinella plummerae*, a shallow infaunal/semi-infaunal opportunistic species that is thought to have been able to tolerate low oxygen conditions (Lamolda, and Peryt, 1995). These species seen are typical of an opportunistic assemblage recolonising the sediment following the disappearance of species in unfavourable and stressful conditions. Infaunal, or potentially infaunal species are thought to be more tolerant of dysoxic or low oxygen conditions, making use of food availability within the sediment and often adopting alternative life strategies in order to survive e.g. metabolic depression or becoming facultive anaerobes (Bernard, 1993).

Following this rapid diversification of benthonic species numbers fall dramatically as bottom water conditions improve and the assemblage returns to a similar diversity and dominance of species as that seen prior to the CTB. Marked changes in carbon lux and bottom water oxygenation are suggested by fluctuations in benthonic foraminiferal abundance and diversity during deposition of the overlying chalks. These changes point towards variable circulation and productivity regimes, and to climate instability during the period following the global blackshale event.

Some planktonic taxa are recorded, but at low levels of abundance. However some new species are seen with the first species of *Dicarinella* being observed, along with new species of *Praeglobotruncana.* This indicates the diversification of species following the disappearance and extinction of foraminiferal species over the CTB, with *Dicarinella*, and later *Marginotruncana* filling the niche left by extinct *Rotalipora*. Interestingly following this initial increase in the number of planktonics, abundance falls again before increasing rapidly to pre-event levels in the nannofossil chalks above the clay layer. This may indicate a fluctuating OMZ during this period of clay deposition, the water column remaining unstable over this time. A fluctuation in conditions is also seen at Site 763 where the black

clays deposited over the CTB show two distinct organic rich layers within the clays beds, indicating complete anoxia did not exist over the whole black shale unit but only at short intervals over the time period (Haq *et al.*, 1990).

Planktonic species also show recovery following the CTB with diversity increasing and species living at all depth habitats, filling all niches, indicating normal stratified ocean conditions to have returned. *Heterohelix,* however, are still present in relatively high numbers and show a second peak in dominance in the *Helvetoglobotruncana helvetica* Zone, coincident with a decline in the numbers of *Dicarinella, Praeglobotruncana* and *Hedbergella.* This possibly suggests the OMZ to have intensified again indicating the oceans still remained unstable through much of the early to mid- Turonian.

4.8.4 Summary

The northwest coast of Australia shows intense environmental change during the mid-Cretaceous. Isotopic and palaeontological change is observed at both Site 766 and Site 762, and although the characteristic CTB black shales are not observed, intensification and expansion of the oxygen minimum zone in this region led to distinct foraminiferal evolution, extinction and diversification patterns at both sites. Situated on the southern margin of the Tethys, many similarities are seen to CTB sediments in the epicontinental seaways of Europe and the USA, the North and South Atlantic Basins and in the Pacific Ocean. The $\delta^{13}C$ excursion observed clearly represents a global event of removal of light carbon from the oceanic reservoir through the burial of organic carbon The extent and form of the carbon isotope excursion at Site 766 is clearly comparable with those seen elsewhere, and is coincident with a warming trend through the Cenomanian and Turonian in both surface and bottom waters. This is not as true at Site 762 where diagenetic alteration of the sediments has occurred. The nature of the diagenesis being interpreted as much as possible in order to fully understand the events seen at Site 762. Changes in the foraminiferal population are however comparable with that seen at Site 766 and sediments

indicate a largely dysoxic water column to have been present at times over the CTB. A full comparison of the events seen in the Indian Ocean and a model of deposition and cause of the events will be given in Chapter 7.

Chapter 5: Palaeoceanography of the eastern Tethys during the mid-Cretaceous

5.1 Introduction

This chapter analyses the palaeoceanographic changes associated with the CTB in the Crimea. During the Cenomanian and Turonian the Crimea lay on the north-eastern flank of the Tethyan margin. Analysis of this region helps to provide a better understanding of environmental conditions at the CTB in the eastern Tethyan region, much previous work having focused on the western region. This enables us to assess changes in the partitioning between carbonate and organic carbon sinks associated with the environmental changes that occurred over the CTB.

Using high-resolution carbon and oxygen isotope analyses of marine carbonates, together with measurements of total organic carbon (TOC), Rock-Eval pyrolysis and petrographic analysis, fluctuations in the global carbon reservoir can be studied, and the environment of deposition assessed. This study, alongside foraminiferal analysis can further determine the condition of the water column and the relative timing of these events.

5.2 Geological background

The Crimean Peninsula is located in the south of the Ukraine, on the northern coast of the Black Sea (Figure 5.1). The peninsula comprises of a range of mountains in the south that make up one-fifth of the region, whilst the larger, northern, part consists of a large plain. The mountains were formed during the Cimmerian (Triassic-Jurassic) and Alpine (Tertiary) orogenies and extend for 200 km, from the northeast to southwest, with a maximum altitude of 1500 m. The Cretaceous sediments are found within the Crimean Mountains and further north on the Crimean Plain. Overall, the sediments range from shallow marine deposits in the north to deeper deposits in the south (Kopaevich and Kuzmicheva, 2002).

Figure 5.1: Location of the Crimea. The study area is shown by the black rectangle and shown in close up in Figure 5.2.

This study concentrates on the outcrops in the mountains of the south. Recent research has focused on a number of Cretaceous sections in this area, and work on the stratigraphy of this region has been presented by Naidin and Alekseev (1981), Naidin (1981), Alekseev (1989), Alekseev *et al.* (1997), Gabdullin *et al.* (1999), Gale *et al.* (1999), Kuzmicheva, (2000) and Kopaevich and Kuzmicheva, (2002), with data on the isotope stratigraphy and geochemistry published by Naidin and Kiyashko (1994a, b).

This study focuses on the sediments found at Aksudere. The section lies about 30 km south of Simferopol. It is one of the most southerly and complete of the Cenomanian – Turonian sections in the region.

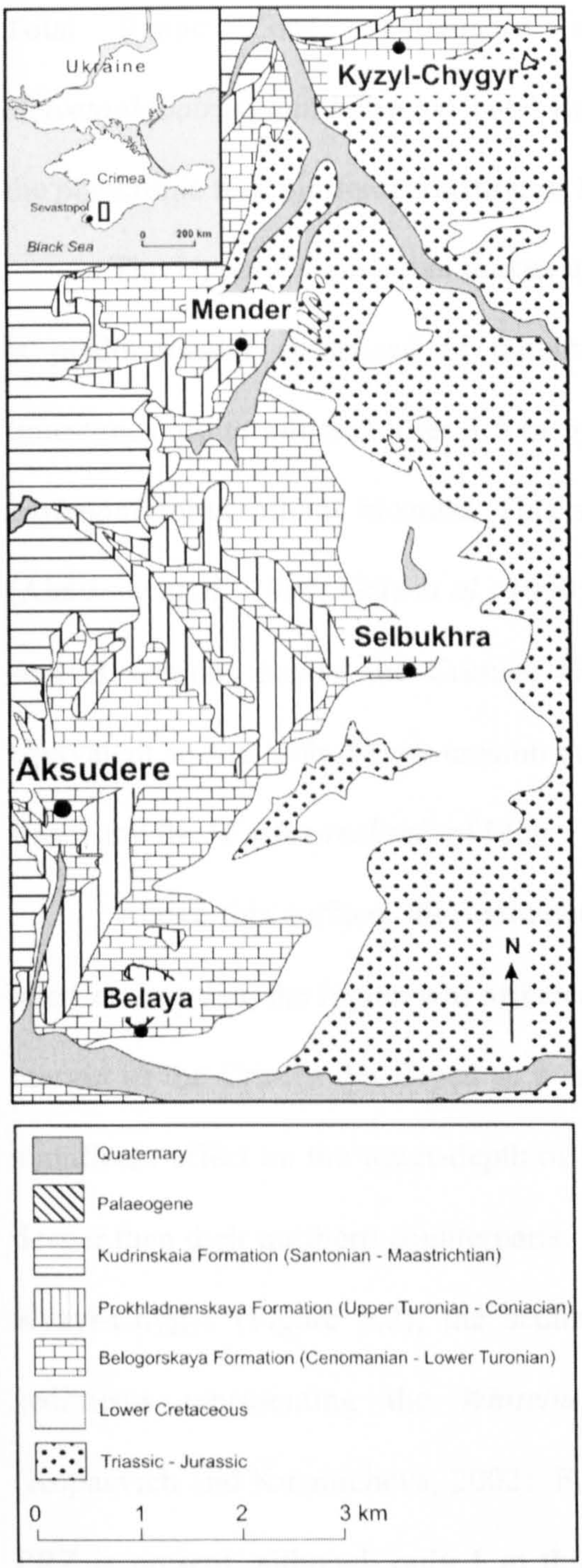

Figure 5.2: Study area, showing outcrop of Upper Cretaceous sediments, and location of Aksudere and other locations with Cenomanian-Turonian sections referred to in the text. (modified from Kopaevich and Kuzmicheva, 2002).

5.3 Sediment description of the Aksudere section

Within southwestern Crimea, the Cenomanian is comprised of ~50-60 m of rhythmically bedded (decimetre-scale) marly chalks, which show an overall decrease in the clay component up through the Cenomanian, and contain a number of erosion surfaces that are recorded across the region (Gale *et al.*, 1999). The section studied at Aksudere includes Upper Cenomanian and Lower Turonian sediments, spanning the *Rotalipora cushmani*

Total Range Zone, *Whiteinella archaeocretacea* Partial Range Zone and *Helvetoglobotruncana helvetica* Total Range Zone. For age determination of the sediments the planktonic foraminiferal zonation of Robaszynski and Caron (1995) was used.

The Upper Cenomanian makes up the lowermost 5 m of the section examined and is predominantly composed of carbonate rich white limestones (Figure 5.3). These limestones are terminated after 3.5 m by an erosion surface, at the top of the *Rotalipora cushmani* foraminiferal biozone. This surface is well documented by many researchers (Alekseev *et al.*, 1997; Gale *et al.*, 1999; Kopaevich and Kuzmicheva, 2002) and occurs in several sections across the Crimea. Gale *et al.* (1999) suggested that this surface is equivalent to the 'sub-plenus erosion surface' of Jeffries (1963) seen in the Anglo-Paris Basin and the '*Fazieswechsel*' of Meyer (1990) in northern Germany.

Above this surface, the sediments vary greatly across the region. During the mid–late Cenomanian, the region was affected by the opening of the Black Sea and the southern margin of the Crimea developed as a continental slope of the passive margin. This had a significant effect on the water-depth of the area, the southern areas becoming significantly deeper than their northern counterparts. In the more northerly sections, such as Mender and Kyzyl-Chygyr (Figure 5.2), the sediments are more condensed and incomplete, with sediments representing the *Whiteinella archaeocretacea* PRZ completely missing (Kopaevich and Kuzmicheva, 2002). Further south, at Selbukhra, the *W. archaeocretacea* PRZ is present, although only 1 m thick. The most southerly sections, at Aksudere and Belaya, however, contain a much thicker sequence (~2.5 m) of *W. archaeocretacea* PRZ sediments.

The uppermost Cenomanian sediments consist of sandy marls, marls and organic-rich claystones, that grade upwards into marls and limestones of early Turonian age. Aksudere is, therefore, one of the most complete sections in SW Crimea, although foraminiferal data indicate that a small stratigraphic gap exists at the late Cenomanian erosion surface discussed above (Kopaevich and Kuzmicheva, 2002).

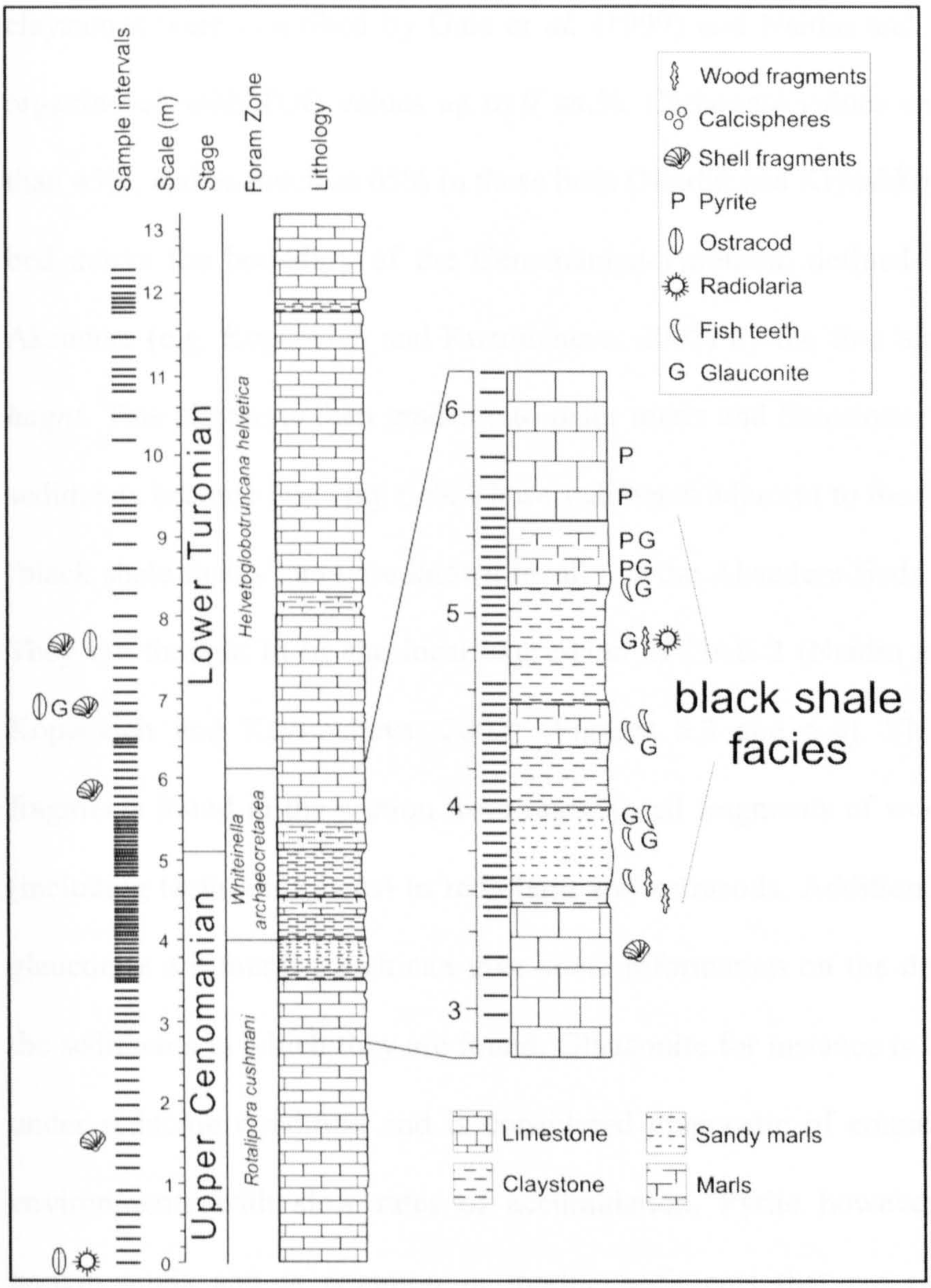

Figure 5.3: Stratigraphical log of Cenomanian-Turonian sediments seen at Aksudere based, upon Alekseev *et al.* (1997) and this study. Foraminiferal zonations after Robaszynski and Caron (1995).

At Aksudere the late Cenomanian erosion surface is directly overlain by a 10 cm thick dark claystone that grades upwards into a 40 cm thick yellow, quartz rich sandy marl. Gale *et al.* (1999) suggested that this was equivalent to Bed 3 of the Plenus Marls, the top of this bed marking the base of the *W. archaeocretacea* PRZ. This is overlain by a second claystone, 30 cm thick and grading up into 20 cm of pale grey marl. Above this lies a third

claystone, 60 cm thick and laminated, it contains some thin quartz sand layers. These dark claystones were described by Gale *et al.* (1999) and Naidin and Kiyashko (1994a, b) as organic-rich with TOC values up to 9 wt.%. Carbonate values were seen to be no lower than 45%, and as much as 65% in these beds (Naidin and Kiyashko, 1994a). The top of this bed marks the boundary of the Cenomanian-Turonian, defined by previous workers at Aksudere (e.g. Kopaevich and Kuzmicheva, 2002) by the first appearance of *Dicarinella hagni*. This claystone then grades into paler marls and limestones of Turonian age, as the sediments become less clay rich. These sediments adjacent to the CTB can be defined as a 'black shale facies', and are known locally as the Aksudere Beds (Alekseev *et al.*, 1997). They are thought to be the local expression of OAE 2 (Naidin and Kiyashko, 1994a, b; Kopaevich and Kuzmicheva, 2002) (Figures 5.3 and 5.4). There are abundant fossil fragments found in the section from macrofossil fragments of wood, shell and fish debris (including teeth and scales) to radiolaria and ostracods. Additionally grains of pyrite and glauconite are found which can give some information on the depositional conditions of the sediments in which they are found. Glauconite for instance is characteristically formed under reducing condition and is considered diagnostic of continental shelf depositional environments with slow rates of accumulation. Pyrite however forms in sulphur-rich anoxic muds and is common in marine sediments that are rich in organic material. Decaying organics use up oxygen and release sulphur, creating conditions ideal for pyrite formation. Both present in abundance in the black shale facies, it can be presumed that low oxygen conditions existed on the sea floor and at the sediment-water interface, abundant deterioration of organic matter was occurring and sedimentation was slow.

The Aksudere section was sampled at 5 to 15 cm intervals throughout the 12.5 m section to obtain 109 samples spanning the Upper Cenomanian to Lower Turonian, *Rotalipora cushmani* to *Helvetoglobotruncana helvetica* Foraminiferal Biozones. The sampling interval can be seen on Figure 5.3.

Figure 5.4: Cenomanian-Turonian boundary 'Black Shale Facies' outcropping in the field at Aksudere. Scale is given by the geological hammer to the right of the rock face.

5.4 Methodology

Samples from the Crimea were processed for foraminiferal and isotopic analysis. Due to the high amounts of organic matter in the boundary samples isotopes measurements were undertaken on samples with the organic matter left in and with the organic matter removed using 5% sodium hypochlorite in order to prevent contamination of the samples from the organic carbon. Unfortunately isotope measurements were not carried out on the organic material. Although some previous studies have undertaken this work (Naidin and Kiyashko, 1994a, b) it was not done at the level of resolution that could have been obtained in this study. Analysis to determine the TOC was carried out using both carbon analyzer and Rock-Eval to determine the nature of the organic matter.

Thin-sections were also obtained from a selection of samples throughout the succession, in order to undertake petrographic analysis of the sediments and to observe any diagenetic alteration of the samples. Details of all methods used are given in Chapter 3.

5.5 Biostratigraphy of the Crimea

Biostratigraphic analysis was carried out on samples from the section in order to determine the relative age of the sediments. Planktonic foraminifera were used primarily, in conjunction with benthonic foraminifera, and evidence from the distribution of nannofossils and radiolaria carried out by other workers. Biostratigraphical work has been undertaken in the Crimea in a number of studies (e.g., Foraminifera - Kopaevich and Walaszczyk, 1990; Alekseev *et al.*, 1997; Kopaevich and Kuzmicheva, 2002; Radiolaria – Bragina, 2004; Palynology – Dodsworth, 2004; Nannofossils – Nikishin *et al.*, 1993).

Bordering the Tethys Ocean, the Crimea was influenced by both the Boreal and Tethyan realms. However, the Tethyan influence dominated from the Albian to Turonian, as sea levels rose and led to the influx of many Tethyan species to the region. The planktonic zonation used is, therefore, based on that of Robaszynski and Caron (1995), using the internationally recognised taxa. Some of the zonal fossils are, however, not as abundant as recorded in completely Tethyan environments. Other species are, therefore, used to determine particular zones, as will be discussed below.

Additionally, due to the preservation of the foraminifera, and processing bias related to the techniques used to liberate the foraminifera from the sediment, some key zonal fossils were absent in this study. The biostratigraphic boundaries are, therefore, based on observations from the foraminiferal analysis of this study and additional data from previous biozonations developed in the region.

The biostratigraphic zonation defined for the Aksudere section is shown in Figure 5.5, with the range charts recorded in Figure 5.6 and the count sheets in Appendix 2.

The Upper Cenomanian is defined by the *Rotalipora cushmani* Zone. The top of this zone is determined by the LO of *R. cushmani* at the base of the black shale facies, and correlates with the top of the basal sandy unit of the BSF, *R. cushmani* being found 50cm above the erosion surface at Selbukhra to the northeast of Aksudere (Alekseev *et al.* 1997). As discussed above this sandy bed has been correlated with Bed 3 of the Plenus Marls by Gale *et al.* (1997) based on the stratigraphy and presence of the erosional surface equivalent to "sub-plenus erosion surface", the top of this unit therefore marks the top of the *R. cushmani* Zone. The assemblages are diverse with abundant *Hedbergella*, *Praeglobotruncana* and *Globigerinelloides*, along with *Heterohelix, Guembelitria* and early *Dicarinella* cf. *imbricata.* Benthonic species are also diverse with a range of agglutinated and calcareous species, both infaunal and epifaunal in habitat. *Gavelinella, Gyroidinoides* and *Tappanina* dominate the benthonic assemblages with species of *Laevidentalina, Lenticulina, Nodosaria, Globulina* and *Pyrulina* also present.

The overlying *Whiteinella archaeocretacea* Partial Range Zone spans the Cenomanian-Turonian boundary from the LO of *R. cushmani* and FO of *H. helvetica.* In this study *R. cushmani* was not found not found in the sandy marls, however it has been found at the nearby section of Selbukhra, (Gale *et al,* 1999). This may be a reworked specimen however for the purposes of this study the *R. cushmani* boundary remains at this level, as defined for the region. Unfortunately *H. helvetica* is largely absent from the Crimean localities and *Dicarinella elata* has, therefore, been used to determine this interval in the Crimea (Kopaevich and Kuzmicheva, 2002). *H. helvetica* has been observed very rarely in this study, but not until higher in the section. The Cenomanian-Turonian boundary is also defined by the FO of *Dicarinella hagni* by a number of authors (Kopaevich, 1996; Tur, 1996). Coincident with the FO of *D. imbricata* is the first appearance of the Turonian nannofossil *Quadrum gartneri* (Kopaevich and Kuzmicheva, 2002) which further constrains the boundary.

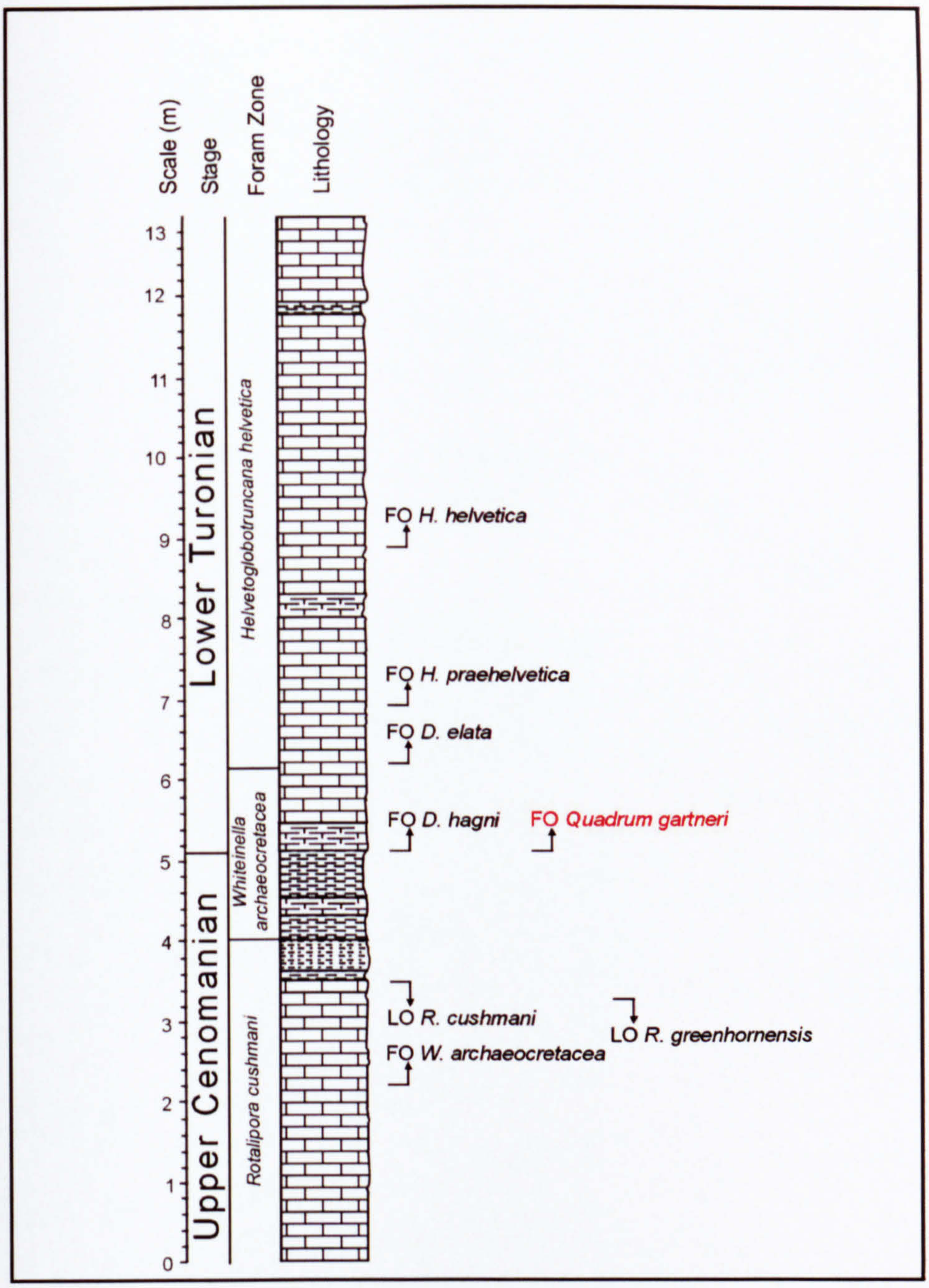

Figure 5.5: Biostratigraphy of the Aksudere section. Nannofossil data is taken from Kopaevich and Kuzmicheva (2002). Zonal boundaries are defined by this study and previous studies (Alekseev *et al.* 1997; Gale *et al.*, 1999; Kopaevich and Kuzmicheva, 2002). Foraminiferal first and last occurrences are those identified during this research. It should be noted the LO of *R. cushmani* in this study, does not mark the top of the *R. cushmani* zone that is defined for the region (see text for more discussion).

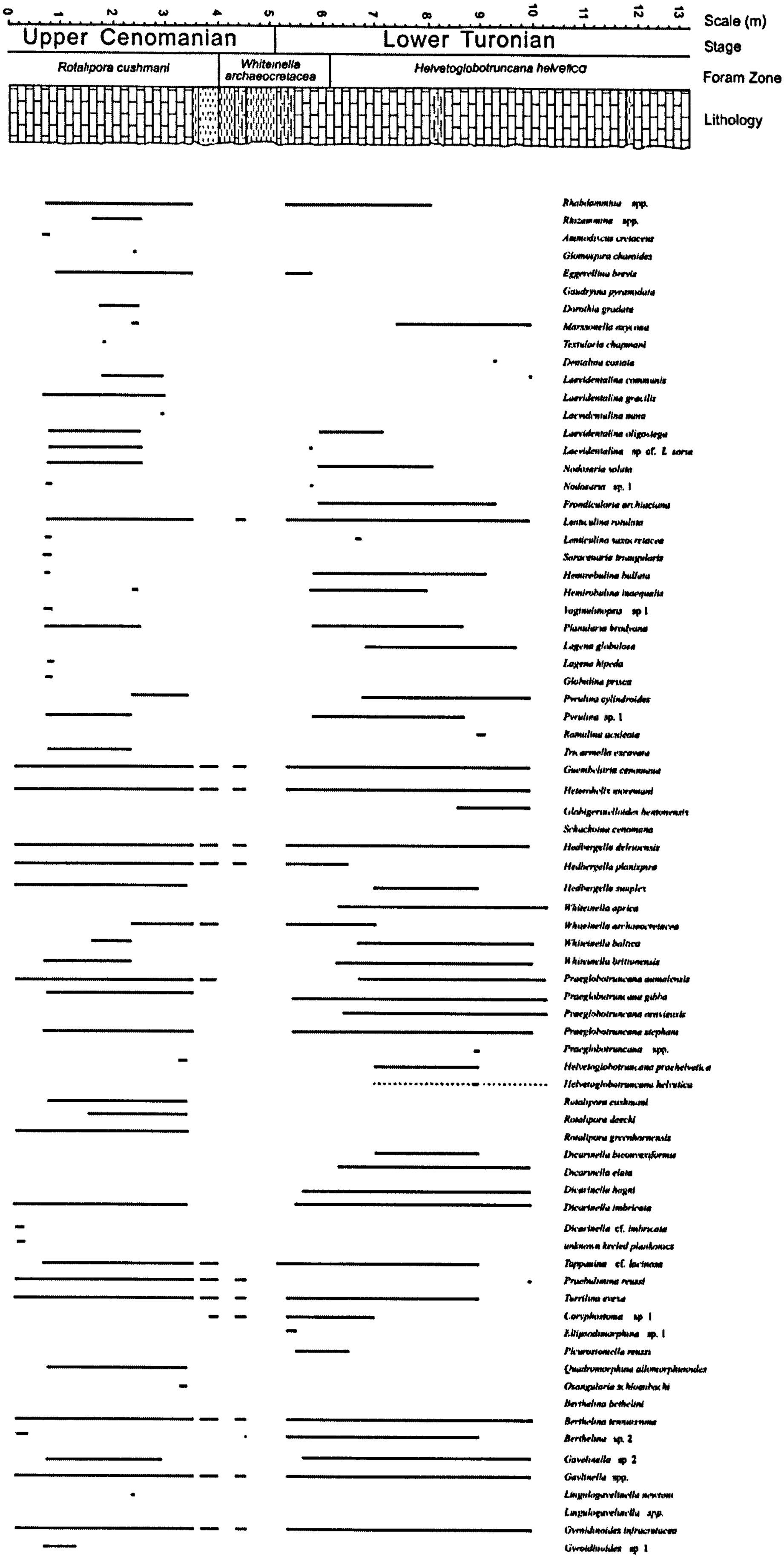

Figure 5.6: Range chart showing the ranges of all foraminiferal species found at Aksudere

The *W. archaeocretacea* Zone is largely made up of the black shale facies and is, therefore, largely barren with a dominance of benthonic species, and rare unkeeled *Hedbergella, Whiteinella* and *Heterohelix*. The upper part of the *W. archaeocretacea* Zone, however, sees an increase of species within the Lower Turonian limestones, with diverse assemblages made up of planktonic and benthonic species typical of the Lower Turonian, including abundant *Praeglobotruncana* and *Dicarinella*.

The overlying *H. helvetica* Zone continues to record typical Lower Turonian assemblages which increase in both numbers and diversity. *Dicarinella, Praeglobotruncana* and *Whiteinella* are present in high numbers with *Heterohelix, Hedbergella* and *Guembelitria* also abundant. Benthonic species are less abundant but agglutinated *Marssonella, Dorothia* and tubular *Rhabdammina* are present with *Laevidentalina, Lenticulina, Pyrulina* and epifaunal *Berthelina, Gavelinella* and *Gyroidinoides*. Further discussion on the abundance of species within these zones can be seen below.

5.6 Results

5.6.1 Foraminiferal results

The results of the foraminiferal distribution of species, genera and morphotypes are shown in Figures 5.7- 5.10. The main features of these distributions are discussed below. Due to the hard lithology of some of the sediments, thin sections were also taken to analyse the parts of the assemblage, the lithology and any diagenetic. Although the observation of any foraminiferal species is taken into account in the following discussion, the full assessment of the thin sections and diagenesis is carried out in section 5.7.

5.6.1.1 Specimen and species distribution

Abundance

Foraminiferal abundance is presented at Aksudere as specimens per gram (SPG)

and not as accumulation rates as seen in Chapter 4. Unfortunately due to the nature of the sediments in the Crimea bulk dry density and linear sedimentation rate were unknown and accumulation rates could not be calculated. Although SPG can be considered to be less accurate than accumulation rates, number of SPG not taking into account the rate of sedimentation. The results in the Indian Ocean (Chapter 4) clearly illustrate that the accumulation rates showed identical trends to the fluctuations in number of specimens per gram. We can therefore postulate that similarly, accumulation rates for the Crimea would also show a similar trend to that of the number of specimens per gram. The abundance of foraminifera at Aksudere show a clear pattern through the Upper Cenomanian and Lower Turonian as this can be seen in Figure 5.7A. Abundance is high through the *R. cushmani* Zone, but a rapid decrease at the top of the zone is observed, coincident with the change in sedimentation and deposition of the first clay layer.

Abundance increases again in the sandy unit, but declines to near zero through most of the *W. archaeocretacea* Zone. At the top of the *W. archaeocretacea* Zone, abundance begins to increase again slowly coincident with the return to carbonate deposition. Abundance continues to rise through the *H. helvetica* Zone, showing just a short decrease near the top of the studied section.

Diversity

Both species richness and Fisher alpha index (Figure 5.7 D and E) show a similar trend and also similar changes in abundance, indicating low diversities to typically exist where abundance is low. Again high diversities decrease rapidly at the top of the *Rotalipora cushmani* Zone. Rather than remaining low through the Black Shale Facies (BSF), however, a number of fluctuations are seen as short increases in diversity possible represent slight shifts and changes in the depositional environment.

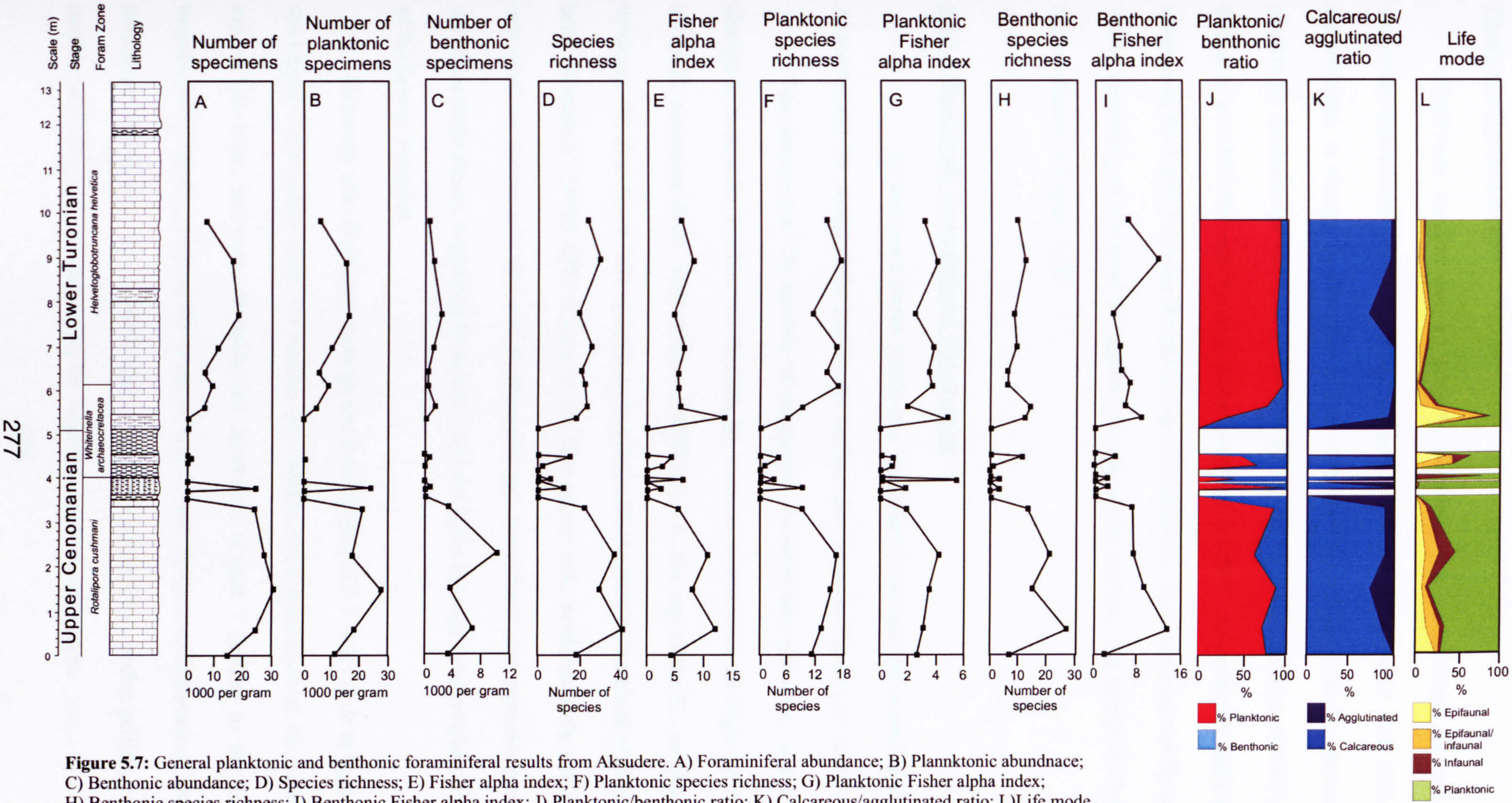

Figure 5.7: General planktonic and benthonic foraminiferal results from Aksudere. A) Foraminiferal abundance; B) Plannktonic abundnace; C) Benthonic abundance; D) Species richness; E) Fisher alpha index; F) Planktonic species richness; G) Planktonic Fisher alpha index; H) Benthonic species richness; I) Benthonic Fisher alpha index; J) Planktonic/benthonic ratio; K) Calcareous/agglutinated ratio; L)Life mode.

Planktonic:Benthonic ratio

Planktonic species can be seen to dominate the assemblages throughout the carbonate depositional units at Aksudere, generally making up more than 80% of the assemblages. A change in the ratio is seen through the section, with the percentage of planktonic foraminifera fluctuating through the Upper Cenomanian from 60-90%, before falling to just 40% through the non-barren zones of the BSF. As carbonate sedimentation resumes in the Early Turonian the percentage of planktonic taxa increases rapidly to values >90%, remaining at this level throughout the rest of the section. The planktonic:benthonic ratio is shown in Figure 5.7D.

5.6.1.2 Planktonic foraminiferal distribution

As discussed above planktonic specimens dominate the assemblages seen at Aksudere and the results of the planktonic analysis are shown in Figures 5.7 and 5.8.

Ten genera and 26 species of planktonic foraminifera are seen, and a distinct change in abundance is observed through the section. Abundances are high through most of the *R. cushmani* Zone, with values ~20000 SPG. At the top of the *R. cushmani* Zone, however, the abundance falls sharply, coinciding with the start of the black shale facies. A brief increase to 24000 SPG is seen in the first sandy unit, predominantly comprised of opportunistic *Heterohelix* spp. and *Hedbergella* spp. Abundance then remains low through the black shale facies, beginning to slowly increase again through the overlying limestones of the Lower Turonian.

Diversity also fluctuates through the core (Figure 5.7 F and G). It is high through the Upper Cenomanian with ~13 species per sample and a maximum of 16. Towards the top of this zone, however, diversity has decreased to just 3 species as the sediments become more marly, marking the onset of anoxic and dysoxic sedimentation. During the limestone deposition the assemblages were dominated by hedbergellids, unkeeled trochospiral morphotypes making up the largest proportion of species.

Keeled species are also present making up ~25% of the assemblage, the deepest dwelling *Rotalipora* are present in low numbers with higher proportions of dicarinellids and praeglobotruncanids. Elongate bi- and triserial forms of *Heterohelix* and *Guembelitria*, and planispiral *Globigerinelloides* are also present, but in lower proportions.

As diversity decreases a change in the proportion of morphotypes is also seen, as *Rotalipora* and, to a lesser extent, *Dicarinella* decline in numbers. *Rotalipora* become extinct and *Dicarinella* disappears completely with the onset of anoxic sedimentation. In the sandy marls numbers of *Praeglobotruncana* have also declined rapidly, and a large increase in *Heterohelix* is seen, dominating the assemblage with the *Hedbergella*. This may be equivalent to the global "*Heterohelix* shift" recorded at other CTB localities (e.g. Keller *et al.*, 2001; Keller and Pardo, 2004; Caron *et al.*, 2006), and will discussed further in section 5.8.

Through the BSF of the *W. archaeocretacea* Zone samples are largely barren of foraminiferal specimens, any foraminifera present being *Guembelitria, Heterohelix* or *Hedbergella* following the LO of keeled species (*Praeglobotruncana*) at a sample level of 3.95 m, within the sandy marl 1.15m below the CTB. The claystone layers of the BSF are seen to be barren of foraminifera, although the underlying marls record the presence of small hedbergellids and heterohelicids, indicating the brief recolonisation of surface waters at this time.

Following the deposition of the last and thickest claystone unit, a slow increase in numbers and diversity of planktonic foraminifera is recorded. An initial increase in *Hedbergella* and *Heterohelix* dominate the overlying marl, with *Praeglobotruncana* species starting to reappear. However, as carbonate deposition re-establishes itself a marked change in dominance is recorded. Tri/biserial and unkeeled trochospiral morphotypes decrease in abundance as keeled trochospiral morphotypes begin to dominate the Lower Turonian samples, with *Praeglobotruncana* and *Dicarinella* species rapidly diversifying with new species of both appearing in the Lower Turonian sediments.

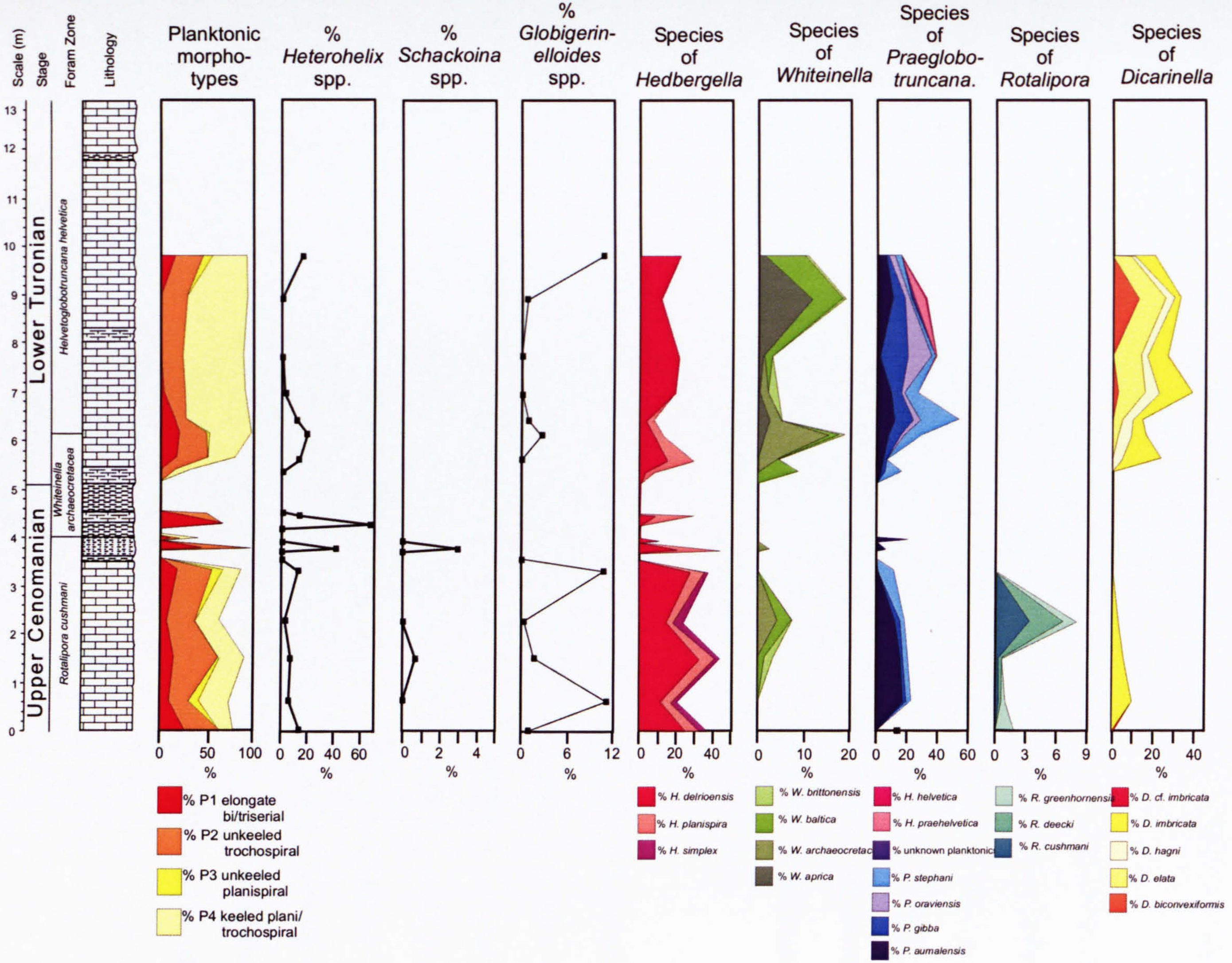

Figure 5.8: Planktonic foraminiferal results from Aksudere, showing planktonic morphotypes and the abundance of each planktonic genus and distribution of species within each genus.

5.6.1.3 Benthonic foraminiferal distribution

The abundance of benthonic foraminifera is low throughout the Aksudere section (Figure 5.7C), with values through the Upper Cenomanian of ~7000-1000 SPG. Through the top of the *R. cushmani* Zone abundance begins to decline, and by the *W. archaeocretacea* Zone the sediments are nearly barren on benthonic foraminifera with no more than 500 SPG in any sample. A slight increase in abundance is onserved in the Lower Turonian limestones, however values remain low with no sign of a return to Upper Cenomanian abundances.

The diversity of the benthonic species is generally much higher than that of the planktonic specimens at Aksudere, and shows a very different pattern to that of benthonic abundance. This is shown in Figure 5.7 H and I. Similar to abundance, diversity decreases through the top of the Upper Cenomanian, and very low diversity is observed through the black shale facies of the *W. archaeocretacea* Zone. However, although abundance remains low through the Lower Turonian, diversity increases markedly, reaching similar Fisher alpha index values to that seen in the Upper Cenomanian, by the *H. helvetica* Zone.

The benthonic specimens that are observed can be simply divided into those with a calcareous test, and those with an agglutinated test. Figure 5.7K shows the ratio of calcareous to agglutinated individuals within the benthonic assemblages. Calcareous species can be seen to dominate throughout the section, generally making up more than 90% of the benthonic specimens present. At times the number of agglutinated species does increase, however, and up to 25% of the benthonic assemblage is seen to be made up of agglutinated specimens at times. This is mainly related to a decrease in calcareous numbers as opposed to an increase in agglutinated taxa. Distribution of benthonic species and morphotypes are shown in Figures 5.9 and 5.10.

Agglutinated benthonic specimens

Only 9 species of 9 genera of agglutinated foraminifera are seen at Aksudere. Each present in only low numbers throughout the section. The Upper Cenomanian records the highest dominance with 6 species present, making up 10% of the benthonic assemblage, predominantly of elongate infaunal species of *Eggerllina, Dorothia* and *Marssonella*, with epifaunal *Glomospira* and *Ammodiscus*, and some fragments of tubular suspension feeders *Rhabdammina* and *Rhizammina*. A second increase in abundance is seen in the Lower Turonian corresponding to specimens of *Rhabdammina* spp. However, tubular species such as this often break up and although each fragment has been counted as one it is likely that the pieces are from only one or two specimens. No real increase in agglutinated dominance is considered to have been observed at this part of the section.

Through the BSF agglutinated species are largely absent with only one *Gaudryina* specimen seen in the marl unit between the second and third claystones. In the Lower Turonian abundance and diversity remains low with a few specimens of *Marssonella, Eggerellina* and *Rhabdammina* the only species present.

Calcareous benthonic specimens

Twenty-six genera and 41 species of calcareous foraminifera are seen at Aksudere, dominating the benthonic assemblages. Through the Upper Cenomanian diversity starts high with a peak of 23 species at sample level 60. With a wide range of infaunal and epifaunal morphotypes, each species is low in abundance, although, there is a dominance of BC2 (plano/concavo-convex, low trochospire) and BC4 (inflated, biconvex) morphotypes. Towards the top of the *R. cushmani* Zone species of morphotype BC9 (infaunal, flattened, biserial species) increase, forming 30% of the benthonic assemblage in the sandy marls. Other morphotypes show consistent numbers throughout the *R. cushmani* Zone, before disappearing in the first clay layer.

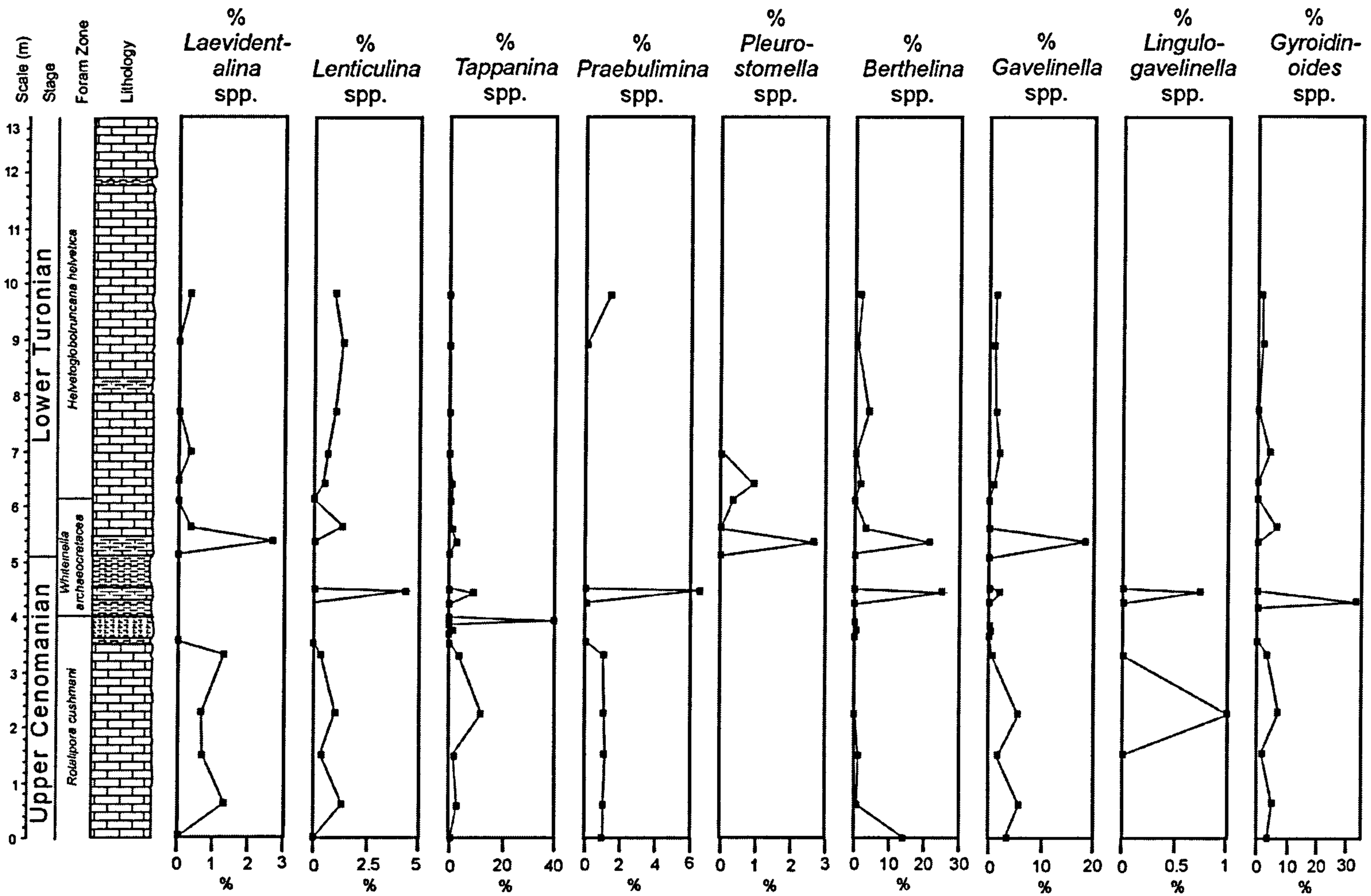

Figure 5.9: Benthonic foraminiferal results from Aksudere.

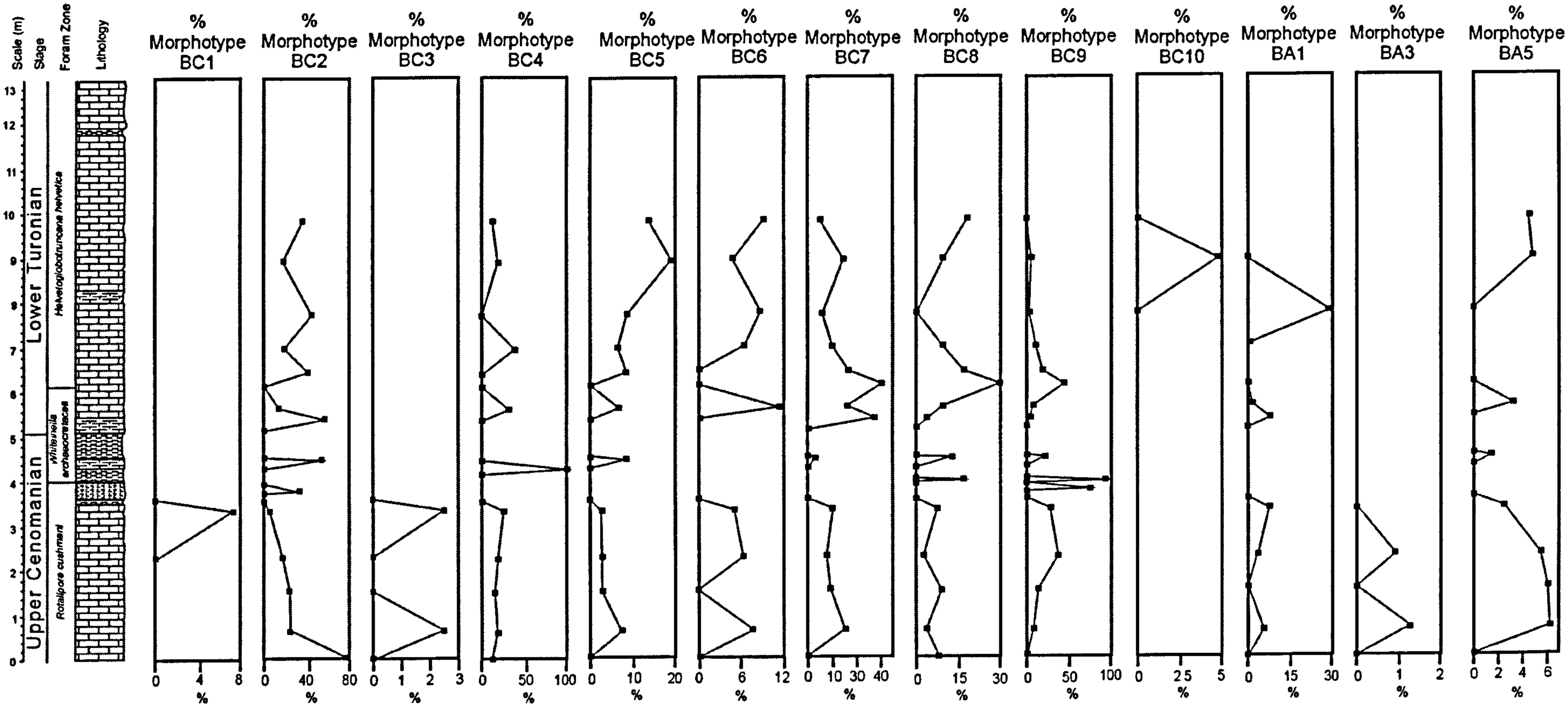

Figure 5.10: Morphotype analysis of benthonic foraminifera at Aksudere. Morphotype values are presented as a percentage of the number of benthonic specimens. **Calcareous hyaline:** BC1 biconvex, trochospiral; BC2 plano/concavo-convex, low trochospiral; BC3 plano/concavo-convex, high trochospiral; BC4 inflated, biconvex trochospiral; BC5 biconvex, lenticular planispiral; BC6 Globular/ovate; BC7 elongate, straight to arcuate, broad to narrow, uniserial; BC8 tapered rounded, elongate tri-bi-uniserial; BC9 tapered flattened, elongate, biserial; **Porcellaneous:** BP1 elongate to ovate quinqueloculine; **Agglutinated:** BA1 tubular or branching; BA2 globular; BA3 planispiral/streptospiral, subsphaerical/flattened; BA4 low trochospire/streptospiral, sphaerical/subsphaerical; BA5 elongate, variably coiled, uni-multiserial.

Through the BSF calcareous benthonics are largely absent, although some specimens are found within the marl units between the organic rich claystones. Within the first sandy marl *Tappanina* is most abundant with rare specimens of *Gavelinella, Berthelina, Coryphostoma* and *Turrilina*,

The first marl unit following the second clay layer in the *W. archaeocretacea* Zone, however, shows a much higher diversity and abundance, with 10 species present at sample level 4.45, 55 cm bellow the CTB. The fauna is dominated by *Berthelina* sp. 2 with *Tappanina* cf. *lacinosa*, *Praebulimina reussi* and *Lenticulina rotulata*, infaunal species of *Hemirobulina*, *Coryphostoma* and *Ellipsodimorphina*, and epifaunal to shallow infaunal *Berthelina tennuissima* and *Lingulogavelinella* spp. are present.

Following the thickest claystone layer and barren zone, foraminifera are again in low abundance in the overlying clays with a few *Praebulimina, Gavelinella* and infaunal elongate morphotypes. At sample level 5.35 m, however, a more diverse assemblage is seen, as more normal marine conditions return to the region. This initial assemblage is similar to that seen in the preceding marls with a high abundance of infaunal calcareous morphotype BC7, *Laevidentalina* and *Pleurostomella* showing a particular increase in numbers, and species of morphotype BC2. It is interesting to notice BC2 is the only morphotype consistently found in each of the marl units, with, to a lesser extent, infaunal morphotypes BC8 and BC9. Through the upper part of the *W. archaeocretacea* Zone and into the *Helvetoglobotruncana helvetica* Zone, more species appear in the assemblages, although as diversity increases, and fluctuates between 9-12 species per sample, abundance remains low. *Gyroidinoides* and *Berthelina* show the greatest abundances, similar to assemblages prior to the BSF deposition, although morphotypes BC7 and BC8 and to a lesser extent BC5 and BC6, show increases into the Lower Turonian.

5.6.1.4 Life mode

Analysis of benthonic morphotypes also enables the inferred life mode of each group to be determined, from epifaunal, to epifaunal/infaunal, and infaunal. Results from the life mode analysis can be seen in Figure 5.7F.

At Aksudere it can be seen that an initial dominance of epifaunal species is rapidly taken over by infaunal species. Similarly in the BSF species are predominantly infaunal, although some epifaunal species are seen in the second marl unit. Following the BSF, at the top of the *W. archaeocretacea* Zone, epifaunal species again dominate the assemblages, up-section, in the Lower Turonian, an even spread of epi- and infaunal species appear to be present.

5.6.1.5 Other biota found at Aksudere

A range of components other than foraminifera were found in the sediments at Aksudere. Although it is beyond the scope of this study to analyse all the biota found in the sediments, it is important to look at the components as they can provide additional information on the depth and depositional environment in which the sediments formed. Figure 5.3 shows the position and type of biota found whilst processing the samples of Aksudere. It can be seen that there is abundant fish debris, including fish teeth (ichthyoliths) and scales, and shell fragments, mainly inoceramid prisms. Ostrocods and radiolaria are also seen, the latter particularly abundant in the BSF. Work has also been carried out on nannofossils in the section (Nikishin *et al.*, 1993), and most recently, work on the Aksudere section has included analysis of the palynology (Dodsworth, 2004) and radiolarians (Bragina, 2004). Reference to this work will be included in the discussion of this chapter.

5.6.1.6 Summary

Overall a simple pattern of diversification and extinction can be seen at Aksudere.

1) The base of the section (in the Upper Cenomanian) is characterised by high diversity and high abundances of species. Deep dwelling, intermediate and shallow dwelling planktonic species are present, along with both epi- and infaunal, agglutinated and calcareous benthonic species.

2) By the top of the *R. cushmani* Zone, *R. cushmani* has disappeared with the other rotaliporid species and diversity has decreased sharply. Planktonic specimens are represented only by small species of *Heterohelix, Guembelitria* and *Hedbergella.* Benthonic species are also reduced to very low numbers of infaunal and shallow infaunal calcareous species. Foraminifera are completely absent in the organic rich layers, and are only recorded in very low numbers in the marls.

3) Following the BSF an increase in diversity and abundance is observed. New species of *Dicarinella* and *Praeglobotruncana* are recorded and benthonic fauna, both epi- and infaunal are seen in slightly higher abundances.

5.6.2 Isotope results

Isotopic analysis was carried out on fine fraction (<63 μm) sediment samples. One sample set was untreated while the other set was treated with sodium hypochlorite, to remove organic matter from the sediments. The raw data can be seen in Appendix 3, and analytical data are presented in Figures 5.11 and 5.12.

The Upper Cenomanian (*Rotalipora cushmani* TRZ) has $\delta^{13}C$ background values of ~2.7‰. These values decrease slightly to 1.9‰ in the lowermost claystone of the Aksudere Beds, then increase rapidly to a peak at the top of the sandy marl at the very top of the *R. cushmani* TRZ. Values then plateau through the *Whiteinella archaeocretacea* PRZ at around 3.3‰, peaking again at 4.4‰ at the top of the upper claystone unit, at the CTB. $\delta^{13}C$ values then decrease slowly through the upper part of the *W. archaeocretacea PRZ* and into the *Helvetoglobotruncana helvetica* TRZ of the Lower Turonian, to steady values ~2.9‰ at a level of 1 m above the CTB.

The $\delta^{18}O$ values show greater fluctuations than the carbon isotope data. $\delta^{18}O$ values of ~ -3.4‰ are observed in the Upper Cenomanian up to the base of the sandy marl. After this point, values decrease rapidly to -5.0‰ at the top of the sandy marl, marking the top of the *R. cushmani* TRZ. Values then fluctuate between -4.0 and -5.0‰ through the whole of the *W. archaeocretacea* PRZ, before decreasing slowly, as the limestones become less marly, to background values of ~ -3.8‰ at 3.5 m above the CTB. These oxygen and carbon isotope values are in the same range as those published in earlier works by Naidin and Kiyashko (1994a, b).

In addition to these main trends, however, are a number of negative excursions not recorded previously, particularly prominent on the $\delta^{13}C$ curve. There are four excursions, the lowest in the sandy marl 1.4 m below the CTB in the *R. cushmani* TRZ, the other three lying in the upper thick claystone unit of the *W. archaeocretacea* PRZ, at 0.6, 0.45 and 0.1 m below the CTB, respectively. In order to rule out contamination of the samples by organic matter, these samples were treated with sodium hypochlorite, as described above.

The results for both treated and untreated samples are nearly identical, which would appear to rule out contamination.

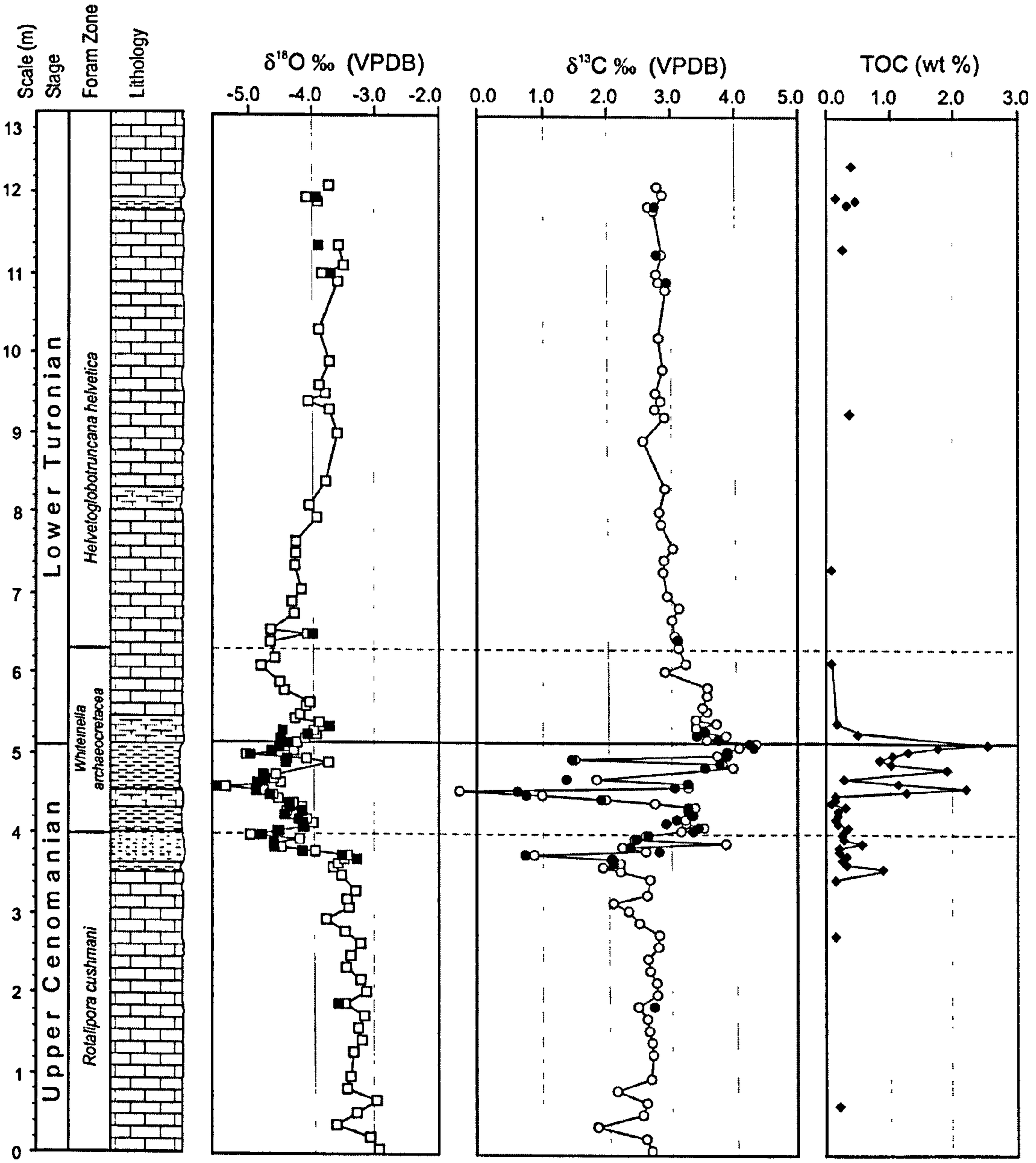

Figure 5.11: Carbon and oxygen isotope results of fine-fraction (<63μm) samples of both untreated (open squares and open circles) and treated (organic carbon removed) (filled squares and filled circles) samples, and TOC results from Aksudere. Dashed lines indicate the Biozone boundaries.

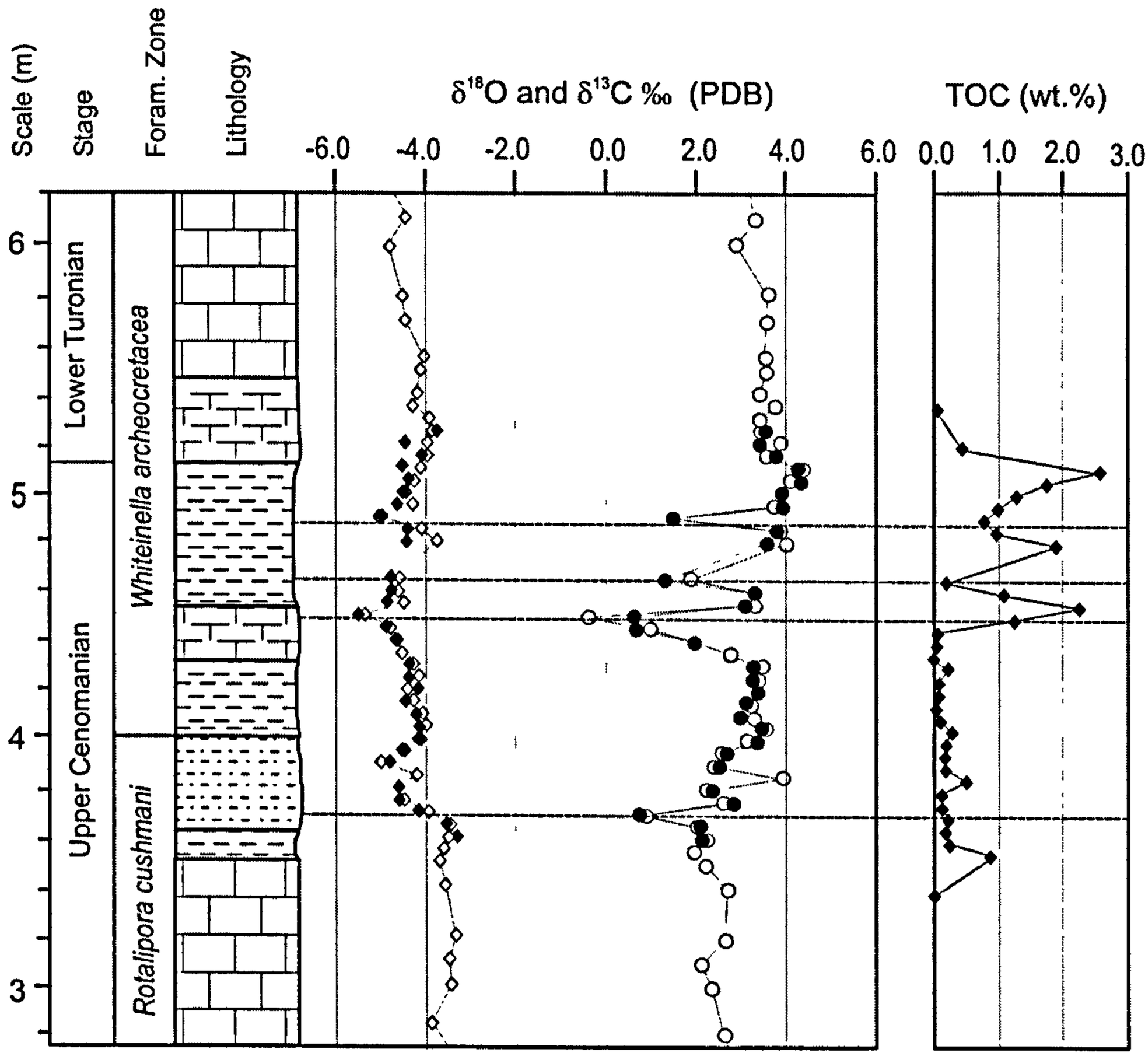

Figure 5.12: Close up of the geochemical changes occurring over the Cenomanian-Turonian boundary at Aksudere.

5.6.3 Geochemical results

5.6.3.1 TOC and Rock Eval analysis

TOC values (Figure 5.11 and 5.12 and Appendix 3) are low in the Upper Cenomanian limestones, reaching no more than 0.1%. A small increase, to 1.0%, is seen in the lowermost thin claystone, although values remain low (<0.5%) through the overlying sandy marl, and into the *W. archaeocretacea* PRZ. TOC values then increase rapidly at the base of the upper claystone unit, peaking at 2.3%, 0.5 m below the CTB. The values then decrease back down to 0.2% over 0.1 m, prior to two subsequent peaks in this unit. TOC increases again to 2.0%, 0.3 m below the CTB, decreases to 0.8% and finally increases to

the largest value of 2.6%, at the CTB. Values then return to near zero 0.15 m above the CTB, and remain low through the *H. helvetica* TRZ of the Lower Turonian.

These TOC values show that organic rich samples lie in the *W. archaeocretacea* PRZ, in the upper claystone (from 0.7 m below the CTB to just below the CTB) and in one sample in the lowermost claystone at the top of the *R. cushmani* TRZ. All samples with TOC >0.5 wt.% were analysed with Rock-Eval pyrolysis. The Rock-Eval pyrolysis data are shown in Figure 5.13. The data indicate that the samples contain mixtures of Type II and III kerogen (organic matter derived from algae, bacteria and marine zooplankton, with some higher plant contribution), as indicated by hydrogen indices ranging from 142 to 321 mg HC/g TOC. The hydrogen indices appear to increase with organic richness, indicating a higher proportion of marine-derived organic matter in the organic-rich layers of the claystones seen 0.5 m and 0.3 m below the CTB and at the CTB.

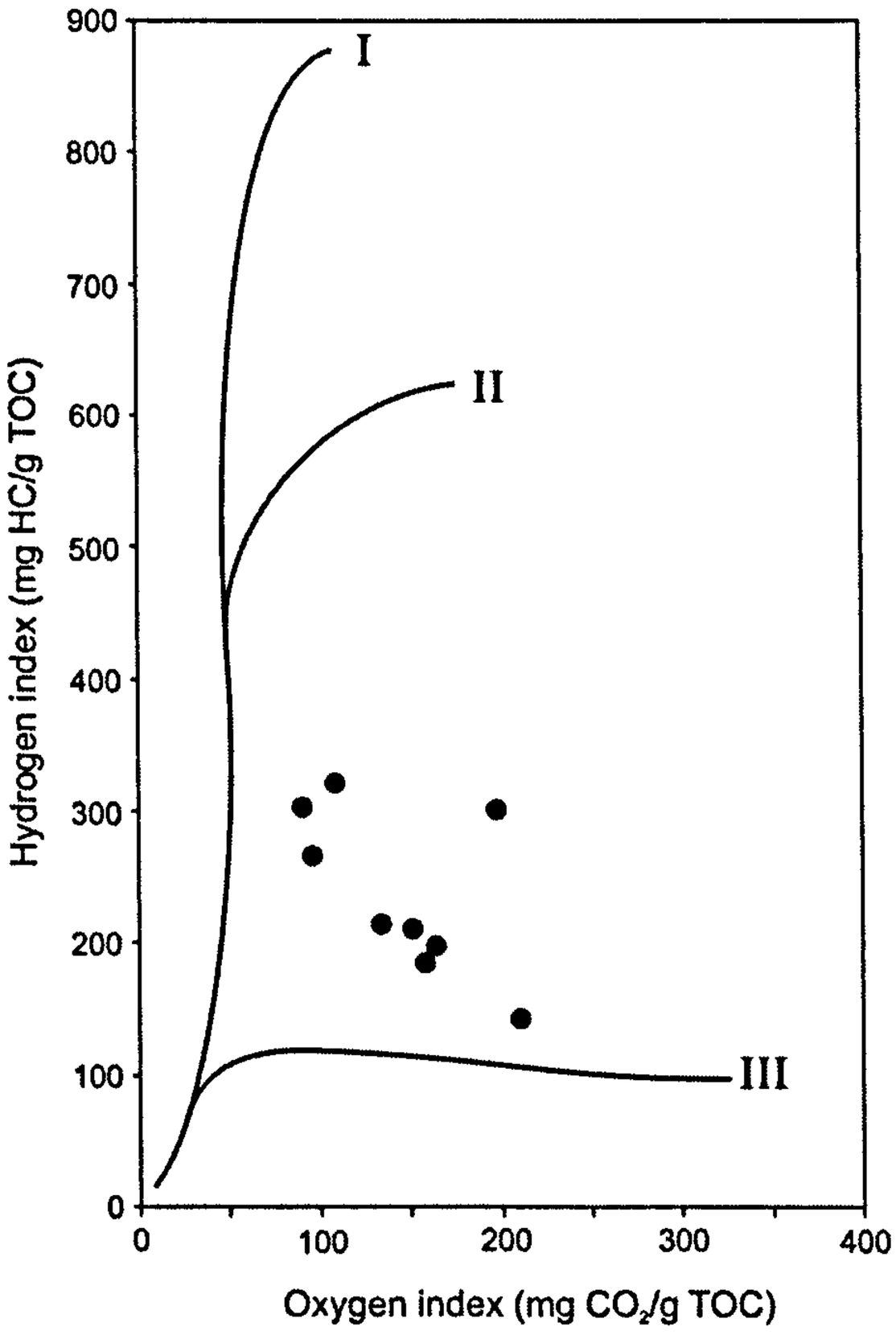

Figure 5.13: Van Krevelen plot indicating nature and source of organic matter in organic rich claystones at Aksudere.

5.7 Palaeoceanographic change in the Crimea

5.7.1 Introduction

The results described above clearly show palaeoenvironmental change within the water column over the Cenomanian-Turonian boundary, with both foraminiferal extinction and diversification, and changes in the water column with respect to the temperature and the carbon cycle. An interpretation and discussion of these results is given below.

The sediments analysed at Aksudere indicate normal marine conditions existed during the lower part of the Upper Cenomanian. A diverse fauna inhabiting all depth habitats indicate an oxygenated and well stratified water column. Over the Cenomanian-Turonian boundary, however, a large change is seen in the foraminiferal population. Benthonic diversity decreases leading to the disappearance and extinction of some benthonic fauna. Deeper dwelling planktonic *Rotalipora* became extinct, and assemblages were left dominated by opportunistic, low oxygen tolerant planktonics such as *Heterohelix* and *Guembelitria.* Coinciding with the deposition of dark organic rich clays, it can be postulated that much of the water column was anoxic at times during the *W. archaeocretacea* Zone. Anoxic conditions did not persist, however, as can be seen by the interbedded organic clays and marls, and the occurrence of foraminiferal species within the marl layers. Isotope data provide more information on the condition of the water column over this time period and is discussed below.

5.7.2 Diagenetic potential at Aksudere

An analysis of the sediments at Aksudere enables the identification of any diagenesis that may occurred in order to determine any affect upon the isotopic data from this site. The limestone sediments at Aksudere are very lithified, causing problems with processing for foraminifera, and suggesting the presence of secondary cements within the sediments. Thin section analysis of these sediments provided sedimentological information on the different

lithologies and the foraminifera present. It also enabled any diagenetic alteration to be determined.

5.7.2.1 Petrographic analysis

Thin sections were taken at a number of levels through the section to analyse the different lithologies and any diagenetic alteration that has occurred. Figure 5.14 shows some of the results of this analysis.

Thin sections of wackestones and mudstones from the Cenomanian limestones (Figure 5.14A) reveal a diverse and abundant microfauna. The microfauna is characterised by single-keeled, large planktonic foraminifera such as *R. cushmani*, *Rotalipora greenhornensis* and *Praeglobotruncana gibba,* and smaller, shallower-dwelling foraminifera, such as *Heterohelix moremani*, *Hedbergella delrioensis*, *Hedbergella planispira*, *Whiteinella* sp. and *Guembelitria cenomana*. These are indicative of the Upper Cenomanian *R. cushmani* TRZ. This microfauna can be seen in Figure 5.14A, where pervasive recrystallisation of the test walls and infilling of the tests with sparry calcite can be seen.

From within the marls below the CTB (Figure 5.14B), a very different assemblage is seen to that of the underlying Cenomanian limestones. These wackestones are dominated by small planktonic species, predominantly *H. moremani* and *H. delrioensis*. There are no larger planktonics and the genus *Rotalipora* has disappeared completely, marking the *W. archaeocretacea* PRZ. The preservation of specimens is generally poor, showing high levels of recrystallisation and infilling. Small grains of detrital glauconite and quartz are also seen, possibly indicating a slight shallowing of sea level at this time. The quartz and glauconite, which is seen in lens shapes within the clay-rich sediments, being deposited by current movement and winnowing over the sea floor.

The thick claystone layer, lying directly below the CTB, appears to be nearly devoid of any foraminifera (Figure 5.14C). Fine laminations within the claystone are

visible. Quartz and glauconite are present, concentrated into thin lenses within the claystone.

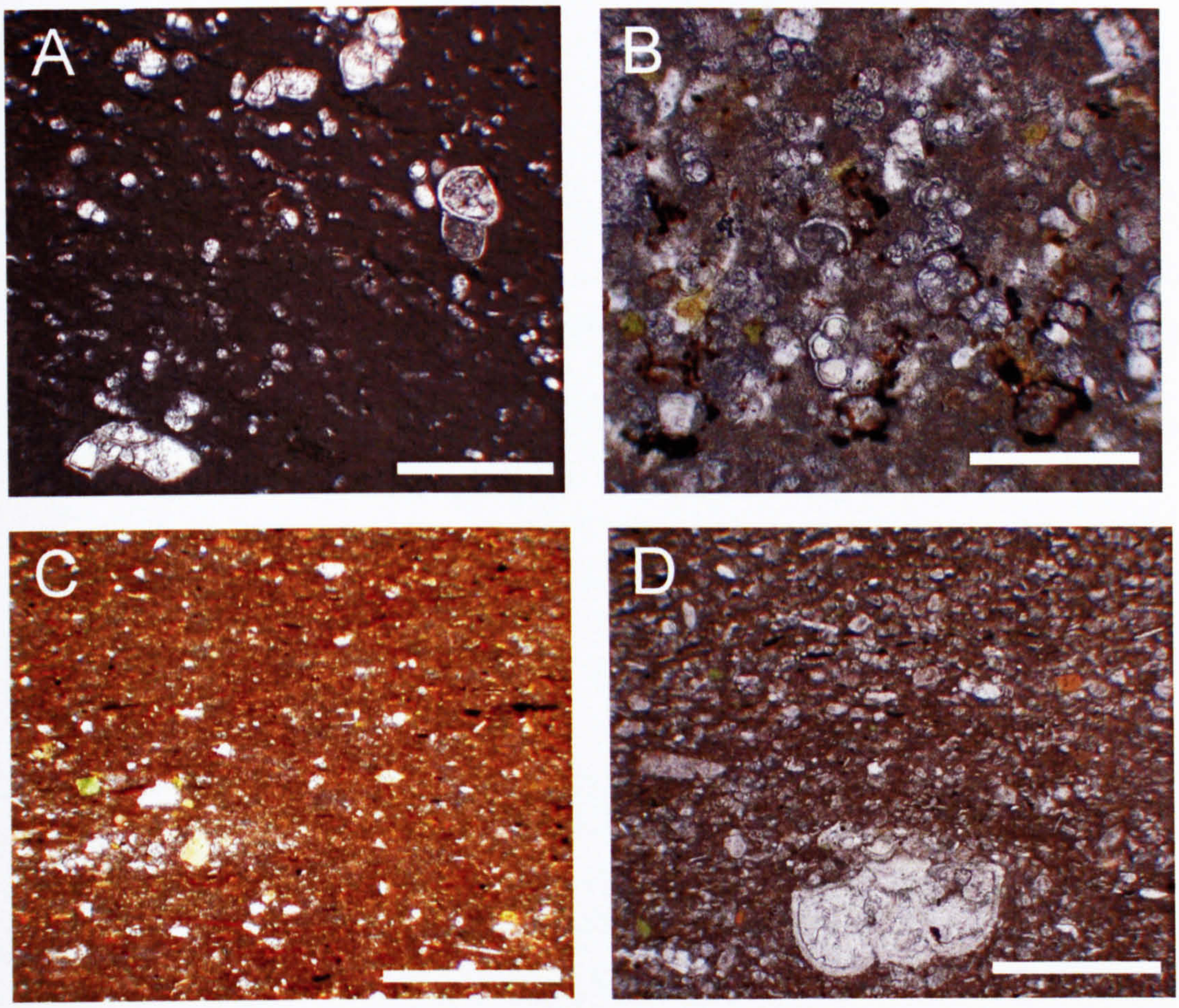

Figure 5.14: Examples of lithologies and microfauna throughout the Aksudere section.

A) Wackestone from Cenomanian limestone, 1.8 m below the Cenomanian-Turonian boundary (CTB). Diverse, high-abundance foraminiferal assemblage including *Rotalipora cushmani* indicating the *Rotalipora cushmani* Biozone. Infilling and recrystallisation of foraminiferal tests with sparry calcite is prevalent. Scale-bar = 500 μm.

B) Wackestone from marls 75cm below the CTB, showing a reduction in diversity of foraminifera and loss of keeled genus, *Rotalipora.* The assemblage is dominated by *Hedbergella* spp. and *Whiteinella* spp., indicating the *Whiteinella*

archaeocretacea Biozone. Again specimens show poor preservation, with infilling and recrystallisation of tests. Scale-bar = 200 μm.

C) Laminated claystone from the CTB, almost devoid of foraminifera. Quartz and glauconite are present. Scale bar = 400 μm.

D) Packstone from Turonian limestones, 6.7 m above CTB, showing a return to higher diversity and abundance. Large foraminifera return and new keeled species, such as *Helvetoglobotruncana helvetica,* are seen, indicating the *Helvetoglobotruncana helvetica* Biozone. Infilling and recrystallisation of foraminiferal tests is prevalent. Scale bar = 500 μm.

Another foraminiferal assemblage is seen in the Turonian limestones (Figure 5.14D). A large increase in the number of specimens and species appear preserved in these packstones. They are dominated by small *H. delrioensis, Whiteinella* spp. and *H. moremani,* with less abundant large planktonic foraminifera present, such as species of *Praeglobotruncana*. These sediments also contain the first occurrences of the keeled species, *Dicarinella hagni* and *Hevetoglobotruncana helvetica*, characteristic of the *H. helvetica* TRZ. The preservation of the foraminifera is again poor, sparry calcite commonly infilling the recrystallised tests. Fragments of inoceramid bivalves are also seen throughout the *H. helvetica* Zone.

5.7.2.2 SEM analysis

Overall it can be seen that the preservation of the foraminifera is poor with abundant infilling of the tests with secondary calcite, and recrystalisation of the test wall. Additional analysis of the foraminifera, and their preservation was undertaken using the SEM analysis. The results of this are shown in Figure 5.15. Each of the specimens show abundant secondary calcite nearly completely infilling the tests. Large crystals of sparry calcite are particularly well seen in the Upper Cenomanian *Whiteinella archaeocretacea*

(see Fig. 5.15 no. 6). The wall structure of the foraminifera can also be seen to be recrystalised, showing no evidence of the original structure or pores to be present.

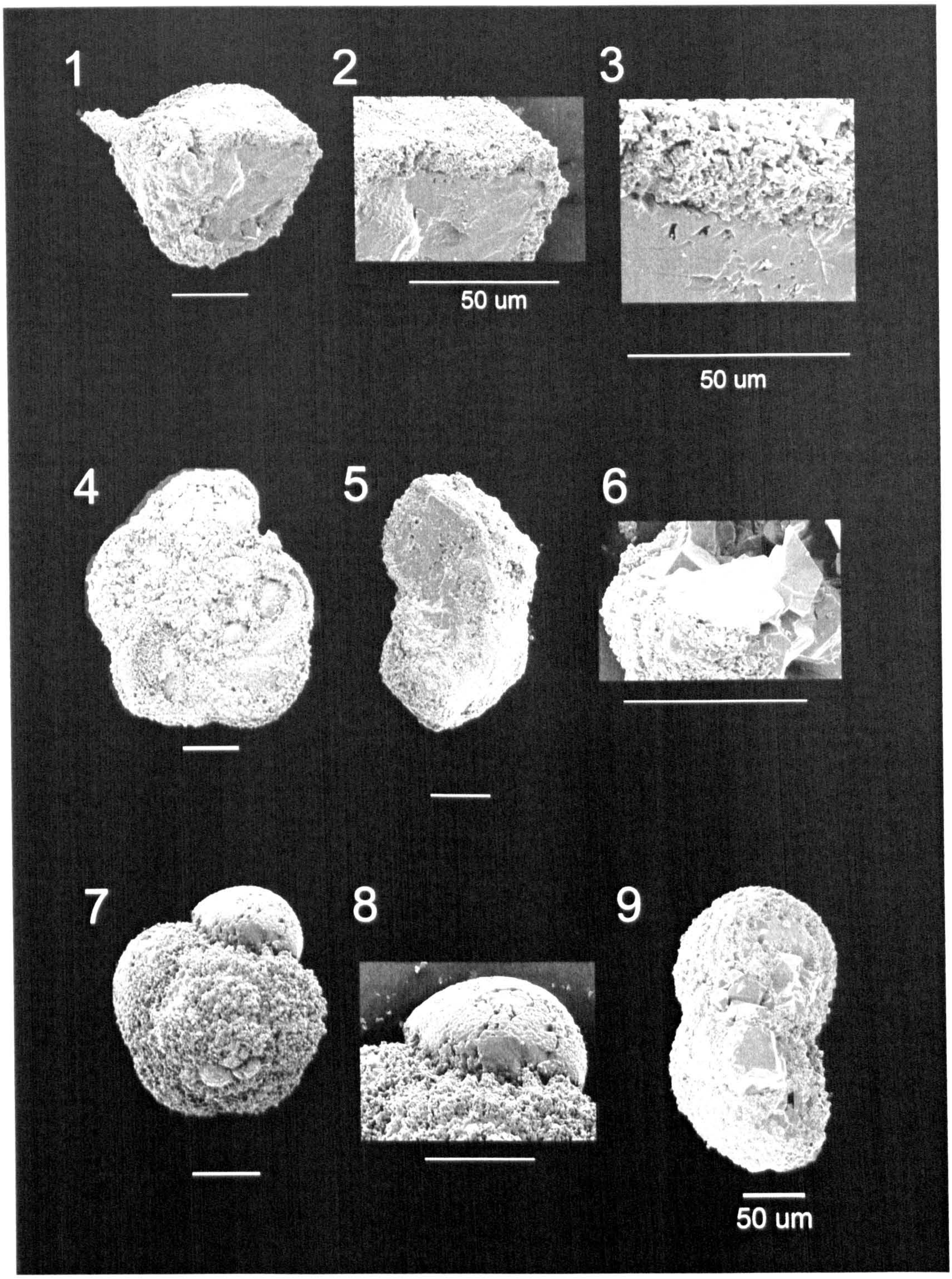

Figure 5.15: Photomicrographs illustrating the preservation of foraminiferal tests at Aksudere. All scale bars are 100 μm unless otherwise stated.

1) *Dicarinella imbricata* AK640, Lower Turonian

2) *Dicarinella imbricata* AK640, Lower Turonian

3) *Dicarinella imbricata* AK640, Lower Turonian

4) *Dicarinella elata* AK640, Lower Turonian

5) *Praeglobotruncana gibba* AK 60 Upper Cenomanian

6) *Whiteinella archaeocretacea* AK225 Upper Cenomanian

7) *Praeglobotruncana aumalensis* AK 225 Upper Cenomanian

8) *Praeglobotruncana aumalensis* AK 225 Upper Cenomanian

9) *Whiteinella archaeocretacea* AK225 Upper Cenomanian

Due to the poor preservation of the specimens at this site it was decided not to analyse the foraminifera using isotopic analysis, and additional care was taken over the interpretation of the fine fraction results, particularly the oxygen isotope values. This will be discussed further in Section 5.8.

5.8. Discussion

Both carbon and oxygen isotope profiles show excursions that are comparable to those seen elsewhere across the CTB. Figure 5.16 shows the correlation of the carbon isotope curve with the profile of Gale *et al.* (1993) from Eastbourne, UK. The shape of the Gale *et al.* (1993) carbon isotope curve is identical to that Paul *et al.* (1999), Keller *et al.* (2001) and Tsikos *et al.* (2004). As indicated above, Gale et al., (1999) suggest that the sandy marl unit lying directly above the erosion surface is probably equivalent to Bed 3 of the Plenus Marls, the erosion surface itself being the equivalent of the 'sub-plenus erosion surface'. At Eastbourne, the carbon excursion begins at the base of the Plenus Marls. In the Crimea, the excursion begins above the erosion surface. This may be due to the longer duration of the erosion event in the Crimea (see below). Both profiles increase rapidly to an initial peak at the top of the *R. cushmani* TRZ. There is a plateau within the lower part of the *W. archaeocretacea* PRZ, with both recording a second peak around the CTB. Both

profiles then decrease slowly to reach pre-excursion values in the *H. helvetica* TRZ. Regionally, the data show that both Crimean and NW European sections may have undergone similar palaeoceanographic change around the CTB, the correlative erosion surface possibly indicating a regional European regression. Foraminiferal data, however, indicate that the duration of this hiatus is longer in the Crimea than in the Anglo-Paris Basin (Kopaevich and Kuzmicheva, 2002).

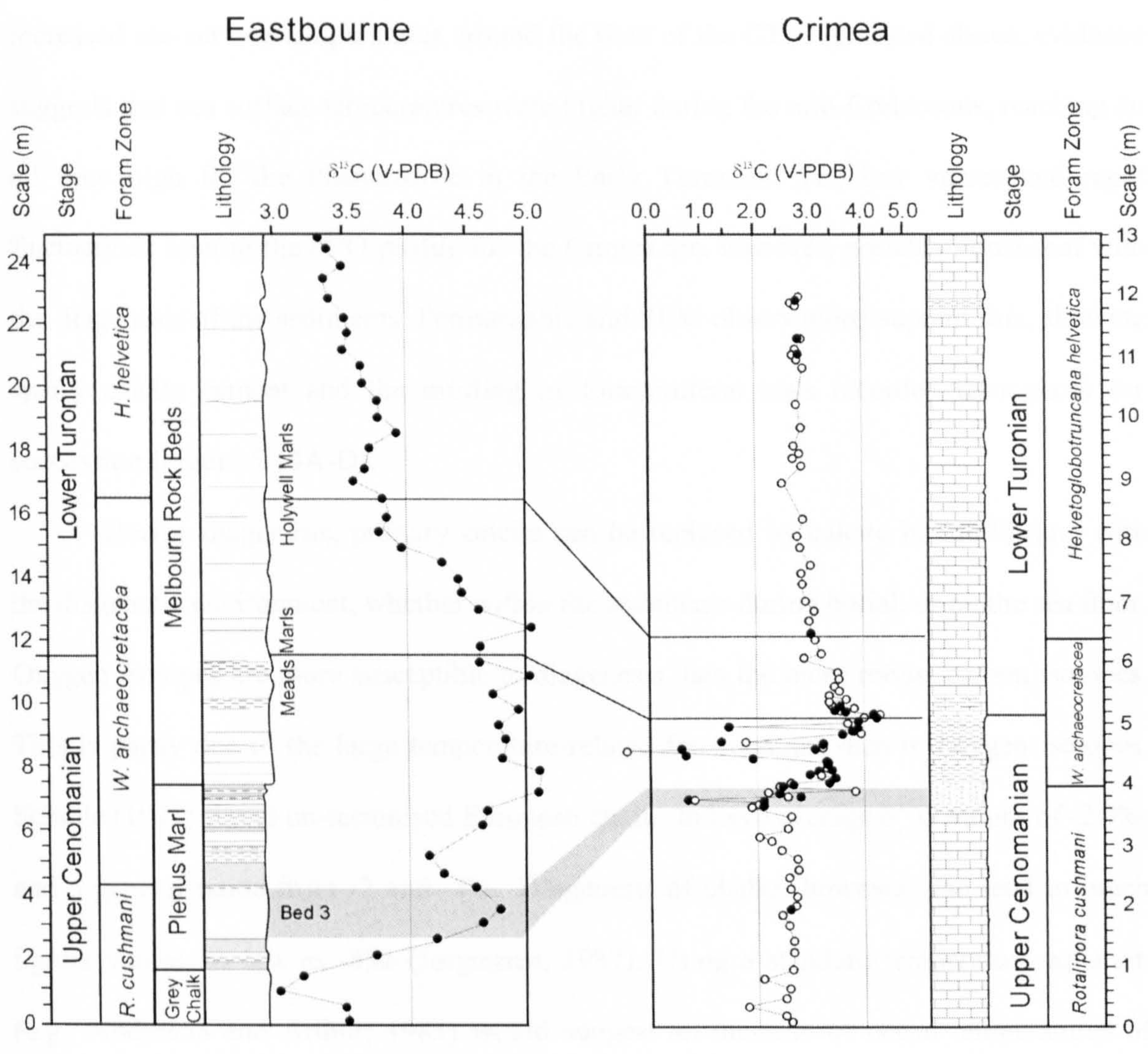

Figure 5.16: Correlation of carbon isotope results from this study with carbon isotope profile from Eastbourne, UK from Gale *et al.* (1993). Eastbourne bed number assignment according to Gale *et al.* (1993). Eastbourne foraminiferal biostratigraphy from Keller *et al.* (2001). Closed circle = treated samples, open circles = untreated samples.

The increased duration of this hiatus in the Crimea was probably due to large-scale tectonics, leading to uplift of the sediments and prolonged exposure of the sediments to erosion. Tectonic rebuilding of the region during the Albian to Cenomanian, and the rifting and/or extension in the Crimean and Caucasus region (Nikishin et al., 1997) may have been a driving mechanism.

In the Aksudere section the oxygen isotope data show a sharp decrease in values coincident with a distinct increase in the carbon isotope values. This may indicate increased sea-surface temperatures around the time of the CTB. As noted above, evidence suggests that sea surface temperatures were higher during the mid-Cretaceous, reaching an all time high for the Phanerozoic in the Early Turonian. The low values and rapid fluctuations seen in the $\delta^{18}O$ profile for the Crimea are, however, possibly consistent with the diagenesis of the sediments. Petrographic and SEM observations support this, showing sparry calcite cement and the infilling of foraminiferal tests recorded throughout the succession (Figure 5.14A-D).

During diagenesis, primary calcite can be replaced by calcite in equilibrium with the diagenetic environment, whether within the sediments during burial, or on the sea floor. Oxygen isotopes are more susceptible to diagenesis than the more robust carbon isotopes. This is partly due to the large temperature-related fractionation seen in oxygen isotopes. Scholle (1977) found un-tectonised European chalks to have average $\delta^{18}O$ values of -2.9‰ and a general range from -2 and -4‰. Diagenesis of chalks, however, can lead to much lighter values, as low as -8‰ (Jørgensen, 1987). Using a standard temperature equation (e.g., Anderson and Arthur, 1983) would suggest an increase of ocean temperatures of ~6°C as the values decrease from –3.5‰ to –5‰ at Aksudere. A similar trend is seen in other Cenomanian-Turonian sections (e.g., Jenkyns *et al.*, 1994). However, these values equate to temperatures of ~30-35°C, considerably warmer than temperatures postulated for the mid-Cretaceous (Barron, 1983; Huber *et al.* 2002) at a palaeolatitude for the Crimea of ~35°N (Smith *et al.*, 1994). Although it is proposed the $\delta^{18}O$ profile has been pushed

towards more negative values through diagenesis, the trend of the $\delta^{18}O$ curve may represent a primary shift in environmental conditions. The profile shows peak values around the CTB, followed by a slight increase and subsequent second negative shift in the Lower Turonian. This pattern is not inconsistent with other CTB studies indicating global warmth in the Turonian particularly Clarke and Jenkyns (2001).

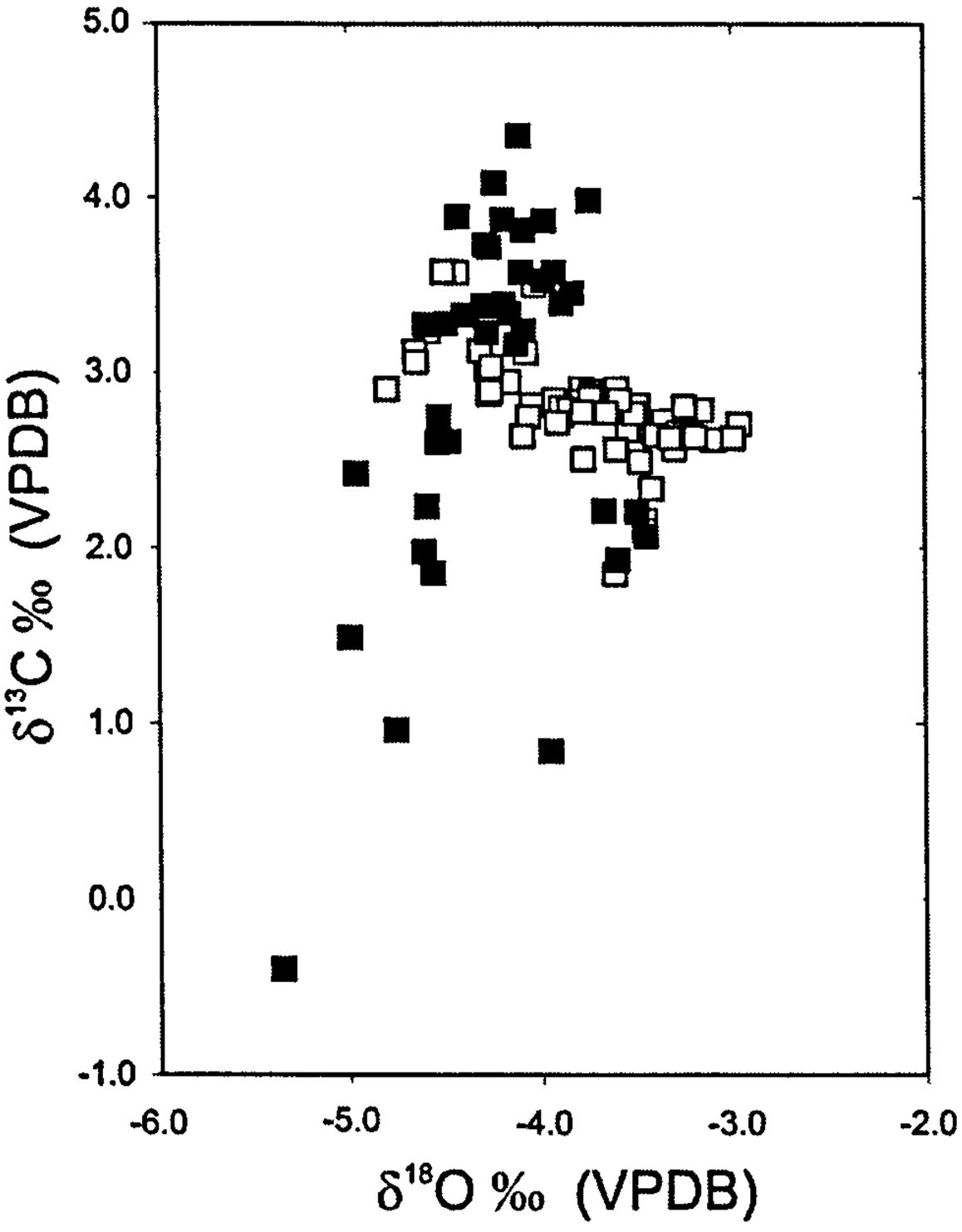

Figure 5.17: Cross-plot of oxygen and carbon isotopes from fine-fraction samples of both treated (organic carbon removed) and untreated (organic carbon present) samples. Carbonate samples = open squares, 'black shale facies' samples = closed squares.

It is likely, therefore, that the $\delta^{18}O$ results at Aksudere were affected by diagenesis shifting the primary signal to more negative values. A cross-plot of $\delta^{13}C$ and $\delta^{18}O$ data (Figure 5.17) shows a weak positive correlation which is typical of sediments thought to have been affected by meteoric diagenesis (e.g., Allan and Matthews, 1982; Marshall, 1992; Buonocunto *et al.*, 2002). This correlation is more defined in the sediments of the

black shale facies (black squares) than in the limestones (white squares). The most negative oxygen isotope values also showing the most negative carbon isotope values.

The positive carbon isotope excursion, also seen in isotope data from organic carbon (Naidin and Kiyashko, 1994a, b), can be interpreted as a response to the abnormally high burial rates of organic carbon that characterise the Cenomanian-Turonian sediments seen globally and at Aksudere. Rock-Eval data indicate that the organic matter in the organic-rich claystones at the CTB of Aksudere is autochthonous, marine-derived carbon predominantly from phytoplankton, with some contribution from higher plant matter.

Although this positive carbon isotope excursion is comparable to those seen at CTB sections globally, the presence of organic black shales at Aksudere and abundant foraminiferal and other micro- and macrofossil data, enables the conditions of the water column at Aksudere to be determined and the local cause of the black shale deposition to be determined.

Prior to the carbon isotope excursion a healthy, diverse foraminiferal population is recorded. Planktonic foraminifera are found from all depth habitats with deep dwelling *Rotalipora,* intermediate dwelling *Dicarinella* and *Whiteinella,* and shallow dwelling *Hedbergella*. This indicates a well stratified water column, with mesotrophic surface waters, as indicated by the dominance of hedbergellids. At this time Aksudere lay on the upper part of the continental slope, at a palaeodepth of ~500m (Kopaevich and Kuzmicheva, 2002). Similar to modern day continental margins, it is may be that upwelling occurred (subject to the right wind patterns) leading to the development of mesotrophic surface waters and a thin oxygen minimum layer.

Through the upper part of the Cenomanian the foraminiferal structure begins to change with the extinction of rotaliporids and a decline in other keeled *Praeglobotruncana* and *Dicarinella* species, leading to the disappearance of these genera following the BSF. This decline is coincident with a decrease in the number of benthonic specimens and is considered to be due to the expansion of the oxygen minimum zone, leading to anoxic

waters on the sea floor, and the intensification of anoxic waters higher in the water column. As the OMZ expanded up through the water column, waters initially became more dysoxic, leading to the initial decrease in the numbers of planktonic individuals, and subsequent decline of the deepest dwelling *Rotalipora,* followed by the intermediate dwelling *Dicarinella* and eventually *Praeglobotruncana*. However, an increase in the numbers of *Heterohelix* is recorded. *Heterohelix* spp. are interpreted as opportunistic and low-oxygen tolerant species based on previous Late Cretaceous and Cenozoic studies (e.g., Kroon and Nederbragt, 1990; Keller, 1993; Keller *et* al., 2001). A shift to *Heterohelix* dominated planktonic assemblages, such as observed at Aksudere, has also been observed globally at a number of CTB successions (e.g. Western Interior Seaway – Leckie *et al.*, 1998; Tunisia – Nederbragt and Fiorentino, 1999; Eastbourne – Keller *et al.*, 2001). This has also been associated with the expansion of the OMZ and has been previously used as a correlative tool in the Western Interior Seaway (Leckie *et al.*, 1998). Now seen to mark an interval of global heterohelicid dominance in the *W. archaeocretacea* Zone, it is recognised as a reliable global biomarker reflecting the expansion of the oxygen minimum zone after sea level transgression and the first peak in the $\delta^{13}C$ excursion (Keller and Pardo, 2004). The peak of *Heterohelix* dominance at Aksudere also corresponds with the onset of the carbon isotope excursion and is therefore considered to represent the global "*Heterohelix* shift", and the onset of localised black shale deposition at Aksudere.

The cause of the expansion and intensification of the OMZ over the CTB is thought to be due to intensified upwelling (e.g. Handoh *et al.* 1999; Kolonic *et al.*, 2005), breaking down water stratification and leading to intensified productivity in the surface waters. Radiolaria and several "blooms" of calcispheres (Kopaevich and Kuzmicheva, 2002) have been found in the black shales indicating highly productive surface waters.

Bottom waters were not completely anoxic during the deposition of the black shale facies however, as can be seen by the fluctuation between marls and organic rich shales, and the presence of some benthonic and planktonic species within the marl units. It is

thought, however, that the bottom waters may have remained dysoxic, accounting for the marly nature of the sediments, and largely infaunal and low oxygen tolerant benthonic species that are seen in the marls. *Tappanina lacinosa,* for example, has been used by Kuhnt and Wiedmann (1995) to define a biofacies indicative of slightly enhanced phytodetritus and mildly dysaerobic bottom waters. This correlates well with the abundance of *Tappanina lacinosa* in the marl units of Aksudere.

This fluctuation in anoxia may be due to pulses of upwelling and productivity at Aksudere, the OMZ becoming reduced temporarily over this period. Kopaevich and Kuzmicheva (2002) believe that the impoverished fauna of small-sized, low diversity, non-keeled morphotypes are typical of Boreal faunas (Weiss, 1982) and their dominance in the Crimea, indicates the presence of a relatively cold water mass in the Crimean area. Similar faunas have been interpreted elsewhere in the western Tethys as indicators of coastal upwelling of cold oceanic water (Kuhnt *et al*, 1986). It may be that the small sized, low diversity, non-keeled morphotypes seen in this study are purely a result of oxygen depleted waters. The evidence from the radiolaria and other microfossils suggests that the intensification and expansion of the OMZ may have been due to upwelling along the coastal margin of the Crimea over the CTB. It must be noted that the increase in abundance of radiolaria at this level may also be due to condensation of the sediments, and this is taken into account in the interpretation of Aksudere.

Following the deposition of the BSF, and return to carbonate sedimentation, the foraminiferal population is seen to recover fully. With an increase in keeled *Dicarinella,* filling the niche of the extinct *Rotalipora*, and the presence of abundant intermediate and surface dwellers indicating a normal ocean stratification, with mesotrophic surface waters. Diverse but low abundances of benthonic species also indicate oxygenated conditions had returned to the sea floor.

As described above, in addition to the long-term trends in the isotope profiles, there are a number of negative carbon isotope events seen clearly in the carbon isotope data, but

also to a lesser extent in the oxygen data. It is possible that negative values arise from contamination of the carbonate from organic matter. However, the similarity between carbon and oxygen isotope values of both the untreated samples and the samples with the organic material chemically removed rules out this possibility. It can be postulated, therefore, that the negative values are a result of environmental effects and/or diagenesis.

Environmental effects

Negative carbon excursions have been considered to be a result of changes in ocean circulation and chemistry. Recent work, however, has focused on the effect of the introduction of isotopically light carbon into the system from magmatically derived CO_2 and methane (e.g., Jahren *et al.*, 2001; Bralower *et al.*, 1994; Price, 2003).

There is a great deal of evidence for volcanism during the Cretaceous and around the CTB (Kerr, 1998). Widespread ocean plateau volcanism (for example the Caribbean-Colombian and Ontong Java plateaus in the Pacific and Kerguelen Plateau in the Indian Ocean) caused the expulsion of isotopically light (6-7‰) carbon into the atmosphere and carbon cycle. Volcanism has been suggested to account for negative isotope shifts in the early Aptian (OAE 1a) (e.g., Bralower *et al.*, 1994; Larson and Erba, 1999; Price, 2003). However, no direct effect upon carbon isotope profiles has been suggested for the CTB.

Methane is also a viable source of light carbon (isotopic values ~-60‰), able to produce the rapid and large negative shifts observed at a number of OAEs (e.g., the Toarcian and Aptian OAEs) (Hesselbo *et al.*, 2000; Jahren *et al.*, 2001; Beerling *et al.*, 2002). Negative excursions have been seen prior to the positive excursion at the CTB (e.g., Pratt, 1985; Arthur *et al.*, 1988; Hasegawa, 1997), although none have been convincingly attributed to methane hydrate dissociation.

In the Crimean section, the negative carbon isotope events occur during the positive isotope excursion, as opposed to preceding it. Negative excursions, similar to those seen in the Crimea, are observed at the Devonian Frasnian–Famennian boundary (364 Ma),

interrupting the positive $\delta^{13}C$ excursion seen in South China and Canada (e.g., Wang *et al.*, 1996; Chen *et al.*, 2002). Dissociation of methane hydrates has been suggested, the late Frasnian regression triggering their release, leading to increased levels of ^{12}C in the biosphere, rapid global warming, rapid sea-level rise and oceanic anoxia. Similarly, at the CTB a section in New Jersey (USA) was found to have two negative peaks, both short (10 kyr) and large (>5‰); it was postulated that methane release was a possible mechanism to explain such a signal (Wright et al., 2001). The presence of coincident negative oxygen isotope shifts and negative carbon isotope shifts, however, would suggest such a signal was more likely to be diagenetic in origin (see below).

At Aksudere, it is also unlikely that the negative shifts are due to the introduction of light carbon from methane or volcanism. No global negative signal is seen at the CTB, unlike for the events discussed above, which would be expected with such a large influx of methane or volcanically sourced ^{12}C into the biosphere.

Diagenetic signal

The presence of an erosion surface at the base of the Aksudere Beds, and the sandy nature of the sediments, indicates a possible regression in the region, just below the CTB. During the lowering of sea level, organic matter can become oxidised leading to localised diagenetic environments with relatively high amounts of ^{12}C and potentially ^{16}O (e.g., Malone *et al.*, 2001; Jarvis *et al.*, 1988). During diagenesis, this light carbon and oxygen would be incorporated into reprecipitated calcite, leading to negative excursions on the $\delta^{13}C$ and $\delta^{18}O$ isotope profiles. Through lithological and palaeontological investigation, Alekseev *et al.* (1997) suggest that the black shale facies (Aksudere Beds) are a result of a short-term regression during the global eustatic transgressive interval of the CTB. Although Gale *et al.* (1999) propose that the organic rich marls represent a transgressive system, it is possible that there were short-lived, localised regressions, possibly related to local tectonic activity, overprinting the overall transgressive trend. The presence of detrital

quartz grains in layers throughout the section at Aksudere (Fig. 3 A-D) and the presence of regional erosion surfaces support this fluctuation in sea level.

Coinciding with the negative excursions on the $\delta^{13}C$ profile are lowered values of TOC (Figure 5.12). Similar fluctuations in TOC levels in the upper claystone layer were identified by Naidin (1993) and Naidin and Kiyashko (1994a, b). Although Naidin (1993) suggested that they represented fluctuations of pelagic productivity that were controlled by climatic fluctuations and Milankovitch cycles, deterioration of organic matter has also been thought to affect other Cenomanian-Turonian localities. Jenkyns *et al.* (1994) attributed a dampening of the Cenomanian-Turonian positive excursion, in the stratigraphical vicinity of the "Livello Bonarelli" at Gubbio, to early diagenetic degradation of organic matter in the claystone.

In addition to the oxidation of organic matter, both $\delta^{13}C$ and $\delta^{18}O$ values could also be lowered during exposure of the sediments to meteoric water during sea-level fall. Meteoric water has lower $\delta^{18}O$ than marine water and can be accompanied by low $\delta^{13}C$ where the waters contain isotopically light carbon from soil-derived CO_2 (e.g., Allan and Matthews, 1982; Marshall, 1992). During early diagenesis it is possible that the carbonates partially equilibrate with these fluids, causing lower $\delta^{13}C$ and $\delta^{18}O$ (e.g., van Buchem *et al.*, 1999). The isotope data, therefore, appears to show the influence of post-depositional oxidation and degradation of organic matter, during early diagenesis, associated with a fall in sea level and the influx of meteoric waters to the sediments.

5.9 Conclusions

The Cenomanian-Turonian section at Aksudere clearly shows a carbon isotope profile reflecting enhanced drawdown of ^{12}C into organic-rich sediments, and the enrichment of marine waters in ^{13}C. This $\delta^{13}C$ excursion can be directly correlated with carbon isotope profiles seen elsewhere in NW Europe (e.g., Eastbourne, UK), indicating

the widespread nature of the changes to the ocean-atmosphere CO_2 reservoir, caused by global factors.

Synchronous with the positive excursion are increased TOC values, indicating the isotope excursion synchronous with the deposition of organic-rich sediments, possibly in anoxic bottom conditions. A decline in the diversity and abundance of foraminifera is also seen, the black shale layers being barren in foraminifera and rich in radiolaria, indicating enhanced upwelling and productivity in the region at this time. It is likely that the degree of anoxia fluctuated through the *W. archaeocretacea* PRZ, in which the Aksudere Beds were deposited. The presence of marls interbedded with the organic-rich claystones indicate that dysoxic conditions prevailed intermittently. Low oxygen tolerant, opportunistic, foraminifera are recorded in these units. Although the region was undergoing a global transgression, it is possible that the activation of geodynamic processes led to local, short, periodic regressions. These regressions are seen by a number of small hiatuses in the region, and sandy layers within the deeper-water sediments. Additionally, a regional regression may have occurred at the base of the *W. archaeocretacea* PRZ, correlative with the sub-plenus erosion surface (e.g. Gale *et al.*, 1999) of the Anglo-Paris Basin.

Coincident with the positive carbon excursion is an apparent negative excursion in the $\delta^{18}O$ profile, possibly indicating warming over the CTB into the early Turonian. The $\delta^{18}O$ values are, however, considered to have been diagenetically altered, shifting the primary signal to more negative values. Negative excursions seen on the $\delta^{13}C$ profile are interpreted as being, in part, an effect of diagenesis. Coinciding with the most negative $\delta^{18}O$ values, the $\delta^{13}C$ values indicate post depositional oxidation of organic matter during localised exposure of the sediments to oxic or meteoric conditions during a lowering of sea level or tectonic uplift.

Chapter 6: Palaeoceanography of northwest Europe during the mid-Cretaceous

6.1 Introduction

North-west Europe is one of the most studied regions of the world for Cenomanian-Turonian Boundary. High sea levels in the mid-Cretaceous led to the formation of widespread epicontinental seaways over much of the continental landmass, particularly in southern and eastern parts of the UK, northern France, Germany and Poland, whilst deep basins existed on the continental margin of western Tethys in Italy, and much of the modern Mediterranean Sea. This led to widespread deposition of Cenomanian and Turonian sediments, at a variety of palaeodepths over Europe. Many of these successions have been studied because of accessibility and completeness. The region was also influenced by the opening of the North Atlantic Ocean situated to the west of the UK, France and Portugal. Whilst lnks to the Tethys Ocean existed between Spain and North Africa. As the North Atlantic Ocean opened this link would have had quite an effect on circulation in northwest Europe and the palaeoceanographic conditions (Poulsen *et al.*, 2001).

Much of this research has concentrated on the expanded sections of deep water epicontinental regions (e.g. Eastbourne) and deep water basins on the continental margin of Tethys (e.g. Gubbio). Little data are avaliable from more from shallow water carbonate successions. In order to fully interpret the 'global' events surrounding the CTB, it is important that all palaeodepths are analysed in order to determine the causes and effects in all marine environments. This chapter looks at two shallow water successions, one located in Portugal and the other in the French Alps. These are then compared to one of the most expanded and complete sections of the Cenomanian–Turonian boundary at Eastbourne (Sussex, UK). The locations of these sections are shown in Figure 6.1.

Figure 6.1: Locality map of north-west Europe showing the three sites discussed in this chapter (shown as black circles), and other important CTB sites (shown as white circles).

In order to determine the events at the shallower localities, where many of the events may be missing or not recorded, Eastbourne is described below in order to set in context the faunal changes observed in Portugal and the Alps.

6.2 Mid-Cretaceous palaeoceanographic change at Eastbourne

Numerous studies have been undertaken of the Cenomanian-Turonian sections on the south coast of England, both on the major faunal turnovers (e.g., Jarvis *et al.*, 1988;

Hart *et al.* 1993; Lamolda *et al.*, 1994; Paul *et al.*, 1999; Keller *et al.*, 2001) and the $\delta^{13}C$ excursion observed (e.g., Gale *et al.* 1993; Paul *et al.*, 1999; Keller *et al.*, 2001; Tsikos *et al.*, 2004). A high resolution detailed chronology of both geochemical and palaeontological events has therefore been determined for Eastbourne, and this chronology has been used to aid correlation of other CTB sections globally.

Located on the south coast of England (Figure 6.1), Eastbourne shows one of the most expanded sections of Cenomanian-Turonian sediments in the UK. Four times thicker than the successions at Dover and twenty times thicker than that seen at South Ferriby (Gale *et al.*, 1993), the Cenomanian-Turonian sediments at Eastbourne are comprised of alternating chalks, marly chalks and rhythmically (Milankovitch driven) bedded marls (e.g., Gale, 1989). The succession is divided into three distinct units. The Grey Chalk Member (of the Lower Chalk Formation), the Plenus Marl Formation and Ballard Cliff Member (of the White chalk Formation). A log of the section at Gun Gardens west of the promenade at Eastbourne is shown in Figure 6.2.

It is thought that sediments at Eastbourne were deposited during a globally warm climatic interval, accompanied by high global sea levels and widespread ocean anoxia (Keller *et al.*, 2001). However, it has been proposed that the Plenus Marls were possibly deposited during a sea-level regression, with increased erosion and accelerated detrital input (Jeans *et al.*, 1991; Lamolda *et al.*, 1994), followed by a transgression as carbonate sedimentation returns. Although no, or very low levels of organic matter are found at Eastbourne (no more than 0.26% TOC; Tsikos *et al.*, 2004), the Plenus Marls are considered to be coeval with the organic rich shales seen elsewhere over the CTB. This is further verified by the global $\delta^{13}C$ isotope excursion seen at Eastbourne.

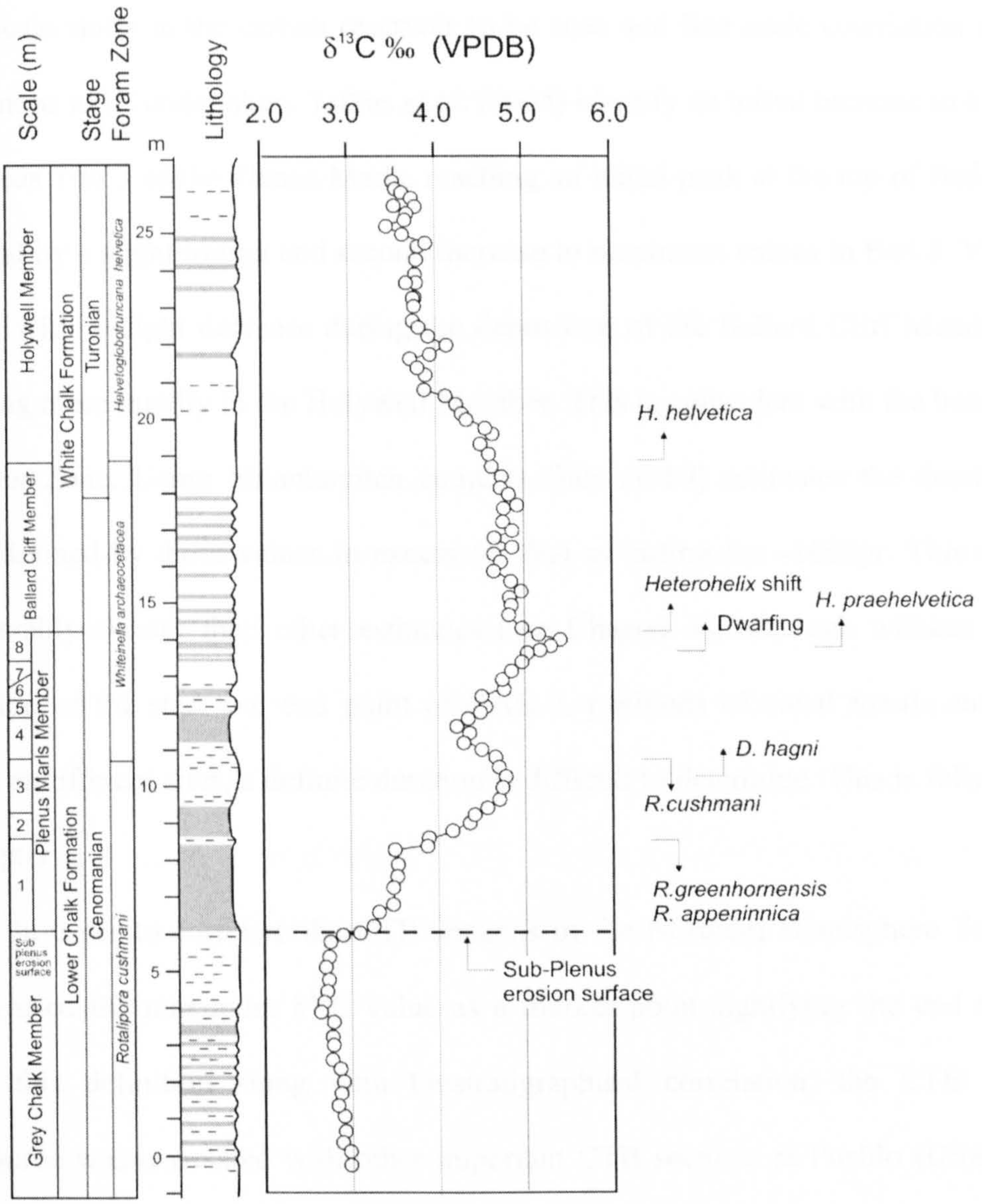

Figure 6.2: The Upper Cenomanian to Lower Turonian succession at Eastbourne. The geochemical data are taken from Tsikos *et al.* (2004). Faunal data is taken from Keller *et al.* (2001). The stratigraphic log is modified from Gale *et al.* (1993) and Keller *et al.* (2001).

The positive carbon isotope excursion begins in Bed 1 of the Plenus Marls (Jefferies, 1963) and reaches a maximum in Beds 7-8. Documented by a number of authors (e.g., Jarvis *et al.*, 1988; Gale *et al.*, 1993; Lamolda *et al.*, 1994; Paul *et al.*, 1999) the most recent study provided by Tsikos *et al.* (2004) shows the highest resolution to date, and although the same magnitude and general trends are seen the increased resolution enables

small scale shifts in the carbon reservoir to be seen and fine scale correlation with other successions to be undertaken. Tsikos *et al.* (2004) identify an initial increase in $\delta^{13}C$ values over Beds 1 to 3 of the Plenus Marls, reaching an initial peak at the top of Bed 3. This is followed by a slight trough and second increase to maximum values in Bed 8. Values then plateau with a slight decrease during the deposition of the Ballard Cliff Member, before declining more rapidly in the Holywell Member. This is coincident with the base of the *H. helvetica* Zone. Using Milankovitch couplets Gale (1989) estimates the duration of the OAE (defined by those values in excess of 3‰) as lasting for ~100kyr. This duration is considerably shorter than other estimates (see Chapter 1), although without an agreed definition of the start and end point of OAE 2, positions of zonal fossils and the $\delta^{13}C$ profile at different sites, a definite duration is difficult to determine. This is fully discussed in Chapter 1.

In order to correlate the CTB sections of the Northern Hemisphere Tsikos *et al.* (2004) used the maximum $\delta^{13}C$ value as a marker point signifying the end of OAE 2. Using this definition along with biostratigraphical correlation, the CTB section at Eastbourne was correlated with other important CTB sections at Pueblo (USA), Tarfaya (Morocco) and Gubbio (Italy). It is important to understand this correlation in terms of chemo- and biostratigraphical events. This enables sections which are incomplete, or shallow water in nature and don't record all the events surrounding the CTB, to be correlated to the larger scale events seen at localities such as Eastbourne.

In addition to the isotopic chemostratigraphy, faunal turnover is also very similar to that seen at other global sections. With the extinction and diversification of many foraminiferal species over the CTB, Keller *et al.* (2001) identify two major faunal turnover phases. The first, seen in Beds 1-3 of the Plenus Marls, is marked by the extinction of *Rotalipora*, and the first appearance of *Dicarinella*. This is coincident with increased surface productivity (abundant *Whiteinella*), subsequent reduced oxygen conditions in surface waters (marked by abundant *Heterohelix*), and the first positive $\delta^{13}C$ shift. Keller *et*

al. (2001) also suggest a possible marine regression or lowstand, in these lowermost beds of the Plenus Marls. The second faunal turnover occurs in Beds 7-8, coincident with the maximum $\delta^{13}C$ excursion. Increased surface productivity is observed again with an increase in hedbergellids and whiteinellids. This is followed by the temporary disappearance of over 50% of species. Jarvis *et al.* (1988) describe this extinction as stepwise, as the OMZ rose through the water column, leading to the disappearance of deeper dwelling species, followed by intermediate and more shallow water dwellers. Dysoxic conditions on the sea floor at this time led to the proliferation of low oxygen tolerant opportunists, whilst less tolerant benthos disappeared.

Many of the remaining species became dwarfed, and *Heterohelix* again dominates the surface waters. This indicates low oxygen waters and the expansion of the OMZ, coincident with a major transgression at this time (Jarvis *et al.*, 1988; Keller *et al.*, 2001). This dominance of *Heterohelix* is known as the "*Heterohelix* shift" and is commonly observed at the CTB, often associated with a flood of calcispheres (Hart *et al.*, 2002), as discussed in Chapter 4. Further discussion of the "*Heterohelix* shift" and its use as a global biomarker is discussed in Chapter 5.

Following this second the faunal turnover, fauna returns to more typical assemblages associated with normal marine sedimentation and, by the base of the *H. helvetoglobotruncana* Zone (approximately) typical assemblages of the Lower to Middle Turonian appear (Paul *et al.*, 1999). Figure 6.2 shows the overall changes, both chemo- and biostratigraphical seen at Eastbourne.

6.3 Mid-Cretaceous palaecoceanographic change on the west coast of Portugal

The Lusitanian Basin is found in western Central Portugal. Extending over 23,000 km^2 it was one of the marginal basins associated with the opening of the North Atlantic Ocean. Mid-Cretaceous successions are found along the Rio Mondego (inland of the town

of Figueira da Foz) and at Praia da Vitória (immediately north of the town of Nazaré). These are shown in Figure 6.3.

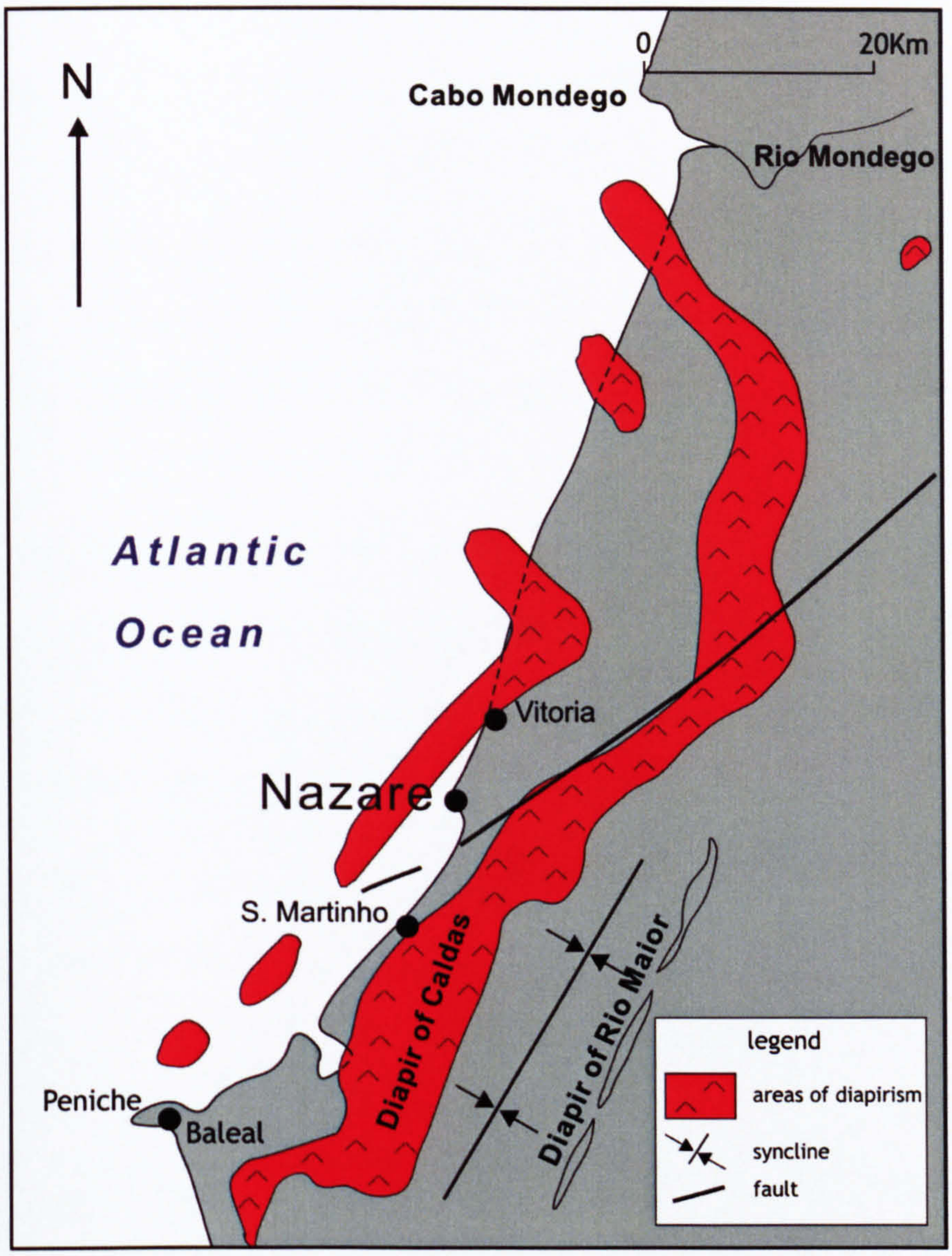

Figure 6.3: Location of Nazaré and the Rio Mondego (modified from Hart *et al.*, 2005)

These sections are found on the Western Portuguese Margin are part of a larger (mega) sequence that extends from the Upper Aptian to Lower Campanian (Wilson, 1988; Pinheiro *et al.*, 1996). Within this succession is an extensive carbonate platform of mid-Cenomanian to early Turonian age. This platform wedges out towards the basin margin and is thought to be coincident with the sea-level highstand of the mid-Cretaceous

(Hancock, 1989), suggesting a response of the sediments to global events rather than local tectonic control.

Figure 6.4 shows the outline log of the succession based on the work of Callapez (1998, 1999) together with data on the ranges of important foraminifera. The nature of the sediments has meant that the analysis of the foraminiferal assemblages has been based on thin sections. This can create problems and provide incomplete information on the assemblages due to the number of fauna recorded being largely dependant on the number of thin sections studied and problems of identification. Many 'smaller' benthonic foraminifera are impossible to identify at species, or even genus, level when using thin sections.

Planktonic specimens found in the succession can prove useful indicators of environment and depth. Very few planktonic foraminifera are recorded, which confirms the shallow water environment that represents the greater part of this succession. The specimens found are predominantly shallow water dwelling, with *Heterohelix* sp. cf. *H. moremani, Guembelitria cretacea, Hedbergella delrioensis* and *Whiteinella* spp. dominating the planktonic assemblages. Occasional very rare, specimens of *Helvetoglobotruncana praehelvetica* are also present, probably the direct results of the shallow water depths. All the planktonic taxa recorded are small in size, representing either juveniles or size-limited species due to the shallow water environment. Benthonic species are less diagnostic of environment, although the large benthonic orbitolinids and praealveolinids probably hosted algal symbionts (Lee and Anderson, 1991). This limits the water depth to 25-30 metres. Some thin sections contain abundant milioliids with few other species and are indicative of lagoonal, possibly hypersaline environments.

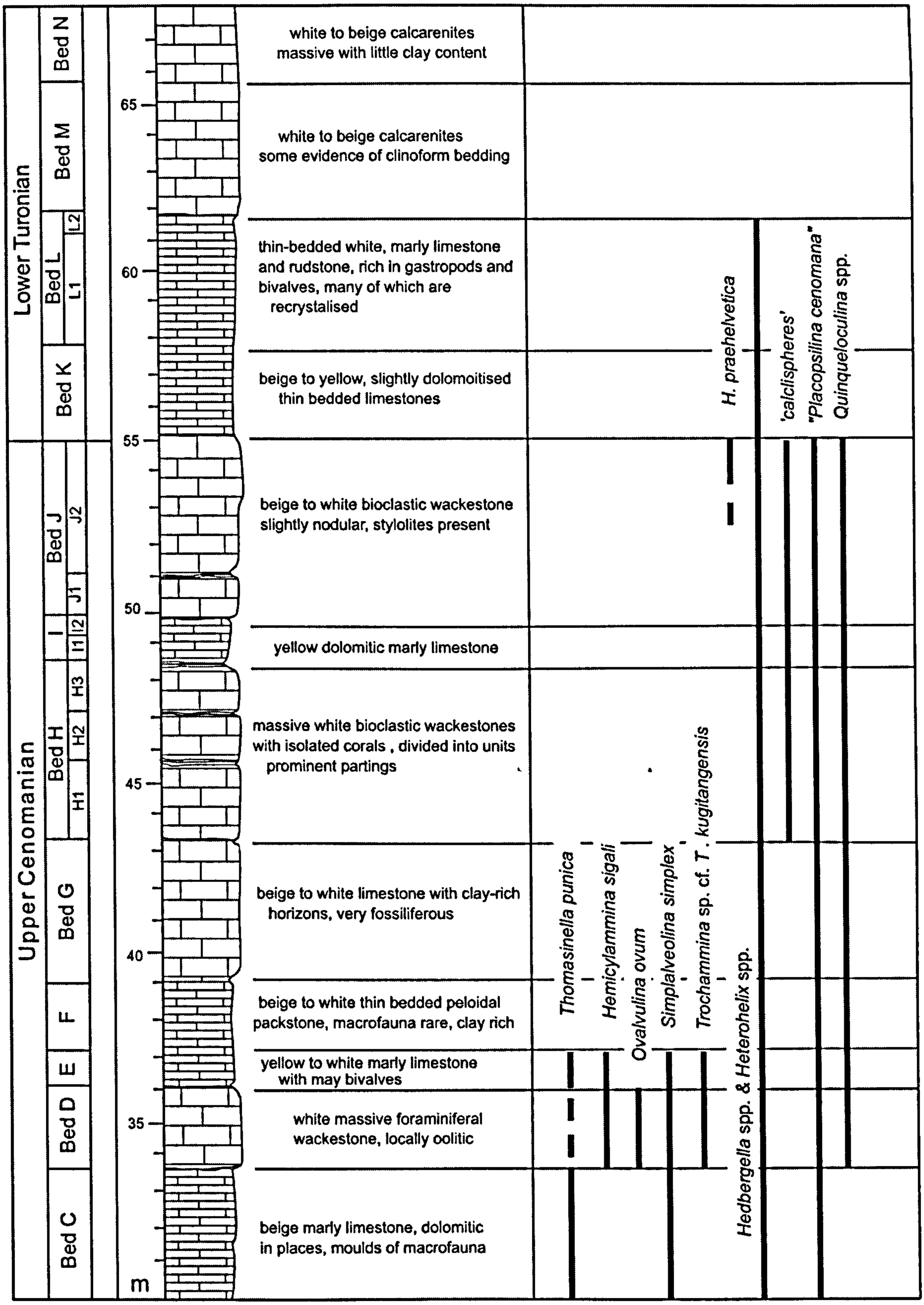

Figure 6.4: Log of the Cenomanian-Turonian succession of the valley of Rio Mondego with notes on lithology of the sediments and the range of the characteristic foraminifera.

A brief description of the sediments and foraminifera is given with corresponding thin section photomicrographs, in order to show the change in assemblages over the CTB. Beds C and D contain by a high diversity benthonic fauna (highest seen in the section) with only a few small *Hedbergella* spp. and *Heterohelix* spp. Benthonic species include *Ammobaculites* spp., *Dorothia* spp., *Marssonella oxycona, Lenticulina* spp., *Quinqueloculina* spp., and *Gavelinella* spp. The adherent agglutinated species "*Placocsilina cenomana*" (this genus is under review – Hart, *pers. comm.*) is also present, along with a diverse fauna of larger benthonic species of which *Simplalveolona simplex, Thomasinella punica, Ovalvulina ovum* are just a few. *Hemicyclammina sigali*, a Cenomanian marker in many Tethyan areas (Maync, 1953; Sartorio and Venturini, 1988) is also present in these beds, aiding correlation and dating of these beds. Other bioclasts present include molluscan fragments, echinoids, bryozoans, ostracods and fragments of dasycladacean algae. Figure 6.5 A-B shows examples of the assemblages recorded.

These faunas, with the associated calcareous algae, represent a mid-carbonate ramp assemblage with both shallow and slightly deeper water environments represented. A similarly diverse assemblage is seen in the Naith Formation of the Oman Mountains, representing a mid-Late Cenomanian age and containing a similar benthos, including *Hemicyclammina sigali* (Kennedy and Simmons, 1991).

Through Beds E and F the majority of the Cenomanian microfauna disappears, although benthonic foraminifera are still present at slightly lower diversities and small *H. delrioensis* are also recorded. By Bed G foraminifera are still present but are less common, and in Bed H the foraminiferal assemblage is reduced to rare, indeterminate agglutinated taxa, with very small *Hedbergella* spp. and *Guembelitria* spp. Interestingly this bed records the first occurrence of calcispheres (Hart, 1991).

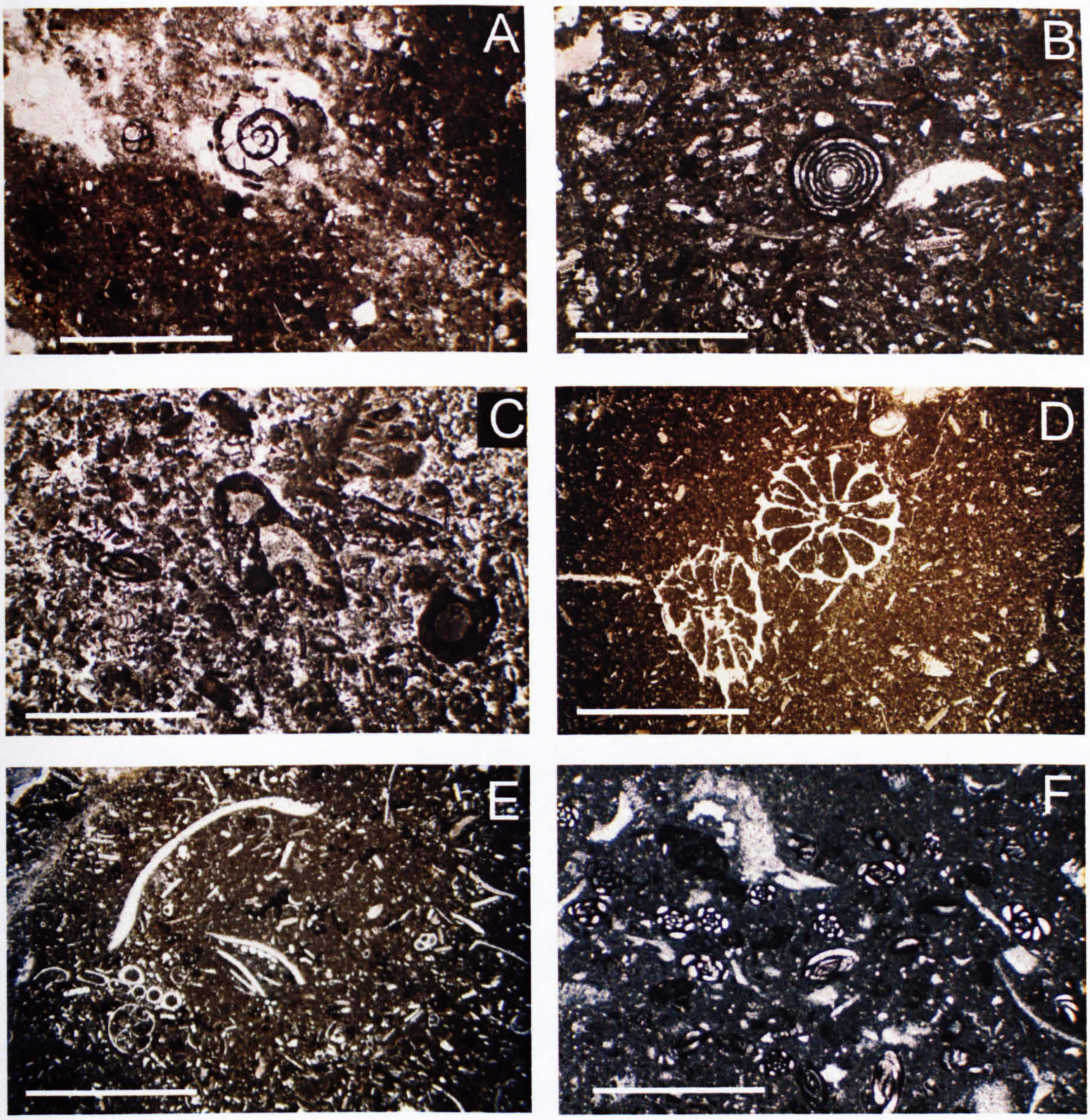

Figure 6.5: Photomicrographs of representative lithologies and foraminifera. All scale bars are 2mm, except F which is 500μm. A) Bed C, foraminiferal wackestone with *Hemicyclammina sigali*; B) Bed C, foraminiferal wackestone with *Simplalveolina simplex*; C) Bed F, peloidal packstone with *Ammobaculites* sp., *Quinqueloculina* sp., *Textularia* sp. and other smaller foraminifera; D) Bed H, bioclastic wackestone with scleractinian corals, echinoid spines and rare small planktonic foraminifera; E) Bed J, foraminiferal wackestone with bivalve fragments, serpulids and "*Placopsilina cenomana*"; F) Bed J, Foraminiferal wackestone with abundant *Quinqueloculina* spp. and *Nautiloculina* spp.

This latest Cenomanian-earliest Turonian flood of calcispheres is exceptionally widespread in Europe, North Africa and the Middle East, and in the Oman Mountains they have been recorded in comparable shallow environments (Kennedy and Simmons, 1991).

In Bed J foraminifera are still rare, however, *Hevetoglobotruncana praehelvetica* makes its first appearance. This species has been associated with the occurrence of the calcispheres (Kennedy and Simmons, 1991), and is also characteristic of the Juddii Zone in many areas (e.g., Eastbourne – see Figure 6.2). Examples of thin sections from Bed J are shown in Figure 6.5 E-F. The top of this bed is marked by a hiatus and this defines the Cenomanian-Turonian Boundary. The beds following the CTB contain rare and un-diagnostic foraminifera including *Marssonella oxycona, Heterohelix globosa, Heterohelix moremani* and *Hedbergella/Whiteinella* spp.

The sequence of the foraminifera from the succession along the Rio Mondego, shows some similarities to other sections in Northwest Europe. Evidence of the Late Cenomanian event is clear with the disappearance of most Cenomanian species by the top of Bed F, and the presence of calcispheres. Although many of the more typical species and events (such as black shale deposition) are not observed within the shallow margin of the shallow section of the Lusitanian Basin section, it is possible to correlate the sediments and record the faunal turnover.

6.4 Mid-Cretaceous palaecoceanographic change at Flaine in the French Alps

Flaine is located in France, 69 km to the southeast of Geneva, and lies on the Helvetic Shelf of the Western Alps (Ramsey, 1963). During the mid-Cretaceous this region lay on the Tethyan margin and is represented by a shallow water condensed mid-Cretaceous succession, followed by widespread deepening and a change in sedimentation at the start of the Turonian. Although highly condensed this section contains important biomarkers enabling correlation across the region and with other CTB sections. During the Early Cretaceous a carbonate platform developed, leading to the deposition of the

Urgonian limestones (Barremo-Aptian). These are shallow water limestones with abundant rudists and orbitolinids (especially in the marl interbeds). Between the Lower and Upper Aptian this platform was abruptly submerged, and starved conditions created a bioeroded and mineralised discontinuity surface at the top of the Urgonian limestones. This surface was then overlain by Upper Aptian argillaceous sandstones and sandy limestones. Parts of this succession are extremely fossiliferous, including bryozoans, oysters, brachiopods and serpulids (Pairis *et al*, 1986). These were deposited in a siliciclastic platform environment below storm wave base. At Flaine these sandy deposits are particularly rich in large bivalve *Epicyprina* sp (Pairis *et al*, 1986), these are shown in Figure 6.7 A-B.

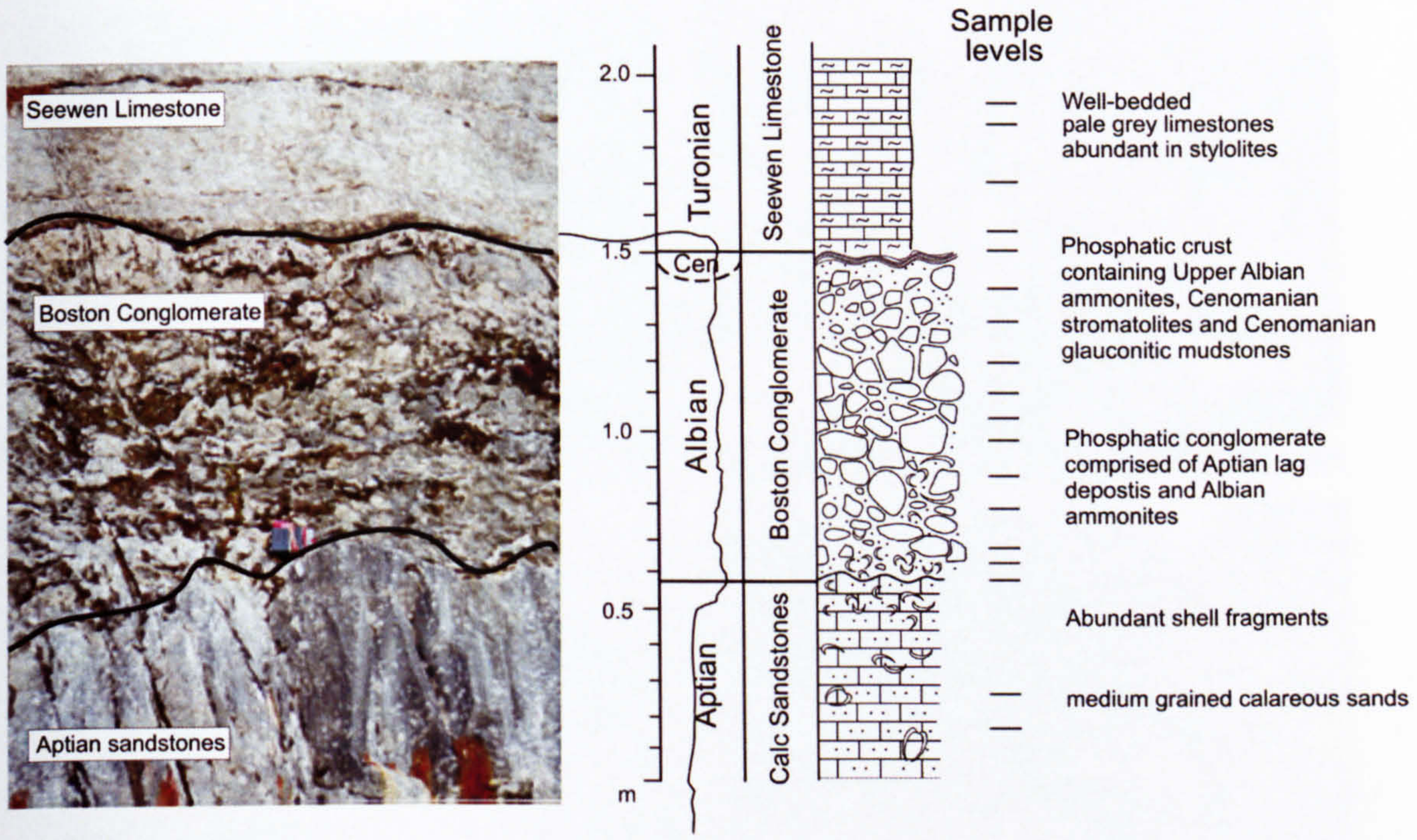

Figure 6.6: Photograph of the Aptian to Turonian succession seen at Flaine and simplified log of the section.

At the end of the Aptian a major change in sedimentation occurred. This is coincident with the beginning of phosphatic deposition and the appearance of a rough submarine topography caused by large scale erosional gullies being cut into the siliciclastic deposits. A subsequent deepening is suggested by the appearance of numerous ammonites and planktonic foraminifera (such as *Hedbergella* spp.). During the Early and Middle

PAGE
MISSING
IN
ORIGINAL

detrital sediments) is overlain by the basal Turonian chalk that is free of detrital grains. This appears to indicate Cornubia was drowned at this time and the source of sediment removed (Smith 1957; Carter and Hart 1977) as is seen at Flaine.

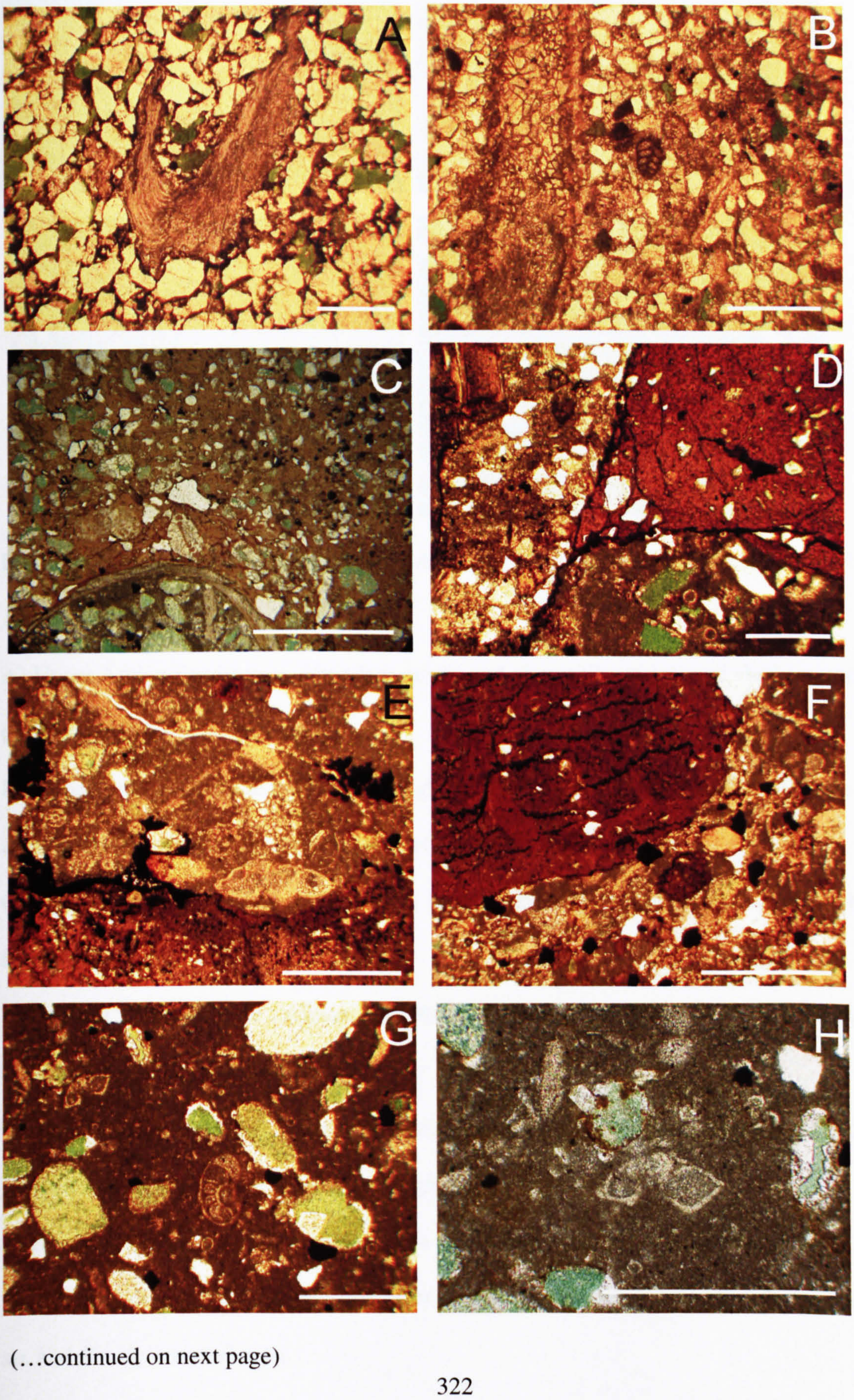

(…continued on next page)

(….continued from previous page)

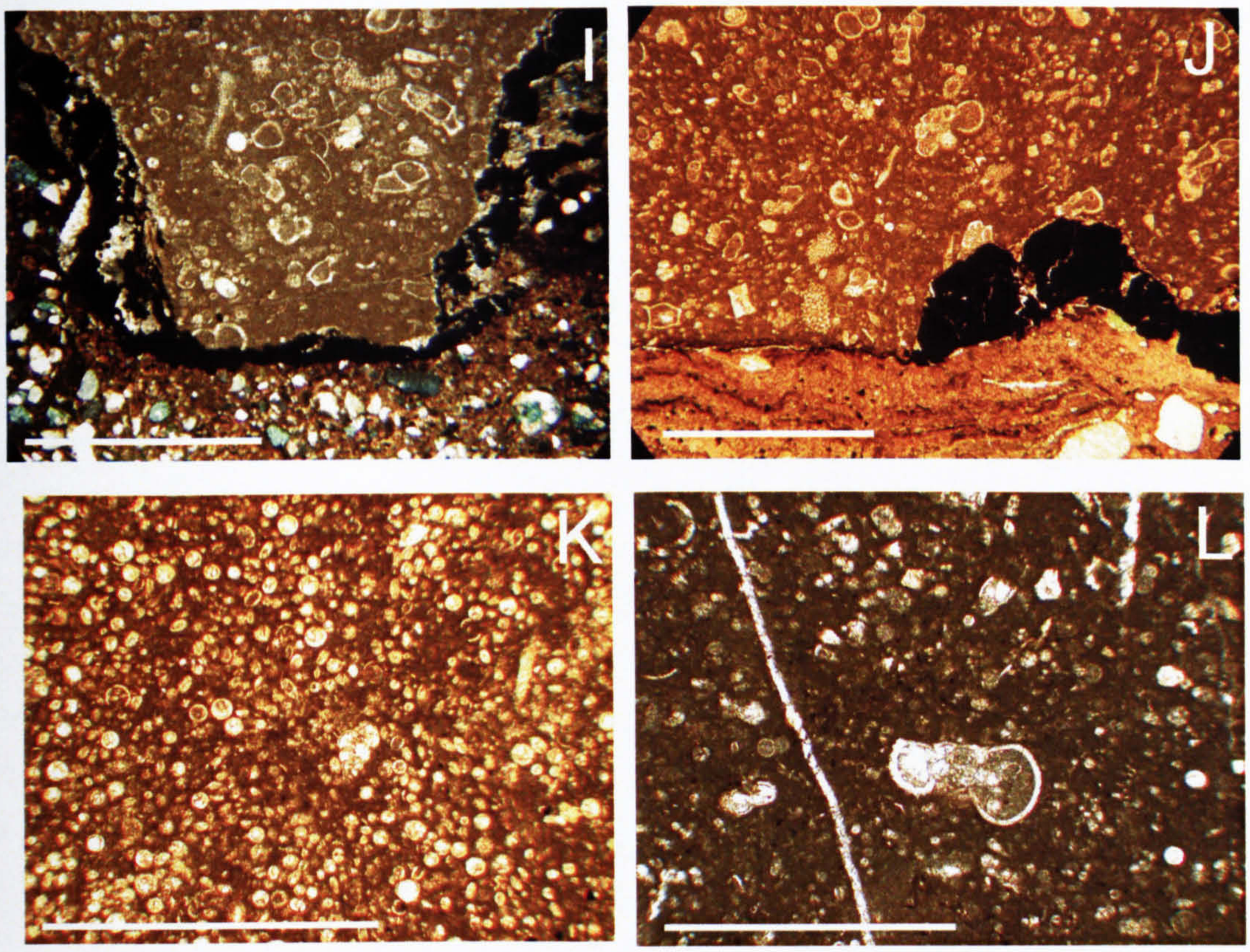

Figure 6.7: Thin section photo-micrographs of the Aptian- Turonian succession at Flaine.

All scale bars 500 μm.

A) Upper Aptian Sandstones. Abundant quartz and glauconite grains, and shell fragment of the bivalve *Epicyprina* sp.

B) Upper Aptian Sandstones. Quartz and glauconite rich sands. Recrystalised bivalve shell and benthonic foraminifera present, possibly *Spiroplectammina* spp.

C) Glauconitic Cenomanian muds from within the Boston Conglomerate, large benthonic foraminifera present.

D) Boston Conglomerate. Albian phosphatic crust, Aptian sandstone lag deposit and Cenomanian glauconitic mudstone.

E) Boston Conglomerate. Phosphatic crust and Lower-Middle Cenomanian glauconitic mudstone with a specimen of *Rotalipora appeninnica*.

F) Boston Conglomerate. Phosphatised bio-microbial film and Cenomanian mudstone.

G) Boston Conglomerate. Mid-Upper Cenomanian glauconitic mudstone with *Gavelinella* sp. and *Rotalipora cushmani*.

H) Boston Conglomerate. Close up of *Rotalipora cushmani* in section G.

I) Cenomanian-Turonian boundary between Boston conglomerate and Seewen Limestones. The boundary is marked by a pyritised algal layer. The undulating nature of the boundary can be seen. The Seewen Limestone infilling the 'topography'.

J) Cenomanian-Turonian boundary between the Boston conglomerate and Seewen Limestones. The boundary is marked by layered Cenomanian stromatolites. The Seewen Limestone is abundant in planktonic foraminifera including hedbergellids, praeglobotruncanids and dicarinellids.

K) Turonian Seewen Limestones. Packstone with abundant calcispheres and a specimen of *Heterohelix globosa*.

L) Turonian Seewen Limestone. Wackestone with *Helvetoglobotruncana helvetica*, calcispheres and smaller planktonics.

Interestingly there is no or evidence of organic rich sediments seen at the CTB on the Helvetic Shelf, although the sections clearly span the CTB with the presence of *R. cushmani* (Figure 6.7 G and H) and other typical Upper Cenomanian species, to the Lower Turonian *W. archaeocretacea* and *H. helvetica* in the Seewen Limestones. This may be due to the condensed nature of the sediments not recording the event. As no evidence is found for the event over the whole region it is suggested the area was situated on a submarine "high", above the anoxic water, but deep or isolated enough to keep out the detrital sediments.

It can be seen therefore that like Portugal the sediments of Flaine can be dated and constrained over the CTB, and although no deposition of black shales is seen, evidence of the Late Cenomanian extinction event is clear.

6.4 Summary

The fragmentary successions at Flaine and central Portugal have been dated and the CTB identified. No organic-rich sediments or black shales are recorded. In both areas, and despite working only with thin sections, the faunal changes at the CTB can be correlated with the events documented in the expanded succession at Eastbourne. With little work carried out on the effects of the CTBE in shallow environments, it is important that these are studies at in more detail. Understanding the effects of oxygen deficiency in deeper waters and the effect this has on the shallower environment being of most importance.

Chapter 7: Synthesis

7.1 Introduction

The previous chapters have discussed the results and local effects of the mid-Cretaceous events on the sedimentation and biota of the sites investigated in this study. This chapter aims to focus on a more regional and global perspective. Considering each site in the context of global change in the mid-Cretaceous and, more specifically, at the CTB.

7.2 Regional events in the Southern High Latitudes

7.2.1 Summary of results in the southeast Indian Ocean

In order to set the results from Site 766 and Site 762 in a regional and global context the key findings are summarised below.

7.2.1.1 Site 766

Site 766 which was drilled on Exmouth Plateau, northeast Indian Ocean, recorded a succession from the Pleistocene to the early Cretaceous (Valanginian). The mid-Cretaceous succession records the following features.

1) **Upper Albian**

   a) Data indicate the existence of a normally stratified water column with productive surface waters (hedbergellid dominated), a thin oxygen minimum zone (of fluctuating thickness), and well oxygenated bottom waters (abundant diverse benthos).

   b) In the late Albian $\delta^{13}C$ and $\delta^{18}O$ values are observed comparable to those associated with OAE 1D, indicating changes in the global carbon flux and a possible short-term warming event. No lithological expression of this is

seen event, and it is likely that the isotopes values are recording a global, as opposed to local, ocean-wide change.

c) Palaeotemperatures, estimated from benthonic foraminifera, show that significantly lower temperatures existed in the bottom waters, indicating that a marked thermal gradient existed in the Southern Tethys at this time.

d) Bottom waters are, however, markedly warmer than seen in low latitudes today, and are in line with other mid-Cretaceous studies of bottom waters temperatures (Huber *et al.*, 1995)

2) Cenomanian

a) An influx of Tethyan planktonic species indicates a rise in sea level through the Cenomanian of the Southern Tethys. This appears to be a response to a global eustatic rise.

b) There was a well-stratified, productive water column, with deep dwelling, intermediate and surface dwelling planktonic foraminifera present in the water column. A marked vertical gradient of $\delta^{18}O$ and $\delta^{13}C$ is recorded.

c) Evidence of a mid-Cenomanian event is seen in the $\delta^{18}O$ data, but this is not recorded in the $\delta^{13}C$ profile or Sr/Ca ratios. There is, therefore, no real expression of the MCE event at Site 766.

d) Bottom waters remained warm and oxygenated, with an increase of organic matter as conditions become more eutrophic in the Late Cenomanian.

3) Cenomanian-Turonian

a) $\delta^{13}C$ values increase markedly over the latest Cenomanian which indicates a global burial of light carbon. The $\delta^{13}C$ data show a similar magnitude and overall trend to many other isotope studies across the CTB. There is strong evidence of a global signal.

b) There are marked changes in the planktonic assemblages just prior to the first $\delta^{13}C$ peak, with the extinction of the rotaliporids, and the reduction of surface dwellers to hedbergellids and schackoinids. This indicates the presence of eutrophic waters and an expanded OMZ.

c) During the first $\delta^{13}C$ peak carbonate sedimentation stopped abruptly and radiolarian rich, zeolitic clays with high levels of manganese were deposited. These clays contain no organic matter, indicating deposition under the influence of oxic bottom waters. However, the lack of carbonate in the clays indicate deposition was possibly below the CCD.

d) The abundance of radiolaria indicates extremely productive surface waters during clay deposition.

e) Coincident with the slight decrease in $\delta^{13}C$ values at the top of the *W. archaeocretacea* Zone carbonate deposition resumes, and a rapid decrease in fine fraction and benthonic oxygen isotope values is seen. This indicates an increase in temperatures through the water column.

f) The sea floor was well oxygenated as benthonic species are recorded in these carbonate sediments.

g) Planktonic diversification is recorded with the influx of *Dicarinella* species which fill the niche vacated by rotaliporids. This indicates the return of a well stratified water column with oligotrophic surface conditions.

h) Coincident with the second $\delta^{13}C$ peak, however, productivity increases and an increase in the hedbergellids indicates the presence of meso- to eutrophic surface waters.

i) Mesotrophic waters remain throughout the Turonian as the hedbergellids, with an increase in heterohelicids and schackonids, dominate the surface waters as carbon and oxygen isotopes return to background levels.

7.2.1.2 Site 762

Site 762 was also drilled on the Exmouth Plateau. This site recovered sediments of Pleistocene to the early Cretaceous age. The mid-Cretaceous succession records the following features.

1) Albian

a) Isotope results from the Albian show intense alteration indicative of sea floor diagenesis. No environmental interpretation can, therefore, be attempted for these samples. A full analysis of the diagenesis is presented in Chapter 4.

2) Cenomanian

a) Pelagic carbonate sedimentation indicates the presence of normal open ocean conditions during the Cenomanian.

b) Diverse planktonic assemblages with an abundant Tethyan fauna indicate a normally, stratified water column with mesotrophic to oligotrophic surface waters.

c) Diverse benthonic assemblages of both epi- and infaunal species indicate the presence of oxygenated bottom waters.

d) In the upper part of the *Rotalipora cushmani* Zone an intensification and expansion of the OMZ is seen as surface waters become enriched in *Heterohelix* spp., and benthonic assemblages become dominated by infaunal morphotypes. This is coincident with a build up in $\delta^{13}C$ values from 2‰ to nearly 4‰ at the CTB.

e) Oxygen isotopes decline in value during the upper part of the *R. cushmani* Zone from -2 to -3‰, reaching a minimum at the CTB.

3) Cenomanian-Turonian boundary

a) The boundary is marked by the deposition of clay-rich black shales, with low amounts of organic matter (<2%). This indicates deposition in dysoxic waters. Up-

section the black shales pass back into carbonate rich chalks. Abundant in radiolaria, enhanced productivity is suggested as the cause for expansion of the OMZ at this time.

b) Just prior to the CTB, *Heterohelix* spp. are seen to dominate assemblages as hedbergellids decrease in numbers and the rotaliporids have become extinct. This indicates a further expansion of the OMZ. Benthonic species become reduced to infaunal low oxygen tolerant species, which indicates the presence of dysoxic bottom waters.

c) Following the deposition of the black claystone, a diverse and abundant benthos of opportunistic, low oxygen tolerant species are recorded, indicative of 'disaster taxa' recolonising the sediments. Abundance rapidly falls as inter-specific competition increases and more favourable conditions return to the sea floor.

d) Planktonic assemblages become more diverse with all niches (from shallow to deep dwelling) occupied. Abundance increases slowly following the CTB, although a second decline in abundance is seen. However, coincident with a second increase of 0.5‰ in $\delta^{13}C$ values, and a huge increase in numbers of *Heterohelix.* This indicates unstable conditions remaining through into the Lower Turonian.

7.2.2 Regional effects of mid-Cretaceous events in the southeast Indian Ocean

The key results identified above enable a picture of the events in the southeast Indian Ocean to be defined. These changing palaeoenvironments can be related to global events seen in the mid-Cretaceous. Marine temperatures in the southeast Indian Ocean were much higher than those seen at similar latitudes today, with surface waters ranging from 19°C in the Albian to 24°C in the Early Turonian. Bottom water temperatures are also much higher, ranging from 13°C in the Albian to 18°C in the Early Turonian. These temperatures are similar to those observed for the same time period at other sites in the southern high latitudes, such as the Falkland Plateau (~61°S) and the Naturaliste Plateau

(~58°S) (Huber *et al.*, 1995). A similar trend is also seen in Clarke and Jenkyns' (1999) composite palaeotemperature curve for surface waters based, on data from Sites 766, 762 and 763. This curve shows similar values for the Late Albian. However, although the trends in the Cenomanian and Turonian remain the same, Clarke and Jenkyns' (1999) absolute temperature estimates are much lower. However, due to the similarities in temperatures and thermal gradients obtained in this study to other high latitude sites (e.g., Huber *et al.* 2002), leads to the conclusion that these are valid palaeotemperature estimates for the mid-Cretaceous. It is widely accepted that increased levels of carbon dioxide in the atmosphere led to increased sea surface temperatures with a lowered pole to equator gradient (e.g., Barron, 1983). Certainly the data presented here support a high latitude warm water scenario. Circulation driven by warm saline bottom waters (e.g., Brass *et al.*, 1982) generated in the low latitude epicontinental seas may also have contributed to the warm bottom waters observed in the Indian Ocean (cf. Brady *et al.* 1998; Poulsen *et al.*, 2001). These warm waters would have been sluggish and more prone to anoxia than modern cold, deep water (DeBoer, 1986). However, in a study of mid-Cretaceous ocean circulation using the "Parallel Ocean Climate Model", Poulsen *et al.* (2001) demonstrated the effect of the presence or absence of a marine connection between the North and South Atlantic. Within the simulations for the mid-Cretaceous, the Pacific-Indian ocean basins were dominated by thermohaline circulation with deep water production in the Southern Ocean (analogus to modern Antarctic Bottom Water). The warm temperatures seen in the bottom waters of the southeast Indian Ocean in this study, however, appear to contradict this high latitude production of (relatively cool) deep water.

At both sites isotopic analysis of the carbonates show positive carbon isotope excursions, related to OAE 1d (Site 766) and OAE2 (Sites 766 and 762). The absence of organic rich sediments indicates that the isotope signals may be recording a global (as opposed to a regional) perturbation in the global carbon reservoir. Through the Albian and lower part of the Cenomanian both sites exhibit open ocean, normally stratified water

columns, with mesotrophic surface waters and most likely a thin oxygen minimum zone, as seen in modern continental margins.

At the CTB, however, a change in sedimentation is seen at both sites, along with a marked faunal turnover in both benthonic and planktonic populations. This indicates a large change in the water column, even if fully anoxic bottom waters did not exist at either site. Cenomanian-Turonian organic carbon rich sediments are, however, recorded at Site 763, 84 km south of Site 762. Two distinct organic rich layers are seen, with up to 15% TOC within the CTB claystone sediments (Haq *et al.*, 1990). A depositional model must, therefore, take this into account in order to interpret what happened in the water column to produce the effects seen in the southeast Indian Ocean. To produce organic rich sediments at Site 763 bottom waters must have become anoxic either from becoming stagnant, enhancing the preservation of the organic matter, or from increased productivity creating an expanded oxygen minimum zone impinging on the sea floor.

Ruttköller *et al.* (1992) postulate that the CTB in the southeast Indian Ocean represents a time of world-wide oxygen depletion in bottom waters which improved preservation of the organic matter produced in overlying waters. Differences in surface palaeo-productivity would, in this model be responsible for the site-to-site contrasts. Pancost *et al.* (2004) examined the black shales of Site 763 and the presence of biomarkers, as part of their study on photic zone euxinic conditions over the CTB. They concluded that intensification of the oxygen minimum zone was the only logical explanation for the occurrence of Chlorobiaceae biomarkers (indicative of euxinic conditions) in sediments such as those found at Site 763. These sediments were deposited on topographic highs and nearby to sites characterised by low organic carbon contents (e.g., Site 762). Bottom water stagnation in contrast, would expect similarly anoxic waters to be observed at the nearby Site 762. Thurow *et al.* (1992) also conclude that the presence of organic rich shales at Site 763 is due to an intensified and expanded OMZ, as a result of high productivity in shallow environments, causing the OMZ expanding vertically and

laterally. In the Thurow *et al.* (1992) model, nutrients being leached from flooded lowland areas are transported to the oceans, as a result of sea level rise. This fits well with the data presented in this study, and may explain how Site 762 was not completely anoxic but showed evidence of an expanded OMZ and dysoxic bottom waters. However, Thurow *et al.* (1992) suggest that no enhanced productivity in the surface waters above Site 766 took place. Instead they suggest that the radiolarians observed in the CTB clays (suggested here to represent enhanced productivity) were re-deposited from an upslope location similar to site 762. Radiolaria at site 766 are, however, well preserved and found in high abundance and diversity of specimens within the CTB clays. This is not indicative of down-slope movement and there is additionally no evidence of turbiditic deposition at Site 766. Although the abundance of radiolaria could be a product of condensation of the sediments foraminiferal evidence also indicates productive waters just prior to the CTB with abundant hedbegellids indicative of eutrophic conditions.

It is likely that enhanced productivity, as a result of increased nutrient flux from the continent, did initially cause the expansion and intensification of the OMZ. However evidence shows that local productivity would have also affected the expansion of the OMZ. This intensification meant the sequestration of manganese and other trace metals from the OMZ into the water column and deposition of them into the sediments on the oxic sea floor, as discussed in Chapter 4.

At Site 762, however, fluctuating conditions from slightly anoxic to dysoxic bottom water conditions are thought to have prevailed, as seen from the deposition of low levels of TOC and the absence of benthonic foraminifera at the base of the claystone unit. This is followed by more dysoxic claystone deposition with limited fauna of low oxygen tolerant benthonic species. Fluctuations in bottom water conditions are also seen at Site 763 with the deposition of two organic rich layers within the CTB clay unit (Haq *et al.*, 1990), indicating a fluctuation from completely anoxic to dysoxic bottom waters over the CTB interval. This would suggest that Site 763 was located very close to the base of the OMZ,

as local productivity variations caused the base to fluctuate as the OMZ expanded and receded. This may explain the dysoxic to weakly anoxic waters in which the sediments leading up to, and during, the CTB were deposited at the slightly deeper and more ocean-ward Site 762.

Shallower onshore sites of Cenomanian-Turonian sediments have also been analysed and comparable events to those seen in the open ocean are observed. The mid-Cretaceous succession of the Giralia Anticline in the Canarvon Basin (Howe *et al.*, 2000), records a 50m sea level rise over the CTB (Haig *et al.*, 1996). Temperatures comparable to those seen in this study and Huber *et al.* (1995) were suggested. Unfortunately the CTB sediments are missing from the Giralia section and no information on the actual CTBE recorded. Faunal turnover across the boundary interval was recorded, however, and although no significant 'mass' extinction was observed a similar turnover of foraminifera as seen in the deeper environments is present. Figure 7.1 shows the model proposed for the environmental changes seen around the CTB in the Indian Ocean.

7.3 Regional events in the Northern Hemisphere

Cenomanian-Turonian boundary sections in the northern hemisphere have been widely researched, particularly the epicontinental seaways of northwest Europe (e.g. Jarvis *et al.*, 1988; Keller *et al.*, 2001), the Tethyan margin (e.g., Coccioni and Luciani, 2004), the North Atlantic (Kuhnt and Wiedmann, 1995; Huber *et al.*, 1999; Gustafsson *et al.*, 2003; Kolonic *et al.*, 2005) and the Western Interior Seaway (e.g., Leckie *et al.*, 1998; Keller and Pardo, 2004). This section looks at the depositional environment of the north east Tethyan margin and shallower Tethyan and Atlantic successions in the context of the regional and global environmental changes in these areas.

In order to discuss the results of Crimea in a regional and global context the general trends and results are summarised below. More in depth discussion of the smaller localised events at the sites can be seen in Chapter 5.

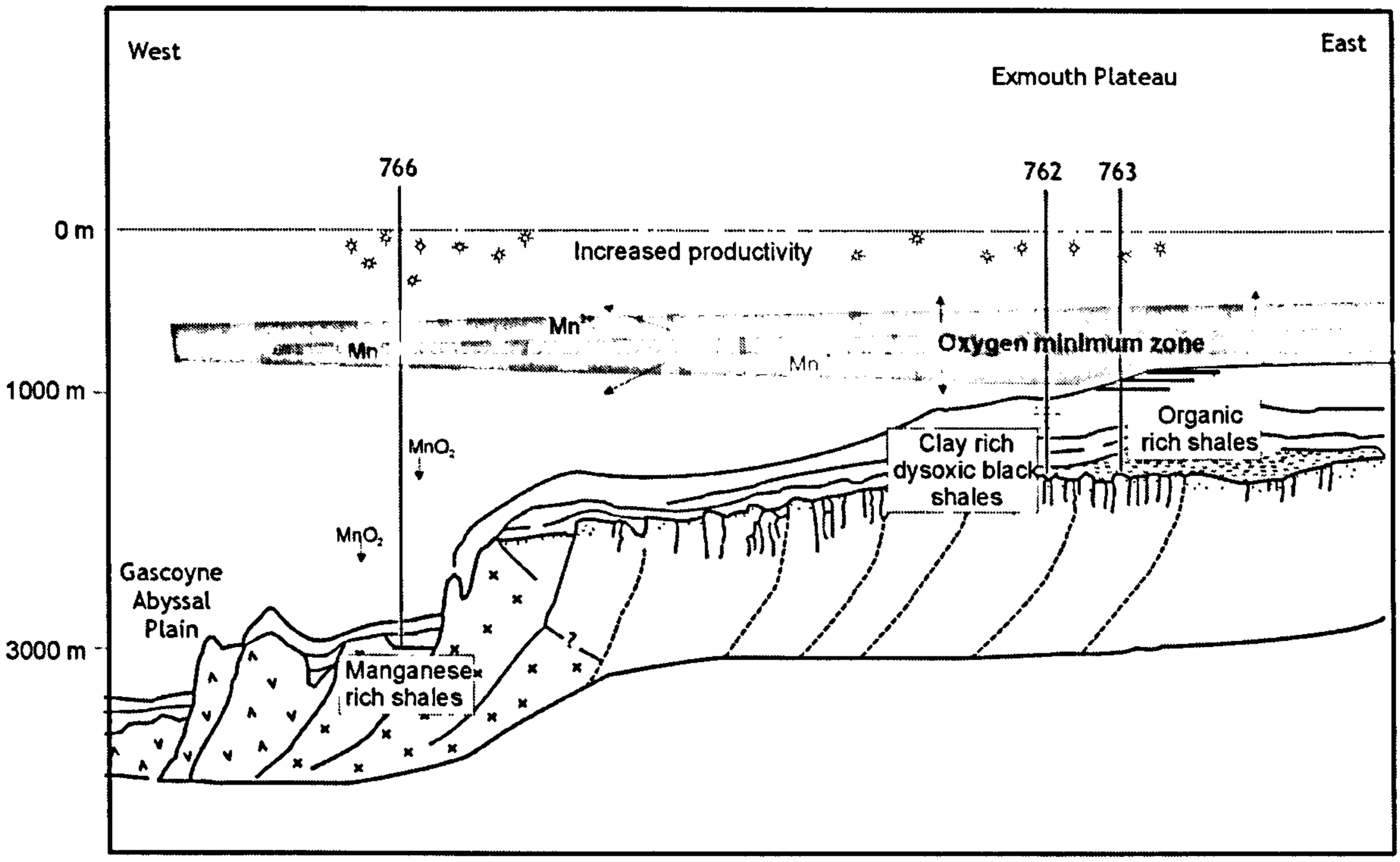

Figure 7.1: Transect of the northwest Australian margin showing proposed environmental conditions at the Cenomanian-Turonian Boundary that produced the sediments and faunal changes described in the text. Cross section modiefied from Gradstein (1992).

7.3.1 Summary of events in the Crimea

1) Upper Cenomanian

a) Data indicate deposition of carbonate rich, limestone sediments in a normally stratified water column with productive surface waters (hedbergellid dominated), a thin oxygen minimum zone (of fluctuating thickness), and well oxygenated bottom waters (abundant, diverse benthos).

2) Cenomanian-Turonian Boundary

a) In the upper part of the Upper Cenomanian rotaliporids became extinct and praeglobotruncanids and dicarinellids temporarily disappeared from the planktonic assemblage as the OMZ expanded and low oxygen tolerant

Heterohelix spp. thrived in the surface waters. Benthonic species also decline as bottom waters become dysoxic.

b) $\delta^{13}C$ values begin to increase in line with global and local environmental changes and deposition of the black shale facies began in anoxic to dysoxic bottom waters.

c) Intensification of the OMZ led to impoverished surface and bottom waters. Fluctuations in the intensity of the OMZ, due to changes in surface productivity, led to changes from anoxic to dysoxic bottom and surface waters, as indicated by the presence of the intermittent marl formation. These marls record impoverished benthonic and planktonic assemblages (predominantly low oxygen tolerant faunas).

d) The $\delta^{13}C$ profile shows a positive isotope excursion over the CTB. This is, however, punctuated by short, rapid negative shifts consistent with diagenesis and the deterioration of organic matter as discussed in chapter 5.

e) $\delta^{18}O$ values also record peak values over the CTB and into the Turonian. Although effected by diagenesis, it is thought that the trends in the record represent an environmental signal of increased sea surface temperatures in the Crimea over the CTB.

3) Lower Turonian

a) A return to carbonate sedimentation is observed, as normal ocean conditions resume with mesotrophic surface water and abundant planktonic foraminifera in deep, intermediate and surface waters. A diverse benthos returns to the sea floor.

7.3.2 Regional effects of the mid-Cretaceous events in the northeast Peri-Tethys

As discussed in Chapter 5 the cause of the events seen at Aksudere in the Crimea is

thought to be due to the expansion and intensification of the OMZ as a result of increased upwelling of cold water from the Boreal realm. This may account for the dominance of hedbergellids in the surface waters at Aksudere, considered by Petrizzo (2002) as indicators of cold or unstable water conditions, thriving in eutrophic surface waters. Without the evidence of reliable oxygen isotope data from surface and bottom waters it is difficult to determine whether a temperature gradients existing in the water column at that time and the influx of cold or warm temperatures cannot be verified in this study. However the presence of a Tethyan fauna (rotaliporids and dicarinellids) indicate a connection to the Tethyan realm, possibly bringing warmer waters into the region. Baraboshkin *et al.* (2003) have described the Cretaceous palaeogeography of the north-eastern Peri-Tethys. They recognise the presence of a longitudinal strait on the Russian Platform, comparable with that of the Western Interior Seaway, regulating the Boreal (cool) and Tethyan (warm) water mass movements. Tectonic rebuilding of the region and rifting in the Caucasus and Crimea (Nikishin *et al.*, 1997) in the Albian-Cenomanian subsequently led to the closing of this longitudinal strait and the opening of a latitudinal sea connecting the northeast Peri-Tethys with other European basins. This would have led to faunal exchange and cool/warm water mixing. Such an event, may have contributed, therefore, to upwelling and influx of Tethyan fauna into the Crimea during the late Cenomanian, as sea transgressed.

Kopaevich and Kuzmicheva (2002) in their study of the CTBE analysed a number of sites in the southwestern Crimea, from southern continental slope (Aksudere) to shallow inner shelf environments (Kyzul-Chygyr). These sites are shown in Figure 5.2. Only the most southern sites show an expression of the OAE, the more shallow water settings are missing part or all of the *Whiteinella archaeocretacea* Zone. This hiatus, seen also at Aksudere at the base of the black shale facies, however, represents a much shorter time period than at the more northern sections. As indicated in Chapter 5 this erosion surface is considered to be correlative with the sub-Plenus erosion surface of the Anglo-Paris Basin and 'Faziewechsel' of northern Germany. This would indicate a widespread regional

regression followed by a transgression during the deposition of the black shale facies. Similar regressive conditions are also seen on the Russian Platform and in the North Caucasus, followed by an uppermost Cenomanian transgressive pulse (Baraboshkin *et al.*, 2003). This correlation with the northern European epicontinental seas further indicates the wide-scale effects of the events surrounding the CTB and the global effects of the causal mechanisms. Kopaevich and Kuzmicheva (2002) believe that the increase in the duration of the hiatus in the northern sections is due to tectonic rebuilding of the region (as discussed above). The mid-Late Cretaceous opening of the Black Sea Basin caused a significant changes in water depth in the region and the development of small fault-bounded blocks on the continental margin on which successions with varying degrees of completeness were deposited. The sediments of the southwestern Crimea, therefore, were deposited on small fault blocks with graben and half graben structures. Kopaevich and Kuzmicheva (2002) concluded that the CTB black shales were deposited only in small, deep depressions in the southern part of the area. As none of the other sections in the area have been investigated in this study it is impossible to verify this suggestion. However, it does appear that the tectonically active environment caused changes in the region related to black shale deposition and subsequent early diagenesis of the sediments as discussed in Chapter 5.

7.4 Global effects of the Cenomanian-Turonian Boundary events in the Tethys, Atlantic and Indian Oceans

As indicated above there are clear links between geographically separate sites and the events surrounding the CTB. Figure 7.2 shows a correlation of the three main sites analysed in this study drawing attention to the interplay between global and local effects of the geochemical and faunal changes.

Eastbourne was chosen for correlative purposes over the proposed Turonian GSSP at Pueblo due to the recent high resolution chemo- and biostratigraphical work that has

been undertaken on this section (Paul *et al.*, 1999; Keller *et al.*, 2001; Tsikos, *et al.*, 2004), and the location of Eastbourne in the north-west margins of the Tethyan Ocean. This provides a picture of the northern, north-eastern and southern parts of the Tethys. Any correlation with Pueblo and the Western Interior Seaway will be given in the text as necessary.

Figure 7.2 shows the $\delta^{13}C$ curve produced from data at each site. Evaluation and comparison of these data is undertaken on the assumption that OAE 2 was a global event creating a perturbation of the global marine carbon reservoir, as a result of enhanced burial of organic matter and the drawdown of light carbon from the ocean waters. Such a global event should, therefore, be reflected in the isotopic composition of the sediments, whether or not they are organic rich. Local effects, due to regional or localised events in the water column and diagenetic, post depositional processes may, however, affect this global signal. In extreme cases such processes may remove the signal completely. For correlation purposes the level of claystone, or carbonate poor, deposition at each location has been highlighted along with the extent of the OAE based on the carbon isotope stratigraphy. As discussed in the Introduction, and Chapters 5 and 6, a stratigraphy based on the geometry of the $\delta^{13}C$ curve has been defined, and used, along with biostratigraphical markers, to compare the carbon isotope curves from different sites (e.g., Gale *et al.*, 1993; Tsikos *et al.*, 2004). Most recently Paul *et al.* (1999) and Tsikos *et al.* (2004) have described the profile of very similar curves from Eastbourne, improving on past curves by their high resolution. This is described in more detail in Chapter 5. This 'typical' profile was used by Tsikos *et al.* (2004) to determine the end of the OAE in order to correlate the start and finish of the event at each site. They define this end point as the final peak of the plateau phase of the curve before $\delta^{13}C$ values begin to decline back to background levels This marks the end of organic carbon burial and the return of light carbon to ocean waters. This definition of the 'end-point' of OAE 2 is utilised in this study, to aid the characterisation of the profiles.

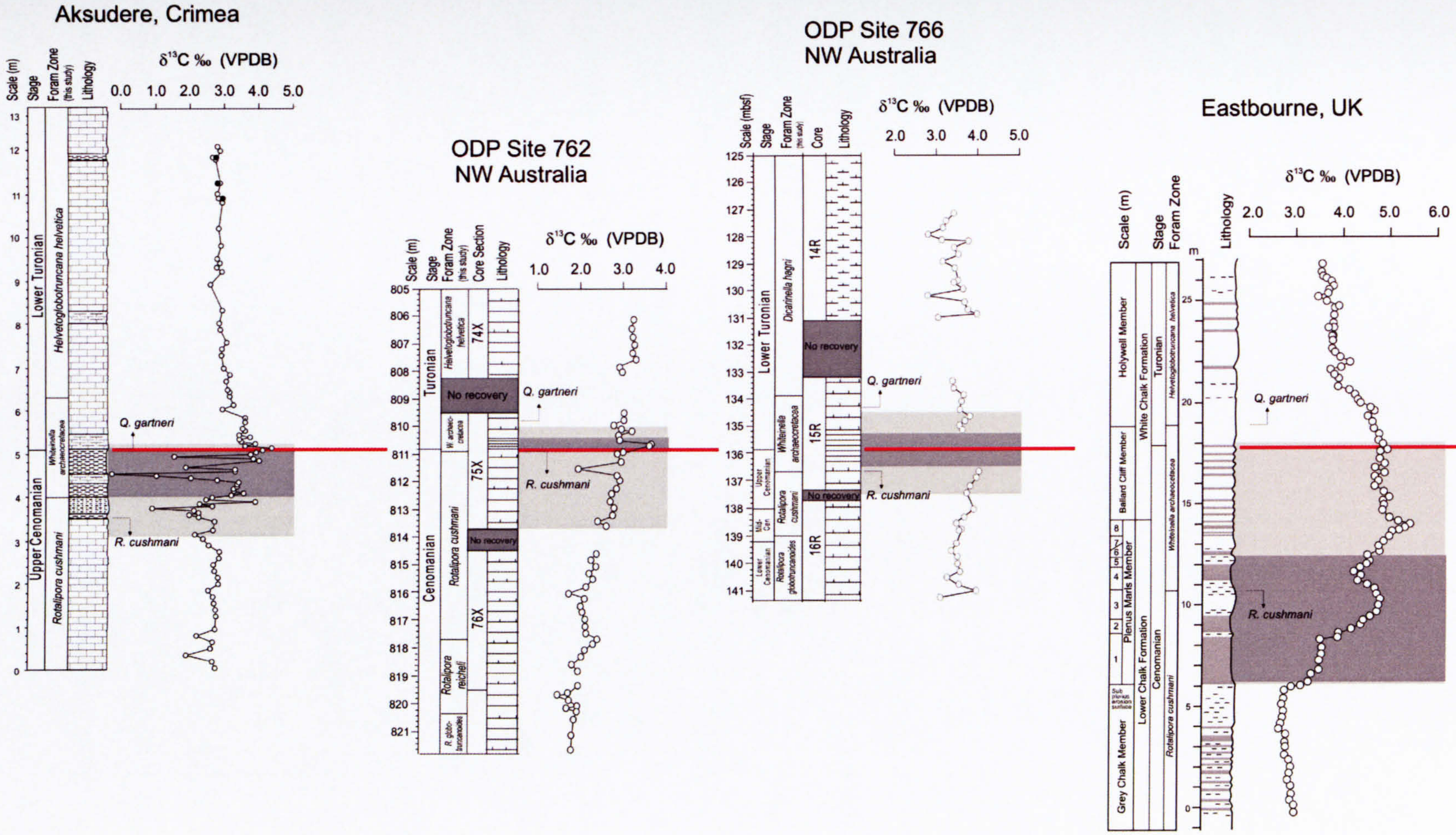

Figure 7.2: Chemo- and biostratigraphical correlation between Cenomanian-Turonian sections at Aksudere (Crimea), ODP Sites 766 and 762 (NW Australia), and Eastbourne (after Tsikos *et al*., 2004). First occurrence of *Quadrum gartneri* in the Crimea from Kopaevich and Kuzmicheva (2002); at ODP Site 766 from Gradstein *et al.* (1990); at Site 762 from Haq *et al.* (1992).Foraminiferal zonation for Eastbourne taken from Keller *et al*. (2001).

Both start and end point are difficult to determine in the ODP cores due to the condensed nature of the CTB sediments, lack of recovery in parts of the core and, at Site 762 due to the diagenetic signal, the possible overwriting of any primary signal at this site.

However, using the duration of the OAE, the deposition of carbonate poor clays and biostratigraphical markers *R. cushmani* and *Q. gartneri*, information on the relative timing of the global isotope curve and the relationship with the localised expression of the OAE at each site can be seen.

All sites show the start of the $\delta^{13}C$ excursion in the upper part of the Cenomanian *R. cushmani* Zone, *Rotalipora* spp. not becoming extinct until after the onset of global sequestration of light carbon at these sites. At the more expanded sites of Eastbourne and the Crimea the end of the OAE can be easily located at the maximum $\delta^{13}C$ value, just before values begin to decrease in the early Turonian. This maximum $\delta^{13}C$ value at both sites lies nearly on the CTB and correlates well with the first occurrence of nannofossil *Quadrum gartneri*. Further discussion on the correlation of these sites is presented in Chapter 5. A marked difference is seen, however, between to two highly correlative sites, related to the position of the carbonate poor sediments within the OAE. Although the $\delta^{13}C$ records a global signal the deposited sediments are a reflection of local changes in the water column. At Eastbourne no organic rich sediments are deposited, as the bottom water conditions at this location never become fully anoxic. Clay rich marly sediments are, however, concentrated in the bottom 4 beds of the Plenus Marls. In contrast, in the Crimea, organic rich clays are deposited, but in the upper part of the OAE event. Although organic rich sediments are deposited at Aksudere, the start of the isotope excursion prior to local deposition of organic rich sediments, indicates further the global nature of the carbon isotope excursion. Tsikos *et al.* (2004) suggest that these sediments are diachronous depending on the local palaeoceanographic settings. The clay rich sediments of the Plenus Marls, relative to those above and below, possibly represent a response to a regional rise in

nutrient levels that favoured the production of organic-walled plankton at the expense of calcareous nannoplankton (Tsikos *et al.*, 2002).

The end point of OAE 2 at both ODP sites, in the absence of such correlative curves as seen at Eastbourne, Pueblo and the Crimea, is placed at points where the values begin to decrease. As mentioned above, missing portions of the core prevent accurate placement of these boundaries. However, with the correlation of the other sites with biostratigraphic markers, particularly *Q. gartneri* marking the end of the OAE at Eastbourne and the Crimea, and additionally at Gubbio (Italy) and Pueblo (USA) (Tsikos *et al.*, 2004), the postulated end of OAE 2 at both site 766 and 762 can be seen to correlate well with the FO of *Q. gartneri.*

Interestingly Site 766 is the only site at which the CTB lies much lower than the FO of *Q. gartneri*. This may be due to the low resolution of nannofossil sampling undertaken at Site 766 by ship-board workers, or the possibility that the CTB based on foraminiferal biostratigraphy needs further resolution to constrain the boundary. As discussed in previous chapters, the FO of *Dicarinella hagni*, is often associated with the CTB, although, in the absence of other zonally important microfossils, the boundary could not be constrained more accurately in this study.

At the sites analysed in this study it is clearly shown that that organic rich sediments, and oxic claystone equivalents, are deposited at each site following the onset of OAE 2. This is not true of Eastbourne, however, where the clay rich sediments are deposited almost coincident with the onset of the $\delta^{13}C$ excursion. At Eastbourne, however *R. cushmani* does not become extinct until the top of the clay rich sediments, equivalent to the 2^{nd} $\delta^{13}C$ peak. Although the sediments suggest oxic conditions existed during the deposition of the Plenus Marls, Jarvis *et al.* (1988) suggest that the bottom waters became highly depleted in oxygen on the basis of foraminiferal evidence. This shows a stepwise extinction of deeper to shallow dwelling foraminifera, consistent with rising anoxic to dysoxic waters in the

water column. This may be due to rising anoxic environments in the adjacent Atlantic Ocean (DSDP Site 551 – Goban Spur, Gustafsson *et al.* 2003), the upper portion of the oxygen minimum zone impinging on the shallow shelf seas at its maximum expansion, coincident with the peak in $\delta^{13}C$ values (Jarvis *et al.*, 1988). A change in productivity as mentioned above may have led to the change to clay sedimentation (Tsikos *et al.*, 2004), coincident with enhanced productivity in parts of the Atlantic Ocean (Goban Spur), enhanced preservation in poorly circulated basins (Kuhnt and Wiedmann, 1995) or euxinic conditions in deep basins (Pancost *et al.*, 2004), leading to the ocean wide anoxia and deposition of organic sediments (Jarvis *et al.*, 1988; Thurow *et al.*, 1992). The presence of widespread organic sediments in the North Atlantic and equivalent sediments in the adjacent epicontinental seas at the start of the $\delta^{13}C$ excursion, leads to the suggestion that the onset of anoxia in the North Atlantic caused the start of the global $\delta^{13}C$ excursion. Deposition of organic rich sediments in the Indian Ocean, Western Interior Seaway and north-east Peri-Tethys occurring later in the OAE, after the onset of the $\delta^{13}C$ positive shift. This may indicate a spread of anoxia through the oceans, originating in the North Atlantic basins (e.g., Cape Verde Basin - de Graciansky *et al.* 1986). The timing of organic deposition is related to the ocean circulation and the local palaeoceanographic setting, as well as the latitudinal position. This may also affect the timing of organic carbon deposition, as cooler high latitude waters increase in temperature later than at the warmer equatorial and tropical low latitudes, the cooler water being less prone to oxygen depletion and delaying the onset of anoxia.

It is clear that a record of OAE 2 is seen in all sections, both with or without organic rich sediments being recorded. OAE2 is constrained by biostratigraphical events that demonstrate that it is a globally synchronous event, through the Late Cenomanian and over the CTB. Site 762, however, exhibits a very diagenetically altered carbon isotope profile, even though the increase in $\delta^{13}C$ values and the CTB peak is coincident with what

would be expected. The correlation of *Q. gartneri* with the end of the OAE proved invaluable at correlating this site with the others in this study. This indicates the importance of utilising chemo- and biostratigraphical markers together, particularly at sites where stable isotope profiles fail to provide conclusive stratigraphic resolution.

Chapter 8: Conclusions

The aim of this research project has been to assess the palaeoceanographical and palaeoenvironmental changes in the mid-Cretaceous, and particularly the Cenomanian-Turonian boundary. The distribution of foraminifera and the stable isotope stratigraphy have been the principal proxies used in this investigation. In order to achieve these aims it was proposed to provide a foraminiferal and geochemical analysis of a series of sites located in both the northern and southern hemispheres, from Tethyan, Boreal and Austral realms. At each of these sites a taxonomic analysis of planktonic and benthonic foraminiferal species was undertaken to provide a biostratigraphical framework (particularly of the previously unzoned Albian to Turonian succession of the eastern Indian Ocean) and to provide a critical analysis of the palaeoenvironmental changes of the mid-Cretaceous and the Cenomanian-Turonian boundary. This study has achieved these aims as set out in Chapter 1.

As discussed throughout this study a number of sites from shallow to deep settings were analysed, and assessed with regards to local, regional and global changes, in order to investigate the events of the mid-Cretaceous. With so much previous study, with regard to this time period, a well formed structure of many of the palaeoceanographical events associated with the mid-Cretaceous have already been defined. However many questions still remain and with different local conditions effecting each location along with the large scale global changes there is much work remaining to be done, particularly at high resolution, such as seen here, in order to analyse the small and large scale events and look at timing and correlation globally.

Each site analysed in this study shows the effects of both global and local palaeoenvironmental change. The stable isotope data record both global perturbations

associated with OAE 1d and OAE 2 and smaller scale regional and local palaeoceanographical changes. Foraminifera aid correlation of the events and help to define the conditions in the water column that are related to the local palaeoceanography. Increased productivity is observed at all sites and this explains the deposition of both the organic-rich sediments and the associated sediments and microfauna (e.g., radiolaraia). This productivity is in turn related to upwelling (e.g., Handoh *et al.,* 1999; Kolonic *et al.,* 2005) of warm saline bottom waters and the increased nutrient runoff from the flooded epicontinental seas and continental margins. But what caused these events? Although productivity has proved to be the key feature in sites on the margins of the Tethys Ocean for the preservation of organic sediments, other sites of organic deposition do not indicate productive surface waters. Enhanced preservation of organic matter in poorly circulated silled basins of the Atlantic, and other regions, also lead to deposition of organic rich shales and expansion of the OMZ to shallow depths (e.g., Tyson, 1995; Kuhnt and Wiedmann, 1995). Additionally, data from shallow water sites in Portugal (eastern margin of the North Atlantic Ocean) and Flaine (shallow part of the Tethyan carbonate platform) indicate that even in these shallow regions where no organic matter is deposited, evidence of the events surrounding the CTB are recorded. This includes dramatic faunal turnover and the widespread calcisphere 'event'. In order to fully determine the cause of all the palaeoceanographic changes at the CTB, it is important that all palaeodepths and environments are examined, not just open shelf and open oceanic sequences that are rich in microfauna and flora.

A global sea level rise related to enhanced tectonic activity would have led to increased productivity in continental margins, and an increase in the production of warm saline bottom water (e.g., Brass *et al.,* 1982; Barron and Peterson 1990). An increase in atmospheric CO_2 (Berner and Kothavala, 2001) may have led to increases in temperature and further warmed the oceans which, linked with low latitude driven circulation of warm

waters, may have caused sluggish low oxygen environments and the preservation of organic matter in other regions. Faunal turnover in sites where no organic deposition is seen may be due low oxygen bottom waters (e.g., Eastbourne) or a highly intensified OMZ higher in the water column (e.g., Indian Ocean Site 766). Shallow environments would become increasingly stressed as deeper areas become more anoxic, which is reflected in the assemblages observed in Portugal and the Alps.

Therefore, although each of the sites examined in this study indicate a global event, most likely a reaction to enhanced sea level and temperatures, coincident with tectonic and igneous activity, the local events need to be fully analysed in order to determine the timing and extent of the events at each site. Foraminifera prove extremely important in precisely constraining and dating events, and enabling a better understanding of conditions in the water column.

Analysis of the data do, however, also indicate a degree of diagenetic alteration. Trace elements and SEM analysis of the foraminifera enable a better understanding of the diagenesis. It is important to look for and understand the nature and timing of the diagenesis in order to fully evaluate the isotopes (e.g., Pearson *et al*, 2001), as demonstrated in this study. The Cenomanian-Turonian section at Aksudere clearly shows a carbon isotope profile reflecting enhanced drawdown of ^{12}C, but also a negative carbon isotope excursion. Negative carbon isotope excursions have been considered to be a result of changes in ocean circulation and chemistry. Recent work, however, has focused on the effect of the introduction of isotopically light carbon into the system from magmatically derived CO_2 and methane (e.g., Jahren *et al.*, 2001; Bralower *et al.*, 1994). Coinciding with the most negative $\delta^{18}O$ values and realtively low values of TOC, the $\delta^{13}C$ values indicate post depositional oxidation of organic matter during localised exposure of the sediments to oxic or meteoric conditions during a lowering of sea level or tectonic uplift.

Data from the Indian Ocean also highlights the necessity to provide a full diagenetic evaluation. Where Site 766 reveals well preserved foraminifera, indicating a predominantly primary environmental signal to be preserved, adjacent Site 762 records foraminifera highly affected by diagenetic alteration. This alteration has been determined as occurring both (early) on the seafloor (cf. Pearson, *et al.*, 2001), and later at depth during burial. The isotopic data from foraminiferal analysis, in particular the oxygen isotopes, do not, therefore, record a primary environmental signal. The use of biostratigraphical markers, are therefore particularly important. The correlation of *Q. gartneri* with the end of the OAE proving invaluable at correlating this site with others in this study and elsewhere. This indicates the importance of utilising chemo- and biostratigraphical markers together, particularly at sites where stable isotope profiles fail to provide conclusive stratigraphic resolution.

Future work

This work has highlighted that although numerous studies have been undertaken on the events surrounding the mid-Cretaceous and Cenomanian-Turonian boundary, many questions remain to be fully evaluated. The necessity for high resolution studies in a range of palaeoenvironmental settings and the full evaluation of diagenetic processes in all sediments analysed, being paramount.

In this study and many others, the global extent of OAE 2 has been demonstrated. A number of other events (e.g., OAE1d Breistroffer Upper Albian; OAE3 Santonian-Campanian) are restricted to certain portions of the globe. For example to date OAE 1d is recorded only recorded fully in SE France, although the isotope signal is recorded in northeast England and areas of the Atlantic, Pacific and Western Interior Seaway. The carbon isotope signal of the eastern Indian Ocean (of this study), however, also records a

profile consistent with this event. Hence a full evaluation of the extent of this event in the Southern Hemisphere is required.

As noted above the need to constrain diagenesis in order to provide, in particular, reliable palaeotemperature estimates, and evidence of carbon cycling, is of great importance. Much recent debate has focused on (early) sea floor diagenesis and the preservation of isotopic signals in pristine "glassy" foraminifera (e.g., Pearson *et al.*, 2001; Wilson *et al.*, 2002). In order to fully determine the extent and impact of sea floor diagenesis on foraminiferal isotope data, further studies are required, particularly, with regards to textural evidence, in order to determine the timing of diagenetic events and the true extent of the pervasive nature of early sea fl

oor diagenesis.

References

Alekseev, A.S., 1989. Upper Cretaceous System. In: Mazarovich, O.A., Mileev, V.S. (Eds.), *Geological structure of the Kacha uplift of Mountainous Crimea. Mesozoic stratigraphy.* Moscow University Press, Moscow, 123-157. [In Russian]

Alekseev, A. S., Vengertsev, V. S., Kopaevich, L. F., Kuzmicheva, T. A., 1997. Lithology and micropaleontology of Cenomanian-Turonian boundary interval in South-Western Crimea. In: Milanovsky, E. E. (eds). *Essays on the geology of the Crimea. Transactions of the A. A. Bogdanov Crimean geological scientific-educational center*, Moscow, MSU, Geological Faculty Publication 1, 54-73. [In Russian]

Allan, J. R., Matthews, R. K., 1982. Isotope signatures associated with early diagenesis. *Sedimentology*, 29, 797-817.

Anderson, T. F., Arthur, M. A., 1983. Stable isotope of oxygen and carbon and their application to application to sedimentologic and palaeoenvironmental problems. In: Arthur, M. A., Anderson, T. F., Kaplan, I. R., Veizer, J., Land, L. S. (eds). *Stable Isotopes in Sedimentary Geology Society of Economic Palaeontologists and Mineralogists Short Course* 10, 1-151.

Arthur, M. A. and Schlanger, S. O. 1979. Cretaceous 'oceanic anoxic events' as a causal factor in development of reef-reservoired giant oil fields. *American Association of Petroleum Geology Bulletin*, 63, 870–885.

Arthur, M.A., Dean, W.E., Pratt, L.M., 1988. Geochemical and climatic effects of increased marine organic carbon burial at the Cenomanian/Turonian boundary. *Nature*, 335, 714–717

Arthur, M. A., Schlanger, S. O. and Jenkyns, H. C., 1987. The Cenomanian-Turonian oceanic anoxic event, II. Palaeoceanographic controls on organic-matter production and preservation. In: Brooks, J. and Fleet, A. J. (eds) *Marine Petroleum source Rocks*, Geological Society Special Publication, 26,401-420.

Arthur, M. A., Dean, W. E., and Pratt, L. M., 1988. Geochemical and climatic effects of increased marine organic carbon burial at the Cenomanian/Turonian boundary. *Nature*, 335, 714-717.

Ball, D. F., 1964. Loss-on-ignition as an estimate of organic matter and organic carbon in non-calcareous soils. *Journal of Soil Science,* 15: 84–92.

Baraboshkin, E. Y., Alekseev, A. S. and Kopaevich, L. F., 2003. Cretaceous palaeogeography of the North-Eastern Peri-Tethys. *Palaeogeography, Palaeoclimatology, Palaeoecology*. 196, 177-208.

Barron, E. J. 1983. A warm equable Cretaceous: The nature of the problem. *Earth Science Reviews*, 19, 305-338.

Barron, E. J. and Peterson, W.H. 1990 Mid-Cretaceous ocean circulation: Results from model sensitivity studies. *Paleoceanography* 5, 319-337.

Barron, E.J., Fawcett, P.J., Peterson, W.H., Pollard, D., Thompson, S., 1995. A 'simulation' of mid-Cretaceous climate. *Paleoceanography* 10, 953-962.

Bartenstein, H., 1954. Revision von Berthelins Mémoire 1880 über die Alb. Foraminiferen von Montcley. *Senckenbergiana lethaea*, 35, 37-50.

Bartenstein, H. 1979 Worldwide zonation of the Lower Cretaceous using benthonic foraminifera. *Newsletters on Stratigraphy*, 7, 142-154.

Bartenstein, H. and Brand, E., 1951. Mikropaläontologie Untersuchungen zur Stratigraphie des nordwestdeutschen Valendis. *Abhandlungen der Senckenbergischen Naturforschenden Gesellschaft*, 458, 239-336.

Bartenstein, H. and Bolli, H. M., 1986. The foraminifera in the Lower Cretaceous of Trinidad, W.I part 5: Maridale Formation, upper part; *Hedbergella rohri* zone. *Eclogae Geologicae Helvetiae*, 7, 945-999.

Basov, I. A. and Krasheninnikov, V. A., 1983. Benthic Foraminiers in Mesozoic and Cenozoic sediments of the southwestern Atlantic as an indicator of palaeoenvironment, Deep Sea Drilling Project Leg 71

Beerling, D. J., Lomas, M. R. and Gröcke, D. R., 2002. On the nature of methane gas-hydrate dissociation during the Toarcian and Aptian oceanic anoxic events. *American Journal of Science*, 302, 28-49.

Bengtsson, L. and M. Enell, 1986. Chemical analysis. In Berglund, B. E. (ed.), Handbook of Holocene Palaeoecology and Palaeohydrology. John Wiley & Sons, Chichester, 423–451.

Berger, W. H. and Vincent, E., 1986. Deep-sea carbonates: reading the carbon-isotope signal. *Geologische Rundschau*, 75 (1), 249-269.

Bernard, J. M., 1993. Experimental and field evidence of Antarctic foraminiferal tolerance to anoxia and hydrogen sulphide. *Marine Micropalaeontology*, 20, 203-213.

Berner, R.A. and Kothavala, Z., 2001. GEOCARB III: A revised model of atmospheric CO2 over Phanerozoic time. *American Journal of Science.* 301, 182-204.

Berthelin, G., 1880. Mémoire sur les foraminifères fossils de l'Etage Albien de Moncley (Doubs). *Soc. Geol. France, Mem.,* ser. 3, 1, 1-84.

Bettenstaedt, F., 1952. Stratigraphisch wichtige Foraminiferen-Arten aus dem Barrême vorwiegend Nordwest-Deutschlands. *Senckenbergiana, Francfort-sur-le-Main*, 33, 263-295.

Bolli, H. M., Loeblich, A. R., Jr. and Tappan, H., 1957. Studies in Foraminifera: lanktonic foraminiferal families Hantkeninidae, orbulinidae, Globorotaliidae and Globotruncanidae. *Bull. U.S. National Mus.*, 215, 3-50.

Bornemann, A., Pross, J., Reichelt, K., Herrle, J. O., Hemleben, C. and Mutterlose, J., 2005. Reconstruction of short-term palaeoceanographic changes during the formation if the Late Albian 'Niveau Breistroffer' black shales (Oceanic Anoxic Event 1d, SE France). *Journal of the Geoloical Sciety, London*, 162, 623-639.

Brady, E. C., DeConto, R. M. and Thompson, S. L. 1998 Deep water formation and poleward ocean heat transport in the warm climate extreme of the Cretaceous (80 Ma), *Geophysical Research Letters*, 25, 4205– 4208,.

Bragina, L. G., 2004. Cenomanian-Turonian radiolarians of northern Turkey and the Crimean mountains. *Paleontological Journal*, 38, Suppl. 4, S325-S456.

Brand, U. and Veizer, J., 1980. Chemical diagenesis of a multicomponent carbonate system-1:Trace elements. *Journal of Sedimentary Petrology*, 50, 1219-1236.

Bralower, T. J., and Siesser, W. G., 1992, Cretaceous calcareous nannofossil stratigraphy of sediments recovered on ODP Leg 122, Exmouth Plateau, N.W. Australia. *in* von Rad, U., Haq, B. U., et al., eds., *Initial Reports of the Ocean Drilling Program, Scientific Results*, v. 122, p. 529-556.

Bralower, T. J., Arthur, M. A., Leckie, R. M., Sliter, W. V., Allard, D. J. and Schlanger, S. O., 1994. Timing and paleoceanography of oceanic dtsoxia/anoxia in the Late Barremian to Early Aptian (Early Cretaceous). *Palios*, 9, 335-369.

Bralower, T. J., Fullagar, P. D., Paull, C. K., Dwyer, G. S. and Leckie, R. M., 1997. Mid-Cretaceous strontium-isotope stratigraphy of deep sea sections. *Geological Society of America Bulletin*, 109, 1421-1442.

Bralower, T. J., Kelly, D. C. and Leckie, R. M., 2002 Biotic effects of abrupt Paleocene and Cretaceous climate events. *Joides Journal,* 1-6.

Bralower, T.J., Premoli Silva, I., and Malone, M., 2002, *Proceedings of the Ocean Drilling Program, Initial reports,* Volume 198: College Station, Texas, Ocean Drilling Program.

Brasier, M. D. 1980. *Microfossils*. Allen and Unwin, London. 193 pp.

Brass, G. W., Southam, J. R. and Peterson, W. H. 1982. Warm saline bottom water in the ancient ocean. *Nature*, 296, 620-623.

Bréhéret, J. –G., 1994. The Mid-Cretaceous organic-rich sediments from the Vocontian Zone of the French Southeast Basin. In: Mascle, A (ed.) *Hydrocarbon and Petroleum Geology of France*. Special Publication of the European Association of Petroleum Geoscientists, 4, 295-320.

Brotzen, F., 1942. Die Foraminiferengattung *Gavelinella* nov. gen. und die Systematik der Rotaliiformes: *Årsbok Sveriges Grologiska Undersökning,* 36, 1-60.

Brotzen, F., 1945. De geologiska resultaten från borrningara vid Höllviken; Preliminär rapport-Del I: Kritan: *Årsbok Sveriges Grologiska Undersökning*, 38, 1-64.

Brumsack, H., 1986. Trace metal accumulation in black shales from the Cenomanian/Turonian boundary event. In: Walliser, O. (eds.) *Global Bio-Events*, Lecture Notes in Earth Sciences, 8, 337-343.

Buonocunto, F. P., Sprovieri, M., Bellanca, A, D'Argenio, B., Ferreri, V., Neri, R., Ferruzza, G., 2002. Cyclostratigraphy and high-frequency carbon isotope fluctuations in Upper Cretaceous shallow-water carbonates, southern Italy. *Sedimentology*. 49, 1321-1337.

Calvert, S. E. and Pedersen, T. F., 1987 Organic carbon accumulation and preservation in marine sediments: how important is anoxia? In: Whelan, J. K. and Farrington, J. W. *Productivity, Accumulation and Preservation of Organic Matter in recent and Ancient Sediments.* Columbia University Press, New York. 231-263.

Carbonnier, A., 1952. Sur un giesment de foraminifères d'âge Cénomanien supérieur de la region de Taza (Maroc). *Bulletin de la Société Géologique de France*, 2, 111-122.

Caron, M., 1985. Cretaceous planktic foraminifera. In: Bolli, H. M., Saunders, J. B. and Perch-Nielsen, K. (Eds.), *Plankton Stratigraphy*, Cambridge University Press, 17-86.

Caron, M. and Homewood, P., 1982. Evolution of early planktonic foraminiferas. *Marine Micropaleontology* 7, 453-62.

Caron, M., Robaszynski, F. and Amedro F. et al. 1999 Estimation de la duree de l'evenement anoxique global au passage Cenomanian/Turonien: approche cyclostratigraphique dans la formation Bahloul en Tunisie central. *Bulletin de la Societi Geologique de France*, 170, 513-527.

Caron, M., Dall'Agnolo, S., Accarie, H., Barrera, E., Kaufman, E. G., Amédro, F. and Robaszynski, F., 2006. High-resolution stratigraphy of the Cenomanian–Turonian boundary interval at Pueblo (USA) and wadi Bahloul (Tunisia): stable isotope and bio-events correlation. *Geobios*, 39, 171-200.

Callapez, P. M., 1998. *Estratigrafia e Paleobiologia do Cenomaniano-Turoniano O significado do eixo da Nazaré-Leiria-Pombal.* Unpublished PhD Thesis, University of Coimbra, 1-479.

Callapez, P. M., 1999. The Cenomanian-Turonian of the western Portuguese Basin: Stratigraphy and Paleobiology of the Central and Northern Sectors. *European Palaeontological Workshop, Field Guide B, July 25th, 1999.*

Carsey, D. O., 1926. Foraminifera of the Cretaceous of Central Texas. *Univ. of Texas Bureau of Econ. Geol and Tech. Bull.*, 2612, 1-56.

Carter, D. J. and Hart, M. B., 1977. Aspects of mid-Cretaceous stratigraphical micropalaeontology. *Bulletin of the British Museum (Natural History), Geology series*, 29, 1-135.

Caus, E., Teixell, A and Bernaus, J.M., 1997. Depostional model of a Cenomanian-Turonian extensional basin (Sopeira Basin, NE Spain): interplay between tectonics, eustacy and biological productivity. *Palaeogeograhy, Palaeoclimatology, Palaeoecology,* 129, 23-36.

Chapman, F. 1891-1898. The Foraminifera of the Gault of Folkestone. *Journal of the Royal Microscopical Society*, London.

Chen, D., Tucker, M. E., Shen, Y., Yans, J. and Preat, A., 2002. Carbon isotope excursions and sea-level change: implications for the Frasnian-Famennian biotic crisis. *Journal of the Geological Society*, 159, 623-626.

Clarke, L. J. and Jenkyns, H. C., 1999. New oxygen isotope evidence for long-term Cretaceous climatic change in the southern Hemisphere. *Geology*, 27 (8), 699-702.

Coccioni, R. and Galeotti, S., 2003. The mid-Cenomanian event: prelude to OAE 2. *Palaeogeography, Palaeoclimatology, Palaeoecology*, 190, 427-440.

Coccioni, R. and Luciani, V., 2004. Planktonic foraminifera and environmental changes across the Bonarelli event (OAE2, latest Cenomanian) in its type area: a high resolution study from the Tethyan reference Bottaccione section (Gubbio, central Italy). *Journal of Foraminiferal Research,* 34 (2), 109-129.

Corfield, R. M., Hall, M. A. and Brasier, M. D., 1990. Stable isotope evidence forforaminiferal habitats during the development of the Cenomanian/Turonian oceanic anoxic event. *Geology*, 18, 175-178.

Corliss, B. H., 1985. Micro-habitats of benthic foraminifera within deep sea sediments. *Nature*, 314, 435-438.

Courtillot, V. 1992. Mass extinction in the last 300 million years: One impact and seven flood basalts? *Israel Journal of Science,* 43, 255-266.

Cushman, J. A., 1926. The foraminifea of the Velasco shale of the Tampico embayment. *Bull. Am. Assoc. Petroleum Geologists*, 10, 581-612.

Cushman, J. A., 1936. New Genera and species of the families Verneuilinidae and Valvulinidae and of the subfamily Virgulininae. *Special Publication from the Cushman Laboratory of Foraminiferal Research,* 6, 1-71.

Cushman, J. A., 1938. Additional new species of American Cretaceous foraminifera. *Contributions from the Cushman Laboratory of Foraminiferal Research*, 14, 31-52.

Cushman, J. A., 1946. Upper Cretaceous Foraminifera of the Gulf Castal region of the United States and adjacent areas. *U.S. Geological Survey Prof. Paper*, 206, 1-241.

Cushman, J. A. and Wickenden, R. T. D., 1928. A new foraminiferal genus from the Upper Cretaceous. *Contributions from the Cushman Laboratory of Foraminiferal Research*, 4, 12-13.

Cushman, J. A. and Parker, F. L., 1936. Some American Eocene buliminas. *Contributions from the Cushman Laboratory of Foraminiferal Research*, 12, 39-45.

Dam, A. ten, 1947. On foraminifera of the Netherlands No. 9. Sur quellques espèces nouvelles ou peu connues dans le Crétacé Inférieur (Albien) des Payes-Bas. *Geologie Mijnb.*, The Hague, 8, 25-29.

Dam, A. ten, 1950. Les Foraminifères de l'Albien des Pays-Bas. *Mém. Soc. Géol. Fr.*, Paris, 29, 1-66.

Dean, W. E. Jr., 1974. Determination of carbonate and organic matter in calcareous sediments and sedimentary rocks by loss on ignition: Comparison with other methods. *Journal of Sedimentary Petrology*, 44, 242–248.

DeBoer, P. L., 1986. Changes in organic carbon burial during the Early Cretaceous. In: Summerhayes, C. P. and Shackleton, N. J. (eds.). *North Atlantic Palaeoceanography*. Geological Society, London Special Publication, 21, 321-331.

Dodsworth, P., 2004. The palynology of the Cenomanian-Turonian (Cretaceous) boundary succession of Aksudere in Crimea, Ukraine. *Palynology*. 28, 129-141.

Douglas, R. G. and Rankin, C., 1969. Cretaceous planktonic foraminifera from Bornholm and their zoogeographic significance. *Lethaia*, 2, 185-217.

Dryden,A. L. 1931. Accuracy in percentage representation of heavy mineral frequency. *Proceedings of the National Academy of Science*, 17, 233-238.

Duxbury, A.C. and Duxbury. A.B 2005 *An introduction to the world's oceans.* 8th edition. Boston, McGraw-Hill Higher Education. 514 p.

Egger, J. G. 1899. Foraminiferen und ostrakoden aus den Kreidemergeln der oberbayerischen alpen, *Abh. Bayer. Akad. Wiss. Munchen, Math.-Naturw/ Kl.*, 21, 1-230.

Ehrenberg, C. G., 1843. Verbreitung und Einfuss mikroskoposchen Lebens in Sud- und Nord-amerika. *Abhandlungen der Koniglichen akademie der Wissenschaftan zu Berlin, Physik*, 291-446.

Eicher, D. L., 1965. Foraminifera and biostratigraphy of the Graneros Shale. *Journal of Paleontology*, 39, 875-909.

Eicher, D. L. and Worstell, P., 1970. Cenomanian and Turonian Foraminifera from the Great Plains, United States. *Micropaleontology*, 16, 269-324.

Erba, E. 1994. Nannofossil and superplumes: The early Aptian "nannoconid crisis". *Paleoceanography* 9, 483-501.

Erba, E., 2004. Calcareous nannofossils and Mesozoic oceanic anoxic events. *Marine Micropaleontology*, 52, 85-106.

Erbacher, J., Hemleben, C., Huber, B. T. and Markey, M., 1999. Correlating environmental changes during early Albian oceanic anoxic event 1B using benthic foraminiferal paleoecology. *Marine Micropaleontology*, 38, 7-28.

Erbacher, J., Huber, B. T., Norris, R. D. and Markey, M., 2001. Increased thermohaline stratification as a possible cause for an ocean anoxic event in the Cretaceous period. *Nature*, 409, 325-327.

Espitalie, J., Laporte, J.L., Madec, M., Marquis, F., Leplat, P., Paulet, J. and Boutefeu A.1977, Methode rapide de caracterisation des roches meres de leur potentiel petrolier et de leur degre d'evolution: *Revue de l'Institute Francais du Petrole,* 32, 23-42.

Exon, N. F. and R. T. Buffler, Mesozoic seismic stratigraphy and tectonic evolution of the western Exmouth Plateau, *Proceedings of Ocean Drilling Prog., Sci. Results,* 122, 61-82, 1992

Fairbanks, R.G., Wiebe, P.H. and Be, A.W.H. 1980 Vertical distribution and isotope composition of living planktonic foraminifera in the western North Atlantic. *Science* 207, 61-63.

Fasssell, M. L. and Bralower, T.L., 1999. Warm, equable mid-Cretaceous: Stable isotope evidence. In: Barrera, E and Johnson, C. C. (eds.) *Evolution of the Cretaceous Ocean-Climate System*, Boulder, Colorado, Geological Society of America Special Paper, 332, 121-142.

Fox, S. K., Jr., 1954. Cretaceous foraminifera from the Greenhorn, Carlile and Cody Formations, South Dakota, Wyoming. *U.S. Geol. Surv. Prof. Paper*, 254-E, 97-124.

Frakes, L.A., Francis, J.E., Syktus, J.I., 1992. *Climate Modes of the Phanerozoic.* Cambridge University Press, Cambridge 274p.

Franke, A., 1928. Die foraminiferen der Oberen Kreide Nord- und Mitteldeutschlands. *Abhandlungen der Preussischen Geologischen Landesanstalt, Neue Folge*, 11, 1-207.

Fullerton, L. G., Sager, W. W. and Handschumacher, D. W. 1989. Late Jurassic – Early Cretaceous Evolution of the Eastern Indian Ocean adjacent to northwest Australia. *Journal of Geophysical Research,* 94, 2937 – 2953.

Gabdullin, R., Guzhikov, A., Dundin, I., 1999. Origin of rhythmically bedded Cenomanian carbonate rocks of the Bakhchisarai region (SW Crimea). Geologica Carpathica. 50, 49-61.

Gale, A. S., 1989. A milankovitch scale for Cenomanian time. *Terra Nova,* 1, 420-425.

Gale, A. S., 2000. The Cretaceous world. In: Culver, S. J. and Rawson, P. F. (eds.) *Biotic Response to Global Change*, Cambridge University Press, 4-19.

Gale, A. S., Jenkyns, H. C., Kennedy, W. J. and Corfield, R. M., 1993. Chemostratigraphy verses biostratigraphy: data from around the Cenomanian-Turonian boundary. *Journal of the Geological Society, London*, 150, 29-32.

Gale, A. S., Hancock, J. M., Kennedy, W. J., 1999. Biostratigraphical and sequence correlation of the Cenomanian successions in Mangyshlak (W. Kazakhstan) and Crimea (Ukraine) with those in southern England. *Bulletin de l'Institut Royal des Sciences Naturelles de Belgique Sciences de la Terre.* 69, Supp. A, 67-86.

Gale, A. S., Smith, A. B., Monks, N. E. A., Yung, J. A., Howard, A., Wray, D. S. and Huggett, J. M., 2000. Marine biodiversity through the Late Cenomanian-Early Turonian: palaeoceanographic controls and sequence stratigraphic biases. *Jounral of the Geological Society, London*, 157, 745-757.

Gale, A.S., Kennedy, W.J., Voigt, S. and Walaszczyk, I. 2005. Stratigraphy of the Upper Cenomanian–Lower Turonian Chalk succession at Eastbourne, Sussex, UK: ammonites, inoceramid bivalves and stable carbon isotopes. *Cretaceous Research*, 26, 480–487

Gandolfi, R., 1942. Ricerche micropaleontologiche e stratigrafiche sulla Scaglia e sul flysch cretacici dei Dintorni di Balerna (Canton Ticino). *Riv. Ital. Paleont.*, 48, 1-160.

Gawor-Biedowa, E., 1972. The Albian, Cenomanian and Turonian forminifers of Poland and their stratigraphic importance. *Acta Palaeontologica Polonica,* 17, 1-151.

Giraud, F., Olivero, D., Baudin, F., Reboulet, S., pittet, . and Proux, O. 2003. minor changes in surface water fertility across the oceanic anoxic event 1d (latest Albian, SE France) evidenced by calcareous nannofossils. *International Journal of Earth Sciences*, 92, 267-284.

Grabert, B., 1959. Phylogenetische Untersuchungen an *Gaudryina* und *Spiroplectinata* (foram.) besonders aus dem nordwestdeutschen Apt. und Alb. *Abh. Senckenb. Naturforsch. Ges.*, Frankfurt am Maim, 498, 1-71.

Gradstein, F. M. 1992. Legs 122 and 123, Northwestern Australian margin—a stratigraphic paleogeographic summary. P*roceedings of the Ocean Drilling Program Scientific Results*, 123, 801 – 816.

Gradstein, F. M., Ludden, J. N., *et al.*, 1990. Proceedings of the Ocean Drilling Program Initial Reports, 123: College Station, TX (Ocean Drilling Program).

Gradstein, F.M., Agterberg, F.P., Ogg, J.G., Hardenbol, J., Van Veen, P., Thierry, J., and Huang Zehui, 1995, A Triassic, Jurassic and Cretaceous time scale, in Berggren, W.A., Kent, D.V., Aubrey, M.-P., and Hardenbol, J., eds., Geochronology, Time Scales and Global Stratigraphic Correlation: *SEPM (Society for Sedimentary Geology) Special Publication* No. 54, p. 95-126.

Gradstein, F. Ogg, J. and Smith A. 2004. *A Geologic Time Scale. Cambridge*, 589 p.

Graves, R. W. and Ellison, S., 1941. Conodonts of the Marathon Basin, Texas. *Missouri Univerisity, School of Mines and Metallurgy, Bulletin Technical Series*, 14, 1-26.

Grocke, D. R., Hesselbo, S. P. and Jenkyns, H. C., 1999. Carbon-isotope composition of the Lower Cretaceous fossil wood: Ocean-atmosphere chemistry and relation to sea level. *Geology*, 27, 155-158.

Grzybowski, J., 1896. Otwornice czerwonych iow z Wadowic. *Akademia Umiejetnosci w Krakowie, Rozprawy Wydzial Matematyczno-Przyrodniczy*, serya 2, 10, 261-308.

Gustafsson, M., Holbourn, A. and Kuhnt, W. 2003, Changes in Northeast Atlantic temperature and carbon flux during the Cenomanian/Turonian palaeoceanographic event: the Goban Spur stable isotope record. *Palaeogeography, Palaeoclimatology, Palaeoecology*, 201, 51-66.

Haig, D.W., 1992. Aptian-Albian foraminifers from Site 766, Cuvier Abyssal Plain, and comparison with coeval faunas from the Australian region. In Gradstein, F.M., Ludden,

J.N., et al., *Proceedings of ODP, Scientific Results*, 123: College Station, TX (Ocean Drilling Program), 271-297.

Haig, D. W., Watkins, D. K. and Ellis, G., 1996. Mid-Cretaceous calcareous and siliceous microfossils from the basal Gearle Siltstone, Giralia Anticline, southern Canarvon Basin. *Alcheringa*, 20, 41-68.

Haig, D. W., 2005. Foraminiferal evidence for inner neritic deposition of Lower Cretaceous (Upper Aptian) radiolarian-rich black shales on the Western Australian margin. *Journal of Micropalaeontology*, 24, 55-75.

Hallam, A., 1992. Phanerozoic sea-level changes. Columbia University Press, New York. 266 pp.

Hallam, A. and Wignall, P. B., 1997 Mass Extinctions and their Aftermath. Oxford University Press

Hallam, A. and Wignall, P. B., 1999. Mass extinctions and sea level changes. *Earth Science Reviews*, 48, 217-250.

Handoh, I. C., Bigg, G. R. Jones, E. J. W. and Inoue M. 1999 An ocean modeling study of the Cenomanian Atlantic: equatorial paleo-upwelling, organic-rich sediments and the consequences for a connection between the proto-North and South Atlantic, *Geophysical Research Letters*, 26, 223–226.

Hancock, J. M., 1989. Sea-level changes in the British region during the Late Cretaceous. *Proceedings of the Geologists' Associations*, 100, 565-594.

Hancock, J. M. and Kaufmann E. G., 1979. The great ransgressions of the Late Cretaceous. *Journal of the Geological Society, London*, 136, 175-186.

Handoh, I. C. and Lenton, T. M., 2003. Periodic mid-Cretaceous oceanic anoxic events inked by oscillations of the phosphorus and oxygen biogeochemical cycles. *Global Biogeochenical Cycles*, 17, 3/1-11.

Haq, B. U., Hardenbol, J., Vail, P.R., 1987. Chronology of the fluctuating sea-level since the Triassic. *Science*. 235, 1156-1167.

Haq, B. U., Von Rad, U., O'Connel, S., *et al.*, 1990. Proceeedings of the Ocean Drilling Program Initial Reports, 122: College Station, TX (Ocean Drilling Program).

Haq, B.U., Boyd, R.L., Exon, N.F. and Von Rad, U. 1992. Evolution of the central Exmouth Plateau: a post-drilling perspective. In: Dearmont, L.H. and Mazzullo, E.K. (eds) *Proceedings of the Ocean Drilling Program, Scientific Results*, 122. Ocean Drilling Program, College Station, TX, 801-816.

Hardenbol, J., Thierry, J., Farley, M.B., Jacquin, T., Graciansky, P-C. de, and Vail, P.R., 1998, Mesozoic and Cenozoic sequence chronostratigraphic framework of European Basins. in Graciansky, P-C. de, Hardenbol, J., Jacquin, T., and Vail, P.R. (eds.), *Mesozoic and Cenozoic sequence stratigraphy of European Basins: SEPM Special Publication* 60, p. 3-13.

Harries, P. J., 1993. Dynamics of survival following the Cenomanian-Turonian (Upper Cretaceous) mass extinction event. *Cretaceous Research*, 14, 563-583.

Hart, M. B., 1991. The Late Cenomanian calcisphere global bioevent. *Annual Proceedings of the Ussher Society, January 1991.* 7, 413-417.

Hart, M.B., 1996. Recovery of the food chain after the Late Cenomanian extinction event. In: Hart, M. B. (ed.), *Biotic recovery from Mass Extinction Events*, Geological Society Special Publication, 102, 265-277.

Hart, M. B., 1999. The evolution and biodiversity of Cretaceous planktonic foraminiferida. *Geobios*, 32, 247-255.

Hart, M.B., and Bailey, H.W. 1979. The distribution of planktonic Foraminiferida in the Mid-Cretaceous of NW Europe. In: *Aspekte der Kreide Europas* (eds J. Wiedmann) 6, 527-42 International Union of Geological Sciences, Series A.

Hart, M. B., Bigg, P. J. 1981. Anoxic events in the Late Cretaceous chalk seas of northwest Europe. In: Neale, J. W. and Braisier, M. B. (eds). Microfossils from Recent and Fossil shelf seas. British Micropalaeontological Society, London. Ellis Horwood. 177-185.

Hart, M. B. and Leary, P. N., 1991. Stepwise extinctions: the case for the Late Cenomanian event. *Terra Nova*, 3, 142-147.

Hart, M. B., Bailey, H. W., Crittenden, S., Fletcher, B. N., Price, R. J. and Swiecicki, A., 1989. Cretaceous. In: Jenkins, D. G. and Murray, J. W. (eds.), *Stratigraphic Atlas of Fossil Foraminifera*, Ellis Harwood Limited, 273-371.

Hart, M. B., Dodsworth, P. and Duane, A. M., 1993. The late Cenomanian Event in eastern England. *Cretaceous Research*, 14, 495-508.

Hart, M. B., Monteiro, J. F., Watkinson, M. P. and Price, G. D., 2002. Correlation of events at the Cenomanian/Turonian boundary: evidence from Southern England and Colorado. In: Wagreich, M. (ed.), *Aspects of Cretaceous Stratigraphy and Palaeobiogeography.* Österreichische Akademie der Wissenschaften Schriftenreihe der Erdwissenschaftlichen Kommissionen, 15, 35-46.

Hasegawa, T., 1997. Cenomanian-Turonian carbon isotope events recorded in terrestrial organic matter from northern Japan. *Palaeogeography, Palaeoclimatology, Palaeoecology*, 130, 251-273.

Hasegawa T, Pratt L.M, Maeda H., Shigeta Y, Okamoto T, Kase T. and Uemura K. 2003 Upper Cretaceous stable carbon isotope stratigraphy of terrestrial organic matter from Sakhalin, Russian Far East: a proxy for the isotopic composition of paleoatmospheric CO_2 *Palaeogeography Palaeoclimatology Palaeoecology* 189, 97-115

Haupt, B. J. and Seidov, D., 2001. Warm deep-water ocean conveyer during Cretaceous time. *Geology*, 29 (4), 295-298.

Hay W.W 1995 Cretaceous paleoceanography Geologica Carpathica 46 (5): 257-266.

Hemleben, C., Spindler, M. and Anderson, O. R., 1989. Modern Planktonic Foraminifera: Springer-Verlag, Berlin, 363 pp.

Hesselbo, S. P., Gröcke, D. R., Jenkyns, H. C., Bjerrum, C. J., Farrimond, P., Morgans Bell, H. S., Gren, O. R., 2000. Massive dissociation of gas hydrate during a Jurassic oceanic anoxic event. Nature. 406, 392-395.

Holbourn, A. E. L. and Kaminski M. A., 1995. Lower Cretaceous benthic foraminifera from DSDP Site 263: Micropalaeontological constraints for the early evolution of the Indian Ocean. *Marine Micropaleontology*, 26, 425-460.

Holbourn, A. E. L. and Kaminski, M. A. 1997. Cretaceous deep-water benthic foraminifera of the Indian Ocean. *Grzybowski Foundation Special Publication*, 4: 1-175.

Holboun, A. E. L. and Kuhnt, W., 1998. Turonian–Santonian benthic foraminifer assemblages from Site 959d (Côte D'ivoire-Ghana Transform Margin, Equatorial Atlantic): Indication of a Late Cretaceous oxygen minimum zone. In: Mascle, J., Lohmann, G. P. and Moullade, M. (Eds.) *Proceedings of the Ocean Drilling Program, Scientific Results,* 159, 375-387.

Holbourn, A. and Kuhnt, W., 2002. Cenomanian-Turonian palaeoceanographic change on the Kerguelen Plateau: a comparison with Northern Hemisphere records. *Cretaceous Research*, 23, 333-349.

Howe, R. W., Haig, D. W. and Apthorpe, M. C., 2000. Cenomanian-Coniacian transition from siliciclastic to carbonate marine deposition, Giralia Anticline, Southern Canarvon Platform, Western Australia. *Cretaceous Research*, 21, 517-551.

Huber, B. T., Hodell, D. A. and Hamilton, C. P., 1995. Middle-Late Cretaceous climate of the southern high latitudes: stable isotopic evidence for minimal equator-to-pole thermal gradients. *GSA Bulletin*, 107 (10), 1164-1191.

Huber, B.T., 1998. Perspectives - paleoclimate - tropical paradise at the Cretaceous poles? Science 282, 2199-2200.

Huber, B. T., Leckie, R. M., Norris, R. D., Bralower, T. J. and CoBane, E., 1999. Foraminiferal assemblage and stable isotopic change across the Cenomanian-Turonian boundary in the subtropical north Atlantic. *Journal of Foraminiferal Research*, 29 (4), 392-417.

Huber, B. T., Norris, R. D. and MacLeod, K. G., 2002. Deep-sea palaeotemperature record of extreme warmth during the Cretaceous. *Geology*, 30, 123-126.

Hunt, J. M. 1979. *Petroleum Geochemisty and Geology*: San Francisco, W. H. Freeman.

Hut, P., Alvarez, W., Elder, W. P., Hansen, T. A., Kaufmann, E. G., Shoemaker, E. M. and Weisman, P. R. 1987. Comet showers as causes of mass extinctions. *Nature*, 329, 118-126.

Jahren, A. H., Arens, N. C., Sarmiento, G., Guerrero, J., Amundson, R., 2001. Terrestrial record of methane hydrate dissociation in the Early Cretaceous. Geology. 29, 159-162.

Jahren, A. H., Arens, N. C., Sarmiento, G., Guerrero, J. and Amundson, R., 2001. Terrestrial records of methane dissociation in the Early Cretaceous. *Geological Society of America*, 29 (2), 159-162.

Jarvis, I., Carson, G. A., Cooper, M. K. E., Hart, M. B., Leary, P. N., Tocher, B. A., Horne, D. Rosenfeld, A., 1988. Microfossil assemblages and the Cenomanian-Turonian (late Cretaceous) oceanic anoxic event. Cretaceous Research. 9, 3-103.

Jeans, C. V., Long, D., Hall, M. A., Bland, D. J. and Cornford, C., 1991. The geochemistry of the Plenus Marls at Dover, England: evidence of fluctuating oceanographic conditions and of glacial control during the development of the Cenomanian-Turonian $\delta^{13}C$ anomaly. *Geological Magazine,* 128, 603-632.

Jeffries, R. P. S., 1963. The stratigraphy of the *Actinocamax plenus* subzone (Turonian) in the Anglo-Paris basin. Proceedings of the Geologists' Association. 74, 1-33.

Jenkyns, H. C., 1980. Cretaceous anoxic events from continents to oceans. Journal of the Geological Society, London. 137, 171-188.

Jenkyns, H. C., Gale. A. S. and Corfield, R. M., 1994. Carbon- and oxygen-isotope stratigraphy of the Italian Scaglia and its palaeoclimatic significance. *Geological Magazine*, 131 (1), 1-34.

Jenkyns, H. C. and Wilson, P. A., 1999. Stratigraphic paleoceanography, and evolution of Cretaceous Pacific guyots: relics from a greenhouse Earth. *American Journal of Science*, 299, 341-392.

Jones, R.W., 1986. Distribution of morphogroups of Recent agglutinating foraminifera in the Rockall Trough – a synopsis. *Proceedings of the Royal society of Edinburgh*, 88B, 55-58.

Jones, R.W. and Charnock, M.A., 1985. 'Morphogroups' of agglutinating foraminifera. Their life positions and feeding habits and potential applicability in (paleo) ecological studies.

Review Paleobiol., 4, 311–320.

Jones, J. P. and Parker, W. K., 1860. On the Rhizopodal fauna of the Mediterranean compared with that of the Italian and some other Tertiary deposits. *Quarterly Journal of the Geological Society of London*, 16, 292-307.

Kaiho, K., 1994. Planktonic and benthonic foraminiferal extinction events during the last 100 m.y. *Palaeogeography, Palaeoclimatology, Palaeoecology,* 111, 45-71.

Kaiho, K and Saito , S. 1994. Oceanic crust production and climate during the last 100 Myr. *Terra Nova*, 6, 376–384.

Katz, B.J., 1983, Limitations of 'Rock-Eval' pyrolysis for typing organic matter: *Organic Geochemistry*, 4, 195-199

Keller, B. M., 1935. Microfauna from the Dneiper-Donetz Basin (Chalk). *Byull. Moskov Obshch Ispyaley Prirody Otdel Geol.*, 13, 522-558.

Keller, G., 1993. The Cretaceous/Tertiary boundary transitionin in the Antarctic Ocean and its global implications. *Marine Micropaleontology*, 21, 1-45.

Keller, G., 2002. *Guembelitria* dominated late Maastrichtian planktic foraminiferal assemblages mimic early Danian in the Eastern Desert of Egypt. *Marine Micropalaeontology*, 47, 71-99.

Keller, G., Han, Q., Adatte, T. and Burns, S. J., 2001. Palaeoenvironments of the Cenomanian-Turonian transition at Eastbourne, England. *Cretaceous Research*, 22, 391.

Keller, G. and Pardo, A., 2004. Age and paleoenvironment of the Cenomanian-Turonian global stratotype section and point at Pueblo, Colorado. *Marine Micropaleontology*, 51, 95-128.

Kennedy, W. J. and Simmons, M. D., 1991. Mid-Cretaceous ammonites and associated microfossils from the Central Oman Mountains. *Newsletters in Stratigraphy*, 25, 127-154.

Kennedy, W.J., Gale, A.S., Bown, P.R., Caron, M., Davey, R.J., Gröcke, D., and Wray, D.S., 2000. Integrated stratigraphy across the Aptian-Albian boundary in the Marnes Bleues, at the Col de Pré-Guitterd, Arnayon (Drôme), and at Tortonne (Alpesde-Haute-Provence),

France: a candidate global boundary stratotype section and boundary point for the base of the Albian Stage. *Cretaceous Research*, 223:591–720.

Kerr, A. C., 1998. Oceanic plateau formation: a cause of mass extinction and black shale deposition around the Cenomanian-Turonian boundary? *Journal of the Geological Society, London*, 155, 619-626.

Klinkhammer, G. P. and Bender, 1980. The distribution of manganese in the Pacific Ocean. *Earth and Planetary Science Letters*, 46, 361-384.

Kolonic S., Wagner T., Forster A., Damste J.S.S, Walsworth- Bell B., Erba E, Turgeon S., Brumsack HJ, Chellai EI, Tsikos H, Kuhnt W. and Kuypers M.M.M. 2005 *Paleoceanography*, 20 (1): Art. No. PA1006.

Kopaevich, L. F. and Walaszczyk, I., 1990. An integrated Inoceramid – Foraminiferal Biostratigraphy of the Turonian and Coniacian Strata in South-Western Crimea, Soviet Union. *Acta. Geol. Polonica,* 40, 83-95.

Kopaevich, L. F. and Kuzmicheva, T. A., 2002. The Cenomanian-Turonian boundary in southwestern Crimea, Ukraine: Foraminifera and palaeogeographic implications. In: Wagreich, M. (Ed.), *Aspects of Cretaceous Stratigraphy and Palaeobiology.* Österreichische Akademie der Wissenschaften, Schriftenreihe der Erdwissenschaftlichen Kommissionen 15, 129-149.

Koutsoukos, E. A. M. and Hart, M. B., 1990, Cretaceous foraminifera morphogroup distribution patterns, palaeocommunities and trophic structures: a case study from the Sergipe Basin , Brazil. *Transactions of the Royal Society of Edinburgh*, 81, 221-246.

Krasheninnikov, V. A., 1974. Upper Cretaceous benthonic agglutinated foraminifera, Leg 27 of the Deep Sea Drilling Project. In: *Initial reports of the Deep Sea Drilling Project.*, 27, 631-661.

Kroon, D. and Nederbragt, A. J., 1990. Ecology and paleoecology of triserial planktic foraminifera. *Marine Micropaleontology*, 16, 25-38.

Kroon, D., Norris, R. and Wilson P. 2002 Exceptional global warmth and climatic transients recorded in oceanic sediments. *JOIDES Journal,* 2811-15.

Kuhnt, W., Thurow, J., Wiedmann, J. and Herbin, J. P., 1986. Oceanic anoxic conditions around the Cenomanian/Turonian Boundary and the response of the biota. *Mitt. Geol.-Paläont. Inst. Univ. Hamburg*, 60, 205-246.

Kuhnt, W., and Kaminski, M. A., 1990. Paleoecology of Late Cretaceous to Paleocene deep-water agglutinated foraminifera from the North Atlantic and Wetern Tethys. In: Hembleben, C., Kaminski, M. A., Kuhnt, W. and Scott, D. B. (eds.), *Biostratigraphy, Paleoceanography and Taxonomy of Agglutinated Foraminifera*, Kluwer academic Publishers, The Netherlands, pp. 433-505.

Kuhnt, W. and Wiedmann, J., 1995. Cenomanian-Turonian source rocks: paleobiogeographic and palaeoenvironmental aspects. In: Huc, A. –Y. (Ed.). *Paleogeography, Palaeoclimate and Source Rocks AAPG Studies in Geology*. 40, 213-231.

Kuhnt, W. and Kaminski, M., 1997. Cenomanian to Lower Eocene deep-water agglutinated foraminifera from the Zumaya section, Northern Spain. *Annales Societatis Geologorum Poloniae,* 67, 257-270.

Kuhnt, W., Nederbragt, A. and Leine, L., 1997. Cyclicity of Cenomanian-Turonian organic-carbon-rich sediments in the Tarfaya Atlantic Coastal Basin (Morocco). *Cretaceous Research*, 18, 587-601.

Kump, L.R. and Arthur, M. A., 1999. Interpreting carbon-isotope excursions: carbonates and organic matter. *Chemical Geology*, 161, 181-198.

Kurtz, A. C., Kump, L. R., Arthur, M. A., Zachos, J. C. and Paytan, A., 2003. Early Cenozoic decoupling of the global carbon and sulfer cycles. *Paleoceanography*, 18 (4), Art. No. 1090

Kuzmicheva, T. A,. 2000. The Cenomanian-Turonian boundary of the Belaya mountain (southwestern Crimea). *Vestnik Moskovskogo Universiteta, Seriya 4. Geologiya.* 1, 70-73. [In Russian]

Kuznetsova, K. I., 1974. Distribution of benthonic foraminifera in Upper Jurassic and Lower Cretaceous deposits at site 261, DSDP Leg 27, in the eastern Indian Ocean. In: *Reports of the Deep sea Drilling Project*, 27, 673-681.

Lalicker, C. G., 1935. New Cretaceous Textulariidae. *Contributions from the Cushman Laboratory of Foraminiferal Research*, 11, 1-13.

Lamarck, J. N., 1804. Suite des mémoires sur les fossils des environs de Paris. *Annales Muséum National d'Histoire Naturelle*, 5, 179-188.

Lamolda, M.A. 1977. Three new species of planktonic foraminifera from the Turonian of northern Spain. *Micropaleontology*, 23, 470-477.

Lamolda, M. A., 1984. Benthic microforaminifera from the Basco-Cantabrian Albian-Turonian. Benthos '83; 2nd *International Symposium of benthic foraminifera,* p. 355-359.

Lamolda, M. A., Gorostidi, A. and Paul, C. R. C., 1994, Quantitative estimates of calcareous nannofossil changes across the Plenus Marls (latest Cenomanian), Dover, England: implications for the greatest generation of the Cenomanian-Turonian Boundary Event. *Cretaceous Research*, 5, 143-164.

Lamolda, M. A. and Peryt, D., 1995. Benthonic foraminiferal response to the Cenomanian/Turonian boundary event in the Ganuza Section, Northern Spain. *Revista Española de Paleontologia*, 8, 101-118.

Lamolda, M. A., Gorostidi, A., Martinez, R., López, G. and Peryt, D. 1997. Fossil occurrences in the Upper Cenomanian-Lower Turonian at Ganuza, northern Spain: an approach to Cenomanian/Turonian boundary chronostratigraphy. *Cretaceous Research*, 18, 331-353.

Larson, R. L., 1991. Geological consequences of superplumes. *Geology*, 19, 963-966.

Larson, R. L. and Erba, E., 1999. Onset of the mid-Cretaceous greenhouse in the Barremian-aptian: igneous events and the biological, sedimentary, and geochemical responses. *Paleoceanography*, 14 (4), 663-678.

Lawrence, J.R., Drever, J.I. Anderson, T.F. and Brueckner, H.K., 1979. Importance of alteration of volcanic material in the sediments of Deep Sea Drilling Site 323: chemistry, $^{18}O/^{16}O$ and $^{87}Sr/^{67}Sr$. *Geochem. Cosmochim. Acta*, 43: 537-588.

Leary, P. N. and Hart, M. B., 1989. The use if the ontogeny of deep water dwelling planktonic foraminifera to assess basin morphology, the development of water masses, eustasy and the position of the oxygen minimum zone in the water column. *Mesozoic Research*, 2, 67-74.

Leckie, R. M., 1987, Paleoecology of mid-Cretaceous planktonic foraminifera: a comparison of open ocean and epicontinental sea assemblages. *Micropaleontology*, 33(2), 164-176.

Leckie, R. M., Yuretich, R. F., West, O. L. O., Finkelstein, D. and Schmidt, M., 1998. Paleoceanography of the southwestern Western Interior Sea during the time of the Cenomanian-Turonian boundary (Late Cretaceous). In: Dean, W. and Arthur, M. A. (eds.) *Stratigraphy and Paleoenvironments of the Cretaceous Western Interior Seaway, USA,* SEPM Concepts in Sedimentology and Paleontology, 6, 101-126.

Lee, J. J. and Anderson, O. R., 1991. Symbiosis in foraminifera. In: Lee, J. J. and Anderson, O. R. (eds.), *Biology of Foraminifera*, Acedemic Press, London. 1-716.

Lipps, J. H., 1979. Ecology and paleoecology of planktic foraminifers. In: Lipps, J. H. *et al.* (eds.) *Foraminiferal ecology and palaecology*: Society of Economy Paleontologists and Mineralogists, Sort Course No. 6, p. 62-104.

Lirer, 2000. A new technique for retrieving calcareous microfossils from lithified lime deposits. *Micropaleontology*, 46, 365-369.

Loeblich, A. R. and Tappan, H., 1987. *Foraminiferal Genera and their Classification*. Van Nostrand Reinhold, New York. pp. 970.

Ludbrook, N. H., 1966. Cretaceous biostratigraphy of the Great Artesian Basin in South Australia. *Bulletin of the Geological Survey of south Australia*, 40, 1-223.

MacArthur, R. H. and Wilson, E. O., 1967. *The Theory of Island Biogeography*: Princeton University Press, Princeton, 167 pp.

MacLeod, K.G., Huber, B.T., and Ducharme, M.L., 1999. Paleontological and geochemical constraints on changes in the deep ocean during the Cretaceous greenhouse interval, in Huber, B.T., MacLeod, K. G., and Wing, S.L., eds., *Warm Climates in Earth History:* Cambridge, Cambridge University Press. p. 241-274.

Malaprism M., 1965. les Gavelinellidae et formes affines du gisement Albien de Courcelles (Aube): *Revue de Micropaléontologie*, 8, 131-150.

Malone, M. J., Slowey, N. C. and Henderson, G. M., 2001. Early diagenesis of shallow-water periplatform carbonate sediments, leeward margin, Great Bahama Bank (Ocean Drilling Project Leg 166). *Geological Society of America Bulletin*, 113 , 881-894.

Marie, P., 1941. Les foraminifères de la Craie à *Belemnitella mucronata* du Bassin de Paris. *Mem. Mus. Nat. Hist., n. ser.*, 12, 1-296.

Marshall, J. D., 1992. Climatic and oceanographic isotoic signals from the carbonate rock record and their preservation. *Geological magazine*, 192 (2), 143-160.

Martin, J. H. and Knauer, 1984. VERTEX: manganese transport through the oxygen minima. *Earth and Planetary Science Letters*, 67, 35-47.

Maync, W., 1953. *Hemicyclammina sigali* n. gen. N. sp. from the Cenomanian of Algeria. *Contributions from the Cushman Foundation for Foraminiferal Research, Washington D.C.*, 4, 148-150.

Maync, W., 1973. Lower Cretaceous foraminiferal fauna from Gorringe Bank, eastern North Atlantic. In: Ryan, W. B. F., Hsu, J. J., *et al.*, *Initial Reports of the Deep Sea Drilling Project*, 13, 1075-1112.

McCrea, J. M., 1950. On the isotope chemistry of carbonates and a paleotemperature scale. *Journal of Chemistry and Physics*,18, 849-857.

Menegatti, A. P., Weissert, H., Brown, R. S., Tyson, R. V., Farrimond, P., Strasser, A. and Caron, M., 1998. High resolution $\delta^{13}C$ stratigraphy through the early Aptian "Livello Selli" of the Alpine Tethys. *Paleoceanography*, 13 (5), 530-545.

Meyer, T., 1990. Biostratigraphische und sedimentologische Untersuchungen in der Plänerfazies des Cenoman von Nord-westdeutschland. *Mitteilungen aus dem Geologischen Institut der Universität Hanover*. 30, 1-114.

Meyers, S.R., Sageman, B.B., Hinnov, L.A., 2001. Integrated quantitative stratigraphy of the Cenomanian–Turonian Bridge Creek Limestone Member using evolutive harmonic analysis and stratigraphic modelling. *Journal of Sedimentary Research* 71,644– 682.

Meyn, H. and Vespermann, J., 1994. Taxonomische Revision von Foraminiferen der Unterkreide SE-Niedersachsens nach ROEMAR (1839, 1841, 1842), KOCH (1851) und REUSS (1853). *Senckenbergiana lethaea,* 74, 49-272.

Mitchell, S. F. and Carr, I. T., 1998. Foraminiferal response to mid-Cenomanian (Upper Cretaceous) palaeoceanographic events in the Anglo-Paris Basin (Northwest Europe). *Palaeogeography, Palaeoclimatology, Palaeoecology*, 137, 103-125.

Montagu, G., 1803. *Testacea Britannica or History of British Shells, Marine Land and Freashwater, Including Most Minute.* J. S. Hollis, Romsey, England.

Monteiro, J. F., Munha, J. and Ribeiro, A. 1998a. Impact ejecta horizon near the Cenomanian-Turonian Boundary, north of Nazaré, Portugal. – Com. V Congresso Nacional de Geologia, Novembro 1998, 4pp. [not numbered]

Monteiro, J. F., Munha, J. and Ribeiro, A, 1998b. Impact ejecta horizon near the Cenomanian-Turonian boundary, north of Nazaré, Portugal. *Meteoritics Planet. Sci.* 33, A112-A113.

Morozova, V. G., 1948. [Foraminifera of Lower Cretaceous strat of the G. Sochi Region (southwest Caucasus)]. *Byulletin' Moskovskogo Obshchestva Ispytateley Prirody, Odtel Geologicheskii*, 23, 23-43.

Morrow, A. L., 1934. Foraminifera and ostracoda from the Upper Cretaceous of Kansas. *Journal of Paleontology*, 8, 186-205.

Moullade, M., 1984. Interet des petits foraminiferes benthiques "profonds," pour la biostratigraphie et l'analyse des paleoenvironnements oceaniques Mésozoïques. *In* Oertli,

H.J. (Ed.), *BENTHOS '83: Proc. 2nd Int. Symp. Benthic Foraminifera. Bull. Cent. Rech. Expl.-Prod. Elf-Aquitaine*, 6, 429-464.

Murray, J.W, 1991, *Ecology and Palaeoecology of Benthic Foraminifera*, Longman Scientific and Technical (John Wiley), 365 pp.

Mutter, J.C., Larson, R.L. and Group N.A.S. 1989 Extension of the Exmouth Plateau, offshore north-western Australia. Deep seismic reflection/refraction evidence for simple and pure shear mechanisms. *Geology*, 17, 15-18.

Naidin, D. P., 1981. The Russian Platform and the Crimea. In: Reyment, R. A., Bengtston, P. (eds). *Aspects of Mid-Cretaceous Regional Geology,* Academic Press. 29-68.

Naidin, D. P., 1993. Late Cretaceous events in the east of the European paleobiogeographic province 2. Cenomanian/Turonian and Maastrichtian/Danian events. *Bulletin of the Moscow Society of Naturalists Geological Series*, 68, 33-53. [In Russian]

Naidin, D. P., Alekseev, A. S., 1981. Importance of ocean drilling data for interpretation and life of fauna in the Cenomanian of the Crimean highlands. In: Krassilov, V. (Ed.). *Evolution of organisms and biostratigraphy of the Mid-Cretaceous*. Vladivostok. 7-21. [In Russian]

Naidin, D.P., Kiyashko, S.I., 1994a. Cenomanian/Turonian boundary deposits in the Crimean highlands. 1. Lithology, organic deposits and some elements contents. *Bulletin of the Moscow Society of Naturalists*, Geological Series 69, 28-42. [In Russian, English Abstract]

Naidin, D.P., Kiyashko, S.I., 1994b. Cenomanian/Turonian boundary deposits in the Crimean highlands. 2. Isotopic composition of carbon and oxygen; environment of organic carbon accumulation. *Bulletin of the Moscow Society of Naturalists*, Geological Series 69, 28-42. [In Russian, English Abstract]

Nederbragt, A. J., Erlich, R. N., Fouke, B. W. and Ganssen, G. M., 1998. Palaeoecology of the biserial planktonic foraminifer *Heterohelix moremani* (Cushman) in the late Albian to middle Turonian Circum-North Atlantic. *Palaeogeography, Palaeoclimatology, Palaeoecology*, 144, 115-133.

Nederbragt, A. J. and Fiorentino, A., 1999. Stratigraphy and paleoceanography of the Cenomanian-Turonian boundary event in Oued Mellegue, northwestern Tunisia. *Cretaceous Research*, 20, 47-62.

Nederbragt, A. J., Fiorentino, A. and Klosowska, B. 2001. Quantitative analysis of calcareous microfossils across the Albian-Cenomanian boundary oceanic anoxic event at DSDP Site 547 (North Atlantic). *Palaeogeography, Palaeoclimatology, Palaeoecology*, 166, 401-421.

Nederbragt, A. J., Thurow, J., Vonhof, H. and Brumsack, H-J. 2004 Modelling oceanic carbon and phosphorous fluxes: implications for the cause of late Cenomanian oceanic anoxic event (OAE2). *Journal of the Geological Society, London*, 161, 721-728.

Nikishin, A. M., Alekseev, A. S., Kopaevich, L. F., Yanin, B. T., Baraboshkin, E. Yu. And Yutsis, V. V., 1993. Cretaceous-Eocene sedimentation in the Shelf Alma Basin of Cimmerian mobile belt (Crimea): eustatic and tectonic influences. In: Vail, P. R. (Ed.) *Book 4. Sequence Stratigraphy Workshop*. May 20-May 30. Crimea, Ukraine. Vrihe Universitat Amsterdam – Moscow State University.

Nikishin, A. M., Cloetingh, S., Bolotov, S. N., Baraboshkin, E. Y., Kopaevich, L. F., Nazarevich, B. P., Panov, D. I., Brunet, M. F., Ershov, A. V., Ilina, V. V., Kosova, S. S., Stephenson, R. A., 1997. Scythian Platform: chronostratigraphy and polyphase stages of tectonic history. Memoirs du Museum National d'Histoire Naturelle. 177, 151-162.

Norris, R. D. and Wilson, P. A. 1998. Low-latitude sea-surface temperatures for the mid-Cretaceous and the evolution of planktic foraminifera. *Geology*, 26 (9), 823-826.

Norris, R. D, Bice, K. L., Magno, E. A. and Wilson, P. A., 2002. Jiggling the tropical thermostat during the Cretaceous hot house. *Geology*, 30, 299-302.

Ogg, J.G., Karl, S.M., and Behl, R.J., 1992. Jurassic through Early Cretaceous sedimentation history of the central equatorial Pacific and of Sites 800 and 801. In Larson, R.L., Lancelot, Y., et al., Proc. *ODP, Sci. Results,* 129: College Station, TX (Ocean Drilling Program), 571-613.

Opdyke, B. N., Erba, E., Larson, R. and Herbert, T. 2001. Hot LIPs, Methane and the Carbon History of the Apticore. *Journal of Conference Abstracts* 6, p. 203.

d'Orbigny, A., 1826. Tableau méthodique de la classe des Céphalopodes. *Ann. Sci. Nat.*, ser. 1, 7, 245-314.

d'Orbigny, A., 1840. Mémoire sur les foraminifères de la Craie blanche du Bassin de Paris. *Mem. Soc. Géol. Fr.*, 4, 1-51.

Pairis, J. L., Delamette, M. and Decrouez, D., 1986. *Guide-book of the field-trip Nr. 3. September, 27th 1986. Mid-Cretaceous and Paleogene of the delphino-Helvetic Zone in the Haute-Savoie, France*. Benthos '86 Museum d'Histoire Naturelle, Genève, Suisse.

Pancost, R. D., Crawford, N., Magness, S., Turner, A, Jekyns, H. C. and Maxwell, J. R., 2004. Further evidence for the development of photic-zone euxinic conditions during Mesozoic oceanic anoxic events. *Journal of the Geological Society, London,* 161, 353-364.

Parker, W. K. and Jones, T. R., 1865. On some foraminifera from the North Atlantic and Arctic Oceans, including Davis Straits and Baffin's bay. *Philosophical Transactions of the Royal Society*, 155, 325-441.

Parrish, J. T., 1995. Paleogeography of C_{org}-rich rocks and the preservation verses production controversy. In: Huc, A. –Y. (Ed.). Paleogeography, Paleoclimate and Source Rocks AAPG Studies in Geology. 40, 1-20.

Paul C. R. C. and Mitchell, 1994. Is famine a common factor in marine mass extinctions? *Geology*, 22, 679-682.

Paul, C. R. C., Lamolda, M. A., Mitchell, S. F., Vaziri, M. R., Gorostidi, A. and Marshall, J. D., 1999. The Cenomanian-Turonian boundary at Eastbourne (Sussex, UK): a proposed European reference section. *Palaeogeography, Palaeoclimatology, Palaeoecology*, 150, 83-121.

Pearson, P. N., Ditchfield, P. W., Singano, J., Harcourt-Brown, K. G., Nicholas, C. J., Olsson, R. K., Shackleton, N. J. and Hall, M. A., 2001. Warm tropical sea surface temperatures in the Late Cretaceous and Eocene epochs. *Nature*, 413, 481-487.

Peryt, D. and Lamolda, M., A., 1996. Benthonic foraminiferal mass extinction and survival assemblages from the Cenomanian-Turonian boundary event in the Menoyo section, northern Spain. In: Hart, M. B. (ed.) *Biotic recovery from Mass Extinction Events*. Geological Society Special Publication, 102, 245-258.

Pessagno, E. A., Jr., 1967.Upper Cretaceous planktonic foraminifera from the western Gulf Coastal Plain. *Palaeontographica Americana*, 5, 1-445.

Peters, K.E., 1986, Guidelines for evaluating petroleum source rock using programmed pyrolysis: *American Association of Petroleum Geology Bulletin*, 70, 318-329.

Petrizzo, M. R., 2002. Palaeoceanographic and palaeoclimatic inferences from Late Cretaceous planktonic foraminiferal assemblages from the Exmouth Plateau (ODP Sites 762 and 763, eastern Indian Ocean). *Marine Micropaleontology*, 45, 117-150.

Phleger F.B. 1960 Ecology and Distribution of Recent Foraminifera. Baltimore, John Hopkins Press.

Pinheiro, L. H., Wilson, R. C. L., Pena dos Reis, R., Whitmarsh, R. B., Riberiro, A., 1996. The Western Iberian Margin: A Geophysical and Geological Overview. In: Whitmarsh, R. B., Sawyer, D. S., Klaus, A. and Masson, D. G. (eds.). *Proceedings of the Ocean Drilling Program, Scientific Results*, Ocean Drilling Program, College Station, TX, 149, 3-23.

Pirrie, D. and Marshall, J.D. 1990 High latitude Late Cretaceous Palaeotemperatures: new data from James Ross Island, Antarctica. *Geology,* 18, 31-34.

Plummer, H. J., 1927. Foraminifera of the Midway Formation in Texas. *Texas University Bulletin (Bur. Econ. Geol.)*, 2644, 1-206.

Plummer, H. J., 1931. Some Cretaceous foraminifera in Texas, *Bull, University of Texas*, 2644, 1-206.

Poulsen C.J., Barron E.J., Arthur M.A. and Peterson W.H. 2001. Response of the mid-Cretaceous global oceanic circulation to tectonic and CO2 forcings. *Paleoceanography*, 16, 576-592.

Poulsen, C. J., Gendaszek, A. S. and Jacob, R. L., 2003. Did the rifting of the Atlantic Ocean cause the Cretaceous thermal maximum? *Geological Society of America*, 31, 115-118.

Pratt, L. M., 1985. Isotopic studies of organic matter and carbonate in rocks of the Greenhorn marine cycle. In: Pratt, L. M. *et al.* (Eds.). *Fine-grained deposits and biofacies of Cretaceous Western Interior Seaway: Evidence of Cyclic Sedimentary Processes*. Soc. Econ. Paleontol. Mineral., Tulsa, Field Trip Guidebook. 4, 38-48.

Pratt, L. M. and Threlkeld, C.N., 1984. Stratigraphic significance of $^{13}C/^{12}C$ ratios in mid-Cretaceous rocks of the Western Interior, U.S.A. In: Stott, D. F. and Glass, D. L. (eds.) *The Mesozoic of Middle North America. Canadian Society of Petroleum Geologists Memoir* 9, 305-312.

Pratt, L.M., Arthur, M.L.A., Dean W.E. and Scholle, P.A., 1993, Paleoceanographic cycles and events during the Late Cretaceous in the Western Interior Seaway of North America, *Geological Association of Canada, Special Paper,* 39,. 333-354.

Premoli Silva, I. and Sliter, I. P., 1999. Cretaceous paleoceanography: evidence from planktonic foraminiferal evolution. *Geological Society of America,* Special Publication, 332, 301-328.

Price, G. D., 2003. New constraints upon isotope variation during the early Cretaceous (Barremian-Cenomanian) from the Pacific Ocean. *Geological Magazine*, 140 (5), 513-522.

Price, G. D. and Sellwood, B. W., 1999. Isotopic variation in late Cenomanian to early Turonian foraminifera and matrix from DSDP site 551 (Goban Spur, Northeast Atlantic). *Proceedings of the Ussher Society*, 9, 297-299.

Price, G. D. and Hart, M. B., 2002. Isotopic evidence for early to mid-Cretaceous ocean temperature variability. *Marine Micropaleontology*, 46, 45-58.

Prokoph, A., Villenouve, M., Agterberg, F. P. and Volker, R., 2001. Geochronology and calibration of global Milankovitch cyclicity at the Cenomanian-Turonian boundary. *Geology*, 29, 523-526.

Ramsey, J. G., 1963. Stratigraphy, Structure and Metamorphism in the Western Alps. *Proceedings of the Geologists' Association*, 74, 357-392.

Quilty, P. G., 1984. Cretaceous foraminiferids from Exmouth Plateau and Kerguelen Ridge, Indian Ocean. *Alcheringa*, 8, 225-241.

Raup, D. M. and Sepkoski, J. J., Jr.1982 Mass extinctions in the marine fossil record. *Science* 215, 1501–1503.

Renz, O., 1936. Stratigraphie und mikropalaeontologische Untersuchung der Scaglia (Obere Kreide-Tertiar) im zentralen Apennin. *Eclogae Geol. Helv.*, 29, 1-149.

Revets, S. A., 1996. The generic revision of the Anomalinidae, Albaminidae, Cancrisidae and Gavelinellidae. *Cushman Foundation Special Publication*, 34, 57-113.

Revets, S. A., 2001. The revision of *Gavelinella* Brotzen, 1942, *Berthelina* Malapris, 1965 and *Lingulogavelinella* Malpris, 1965. Cushman Foundation for Foraminiferal Research, Special Publication, 37. pp. 1-110.

Reuss, A. E., 1845. Die Versteinerungen der bohmischen Kreideformation. *E. Schweizerbartsohne Verlagsbuchhandlung,* Abtheilung, 1, 1-58.

Reuss, A. E., 1851. Die Foraminiferen und Entomostraceen des Kreidemergels von Lemberg. *Haidinger's Nayurwiss. Abh.*, 4, 17-52.

Reuss, A. E., 1854. Beitrage zur Charakteristik der Kreideschichten in den Ostalpen, besonders im Gosauthale und am Wolfgangsee. *K. Akad. Wiss. Wien, Math.-naturw., Kl., Denkschr.*, 7, 1-156.

Reuss, A. E., 1860. Die foraminiferen der westphalischen Kreideformation. *Sitzungberichte der Kaiserlichen Akademie der Wissenschaften in Wien, Mathemtisch-Naturwissenschaftliche*, 40, 301-342.

Reuss, A. E., 1862. Palaeontologische Beitrage. *Kaiserlichen Akademie der Wissenschaften in Wien, Mathemtisch-Naturwissenschaftliche*, 44, 301-342,

Reuss, A. E., 1863. Die foraminiferen des norddeutschen Hils und Gaukt. *Sitzungsberichte der Kaiserlichten Akademie der Wissenchaften in Wien, Mathemtisch-Naturwissenschaftliche*, 46, 5-100.

Riegraf, W., and Luterbacher, H., 1989. Oberjura-Foraminiferen aus dem Nord- und Siidatlantik (Deep Sea Drilling Project Leg 1-79). *Geologische Rundschau*, 78:999-1045.

Robaszynski, F. and Caron, M., 1979. Atlas de Foraminiferes Planctoniques du Cretace Moyen (Mer Boreale et Tethys). *Cahiers de Micropaleontologie*, 1. Editions du Centre National de le Recherche Scientifique, Paris.

Robaszynski, F. and Caron, M., 1995. Foraminifères planctoniques du Crétacé: commentaire de la zonations Europe-Méditerranée. *Bulletin de la Société géologique de France* 166, 681-692.

Roemar, F. A., 1838. Die Cephalopoden des Nord-Deutschen tertiären Meersandes. *Neues Jahrbuch für Mineralogie, Geognosie, Geologie und Petrefakten-Kunde*. 381-394.

Roemar, F. A., 1841. *die Versteinerungen des norddeutschen Kreidegebirges*. Hannover, 1-145.

Ruttköller, J., Littke, R., Radke, M., Disko, U., Horsfield, B. and Thurow, J., 1992. Petrography and geochemistry of organic matter in Triassic and Cretaceous deep-sea sediments from the Wombat and Exmouth Plateaus and nearby abyssal plains off northwest Australia. In: Von Rad, U., Haq, B. U. *et al.* (eds.). *Proceedings of the Ocean Drilling Program, Scientific Results* 122, 317-328.

Sageman, B.B., Meyers, S.R. and Arthur, M.A. 2006 Orbital time scale and new C-isotope record for Cenomanian-Turonian boundary stratotype. *Geology* 34, 125-128.

Salaj, J. 1996. Tunisian Upper Cretaceous hypostratotypes as possible candidates of Tethyan stratotypes including stratotype boundaries. *Zemni plyn a nafta,* 40, 245-307.

Sartorio, D. and Venturini, S., 1988. *Southern Tethys Biofacies* Agip S.p.A, S. Donato Milanese, 235 pp.

Savin, S.M., Abel, L., Barrera, E., Hodell, D., Keller, G., Kennet, J.P., Killingley, J. and Berger, W.H. 1985 The evolution of Miocene surface and near-surface marine temperatures: Oxygen isotopic evidence. *Memoir of the Geology Society of America* 163, 49-79.

Schacko, G., 1897. Beitrag uebar Foraminiferen aus der Kreide von Moltzow in Meckleburg. *Ver. Freunde Naturg. Mecklenburg, Archiv.* 50, 161-168.

Scheibnerová, V., 1960. Poznáky k rodu Praeglobotruncana Bermudez z kusyckich vrstiev bradlovego pasma. *Ibidem*, 11, 1, 85-93.

Scheibnerová, V., 1974. Aptian-Albian benthonic foraminifera from DSDP Leg 27, Sites 259, 260 and 263, eastern Indian Ocean. In: *Reports of the Deep sea Drilling Project*, 27, 697-741.

Scheibnerová, V., 1976. Cretaceous Foraminifera of the Great Australian Basin. *New South Wales Geological Survey Memoirs on Palaeontology*, 17, 1-265.

Scheibnerová, V., 1978. Aptian and Albian benthic foraminifers of Leg 40, Sites 363 and 364, southern Atlantic. In: *Initial reports of the Deep Sea Drilling Project*, 40, 741-757.

Schlanger, S. O. and Jenkyns, H. C., 1976. Cretaceous oceanic anoxic events: causes and consequences. *Geologie en Mijnbouw*, 55, 179-184.

Schlanger, S.O., Jenkyns, H.C. and Premoli-Silva, I., 1981. Volcanism and vertical tectonics in the Pacific Basin related to global Cretaceous transgressions. *Earth and Planetary Science Letters,* 52, 435-449.

Schlanger, S. O., Arthur, M. A., Jenkyns, H. C. and Scholle, P. A., 1987. The Cenomanian-Turonian Oceanic Anoxic Event I. Stratigraphy and distribution of organic carbon-rich beds and the marine $\delta^{13}C$ excursion. In: Brooks, J. and Fleet, A. J. (eds.), *Marine Petroleum Source Rocks*, Geological Society Special Publication, 26, 371-399.

Scholle, P. A., 1977. Chalk diagenesis and its relation to petroleum exploration: Oil from chalks, a modern miracle? *American Association of Petroleum Geologists Bulletin*. 64, 67-87.

Scholle, P. A., Arthur, M. A., 1980. Carbon isotope fluctuations in cretaceous pelagic limestones: potential stratigraphic and petroleum exploration tool. *American Association of Petroleum Geologist Bulletin.* 64, 67-87.

Schrag, D. P., DePaolo, D. J. and Richter, F. M., 1995. Reconstructing past sea surface temperatures: correcting for diagenesis of bulk marine carbonate. *Geochimica et Cosmochimica Acta*, 59 (11), 2265-2278.

Schrag. D. P., 1999. Effects of diagenesis on the isotope record of late Paleogene tropical sea surface temperatures. *Chemical Geology*, 161, 215-224.

Schulze, F. E., 1875. *Zoologische Ergebnisse der nord-seefahrt, vom 21 Juli bis 9 September, 1872*. I, Rhizpoden. II, Jahresberichte Kommission zur Untersuchung der Deutschen Meer in Kiel für die Jahr 1872, 1873, 99-114.

Sepkoski, J. J., Jr., 1990. The taxonomic structure of periodic extinction, in Sharpton, V. L., and Ward, P. D., Global catastrophies in Earth history: *Geological Society of America Special Paper* 247, p. 33–44.

Sepkoski, J. J., Jr., and Raup, D. M., 1986, Periodicity in marine extinctionevents. In: Elliott, D. K., (Ed.), *Dynamics of extinction*: New York, Wiley,p. 3–36

Severin, K.P., 1983. Test morphology in benthic foraminifera as a discriminator of biofacies. *Marine micropaleontology*, 8, 65-76.

Shackleton, N.J., Kennett, J.P., 1975. Paleotemperature history of the Cenozoic and the initiation of Antarctic glaciation: Oxygen and carbon isotope analyses in DSDP sites 277, 279 and 281. In: Kennett, J.P., Houtz, R.E. et al. (Eds.), Initial Reports of the Deep Sea Drilling Project 29, Washington: U.S. Government Printing Office, 743-756.

Sigal, J., 1948. Notes sur les genres de foraminifères *Rotalipora* Brotzen, 1942 et *Thalmanninella*. Famille des Globorotaliidae. *Rev. Inst. Fr. Petrol. Paris*, 3, 95-103.

Sliter, W. V., 1968. Upper Cretaceous Foraminifera from Southern California and northwestern Baja California, Mexico. *The University of Kansas Pal. Contr.*, 7, 1-141.

Sliter, W. V., 1980. Mesozoic foraminifers and deep-sea benthic environments from the Deep Sea Drilling Project Sites 415-416, eastern North Atlantic. Initial Report of the Deep Sea Drilling Project, 50, 353-427.

Smith, W.E. 1957 The Cenomanian Limestone of the Beer district, South Devon. *Proceedings of the Geologists Association*, 68, 115-133.

Smith, A.G., Smith, D.G., Funnell, B.M., 1994. Atlas of Mesozoic and Cenozoic Coastlines. Cambridge University Press, Cambridge. 99pp.

Stouge, S. and Boyce, D. W., 1983. Fossils of Northwesterns Newfoundland and Southeastern Labrador: Conodonts and triobites. *Mineral Development Division Department of Mines*

Energy Government of Newfoundland and Labrador. ST John's Newfoundland – Report, 83-3.

Tappan, H., 1940. foraminifera from the Grayson Formation of northern Texas. *Journal of Paleontology*, 14, 93-126.

Tappan, H., and Loeblich, AR, 1988. Foraminiferal evolution, diversification and extinction. *Journal of Paleontology,* 62: 695-741.

Tarduno, J. A., Sliter, W.V., Kroenke, L., Leckie, M., Mayer, H., Mahoney, J. J., Musgrave, R., Storey, M. and Winterer, E. L., 1991. Rapid formation of the Ontong Java Plateau bu Aptian mantle plume volcanism. *Science*, 18, 399-403.

Tewari, A., 1996. The Middle to Late Cretaceous microbiostratigraphy (foraminifera) and lithostratigraphy of the Cauvery Basin, Southeast India. Unpublished PhD Thesis.

Thurow, J., Brumsack, H.-J., Rullkötter, J., Littke, R., and Meyers, P., 1992. The Cenomanian/Turonian boundary event in the Indian Ocean—a key to understand the global picture. In Duncan, R.A., Rea, D.K., Kidd, R.B., von Rad, U., and Weissel, J.K. (Eds.), Synthesis of Results from Scientific Drilling in the Indian Ocean. *Geophys. Monograph, American Geophys. Union*, 70, 253–273.

Trujillo, E. F., 1960. Upper Cretaceous foraminifera from near Redding, Shasta County, California. *Journal of Paleontology.*, 34, 290-346.

Tsikos, H., Jenkyns, H. C., Walsworth-Bell, B., Petrizzo, M. R., Forster, A., Kolonic, S., Erba, E., Premoli Silva, I., Baas, M., Wagner, T. and Sinninghe Damsté, J. S., 2004. Carbon-isotope stratigraphy recorded by the Cenomanian-Turonian oceanic anoxic event: correlation and implications based on three key localities. *Journal of the Geological Society, London*, 161, 711-719.

Tur, N. A., Smirnov, J. P. and Huber, B. T., 2001. Late Albian-Coniacian planktic foraminifera and biostratigraphy of the northeastern Caucasus. *Cretaceous Research*, 22, 719-734.

Tyson, R. V., 1995. Sedimentary Organic Matter: Organic Facies and Palynofacies. Chapman and Hall, London. 615 pp.

Voigt, S. and Hilbrecht, H., 1997. Late Cretaceous carbon isotope stratigraphy in Europe: Correlation and relations with sea level and sediment stability. *Palaeogeography, Palaeoclimatology, Palaeoecology*, 134, 39-59.

Von Rad U., Exon N. F., Boyd R. and Haq B. U. 1992. Mesozoic paleoenvironment of the rifted margin off NW Australia (ODPLegs 122/123). In: Duncan R. A., Rea D. K., Kidd R. B., von Rad U. and Weissel J. K. eds. *Synthesis of Results from Scientific Drilling in the Indian Ocean*, pp. 157 – 184.

Wang, K., Geldsetzer, H. H. J., Goodfellow, W. D., Krouse, H. R., 1996. Carbon and sulphur isotope anomalies across the Frasnian-Famennian extinction boundary, Alberta, Canada. *Geology*. 24, 187-191.

Watkins, D. K., 1985, Biostratigraphy and paleoecology of calcareous nannofossils in the Greenhorn marine cycle: in Pratt, L. M., Kauffman, E. G., and Zelt, F. B. eds., *Fine-grained deposits and biofacies of the Cretaceous Western Interior Seaway: Evidence of Cyclic sedimentary Processes*: SEPM, 1985 Midyear Meeting, Golden, Colorado, Field Trip Guidebook, p. 4.

Whittaker, S.G., Kyser, T.K. and Caldwell, W.G.E. 1987 Palaeoenvironmental geochemistry of the Claggett marine cyclotherm in south-central Saskatchewan. *Canadian Journal of Earth Sciences* 24, 967-984.

Wignall, P.B. 1994 Black Shales, Oxford

Williamson, P.E., Swift, M.G., Kravis, S.P., Falvey, D.A., Brassil, F., 1990. Permo-Carboniferous rifting of the Exmouth plateau region (Australia): an intermediate plate model. In: B. Pinet, C. Bois (Eds.), The *potential of deep seismic profiling for hydrocarbon exploration*. Ed. Technip, Paris, pp 237-248.

Wilson, R. C. L., 1988. Mesozoic development of the Lusitanian Basin, Portugal. *Revista de la Sociedad Geológica de España, Madrid*, 1, 393-407.

Wilson, P. A. and Norris, R. D., 2001. Warm tropical ocean surface and global anoxia during the mid-Cretaceous period. *Nature*, 412, 425-429.

Wilson, P. A., Norris, R. D. and Cooper, M. J., 2002. Testing the Cretaceous greenhouse hypothesis using glassy foraminiferal calcite from the core of the Turonian tropics on Demerara Rise. *Geology*, 30, 607-610.

Wonders, A. A. H., 1980. Middle and late Cretaceous planktonic foraminifera of the Western Mediterranean area. *Utrecht Micropaleontological Bulletin*, 24, 1–157.

Wonders, A.A.H., 1992. Cretaceous planktonic foraminiferal biostratigraphy, Leg 122, Exmouth Plateau, Australia. In von Rad, U., Haq, B.U., et al., *Proceedings of ODP, Scientific Results,* 122: College Station, TX (Ocean Drilling Program), 587-599.

Wright, J., 1886. A list of the Cretaceous foraminifera of Keady Hill, County Derry. *Proceeding Belfast Naturalists' Field Club*, Series 2 (2). Appendix 1885-1886, pp. 327-332.

Wright J. D., Miller, K. G., Cramer, B. S., Olsson, R. K., Katz, M. E., Sugarman, P. J., 2001. Transient climate event at the Cenomanian/Turonian Boundary (OAE2). American Geophysical Union, Fall Meeting 2001, abstract #PP32A-0515.

Zachos, J.C., Stott, L.D. and Lohmann, K.C. 1994. Evolution of early Cenozoic marine temperatures. *Paleoceanography* 9, 353-87.

Appendix 1

Taxonomic Plates

Plate 1

1 ***Rhabdammina*** **spp.**, side view, Upper Cenomanian, Crimea AK 60

2, 3 ***Rhizzammina*** **spp.**, side view, Lower Cenomanian, ODP Site 766A, 15R-5 20-22

4 ***Psammosphaera fusca*** Schulze, side view, Upper Albian, ODP Site 766A, 16R-5 135-137

5, 10 ***Hippocrepina gracilis*** Holbourn & Kaminski.
5. side view, Upper Albian, Gascoyne Abyssal Plain, ODP Site 766A, 16R-6 35-37.
10. close up of proloculus, Upper Albian, ODP Site 766A, 16R-6 35-37.

6 ***Ammodiscus cretaceous*** (Reuss), side view, Upper Cenomanian, Crimea AK 60

7 ***Glomospira charoides*** (Jones & Parker), side view, Upper Albian, ODP Site 766A, 16R-4 60-62.

8 ***Glomospira irregularis*** (Grzybowski), side view, Upper Albian, ODP Site 766A, 16R-5 135-137.

9 ***Glomospirella gaultina*** (Berthelin), side view, Upper Albian, ODP Site 766A, 16R-7 10-12.

11 ***Reophax*** **sp. 1**, side view, Upper Cenomanian, ODP Site 762C, 75X-1 110-112.

12 ***Reophax*** **sp. 2**, side view, Upper Cenomanian, ODP Site 762C, 75X-1 110-112.

13 ***Ammosphaeroidina*** **sp. 1**, side view, Upper Albian, ODP Site 766A 16R-5 10-12.

14 ***Spiroplectinella gandolfi*** (Carbonnier), side view, Upper Albian, ODP Site 766A 16R-7 10-12.

15, 20 ***Spiroplectinella*** **sp. 1**
15. side view, Upper Albian, ODP Site 766A 16R-7 10-12.
20. close up of wall structure, ODP Site 766A 16R-7 10-12.
Scale bar is 50 μm.

16 ***Eggerellina brevis*** Marie, side view, Upper Cenomanian, Crimea AK 225.

17-18 ***Eggerellina mariae*** ten Dam
17. side view, Upper Albian, ODP Site 766A 16R-6 110-112.
18. side view, Lower Turonian, ODP Site 766A 15R-2 40-42.

19 ***Spiroplectinata annectans*** (Jones & Parker), side view, Lower Turonian, ODP Site 766A 15R-2 30-32.

21-22 ***Spiroplectinata bettenstaedti*** Grabert.
22. side view, Lower Turonian, ODP Site 766A 15R-2 1-3.
23. side view, Lower Turonain, ODP Site 766A 15R-1 55-57.

23 ***Spiroplectinata complanata*** (Reuss), side view, Lower Turonian, ODP Site 766A 15R-2 30-32.

24-25 ***Gaudryina*** **ex gr** ***dividens*** Grabert
24. side view, Upper Albian, ODP Site 766A 16R-6 110-112.
25. side view, Upper Albian, ODP Site 766A 16R-5 85-87.

Plate 1

1 2 3 4 5

6 7 8 9 10

11 12 13 14 15

16 17 18 19 20

20 um

21 22 23 24 25

Plate 2

1-6 ***Gauryina*** **ex. gr.** ***dividens*** Grabert.
1. side view, Lower Turonian, ODP Site 766A 15R-2 1-3.
2, side view, Upper Albian, ODP Site 766A 16R-CC 7-9.
3. side view, Lower Turonian ODP Site 766A 15R-2 1-3.
4. side view, Lower Turonian ODP Site 766A 15R-2 1-3.
5. side view, Lower Turonian ODP Site 766A 15R-2 1-3.
6. side view, Lower Turonian, ODP Site 766A 15R-1 5-7

7, 8 ***Gaudryina pyramidata*** Cushman
7. side view, Upper Albian, ODP Site 766A 16R-3 135-137.
8. side view, Lower Cenomanian, ODP Site 766A 15R-5 95-97.

9-11 ***Veurneuilina cretacea*** Karrer
9. side view, Lower Turonian ODP Site 766A 15R-2 30-32.
10. side view, Lower Turonian ODP Site 766A 15R-2 30-32.
11. side view, Lower Cenomanian, ODP Site 766A 15R-4 145-147.

12 ***Tritaxia gaultina*** (Morozova), side view, Upper Albian, ODP Site 766A 16R-1 8-10.

13 ***Tritaxia*** **cf.** ***gaultina*** (Morozova), side view, Upper Cenomanian, ODP Site 762C 75X-1 110-111.

14 ***Arenobulimina anglica*** Cushman, side view, Mid-Cenomanian, ODP Site 766A 15R-4 45-47.

15 ***Arenobulimina*** **cf.** ***frankei*** Cushman, side view, Mid-Cenomanian, ODP Site 766A 15R-4 120-121

16-18 ***Remessella*** **sp. 1**
16. side view, Upper Albian, ODP Site 766A 16R-6 35-37.
17. side view, Upper Albian, ODP Site 766A 16R-6 45-47.
18. side view, Upper Cenomanian, ODP Site 762C 75X-1 149-150.

19 ***Dorotha filliformis*** (Berthein), side view, Lower Cenomanian, ODP Site 766A 15R-6 45-47.

20-21 ***Dorothia gradata*** (Berthelin)
20. side view, Upper Albian, 16R-3 135-137.
21. side view, Upper Albian, 16R-1 35-37.

22. ***Dorothia*** **cf.** ***gradata*** (Berthelin), side view, Upper Albian, ODP Site 766A 16R-6 110-112.

23-25 ***Marssonella oxycona*** (Reuss)
23. side view, Lower Cenomanian, ODP Site 766A 15R-5 145-147.
24. side view, Lower Turonian, ODP Site 766A 15R-1 5-7.
25. close up of wall structure, Lower Turonian, ODP Site 766A 15R-1 5-7.
Scale bar 50 μm.

Plate 2

1 2 3 4 5

6 7 8 9 10

11 12 13 14 15

16 17 18 19 20

21 22 23 24 25

Plate 3

1 ***Textularia chapmani*** Lalicker, side view, Upper Cenomanian, Crimea AK 150.

2 ***Quinqueloculina antiqua*** (Franke), side view, Upper Albian, ODP Site 766A 16R-2 85-87.

3 ***Dentalina delicatula*** Cushman, side view, Upper Cenomanian, ODP Site 766A 15R-5 70-72.

4 ***Laevidentalina basiplanata*** (Cushman), side view, Mid-Cenomanian, ODP Site 762C 76X-4 6-8.

5 ***Laevidentalina catenula*** Reuss, side view, Upper Cenomanian, Crimea AK 60.

6 ***Laevidentalina communis*** (d'Orbigny), side view, Upper Cenomanian, Lower Turonian, ODP Site 766A 15R-2 140-142. Scale bar 500 μm

7 ***Laevidentalina cylindroides*** (Reuss), side view, Lower Turonian, ODP Site 766A 15R-1 5-7.

8 ***Laevidentalina gracilis*** (d'Orbigny), side view, Upper Cenomanian, ODP Site 766A 15R-5 95-97.

9-10 ***Laevidentalina nana*** (Reuss)
9. side view, Lower Turonian, ODP Site 766A 14R-5 100-102.
10. side view, Upper Cenomanian, Crimea AK 60.

11-12 ***Laevidentalina oligostega*** (Reuss)
11. side view, Upper Albian, ODP Site 766A 16R-5 135-137
12. side view, Lower Turonian, ODP Site 766A 14R-CC 3-5.

13 ***Laevidentalina*** **sp. cf.** ***L. sororia*** (Reuss), side view, Lower Turonian, ODP Site 766A 14R-CC 3-5.

14 ***Nodosaria aspera*** Reuss, side view, Upper Albian, ODP Site 766A 16R-CC 7-9

15, 20 ***Nodosaria soluta*** Reuss
15. side view, Upper Cenomanian, ODP Site 766A 15R-2 110-112.
20. side view, Lower Turonian, ODP Site 766A 14R-5 100-102.

16 ***Nodosaria*** **sp. 1**, side view, Upper Albian, ODP Site 766A 16R-5 135-137.

17 ***Nodosaria*** **sp. 2**, side view, Lower Turonian, ODP Site 766A 14R-5 100-102

18 ***Pseudonodosaria humilis***, side view, Upper Albian, ODP Site 766A 16R-CC 7-9.

19 ***Pyramidulina sceptrum*** (Reuss), side view, Upper Cenomanian, ODP Site 766A 15R-3 110-112.

21 ***Pyramidulina zippei*** (Reuss), side view, Upper Aptian, ODP Site 766A 16R-7 10-12.

22-23 ***Frondicularia archiaciana*** d'Orbigny
22. side view, Lower Turonian, ODP Site 766A 15R-1 55-57.
23. side view, Upper Cenomanian, ODP Site 766A 15R-4 120-122.

24 ***Lenticulina circumcidanea*** (Berthelin), spiral view, Lower Turonian, ODP Site 766A 14R-5 100-102.

25 ***Lenticulina gaultina*** (Berthelin), spiral view, Lower Turonian, ODP Site 766A 15R-2 1-3.

Plate 3

1 2 3 4 5

6 7 8 9 10

11 12 13 14 15

16 17 18 19 20

21 22 23 24 25

Plate 4

1-3 ***Lenticulina muensteri*** (Roemar)
1. spiral view, Middle Cenomanian, ODP Site 762C 76X-4 57-59.
2. side view, Middle Cenomanian, ODP Site 762C 76X-4 57-59.
3. spiral view, Lower Cenomanian, ODP Site 762C 76X-4 57-59.

4-5 ***Lenticulina pulchella*** (Reuss)
3. spiral view, Upper Cenomanian, ODP Site 766A 15R-4 20-22 .
4. spiral view, Upper Cenomanian, ODP Site 762C 76X-1 97-99.
5. spiral view, Upper Albian, 16R-6 110-112.

6-7 ***Lenticulina rotulata*** Lamarck
6. spiral view, Lower Cenomanian, ODP Site 766A 16R-1 8-10.
7. oblique view, Lower Albian, ODP Site 766A 16R-CC 7-9.

8-10 ***Lenticulina saxocretacea*** Bartenstein
8. spiral view, Lower Turonian, ODP Site 766A 15R-1 130-132.
9. spiral view, Upper Cenomanian, Crimea AK 60.
10. spiral view, Upper Cenomanian, ODP Site 766A 15R-3 35-37.

11-12 ***Lenticulina*** **sp. 1**
11. side view, Lower Turonian, ODP Site 766A 15R-1 130-132
12. side view, Upper Cenomanian, ODPSite 766A 15R-5 95-97

13 ***Marginulinopsis*** **sp. 1**, side view, Upper Albian, ODP Site 766A 16R-3 35-37.

14 ***Saracenaria erlita*** Ludbrook, side view, Upper Cenomanian, Crimea AK 60

15 ***Saracenaria triangularis*** (d'Orbigny), side view, Upper Cenomanian, ODP Site 766A 15R-4 20-22.

16 ***Saracenaria*** **sp. 1**, side view, Upper Albian, ODP Site 766A 16R-3 85-87

17 ***Astacolus calliopsis*** (Reuss), side view, Lower Turonian, ODP Site 766A 14R-CC 4-7.

18 ***Hemirobulina bullata*** (Reuss), side view, Upper Albian, ODP Site 766A 16R-4 85-87.

19 ***Hemirobulina hamulus*** (Chapman), side view, Upper Cenomanian, ODP Site 762C 76X-2 89-91.

20 ***Hemirobulina inaequalis*** (Reuss), side view, Upper Albian, ODP Site 766A 16R-7 10-12.

21 ***Vaginulinopsis harpa*** (Reuss), side view, Lower Cenomanian, ODP Site 766A 16R-1 35-37.

22-23 ***Planularia bradyana*** Chapman, side view, Upper Albian, ODP Site 766A 16R-5 135-137.

24 ***Psilocitharella arguata*** (Reuss), side view, Upper Albian, ODP Site 766A 16R-3 135-137.

25 ***Psilocitharella paucistriata*** (Reuss), side view, Upper Albian, ODP Site 766A 16R-3 85-87.

Plate 4

1 2 3 4 5

6 7 8 9 10

11 12 13 14 15

16 17 18 19 20

21 22 23 24 25

Plate 5

1 *Vaginulina cretacea* Plummer, side view, Upper Albian, ODP Site 766A 16R-5 135-137.

2 *Vaginulina recta* Reuss. side view, Upper Albian, ODP Site 766A 16R-5 135-137.

3 *Lagena globulosa* (Montagu), side view, Lower Cenomanian, ODP Site 766A 16R-1 8-10.

4 *Globulina lacrima* Reuss, side view, Upper Cenomanian, ODP Site 766A 15R-5 95-97.

5 *Globulina prisca* Reuss, side view, Upper Cenomanian, ODP Site 766A 15R-3 110-112

6 *Pyrulina cylindroides* (Roemar), Lower Turonian, ODP Site 766A 15R-1 5-7

7 *Ramulina* **aculaeta**, side view, Upper Albian, ODP Site 766A 16R-6 110-112

8 *Ramulina spandeli*, side view, Lower Cenomanian, ODP Site 766A 16R-2 85-87

9-10 *Ramulina* **sp. 3**
9. side view, Upper Cenomanian, ODP Site 766A 15R-5 20-22
10. side view, Upper Cenomanian, ODP Site 766A 15R-5 20-22

11 *Oolina globosa* Montagu, side view, Upper Cenomanian, ODP Site 766A 15R-4 20-22

12 *Fissurina* **sp. 1**, side view, Upper Cenomanian, ODP 766A 15R-3 110-112

13 *Tricarinella excavata* (Reuss), side view, Upper Cenomanian, ODP Site 766A 15R-3 110-112.

14-15 *Guembelitria cenomana* (Keller).
1. side view, Upper Cenomanian, Crimea AK 60
2. side view, Upper Cenomanian, Crimea AK 60

16 *Heterohelix globulosa* (Ehrenberg), side view, Lower Turonian, ODP Site 766A, 14R-5 50-52.

17 *Heterohelix moremani* (Cushman), side view, Upper Cenomanain, Crimea AK 60.

18 *Heterohelix reussi* (Cushman), side view, Lower Turonian, ODP Site 766, 14R-CC 3-5.

19-20 ***Globigerinelloides bentonensis*** (Morrow),
19. umbilical view, Upper Cenomanian, Crimea AK 60
20. umbilical view, Lower Turonian, 14R-5 100-102.

21-22 ***Globigerinelloides*** **sp. 2**
21. umbilical view, Lower Turonian, ODP Site 766A 15R-1 5-7
22. umbilical view, Lower Turonian, ODP Site 766A 15R-1 5-7

23-24 ***Planomalina buxtorfi***
23. umbilical view, Upper Albian, ODP Site 766A 16R-4 35-37
24. side view, Upper Albian, ODP Site 766A 16R-4 35-37

25. ***Schackoina cenomana*** (Schako), 4 chambered morphotype, umbilical view, Lower Turonian, ODP Site 766A 14R-CC 3-5.

Plate 5

1 2 3 4 5

6 7 8 9 10

11 12 13 14 15

16 17 18 19 20

21 22 23 24 25

Plate 6

1 ***Schackoina cenomana*** (Schako), 4 chambered morphotype, side view, Lower Turonian, ODP Site 766A 14R-CC 3-5.

2 ***Schackoina cenomana*** (Schacko), 3 chambered morphotype, umbilical view, Lower Turonian, ODP Site 766A, 14R-CC 3-5.

3 ***Schackoina cenomana*** (Schacko), 5 chambered morphotype, Lower Turonian, ODP Site 766A, 15R-1 5-7.

4 ***Schackoina multispinata*** (Cushman & Wickenden), umbilical view, Lower Turonian, ODP Site 766A, 14R-CC 3-5.

5 ***Schackoina*** **sp. 1** umbilical view, Lower Turonian, ODP Site 766A, 14R-CC 3-5.

6-8 ***Hedbergella brittonensis*** Loeblich & Tappan.
6. Spiral view, Upper Albian, ODP Site 766A 16R-CC 7-9.
7. Umbilical view, Upper Albian, ODP Site 766A 16R-CC 7-9.
8. Side view, Upper Albian, ODP Site 766A 16R-CC 7-9.

9-10, 14-15 ***Hedbergella delrioensis*** (Carsey)
9. Spiral view, Upper Cenomanian, ODP Site 762C 76X-1 121-123
10. Side view, Upper Albian, ODP Site 766A 16R-CC 7-9.
14. Umbilical view, Upper Albian, ODP Site 766A 16R-CC 7-9.
15. Spiral view, Upper Cenomanian, Crimea AK 60.

11-13 ***Hedbergella planispira*** (Tappan)
11. umbilical view, Lower Turonian, ODP Site 766A 14R-5 50-52
12. side view, Lower Turonian, ODP Site 766A 14R-5 50-52
13. umbilical view, Lower Turonian, ODP Site 766A 15R-1 5-7.

16-19 ***Hedbergella planispira*** (Tappan)
16. spiral view, Lower Turonian, ODP Site 766A 15R-1 5-7
17. side view, Lower Turonian, ODP Site 766A 15R-1 5-7
18. close up, Lower Turonian, ODP Site 766A 15R-1 5-7
19. umbilical view, Lower Turonian, ODP Site 766A 15R-1 5-7

20 ***Hedbergella planispira*** (Tappan) spiral view, Upper Albian, ODP Site 766A 16R-6 35-37.

21-22 ***Hedbergella planispira*** (Tappan)
21. Spiral view, Upper Albian, ODP Site 766A 16R-CC 7-9. Scale bar 50μm.
22. Umbilical view, Upper Albian, ODP Site 766A 16R-CC 7-9. Scale bar 50μm.

23-25 ***Hedbergella simplex*** (Morrow)

23. spiral view, Upper Albian, ODP Site 766A 16R-CC 7-9

24. umbilical view, Upper Albian, ODP Site 766A 16R-CC 7-9

25. spiral view, Lower Turonian, ODP Site 766A 14R-5 119-121

Plate 6

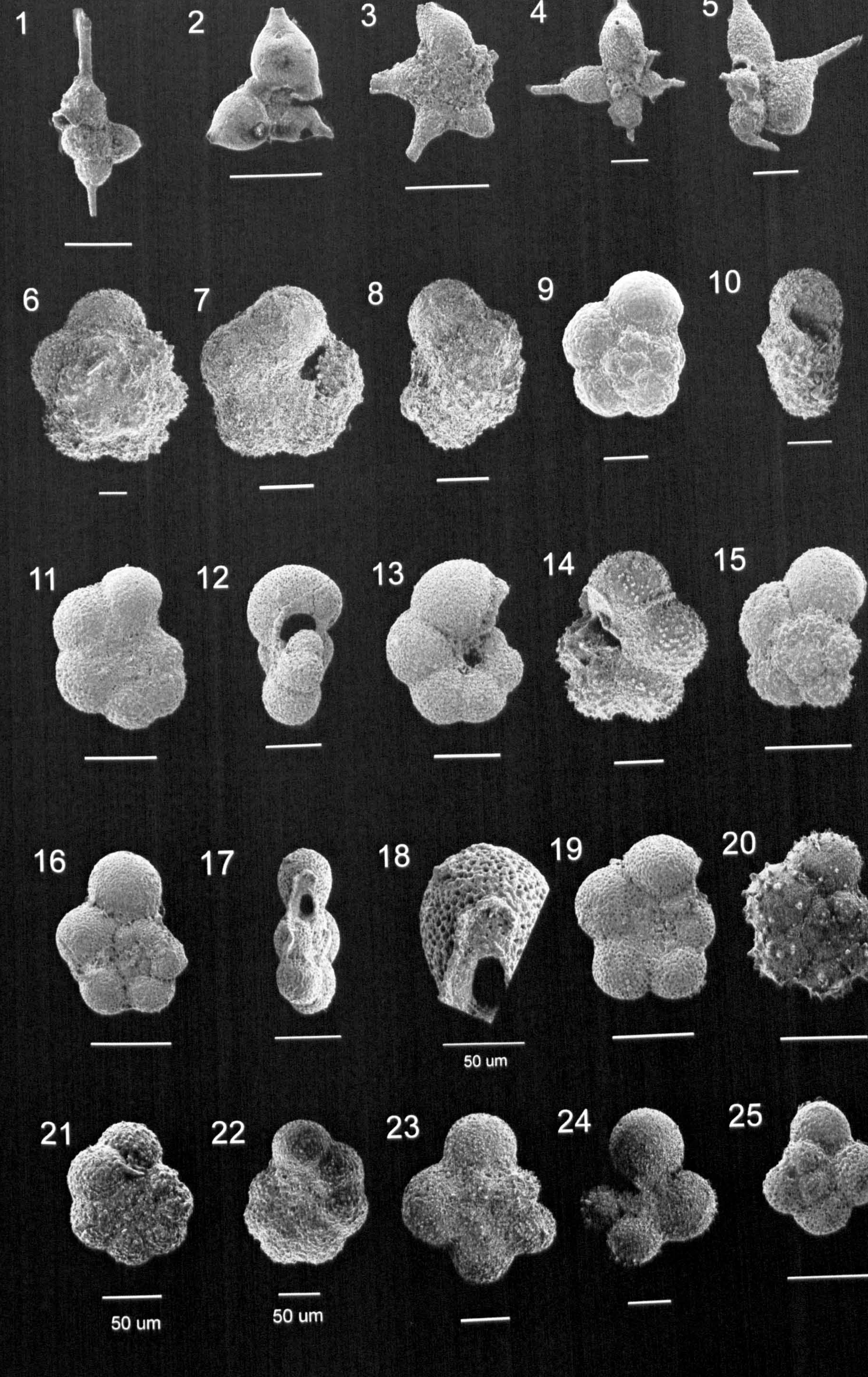

Plate 7

1 ***Hedbergella simplex*** (Morrow) umbilical view, Lower Turonian, ODP Site 766A 14R-5 119-121

2 ***Hedbergella simplicissima*** (Magne and Sigal) spiral view, Upper Albian, ODP Site 766A 16R-6 110-112

3-4 ***Whiteinella archaeocretacea*** Pessagno
3. spiral view, Lower Turonian, ODP Site 766A 15R-1 130-132
4. umbilical view, Lower Turonian, ODP Site 766A 15R-1 130-132

6-7, 11-12 ***Whiteinella baltica*** Douglas and Rankin
6. spiral view, Lower Turonian, ODP Site 766A 15R-2 40-42
7. umbilical view, Lower Turonian, ODP Site 766A 15R-1 130-132
11. spiral side, Lower Turonian, ODP Site 766A 15R-1 130-132
12. umbilical side, Lower Turonian, ODP 766A 15R-2 40-42

5, 9, 10 ***Whiteinella brittonensis*** (Loeblich and Tappan)
5. spiral view, Lower Turonian, ODP Site 766A 14R-5 50-52
9. side view, Lower Turonian, ODP Site 766A 14R-5 50-52
10. umbilical view, Lower Turonian, ODP Site 766A 14R-5 50-52

8, 13 ***Whiteinella hessi***
8. spiral view, Upper Albian, ODP Site 766A 16R-CC 7-9
13. umbilical view, Lower Turonian, ODP Site 766A 14R-5 50-52

14-15 ***Whiteinella paradubia*** (Sigal)
14. spiral view, Upper Albian, ODP Site 762C 76X-4 57-59
15. side view, Upper Albian, ODP Site 762C 76X-4 57-59

16-19 ***Praeglobotruncana aumalensis*** (Sigal)
16. spiral view, Upper Cenomanian, AK 150 Crimea
17. umbilical view, Upper Cenomanina, AK 150, Crimea
18. spiral view, Upper Cenomanian, ODP Site 766 15R-4 20-22
19. umbilical view, Upper Cenomanian, Crimea AK 60

20, 24-25 ***Praeglobotruncana delrioensis*** (Plummer)
20. spiral view, Lower Cenomanian, ODP Site 766A 15R-6 45-47
24. side view, Lower Turonian, ODP Site 766A 14R-5 50-52
umbilical view, Lower Turonian, ODP Site 766A 14R-5 50-52

21-23 ***Praeglobotrunca gibba*** Klaus
21. spiral view, Upper Cenomanian, Crimea AK 60
22. side view, Lower Turonian, ODP Site 766A 15R-1 5-7
23. umbilical view, Upper Cenomanian, Crimea AK 60

Plate 7

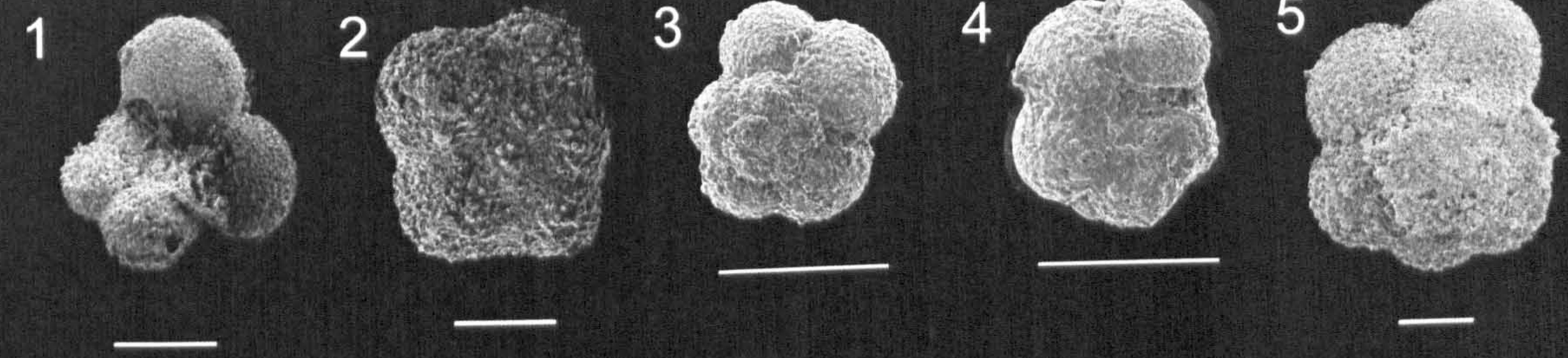

Plate 8

1-2, 6 ***Praeglobotruncana oraviensis*** Schiebnerova
1. spiral view, Lower Turonian, Crimea AK770
2. side view, Lower Turonian, Crimea AK770
6. umbilical view, Lower Turonian, Crimea AK770

3-4 ***Praeglobotruncana inornata*** (Bolli)
3. spiral view, Mid-Cenomanian, ODP Site 762C 75X-3 100-102
4. umbilical view, Mid-Cenomanian, ODP Site 762C 75X-3 100-102

7-9 ***Praeglobotruncana stephani*** (Gandolfi)
7. spiral view, Lower Turonian, ODP Site 766A 14R-5 100-102
8. umbilical view, Lower Turonian, ODP Site 766A 14R-5 100-102
9. spiral view, Upper Cenomanian, Crimea AK60

5, 10, 15 ***Helvetoglobotruncana praehelvetica*** (Trujuillo)
5. spiral view, Upper Cenomanian, ODP Site 766A 15R-6 45-47
10. side view, Lower Turonian, ODP Site 766A 14R-5 50-52
15. umbilical view, Upper Cenomanian, ODP Site 766A 15R-3 110-112

11-13 ***Rotalipora appenninica*** (Renz)
11. spiral view, Upper Albian, ODP Site 766A 16R-2 85-87
12. side view, Upper Albian, ODP Site 766A 16R-2 85-87
13. umbilical view, Upper Albian, ODP Site 766A 16R-2 85-87

14, 18-19 ***Rotalipora brotzeni*** (Sigal)
14. spiral view, Lower Cenomanian, ODP Site 762C 76X-4 57-59
side view, Lower Cenomanian, ODP Site 762C 76X-4 57-59
19. umbilical view, Mid-Cenomanian, ODP Site 766A 15R-4 120-121

16-17 ***Rotalipora cushmani*** (Morrow)
16. spiral view, Upper Cenomanian, Crimea AK 225
17. umbilical view, Upper Cenomanian, Crimea AK 225

20, 24-25 ***Rotalipora deecki*** (Franke)
20. spiral view, Upper Cenomanian, ODP Site 766A 15R-4 20-22
24. side view, Upper Cenomanian, ODP Site 762C 75X-2 26-28
25. umbilical view, Upper Cenomanian, ODP Site 766A 15R-3 110-112

21 ***Rotalipora greenhornensis*** (Morrow), spiral view, Upper Cenomanian, Crimea AK 225

22 ***Rotalipora globotruncanoides*** Sigal, spiral view, Upper Cenomanian, ODP Site 766A 15R-4 120-122

23 ***Rotalipora montsalvensis*** Mornod, spiral view, Upper Cenomanian, ODP Site 766A 15R-6 45-47

Plate 8

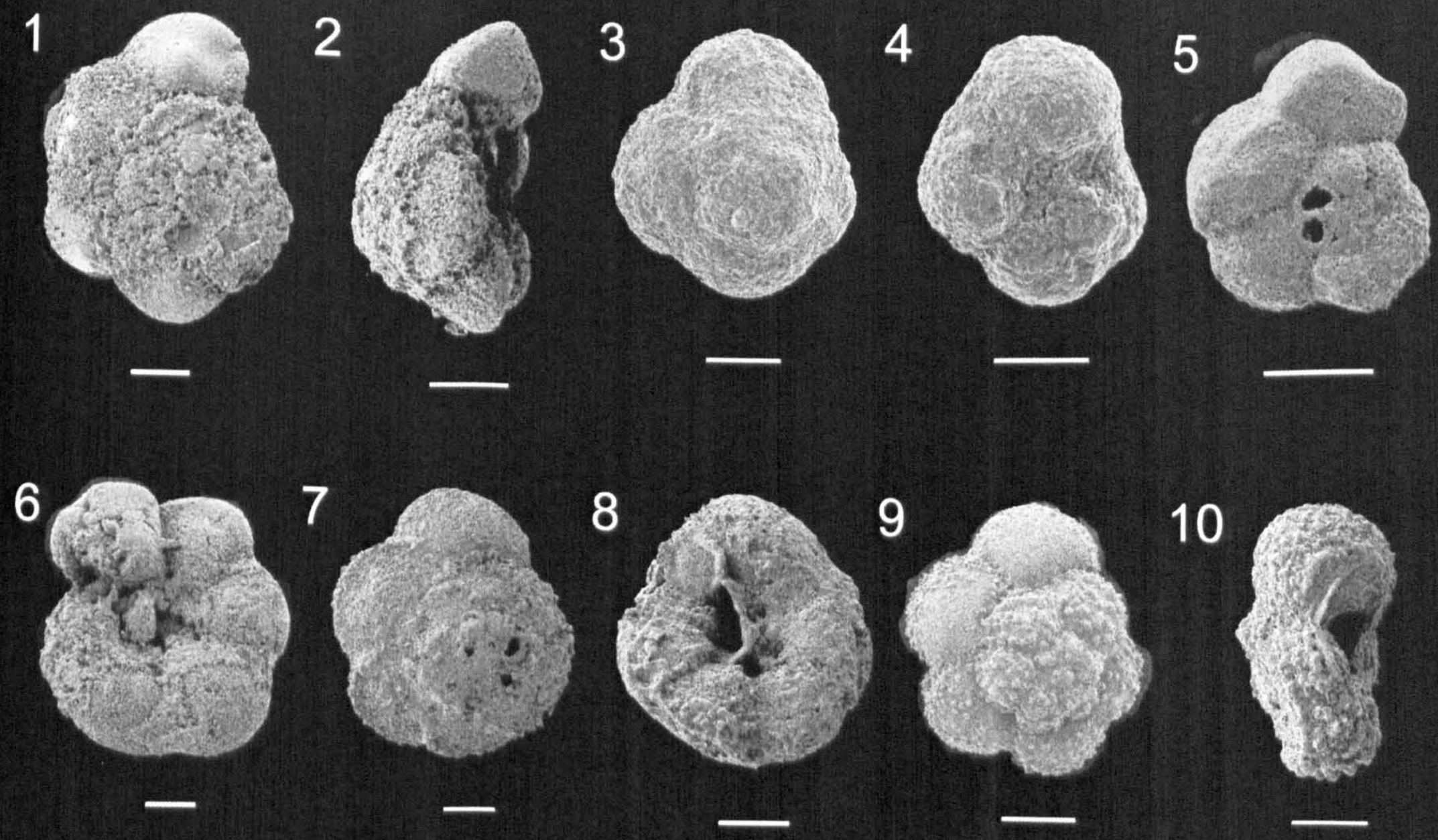

Plate 9

1-3 ***Rotalipora reicheli*** Mornod
1. spiral view, Mid Cenomanian, ODP Site 762C 76X-4 55-57
2. side view, Mid Cenomanian, ODP Site 762C 76X-4 55-57
3. umbilical view, Mid Cenomanian, ODP Site 762C 76X-4 55-57

4-5, 10 ***Rotalipora ticinensis*** (Gandolfi)
4. spiral view, Upper Albian, ODP Site 766A 16R-2 85-87
5. side view, Upper Albian, ODP Site 766A 16R-2 85-87
10. umbilical view, Upper Albian, ODP Site 766A 16R-2 85-87

6-7 ***Dicarinella algeriana*** (Caron)
6. spiral view, Upper Cenomanian, Crimea AK 60
7. umbilical view, Upper Cenomanian, Crimea AK 60

8 ***Dicarinella canaliculata*** (Reuss), oblique side view, Lower Turonian, ODP Site 766A 15R-1 5-7

9 ***Dicarinella elata*** (Lamolda), spiral view, Lower Turonian, Crimea AK 640

11-13 ***Dicarinella hagni*** (Schiebnerova)
11. spiral view, Lower Turonian, ODP Site 766A 15R-1 55-57
12. side view, Lower Turonian, ODP Site 766A 15R-1 55-57
13. umbilical view, Lower Turonian, ODP Site 766A 15R-1 55-57

14-15, 19-20 ***Dicarinella imbricata*** (Mornod)
14. spiral view,
15. spiral view, Lower Turonian, ODP Site 766A 15R-1 55-57
19. side view, Lower Turonian, ODP Site 766A 15R-1 55-57
20. umbilical view, Lower Turonian, ODP Site 766A 15R-1 55-57

16. ***Dicarinella*** **cf.** ***imbricata*** (Mornod), spiral view, Upper Cenomanian, Crimea AK 225

17 ***Marginotruncana*** **cf** ***marianosi*** (Douglas), spiral view, Lower Turonian, ODP Site 766A 15R-1 55-57

18 ***Marginotruncana sigali*** (Reichel), spiral view, Lower Turonian, ODP Site 762C 74X-3 40-41

21 ***Bolivina*** **sp. 1,** side view, Upper Albian, ODP Site 766A 16R-5 10-12

22-23 ***Bolivina*** **sp. 2**
21. side view, Upper Albian, ODP Site 766A 16R-1 110-112
22. side view, Upper Cenomanian, ODP Site 766A 15R-4 20-22

24 ***Bolivinoides*** **sp. 1** side view, Upper Cenomanian, ODP Site 766A 15R-3 110-112

25-26 ***Tappanina*** **cf.** ***lacinosa*** Eicher & Worstell
24. side view, Lower Turonian, ODP Site 766A 15R-1 130-132

Plate 9

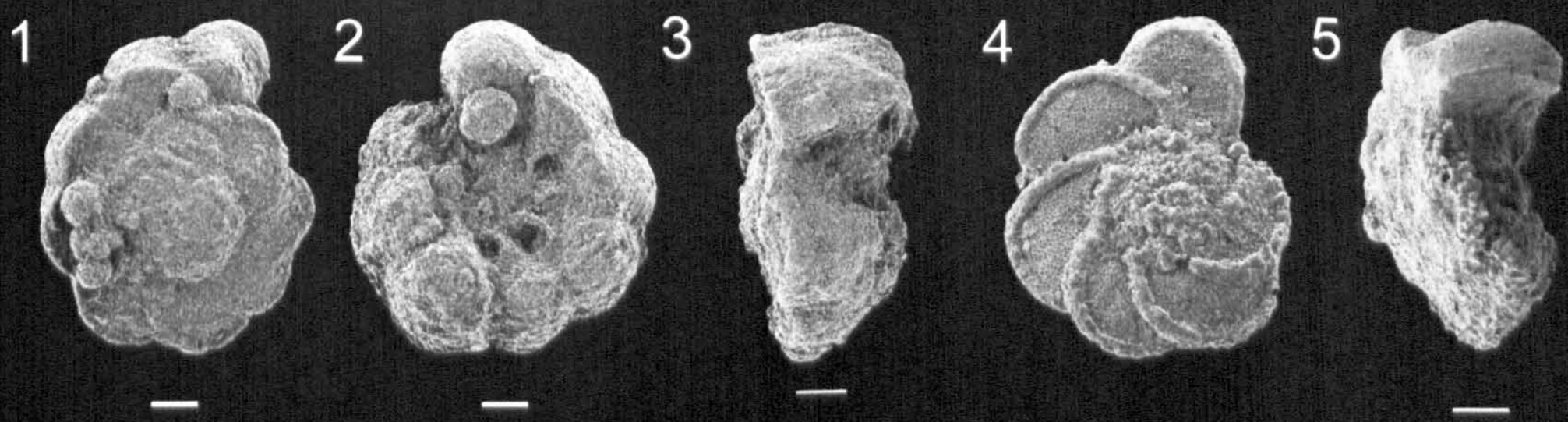

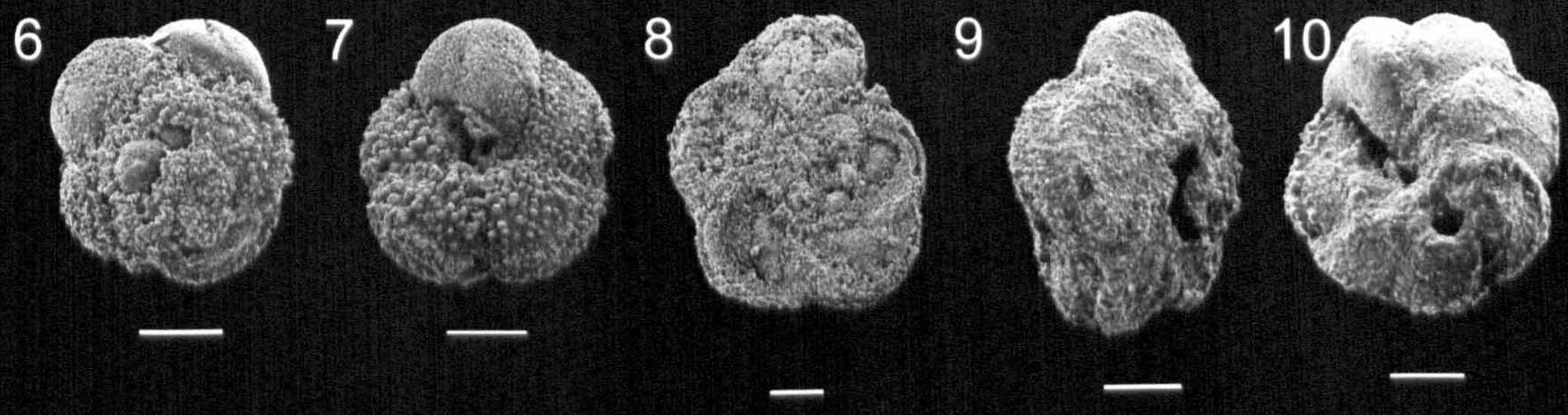

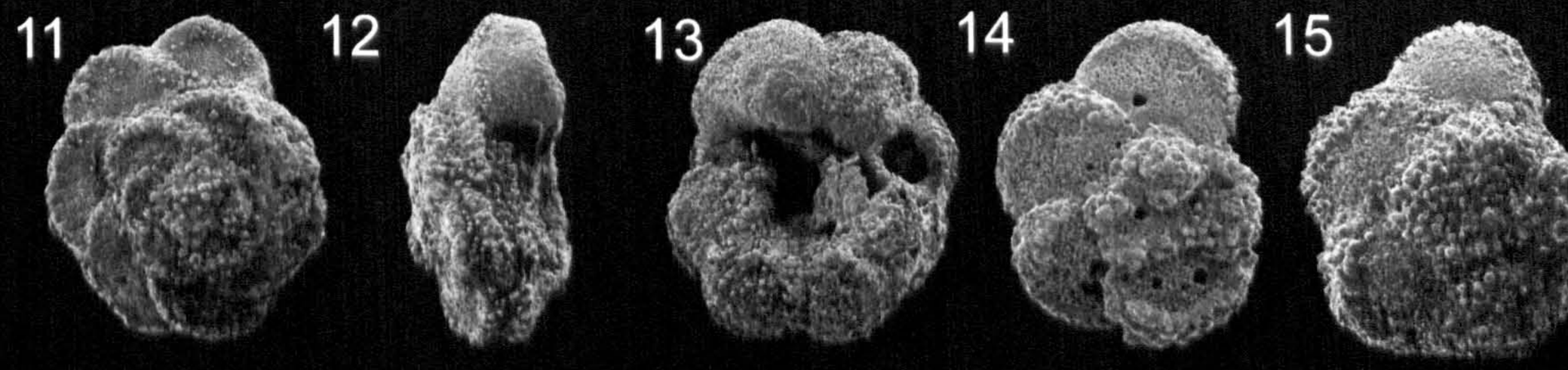

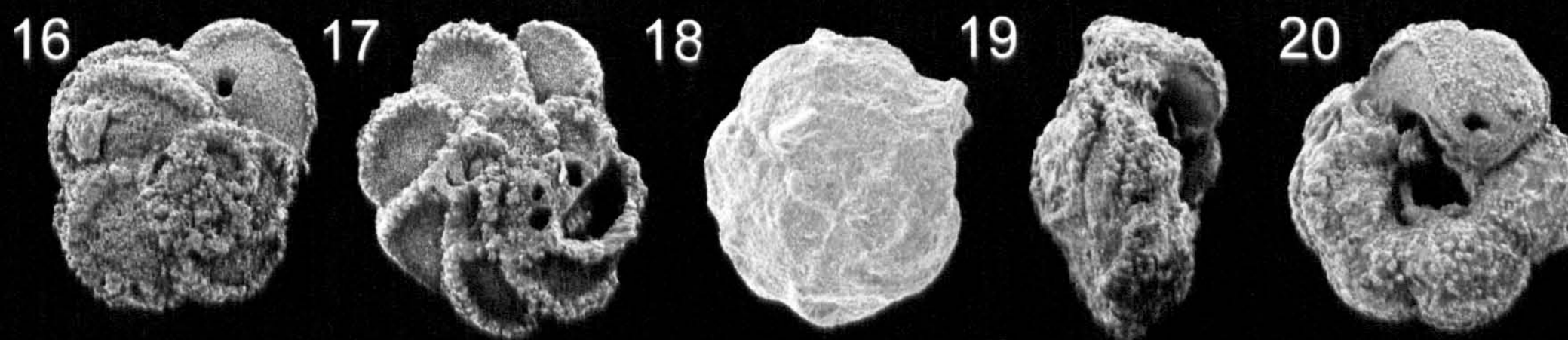

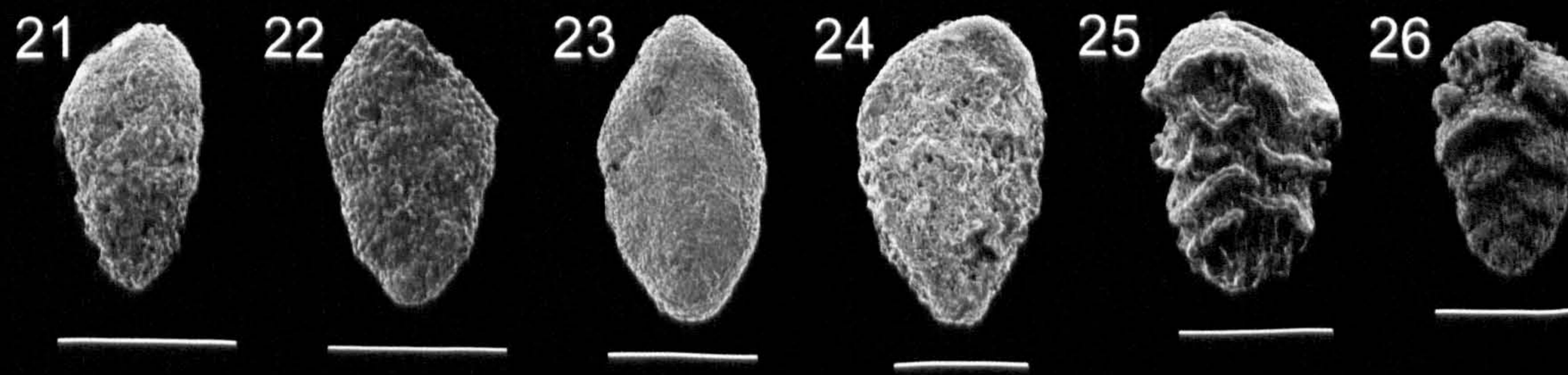

PAGE NUMBERING AS ORIGINAL

Plate 10

1 ***Spirobolivina australis*** Schiebnerova, side view, Upper Cenomanian, ODP Site 766A 16R-1 8-10

2 ***Cuneus* cf. *ludbrookae*** Haig, side view, Upper Cenomanian ODP Site 766A 15R-4 120-121.

3-4 ***Neobulimina australiana*** Ludbrook
3. side view, Upper Cenomanian, ODP Site 766A 15R-4 20-22
4. side view, Upper Albian, ODP Site 766A 16R-7 10-12

5-7 ***Praebulimina nannina*** (Tappan)
5. side view, Lower Turonian, ODP Site 766A 15R-2 1-3
6. side view, Upper Albian, ODP Site 766A 16R-5 135-137
7. side view, Lower Turonian, ODP Site 766A 14R-5 50-52

8-9 ***Praebulimina reussi*** (Morrow)
8. side view, Lower Turonian, ODP Site 766A 15R-1 130-132
9. side view, Lower Turonian, ODP Site 766A 15R-2 1-3

10-11 ***Praebulimina* cf. *reussi*** (Morrow)
10. side view, Upper Albian, ODP Site 766A 16R-5 10-12
11. side view, Upper Albian, ODP Site 766A 16R-5 85-87

12 ***Praebulimina robusta*** (Klasz, Magné & Rérat), side view, Lower Turonian, ODP Site 766A 14R-5 119-121

13-14 ***Praebulimina* sp. 1**
13. side view, Lower Turonian, ODP Site 766A 15R-1 5-7
14. side view, Lower Turonian, ODP Site 766A 15R-1 5-7

15 ***Praebulimina* sp. 2**, side view, Upper Albian, ODP Site 766A 16R-5 135-137

16-19 ***Turrilina evexa*** (Loeblich and Tappan)
16. spiral view, Mid-Cenomanian, ODP Site 766A 16R-1 110-112
17. side view, Upper Albian, ODP Site 766A 16R-5 10-12
18. side view, Upper Cenomanian, ODP Site 762C 76X-1 24-26
19. side view, Upper Albian, ODP Site 766A 16R-3 85-87

20 ***Bulimina fabilis*** (Cushman & Parker), side view, Lower Turonian, ODP Site 766A 14R-5 50-52

21 ***Cassidella* sp. 1**, side view, Lower Turonian, 15R-2 30-32

22 ***Coryphostoma* sp. 1** side view, Upper Albian, ODP Site 766A 16R-6 35-37

23 ***Ellipsodimorphina* sp. 1** side view, Upper Albian, ODP Site 766A 16R-3 8-10

24 ***Ellipsoglandulina*** **sp. 1** side view, Upper Albian, ODP Site 766A 16R-3 8-10

25 ***Nodosarella*** **sp. 1** side view, Lower Cenomanian, ODP Site 766A 15R-2 1-3

Plate 10

1


2


3
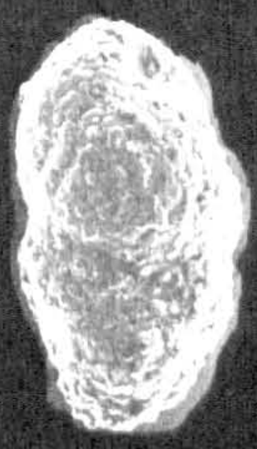

4


5


6


7


8


9


10
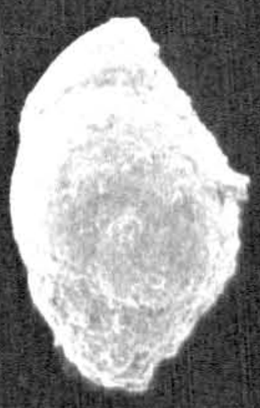

11


12


13


14


15
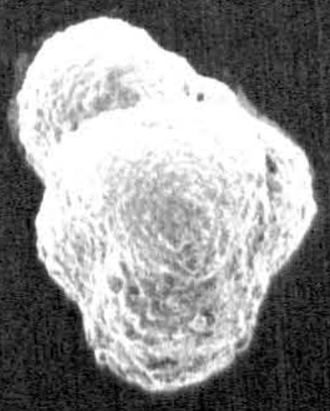

16


17


18


19


20


21


22


23


24
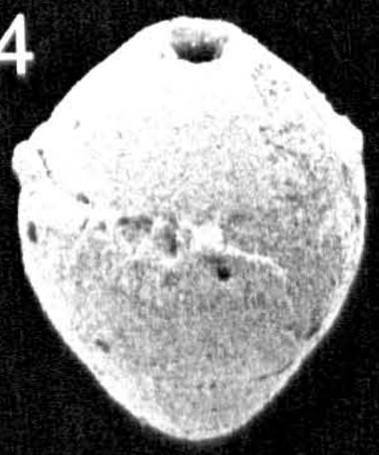

25


Plate 11

1 ***Pleurostomella nitida*** Morrow, side view, Lower Turonian, ODP Site 766A 14R-5 100-102

2-5 ***Pleurostomella reussi*** Berthelin
2. side view, Upper Albian, ODP Site 766A 16R-6 35-37
3. side view, Upper Albian, ODP Site 766A 16R-4 60-62
4. side view, Upper Albian, ODP Site 766A 16R-7 10-12
5. side view, Upper Albian, ODP Site 766A 16R-5 135-137

6-7 ***Pleurostomella subnodosa*** Reuss
6. side view, Lower Turonian, ODP Site 766A 15R-1 5-7
7. close up of aperture, Lower Turonian, ODP Site 766A 15R-1 5-7

8 ***Pleurostomella subnodosa*** Reuss, side view, Lower Turonian, ODP Site 766A 15R-2 30-32

9 ***Pleurostomella*** **sp. 1**, side view, Upper Cenomanian, ODP Site 766A 15R-3 110-112

10 ***Eurycheilostoma? hettgottensis*** (Ludbrook), side view, Upper Cenomanian, ODP Site 766A 15R-3 35-37

11 ***Eurycheilostoma? moorei***, Haig, side view, Upper Cenomanian, ODP Site 766A 16R-1 8-10

12-17 ***Iuliusina grata*** Fuchs
12. 6 chambered morphotype, spiral view, Upper Albian, ODP Site 766A 16R-3 35-37
13. 6 chambered morphotype, umbilical view, Lower Turonian, ODP Site 766A 15R-2 1-3
14. 5 chambered morphotype, spiral view, Lower Turonian, ODP Site 766A 15R-2 1-3
15. 5 chambered morphotype, umbilical view, Lower Turonian, ODP Site 766A 16R-1 110-112
16. 4 chambered morphotype, spiral view, Lower Turonian, ODP Site 766A 15R-2 1-3
17. 4 chambered morphotype, umbilical view, Lower Turonian, ODP Site 766A 15R-2 1-3

18-20, 25 ***Gubkinella*** **sp.1**
18. oblique view, Upper Cenomanian, ODP Site 766A 15R-4 20-22
19. side view, Upper Cenomanian, ODP Site 766A 15R-3 35-37
20. spiral view, Upper Cenomanian, ODP Site 766A 15R-3 35-37
25. oblique umbilical view, Upper Cenomanian, ODP Site 766A 15R-3 35-37

21-22 ***Quadrimorphina allomorphinoides*** (Reuss)
21. spiral view, Upper Albian, ODP Site 766A 16R-5 135-137

22. umbilical view, Upper Albian, ODP Site 766A 16R-5 135-137

23-24 ***Charltonina australis*** Schiebnerová
23. spiral view, Upper Albian, ODP Site 766A 16R-5 135-137
24. umbilical view, Upper Albian, ODP Site 766A 16R-5 135-137

Plate 11

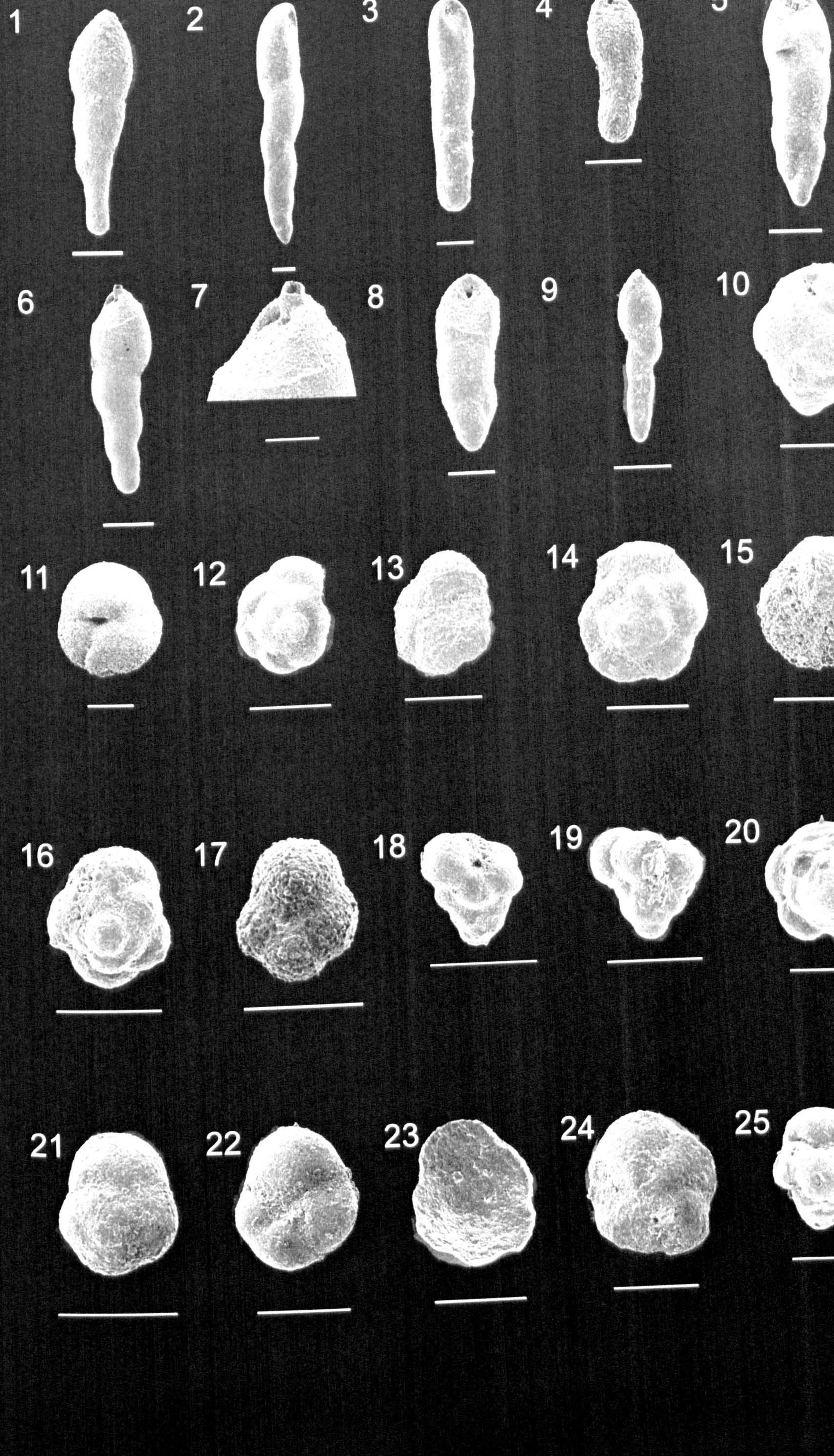

Plate 12

1 ***Charltonina*** **cf.** ***australis*** Schiebnerová, spiral view, Upper Albian, ODP Site 766A 16R-5 135-137

2 ***Charltonina*** **sp. 1**, spiral view, Upper Albian, ODP Site 766A 16R-6 35-37

3-5 ***Conorotalites aptiensis*** (Bettenstaedt)
3. spiral view, Upper Albian, ODP Site 766A 16R-5 10-12
4. umbilical view, Upper Albian, ODP Site 766A 16R-5 10-12
5. oblique spiral view, Upper Albian, ODP Site 766A 16R-5 10-12

6-7 ***Osangularia schloenbachi*** (Reuss)
6. spiral view, Upper Albian, ODP Site 766A 16R-1 8-10
7. umbilical view, Upper Albian, ODP Site 766A 16R-4 60-62

8-10 ***Berthelina berthelini*** (Keller)
8. spiral view, Upper Albian, ODP Site 766A 16R-5 85-87
9. side view, Upper Albian, ODP Site 766A 16R-5 85-87
10. umbilical view, Upper Albian, ODP Site 766A 16R-6 110-112

11-12, 16-17 ***Berthelina*** **cf.** ***berthelini*** (Keller)
11. spiral view, Upper Albian, ODP Site 766A 16R-4 60-62
12. spiral view, Upper Albian, ODP Site 766A 16R-3 135-137
16. umbilical view, Upper Albian, ODP Site 766A 16R-7 10-12
17. oblique side view, Upper Albian, ODP Site 766A 16R-5 135-137

13-18 ***Berthelina cenomanica*** (Brotzen)
13. spiral view, Upper Cenomanian, ODP Site 766A 15R-4 145-147
18. umbilical view, Upper Cenomanian, ODP Site 766A 15R-5 120-122

14-15, 19 ***Berthelina*** **cf.** ***daktoensis*** (Fox)
14. spiral view, Upper Albian, ODP Site 766A 16R-3 85-87
15. side view, Upper Albian, ODP Site 766A 16R-3 35-37
19. umbilical view, Upper Albian, ODP Site 766A 16R-3 35-37

20, 25 ***Berthelina*** **cf.** ***tenuis*** (Bukalova)
20. spiral view, Lower Turonian, ODP Site 766A 15R-1 55-57
25. umbilical view, Lower Turonian, ODP Site 766A 15R-1 55-57

21-22 ***Berthelina*** **cf.** ***tenuissima*** (Gawor-Biedowa)
21. umbilical view, Lower Turonian, ODP Site 766A 15R-2 40-42
22. umbilical view, Upper Cenomanian, Crimea AK 445

23-24 ***Berthelina*** **sp. 2**
23. spiral view, Upper Albian, ODP Site 766A 16R-6 110-112
24. spiral view, Upper Albian, ODP Site 766A 16R-6 110-112

Plate 12

1
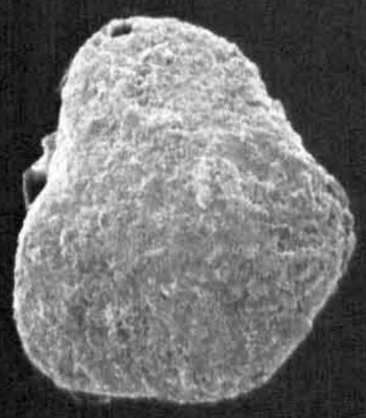

2
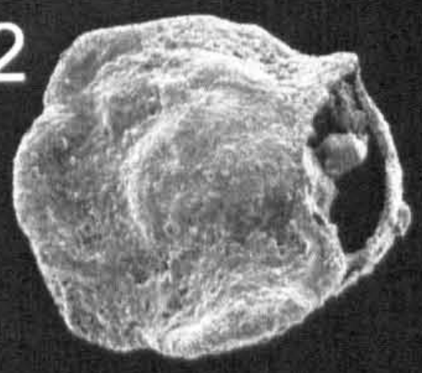

3
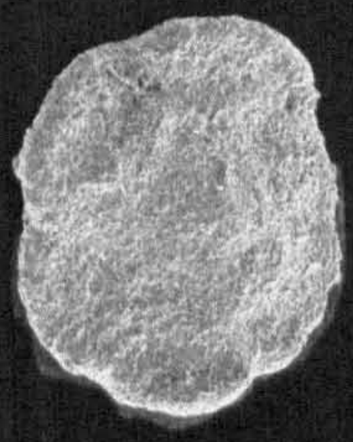

4
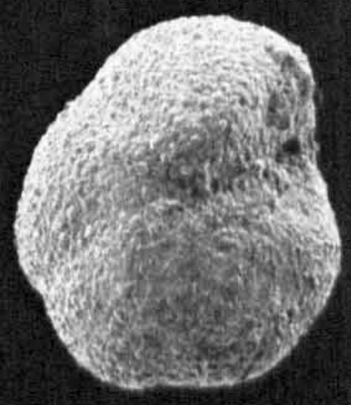

5


6


7
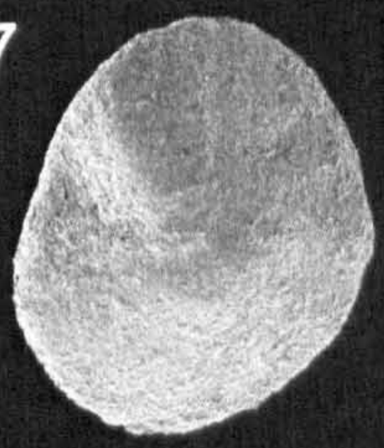

8


9


10
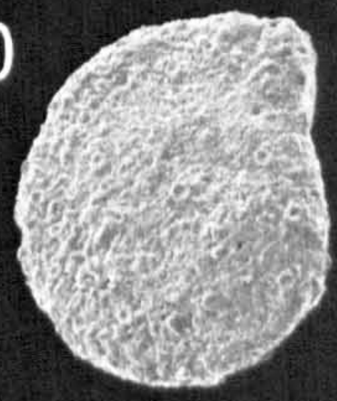

11
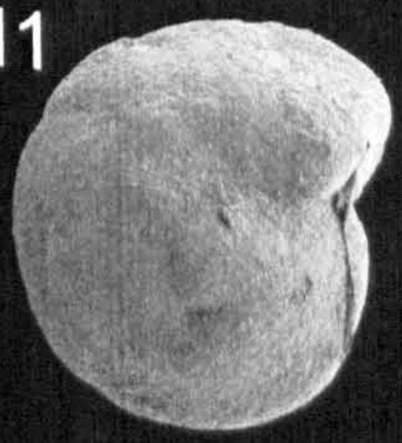

12
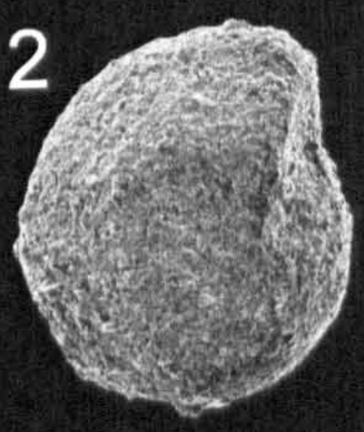

13


14


15


16


17


18


19


20
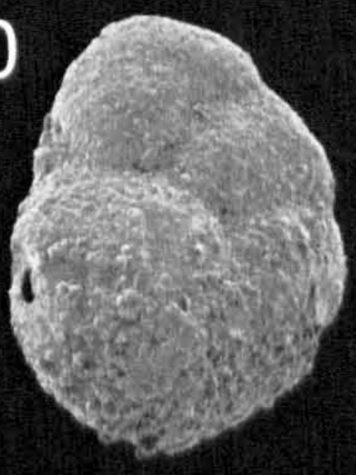

21
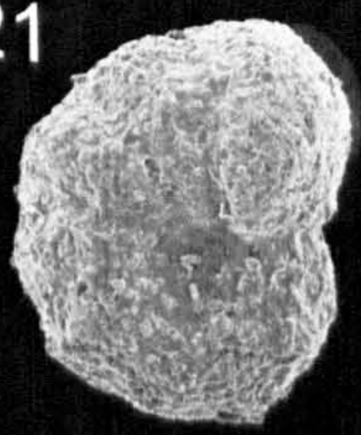

22


23
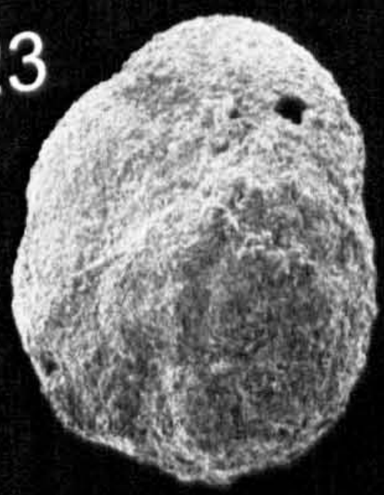

24


25


Plate 13

1 ***Berthelina*** **sp. 2,** umbilical view, Lower Turonian, ODP Site 766A 15R-1 130-132

2-3, 4 ***Berthelina*** **sp. 3**
2. spiral view, Lower Turonian, ODP Site 766A 15R-2 30-32
3. umbilical view, Upper Cenomanian, ODP Site 766A 15R-2 30-32
4. oblique umbilical view, Upper Cenomanian, ODP Site 766A 15R-5 119-121

5-9, 10 ***Gavelinella*** **cf.** ***plummerae*** (Tappan)
5. spiral view, Lower Turonian, ODP Site 766 15R-1 130-132
9. side view, Lower Turonian, ODP Site 766 15R-1 130-132
10. umbilical view, Lower Turonian, ODP Site 766 15R-1 130-132

6-7 ***Gavelinella tormarpensis*** Brotzen
6. spiral view, Lower Turonian, ODP Site 766 15R-1 130-132
7. umbilical view, Upper Albian, ODP Site 766A 16R-7 10-1215R-1 55-57

8, 13 ***Gavelinella*** **sp. 1**
8. spiral view, Lower Turonian, ODP Site 766 15R-1 55-57
13. umbilical view, Lower Turonian, ODP Site 766 15R-1 55-57

11-12 ***Gavelinella*** **sp. 2**
11. spiral view, Upper Cenomanian, Crimea AK 225
12. umbilical view, Upper Cenomanian, Crimea AK 225

14-15 ***Gavelinella*** **sp. 3**
14. spiral view, Upper Cenomanian, ODP Site 766A 15R-3 110-112
15. umbilical view, Upper Cenomanian, ODP Site 766A 15R-3 110-112

16 ***Gavelinella*** **sp. 4,** umbilical view, Upper Albian, ODP Site 766A 16R-7 10-12

17-18 ***Gavelinella*** **sp. 5**
17. spiral view, Upper Cenomanian, ODP Site 762C 75X-2 95-97
18. umbilical view, Upper Cenomanian, ODP Site 762C 75X-2 95-97

19 ***Gavelinella*** **sp. 6,** spiral view, Lower Turonian, ODP Site 766A 14R-5 100-102

20 ***Lingulogavelinella albiensis*** Malapris, spiral view, Upper Cenomanian, ODP Site 766 15R-5 70-72

21 ***Lingulogavelinella indica*** Schiebnerová, umbilical view, Upper Cenomanian, ODP Site 766A 15R-5 20-22

22-23 ***Lingulogavelinella newtoni*** (Eicher & Worstell)
22. umbilical view, Upper Cenomanian, ODP Site 766A 15R-3 110-112
23. spiral view, Lower Turonian, ODP Site 766A 15R-2 1-3

24 ***Lingulogavelinella*** **sp. 1** umbilical view, Lower Turonian, ODP Site 766A 15R-2 1-3

25 ***Anomalina? santoodnae*** Ludbrook, umbilical view, Lower Turonian, ODP Site 766A 15R-2 1-3

Plate 13

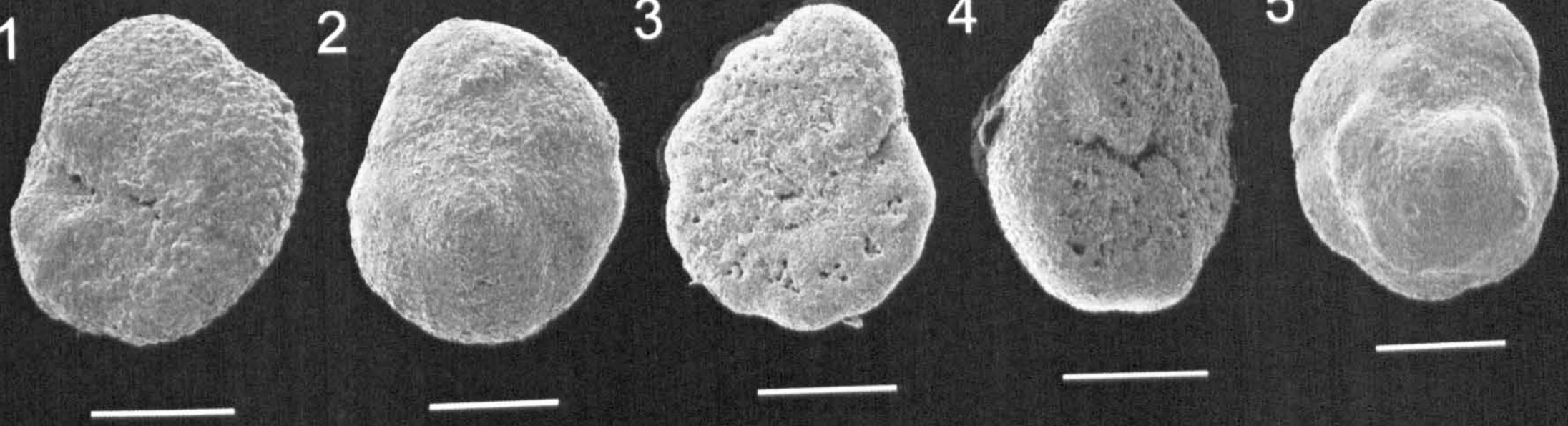

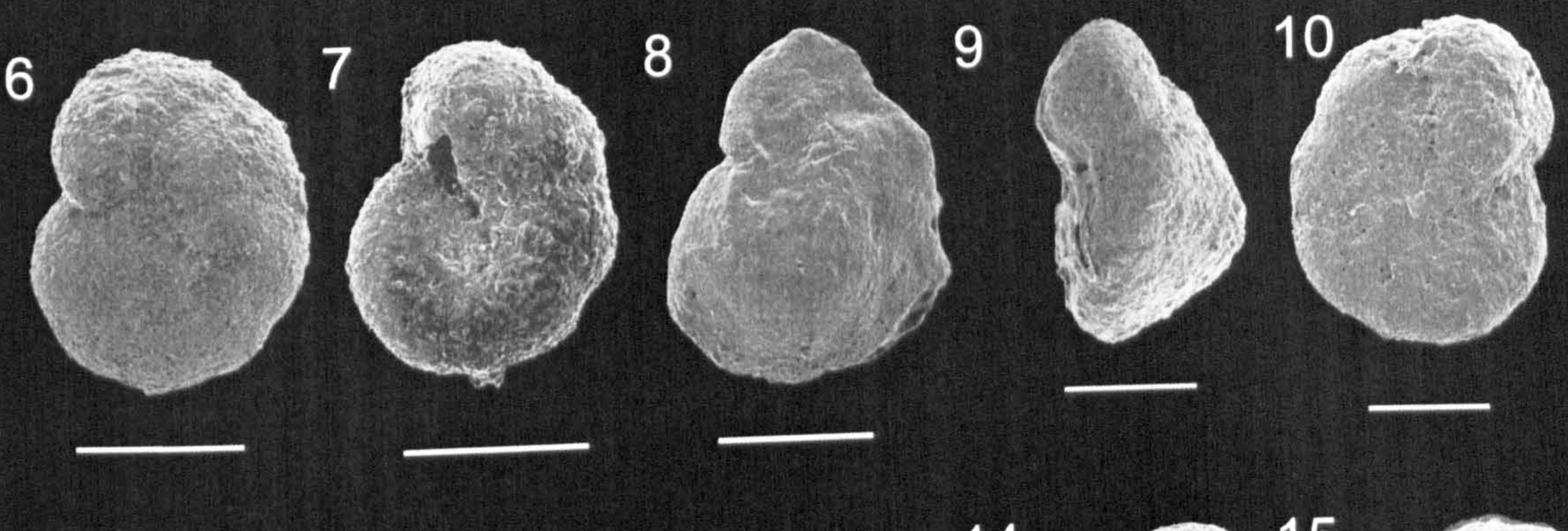

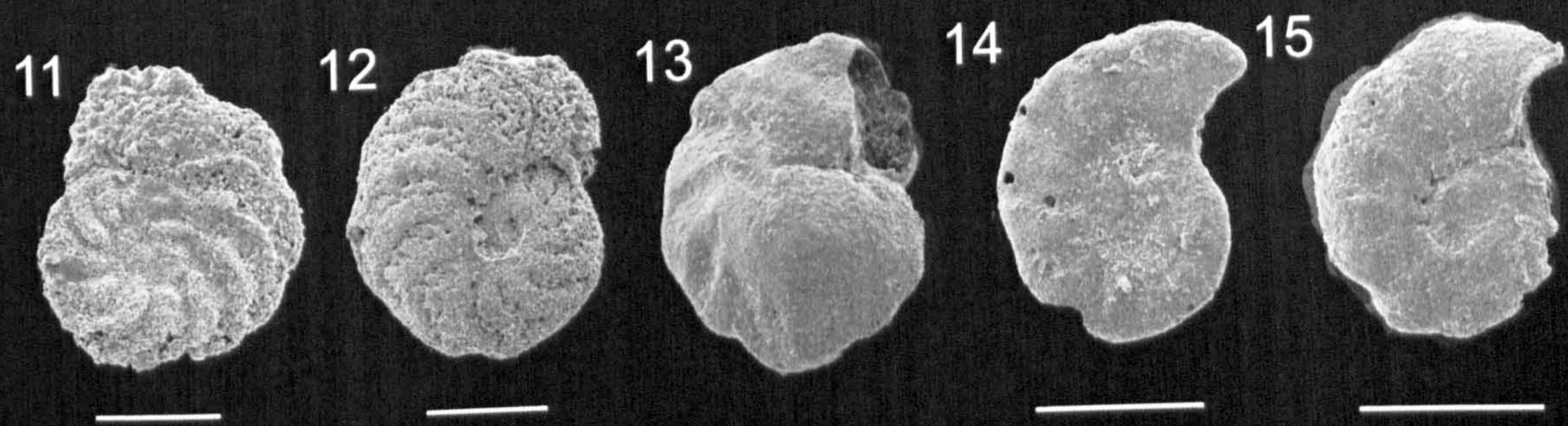

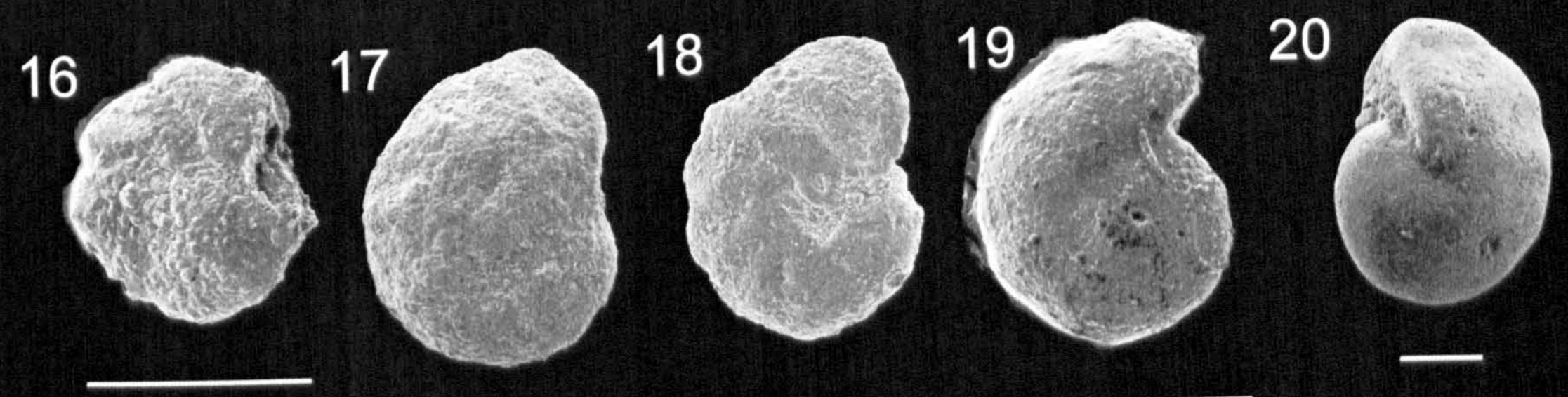

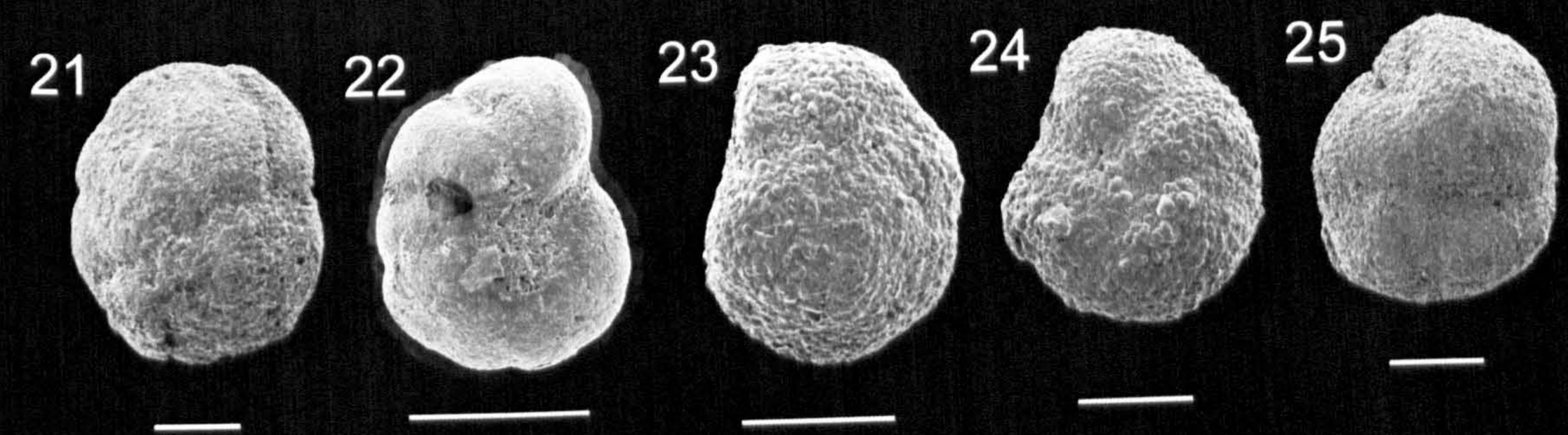

Plate 14

1-3 ***Gyroidinoides infracretacea*** Morozova
1. umbilical view, Upper Albian, ODP Site 766A 16R-6 35-37
2. side view, Mid Cenomanian, ODP Site 766A 16R-1 8-10
3. umbilical view, Upper Albian, ODP Site 766A 16R-5 10-12

4-5, 10 ***Gyroidinoides infracretacea*** Morozova
4. umbilical view, Upper Albian, ODP Site 766A 16R-5 10-12
5. oblique side view, Upper Albian, ODP Site 766A 16R-3 85-87
10. spiral view, Upper Albian, ODP Site 766A 16R-3 85-87

6-7 ***Gyroidinoides infracretacea*** Morozova **large ap flap**
6. umbilical view, Upper Albian, ODP Site 766A 16R-5 10-12
7. side view, Upper Albian, ODP Site 766A 16R-5 10-12

8-9 ***Gyroidinoides infracretacea*** Morozova **Crimea**
8. umbilical view, Upper Cenomanian, Crimea AK 60
9. side view, Upper Cenomanian, Crimea AK 60

11-13 ***Gyroidinoides infracretacea***
11. umbilicial view, Lower Turonian, ODP Site 766A 15R-2 1-3
12. side view, Lower Turonian, ODP Site 766A 15R-2 1-3
13. spiral view, Lower Turonian, ODP Site 766A 15R-2 1-3

14-15, 20 ***Gryroidinoides*** **sp.1**
14. umbilical view, Upper Albian, ODP Site 766A 16R-5 135-137
15. side view, Upper Albian, ODP Site 766A 16R-5 135-137
20. spiral view, Upper Albian, ODP Site 766A 16R-5 85-87

16-17 ***Gyroidinoides*** **sp. 2**
16. umbilical view, Lower Albian, ODP Site 766A 16R-4 85-87
17. side view, Lower Albian, ODP Site 766A 16R-4 60-62

18-19 ***Gyroidinoides*** **sp. 3**
18. umbilical view, Lower Albian, ODP Site 766A 16R-4 85-87
19. umbilical view, Lower Albian, ODP Site 766A 16R-7 10-12

21 ***Gyroidinoides*** **sp. 4**, Lower Albian, ODP Site 766A 16R-6 35-37

22-23 ***Valvulineria gracillima*** Ten Dam
22. umbilical view, Mid-Cenomanian ODP Site 762 76X-3 9-11
23. broken umbilical view, Upper Albian, ODP Site 766A 16R-7 10-12

24-25 ***Valvulineria gracillima*** Ten Dam
24. umbilical view, Upper Albian, ODP Site 766A 16R-1 110-112
25. spiral view, Lower Turonian, ODP Site 766A 15R-2 30-32

Plate 14

1
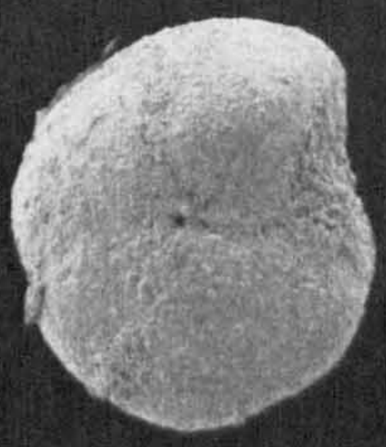

2
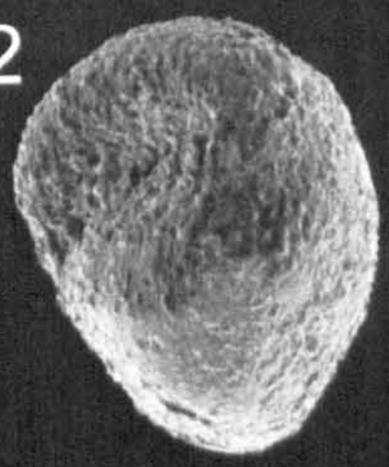

3


4


5


6


7
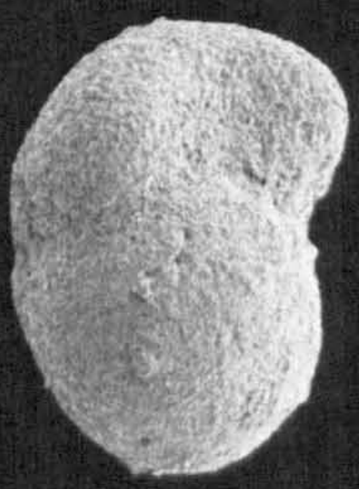

8
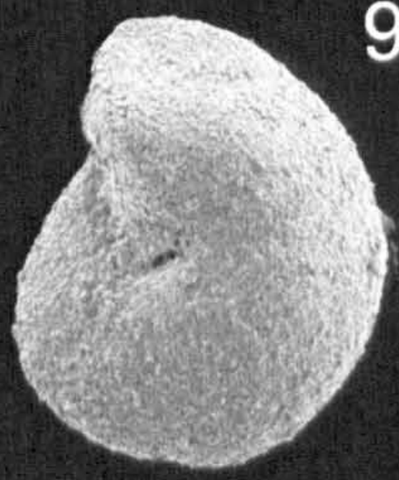

9


10
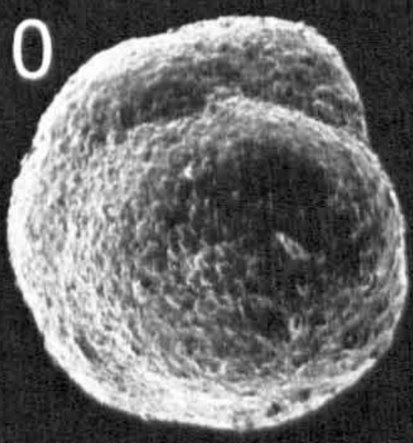

11
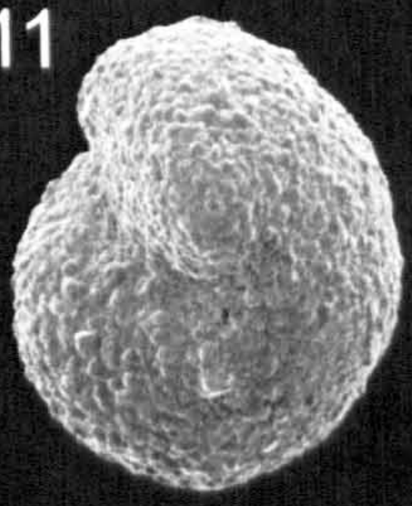

12
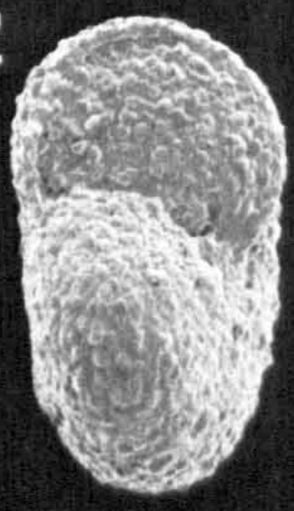

13
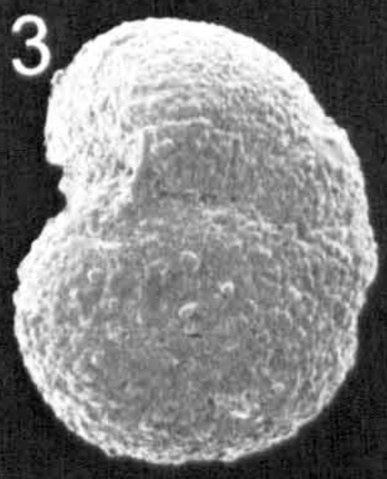

14


15


16


17


18


19


20


21
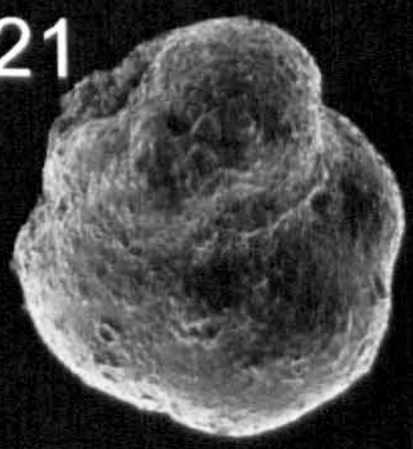

22
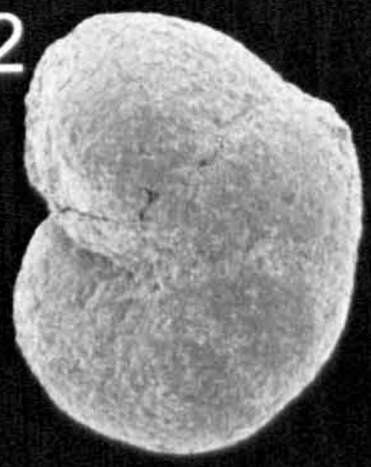

23
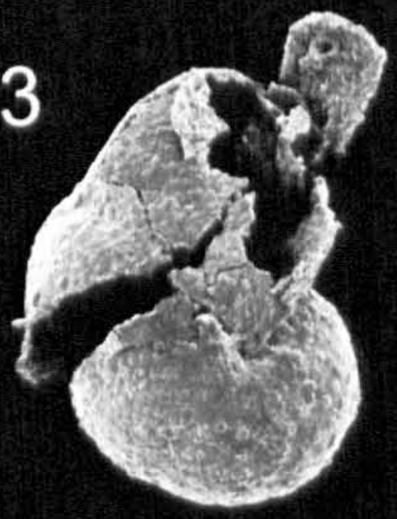

24
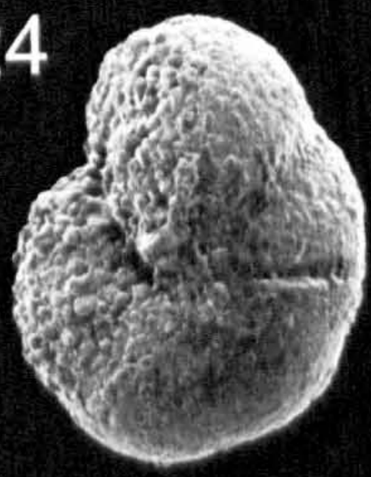

25


Plate 15

1 *Valvulineria lenticula* (Reuss) umbilical view, Lower Turonian, ODP Site 766A 15R-2 1-3

2 *Valvulineria* **sp. 1**, umbilical view, Upper Cenomanian, ODP Site 766A 15R-5 70-72

3-5 ***Schiebnerova proindica*** Quilty
3. spiral view, Upper Albian, ODP Site 766A 16R-4 85-87
4. side view, Upper Albian, ODP Site 766A 16R-3 35-37
5. umbilical view, Upper Albian, ODP Site 766A 16R-3 8-10

Plate 15

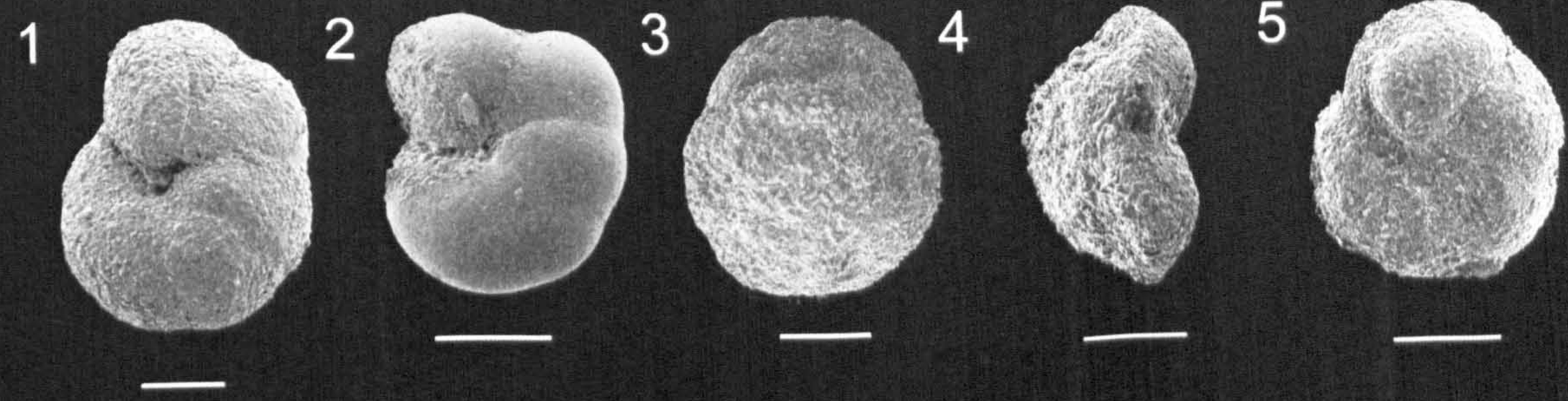

Appendix 2

Foraminiferal Count Sheets

Foraminiferal Count Sheets of all > 63µm samples picked from ODP Site 766

P = present in sample

Samples (Core, section, interval)	mbsf	Rhizammina spp.	Psammosphaera fusca	Hippocrepina gracilis	Glomospira charoides	Glomospira irregularis	Glomospirella gaultina	Reophax sp. 2	Ammosphaeroidina sp. 1	Spiroplectinella gandolfi	Spiroplectinella sp. 1	Eggerellina manae	Spiroplectinata annectans	Spiroplectinata bettenstaedti	Spiroplectinata complanata	Gaudryina ex. gr. dividens	Gaudryina pyramidata	Verneuilina cretacea	Tritaxia gaultina	Tritaxia sp. cf. T. gaultina	Arenobulimina anglica	Arenobulimina cf. frankei	Remesella sp. 1
123-766C-14R-4 149-151	129.59																						
123-766C-14R-5 1-3	129.61																						
123-766C-14R-5 25-27	129.85																						
123-766C-14R-5 50-52	130.10																						
123-766C-14R-5 75-77	130.35																						
123-766C-14R-5 100-102	130.60																			6			
123-766C-14R-5 119-121	130.79															1	12	4					
123-766C-14R-CC 3-5	130.88																						
123-766C-15R-1 5-7	133.25				1										1	3	6	4					
123-766C-15R-1 30-32	133.50																						
123-766C-15R-1 55-57	133.75													7		2		2		15			
123-766C-15R-1 80-82	134.00																						
123-766C-15R-1 105-107	134.25																						
123-766C-15R-1 130-132	134.50	1												1		22		3		9			
123-766C-15R-2 1-3	134.71													2		31		2		34			
123-766C-15R-2 10-12	134.80																						
123-766C-15R-2 20-22	134.90																						
123-766C-15R-2 30-32	135.00										1		2		1		5	15					
123-766C-15R-2 40-42	135.10	6										4			1					11			
123-766C-15R-2 50-52	135.20																						
123-766C-15R-2 60-62	135.30																						
123-766C-15R-2 70-72	135.40	BARREN																					
123-766C-15R-2 80-82	135.50	BARREN																					
123-766C-15R-2 90-92	135.60	BARREN																					
123-766C-15R-2 100-102	135.70	BARREN																					
123-766C-15R-2 110-112	135.80	BARREN																					
123-766C-15R-2 120-122	135.90																						
123-766C-15R-2 130-132	136.00																						
123-766C-15R-2 140-142	136.10																						
123-766C-15R-3 10-12	136.30																						
123-766C-15R-3 35-37	136.55				1				1		2	7				6	4	2	4				
123-766C-15R-3 58-60	136.78																						
123-766C-15R-3 85-87	137.05																						
123-766C-15R-3 110-112	137.30																3	2				1	
123-766C-15R-4 20-22	137.90								1		1						7		2				
123-766C-15R-4 45-47	138.15				2						1	6				1	10		4		2		
123-766C-15R-4 70-72	138.40																						
123-766C-15R-4 95-97	138.65																						
123-766C-15R-4 120-122	138.90				1				1		2	3				3	8		4			2	2
123-766C-15R-4 145-147	139.15	11	11		1							2				3	7	3	1				
123-766C-15R-5 20-22	139.40	P															P						
123-766C-15R-5 45-47	139 65																						
123-766C-15R-5 70-72	139.90										1	1				2	4		2				1
123-766C-15R-5 95-97	140.15		5						3		6	6				3	6		2			5	
123-766C-15R-5 120-122	140.40								2		6	1					16						
123-766C-15R-5 145-147	140.65		10							3		1					22						
123-766C-15R-6 20-22	140.90																						
123-766C-15R-6 45-47	141.15																						
123-766C-16R-1 8-10	142.98	1	2						3		2	4				1	16		6			4	1
123-766C-16R-1 35-37	143 25	1	2		1				1	3		8					13		5			1	

Samples (Core, section, interval)	mbsf	Dorothia filiformis	Dorothia gradata	Dorothia cf. gradata	Marssonella oxycona	Textularia chapmani	Quinqueloculina antiqua	Dentalina delicatula	Laevidentalina basiplanata	Laevidentalina communis	Laevidentalina cylindroides	Laevidentalina gracilis	Laevidentalina nana	Laevidentalina oligostega	Laevidentalina sp. cf. L. sona	Nodosaria aspera	Nodosaria soluta	Nodosaria sp. 1	Nodosaria sp. 2	Pseudonodosaria humilis	Pyramidulina sceptrum	Pyramidulina zippei	Frondicularia archiaciana	Lenticulina circumcidanea
123-766C-14R-4 149-151	129.59																							
123-766C-14R-5 1-3	129.61																							
123-766C-14R-5 25-27	129.85																							
123-766C-14R-5 50-52	130.10																							
123-766C-14R-5 75-77	130.35																							
123-766C-14R-5 100-102	130.60									1			1				1		1					1
123-766C-14R-5 119-121	130.79														3									
123-766C-14R-CC 3-5	130.88											1	1	1	1		1							
123-766C-15R-1 5-7	133.25				3						1									1				
123-766C-15R-1 30-32	133.50																							
123-766C-15R-1 55-57	133.75				4																		1	
123-766C-15R-1 80-82	134.00																							
123-766C-15R-1 105-107	134.25																							
123-766C-15R-1 130-132	134.50																							
123-766C-15R-2 1-3	134.71																							
123-766C-15R-2 10-12	134.80																							
123-766C-15R-2 20-22	134.90																							
123-766C-15R-2 30-32	135.00																							
123-766C-15R-2 40-42	135.10																							
123-766C-15R-2 50-52	135.20																							
123-766C-15R-2 60-62	135.30																							
123-766C-15R-2 70-72	135.40																							
123-766C-15R-2 80-82	135.50																							
123-766C-15R-2 90-92	135.60																							
123-766C-15R-2 100-102	135.70																							
123-766C-15R-2 110-112	135.80																							
123-766C-15R-2 120-122	135.90																							
123-766C-15R-2 130-132	136.00																							
123-766C-15R-2 140-142	136.10									P														
123-766C-15R-3 10-12	136.30																							
123-766C-15R-3 35-37	136.55				1									1										
123-766C-15R-3 58-60	136.78				P																			
123-766C-15R-3 85-87	137.05																							
123-766C-15R-3 110-112	137.30																1				1			
123-766C-15R-4 20-22	137.90				8	1																		
123-766C-15R-4 45-47	138.15				18													1						
123-766C-15R-4 70-72	138.40																							
123-766C-15R-4 95-97	138.65																							
123-766C-15R-4 120-122	138.90	1			3	1																	1	
123-766C-15R-4 145-147	139.15				5																			
123-766C-15R-5 20-22	139.40																P							
123-766C-15R-5 45-47	139 65																							
123-766C-15R-5 70-72	139.90				1			1																
123-766C-15R-5 95-97	140.15			1								2												
123-766C-15R-5 120-122	140.40			1	9																			
123-766C-15R-5 145-147	140.65				4																			
123-766C-15R-6 20-22	140.90																							
123-766C-15R-6 45-47	141.15	1																						
123-766C-16R-1 8-10	142.98		9															1						
123-766C-16R-1 35-37	143 25		11	4										1										

Samples (Core, section, interval)	mbsf	Lenticulina gaultina	Lenticulina muensteri	Lenticulina pulchella	Lenticulina rotulata	Lenticulina saxocretacea	Lenticulina sp. 1	Marginulinopsis sp. 1	Saracenaria erlita	Saracenaria triangularis	Saracenaria sp. 1	Astacolus calliopsis	Hemirobulina bullata	Hemirobulina inaequalis	Vaginulinopsis harpa	Planularia bradyana	Psilocitharella arguta	Psilocitharella paucistriata	Vaginulina cretacea	Vaginulina recta	Lagena globulosa	Globulina lacrima	Globulina prisca
123-766C-14R-4 149-151	129.59																						
123-766C-14R-5 1-3	129.61																						
123-766C-14R-5 25-27	129.85																						
123-766C-14R-5 50-52	130.10																						
123-766C-14R-5 75-77	130.35																						
123-766C-14R-5 100-102	130.60	1			1										1	1							
123-766C-14R-5 119-121	130.79																						1
123-766C-14R-CC 3-5	130.88											1											
123-766C-15R-1 5-7	133.25						2																
123-766C-15R-1 30-32	133.50																						
123-766C-15R-1 55-57	133.75																						
123-766C-15R-1 80-82	134.00																						
123-766C-15R-1 105-107	134.25																						
123-766C-15R-1 130-132	134.50					1	1																
123-766C-15R-2 1-3	134.71	1																					
123-766C-15R-2 10-12	134.80																						
123-766C-15R-2 20-22	134.90																						
123-766C-15R-2 30-32	135.00															1							
123-766C-15R-2 40-42	135.10																						
123-766C-15R-2 50-52	135.20																						
123-766C-15R-2 60-62	135.30																						
123-766C-15R-2 70-72	135.40																						
123-766C-15R-2 80-82	135.50																						
123-766C-15R-2 90-92	135.60																						
123-766C-15R-2 100-102	135.70																						
123-766C-15R-2 110-112	135.80																						
123-766C-15R-2 120-122	135.90																						
123-766C-15R-2 130-132	136.00																						
123-766C-15R-2 140-142	136.10																						
123-766C-15R-3 10-12	136.30																						
123-766C-15R-3 35-37	136.55					1																	
123-766C-15R-3 58-60	136.78																						
123-766C-15R-3 85-87	137.05																						
123-766C-15R-3 110-112	137.30																						1
123-766C-15R-4 20-22	137.90			1						1													
123-766C-15R-4 45-47	138.15																1						
123-766C-15R-4 70-72	138.40																						
123-766C-15R-4 95-97	138.65																						
123-766C-15R-4 120-122	138.90																						
123-766C-15R-4 145-147	139.15		1																				
123-766C-15R-5 20-22	139.40																						
123-766C-15R-5 45-47	139 65																						
123-766C-15R-5 70-72	139.90		1																				
123-766C-15R-5 95-97	140.15						1															1	
123-766C-15R-5 120-122	140.40																						
123-766C-15R-5 145-147	140.65															1							
123-766C-15R-6 20-22	140.90																						
123-766C-15R-6 45-47	141.15																						
123-766C-16R-1 8-10	142.98				1											1					1		
123-766C-16R-1 35-37	143 25		1												1								

Samples (Core, section, interval)	123-766C-16R-1 60-62	123-766C-16R-1 85-87	123-766C-16R-1 110-112	123-766C-16R-1 135-137	123-766C-16R-2 10-12	123-766C-16R-2 35-37	123-766C-16R-2 60-62	123-766C-16R-2 85-87	123-766C-16R-2 110-112	123-766C-16R-2 135-137	123-766C-16R-3 8-10	123-766C-16R-3 35-37	123-766C-16R-3 60-62	123-766C-16R-3 85-87	123-766C-16R-3 110-112	123-766C-16R-3 135-137	123-766C-16R-4 10-12	123-766C-16R-4 35-37	123-766C-16R-4 60-62	123-766C-16R-4 85-87	123-766C-16R-4 110-112	123-766C-16R-4 135-137	123-766C-16R-5 10-12	123-766C-16R-5 35-37	123-766C-16R-5 60-62	123-766C-16R-5 85-87	123-766C-16R-5110-112	123-766C-16R-5 135-137	123-766C-16R-6 10-12	123-766C-16R-6 35-37	123-766C-16R-6 60-62	123-766C-16R-6 85-87	123-766C-16R-6 110-112	123-766C-16R-6 135-137	123-766C-16R-7 10-12	123-766C-16R-CC 7-9
mbsf	143.50	143.75	144.00	144.25	144.50	144.75	145.00	145.25	145.50	145.75	145.98	146.25	146.50	146.75	147.00	147.25	147.50	147.75	148.00	148.25	148.50	148.75	149.00	149.25	149.50	149.75	150.00	150.25	150.50	150.75	151.00	151.25	151.50	151.75	152.00	152.16
Rhizammina spp.																												1		1			2		1	
Psammosphaera fusca			7																				1					1								
Hippocrepina gracilis																														1						
Glomospira charoides																			1				1			1		1					2		1	
Glomospira irregularis																												1								
Glomospirella gaultina																												2							1	
Reophax sp. 2												2																								
Ammosphaeroidina sp. 1			2		2						1	1		1									1					1					3			
Spiroplectinella gandolfi																1				1			1					1							1	
Spiroplectinella sp. 1								1			3	3				1				1															2	
Eggerellina manea			12		1						3	7		6		1			1				1										3			
Spiroplectinata annectans																																				
Spiroplectinata bettenstaedti																																				
Spiroplectinata complanata																																				
Gaudryina ex. gr. dividens																			18	2			10			2		7		5			6		3	2
Gaudryina pyramidata			8					6						2		2																				
Verneuilina cretacea														4																						
Tritaxia gaultina					3			1						4		3			9				3			1		1		1			2		1	1
Tritaxia sp. cf. T. gaultina																																				
Arenobulimina anglica																																				
Arenobulimina cf frankei								2																												
Remesella sp. 1			2					1			1	2		3					12	1			2			1		1		1					1	
Dorothia filiformis																																				
Dorothia gradata					2						1					2							1					1					1			
Dorothia cf. gradata								2												1													2			
Marssonella oxycona																																				
Textularia chapmani																																				
Quinqueloculina antiqua								1																												
Dentalina delicatula																																				
Laevidentalina basiplanata											1									3										1						
Laevidentalina communis																																			2	
Laevidentalina cylindroides																																				
Laevidentalina gracilis																														1						
Laevidentalina nana								1																												
Laevidentalina oligostega																												3								
Laevidentalina sp. cf. L. sona																																				
Nodosaria aspera																																				1
Nodosaria soluta																																				
Nodosaria sp. 1																																				
Nodosaria sp. 2																												1								
Pseudonodosaria humilis																																				1
Pyramidulina sceptrum																																				
Pyramidulina zippei																																			1	
Frondicularia archiaciana																																				
Lenticulina circumcidanea														1																						
Lenticulina gaultina																							1													
Lenticulina muensteri																																				
Lenticulina pulchella																												1					1			
Lenticulina rotulata																																				1
Lenticulina saxocretacea																																	3			
Lenticulina sp. 1												1																								
Marginulinopsis sp. 1												1																								
Saracenaria erlita																																				
Saracenaria triangulans																																				
Saracenaria sp. 1														1																						
Astacolus calliopsis																																				
Hemirobulina bullata																				1																
Hemirobulina inaequalis																																			1	
Vaginulinopsis harpa																																				
Planularia bradyana			1									1											2					1					1		1	
Psilocitharella arguta																1																				
Psilocitharella paucistriata														1																						
Vaginulina cretacea														1														1								
Vaginulina recta																												1					1			
Lagena globulosa																																				
Globulina lacrima																																				
Globulina prisca																																				

Samples (Core, section, interval)	Pyrulina cylindroides	Ramulina aculeata	Ramulina spandeli	Ramulina sp. 3	Oolina globosa	Fissurina sp. 1	Tricarinella excavata	Heterohelix globulosa	Heterohelix moremani	Heterohelix reussi	Globigerinelloides bentonensis	Globigerinelloides sp. 2	Planomalina buxtorfi	Schackoina cenomana	Schackoina multispinata	Schackoina sp. 1
123-766C-14R-4 149-151																
123-766C-14R-5 1-3																
123-766C-14R-5 25-27																
123-766C-14R-5 50-52								10	9			19		16	4	
123-766C-14R-5 75-77																
123-766C-14R-5 100-102									10	10	2	10		9		
123-766C-14R-5 119-121		1					1		3					21		2
123-766C-14R-CC 3-5									85	8				27	3	1
123-766C-15R-1 5-7	2	1										9		39		
123-766C-15R-1 30-32									P					P		
123-766C-15R-1 55-57																
123-766C-15R-1 80-82																
123-766C-15R-1 105-107																
123-766C-15R-1 130-132														1		
123-766C-15R-2 1-3																
123-766C-15R-2 10-12																
123-766C-15R-2 20-22																
123-766C-15R-2 30-32					1									2		
123-766C-15R-2 40-42																
123-766C-15R-2 50-52																
123-766C-15R-2 60-62									P							
123-766C-15R-2 70-72																
123-766C-15R-2 80-82																
123-766C-15R-2 90-92																
123-766C-15R-2 100-102																
123-766C-15R-2 110-112																
123-766C-15R-2 120-122																
123-766C-15R-2 130-132								10								
123-766C-15R-2 140-142																
123-766C-15R-3 10-12																
123-766C-15R-3 35-37		1												1		
123-766C-15R-3 58-60																
123-766C-15R-3 85-87																
123-766C-15R-3 110-112						1	2		1				1®	6		
123-766C-15R-4 20-22					1									1		
123-766C-15R-4 45-47		1												1		
123-766C-15R-4 70-72																
123-766C-15R-4 95-97																
123-766C-15R-4 120-122							1							2		
123-766C-15R-4 145-147		2														
123-766C-15R-5 20-22		P		2												
123-766C-15R-5 45-47																
123-766C-15R-5 70-72													1®	1		
123-766C-15R-5 95-97		1												3		
123-766C-15R-5 120-122		1														
123-766C-15R-5 145-147																
123-766C-15R-6 20-22																
123-766C-15R-6 45-47												3	1®	7		
123-766C-16R-1 8-10													P			
123-766C-16R-1 35-37																

Samples (Core, section, interval)	Hedbergella brittonensis	Hedbergella delrioensis	Hedbergella planispira	Hedbergella simplex	Whiteinella aprica	Whiteinella archaeocretacea	Whiteinella baltica	Whiteinella brittonensis	Whiteinella hessi	Praeglobotruncana aumalensis	Praeglobotruncana delrioensis	Praeglobotruncana gibba	Praeglobotruncana inornata	Praeglobotruncana stephani	Helvetoglobotruncana praehelvetica
123-766C-14R-4 149-151															
123-766C-14R-5 1-3															
123-766C-14R-5 25-27															
123-766C-14R-5 50-52		33	12	45		16	4	17	30	4		5		42	4
123-766C-14R-5 75-77															
123-766C-14R-5 100-102		94	37	29	5	13								4	1
123-766C-14R-5 119-121		27	16	18						1			13		
123-766C-14R-CC 3-5		96	26	50		1				1			1		
123-766C-15R-1 5-7		11	95	39		8				4		1			
123-766C-15R-1 30-32		P													
123-766C-15R-1 55-57		2	5			4				2			2	13	
123-766C-15R-1 80-82															
123-766C-15R-1 105-107															
123-766C-15R-1 130-132		10	42			6	15								
123-766C-15R-2 1-3															
123-766C-15R-2 10-12															
123-766C-15R-2 20-22															
123-766C-15R-2 30-32		8	5												
123-766C-15R-2 40-42		52	5	20		10	13								
123-766C-15R-2 50-52										P					
123-766C-15R-2 60-62		P	P	P		P	P								
123-766C-15R-2 70-72															
123-766C-15R-2 80-82															
123-766C-15R-2 90-92															
123-766C-15R-2 100-102															
123-766C-15R-2 110-112															
123-766C-15R-2 120-122															
123-766C-15R-2 130-132		P		P											
123-766C-15R-2 140-142															
123-766C-15R-3 10-12															
123-766C-15R-3 35-37		9	17												
123-766C-15R-3 58-60															
123-766C-15R-3 85-87															
123-766C-15R-3 110-112		41	152	22											1
123-766C-15R-4 20-22		16	136	7			1			2	5			2	
123-766C-15R-4 45-47	1	3	9	1											
123-766C-15R-4 70-72															
123-766C-15R-4 95-97															
123-766C-15R-4 120-122	2	46	71	1									2	1	
123-766C-15R-4 145-147		10	21												
123-766C-15R-5 20-22															
123-766C-15R-5 45-47															
123-766C-15R-5 70-72		13	59	1											
123-766C-15R-5 95-97		9	124												
123-766C-15R-5 120-122		1	1												
123-766C-15R-5 145-147		3	11												
123-766C-15R-6 20-22															
123-766C-15R-6 45-47		80	186	9							3				2
123-766C-16R-1 8-10	1	2	4												
123-766C-16R-1 35-37		2													

Samples (Core, section, interval)	Rotalipora appenninica	Rotalipora brotzeni	Rotalipora cushmani	Rotalipora deecki	Rotalipora greenhornensis	Rotalipora globotruncanoides	Rotalipora montsalvensis	Rotalipora ticinensis	Dicarinella canaliculata	Dicarinella hagni	Dicarinella imbricata	Marginotruncana cf. marianosi	Bolivina sp. 1	Bolivina sp 2	Bolivinoides sp. 1	Tappanina cf. laciniosa	Spirobolivina australis
123-766C-14R-4 149-151																	
123-766C-14R-5 1-3																	
123-766C-14R-5 25-27																	
123-766C-14R-5 50-52									9	4	16						
123-766C-14R-5 75-77																	
123-766C-14R-5 100-102									P	20	3	1	1	2			
123-766C-14R-5 119-121									P	P	2		12	2			
123-766C-14R-CC 3-5									1	2	3						
123-766C-15R-1 5-7									4	1	2		4				
123-766C-15R-1 30-32										P	P						
123-766C-15R-1 55-57										130	75	1					
123-766C-15R-1 80-82																	
123-766C-15R-1 105-107																	
123-766C-15R-1 130-132													11			2	
123-766C-15R-2 1-3													2				
123-766C-15R-2 10-12																	
123-766C-15R-2 20-22																	
123-766C-15R-2 30-32													9				
123-766C-15R-2 40-42													1				
123-766C-15R-2 50-52																	
123-766C-15R-2 60-62																	
123-766C-15R-2 70-72																	
123-766C-15R-2 80-82																	
123-766C-15R-2 90-92																	
123-766C-15R-2 100-102																	
123-766C-15R-2 110-112																	
123-766C-15R-2 120-122																	
123-766C-15R-2 130-132																	
123-766C-15R-2 140-142																	
123-766C-15R-3 10-12																	
123-766C-15R-3 35-37													10				
123-766C-15R-3 58-60			P	P													
123-766C-15R-3 85-87																	
123-766C-15R-3 110-112			1	5	1									3	1		
123-766C-15R-4 20-22			1	13	1								1	2		1	
123-766C-15R-4 45-47						2							5	1			
123-766C-15R-4 70-72																	
123-766C-15R-4 95-97																	
123-766C-15R-4 120-122		2	6			11											
123-766C-15R-4 145-147																5	
123-766C-15R-5 20-22																	
123-766C-15R-5 45-47																	
123-766C-15R-5 70-72													1	1			
123-766C-15R-5 95-97													2				
123-766C-15R-5 120-122													2				
123-766C-15R-5 145-147													4			2	
123-766C-15R-6 20-22																	
123-766C-15R-6 45-47	24						5										
123-766C-16R-1 8-10	1																5
123-766C-16R-1 35-37													1				1

Samples (Core, section, interval)	Cuneus cf ludbrookae	Neobulimina australiana	Praebulimina nannina	Praebulimina reussi	Praebulimina cf. reussi	Praebulimina robusta	Praebulimina sp. 1	Praebulimina sp. 2	Turrilina evexa	Bulimina fabilis	Cassidella sp. 1	Coryphostoma sp. 1	Ellipsodimorphina sp 1	Ellipsoglandulina sp 1	Nodosarella sp. 1	Pleurostomella nitida
123-766C-14R-4 149-151																
123-766C-14R-5 1-3																
123-766C-14R-5 25-27																
123-766C-14R-5 50-52			3							1						
123-766C-14R-5 75-77																
123-766C-14R-5 100-102			4	5					4							2
123-766C-14R-5 119-121						9			6							
123-766C-14R-CC 3-5																
123-766C-15R-1 5-7			1	4			3		8							
123-766C-15R-1 30-32																
123-766C-15R-1 55-57			2												1	
123-766C-15R-1 80-82																
123-766C-15R-1 105-107																
123-766C-15R-1 130-132			3	7					4							
123-766C-15R-2 1-3			2	21					7						1	
123-766C-15R-2 10-12																
123-766C-15R-2 20-22																
123-766C-15R-2 30-32			33						5		1					
123-766C-15R-2 40-42				2			2		1							
123-766C-15R-2 50-52																
123-766C-15R-2 60-62																
123-766C-15R-2 70-72																
123-766C-15R-2 80-82																
123-766C-15R-2 90-92																
123-766C-15R-2 100-102																
123-766C-15R-2 110-112																
123-766C-15R-2 120-122																
123-766C-15R-2 130-132																
123-766C-15R-2 140-142																
123-766C-15R-3 10-12																
123-766C-15R-3 35-37			1				3		2		1					
123-766C-15R-3 58-60																
123-766C-15R-3 85-87																
123-766C-15R-3 110-112			3	4												
123-766C-15R-4 20-22		1	2	3												
123-766C-15R-4 45-47			3	1				1								
123-766C-15R-4 70-72																
123-766C-15R-4 95-97																
123-766C-15R-4 120-122	1		1				1	2					3			
123-766C-15R-4 145-147			21										1			
123-766C-15R-5 20-22			P													
123-766C-15R-5 45-47																
123-766C-15R-5 70-72			25										1			
123-766C-15R-5 95-97			6						3				1			
123-766C-15R-5 120-122			7						43							
123-766C-15R-5 145-147			7													
123-766C-15R-6 20-22																
123-766C-15R-6 45-47																
123-766C-16R-1 8-10			13						1			5				
123-766C-16R-1 35-37			3						4							

Samples (Core, section, interval)	*Pyrulina cylindroides*	*Ramulina aculeata*	*Ramulina spandeli*	*Ramulina* sp. 3	*Oolina globosa*	*Fissurina* sp. 1	*Tricannella excavata*	*Heterohelix globulosa*	*Heterohelix moremani*	*Heterohelix reussi*	*Globigerinelloides bentonensis*	*Globigerinelloides* sp. 2	*Planomalina buxtorfi*	*Schackoina cenomana*	*Schackoina multispinata*	*Schackoina* sp. 1	*Hedbergella brittonensis*	*Hedbergella delrioensis*	*Hedbergella planispira*	*Hedbergella simplex*	*Whiteinella aprica*	*Whiteinella archaeocretacea*	*Whiteinella baltica*	*Whiteinella brittonensis*	*Whiteinella hessi*
123-766C-16R-1 60-62																									
123-766C-16R-1 85-87																									
123-766C-16R-1 110-112																		12	25						
123-766C-16R-1 135-137																									
123-766C-16R-2 10-12													3	3				59	202						
123-766C-16R-2 35-37																									
123-766C-16R-2 60-62																									
123-766C-16R-2 85-87			1										4					13	35	2					
123-766C-16R-2 110-112																									
123-766C-16R-2 135-137																									
123-766C-16R-3 8-10														2				2	217						
123-766C-16R-3 35-37														1				18	160	2					
123-766C-16R-3 60-62																									
123-766C-16R-3 85-87														2				5	169	1					
123-766C-16R-3 110-112																									
123-766C-16R-3 135-137																		12	197						
123-766C-16R-4 10-12																									
123-766C-16R-4 35-37													7	6				54	221	9					
123-766C-16R-4 60-62																			25						
123-766C-16R-4 85-87																		34	278	2					
123-766C-16R-4 110-112																									
123-766C-16R-4 135-137																									
123-766C-16R-5 10-12																		6	19						
123-766C-16R-5 35-37																									
123-766C-16R-5 60-62																									
123-766C-16R-5 85-87													2	1				48	215	2					
123-766C-16R-5110-112																									
123-766C-16R-5 135-137																		21	113	3					
123-766C-16R-6 10-12																									
123-766C-16R-6 35-37											1						4	55	191	6					
123-766C-16R-6 60-62																									
123-766C-16R-6 85-87																									
123-766C-16R-6 110-112		3																13	87	11					
123-766C-16R-6 135-137																									
123-766C-16R-7 10-12																		41	181	8					
123-766C-16R-CC 7-9																	38	112	121	33					2

Samples (Core, section, interval)	*Praeglobotruncana aumalensis*	*Praeglobotruncana delrioensis*	*Praeglobutruncana gibba*	*Praeglobotruncana inornata*	*Praeglobotruncana stephani*	*Helvetoglobotruncana praehelvetic[a]*	*Rotalipora appenninica*	*Rotalipora brotzeni*	*Rotalipora cushmani*	*Rotalipora deecki*	*Rotalipora greenhornensis*	*Rotalipora globotruncanoides*	*Rotalipora montsalvensis*	*Rotalipora ticinensis*	*Dicarinella canaliculata*	*Dicarinella hagni*	*Dicarinella imbricata*	*Marginotruncana* cf. *marianosi*
123-766C-16R-1 60-62																		
123-766C-16R-1 85-87																		
123-766C-16R-1 110-112																		
123-766C-16R-1 135-137																		
123-766C-16R-2 10-12		1					5							8				
123-766C-16R-2 35-37																		
123-766C-16R-2 60-62																		
123-766C-16R-2 85-87		5					38							73				
123-766C-16R-2 110-112																		
123-766C-16R-2 135-137																		
123-766C-16R-3 8-10																		
123-766C-16R-3 35-37														1				
123-766C-16R-3 60-62																		
123-766C-16R-3 85-87																		
123-766C-16R-3 110-112																		
123-766C-16R-3 135-137																		
123-766C-16R-4 10-12																		
123-766C-16R-4 35-37							2							4				
123-766C-16R-4 60-62																		
123-766C-16R-4 85-87																		
123-766C-16R-4 110-112																		
123-766C-16R-4 135-137																		
123-766C-16R-5 10-12																		
123-766C-16R-5 35-37																		
123-766C-16R-5 60-62																		
123-766C-16R-5 85-87																		
123-766C-16R-5110-112																		
123-766C-16R-5 135-137																		
123-766C-16R-6 10-12																		
123-766C-16R-6 35-37																		
123-766C-16R-6 60-62																		
123-766C-16R-6 85-87																		
123-766C-16R-6 110-112																		
123-766C-16R-6 135-137																		
123-766C-16R-7 10-12																		
123-766C-16R-CC 7-9																		

Samples (Core, section, interval)	*Bolivina* sp. 1	*Bolivina* sp. 2	*Bolivinoides* sp 1	*Tappanina* cf. *laciniosa*	*Spirobolivina australis*	*Cuneus* cf. *ludbrookae*	*Neobulimina australiana*	*Praebulimina nannina*	*Praebulimina reussi*	*Praebulimina* cf. *reussi*	*Praebulimina robusta*	*Praebulimina* sp. 1	*Praebulimina* sp. 2	*Turrilina avexa*	*Bulimina fabilis*	*Cassidella* sp. 1	*Coryphostoma* sp. 1	*Ellipsodimorphina* sp. 1	*Ellipsoglandulina* sp 1	*Nodosarella* sp. 1	*Pleurostomella nitida*
123-766C-16R-1 60-62																					
123-766C-16R-1 85-87																					
123-766C-16R-1 110-112		14						12						11			2				
123-766C-16R-1 135-137																					
123-766C-16R-2 10-12								1									1				
123-766C-16R-2 35-37																					
123-766C-16R-2 60-62																					
123-766C-16R-2 85-87								1													
123-766C-16R-2 110-112																					
123-766C-16R-2 135-137																					
123-766C-16R-3 8-10	3				2			3									1	1	1		
123-766C-16R-3 35-37	1							1						2				1			
123-766C-16R-3 60-62																					
123-766C-16R-3 85-87	6								4					7							
123-766C-16R-3 110-112																					
123-766C-16R-3 135-137	2				1			4		1							1				
123-766C-16R-4 10-12																					
123-766C-16R-4 35-37																					
123-766C-16R-4 60-62	6							3									4				
123-766C-16R-4 85-87					1			1	1												
123-766C-16R-4 110-112																					
123-766C-16R-4 135-137																					
123-766C-16R-5 10-12	10				2			3	3					2			3				
123-766C-16R-5 35-37																					
123-766C-16R-5 60-62																					
123-766C-16R-5 85-87					1			1	2	1											
123-766C-16R-5110-112																					
123-766C-16R-5 135-137								12					2	3			4				
123-766C-16R-6 10-12																					
123-766C-16R-6 35-37														1			1				
123-766C-16R-6 60-62																					
123-766C-16R-6 85-87																					
123-766C-16R-6 110-112	1							2													
123-766C-16R-6 135-137																					
123-766C-16R-7 10-12							1	4													
123-766C-16R-CC 7-9																					

Samples (Core, section, interval)	Pleurostomella reussi	Pleurostomella subnodosa	Pleurostomella sp. 1	Eurycheilostoma? heitgottensis	Eurycheilostoma? moorei	Iuhusina grata	Quadromorphina allomorphinoides	Gubkinella sp. 1	Charltonina australis	Charltonina cf. australis	Charltonina sp. 1	Conorotalites aptiensis	Osangularia schloenbachi	Berthelina berthelini	Berthelina cf. berthelini	Berthelina cenomanica	Berthelina cf. daktoensis	Berthelina tenuis	Berthelina tennuissima	Berthelina sp. 2	Berthelina sp. 3	Gavelinella cf. plummerae	Gavelinella tormarpensis	Gavelinella sp. 1	Gavelinella sp. 3	Gavelinella sp. 4	Gavelinella sp. 6	Lingulogavelinella albiensis	Lingulogavelinella globulosa	Lingulogavelinella indica	Lingulogavelinella newtoni	Lingulogavelinella sp. 1	Anomalina? Santoodnae	Gyroidinoides infracretacea	Gyroidinoides sp. 1	Gyroidinoides sp. 2	Gyroidinoides sp. 3	Gyroidinoides sp. 4	Valvulinera gracillima	Valvulinera lenticula	Valvulinera sp. 1	Schiebnerova proindica		Radiolaria	Ostrocods	Pithonella	Fish debris	Shell fragments	Inoceramids	Wood	Pyrite	Glauconite	number of foraminifera picked	weight of sample picked (g)
123-766C-14R-4 149-151																																														P								
123-766C-14R-5 1-3																																																						
123-766C-14R-5 25-27																																																						
123-766C-14R-5 50-52																																																					303	0.0032
123-766C-14R-5 75-77																																																						
123-766C-14R-5 100-102						5												9		2		4					1							13																			315	0.00333
123-766C-14R-5 119-121						24							18	15				2		3	74	5												8					13					P		P							317	0.005
123-766C-14R-CC 3-5						1						1																											1							P							314	0.0072
123-766C-15R-1 5-7	4	2	1										5	2						16		4											2	4					5							P							303	0.0164
123-766C-15R-1 30-32																																												P										
123-766C-15R-1 55-57	2					3												8		22		3		4					1					4					4					P		P		P					319	0.0508
123-766C-15R-1 80-82																																																						
123-766C-15R-1 105-107																																																						
123-766C-15R-1 130-132	3					16		6				1								85	13	6	5										4	18	5									P		P							301	0.00278
123-766C-15R-2 1-3	1	1				36								10						83		14		2					1	3	5	2	2	14	22				4	2				P		P	P						305	0.0029
123-766C-15R-2 10-12																																																						
123-766C-15R-2 20-22																																																						
123-766C-15R-2 30-32	1	1	1			3		35						7							111	7												33	6				7							P							301	0.00134
123-766C-15R-2 40-42		6	1			18									4	8			4	105													2	25								4		P			P			P			305	0.0011
123-766C-15R-2 50-52																																												P										
123-766C-15R-2 60-62																																												P										
123-766C-15R-2 70-72																																												P									0	
123-766C-15R-2 80-82																																												P									0	
123-766C-15R-2 90-92																																												P									0	
123-766C-15R-2 100-102																																												P									0	
123-766C-15R-2 110-112																																												P									0	
123-766C-15R-2 120-122																																												P										
123-766C-15R-2 130-132																																												P										
123-766C-15R-2 140-142																																												P			P							
123-766C-15R-3 10-12																																																						
123-766C-15R-3 35-37	1			2				38	4				21	6	14	2					31				2									31	3		27		10			34		P		P	P						301	0.00159
123-766C-15R-3 58-60																																												P										
123-766C-15R-3 85-87																																												P										
123-766C-15R-3 110-112			1				2	1	7				3	11		3									4						2			8		1	1		8			1			P								306	0.00914
123-766C-15R-4 20-22								2	16				4	8	9	2				29														24			3					9		P	P								324	0.00244
123-766C-15R-4 45-47	3								11			1	14	1	24	1					102										1			23		7	9		3			27											302	0.00108
123-766C-15R-4 70-72																																																						
123-766C-15R-4 95-97																																																						
123-766C-15R-4 120-122	1						1		15			8	19	2	7						14													19		3	14					27		P									315	0.0149
123-766C-15R-4 145-147	2						1		13			8	11	6	29	2					51													36		4	7		1			26		P									302	0.00379
123-766C-15R-5 20-22																		P			P									2				P										P										
123-766C-15R-5 45-47																																																						
123-766C-15R-5 70-72									26			4	11	7	18	2					52				2			2						46		12					2	13			P								313	0.01235
123-766C-15R-5 95-97									3			2	38	6	10	2									1									30		2	9					22											315	0.01071
123-766C-15R-5 120-122									34			2	7	17	29	3				13	60													32			18					7											312	0.00132
123-766C-15R-5 145-147									15			2	6	9	89	2				54	11													20		9	1					16		P									302	0.00109
123-766C-15R-6 20-22																																																						
123-766C-15R-6 45-47									4							3																																					327	0.0286
123-766C-16R-1 8-10	4			1	3				12			1	20	32	27					81														6		18	8		4			6											308	0.0039
123-766C-16R-1 35-37	3								11			13	38	11	31			1		19	5													54		14	4		9			24											301	0.0062

Samples (Core, section, Interval)	Pleurostomella reussi	Pleurostomella subnodosa	Pleurostomella sp. 1	Eurycheilostoma? heltgottensis	Eurycheilostoma? moorei	Iuiusina grata	Quadromorphina allomorphinoides	Gubkinella sp. 1	Charltonina australis	Charltonina cf. australis	Charltonina sp. 1	Conorotalites aptiensis	Osangularia schloenbachi	Berthelina bethelni	Berthelina cf. bethelni	Berthelina cenomanica	Berthelina cf. daktoensis	Berthelina tenuis	Berthelina tennuissima	Berthelina sp. 2	Berthelina sp. 3	Gavelinella cf. plummerae	Gavelinella tormarpensis	Gavelinella sp. 1	Gavelinella sp 3	Gavelinella sp. 4	Gavelinella sp. 6	Lingulogavelinella albiensis	Lingulogavelinella globulosa	Lingulogavelinella indica	Lingulogavelinella newtoni	Lingulogavelinella sp. 1	Anomalina? Santoodnae	Gyroidinoides infracretacea	Gyroidinoides sp. 1	Gyroidinoides sp. 2	Gyroidinoides sp. 3	Gyroidinoides sp. 4	Valvulineria gracillima	Valvulineria lenticula	Valvulineria sp. 1	Schebnerova proindica		Radiolaria	Ostrocods	Pithonella	Fish debris	Shell fragments	Inoceramids	Wood	Pyrite	Glauconite	number of foraminifera picked	weight of sample picked (g)
123-766C-16R-1 60-62																																																						
123-766C-16R-1 85-87																																																						
123-766C-16R-1 110-112						1							25	7	49	6				10	13										2			17	11	13	3		6			28											299	0.0023
123-766C-16R-1 135-137																																																						
123-766C-16R-2 10-12						1	2		7					3	1					2														4					1			1											313	0.01538
123-766C-16R-2 35-37																																																						
123-766C-16R-2 60-62																																																						
123-766C-16R-2 85-87													7	2	5										4						1			1		4	1		5			9											226	0.02577
123-766C-16R-2 110-112																																																						
123-766C-16R-2 135-137																																																						
123-766C-16R-3 8-10	1						2		8			3	9	1	6		8																	12		2			6			12				P							312	0.00169
123-766C-16R-3 35-37						2	4		13			7	19	2	6		5			18														25		4			7			9				P							326	0.00182
123-766C-16R-3 60-62																																																						
123-766C-16R-3 85-87	2						1		6			1	14	7			5			4														23		3			5			1											290	0.00445
123-766C-16R-3 110-112																																																						
123-766C-16R-3 135-137	1						1		18				9		3		14			9														4		11	4		7			7				P							317	0.00324
123-766C-16R-4 10-12																																																						
123-766C-16R-4 35-37												1	3			2				1																																	310	0.0744
123-766C-16R-4 60-62	2						2		11			1	55	5	3	2	1			23														39	9	17	7		3			42					P						301	0.0071
123-766C-16R-4 85-87	4						3		7			2	4	2	2					2																3	10		2			5											373	0.0038
123-766C-16R-4 110-112																																																						
123-766C-16R-4 135-137																																																						
123-766C-16R-5 10-12	2						6					5	31	6	18	1				18														31	16	15	2		7			5											235	0.0025
123-766C-16R-5 35-37																																																						
123-766C-16R-5 60-62																																																						
123-766C-16R-5 85-87	1						2		3				4	5	4					3														3	1	1	1		1			3				P							310	0.0259
123-766C-16R-5110-112																																																						
123-766C-16R-5 135-137	6	1					6		18	3			13	7	8	1				29														5	4		2		14					P		P							301	0.0089
123-766C-16R-6 10-12																																																						
123-766C-16R-6 35-37	2								4		1			5	1	1				1														4	2	1		1	5														298	0.0052
123-766C-16R-6 60-62																																																						
123-766C-16R-6 85-87																																																						-
123-766C-16R-6 110-112	2								12				14	4	6	4				8														61					17			33											305	0.0031
123-766C-16R-6 135-137																																																						
123-766C-16R-7 10-12	1												8	1	3	3				3						2	2				3			14	2		4		4			4						P					305	0.0063
123-766C-16R-CC 7-9	2											1	3		1					1										3				4								2											329	0.0045

Foraminiferal Count Sheets of all > 63μm samples picked from ODP Site 762

P = present in sample

| Samples (Core, section, interval) | mbsf | | Rhabdammina sp 1 | Ammodiscus cretaceus | Reophax sp 1 | Reophax sp 2 | Ammosphaeroidina sp 1 | Spiroplectinella gandolfi | Spiroplectinella sp 1 | Eggerellina brevis | Spiroplectinata bettenstaedti | Gaudryina ex gr dividens | Gaudryina pyramidata | Verneuilina cretacea | Tritaxia gaultina | Tritaxia sp cf T. gaultina | Arenobulimina cf frankei | Dorothia conicula | Dorothia gradata | Marssonella oxycona | Textularia chapmani | Laevidentalina basiplanata | Laevidentalina gracilis | Laevidentalina nana | Laevidentalina sp cf L sona | Nodosaria soluta | Nodosaria sp 1 | Lenticulina circumcidanea | Lenticulina muenster | Lenticulina pulchella | Lenticulina rotulata | Lenticulina saxocretacea | Lenticulina subangulata | Marginulinopsis sp 1 | Vaginulinopsis harpa | Lagena globulosa | Globulina lacrima | Globulina prisca | Pyrulina cylindroides | Ramulina aculeata | Tricarinella excavata | Guembelitria cenomana | Heterohelix moremani | Heterohelix reussi | Globigerinelloides bentonensis | Schackoina cenomana | Hedbergella delrioensis | Hedbergella planispira | Hedbergella simplex | Whiteinella archaeocretacea | Whiteinella brittonensis | Praeglobotruncana delrioensis | Praeglobotruncana gibba | Praeglobotruncana inornata | Praeglobotruncana oraviensis | Praeglobotruncana stephani | Praeglobotruncana spp | Helvetoglobotruncana praehelvetica | Rotalipora appenninica | Rotalipora brotzeni | Rotalipora cushmani | Rotalipora deeckl | Rotalipora greenhornensis | Rotalipora globotruncanoides | Rotalipora micheli | Rotalipora montsalvensis | Rotalipora reicheli | Rotalipora spp | Dicarinella algeriana | Dicarinella canaliculata | Dicarinella hagni | Dicarinella imbricata | Dicarinella spp | Marginotruncana sigali | Bolivina sp 1 | Bolivinoides sp 1 | Tappanina cf lacinosa | Sprobolivina australis | Praebulimina nannina | Praebulimina reussi | Praebulimina cf reussi | Turrilina evexa | Pleurostomella reussi | Pleurostomella subnodosa | Julusina grata |
|---|---|---

Samples (Core, section, interval)	Quadromorphina allomorphinoides	Gublonella sp 1	Charltonina australis	Conorotalites aptiensis	Osangularia schloenbachi	Bertheline bethelmi	Bertheline cenomanica	Bertheline tennuissima	Bertheline sp 2	Bertheline sp 3	Gavelinella cf plummerae	Gavelinella formarpensis	Gavelinella sp 3	Gavelinella sp 4	Gavelinella sp 5	Gavinella spp	Lingulogavelinella globulosa	Lingulogavelinella sp 1	Lingulogavelinella spp	Gyroidinoides infracretacea	Gyroidinoides sp 2	Gyroidinoides sp 3	Gyroidinoides spp	Valvulineria gracilima	Valvulineria lenticula	Schebnerova prandica	Radiolaria	Ostrocods	Pithonella	Fish debris	Shell fragments	Inoceramids	Wood	Pyrite	Glauconite	number of foraminifera picked	weight of sample picked (g)
74X-2 19-22																7							2				P									240	0.00891
74X-2 50-53																																				240	0.00891
74X-2 70-82																																				0	0
74X-2 111-113																																				0	0
74X-2 137-140																																				0	0
74X-3 10-13																																				0	0
74X-3 40-41										10	2					11				2																300	0.00953
74X-CC 14-16																																				262	0.02196
75X-1 5-6																																				0	0
75X-1 27-29					4					103										5																398	0.04304
75X-1 45-48																																				0	0
75X-1 60-62																																				0	0
75X-1 70-72					2					3	2	2				3				2				P												311	0.03602
75X-1 80-82																																				0	0
75X-1 90-91																																				0	0
75X-1 99-100																																				240	0.03545
75X-1 110-111					18					92						1				14				P	P	P										289	0.73563
75X-1 120-121				22	13					68						3				5				P	P	P										330	0.86034
75X-1 129-131																								P												0	1.34236
75X-1 140-142																				3				3												301	0.0079
75X-1 149-150													4	5	1					1																313	0.03075
75X-2 26-28														1											1	P										302	0.01522
75X-2 51-53																				2																0	
75X-2 75-77																																				240	0.03545
75X-2 95-97				1	2	3				4						2	4								1	P										316	0.01649
75X-2 121-123																				2	4															0	
75X-2 140-142																								P												306	0.01914
75X-3 15-17				1																2	3															0	
75X-3 40-42																								P												310	0.0192
75X-3 62-64																				2																0	
75X-3 90-92				1												1								P												325	0.05013
75X-CC 13-16																				2	P				1	P										0	
76X-1 5-7																								P												316	0.02181
76X-1 24-26																5				8																0	
76X-1 49-51																								1												0	
76X-1 74-76																				1																316	0.02181
76X-1 97-99				1												3																				0	
76X-1 121-123					1																															0	
76X-1 145-147																																				0	
76X-2 15-17				1	2	1				4										5				1	P											321	0.02511
76X-2 40-42																								P												0	
76X-2 64-67																																				0	
76X-2 89-91					8											7				1	12															293	0.02843
76X-2 114-116																																				0	
76X-2 140-142																																				0	
76X-3 9-11					9	4														1	13	7														233	0.3754
76X-3 28-30																																				0	
76X-3 50-53																																				0	
76X-3 74-76																																				0	
76X-3 100-102					5		1		2											3				2	P										288	0.01423
76X-3 124-126																																				0	
76X-4 6-8					1															1	1			1	P										312	0.01864
76X-4 25-27					4	1														1	2															0	
77X-1 5-7																																				0	
76X-4 57-59				1	5	1			1																											311	0.01462

Foraminiferal Count Sheets of all > 63µm samples picked from the Aksudere section, Crimea

P = present in sample

| sample interval | AK 9.80 | AK 9.50 | AK 9.40 | AK 9.30 | AK 9.20 | AK 8.90 | AK 8.80 | AK 8.30 | AK 8.00 | AK 7.85 | AK 7.70 | AK 7.55 | AK 7.40 | AK 7.25 | AK 7.10 | AK 6.95 | AK 6.80 | AK 6.65 | AK 6.50 | AK 6.45 | AK 6.40 | AK 6.30 | AK 6.20 | AK 6.10 | AK 6.00 | AK 5.90 | AK 5.80 | AK 5.70 | AK 5.60 | AK 5.55 | AK 5.50 | AK 5.45 | AK 5.40 | AK 5.35 | AK 5.30 | AK 5.25 | AK 5.20 | AK 5.15 | AK 5.10 | AK 5.05 | AK 5.00 | AK 4.95 | AK 4.90 | AK 4.85 | AK 4.80 | AK 4.65 | AK 4.60 | AK 4.55 | AK 4.50 | AK 4.45 | AK 4.40 | AK 4.35 | AK 4.30 | AK 4.25 | AK 4.20 | AK 4.15 | AK 4.10 | AK 4.05 | AK 4.00 | AK 3.95 | AK 3.90 | AK 3.85 | AK 3.80 | AK 3.75 | AK 3.70 | AK 3.65 | AK 3.60 | AK 3.55 | AK 3.50 |
|---|---|---

sample interval	AK 3.40	AK 3.30	AK 3.20	AK 3.10	AK 3.00	AK 2.85	AK 2.70	AK 2.55	AK 2.40	AK 2.25	AK 2.10	AK 1.95	AK 1.80	AK 1.65	AK 1.50	AK 1.35	AK 1.20	AK 0.90	AK 0.75	AK 0.60	AK 0.45	AK 0.30	AK 0.15	AK 0
Rhabdammina spp		3								2										4				
Rhizammina spp										2					7									
Ammodiscus cretaceus																				1				
Glomospira charoides										1														
Eggerelina brevis		1								2										5				
Gaudryina pyramidata																								
Dorothia gradata										2					1									
Marssonella oxycona										2														
Textularia chapmani															1									
Dentalina costata																								
Laevidentalina communis	2														1									
Laevidentalina gracilis	1														1					1				
Laevidentalina nana	1																							
Laevidentalina oligostega										1										2				
Laevidentalina sp. cf. *L. sana*										1										1				
Nodosaria soluta										1					1									
Nodosaria sp. 1																				1				
Frondicularia archiaciana																								
Lenticulina rotulata	1									3					1					2				
Lenticulina saxocretacea																				2				
Saracenaria triangularis																				2				
Hemirobulina bullata																				2				
Hemirobulina inaequalis										1														
Vaginulinopsis sp. 1																				1				
Planularia bradyana										2										1				
Lagena globulosa																				1				
Lagena hispida																				2				
Globulina prisca																				2				
Pyrulina cylindroides	2									2										2				
Pyrulina sp. 1										5										2				
Ramulina aculeata																								
Tricarinella excavata										2										2				
Guembelitria cenomana	20									15					29					10				32
Heterohelix moremani	36									6					18					14				20
Globigerinelloides bentonensis	33									1					5					34				2
Schackoina cenomana															2									
Hedbergella delrioensis	85									42					97					35				58
Hedbergella planispira	23									14					27					16				16
Hedbergella simplex	5									15					8					11				10
Whiteinella aprica																								
Whiteinella archaeocretacea										12														
Whiteinella baltica										8					4									
Whiteinella brittonensis										1					5					1				
Praeglobotruncana aumalensis	2	P								30					47					52				1
Praeglobutruncana gibba										11					6					9				
Praeglobotruncana gravelensis																								
Praeglobotruncana stephani	29									6					4					4				
Praeglobotruncana spp		P																						
Helvetoglobotruncana praehelvetica		P																						
Helvetoglobotruncana helvetica		P								10					1					1				
Rotalipora cushmani		P								2					1									
Rotalipora deeckii		P								4										1				4
Rotalipora greenhornensis		P																						
Dicarinella biconvexiformis																								
Dicarinella stata																								
Dicarinella hagni																								
Dicarinella imbricata	33									10					18					31				1
Dicarinella cf. *imbricata*																								1
unknown keeled planktonics																								23
Tappanina cf. *lecanosa*	10									37					4					6				
Praebulimina reussi	3									3					3					3				2
Turrilina evexa																								2
Coryphostoma sp. 1																								
Ellipsodimorphina sp. 1																								
Pleurostomella reussi																								
Quadrimorphina allomorphinoides	1																			2				
Osangularia schloenbachi	3																							
Berthelina bertheloti																				2				
Berthelina tennuissima															3									
Bertheina sp. 2																								2
Gavelinella sp. 2	2									17					4					17				
Gavinella spp															1					1				6
Lingulogavelinella newtoni										3														
Lingulogavelinella spp																								
Gyrodinoides infracretacea	10									21					3					14				7
Gyrodinoides sp. 1															2					1				
Radiolaria																								P
Ostracods																								P
Fish debris																								
Shell fragments	P														P									
Inoceramids																								
Glauconite																								
Pyrite																								
Wood																								
Organic matter																								
number of foraminifera picked	306	303	302	305	227																			
number of species picked	22	30	29	30	17																			
weight of sample picked	0.01274	0.01109	0.0098	0.01243	0.01582																			

Appendix 3

All isotopic and trace element data tables

Sample	Depth	Fine fraction results			*Berthelina* spp. results			*Hedbergella* spp. results		
		$\delta^{13}C$	$\delta^{18}O$	T°C α_w=-1	$\delta^{13}C$	$\delta^{18}O$	T°C α_w=-1	$\delta^{13}C$	$\delta^{18}O$	T°C α_w=-1
123-766C-14R-3 50-52	127.10	3.40	-1.19	16.8						
123-766C-14R-3 75-77	127.35	3.22	-1.64	18.7						
123-766C-14R-3 100-102	127.60	3.15	-1.48	18.0						
123-766C-14R-3 125-127	127.85	2.78	-1.52	18.2						
123-766C-14R-3 149-151	128.09	3.11	-2.00	20.3						
123-766C-14R-4 1-3	128.11	3.79	-2.06	20.5						
123-766C-14R-4 25-27	128.35	3.42	-1.39	17.6						
123-766C-14R-4 50-52	128 60	3.52	-2.35	21.8						
123-766C-14R-4 75-77	128 85	3.14	-1.84	19.6						
123-766C-14R-4 100-102	129.10	3 44	-1.98	20.2						
123-766C-14R-4 149-151	129.59	3.50	-2 03	20.4						
123-766C-14R-5 1-3	129.61	3.42	-2.42	22.1						
123-766C-14R-5 25-27	129.85	3.63	-2.18	21.1				3.1	-1.4	17.8
123-766C-14R-5 50-52	130.10	2.78	-1.99	20.2				3 6	-1.8	19.3
123-766C-14R-5 75-77	130.35	3.68	-1.78	19.3	2.5	-0.9	15.7			
123-766C-14R-5 100-102	130 60	3.75	-2.04	20 4	2.4	-0.9	15.5			
123-766C-14R-5 119-121	130.79	3.98	-1.94	20.0	2.3	-0.9	15.6			
123-766C-14R-CC 3-5	130.88	3.03	-1.79	19.4						
123-766C-15R-1 5-7	133.25	3.39	-2.04	20.4	2.1	-1.2	16.9	2.7	-1.7	18.9
123-766C-15R-1 30-32	133.50	3.42	-1.79	19.4						
123-766C-15R-1 55-57	133.75	3.67	-1.72	19.0						
123-766C-15R-1 80-82	134.00	3.63	-2.42	22.1						
123-766C-15R-1 105-107	134.25	3.59	-2.64	23.1						
123-766C-15R-1 130-132	134.50	3.81	-2.23	21.3						
123-766C-15R-2 1-3	134.71	3.69	-2.69	23.4	2.6	-1.4	17.6			
123-766C-15R-2 10-12	134.80	3.59	-2.65	23.2						
123-766C-15R-2 20-22	134.90	3 64	-2 84	24 1	2 5	-1 5	18 0			
123-766C-15R-2 30-32	135.00	No Carbonate								
123-766C-15R-2 40-42	135.10									
123-766C-15R-2 50-52	135.20									
123-766C-15R-2 60-62	135.30									
123-766C-15R-2 70-72	135 40									
123-766C-15R-2 80-82	135.50									
123-766C-15R-2 90-92	135.60									
123-766C-15R-2 100-102	135.70									
123-766C-15R-2 110-112	135.80									
123-766C-15R-2 120-122	135.90									
123-766C-15R-2 130-132	136.00									
123-766C-15R-2 140-142	136.10									
123-766C-15R-3 10-12	136.30				2.0	-0.4	13.6			
123-766C-15R-3 35-37	136.55	4.05	-1.73	19.1	2.0	-0 5	13.8			
123-766C-15R-3 58-60	136.78	3.99	-1.74	19.1						
123-766C-15R-3 85-87	137.05	3.81	-1.83	19.5	2.1	-0.7	14.8			
123-766C-15R-3 110-112	137.30	3.75	-1.73	19.1	2.2	-0.3	13.2			
123-766C-15R-4 20-22	137.90	3.91	-1.50	18.1	2.1	-0.4	13 8			
123-766C-15R-4 45-47	138.15	3.69	-1.64	18.7	1.9	-0.2	12.7			
123-766C-15R-4 70-72	138.40	3.51	-1.61	18.6	2.0	0.1	11.5			
123-766C-15R-4 95-97	138 65	3 62	-1.70	19 0				3 4	-0 3	13 2

Sample	Depth	Fine fraction results			*Berthelina* spp. results			*Hedbergella* spp. results		
		$\delta^{13}C$	$\delta^{18}O$	T°C α_w=-1	$\delta^{13}C$	$\delta^{18}O$	T°C α_w=-1	$\delta^{13}C$	$\delta^{18}O$	T°C α_w=-1
123-766C-15R-4 120-122	138.90	3.58	-1.94	20.0						
123-766C-15R-4 145-147	139.15	3.50	-1.93	20.0						
123-766C-15R-5 20-22	139 40	3.37	-1.59	18.5	1.8	-0 6	14.2			
123-766C-15R-5 45-47	139 65	3.52	-1 68	18.9	1.6	-0.4	13.6			
123-766C-15R-5 70-72	139 90	3 54	-1 48	18 0	1.3	-0 5	13.9			
123-766C-15R-5 95-97	140.15	3 58	-1.61	18 6						
123-766C-15R-5 120-122	140.40	3.28	-1.71	19.0	2.2	-0.3	13.1			
123-766C-15R-5 145-147	140.65	3 57	-1.70	19.0						
123-766C-15R-6 20-22	140.90	3.98	-1.67	18.8						
123-766C-15R-6 45-47	141.15	3.11	-1 47	18 0						
123-766C-16R-1 8-10	142.98	3.46	-1.38	17 6	1.5	-0.2	12.9			
123-766C-16R-1 35-37	143.25	3.52	-1.65	18.7	1.5	-0.1	12.4			
123-766C-16R-1 60-62	143.50	2.99	-1.71	19 0						
123-766C-16R-1 85-87	143.75	3.50	-1.76	19 2	1.7	-0.5	14.0			
123-766C-16R-1 110-112	144.00	3.34	-1.78	19.3						
123-766C-16R-1 135-137	144.25	3.13	-1.71	19.0	1.1	-0 4	13.6			
123-766C-16R-2 10-12	144.50	3.18	-1 70	19 0	1.4	-0.6	14.2			
123-766C-16R-2 35-37	144.75	3.24	-1.69	18.9						
123-766C-16R-2 60-62	145.00	3.38	-1.66	18 8						
123-766C-16R-2 85-87	145.25	3.06	-1.72	19.0						
123-766C-16R-2 110-112	145.50	3.16	-1 94	20 0						
123-766C-16R-2 135-137	145.75	3.23	-1.77	19 3						
123-766C-16R-3 8-10	145.98	3.23	-1 68	18 9						
123-766C-16R-3 35-37	146.25	3 17	-1 66	18.8						
123-766C-16R-3 60-62	146.50	3.09	-1 69	18.9						
123-766C-16R-3 85-87	146.75	2.96	-1.76	19 2						
123-766C-16R-3 110-112	147.00	3.24	-2.22	21.2						
123-766C-16R-3 135-137	147 25	3.21	-1.84	19 6						
123-766C-16R-4 10-12	147.50	3 07	-1 72	19 0						
123-766C-16R-4 35-37	147.75	3.09	-1.89	19 8						
123-766C-16R-4 60-62	148.00	3.35	-2.07	20.6						
123-766C-16R-4 85-87	148.25	3.39	-1.72	19.0						
123-766C-16R-4 110-112	148.50	3.54	-1.97	20.1						
123-766C-16R-4 135-137	148.75	3.50	-1.95	20.1						
123-766C-16R-5 10-12	149.00	3.79	-1.73	19 1						
123-766C-16R-5 35-37	149 25	3.78	-1.86	19.7						
123-766C-16R-5 60-62	149.50	3.28	-1.89	19 8						
123-766C-16R-5 85-87	149.75	3.31	-1.87	19.7						
123-766C-16R-5110-112	150.00	3.57	-1.92	19.9						
123-766C-16R-5 135-137	150.25	3.64	-2.22	21.2						
123-766C-16R-6 10-12	150.50	3.63	-2 08	20 6						
123-766C-16R-6 35-37	150 75	3.52	-1.94	20.0						
123-766C-16R-6 60-62	151.00	3.41	-1.88	19.7						
123-766C-16R-6 85-87	151.25	3.59	-2.04	20 4						
123-766C-16R-6 110-112	151.50	3.58	-1.75	19.2						
123-766C-16R-6 135-137	151.75	3.20	-1 64	18.7						
123-766C-16R-7 10-12	152.00	3.13	-1.77	19.3						
123-766C-16R-CC 7-9	152 16	3 37	-1 81	19 4						

Table 1: All isotope values obtained from fine fraction and foraminiferal isotope analysis. Palaeotemperature estimates are calculated using the equation of Anderson and Arthur (1983) using the SMOW isotope value for Cretaceous water of -1.

Sample	Depth	Mn (ppm)	Mn/Ca	Fe (ppm)	Fe/Ca	Mg (ppm)	Mg/Ca	Sr (ppm)	Sr/Ca	Ca (ppm)
123-766C-14R-3 50-52	127.10	321.67	0.00690	1012.00	0.02170	5494.37	0 11781	239 64	0 00514	46637.02
123-766C-14R-3 75-77	127 35	299 44	0 00151	906 56	0.00456	3687 83	0 01854	533 42	0.00268	198912 54
123-766C-14R-3 100-102	127.60	327.06	0 00392	1042.45	0 01249	4313.36	0 05166	337 32	0 00404	83493 00
123-766C-14R-3 125-127	127 85	444.26	0 01530	1189 88	0 04097	6132 98	0 21116	168 71	0 00581	29044 00
123-766C-14R-3 149-151	128 09	375 07	0 00445	1189 91	0 01411	5360.29	0 06354	320 69	0 00380	84355 83
123-766C-14R-4 1-3	128.11	339 98	0.00163	955.38	0.00458	3723.03	0.01786	534 91	0.00257	208486.56
123-766C-14R-4 25-27	128 35	295 89	0 00099	605 78	0 00203	1865.42	0 00625	536.30	0 00180	298531.12
123-766C-14R-4 50-52	128 60	285 21	0.00123	934.72	0.00404	4022 23	0.01737	425 83	0.00184	231562.94
123-766C-14R-4 75-77	128 85	416 74	0.00552	978 11	0.01295	3855 54	0 05106	257 25	0 00341	75515 92
123-766C-14R-4 100-102	129.10	281.01	0 00145	696.23	0 00360	2974 36	0 01540	446 69	0 00231	193194 05
123-766C-14R-4 149-151	129 59	333.54	0 00122	701.11	0 00256	3574 73	0.01304	537.15	0 00196	274228 02
123-766C-14R-5 1-3	129 61	337.33	0.00105	415 92	0.00129	2211 31	0 00685	664.72	0.00206	322668 82
123-766C-14R-5 25-27	129 85	320.15	0 00095	285.21	0.00084	1959 35	0.00580	665 99	0 00197	337564 21
123-766C-14R-5 50-52	130.10									
123-766C-14R-5 75-77	130 35	452 54	0.00212	1090.21	0.00511	4184 55	0.01963	437.17	0.00205	213157.26
123-766C-14R-5 100-102	130 60	452 51	0 00161	865.05	0.00307	4152.93	0.01473	572 43	0.00203	281867.60
123-766C-14R-5 119-121	130.79	339.12	0 00120	692.28	0.00245	4659.84	0.01646	594.57	0.00210	283134 69
123-766C-14R-CC 3-5	130 88	356 56	0.00114	935.27	0 00299	4160 21	0 01329	730.73	0 00233	313091 71
123-766C-15R-1 5-7	133.25	387.81	0 00178	1282.34	0 00590	5448 58	0 02506	458 97	0.00211	217440 86
123-766C-15R-1 30-32	133 50	302 96	0 00613	1180.62	0.02387	8360 86	0 16907	153 26	0 00310	49452.65
123-766C-15R-1 55-57	133.75	320.62	0.00155	958 92	0.00465	4129.41	0 02000	408 11	0 00198	206428 38
123-766C-15R-1 80-82	134.00	322 77	0 00125	476 82	0 00184	2030 18	0.00784	575.12	0.00222	258832.16
123-766C-15R-1 105-107	134.25	405 91	0 00170	553 46	0 00232	3036.22	0 01275	581 74	0 00244	238186 55
123-766C-15R-1 130-132	134 50	275.56	0 00509	573 80	0.01060	4022 99	0 07434	211 78	0 00391	54116 01
123-766C-15R-2 1-3	134.71	210 12	0 00099	414 60	0 00195	3028 07	0 01424	471 56	0.00222	212640 32
123-766C-15R-2 10-12	134 80	311 92	0 00229	750.14	0.00550	5393.94	0 03958	353 88	0 00260	136289 40
123-766C-15R-2 20-22	134 90	280 27	0 00203	496 11	0 00359	5035 23	0 03641	369 36	0 00267	138289 70
123-766C-15R-2 30-32	135 00	247 24	0.00156	221.78	0.00140	3259 00	0 02062	396.03	0.00251	158063.47
123-766C-15R-2 40-42	135 10	236.68	0.00401	435.79	0.00739	4943.73	0.08378	255 03	0 00432	59006 71
123-766C-15R-2 50-52	135 20	329 22	0 08573	409 13	0 10654	4368.30	1 13753	140 81	0 03667	3840.15
123-766C-15R-2 60-62	135.30	412.58	0 07133	624 51	0.10797	4563.35	0.78893	148.39	0.02565	5784 20
123-766C-15R-2 70-72	135 40	303 89	0 06780	365.89	0.08163	4739 03	1 05729	147.59	0 03293	4482 22
123-766C-15R-2 90-92	135 60	342 11	0 12575	509.31	0.18721	1616 34	0 59413	89 65	0.03295	2720 50
123-766C-15R-2 100-102	135 70	401.49	0 09273	597 50	0.13800	5455.75	1 26006	155.70	0 03596	4329 74
123-766C-15R-2 110-112	135 80	485 40	0.12074	555.17	0.13809	4118 25	1.02435	176 65	0 04394	4020.35
123-766C-15R-2 120-122	135.90	311 27	0 07153	423.49	0 09732	4752 23	1 09206	169 82	0 03902	4351 61
123-766C-15R-2 130-132	136 00	1125.19	0.19528	514.69	0 08933	5598 76	0 97171	203 53	0 03532	5761.79
123-766C-15R-2 140-142	136 10	1018 39	0 25829	1263 30	0.32041	6569 11	1.66612	215 06	0 05455	3942.77
123-766C-15R-3 10-12	136.30	157.32	0 04754	269 19	0 08134	5361.43	1 62007	129 86	0 03924	3309 39
123-766C-15R-3 35-37	136 55	209 89	0 00172	412.75	0 00338	4556 02	0.03733	390.00	0 00320	122062 09
123-766C-15R-3 58-60	136.78									
123-766C-15R-3 85-87	137.05	290 33	0 00129	138 89	0 00062	1792 16	0 00799	583 81	0 00260	224326.25
123-766C-15R-3 110-112	137.30	338.73	0 00139	98 72	0 00040	395 77	0 00162	622 37	0 00255	244479 76
123-766C-15R-4 20-22	137 90	310 98	0 00131	111 86	0.00047	2171.13	0 00918	564.75	0 00239	236503 66
123-766C-15R-4 45-47	138 15	422.95	0 00148	162 66	0.00057	1710 35	0 00598	657 89	0.00230	285908.74
123-766C-15R-4 70-72	138 40	264 63	0.00112	115 08	0.00049	2217.62	0 00940	649 59	0.00275	235885.37
123-766C-15R-4 95-97	138 65	272 58	0.00124	202 58	0 00092	2563.33	0 01166	563 82	0 00256	219864 79
123-766C-15R-4 120-122	138.90	320 90	0 00118	94.44	0 00035	2009.70	0 00739	816.81	0 00300	272025.17
123-766C-15R-4 145-147	139 15	278 47	0 00111	138 60	0 00055	2811.32	0 01116	709 65	0 00282	251912.86
123-766C-15R-5 20-22	139 40	290.51	0 00157	97.36	0 00053	3524 65	0 01903	507 95	0 00274	185216 54
123-766C-15R-5 45-47	139 65	342.86	0.00121	70 53	0.00025	2459 28	0 00867	671.74	0 00237	283615.09
123-766C-15R-5 70-72	139 90	259 84	0 00129	75 94	0.00038	2223.19	0 01104	510 10	0.00253	201461 53
123-766C-15R-5 95-97	140.15									
123-766C-15R-5 120-122	140 40	211 96	0 00163	88 43	0.00068	2665 59	0 02050	391.32	0.00301	130043.55
123-766C-15R-5 145-147	140 65	225 31	0 00199	147 08	0 00130	2842.14	0 02507	301 82	0.00266	113386 04
123-766C-15R-6 20-22	140 90	261.08	0.00712	152 48	0 00416	3212 04	0 08759	201 63	0 00550	36670 66
123-766C-15R-6 45-47	141 15	262.74	0 00248	51.13	0 00048	2338 07	0 02203	275.30	0 00259	106154 96
123-766C-16R-1 8-10	142 98	233.54	0 00176	50 40	0 00038	3008 84	0.02267	250 84	0.00189	132713 97
123-766C-16R-1 35-37	143 25	282 98	0 00162	105 33	0 00060	3545 63	0 02028	371 39	0 00212	174824 96
123-766C-16R-1 60-62	143 50	273 93	0.00173	158.87	0 00100	3725 90	0.02355	407.97	0.00258	158191.02
123-766C-16R-1 85-87	143.75	260 56	0 00251	98 46	0 00095	2778 55	0 02681	262.21	0 00253	103632.19
123-766C-16R-1 110-112	144 00	286 19	0 00215	142 57	0 00107	2636 22	0 01982	324.15	0 00244	132989.54
123-766C-16R-1 135-137	144 25	206 62	0.00098	127.56	0 00060	2571 47	0 01217	471 11	0 00223	211255.14
123-766C-16R-2 10-12	144 50	232.97	0 00123	76.01	0 00040	2337.35	0 01236	481 93	0 00255	189053 60
123-766C-16R-2 60-62	145 00	382.03	0.00207	1832.99	0 00993	5415 40	0.02934	425 25	0 00230	184582.31
123-766C-16R-2 85-87	145 25	236.62	0 00121	167.06	0 00086	2392.71	0 01226	438 07	0 00224	195160 67
123-766C-16R-2 110-112	145 50	250.46	0.00091	78 50	0.00029	2036 73	0 00740	638 48	0.00232	275365 39
123-766C-16R-2 135-137	145.75	253 23	0.00095	69 39	0.00026	2031.27	0 00763	615.06	0 00231	266059.89
123-766C-16R-3 8-10	145 98	229 38	0 00101	60 70	0 00027	1918 71	0.00846	502 80	0 00222	226893.41
123-766C-16R-3 35-37	146 25	243 03	0 00119	89 86	0 00044	2459 06	0 01204	527.32	0 00258	204249.74
123-766C-16R-3 60-62	146 50	239 38	0.00102	124 27	0 00053	2377 97	0.01012	537.39	0 00229	235046.26
123-766C-16R-3 85-87	146.75	216 63	0 00102	80.05	0.00038	2444.13	0 01151	476.78	0 00225	212343 28
123-766C-16R-3 110-112	147.00	246 30	0 00114	74 07	0.00034	2060 60	0 00956	559.48	0.00259	215620 83
123-766C-16R-3 135-137	147.25	222 51	0.00107	78 49	0 00038	2210 56	0 01065	485.64	0.00234	207499.22
123-766C-16R-4 10-12	147.50	227 63	0 00160	100.51	0 00070	1669 51	0 01171	370.13	0.00260	142573 42
123-766C-16R-4 35-37	147.75	245 60	0.00115	110 77	0 00052	2332 05	0 01091	511 00	0.00239	213666 80
123-766C-16R-4 60-62	148 00	220 27	0.00096	118.79	0.00052	1882.60	0.00823	562.99	0.00246	228674.17
123-766C-16R-4 85-87	148 25	222 20	0 00119	128.56	0 00069	2140 68	0.01142	459.74	0 00245	187445.02
123-766C-16R-4 110-112	148 50	263 20	0 00343	101 89	0 00133	2139 94	0 02791	222 78	0 00291	76663.50
123-766C-16R-4 135-137	148 75	264 53	0.00157	78 39	0.00047	2221 73	0.01319	413 20	0.00245	168469.34
123-766C-16R-5 10-12	149 00	189 60	0 00089	81 23	0 00038	1851.17	0 00871	463 52	0.00218	212559 32
123-766C-16R-5 35-37	149.25	218 86	0.00106	83 04	0 00040	2013 54	0.00974	425 93	0 00206	206723.81
123-766C-16R-5 60-62	149.50	227.49	0.00095	61.21	0.00026	2021 65	0.00847	523.76	0 00219	238688.71
123-766C-16R-5 85-87	149.75	212 76	0 00110	71.22	0.00037	2160 31	0 01118	439 46	0 00228	193150 48
123-766C-16R-5110-112	150.00									
123-766C-16R-5 135-137	150.25	174.23	0 00088	68.94	0.00035	2051.94	0 01037	484 57	0 00245	197903.13
123-766C-16R-6 10-12	150 50	244 61	0.00085	178.24	0 00062	1950 21	0.00675	672 33	0.00233	288787.80
123-766C-16R-6 35-37	150.75	183 81	0.00073	93 89	0 00037	2338.05	0 00933	504 91	0 00201	250641 57
123-766C-16R-6 60-62	151 00	197.07	0 00096	73 65	0.00036	2345 32	0.01148	477 44	0.00234	204256 29
123-766C-16R-6 85-87	151.25	215.66	0.00098	104 49	0 00047	2393.51	0 01085	551 99	0 00250	220564 83
123-766C-16R-6 110-112	151 50	203.20	0.00134	83.21	0 00055	2501 80	0 01652	343.50	0 00227	151455 04
123-766C-16R-6 135-137	151 75	237.44	0 00123	97 00	0.00050	2544 35	0 01317	414 07	0 00214	193224 27
123-766C-16R-7 10-12	152 00	264.96	0.00190	144.63	0.00104	2907.35	0 02083	328.16	0.00235	139558.20
123-766C-16R-CC 7-9	152 16	281 98	0 00106	455 51	0 00171	2599 05	0 00978	511 90	0 00193	265639 01

Table 2: Trace element data obtained from Site 766 samples. Data are presented as both ppm and at a ratio with calcium.

Sample	Depth	Fine fraction results		*Hedbergella* spp. results		*Berthelina* spp. results		*Gyroidinoides* spp. results		*Rotalipora* spp. results		*Planomalina buxtorfi* results		*Praeglobotruncana* spp.		*Dicarinella* spp. results		*Marginotruncana* spp.	
		$\delta^{13}C$	$\delta^{18}O$	$\delta^{13}C$	$\delta^{18}O$	$\delta^{13}C$	$\delta^{18}O$	$\delta^{13}C$	$\delta^{18}O$	$\delta^{13}C$	$\delta^{18}O$	$\delta^{13}C$	$\delta^{18}O$	$\delta^{13}C$	$\delta^{18}O$	$\delta^{13}C$	$\delta^{18}O$	$\delta^{13}C$	$\delta^{18}O$
122-762C-74X-2 19-22	806.19	3.3	-2.4	2.7	-3.3											2.6	-3.1		
122-762C-74X-2 50-53	806.50	3.2	-2.6	2.7	-3.5	2.3	-2.6									2.7	-3.2		
122-762C-74X-2 79-82	806.79	3.2	-2.7	2.4	-3.6											2.7	-3.2		
122-762C-74X-2 111-113	807.11	3.3	-2.5	2.7	-3.0	2.4	-2.7									2.6	-3.1	2.9	-3.3
122-762C-74X-2 137-140	807.37	3.2	-2.5	2.4	-4.1	2.2	-2.3									2.9	-2.8	2.9	-3.5
122-762C-74X-3 10-13	807.60	3.3	-2.1	2.5	-3.3	2.3	-3.2									2.6	-2.8		
122-762C-74X-3 40-41	807.90	2.9	-2.5			2.0	-3.2									2.4	-3.3	2.5	-3.4
122-762C-74X-CC 14-16	808.05	3.0	-2.6			2.0	-2.1									2.2	-3.5	2.4	-3.3
122-762C-75X-1 5-6	809.55	3.0	-2.0			2.0	-2.3							2.3	-3.2			2.3	-3.3
122-762C-75X-1 27-29	809.77	3.0	-2.3	1.7	-3.5									2.0	-2.9	3.8	-1.9		
122-762C-75X-1 45-46	809.95	2.8	-2.7	1.9	-3.3									2.2	-3.0	2.3	-2.8		
122-762C-75X-1 60-62	810.10	3.0	-2.9	2.3	-3.2											2.2	-3.1		
122-762C-75X-1 70-72	810.20	3.2	-2.5	2.1	-3.2	1.7	-2.7							2.0	-2.9	2.7	-2.2		
122-762C-75X-1 80-82	810.30	2.9	-2.7	1.9	-3.2	2.0	-2.1							2.0	-1.8	2.1	-2.8		
122-762C-75X-1 90-91	810.40	2.9	-2.7	2.0	-3.1									2.0	-3.0				
122-762C-75X-1 99-100	810.49	3.0	-3.0	2.0	-3.0									1.7	-3.1				
122-762C-75X-1 110-111	810.60	3.7	-2.6																
122-762C-75X-1 120-121	810.70	3.6	-2.8																
122-762C-75X-1 129-131	810.80	NO CARBONATE																	
122-762C-75X-1 140-142	810.90	3.0	-2.7	1.1	-3.5	1.9	-2.4			2.2	-3.2								
122-762C-75X-1 149-150	810.99	2.9	-3.0	2.0	-3.5	2.0	-2.3			2.1	-4.3								
122-762C-75X-2 26-28	811.26	3.0	-2.6	1.9	-3.3	1.8	-2.2			2.4	-2.9								
122-762C-75X-2 51-53	811.51	2.0	-2.3	1.7	-3.3	1.7	-1.9			2.0	-3.0			1.7	-3.0				
122-762C-75X-2 75-77	811.75	2.9	-2.4	1.6	-3.1	1.5	-2.2			1.8	-2.2								
122-762C-75X-2 95-97	811.95	3.0	-2.4			1.7	-2.2			2.0	-3.3			1.3	-3.9				
122-762C-75X-2 121-123	812.21	2.9	-2.3	1.6	-3.2	1.5	-1.8			2.0	-2.4								
122-762C-75X-2 140-142	812.40	2.7	-2.4	1.4	-2.8	1.1	-3.6			1.7	-3.2								
122-762C-75X-3 15-17	812.65	2.7	-2.3	1.6	-3.1	1.5	-2.8			1.9	-2.3								
122-762C-75X-3 40-42	812.90	2.8	-2.1	1.7	-3.2	1.5	-2.5	1.3	-2.3	1.6	-3.2								
122-762C-75X-3 62-64	813.12	2.8	-2.0	1.3	-2.9	1.4	-2.2			1.5	-2.4								
122-762C-75X-3 90-92	813.40	2.4	-2.3							1.5	-3.2								
122-762C-75X-CC 13-16	813.56	2.6	-2.1	1.3	-2.9	1.3	-1.8			1.5	-2.2								
122-762C-76X-1 5-7	814.55	2.4	-2.2	1.3	-3.5	1.5	-1.8			1.6	-3.4			1.4	-3.1				
122-762C-76X-1 24-26	814.74	2.3	-2.6	1.1	-3.2	1.0	-2.0			1.5	-2.3								
122-762C-76X-1 49-51	814.99	2.4	-2.5	1.3	-2.9					1.5	-3.0								
122-762C-76X-1 74-76	815.24	2.2	-2.6	1.1	-3.1	1.1	-2.2			1.6	-2.8								
122-762C-76X-1 97-99	815.47	2.3	-2.3	1.2	-3.3	1.0	-1.8			1.4	-3.1			1.4	-3.1				
122-762C-76X-1 121-123	815.71	2.2	-2.3			1.1	-1.7			1.4	-3.1								
122-762C-76X-1 145-147	815.95	1.7	-2.6	1.1	-3.4	0.8	-2.5			1.2	-3.7			1.2	-3.3				
122-762C-76X-2 15-17	816.15	2.1	-2.3	1.1	-3.0	1.0	-1.3			1.4	-3.4								
122-762C-76X-2 40-42	816.40	2.0	-2.3	1.2	-3.1	1.1	-1.5			1.4	-2.7								
122-762C-76X-2 64-67	816.64	2.1	-2.5	0.9	-3.1	1.1	-2.6			1.0	-3.1								
122-762C-76X-2 89-91	816.89	2.1	-2.5	1.1	-3.8	0.8	-2.2			1.2	-2.7								
122-762C-76X-2 114-116	817.14	2.1	-2.5	0.9	-3.0	0.7	-3.2	1.1	-2.1	1.3	-3.0								
122-762C-76X-2 140-142	817.40	2.2	-1.9	1.0	-3.1			1.1	-2.0	1.2	-2.8								
122-762C-76X-3 9-11	817.59	2.4	-1.6																

Table 3: All isotope data from foraminiferal and fine fraction analysis at Site 762 (continued on next page....)

Sample	Depth	Fine fraction		*Hedbergella*		*Berthelina* spp.		*Gyroidinoides*		*Rotalipora* spp.		*Planomalina*		*Praeglobotrun-*		*Dicarinella* spp.		*Marginotrun-*	
		$\delta^{13}C$	$\delta^{18}O$	$\delta^{13}C$	$\delta^{18}O$	$\delta^{13}C$	$\delta^{18}O$	$\delta^{13}C$	$\delta^{18}O$	$\delta^{13}C$	$\delta^{18}O$	$\delta^{13}C$	$\delta^{18}O$	$\delta^{13}C$	$\delta^{18}O$	$\delta^{13}C$	$\delta^{18}O$	$\delta^{13}C$	$\delta^{18}O$
122-762C-76X-3 28-30	817.78	2.3	-2.1	1.6	-3.4					1.4	-2.9								
122-762C-76X-3 50-53	818.00	2.1	-2.3	0.6	-3.2	0.8	-2.2			1.3	-3.1								
122-762C-76X-3 74-76	818.24	2.1	-2.2	0.6	-3.1	-0.1	-2.6			0.8	-2.6								
122-762C-76X-3 100-102	818.50	1.8	-2.3	0.7	-3.1	0.6	-2.3			0.8	-2.7								
122-762C-76X-3 124-126	818.74	2.0	-2.5	0.8	-3.6	0.4	-2.6			0.8	-3.5								
122-762C-76X-4 6-8	819.06			1.0	-3.6	0.6	-2.3			0.6	-3.3								
122-762C-76X-4 25-27	819.25	2.0	-3.0	1.3	-4.3					0.9	-3.9								
122-762C-77X-1 5-7	819.55	1.7	-2.6	0.3	-3.0	0.5	-1.6			0.5	-3.3								
122-762C-76X-4 57-59	819.57	1.5	-3.1	0.6	-3.7	0.5	-2.6			0.9	-3.9								
122-762C-76X-4 80-83	819.80	1.8	-2.7	0.6	-3.3	0.4	-1.7			0.9	-3.4								
122-762C-76X-4 102-104	820.02	2.0	-2.6	0.0	-3.1	0.4	-1.9			0.6	-3.1								
122-762C-77X-1 55-57	820.05	1.7	-2.5	0.1	-3.3	0.2	-2.1			0.4	-3.2								
122-762C-76X-CC 16-18	820.20	1.9	-2.3	0.2	-3.5	0.4	-2.8			0.5	-3.4								
122-762C-77X-1 98-100	820.48	1.9	-1.9	0.3	-3.1					0.9	-2.9								
122-762C-77X-2 6-8	821.06	1.8	-2.1	0.1	-3.0	0.1	-2.5			0.7	-3.0								
122-762C-77X-2 55-57	821.55	1.8	-2.3	0.1	-3.2	0.2	-2.2			0.4	-3.2								
122-762C-77X-2 100-102	822.00	1.6	-1.2	-0.2	-3.2	0.2	-1.9			0.4	-2.9	0.1	-3.0						
122-762C-77X-3 5-7	822.55	1.9	-2.3	-0.2	-3.3	0.1	-1.9			0.3	-3.3	0.4	-3.0						
122-762C-77X-3 55-58	823.05	2.1	-2.0	-0.1	-3.0	0.1	-1.9			0.6	-3.2	0.3	-3.1						
122-762C-77X-3 100-102	823.50	2.0	-2.1	-0.3	-3.2	0.2	-1.8					0.5	-3.0						
122-762C-77X-4 5-7	824.05	2.0	-2.0	-0.2	-3.2	-0.7	-2.7					0.5	-3.0						
122-762C-77X-4 55-57	824.55	1.5	-2.0	-0.5	-3.2	0.1	-1.5					0.2	-2.9						
122-762C-77X-4 100-102	825.00	1.7	-1.7	-0.5	-2.8	-0.1	-1.5					-0.3	-3.0						
122-762C-77X-5 5-7	825.55	1.0	-1.7	-1.5	-3.8	-0.1	-1.6												
122-762C-77X-5 55-57	826.05	1.6	-0.9	-0.7	-3.5	-0.5	-1.5												
122-762C-77X-5 100-102	826.50	1.7	-1.0	-0.6	-3.2	0.1	-1.3												
122-762C-77X-6 5-7	827.05	2.1	-1.1	0.5	-3.3	0.1	-1.6												
122-762C-77X-6 55-57	827.55	1.2	-1.5	-1.6	-3.4	0.3	-1.3												
122-762C-77X-6 100-101	828.00			-0.8	-2.9	0.5	-0.7												
122-762C-77X-7 15-17	828.65	1.7	-0.7	-0.5	-3.1	0.3	-1.3												
122-762C-78X-1 10-12	829.10	1.1	-0.6	-0.3	-2.4	0.5	-0.9												
122-762C-78X-1 60-62	829.60	1.3	-0.7	0.8	-3.0	0.8	-0.8												
122-762C-78X-1 100-102	830.10	1.4	-0.5			1.0	-0.5												
122-762C-78X-2 10-12	830.60	0.4	-1.4			-1.2	-2.0												
122-762C-78X-2 60-62	831.10	0.1	-1.3	-0.9	-2.2	-1.7	-1.2												
122-762C-78X-2 110-112	831.60	0.5	-0.8	-0.7	-2.3	-0.8	-1.5												
122-762C-78X-CC 10-12	831.81	0.7	-1.2	-0 4	-2.3	-0.3	-1.2												

Table 3: (....continued from previous page) All isotope data from foraminiferal and fine fraction analysis at Site 762

Sample	Depth	Mn (ppm)	Mn/Ca	Fe (ppm)	Fe/Ca	Mg (ppm)	Mg/Ca	Sr (ppm)	Sr/Ca	Ca (ppm)
122-762C-74X-2 19-22	806.19	284.3794	0.001229	21271.31	0 09196	2153.485	0 00931	664.72	0.00287	231312 9
122-762C-74X-2 50-53	806.50	273.8388	0 000859	2962.578	0.00929	1079.498	0 00338	665.99	0.00209	318962 2
122-762C-74X-2 79-82	806.79	502 1781	0 001864	140351 3	0 52097	2723.854	0 01011	437 17	0.00162	269402.5
122-762C-74X-2 111-113	807 11	331.0025	0 001012	18400.27	0.05625	916 3393	0 00280	572.43	0 00175	327136 2
122-762C-74X-2 137-140	807.37	254 0541	0.000935	4366.162	0.01607	1370.252	0 00504	594 57	0.00219	271717.6
122-762C-74X-3 10-13	807.60	325.3145	0.001336	3293.006	0.01352	1144.195	0.00470	730.73	0.00300	243488 5
122-762C-74X-3 40-41	807.90	296.8304	0.00092	17328.41	0.05371	2024.223	0.00627	458 97	0.00142	322631.5
122-762C-74X-CC 14-16	808.05	259 0419	0 000777	6565 314	0 01970	976.2222	0 00293	153.26	0.00046	333248.5
122-762C-75X-1 5-6	809 55	396.5158	0.001511	4185.786	0 01595	1433 225	0 00546	408.11	0.00156	262441.1
122-762C-75X-1 27-29	809 77	443 3815	0 002264	31580.33	0.16125	2250.285	0.01149	575 12	0 00294	195841.9
122-762C-75X-1 45-46	809 95	548.8975	0.002852	15728.85	0 08171	2104.091	0.01093	581.74	0.00302	192484.7
122-762C-75X-1 60-62	810.10	361.5317	0.001517	4883.412	0.02049	872.7005	0.00366	211.78	0.00089	238327.9
122-762C-75X-1 70-72	810.20	309 279	0.001366	7475 347	0.03301	1379 936	0.00609	471.56	0.00208	226444 8
122-762C-75X-1 80-82	810.30	474 8207	0 002184	22366.17	0.10290	2426.588	0 01116	353.88	0 00163	217364 5
122-762C-75X-1 90-91	810.40	456 8558	0 0012	31828 66	0 08359	2479 73	0.00651	369.36	0.00097	380750.4
122-762C-75X-1 99-100	810.49	457.8199	0.001695	41705.78	0.15439	1514 288	0 00561	396.03	0 00147	270124 7
122-762C-75X-1 110-111	810.60	317.9916	0.014138	7598 888	0.33785	660.5361	0 02937	394 63	0.01755	22492.16
122-762C-75X-1 120-121	810.70	219 8626	0 001117	19705.26	0.10015	183 4001	0 00093	243.21	0.00124	196756 3
122-762C-75X-1 129-131	810.79	48.34144	0 000158	50985.77	0.16711	65 34956	0.00021	166.56	0 00055	305098
122-762C-75X-1 140-142	810.90	444 3471	0.001563	16711.31	0 05880	1766.337	0 00621	147.59	0.00052	284218.8
122-762C-75X-1 149-150	810 99	432 4188	0 001486	14668.58	0.05039	1363 626	0 00468	92.60	0 00032	291086.8
122-762C-75X-2 26-28	811.26	438.0241	0.002754	13337 58	0 08386	1327.298	0.00835	89 65	0.00056	159040.5
122-762C-75X-2 51-53	811.51	522.061	0 001921	23077.25	0.08492	1529 377	0.00563	155.70	0.00057	271748.2
122-762C-75X-2 75-77	811.75	518 4899	0.001875	14182 49	0 05128	1070 856	0 00387	176.65	0.00064	276580.8
122-762C-75X-2 95-97	811.95	387.3586	0 001397	19019.22	0.06859	943.7339	0 00340	169.82	0.00061	277274 3
122-762C-75X-2 121-123	812 21	534 6475	0 002114	3883.865	0 01535	1046.719	0 00414	203.53	0 00080	252958 5
122-762C-75X-2 140-142	812.40	342 9385	0 00121	20585.48	0.07262	1500 591	0.00529	185.19	0.00065	283472.6
122-762C-75X-3 15-17	812 65	560.4966	0 002343	35298.05	0.14754	1934.418	0 00809	316.28	0 00132	239248.9
122-762C-75X-3 40-42	812 90	468 1485	0.002221	5595.669	0.02655	746.3121	0 00354	390 00	0.00185	210787.7
122-762C-75X-3 62-64	813.12	389 4279	0.00144	10782.32	0 03986	2195 444	0 00812	583.81	0.00216	270499.2
122-762C-75X-3 90-92	813.40	532.8193	0.002277	32956.6	0.14084	918.1996	0.00392	622 37	0.00266	234007.4
122-762C-75X-CC 13-16	813.56	445.1	0 001624	2493 99	0.00910	1186.796	0 00433	564.75	0.00206	274143.2
122-762C-76X-1 5-7	814.55	468.5825	0 001668	18104.27	0.06443	1433.337	0 00510	657.89	0.00234	280973
122-762C-76X-1 24-26	814.74	447.0648	0 000757	17298 84	0 02931	1293 4	0 00219	649 59	0.00110	590187.9
122-762C-76X-1 49-51	814.99	549.6345	0 001894	1971.113	0.00679	482 9512	0.00166	563.82	0.00194	290260.4
122-762C-76X-1 74-76	815.24	633.7863	0.002245	25513.2	0 09035	1411.176	0 00500	816 81	0.00289	282372.1
122-762C-76X-1 97-99	815 47	603 6121	0.002096	3794 889	0.01317	662.7667	0 00230	709.65	0.00246	288042.5
122-762C-76X-1 121-123	815 71	516.7998	0 001486	5712 817	0.01643	742 2978	0.00213	507.95	0 00146	347715.3
122-762C-76X-1 145-147	815 95	578.2773	0.001971	4591 927	0 01565	728.0296	0.00248	671.74	0.00229	293443 6
122-762C-76X-2 15-17	816.15	560.1425	0.001753	4195 625	0 01313	1128.202	0 00353	510.10	0.00160	319570.9
122-762C-76X-2 40-42	816.40	618 5653	0 002746	3577.791	0.01588	975.3413	0.00433	391.32	0.00174	225266
122-762C-76X-2 64-67	816.64	548.0478	0.002583	5838 636	0.02752	648.0924	0.00305	301.82	0.00142	212170.6
122-762C-76X-2 89-91	816 89	556 8967	0.002596	7968 802	0.03714	398.6356	0.00186	201 63	0.00094	214543.2
122-762C-76X-2 114-116	817.14	534.9772	0 001818	2465.618	0.00838	406.0764	0 00138	275.30	0.00094	294187 9
122-762C-76X-2 140-142	817.40	496.929	0 002518	7052.189	0.03573	308 1115	0 00156	250.84	0.00127	197359.3
122-762C-76X-3 9-11	817.59	475 9408	0.001806	9190 855	0 03487	110.4922	0.00042	371.39	0.00141	263602.5
122-762C-76X-3 28-30	817.78	673.7884	0.003082	11795.13	0 05395	89.78483	0 00041	407.97	0.00187	218617 8
122-762C-76X-3 50-53	818 00	426.2211	0.001681	16499.17	0 06506	1406.352	0 00555	262.21	0.00103	253595.7
122-762C-76X-3 74-76	818.24	256.3688	0 001222	46503 62	0.22160	408 5287	0.00195	324.15	0 00154	209851.1
122-762C-76X-3 100-102	818.50	484.0437	0.003223	5010.573	0.03336	617.1022	0.00411	471.11	0.00314	150206.4
122-762C-76X-3 124-126	818.74	319.5062	0 00135	20923 56	0.08841	644 9309	0.00273	481 93	0.00204	236670.7
122-762C-76X-4 6-8	819 25	375 4333	0 002094	3924.708	0.02189	833 5995	0 00465	419 59	0 00234	179301 8
122-762C-76X-4 25-27	819.55	337.7503	0 001428	13807.48	0.05839	1512 769	0.00640	425.25	0.00180	236484 6
122-762C-77X-1 5-7	819.57	491.2161	0 001945	27988 3	0.11084	1838 336	0 00728	438.07	0.00173	252512 4
122-762C-76X-4 57-59	819.80	506 6344	0.00303	38787.72	0 23198	2200.095	0 01316	638.48	0.00382	167205.3
122-762C-76X-4 80-83	820.02	259.1405	0 001374	10765.25	0.05709	93.7349	0.00050	615.06	0.00326	188581 9
122-762C-76X-4 102-104	820.05	362.5852	0 001788	12260 81	0.06046	1729 061	0 00853	502.80	0 00248	202797 5
122-762C-77X-1 55-57	820 20	333.7491	0.001487	30426 92	0 13554	2017.989	0.00899	527.32	0.00235	224487.3
122-762C-76X-CC 16-18	820 48	458.7292	0 002056	35855.09	0.16073	2240.61	0 01004	537.39	0 00241	223078 5
122-762C-77X-1 98-100	821.06	444 8552	0 00231	8866.995	0 04604	990.3863	0 00514	476.78	0.00248	192582.2
122-762C-77X-2 6-8	821.55	404.0793	0.00196	181920 2	0.88229	2329.813	0 01130	559.48	0.00271	206191.5
122-762C-77X-2 55-57	822.00	370 9271	0.001294	15622.93	0.05451	1113.53	0 00389	485 64	0.00169	286597.8
122-762C-77X-2 100-102	822.55	323 0279	0.001908	11720.65	0 06922	1027.942	0 00607	370.13	0.00219	169329 5
122-762C-77X-3 5-7	823 05	473 569	0 001787	13960.88	0 05268	990.1843	0 00374	511.00	0.00193	265028.7
122-762C-77X-3 55-58	823.50	402 5804	0 001709	14534 28	0.06168	1163.376	0 00494	562 99	0.00239	235628.5
122-762C-77X-3 100-102	824.05	376 0938	0.001801	12914.18	0.06186	797.6714	0.00382	459.74	0.00220	208773.6
122-762C-77X-4 5-7	824.55	384.7262	0.001961	18974 6	0.09672	1029.171	0.00525	222.78	0.00114	196173.4
122-762C-77X-4 55-57	825.00	273.7249	0 00124	14699.45	0 06659	808.5523	0 00366	413.20	0.00187	220748
122-762C-77X-4 100-102	825 55	390 3046	0 001516	13705 51	0.05322	1000.189	0 00388	463.52	0.00180	257518.3
122-762C-77X-5 5-7	826.05	145 9338	0.000468	33497.58	0.10737	806.5904	0 00259	425.93	0.00137	311977.9
122-762C-77X-5 55-57	826.50	307.2131	0.001265	258455.7	1.06398	3064.525	0 01262	523.76	0.00216	242914 7
122-762C-77X-5 100-102	827.05	232.1724	0 001543	139709.3	0.92874	7735.143	0 05142	439.46	0.00292	150428.9
122-762C-77X-6 5-7	827.55	480.4029	0.001491	435795 2	1.35247	17022.13	0.05283	484.57	0 00150	322222.7
122-762C-77X-6 55-57	828.65	358 8847	0 001216	163973 5	0.55580	2834 407	0 00961	672.33	0.00228	295024 4
122-762C-77X-6 100-101	829.10	619.1092	0 001594	69129 16	0.17796	8172.293	0.02104	504 91	0.00130	388447.5
122-762C-77X-7 15-17	829 60	746.0511	0 002086	389895.5	1.09021	6115.702	0 01710	477.44	0 00133	357632 3
122-762C-78X-1 10-12	830.10	482 7525	0.001417	121879 7	0 35783	10516.73	0.03088	551.99	0.00162	340603.5
122-762C-78X-1 60-62	830.60	322.8295	0.001516	52121.08	0.24469	3673.263	0 01724	343.50	0.00161	213009.7
122-762C-78X-1 100-102	831.10	684.4523	0.001579	66010.54	0.15226	4811.255	0.01110	414 07	0.00096	433535.7
122-762C-78X-2 10-12	831 60	654.5953	0.001429	85201 32	0.18600	3250.909	0 00710	328.16	0.00072	458069.4
122-762C-78X-2 60-62	831 81	589 4056	0 001371	67139 86	0 15614	5292 141	0 01231	511 90	0 00119	430009 8

Table 4 : Raw data from geochemical trace element analysis at Site 762.

Sample	Untreated		Organics removed		TOC (%)
	^{13}C (PDB)	^{18}O (PDB)	^{13}C (PDB)	^{18}O (PDB)	
0	2.7	-3.0			
15	2.6	-3.1			
30	1.9	-3.6			
45	2.6	-3.3			
60	2.6	-3.0			0.141
75	2.2	-3.5			
90	2.7	-3.4			
120	2.7	-3.4			
135	2.7	-3.2			
150	2.7	-3.3			
165	2.6	-3 2			
180	2 5	-3.5	2.7	-3 6	
195	2.8	-3.2			
210	2.8	-3.3			
225	2.7	-3.5			
240	2.6	-3.4			
255	2.8	-3.3			
270	2.8	-3.5			0.068
285	2.5	-3.8			
300	2.3	-3.4			
310	2.1	-3.5			
320	2.6	-3.3			
340	2.7	-3 6			0.070
350	2.2	-3.7			
355			1.9	-3.6	0.932
360	2.2	-3.5	2.1	-3 3	0.275
365	2.1	-3.5	2.1	-3 6	0.206
370			0.7	-4.2	0.267
375	2.6	-4.5	2 8	-4.6	0.163
380	2.2	-4.6	2.4	-4.6	0.157
385	3.9	-4.2			0.550
390	2 4	-5.0	2.5	-4.8	0.217
395	2.6	-4.6	2.7	-4.5	0.200
400	3.2	-4 1	3.4	-4 2	0.222
405	3.5	-4.0	3.4	-4.2	0.310
410	3.2	-4.1	2.9	-4.2	0.127
415	3.2	-4.3	3.1	-4.4	0.083
420	3.3	-4.4	3.4	-4.2	0.116
425	3.3	-4.2	3.3	-4.4	0.116
430	3 4	-4.3	3.3	-4.4	0.256
435			2 8	-4 5	0.000
440	2.0	-4.6	2.0	-4.7	0.077
445	1.0	-4.8	0.7	-4.9	0.077
450	-0.4	-5.4	0.6	-5.5	1.291
455	3.3	-4.5	3.1	-4.9	2.331
460	3.3	-4.6	3.3	-4 8	1.134
465	1.9	-4.6	1.3	-4.8	0.233
480	4.0	-3.8	3.5	-4 4	1.961
485	3 8	-4 1	3 8	-4 4	1 010

Sample	Untreated		Organics removed		TOC (%)
	^{13}C (PDB)	^{18}O (PDB)	^{13}C (PDB)	^{18}O (PDB)	
490			1.5	-5.0	0 815
495	3.7	-4.3	3.9	-4.6	1.026
500	3 9	-4 4	3.9	-4.5	1 319
505	4.1	-4.3	4.3	-4 4	1.805
510	4.4	-4.1	4 3	-4.5	2 633
515	3.6	-3.9	3.7	-4.1	
520	3.9	-4.0	3.4	-4.5	0.469
525	3.5	-3.9	3.5	-3.8	
530	3.4	-3.9			
535	3.7	-4.3			0.090
540	3.4	-4.2			
550	3 6	-4.1			
555	3.5	-4.0			
570	3 6	-4.4			
580	3 6	-4.5			
600	2.9	-4.8			
610	3.2	-4.6			0.000
630	3.1	-4.7			
640	3 1	-4.1	3.1	-4.0	
645	3.1	-4.7			
665	3.0	-4.3			
680	3.1	-4.3			
695	2.9	-4.2			
725	2.9	-4.3			0.000
740	2.9	-4.3			
755	3.0	-4.3			
785	2.8	-3.9			
800	2.8	-4.1			
830	2.9	-3.8			
890	2.6	-3.6			
920	2.9	-3.7			0.319
930	2.8	-4.1			
940	2.8	-3.8			
950	2.8	-3.9			
980	2.9	-3.7			
1020	2.8	-3 9			
1080	2.9	-3.6			
1090	2.8	-3.9	2.9	-3.7	
1100	2.8	-3.5			
1125	2.8	-3 6	2 8	-3 9	0.205
1150					
1180	2.7	-3.9			0.280
1185			2.7	-4 0	0.432
1190					0.065
1195					
1200	2.9	-3.8			
1210	2.8	-3.8			
1220					
1230	2 8	-3 7			0 350

Table 5: All isotope values obtained from fine fraction analyses of both treated and untreated fine fraction samples of Aksudere, Crimea. TOC data is also presented.

Appendix 4

Published Papers

ELSEVIER

Cretaceous Research 26 (2005) 853–863

CRETACEOUS RESEARCH

www.elsevier.com/locate/CretRes

Stable isotope analysis of the Cenomanian–Turonian (Late Cretaceous) oceanic anoxic event in the Crimea

Jodie K. Fisher [a,*], Gregory D. Price [a], Malcolm B. Hart [a], Melanie J. Leng [b]

[a] *School of Earth, Ocean and Environmental Sciences, University of Plymouth, Drake Circus, Plymouth, Devon PL4 8AA, UK*
[b] *NERC Isotope Geosciences Laboratory, British Geological Survey, Nottingham NG12 5GG, and School of Geography, University of Nottingham, Nottingham, NG7 2RD, UK*

Received 14 April 2004; accepted in revised form 20 May 2005
Available online 14 November 2005

Abstract

Carbon and oxygen isotope data from Cenomanian–Turonian sediments from the southwest of the Crimea are presented. The sediments consist of limestones, marls and organic-rich claystones, the latter with total organic carbon values up to 2.6 wt. %, representing Oceanic Anoxic Event 2. A shift to more negative $\delta^{18}O$ values through the uppermost Cenomanian into the lowermost Turonian may be the result of warming; however, petrographic analysis shows that the samples have undergone a degree of diagenetic alteration. The carbon isotope data reveal a positive excursion from ~2.7‰ to a peak of 4.3‰ at the Cenomanian/Turonian boundary; values then decrease in the early Turonian. This excursion is comparable to those of other Cenomanian–Turonian sections, such as those seen in the Anglo-Paris Basin, and is thought to be due to global changes in the oceanic carbon reservoir. On this curve are a number of negative $\delta^{13}C$ excursions, just below the Cenomanian/Turonian boundary. It is suggested that these negative excursions are associated with the uptake of light carbon derived from the oxidation and deterioration of organic material during localised exposure of the sediments to oxic or meteoric diagenetic conditions, possibly during sea-level fluctuations.

Keywords: Cenomanian/Turonian boundary; Crimea; Carbon isotopes; Oxygen isotopes; Foraminifera

1. Introduction

There are a number of oceanic anoxic events (OAEs) throughout the Cretaceous Period, from the early Aptian (OAE 1) to the Campanian (OAE 3). Particularly well researched is OAE 2 and the organic-rich black shales deposited during this interval at the Cenomanian/Turonian boundary (CTB) (Schlanger and Jenkyns, 1976; Jenkyns, 1980; Hart and Bigg, 1981; Arthur et al., 1987; Schlanger et al., 1987; Jarvis et al., 1988; Paul et al., 1999; Keller et al., 2001).

Two main models exist for black shale deposition: (1) increased productivity, the increased flux of organic matter to the sea floor exceeding the rate of oxidation (e.g., Parrish, 1995); and (2) enhanced preservation of organic matter on the sea floor (e.g., Tyson, 1995), formed due to the expansion of the oxygen minimum zone (OMZ). Precise mechanisms are, however, still controversial. The dominant mechanism may be related to the palaeoceanographic setting in which deposition occurred (Kuhnt and Wiedmann, 1995).

Associated with these organic-rich sediments is a global positive carbon isotope anomaly (Scholle and Arthur, 1980; Pratt and Threlkeld, 1984; Arthur et al., 1988; Hart et al., 1993; Gale et al., 1993; Jenkyns et al., 1994; Voigt and Hilbrecht, 1997). This excursion has a distinctive profile and has been used for global correlation. In addition to marine carbonates, a carbon excursion has also been described from marine organic carbon and terrestrial organic carbon (e.g., Hasegawa, 1997), indicating the linkage between the ocean-atmosphere CO_2 reservoirs.

At the time of the CTB, widespread faunal diversification and extinction occurred (e.g., Hart, 1996), sea levels increased rapidly (Haq et al., 1987; Hallam, 1992) and global temperatures were significantly warmer than today (Barron, 1983;

* Corresponding author.
E-mail address: jkfisher@plymouth.ac.uk (J.K. Fisher).

0195-6671/$ - see front matter © 2005 Elsevier Ltd. All rights reserved.
doi:10.1016/j.cretres.2005.05.010

Kaiho, 1994), representing an acme for the Late Cretaceous (e.g., Huber, 1998; Clarke and Jenkyns, 1999). It has been suggested that atmospheric levels of CO_2 were 3–12 times higher than at present (Berner and Kothavala, 2001) and both the increase in temperature and rise in sea level have been linked to the anomalous amount of oceanic volcanism during the mid-Cretaceous (Larson, 1991; Kerr, 1998).

Using high-resolution carbon and oxygen isotope analyses of marine carbonates, together with measurements of total organic carbon (TOC), Rock-Eval pyrolysis and petrographic analysis, fluctuations in the global carbon reservoir can be studied, and the environment of deposition assessed. This study is aimed at providing a better understanding of environmental conditions at the CTB in the eastern Tethyan region, much previous work having focused on the west. This enables us to assess changes in the partitioning between carbonate and organic carbon sinks associated with environmental changes that occurred over the CTB.

2. Geological location and depositional setting

The Crimean Peninsula is located in the south of the Ukraine, on the northern coast of the Black Sea (Fig. 1). The peninsula comprises a range of mountains in the south that make up one-fifth of the region, whilst the greater, northern part consists of a large plain. The mountains were formed during the Cimmerian (Triassic–Jurassic) and Alpine (Tertiary) orogenies, and extend for 200 km from the northeast to the southwest, with a maximum altitude of 1500 m. The Cretaceous sediments are found within the Crimean Mountains and further north on the Crimean Plain. These sediments range from shallow marine deposits in the north to deeper deposits in the south (Kopaevich and Kuzmicheva, 2002). This paper concentrates on the outcrops in the mountains of the south. Recent research has focused on a number of Cretaceous sections in this area, and work on the stratigraphy of this region has been presented by Naidin (1981), Naidin and Alekseev (1981), Alekseev (1989), Alekseev et al. (1997), Gabdullin et al. (1999), Gale et al. (1999), Kuzmicheva (2000) and Kopaevich and Kuzmicheva (2002), with data on the isotope stratigraphy and geochemistry published by Naidin and Kiyashko (1994a,b). Our study focuses on the sediments found at Aksudere. The section lies about 30 km south of Simferopol and just north of the Kacha River. It is one of the most southerly and complete of the Cenomanian–Turonian sections in the region.

3. Stratigraphy of the Aksudere section

Within southwest Crimea, the Cenomanian comprises ~50–60 m of rhythmically-bedded (decimetre-scale) marly chalks, which show an overall decrease in the clay component up through the Cenomanian, and contain a number of erosion surfaces, seen across the region (Gale et al., 1999). The section studied at Aksudere includes Upper Cenomanian and Lower Turonian sediments, spanning the *Rotalipora cushmani* Total Range Zone (TRZ), *Whiteinella archaeocretacea* Partial Range Zone (PRZ) and *Helvetoglobotruncana helvetica*

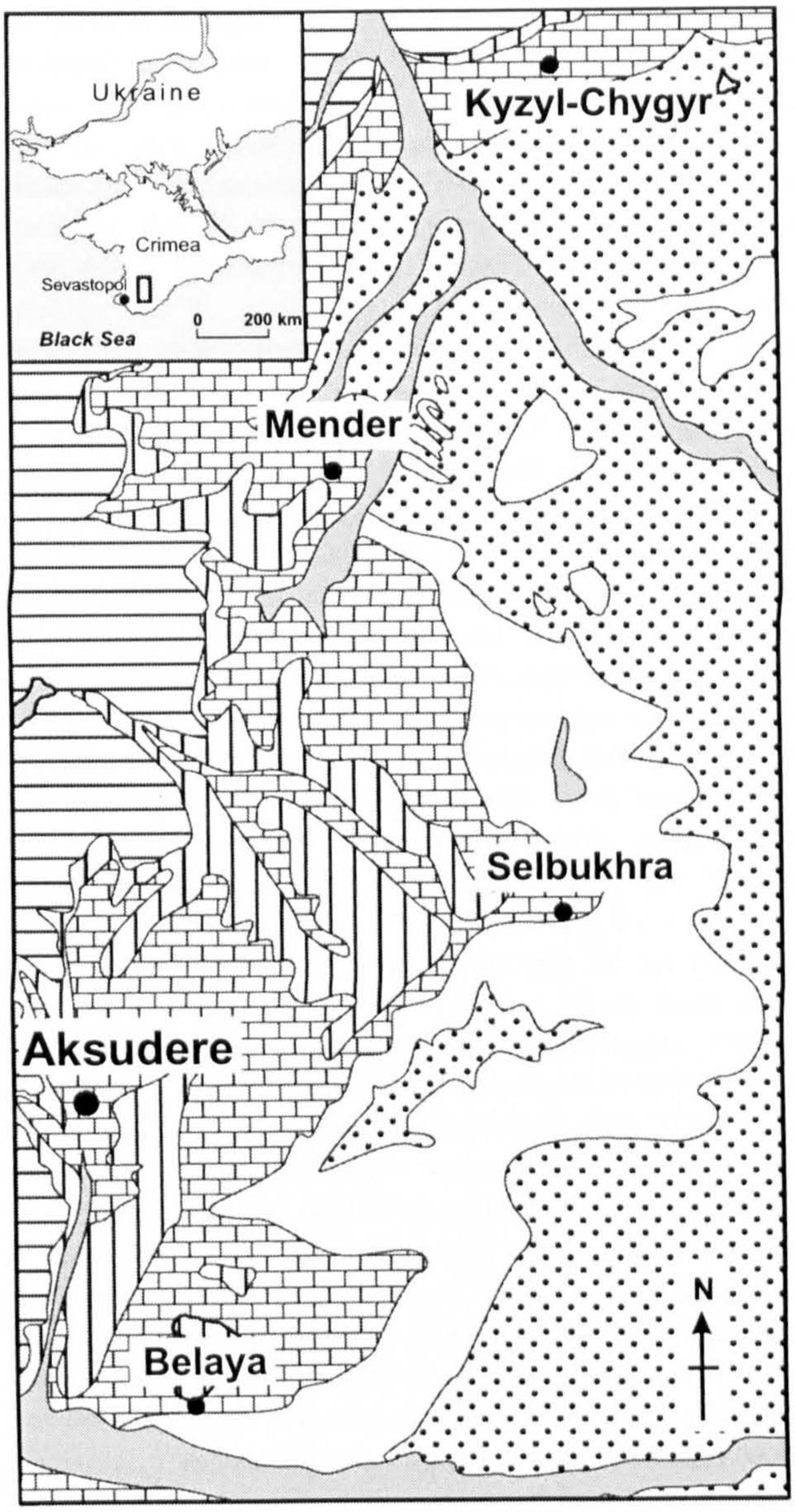

Fig. 1. Study area, showing outcrop of Upper Cretaceous sediments and location of Aksudere and other sites with Cenomanian–Turonian sections referred to in text (modified from Kopaevich and Kuzmicheva, 2002).

TRZ. For age determination of the sediments, the planktonic foraminiferal biozonation of Robaszynski and Caron (1995) was used.

The Upper Cenomanian makes up the lowermost 5 m of the section and is predominantly composed of carbonate-rich white limestones (Fig. 2). These limestones are terminated after 3.5 m by an erosion surface, at the top of the *Rotalipora cushmani* Foraminiferal Biozone. This surface is well documented by many researchers (Alekseev et al., 1997; Gale et al., 1999; Kopaevich and Kuzmicheva, 2002) and occurs in several sections across the Crimea. Gale et al. (1999) suggested that it is equivalent to the "sub-plenus erosion surface" of Jeffries (1963), seen in the Anglo-Paris Basin and the "Fazieswechsel" of Meyer (1990) in northern Germany.

Above this surface, the sediments vary greatly across the region. During the mid–late Cenomanian, the region was affected by the opening of the Black Sea and the southern margin of the Crimea developed as a continental slope of the passive margin. This had a significant effect on the water-depth of the area, the southern areas becoming significantly deeper than their northern counterparts. In the more northerly sections, such as Mender and Kyzyl-Chygyr (Fig. 1), the sediments are more condensed and incomplete, with deposits representing the *W. archaeocretacea* PRZ completely missing (Kopaevich and Kuzmicheva, 2002). Further south, at Selbukhra, the *W. archaeocretacea* PRZ is present, although only 1 m thick. The most southerly sections, at Aksudere and Belaya, however, contain a much thicker sequence (~2.5 m) of *W. archaeocretacea* PRZ sediments. Consisting of sandy marls, marls and organic-rich claystones, these sediments grade upwards into marls and limestones of early Turonian age. Aksudere is, therefore, one of the most complete sections in southwest Crimea, although foraminiferal data indicate that a small stratigraphic gap exists at the late Cenomanian erosion surface discussed above (Kopaevich and Kuzmicheva, 2002).

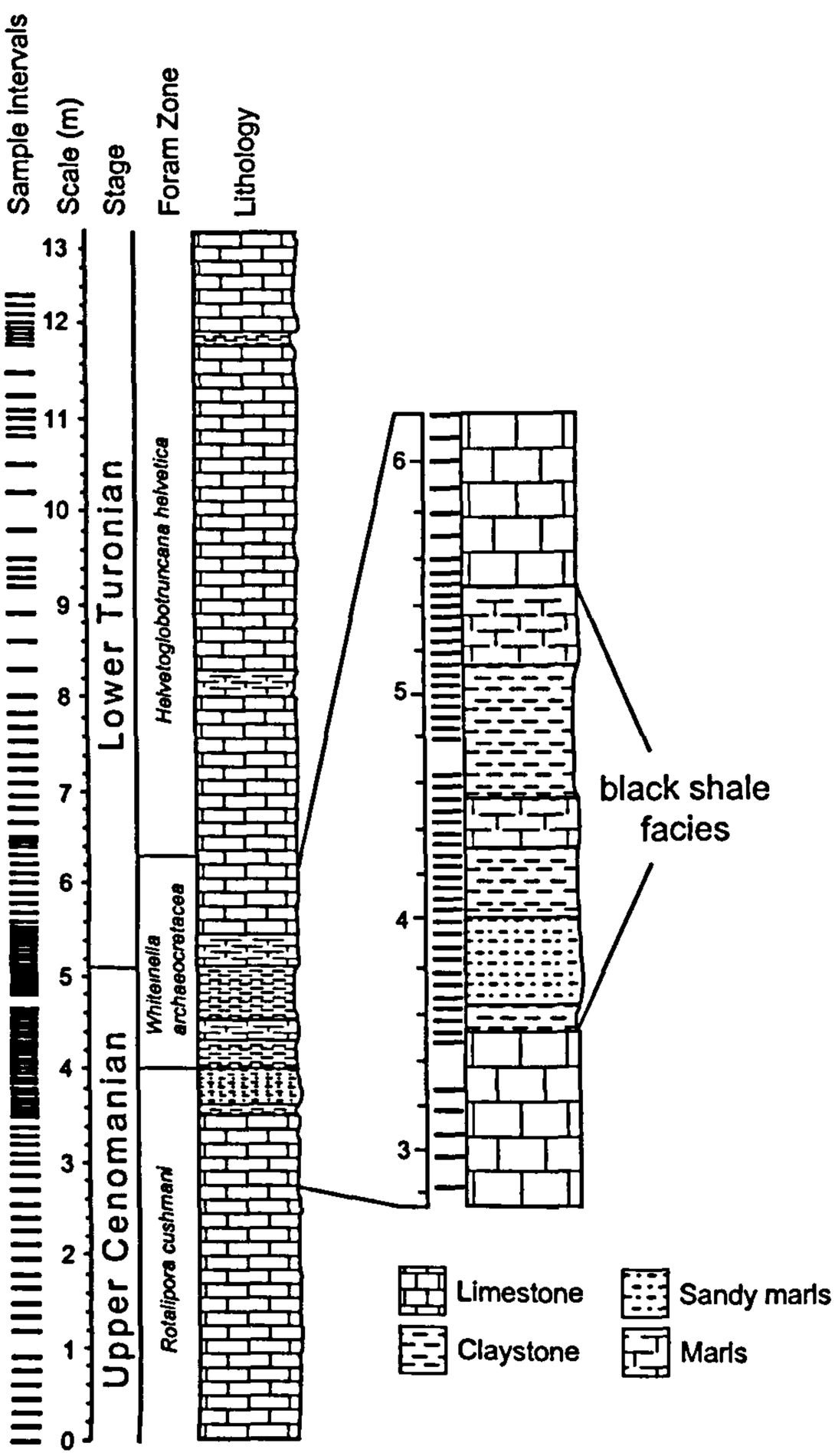

Fig. 2. Stratigraphical log of Cenomanian–Turonian sediments seen at Aksudere, based upon Alekseev et al. (1997) and this study. Foraminiferal biozonations after Robaszynski and Caron (1995).

At Aksudere, the late Cenomanian erosion surface is directly overlain by a 10-cm-thick dark claystone that grades upwards into a 40-cm-thick yellow, quartz-rich sandy marl. Gale et al. (1999) suggested that this was equivalent to Bed 3 of the Plenus Marls, the top of this bed marking the base of the *W. archaeocretacea* PRZ. This is overlain by a second claystone 30 cm thick, and grading up into 20 cm of pale grey marl. Above this lies a third claystone, 60 cm thick and laminated; it contains some thin quartz-sand layers. These dark claystones were described by Gale et al. (1999) and Naidin and Kiyashko (1994a,b) as organic-rich with TOC values up to 9 wt.%. Carbonate values were seen to be no lower than 45%, and as much as 65% in these beds (Naidin and Kiyashko, 1994a). The top of this bed marks the Cenomanian/Turonian boundary, defined by previous workers at Aksudere (e.g., Kopaevich and Kuzmicheva, 2002) by the first appearance of *Dicarinella hagni*. This claystone then grades into paler marls and limestones of Turonian age, as the sediments become less clay-rich. These sediments adjacent to the CTB can be defined as a "black shale facies", and are known locally as the Aksudere Beds (Alekseev et al., 1997). They are thought to be the local expression of OAE 2 (Naidin and Kiyashko, 1994a,b; Kopaevich and Kuzmicheva, 2002) (Fig. 2).

4. Material and methods

The Aksudere section was sampled at 5 to 15 cm intervals throughout the 12.5 m section to obtain 109, samples spanning the Upper Cenomanian–Lower Turonian *Rotalipora cushmani–Helvetoglobotruncana helvetica* foraminiferal biozones. The samples were disaggregated using standard techniques: the softer marls by soaking in a 10% solution of sodium hexametaphosphate (Calgon), and the harder samples using the solvent method of Brasier (1980). All samples were washed over a 63 μm sieve and dried at 40 °C. A portion of the fine (<63 μm) fraction was kept for whole-rock (fine-fraction) isotope analysis, whilst the >63 μm fraction was used for foraminiferal analysis. After drying, the fine-fraction samples were ground and homogenised in an agate pestle and mortar. Samples

were processed a second time in order to obtain fine-fraction samples for treatment with 5% sodium hypochlorite, in order to remove any organic matter from the samples.

Oxygen and carbon isotope analyses on the fine-fraction carbonate were undertaken using standard offline vacuum methods (McCrea, 1950) on samples both treated and untreated with 5% sodium hypochlorite, using a dual-inlet stable isotope mass spectrometer.

The ratios are presented in relation to the heavier isotope using the δ notation and the VPDB scale. Analytical precision, based on duplicate samples, was typically $<0.1‰$ for both oxygen and carbon isotope ratios. Consistency of results was achieved by comparison of laboratory standards against NBS-19.

Analysis to determine the TOC was carried out using a TOC 5000 carbon analyser. A small amount of sample was crushed and homogenised in an agate pestle and mortar, and analysed in a solid sample module 55M-5000A. Samples were duplicated where possible and reproducibility was generally better than 0.1%. All results are given as wt. % TOC. Samples were also analysed with a Rock-Eval 6, at the University of Neuchâtel, to determine the source of organic matter within samples with TOC values >0.5 wt. %.

Thin sections were obtained from a selection of samples throughout the succession, in order to undertake petrographic analysis of the sediments and to observe any diagenetic alteration of the samples.

5. Results

5.1. Petrographic analysis

Thin sections of wackestones and mudstones from the Cenomanian limestones (Fig. 3A) reveal a diverse and abundant microfauna. This is characterised by single-keeled, large planktonic foraminifera such as *Rotalipora cushmani*, *Rotalipora greenhornensis* and *Praeglobotruncana gibba*, and smaller, shallower-dwelling foraminifera, such as *Heterohelix moremani*, *Hedbergella delrioensis*, *Hedbergella planispira*, *Whiteinella* spp. and *Guembelitria cenomana*. These are indicative of the Upper Cenomanian *R. cushmani* TRZ. This microfauna can

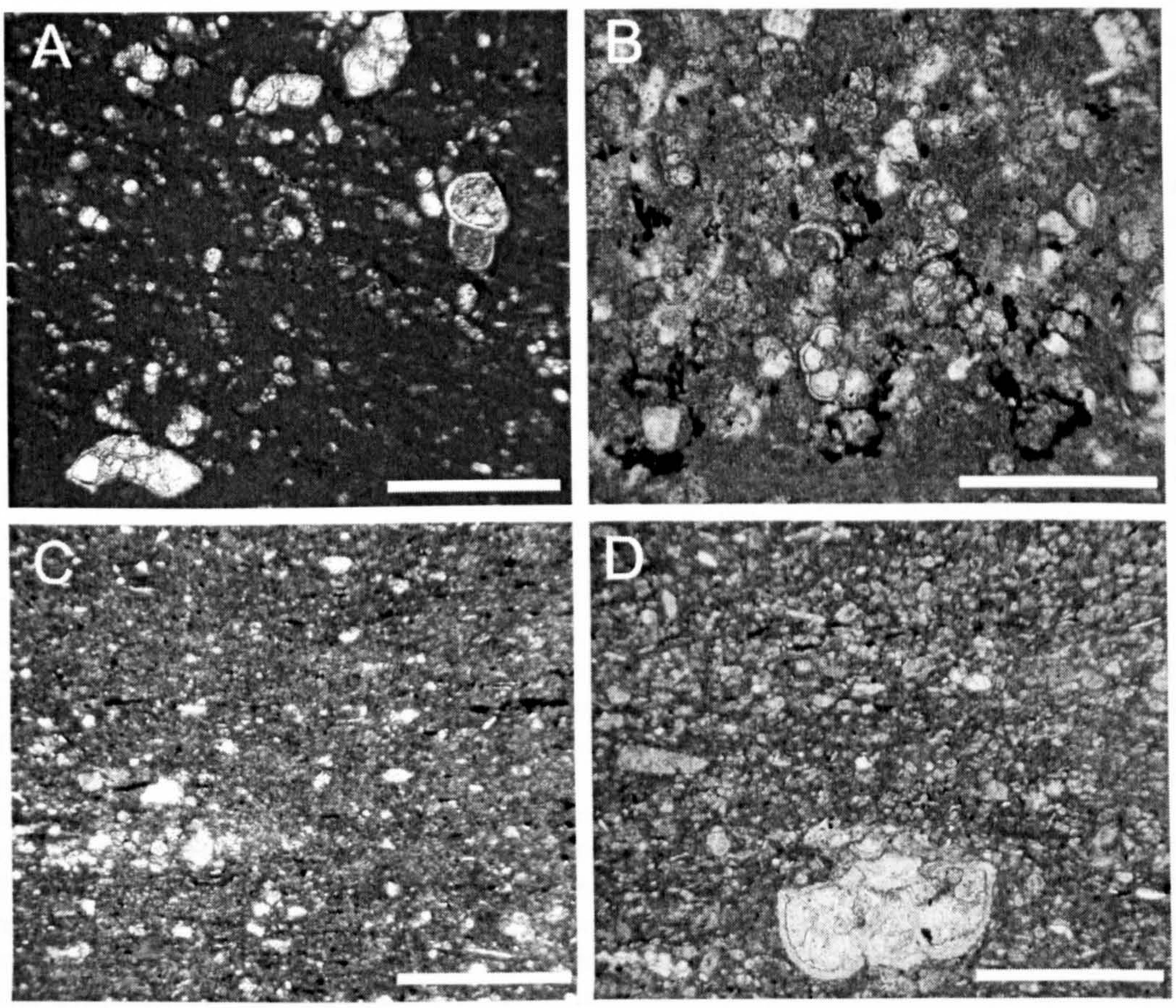

Fig. 3. Examples of lithologies and microfauna throughout the Aksudere section. A, wackestone from Cenomanian limestone, 1.8 m below the CTB. Diverse, high-abundance foraminiferal assemblage including *Rotalipora cushmani* indicating the *R. cushmani* Biozone. Infilling and recrystallisation of foraminiferal tests with sparry calcite is prevalent. B, wackestone from marls 75 cm below the CTB, showing a reduction in diversity of foraminifera and loss of keeled genus, *Rotalipora*. Dominated by *Hedbergella* spp. and *Whiteinella* spp., indicating the *Whiteinella archaeocretacea* Biozone. Again, specimens show poor preservation, with infilling and recrystallisation of tests. C, laminated claystone from the CTB, almost devoid of foraminifera. Quartz and glauconite present. D, packstone from Turonian limestones, 6.7 m above the CTB, showing a return to higher diversity and abundance. Large foraminifera return and new keeled species, such as *Helvetoglobotruncana helvetica*, are seen, indicating the *H. helvetica* Biozone. Infilling and recrystallisation of foraminiferal tests is prevalent. Scale bars represent 500, 200, 400 and 500 μm respectively.

be seen in Fig. 3A, where abundant recrystallisation of the test walls, and infilling of the tests with sparry calcite, can be seen.

Within the marls below the CTB (Fig. 3B), a very different assemblage from that of the underlying Cenomanian limestones is seen. These wackestones are dominated by small planktonics, predominantly *H. moremani* and *H. delrioensis*. There are no larger planktonics and the genus *Rotalipora* has disappeared completely, marking the *Whiteinella archaeocretacea* PRZ. The preservation of species is generally poor, showing high levels of recrystallisation and infilling. Small grains of glauconite and quartz are also seen.

The thick claystone layer, lying directly below the CTB, appears to be nearly devoid of any foraminifera (Fig. 3C); however, fine laminations within the claystone are apparent. Quartz and glauconite are present, concentrated in thin lenses within the claystone.

Another foraminiferal assemblage is seen in the Turonian limestones (Fig. 3D). A large increase in the number of specimens and species appear preserved in these packstones. They are dominated by small *H. delrioensis*, *Whiteinella* spp. and *H. moremani*, with less abundant large planktonic foraminifera present, such as species of *Praeglobotruncana*. These sediments also contain the first occurrences of the keeled species, *Dicarinella hagni* and *Helvetoglobotruncana helvetica*, characteristic of the *H. helvetica* TRZ. The preservation of the foraminifera is again poor, sparry calcite commonly infilling the recrystallised tests. Fragments of inoceramid bivalves are also seen throughout the *H. helvetica* Zone.

5.2. TOC

TOC values (Fig. 4) are low in the Upper Cenomanian limestones, reaching no more than 0.1%. A small increase, to 1.0%, is seen in the lowermost thin claystone; however values remain low (<0.5%) through the overlying sandy marl, and into the *W. archaeocretacea* PRZ. They increase rapidly at the base of the upper claystone unit, peaking at 2.3%, 0.5 m below the CTB. The values then decrease back down to 0.2% over 0.1 m, prior to two subsequent peaks in this unit. TOC increases again to 2.0%, 0.3 m below the CTB, decreases to 0.8% and finally increases to the largest value of 2.6%, at the CTB. They then return to near zero, 0.15 m above the CTB, and remain low through the *H. helvetica* TRZ of the Lower Turonian.

These TOC values show that organic-rich samples lie in the *W. archaeocretacea* PRZ, in the upper claystone (from 0.7 m below the CTB to just below the CTB) and, in one sample, in the lowermost claystone at the top of the *R. cushmani* TRZ. All samples with TOC >0.5 wt. % were analysed with Rock-Eval pyrolysis. The data obtained are shown in Fig. 5. They indicate that the samples contain mixtures of Types II and III kerogen (organic matter derived from algae, bacteria and marine zooplankton, with some higher plant contribution), as indicated by hydrogen indices ranging from 142 to 321 mg HC/g TOC. The hydrogen indices appear to increase with organic richness, indicating a higher proportion of marine-derived organic matter in the organic-rich layers of the claystones, seen 0.5 m and 0.3 m below the CTB and at the CTB.

5.3. Carbon and oxygen isotope ratios

The analytical data are presented in Figs. 4 and 6. The Upper Cenomanian (*R. cushmani* TRZ) has $\delta^{13}C$ background values of ~2.7‰. These values decrease slightly to 1.9‰ in the lowermost claystone of the Aksudere Beds, then increase rapidly to a peak at the top of the sandy marl at the very top of the *R. cushmani* TRZ. Values then plateau through the *W. archaeocretacea* PRZ at around 3.3‰, peaking again at 4.4‰ at the top of the upper claystone unit, at the CTB. $\delta^{13}C$ values then decrease slowly through the rest of the *W. archaeocretacea* PRZ and into the *H. helvetica* TRZ of the Lower Turonian, to steady values of ~2.9‰ at a level 1 m above the CTB.

The $\delta^{18}O$ values show greater fluctuations than the carbon isotope data. $\delta^{18}O$ values of ~−3.4‰ are observed in the Upper Cenomanian, up to the base of the sandy marl. After this point, values decrease rapidly to −5.0‰ at the top of the sandy marl, the top of the *R. cushmani* TRZ. Values then fluctuate between −4.0 and −5.0‰ through the whole *W. archaeocretacea* PRZ before decreasing slowly, as the limestones become less marly, to background values of ~−3.8‰ at 3.5 m above the CTB. These oxygen and carbon isotope values are in the same range as those of Naidin and Kiyashko (1994a,b).

In addition to these main trends, however, four negative excursions not recorded previously are particularly prominent on the $\delta^{13}C$ curve. The lowest is in the sandy marl 1.4 m below the CTB, in the *R. cushmani* TRZ; the other three lie in the upper thick claystone unit of the *W. archaeocretacea* PRZ, at 0.6, 0.45 and 0.1 m below the CTB, respectively. In order to rule out contamination of the samples by organic matter, they were treated with sodium hypochlorite, as described above. The results for both treated and untreated samples are nearly identical, ruling out contamination.

6. Discussion

Both carbon and oxygen isotope profiles show excursions that are comparable to those seen elsewhere across the CTB. Fig. 7 shows the correlation of the carbon isotope curve with the profile of Gale et al. (1993) from Eastbourne, UK. The shape of the latter is identical to those of Paul et al. (1999), Keller et al. (2001) and Tsikos et al. (2004). As indicated above, Gale et al. (1999) suggested that the sandy marl unit lying directly above the erosion surface is probably equivalent to Bed 3 of the Plenus Marls, the erosion surface itself being the equivalent of the "sub-plenus erosion surface". At Eastbourne, the carbon excursion begins at the base of the Plenus Marls. In the Crimea, it begins above the erosion surface. This may be due to the longer duration of the erosion event in the Crimea (see below). Both profiles increase rapidly to an initial peak at the top of the *Rotalipora cushmani* TRZ. Plateauing within the lower part of the *Whiteinella archaeocretacea* PRZ, they both record a second peak around the CTB. Both

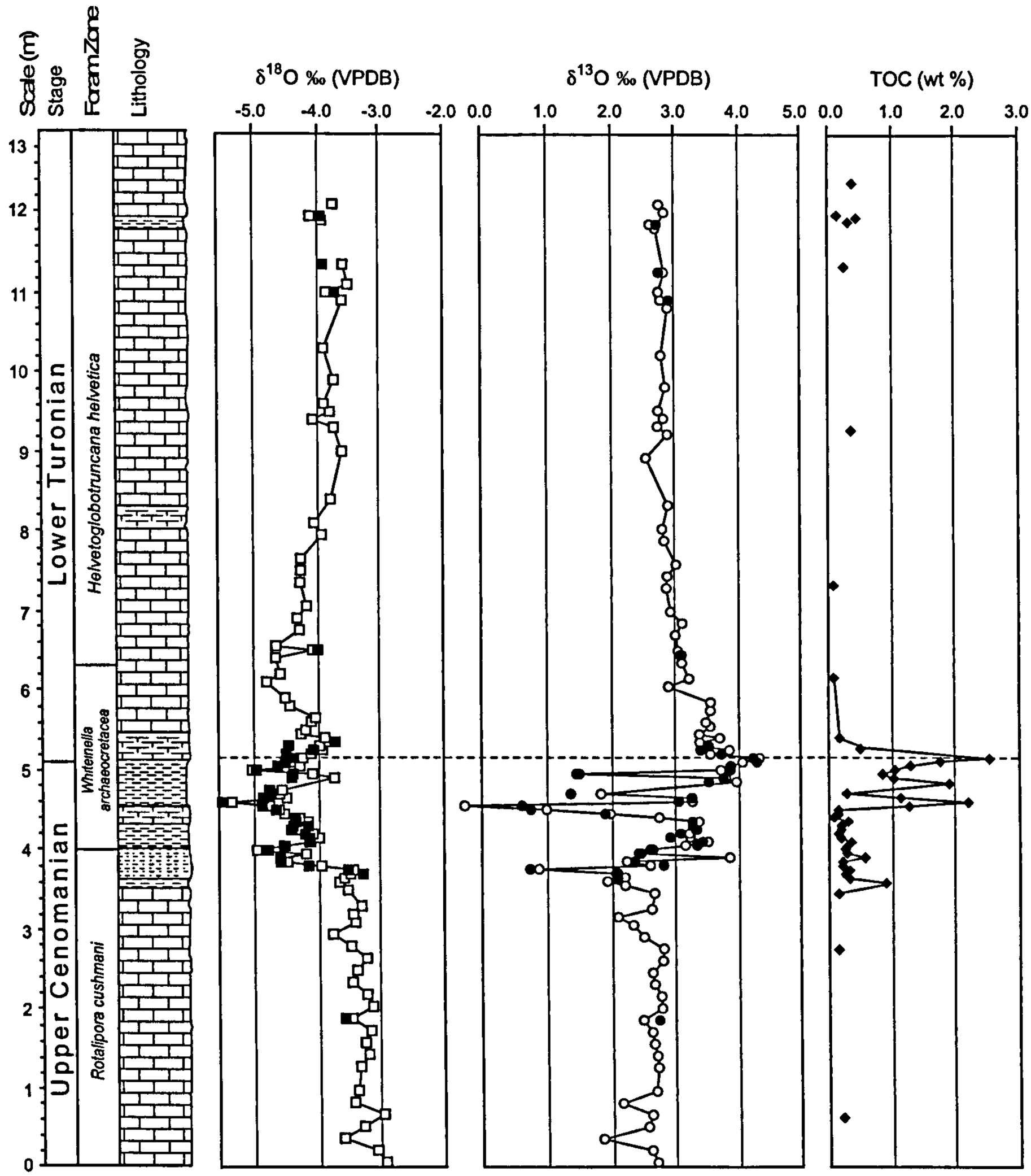

Fig. 4. Carbon and oxygen isotope results of fine-fraction (<63 μm) samples of both untreated (open squares and open circles) and treated (organic carbon removed) (filled squares and filled circles) samples, and TOC results from Aksudere. Foraminiferal biozonation after Robaszynski and Caron (1995).

excursions then decrease slowly to reach pre-excursion values in the *Helvetoglobotruncana helvetica* TRZ. Regionally, the data show that both Crimean and northwest European sections may have undergone similar palaeoceanographic change around the CTB, the correlative erosion surface possibly indicating a regional European regression. Foraminiferal data, however, indicate that the duration of this hiatus is longer in the Crimea than in the Anglo-Paris Basin (Kopaevich and Kuzmicheva, 2002). The increased duration in the Crimea was probably due to large-scale tectonics, leading to uplift and prolonged exposure of the sediments to erosion. Tectonic rebuilding of the region during the Albian–Cenomanian and the rifting and/or extension in the Crimean and Caucasus region (Nikishin et al., 1997) possibly contributing to this.

In the Aksudere section the oxygen isotope data show a sharp decrease in values coincident with a distinct increase in the carbon isotope values. This may indicate increased sea-surface temperatures around the time of the CTB. As noted above, evidence suggests that sea-surface temperatures were higher during the mid-Cretaceous, reaching an all time high for the Phanerozoic in the Turonian. The low values and rapid fluctuations seen in the $\delta^{18}O$ profile for the Crimea are, however, possibly consistent with diagenesis of the sediments. Petrographic observations support this, showing sparry calcite cement and an infilling of foraminiferal tests to be present throughout the succession (Fig. 3A–D), indicating that diagenesis affected sediments throughout the section.

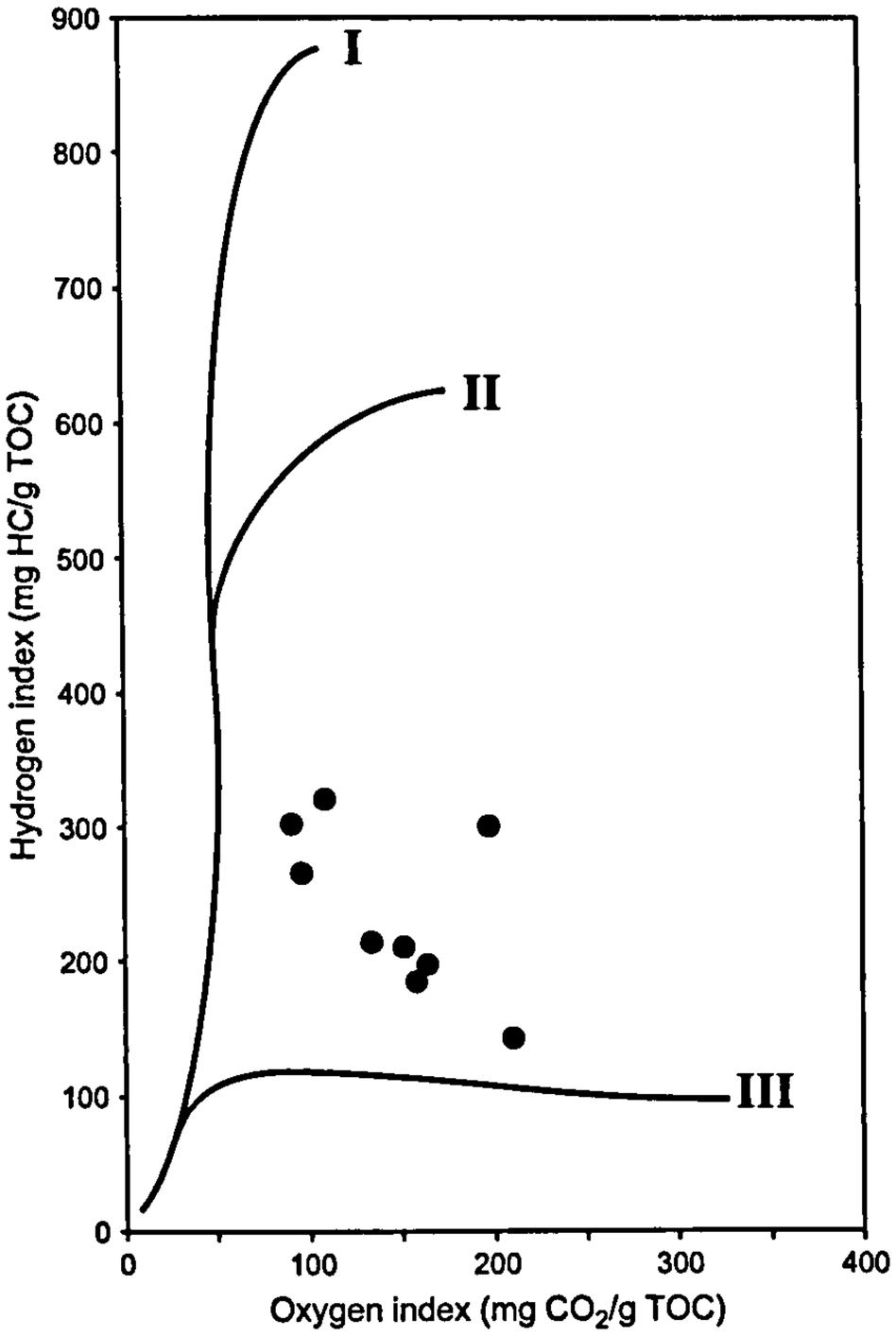

Fig. 5. Van Krevelen plot indicating nature and source of organic matter in organic-rich claystones at Aksudere.

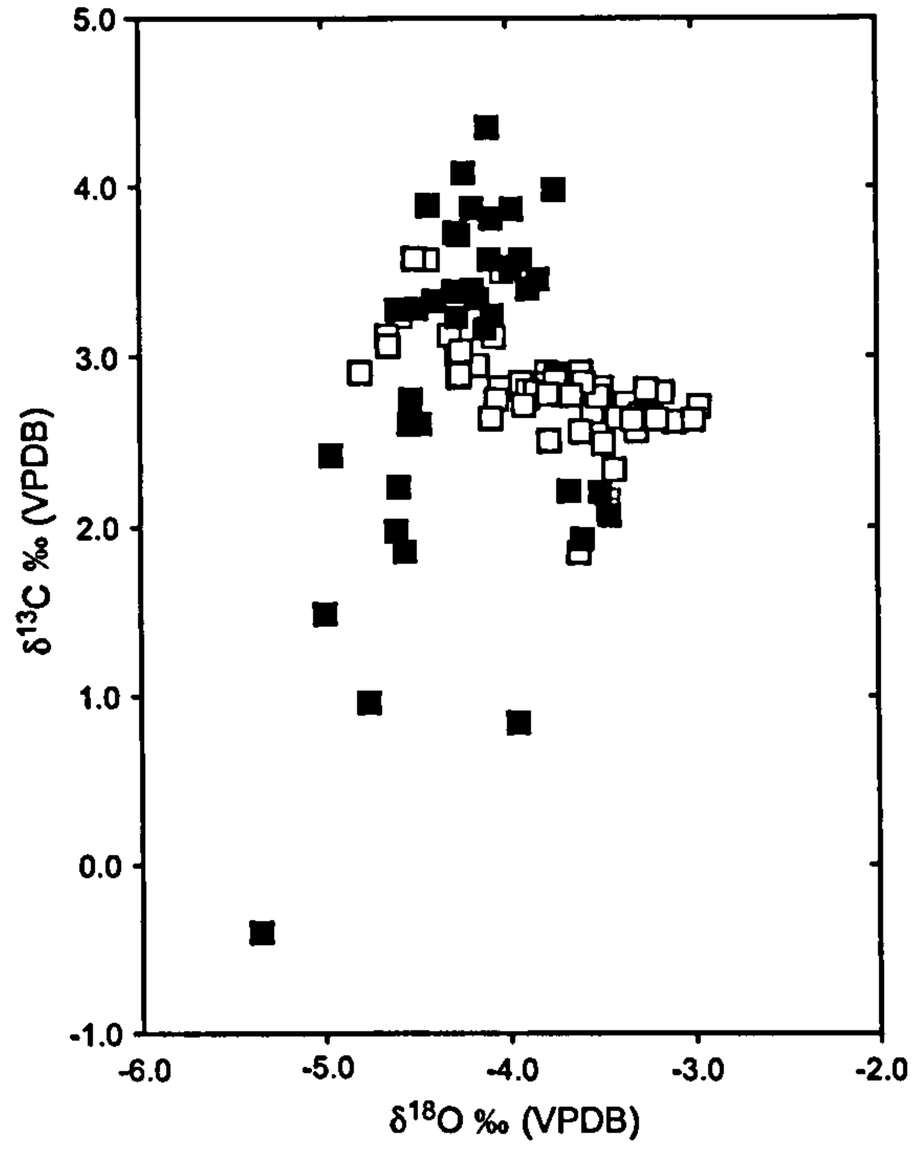

Fig. 6. Cross-plot of oxygen and carbon isotopes from fine-fraction samples of both treated (organic carbon removed) and untreated (organic carbon present) samples. Carbonate samples, open squares; "black shale facies" samples, closed squares.

During diagenesis, primary calcite can be replaced by calcite in equilibrium with the diagenetic environment, whether within the sediments during burial, or on the sea floor. Oxygen isotopes are more susceptible to diagenesis than the more robust carbon isotopes. This is partly due to the large temperature-related fractionation seen in oxygen isotopes. Scholle (1977) found untectonised European chalks to have average $\delta^{18}O$ values of −2.9‰, ranging generally between −2 and −4‰. Diagenesis of chalks, however, can lead to much lighter values, as low as −8‰ (Jørgensen, 1987). Using a standard temperature equation (e.g., Anderson and Arthur, 1983) would suggest an increase of ocean temperatures of ~6 °C as the values decrease from −3.5 to −5‰ at Aksudere. A similar trend is seen in other Cenomanian–Turonian sections (e.g., Jenkyns et al., 1994). However, these values equate to temperatures of ~30–35 °C, considerably warmer than temperatures postulated for the mid-Cretaceous (Barron, 1983) at a palaeolatitude for the Crimea of ~35°N (Smith et al., 1994).

It is likely, therefore, that the $\delta^{18}O$ results at Aksudere were affected by diagenesis shifting the primary signal to more negative values. A cross-plot of $\delta^{13}C$ and $\delta^{18}O$ data (Fig. 6) also shows a weak positive correlation typical of sediments thought to have been affected by meteoric diagenesis (e.g., Allan and Matthews, 1982; Marshall, 1992; Buonocunto et al., 2002).

The positive carbon isotope excursion, also seen in isotope data from organic carbon (Naidin and Kiyashko, 1994a,b), can be interpreted as a response to the abnormally high burial rates of organic carbon that characterise the Cenomanian–Turonian sediments seen globally and at Aksudere. Rock-Eval data indicate that the organic matter in the organic-rich claystones at the CTB of Aksudere is autochthonous, marine-derived carbon predominantly from phytoplankton, with some contribution from higher plant matter.

As described above, in addition to the long-term trends in the isotope profiles, a number of negative carbon isotope events are clearly seen in the carbon isotope data, and also to a smaller extent in the oxygen isotope data. It is possible that negative values arise from contamination of the carbonate from organic matter. However, the similarity between carbon and oxygen isotope values of both the untreated samples and the samples with organic material chemically removed rules out this possibility. It can be postulated, therefore, that the negative values are a result of environmental effects and/or diagenesis.

6.1. Environmental effects

Negative carbon excursions have been considered to be a result of changes in ocean circulation and chemistry. Recent work, however, has focused on the effect of the introduction of isotopically light carbon into the system from magmatically-derived CO_2 and methane (e.g., Bralower et al., 1994; Jahren et al., 2001; Price, 2003).

There is a great deal of evidence for volcanism during the Cretaceous and around the CTB (Kerr, 1998). Widespread ocean plateau volcanism (e.g., the Caribbean-Colombian and Ontong Java plateaus in the Pacific, and the Kerguelen Plateau

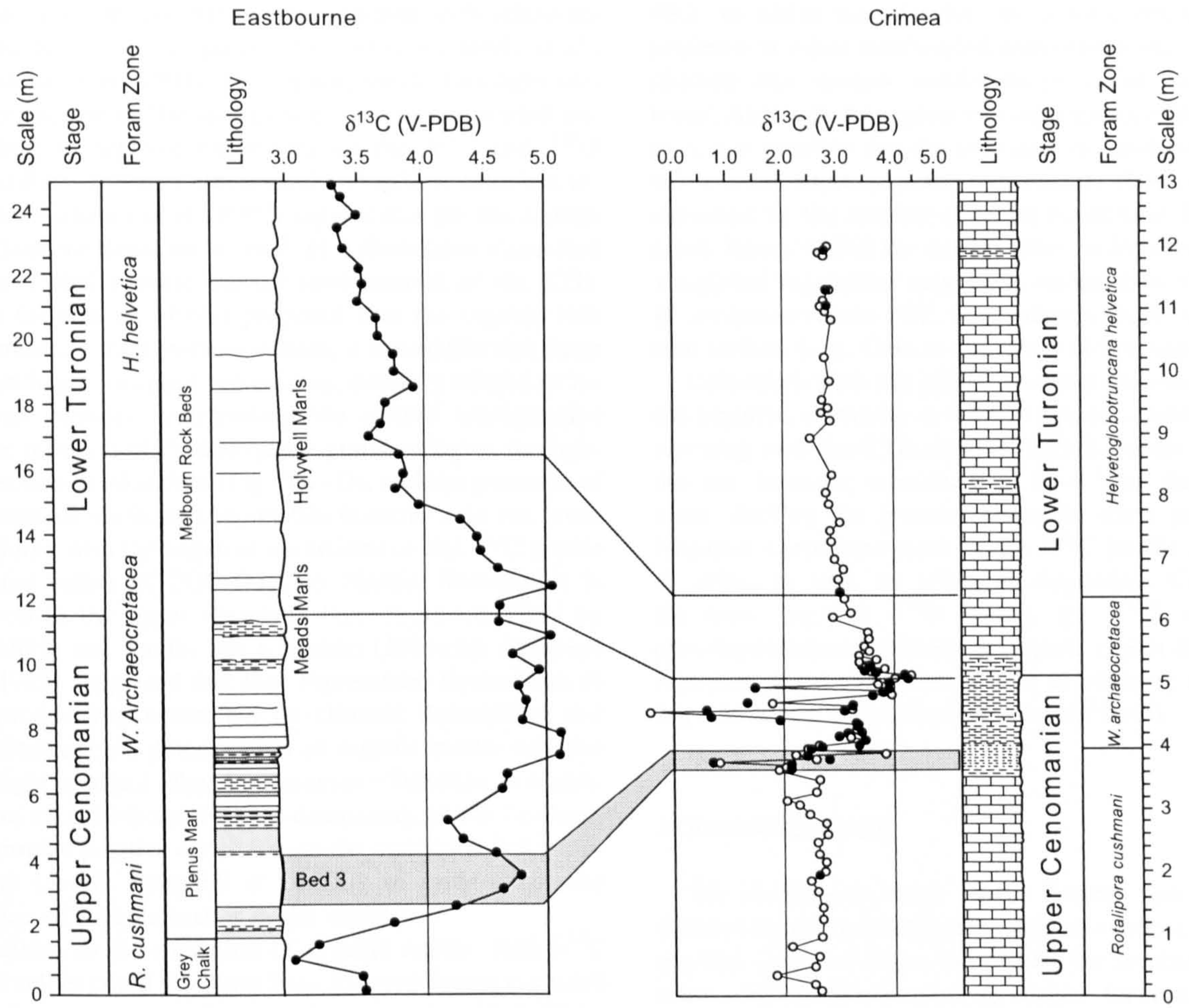

Fig. 7. Correlation of carbon isotope results from this study with carbon isotope profile from Eastbourne, UK from Gale et al. (1993). Eastbourne bed number assignment according to Gale et al. (1993). Eastbourne foraminiferal biostratigraphy from Keller et al. (2001), Crimean biozonation after Robaszynski and Caron (1995). Crimean profile: open circles, untreated values; filled circles, chemically treated (organic carbon removed) values.

in the Indian Ocean) caused the expulsion of isotopically light (typically 6–7‰) carbon into the atmosphere and carbon cycle. Volcanism has been suggested to account for negative isotope shifts in the early Aptian (OAE 1a) (e.g., Bralower et al., 1994; Larson and Erba, 1999; Price, 2003). However, no direct effect upon carbon isotope profiles has been suggested for the CTB.

Methane is also a viable source of light carbon (isotopic values ~ -60‰), able to produce the rapid and large negative shifts observed at a number of OAEs (e.g., the Toarcian and Aptian OAEs) (Hesselbo et al., 2000; Jahren et al., 2001; Beerling et al., 2002). Negative excursions have been seen prior to the positive excursion at the CTB (e.g., Pratt, 1985; Arthur et al., 1988; Hasegawa, 1997), although none has been convincingly attributed to methane hydrate dissociation.

In the Crimean section, the negative carbon isotope events occur during the positive isotope excursion, as opposed to preceding it. Negative excursions, similar to those seen in the Crimea, are observed at the Devonian Frasnian/Famennian boundary (364 Ma), interrupting the positive $\delta^{13}C$ excursion seen in South China and Canada (e.g., Wang et al., 1996; Chen et al., 2002). Dissociation of methane hydrates has been suggested, the late Frasnian regression triggering their release, leading to increased levels of ^{12}C in the biosphere, rapid global warming, rapid sea-level rise and oceanic anoxia. Similarly, at the CTB, a section in New Jersey (USA) was found to have two negative peaks, both short (10 kyr) and large (>5‰); it has been postulated that methane release was a possible mechanism to explain such a signal (Wright et al., 2001). The presence of coincident negative oxygen and carbon isotope shifts, however, would suggest that such a signal was more likely to be diagenetic in origin (see below).

At Aksudere, it is also unlikely that the negative shifts are due to the introduction of light carbon from methane or volcanism. No global negative signal is seen at the CTB, unlike for the events discussed above, which would be expected with such a large influx of methane or volcanically-sourced ^{12}C into the biosphere.

6.2. Diagenetic signal

The presence of an erosion surface at the base of the Aksudere Beds, and the sandy nature of the sediments, indicates a possible regression in the region, just below the CTB. During the lowering of sea level, organic matter can become oxidised,

leading to localised diagenetic environments with relatively high amounts of ^{12}C and potentially ^{16}O (e.g., Jarvis et al., 1988; Malone et al., 2001). During diagenesis, this light carbon and oxygen would be incorporated into reprecipitated calcite, leading to negative excursions on the $\delta^{13}C$ and $\delta^{18}O$ isotope profiles. Through lithological and palaeontological investigation, Alekseev et al. (1997) suggest that the black shale facies (Aksudere Beds) are a result of a short-term regression during the global eustatic transgressive interval of the CTB. Although Gale et al. (1999) proposed that the organic rich marls represent a transgressive system, it is possible that there were short-lived, localised regressions, possibly related to local tectonic activity, overprinting the overall transgressive trend. The presence of detrital quartz grains in layers throughout the section at Aksudere (Fig. 3A–D), and the presence of regional erosion surfaces, support this fluctuation in sea level.

Coinciding with the negative excursions on the $\delta^{13}C$ profile are lowered values of TOC (Fig. 4). Similar fluctuations in TOC levels in the upper claystone layer were identified by Naidin (1993) and Naidin and Kiyashko (1994a,b). Although Naidin (1993) suggested that they represented fluctuations of pelagic productivity controlled by climatic fluctuations and Milankovitch cycles, deterioration of organic matter has also been thought to affect other Cenomanian–Turonian localities. Jenkyns et al. (1994) attributed a dampening of the Cenomanian–Turonian positive excursion, in the stratigraphical vicinity of the Livello Bonarelli at Gubbio, to early diagenetic degradation of organic matter in the claystone.

In addition to the oxidation of organic matter, both $\delta^{13}C$ and $\delta^{18}O$ values could also have been lowered during exposure of the sediments to meteoric water during sea-level fall. Meteoric water has lower $\delta^{18}O$ than marine water and can be accompanied by low $\delta^{13}C$ where the waters contain isotopically light carbon from soil-derived CO_2 (e.g., Allan and Matthews, 1982; Marshall, 1992). During early diagenesis, it is possible that the carbonates partially equilibrate with these fluids, causing lower $\delta^{13}C$ and $\delta^{18}O$ (e.g., van Buchem et al., 1999). The isotope data therefore appear to show the influence of post-depositional oxidation and degradation of organic matter during early diagenesis, associated with a fall in sea level and the influx of meteoric waters to the sediments.

7. Conclusions

The Cenomanian–Turonian section at Aksudere clearly shows a carbon isotope profile reflecting enhanced drawdown of ^{12}C into organic-rich sediments, and the enrichment of marine waters in ^{13}C. This $\delta^{13}C$ excursion can be directly correlated with carbon isotope profiles seen elsewhere in northwest Europe (e.g., Eastbourne, UK), indicating the widespread nature of the changes to the ocean-atmosphere CO_2 reservoir, caused by global factors.

Synchronous with the positive excursion are increased TOC values, indicating the isotope excursion to have occurred synchronously with the deposition of organic-rich sediments, possibly in anoxic bottom conditions. It is likely that the degree of anoxia fluctuated through the *Whiteinella archaeocretacea* PRZ, in which the Aksudere Beds were deposited, with the presence of marls interbedded with organic-rich claystones indicating that dysoxic conditions prevailed intermittently, at times. Although the region was undergoing a global transgression, it is possible that the activation of geodynamic processes led to local, short, periodic regressions. These regressions are indicated by the number of small hiatuses in the region, and sandy layers within the deeper-water sediments. Additionally, a regional regression may have occurred at the base of the *W. archaeocretacea* PRZ, correlative with the sub-plenus erosion surface (e.g., Gale et al., 1999) of the Anglo-Paris Basin.

Coincident with the positive carbon excursion is an apparent negative excursion in the $\delta^{18}O$ profile, possibly indicating warming over the CTB into the early Turonian. The $\delta^{18}O$ values are, however, considered to have been diagenetically altered, shifting the primary signal to more negative values. Negative excursions seen on the $\delta^{13}C$ profile are interpreted as being, in part, an effect of diagenesis. Coinciding with the most negative $\delta^{18}O$ values, the $\delta^{13}C$ values indicate post-depositional oxidation of organic matter during localised exposure of the sediments to oxic or meteoric conditions during a lowering of sea level or tectonic uplift.

Acknowledgements

We particularly thank Roger Bowers and Kevin Solman (University of Plymouth) for technical support, Evgeniy Baraboshkin (Moscow State University) for invaluable field assistance, Hilary Sloane and Jo Green for running the mass spectrometer and isotope samples at NIGL, and Philipp Steinmann at the University of Neuchâtel for undertaking the Rock-Eval analyses. We also thank reviewers Prof. Andy Gale and Dr. Harry Tsikos, and Dr. Jackie Lees for their helpful comments and suggestions, which helped improve an earlier version of the manuscript. JKF acknowledges receipt of a University of Plymouth studentship. All materials used are housed at the University of Plymouth.

References

Allan, J.R., Matthews, R.K., 1982. Isotope signatures associated with early diagenesis. Sedimentology 29, 797–817.

Alekseev, A.S., 1989. Upper Cretaceous System. In: Mazarovich, O.A., Mileev, V.S. (Eds.), Geological Structure of the Kacha Uplift of Mountainous Crimea. Mesozoic Stratigraphy. Moscow University Press, Moscow, pp. 123–157 (in Russian).

Alekseev, A.S., Vengertsev, V.S., Kopaevich, L.F., Kuzmicheva, T.A., 1997. Lithology and micropaleontology of Cenomanian–Turonian boundary interval in south-western Crimea. In: Milanovsky, E.E. (Ed.), Essays on the Geology of the Crimea. Transactions of the A.A. Bogdanov Crimean Geological Scientific-Educational Centre, Moscow; Moscow State University, Geological Faculty Publication 1, 54–74 (in Russian, English abstract).

Anderson, T.F., Arthur, M.A., 1983. Stable isotopes of oxygen and carbon and their application to sedimentologic and palaeoenvironmental problems. In: Arthur, M.A., Anderson, T.F., Kaplan, I.R., Veizer, J., Land, L.S. (Eds.), Stable Isotopes in Sedimentary Geology. Society of Economic Paleontologists and Mineralogists, Short Course 10, 1–151.

Arthur, M.A., Dean, W.E., Pratt, L.M., 1988. Geochemical and climatic effects of increased marine organic carbon burial at the Cenomanian/Turonian boundary. Nature 335, 714–717.

Arthur, M.A., Schlanger, S.O., Jenkyns, H.C., 1987. The Cenomanian–Turonian oceanic anoxic event. II. Palaeoceanographic controls on organic-matter production and preservation. In: Brooks, J., Fleet, A.J. (Eds.), Marine Petroleum Source Rocks. Geological Society, London, Special Publications 26, 401–420.

Barron, E.J., 1983. A warm equable Cretaceous: the nature of the problem. Earth-Science Reviews 19, 305–338.

Beerling, D.J., Lomas, M.R., Gröcke, D.R., 2002. On the nature of methane gas-hydrate dissociation during the Toarcian and Aptian oceanic anoxic events. American Journal of Science 302, 28–49.

Berner, R.A., Kothavala, Z., 2001. GEOCARB III: a revised model of atmospheric CO_2 over Phanerozoic time. American Journal of Science 301, 182–204.

Bralower, T.J., Arthur, M.A., Leckie, R.M., Sliter, W.V., Allard, D.J., Schlanger, S.O., 1994. Timing and paleoceanography of oceanic dysoxia/anoxia in the Late Barremian to Early Aptian (Early Cretaceous). Palaios 9, 335–369.

Brasier, M.D., 1980. Microfossils. Allen and Unwin, London, 193 pp.

van Buchem, F.S.P., Razin, P., Casanova, J., Walgenwitz, F., 1999. Stratigraphic architecture, sediment flux and isotope curves of the Cenomanian carbonate system in northern Oman (Naith Fm.). Journal of Conference Abstracts 4 (2), 11th Bathurst Meeting 13th–15th July, 1999, Cambridge, UK.

Buonocunto, F.P., Sprovieri, M., Bellanca, A., D'Argenio, B., Ferreri, V., Neri, R., Ferruzza, G., 2002. Cyclostratigraphy and high-frequency carbon isotope fluctuations in Upper Cretaceous shallow-water carbonates, southern Italy. Sedimentology 49, 1321–1337.

Chen, D., Tucker, M.E., Shen, Y., Yans, J., Preat, A., 2002. Carbon isotope excursions and sea level change: implications for the Frasnian–Famennian biotic crisis. Journal of the Geological Society, London 159, 623–626.

Clarke, L.J., Jenkyns, H.C., 1999. New oxygen isotope evidence for long-term Cretaceous climatic change in the Southern Hemisphere. Geology 27, 699–702.

Gabdullin, R., Guzhikov, A., Dundin, I., 1999. Origin of rhythmically bedded Cenomanian carbonate rocks of the Bakhchisarai region (SW Crimea). Geologica Carpathica 50, 49–61.

Gale, A.S., Hancock, J.M., Kennedy, W.J., 1999. Biostratigraphical and sequence correlation of the Cenomanian successions in Mangyshlak (W. Kazakhstan) and Crimea (Ukraine) with those in southern England. Bulletin de l'Institut Royal des Sciences Naturelles de Belgique, Sciences de la Terre 69 (Supplement A), 67–86.

Gale, A.S., Jenkyns, H.C., Kennedy, W.J., Corfield, R.M., 1993. Chemostratigraphy versus biostratigraphy: data from around the Cenomanian–Turonian boundary. Journal of the Geological Society, London 150, 29–32.

Hallam, A., 1992. Phanerozoic Sea-level Changes. Columbia University Press, New York, 266 pp.

Haq, B.U., Hardenbol, J., Vail, P.R., 1987. Chronology of fluctuating sea-levels since the Triassic. Science 235, 1156–1167.

Hart, M.B., 1996. Recovery of the food chain after the late Cenomanian extinction event. In: Hart, M.B. (Ed.), Biotic Recovery from Mass Extinction Events. Geological Society, London, Special Publications 102, 265–277.

Hart, M.B., Bigg, P.J., 1981. Anoxic events in the Late Cretaceous chalk seas of northwest Europe. In: Neale, J.W., Braisier, M.B. (Eds.), Microfossils from Recent and Fossil Shelf Seas. British Micropalaeontological Society, Ellis Horwood, Chichester, pp. 177–185.

Hart, M.B., Dodsworth, P., Duane, A.M., 1993. The late Cenomanian event in eastern England. Cretaceous Research 14, 495–508.

Hasegawa, T., 1997. Cenomanian–Turonian carbon isotope events recorded in terrestrial organic matter from northern Japan. Palaeogeography, Palaeoclimatology, Palaeoecology 130, 251–273.

Hesselbo, S.P., Gröcke, D.R., Jenkyns, H.C., Bjerrum, C.J., Farrimond, P., Morgans Bell, H.S., Gren, O.R., 2000. Massive dissociation of gas hydrate during a Jurassic oceanic anoxic event. Nature 406, 392–395.

Huber, B.T., 1998. Perspectives – paleoclimate – tropical paradise at the Cretaceous poles? Science 282, 2199–2200.

Jahren, A.H., Arens, N.C., Sarmiento, G., Guerrero, J., Amundson, R., 2001. Terrestrial record of methane hydrate dissociation in the Early Cretaceous. Geology 29, 159–162.

Jarvis, I., Carson, G.A., Cooper, M.K.E., Hart, M.B., Leary, P.N., Tocher, B.A., Horne, D., Rosenfeld, A., 1988. Microfossil assemblages and the Cenomanian–Turonian (late Cretaceous) oceanic anoxic event. Cretaceous Research 9, 3–103.

Jeffries, R.P.S., 1963. The stratigraphy of the *Actinocamax plenus* Subzone (Turonian) in the Anglo-Paris Basin. Proceedings of the Geologists' Association 74, 1–33.

Jenkyns, H.C., 1980. Cretaceous anoxic events from continents to oceans. Journal of the Geological Society, London 137, 171–188.

Jenkyns, H.C., Gale, A.S., Corfield, R.M., 1994. Carbon- and oxygen-isotope stratigraphy of the English Chalk and the Italian Scaglia and its palaeoclimatic significance. Geological Magazine 131, 1–34.

Jørgensen, N.O., 1987. Oxygen and carbon isotope compositions of upper Cretaceous chalk from the Danish Sub-basin and the North Sea Central Graben. Sedimentology 34, 559–570.

Kaiho, K., 1994. Planktonic and benthic foraminiferal extinction events during the last 100 m.y. Palaeogeography, Palaeoclimatology, Palaeoecology 111, 45–71.

Keller, G., Han, Q., Adatte, T., Burns, S.J., 2001. Palaeoenvironment of the Cenomanian–Turonian transition at Eastbourne, England. Cretaceous Research 22, 391–422.

Kerr, A.C., 1998. Oceanic plateau formation: a cause of mass extinction and black shale deposition around the Cenomanian–Turonian boundary? Journal of the Geological Society, London 155, 619–626.

Kopaevich, L.F., Kuzmicheva, T.A., 2002. The Cenomanian–Turonian boundary in southwestern Crimea, Ukraine: foraminifera and palaeogeographic implications. In: Wagreich, M. (Ed.), Aspects of Cretaceous Stratigraphy and Palaeobiology. Österreichische Akademie der Wissenschaften, Schriftenreihe der Erdwissenschaftlichen Kommissionen 15, 129–149.

Kuhnt, W., Wiedmann, J., 1995. Cenomanian–Turonian source rocks: paleobiogeographic and paleoenvironmental aspects. In: Huc, A.-Y. (Ed.), Paleogeography, Paleoclimate and Source Rocks. AAPG Studies in Geology 40, 213–231.

Kuzmicheva, T.A., 2000. The Cenomanian–Turonian boundary of Belaya Mountain (southwestern Crimea). Vestnik Moskovskogo Universiteta, Seriya 4. Geologiya 1, 70–73 (in Russian).

Larson, R.L., 1991. Latest pulse of earth: evidence for a mid-Cretaceous superplume. Geology 19, 547–550.

Larson, R.L., Erba, E., 1999. Onset of the mid-Cretaceous greenhouse in the Barremian–Aptian: igneous events and the biological, sedimentary, and geochemical responses. Paleoceanography 14, 663–678.

Malone, M.J., Slowey, N.C., Henderson, G.M., 2001. Early diagenesis of shallow-water periplatform carbonate sediments, leeward margin, Great Bahama Bank (Ocean Drilling Project Leg 166). GSA (Geological Society of America) Bulletin 113, 881–894.

Marshall, J.D., 1992. Climatic and oceanographic isotope signals from the carbonate rock record and their preservation. Geological Magazine 129, 143–160.

McCrea, J.M., 1950. On the isotope chemistry of carbonates and a paleotemperature scale. Journal of Chemistry and Physics 18, 849–857.

Meyer, T., 1990. Biostratigraphische und sedimentologische Untersuchungen in der Plänerfazies des Cenoman von Nord-westdeutschland. Mitteilungen aus dem Geologischen Institut der Universität Hanover 30, 1–114.

Naidin, D.P., 1981. The Russian Platform and the Crimea. In: Reyment, R.A., Bengtson, P. (Eds.), Aspects of Mid-Cretaceous Regional Geology. Academic Press, London, pp. 29–68.

Naidin, D.P., 1993. Late Cretaceous events in the east of the European paleobiogeographic province. 2. Cenomanian/Turonian and Maastrichtian/Danian events. Bulletin of the Moscow Society of Naturalists, Geological Series 68, 33–53 (in Russian, English abstract).

Naidin, D.P., Alekseev, A.S., 1981. Importance of ocean drilling data for interpretation and life of fauna in the Cenomanian of the Crimean highlands. In: Krassilov, V. (Ed.), Evolution of Organisms and Biostratigraphy of the Mid-Cretaceous, pp. 7–21, Vladivostok (in Russian).

Naidin, D.P., Kiyashko, S.I., 1994a. Cenomanian/Turonian boundary deposits in the Crimean highlands. 1. Lithology, organic deposits and some element contents. Bulletin of the Moscow Society of Naturalists, Geological Series 69, 28–42 (in Russian, English abstract).

Naidin, D.P., Kiyashko, S.I., 1994b. Cenomanian/Turonian boundary deposits in the Crimean highlands. 2. Isotopic composition of carbon and oxygen; environment of organic carbon accumulation. Bulletin of the Moscow Society of Naturalists, Geological Series 69, 28–42 (in Russian, English Abstract).

Nikishin, A.M., Cloetingh, S., Bolotov, S.N., Baraboshkin, E.Y., Kopaevich, L.F., Nazarevich, B.P., Panov, D.I., Brunet, M.F., Ershov, A.V., Ilina, V.V., Kosova, S.S., Stephenson, R.A., 1997. Scythian Platform: chronostratigraphy and polyphase stages of tectonic history. Memoirs du Museum National d'Histoire Naturelle 177, 151–162.

Parrish, J.T., 1995. Paleogeography of C_{org}-rich rocks and the preservation versus production controversy. In: Huc, A.-Y. (Ed.), Paleogeography, Paleoclimate and Source Rocks. American Association of Petroleum Geologists, Studies in Geology 40, 1–20.

Paul, C.R.C., Lamolda, M.A., Mitchell, S.F., Vaziri, M.R., Gorostidi, A., Marshall, J.D., 1999. The Cenomanian–Turonian boundary at Eastbourne (Sussex, UK): a proposed European reference section. Palaeogeography, Palaeoclimatology, Palaeoecology 150, 83–121.

Pratt, L.M., 1985. Isotopic studies of organic matter and carbonate in rocks of the Greenhorn marine cycle. In: Pratt, L.M., Kauffman, E.G., Zelt, F.B. (Eds.), Fine-Grained Deposits and Biofacies of the Cretaceous Western Interior Seaway: Evidence of Cyclic Sedimentary Processes. Society of Economic Paleontologists and Mineraleralogists, 1985 Midyear Meeting, Golden, Colorado, Field Trip Guidebook 4, pp. 38–48.

Pratt, L.M., Threlkeld, C.N., 1984. Stratigraphic significance of $^{13}C/^{12}C$ ratios in mid-Cretaceous rocks of the Western Interior, USA. In: Stott, D.F., Glass, D.J. (Eds.), The Mesozoic of Middle North America. Canadian Society of Petroleum Geologists, Memoir 9, 305–312.

Price, G.D., 2003. New constraints upon isotope variation during the early Cretaceous (Barremian–Cenomanian) from the Pacific Ocean. Geological Magazine 140, 513–522.

Robaszynski, F., Caron, M., 1995. Foraminifères planctoniques du Crétacé: commentaire de la zonation Europe-Méditerranée. Bulletin de la Société Géologique de France 166, 681–692.

Schlanger, S.O., Jenkyns, H.C., 1976. Cretaceous oceanic anoxic events: causes and consequences. Geologie en Mijnbouw 55, 179–184.

Schlanger, S.O., Arthur, M.A., Jenkyns, H.C., Scholle, P.A., 1987. The Cenomanian–Turonian oceanic anoxic event, I. Stratigraphy and distribution of organic-rich beds and the marine $\delta^{13}C$ excursion. In: Brooks, J., Fleet, A.J. (Eds.), Marine Petroleum Source Rocks. Geological Society, London, Special Publication 26, 371–399.

Scholle, P.A., 1977. Chalk diagenesis and its relation to petroleum exploration: oil from chalks, a modern miracle? American Association of Petroleum Geologists, Bulletin 64, 67–87.

Scholle, P.A., Arthur, M.A., 1980. Carbon isotope fluctuations in Cretaceous pelagic limestones: potential stratigraphic and petroleum exploration tool. American Association of Petroleum Geologists, Bulletin 64, 67–87.

Smith, A.G., Smith, D.G., Funnell, B.M., 1994. Atlas of Mesozoic and Cenozoic Coastlines. Cambridge University Press, Cambridge, 99 pp.

Tsikos, H., Jenkyns, H.C., Walsworth-Bell, B., Petrizzo, M.R., Forster, A., Kolonic, S., Erba, E., Premoli Silva, I., Baas, M., Wagner, T., Sinninghe Damsté, J.S., 2004. Carbon-isotope stratigraphy recorded by the Cenomanian–Turonian Oceanic Anoxic Event: correlation and implications based on three key localities. Journal of the Geological Society, London 161, 711–719.

Tyson, R.V., 1995. Sedimentary Organic Matter: Organic Facies and Palynofacies. Chapman and Hall, London, 615 pp.

Voigt, S., Hilbrecht, H., 1997. Late Cretaceous carbon isotope stratigraphy in Europe: correlation and relations with sea level and sediment stability. Palaeogeography, Palaeoclimatology, Palaeoecology 134, 39–59.

Wang, K., Geldsetzer, H.H.J., Goodfellow, W.D., Krouse, H.R., 1996. Carbon and sulphur isotope anomalies across the Frasnian–Famennian extinction boundary, Alberta, Canada. Geology 24, 187–191.

Wright, J.D., Miller, K.G., Cramer, B.S., Olsson, R.K., Katz, M.E., Sugarman, P.J., 2001. Transient climate event at the Cenomanian/Turonian Boundary (OAE2). American Geophysical Union, Fall Meeting 2001, abstract #PP32A-0515.

ISSN: 1698-6180
www.ucm.es/info/estratig/journal.htm

Journal of Iberian Geology 31 (2) 2005: 311-326

Journal of Iberian Geology
AN INTERNATIONAL PUBLICATION OF EARTH SCIENCES

Micropalaeontology and Stratigraphy of the Cenomanian/Turonian boundary in the Lusitanian Basin, Portugal

Micropaleontología y Estratigrafía del límite Cenomaniense/Turoniense en la Cuenca Lusitánica, Portugal

M. B. Hart[1], P. M. Callapez[2], J. K. Fisher[1], K. Hannant[1], J. F. Monteiro[3], G. D. Price[1], M. P. Watkinson[1]

[1]School of Earth, Ocean & Environmental Sciences, University of Plymouth, Drake Circus, Plymouth PL4 8AA, United Kingdom, M.Hart@plymouth.ac.uk
[2]Departamento de Ciências da Terra, Faculdade de Ciências e Tecnologia da Universidade de Coimbra, 3000 -272 Coimbra, Portugal.
[3]Departamento de Geologia, Faculdade de Ciências da Universidade de Lisboa, Edifício C-2, Campo Grande, 1700 Lisboa, Portugal.

Received: 26/03/04 / Accepted: 10/09/04

Abstract

The mid-Cretaceous carbonate succession exposed along the valley of the Rio Mondego (Lusitanian Basin, Western Portuguese Margin, Portugal) is described and the microfauna documented. This succession records the Cenomanian-Turonian transition within a shallow water environment. The majority of Cenomanian-Turonian boundary sections described in the literature are from deeper-water settings and the unusual benthic foraminifera recorded in this succession are rarely discussed in terms of the latest Cenomanian extinction event. The Rio Mondego succession is discussed in terms of the proposed "ejecta horizon" exposed on the coast at Praia da Vitória, 10 km north of Nazaré.

Keywords: Portugal, Lusitanian Basin, Foraminifera, Cenomanian/Turonian boundary, impact breccia

Resumen

En este trabajo se describe la sucesión de naturaleza carbonática de edad Cretácico medio expuesta en la región del valle del Río Mondego (Cuenca Lusitánica, Margen Occidental de Iberia, Portugal) y su contenido microfósil. La mayoría de las secciones del límite Cenomaniense-Turoniense descritas en la bibliografía registran facies de ambientes marinos de mayor profundidad, mientras que la sección que se presenta en este trabajo muestra dicha transición en depósitos formados en un ambiente marino de aguas poco profundas. Los escasos foraminíferos bénticos que han sido hallados en esta sucesión no habían sido estudiados en detalle previamente en relación al evento de extinción del final del Cenomaniense. En la sucesión del Río Mondego ha sido analizado también el "horizonte de ejecta", expuesto en el litoral de Praia da Vitória, 10 km al norte de Nazaré.

Palabras clave: Portugal, Cuenca Lusitánica, Foraminíferos, Límite Cenomaniense/Turoniense, brecha de impacto

1. Introduction

The Lusitanian Basin, in western Central Portugal, is one of the marginal basins associated with the opening of the North Atlantic Ocean (Fig. 1). It extends over 23,000 km², and is exposed along the coastline of Portugal for over 250 km from Lisbon to Aveiro. The northern margin is ill-defined, connecting to off-shore Mesozoic basins that are surrounded by the Porto and Vigo Seamounts and the Galicia Bank. Off-shore basement horsts within

the basin include the Berlengas and Farilhões Islands. Most of the basin fill is Jurassic in age but Upper Triassic sediments are known from a few areas. Lower and Upper Cretaceous sediments are also present, overlain by a cover of Cenozoic sediments. Two episodes of rifting and extension are recorded, the first being in the late Triassic. The later movements, which gave rise to ocean opening, occurred in the latest Jurassic and earliest Cretaceous (Ribeiro *et al.*, 1979; Wilson, 1988: Proença Cunha and Pena dos Reis, 1995). The basin suffered tectonic inversion in the Cenozoic and, as a result, a large part of its pre-, syn-, and post-rift sequences became exposed (Wilson, 1988). The area close to the Nazaré Fault (Fig. 2) has also been affected by salt diapirs (see Proença Cunha and Pena dos Reis, 1995, fig. 3, and Pena dos Reis, 1998, fig.1), the emplacement of which is important in the geological history of the area.

The mid-Cretaceous successions described herein are located along the Rio Mondego inland of Figueira da Foz and at Praia da Vitória (immediately north of Nazaré). As a part of a larger study of the Cenomanian-Turonian boundary our interest in this area arises from the fact that:

(1) there is a well-documented Cenomanian-Turonian succession in relatively shallow-water sediments as compared to the deeper-water successions normally investigated at this level; and

(2) there is a suggestion that an impact ejecta deposit is present within the Praia da Vitoria succession.

2. The Late Cenomanian Extinction Event

The Late Cenomanian extinction event (= Cenomanian-Turonian Boundary Event [CTBE] or Bonarelli Event or OAE 2) was an important biotic crisis in the history of the Cretaceous world-wide. It is one of the extinction events identified by Raup and Sepkoski (1982) in their analysis of periodic extinctions. It is not one of the 'big five' extinction events of the Phanerozoic record as the majority of the faunal changes are at the species level, rather than higher taxonomic levels. In a recent review Hart *et al.* (2002) have discussed the evidence for the 'event' and listed a number of potential causes.

Much of the data on the CTBE come from localities located within the chalk succession of Western Europe (Eastbourne, Folkestone, etc.), the limestone/shale/marl successions of the Western Interior Seaway of the USA or the carbonate/clay successions drilled as part of DSDP/ODP/IPOD programs in the various oceans of the world. A wide range of potential causes has been assembled (see Hart *et al.*, 2002, p. 36) extending from the purely oceanographic to a bolide impact. In the debate over the potential/probable causes few authors (e.g., Kennedy and Simmons, 1991; Caus *et al.*, 1997) have presented data from a shallow-water, carbonate succession. In the successions from the Lusitanian Basin planktic foraminifera are extremely rare while the larger and smaller benthic taxa are more abundant. The microfaunas are associated with extensive, and well-known, ammonite and rudist faunas first described in detail by Choffat (1885, 1886, 1896, 1897a,b, 1898, 1900). In recent years this original work has been revised by Soares (1966, 1972, 1980), Berthou and Philip (1972), Berthou (1973, 1978, 1984a,b), Berthou *et al.* (1975, 1985), Berthou and Lauverjat (1975, 1976, 1979), Lauverjat (1978, 1982), Lauverjat and Berthou (1973-74), Amédro *et al.* (1980) and Callapez (1998). One of the most accessible reviews (in English) is that of Berthou (1984a) who presented a reinterpretation of Choffat's ammonite stratigraphy of the Cenomanian-Turonian boundary (as well as an overview of the complete Albian-Turonian succession).

Choffat (1900) and Berthou (1984a, fig. 1) identify three regions in the Lusitanian Basin that are characterised, in the Late Cenomanian, by ammonites (north of

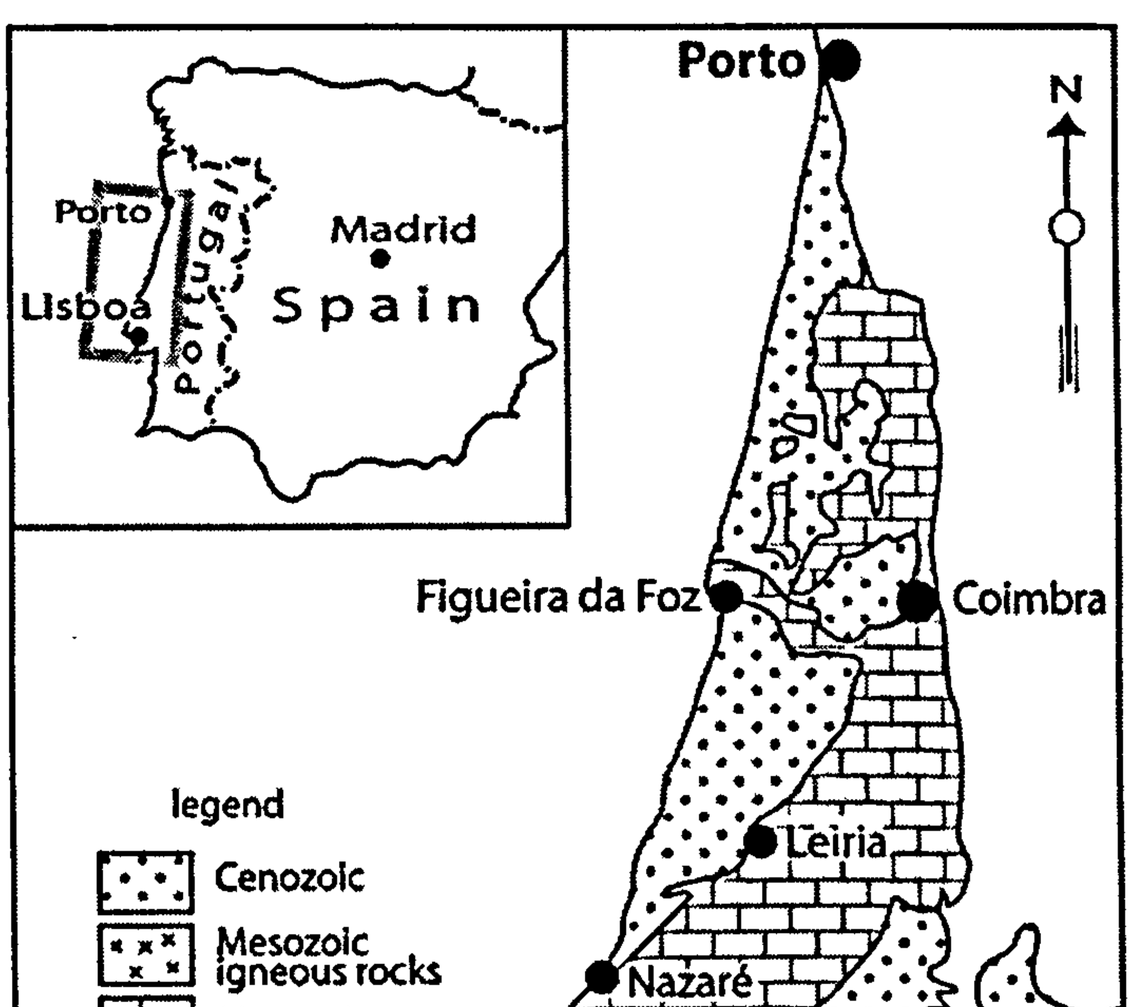

Fig. 1.– Outline geological map of the Lusitanian Basin.
Fig. 1.– Mapa geológico de la Cuenca Lusitánica.

Leiria), rudists (south of Leiria) and echinoderms (east of Leiria). In this account we are considering the foraminifera and biostratigraphy in the area north of Leiria and, in particular, the succession exposed along the Rio Mondego between Figueira da Foz and Coimbra. More recently this area has been investigated by Callapez (1998, 1999) as part of a doctoral study of the region. Callapez (*op. cit.*) has revised the ammonite stratigraphy and provided the framework within which we have investigated the foraminifera.

3. Rio Mondego Succession

The Cenomanian-Turonian carbonate succession of the Western Portuguese Margin is part of a larger (?)megasequence that extends (Fig. 3) from the Upper Aptian to the Lower Campanian (Wilson, 1988; Pinheiro *et al.*, 1996). Within this setting there is an extensive carbonate platform of mid-Cenomanian to early Turonian age (Figs. 3, 4). The carbonate platform wedges out towards the basin margin. It is interesting that the maximum stratigraphical extent of this carbonate succession ranges from mid-Cenomanian to mid-Turonian, coincident with the sea-level highstand of the mid-Cretaceous (Hancock, 1989 and references therein). This is significant as it almost certainly indicates a response to global events rather than local tectonic control. In the Northern Sector (Fig. 3) the succession shown is that inland of Figueira da Foz along the valley of the Rio Mondego (Fig. 2). This part of the succession is shown in Figure 4, which also includes the facies changes and stratigraphy along a section from the coast (Figueira da Foz) inland towards Coimbra. The letters (B, C, D, etc.) are the classic units of Choffat (1900), that have been retained by both Berthou (1984a) and Callapez (1998, 1999). The described succession begins in Salmanha Quarry (Lauverjat and Berthou, 1973-74, fig.1; Callapez, 1999, fig.16) and a range of other overgrown quarries and roadside exposures along the valley of the Rio Mondego. The composite succession shown in Figure 4 indicates that, in the vicinity of Salmanha Quarry, Beds B – O are present. The ammonite zonation used in this diagram is the international standard that is in general use in N.W. Europe and the Western Interior Seaway of the U.S.A. The application of this zonation to successions in Spain and Portugal is slightly controversial and we use the evidence presented in Callapez (1998, 1999). In recent years a number of interpretations of the ammonite zonation have been presented: see, for example, Wiedmann (1980, fig. 7), Wiedmann and Kauffman (1978), Meister *et al.* (1992, figs 24-26), Hardenbol *et al.* (1998, chart 5) and Kassab and Obaidalla (2001, table 3)

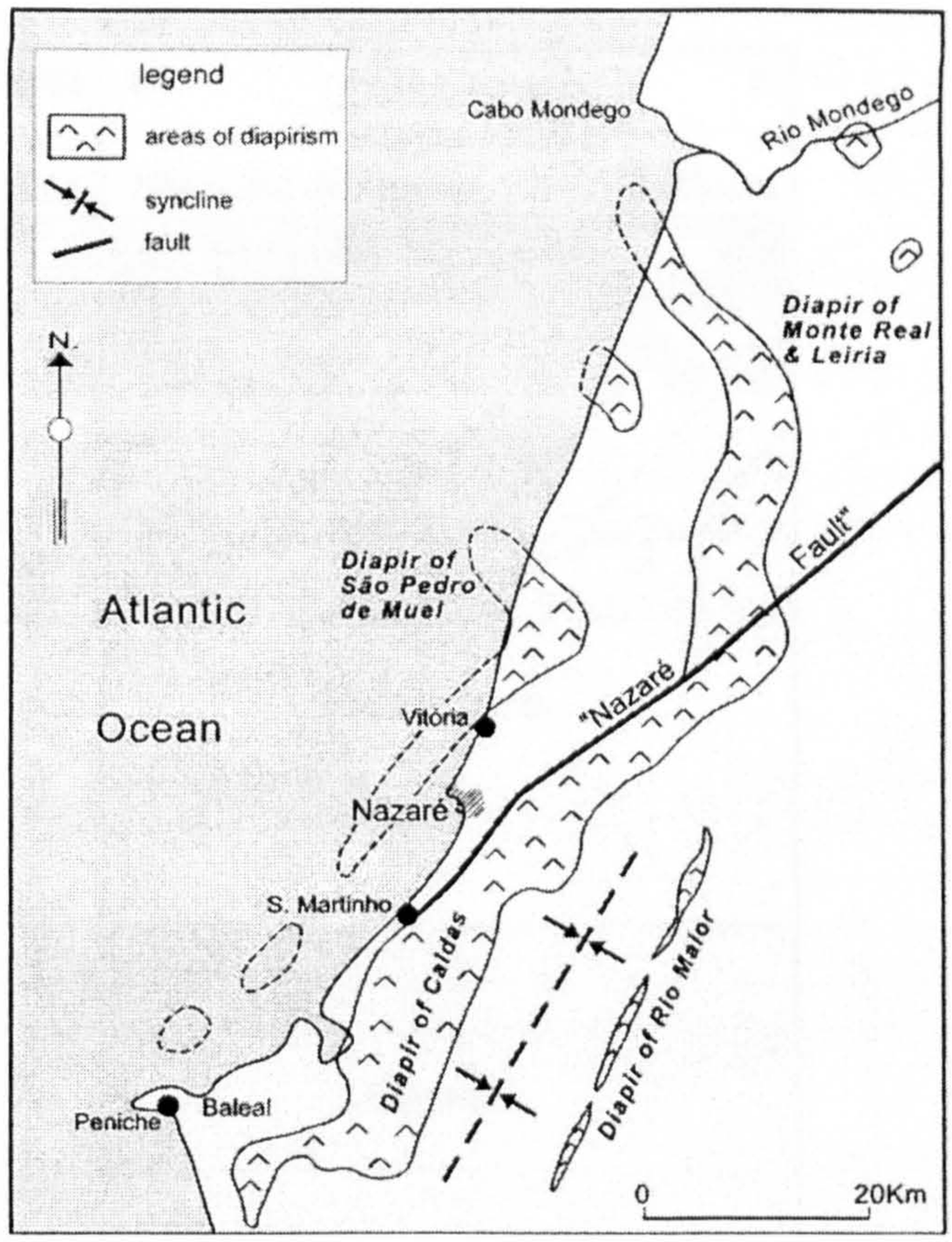

Fig. 2.– Location of Nazaré and the Rio Mondego. The approximate position of salt diapirs associated with the Nazaré–Leiria–Pombal flexure/fault (the Nazaré Fault of Berthou, 1984a) are indicated.

Fig. 2.– Situación de Nazaré y del Río Mondego. Posición aproximada de los diapiros salinos relacionados con la flexión/falla de Nazaré–Leiria–Pombal (Falla de Nazaré, según Berthou, 1984a).

The contemporaneous ammonite assemblages of Northern Spain described by Wiedmann (1980) and Wiedmann and Kauffman (1978) are somewhat different to those in the Lusitanian Basin, except for the common occurrence of *Neolobites* and *Calycoceras* in the basal Upper Cenomanian and the abundance of *Spathites subconciliatus*. The age of the first *Vascoceras* assemblages (a problem Berthou tackled for many years) can be defined as a result of the discovery of *Euomphaloceras septemseriatum* in the same beds. This species is known from assemblages correlative with the Geslinianum Zone. The papers of Kennedy (1984, 1988), Kennedy and Cobban (1991), Kennedy and Juignet (1994) and Kennedy *et al.* (1989) are very helpful in this respect. The hiatus recorded between Beds J and K may be of relatively short duration but is certainly present. The ammonites from the overlying beds are representatives of the middle of the Lower Turonian. *Pseudaspidoceras flexuosum* Zone faunas are not found, despite being typical of many other Tethyan Cenomanian–Turonian boundary successions.

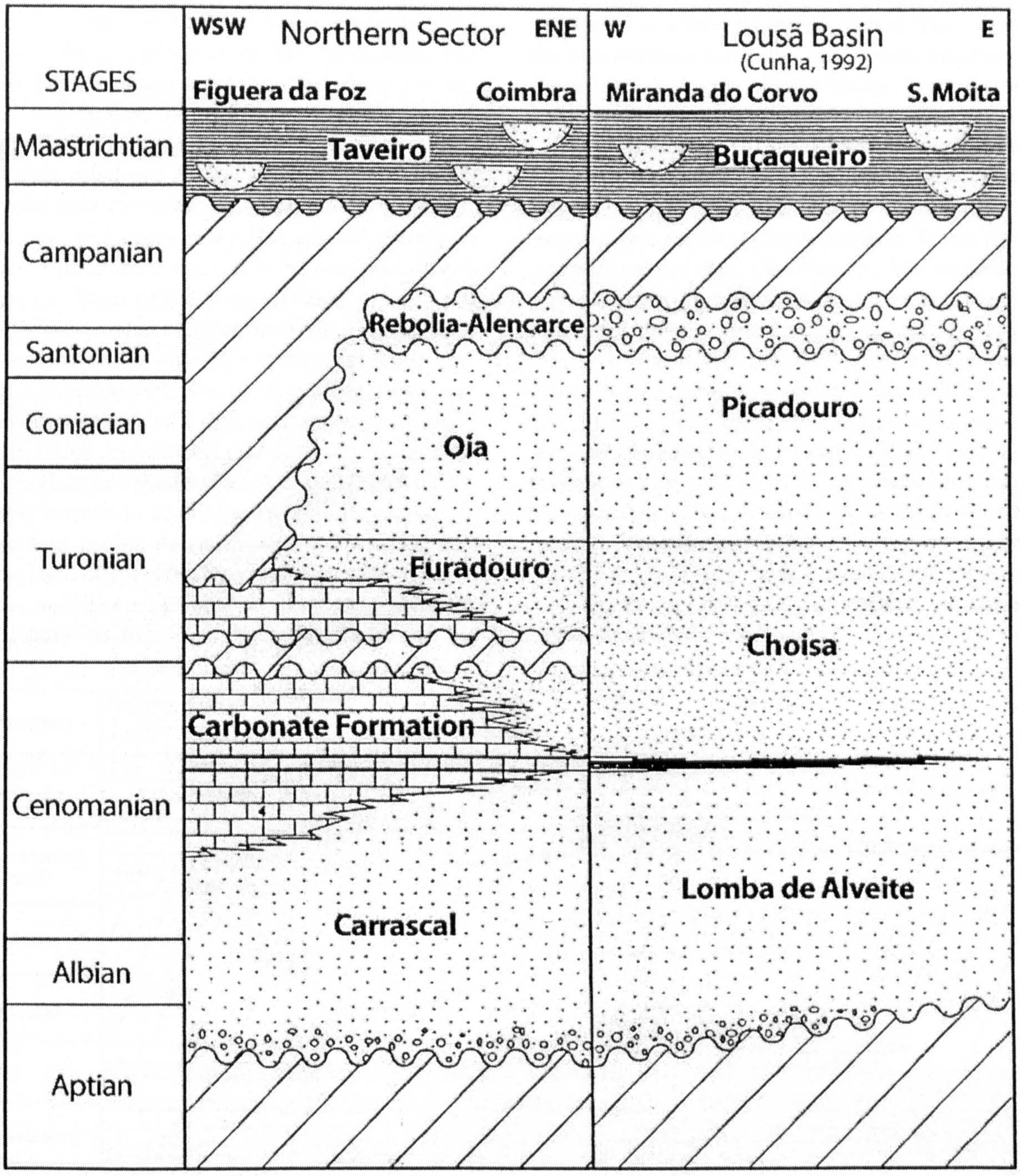

Fig. 3.– Simplified summary of the stratigraphic succession within the Upper Aptian to Lower Campanian 'megasequence' of the Western Portugal Margin (modified after Callapez, 1998, 1999).

Fig. 3.– Resumen simplificado de la sucesión estratigráfica correspondiente a la "megasecuencia" Aptiense superior - Campaniense inferior del Margen occidental de Portugal (modificado de Callapez, 1998, 1999).

3.1. Lithological succession and microfauna

Figure 5 shows an outline log of the succession which is based on the work of Callapez (1998, 1999), together with some data on the ranges of important foraminifera. Such information is necessarily incomplete as working with thin section material always means that:

(1) the fauna recorded for each sample is limited by the number of thin sections studied; and

(2) many 'smaller' benthic foraminifera are impossible to identify at the species (or even genus) level while 'larger' benthic foraminifera (orbitolinids and alveolinids) tend to display more diagnostic features in thin section.

It is significant that very few planktic foraminifera are recorded, confirming the shallow water environments represented by the greater part of the succession. No deeper-water keeled planktic foraminifera (see, for example, Hart and Bailey, 1979; Hart, 1980, Caron and Homewood, 1983; Hart, 1999) have been found. The only species recorded are *Heterohelix* sp. cf. *H. moremani, Guembelitria cretacea, Hedbergella delrioensis, Whiteinella* spp., and (very rare) *Helvetoglobotruncana praehelvetica.* All of these are (probably) surface dwelling forms (upper 50 m of the water column or less). All of the planktic specimens recorded in the thin sections are very small and are either juveniles or size-limited by the shallow water environment. The benthic foraminifera are probably less diagnostic, although one can suggest that:

(1) orbitolinids and alveolinids probably hosted algal symbionts (Lee and Anderson, 1991) and, as a result, were probably limited to 25-30 metres of water; and

(2) abundant milioliids (and little else) almost certainly indicate lagoonal, possibly hypersaline, environments.

Bed B has only been sampled at Tentúgal, inland of Salmanha Quarry. At this locality the sediment is a bivalve-rich rudstone with large macrofossil fragments supported in a lime mudstone matrix. The majority of the fauna comprises turritellid gastropods, bivalves (possibly *Gyrostrea*) and very small planktic foraminifera. Small, indeterminate ostracods are also present.

Bed C is mainly composed of anhedral rhomb-shaped dolomite crystals with rare quartz grains and molluscan fragments. At Tentúgal Bed C is a foraminiferal wackestone with a relatively high diversity fauna that includes *Ammobaculites* spp., *Dorothia* sp., *Marssonella oxycona, Quinqueloculina* spp., *Gavelinella* sp. and planktic forms identified only as *Hedbergella* sp. and *Heterohelix* sp.. Of particular note is the occurrence of *Hemicyclammina sigali, Simplalveolina simplex* (Figs. 6F/G/H and 7A/B) and a form very close to *Thomasinella punica* (*sensu* Arnaud-Vanneau and Prestat, 1984). On many shell fragments (Figs. 6D and 7C) are adherent, agglutinated foraminifera often referred to as "*Placopsilina cenomana*" although this genus does require urgent revision (Hodgkinson, 1992). This assemblage is typical of many mid-Upper Cenomanian successions in shallow-water carbonate-rich environments.

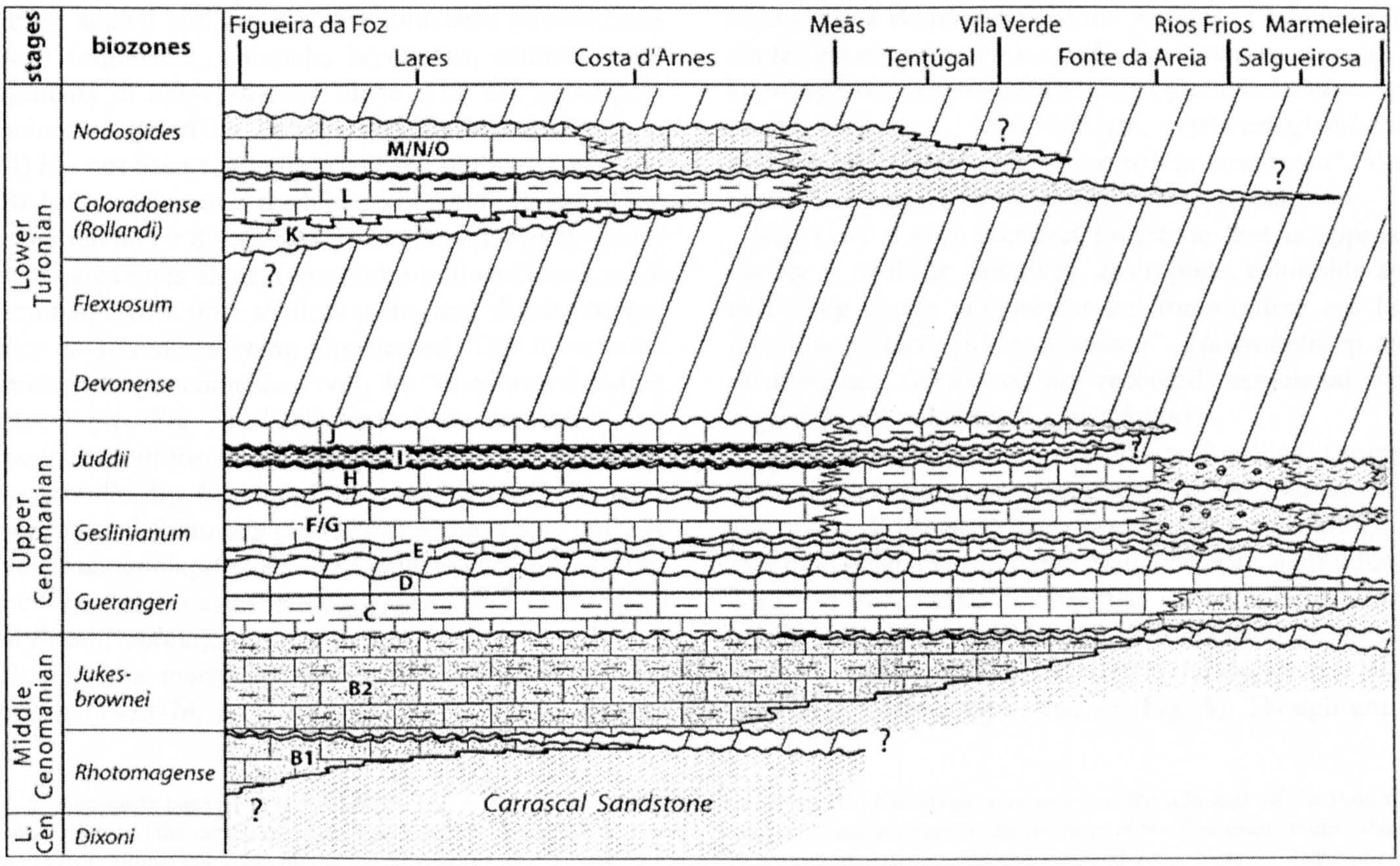

Fig. 4.– Chronostratigraphy and biostratigraphy of the carbonate succession along the Rio Mondego from Figueira da Foz inland towards Tentúgal, Coimbra and Lousã (modified after Callapez, 1998, 1999).

Fig. 4.– Cronoestratigrafía y bioestratigrafía de la sucesión carbonática a lo largo de Río Mondego desde Figueira da Foz hacia el interior por Tentúgal, Coimbra y Lousã (modificado de Callapez, 1998, 1999).

Bed D comprises approximately 2 metres of yellow, marly, limestone. In thin section the rock is a foraminiferal wackestone with a wide range of taxa that includes *Lenticulina* spp., *Marssonella oxycona, Quinqueloculina* spp., *Ovalveolina ovum, Simplalveolina simplex, Hemicyclammina sigali, Nummoloculina* sp., *Pseudocyclammina* sp., *Nummofallotia* sp., *Vidalina* sp., *Trochammina* sp. cf. *T. kugitangensis, Pseudolituonella reicheli* and a few very small specimens of *Hedbergella* and *Heterohelix. Hemicyclammina sigali* is a particularly useful Cenomanian marker in many Tethyan areas (Maync, 1953; Sartorio and Venturini, 1988) and can usually be recognised with little difficulty in thin section. *Trochammina* sp. cf. *T. kugitangensis* was recorded by Lauverjat and Berthou (1973-74) but the form seen in these limestones is much flatter, with sharply angled chambers, than the typically rounded form (holotype) illustrated by Bykova (1947). *Trochammina webbi* Stelck and Wall (1954) and *Trochammina whittingtoni* Tappan (1957) are possible alternative identifications for this taxon, although both are from Northern Canada and Alaska respectively. Unfortunately, neither of these taxa has been illustrated in thin section, but they are much flatter species with a sharply angled periphery. Other bioclasts include molluscan fragments, echinoids, bryozoans, ostracods and fragments of dasycladacean algae. The *Dicyclina schlumbergi* recorded by Lauverjat and Berthou (1973-74, p. 274) has not been encountered during our investigation.

Beds C and D record the highest diversity faunas of the succession under discussion. These faunas, and the associated calcareous algae, represent a mid-carbonate ramp assemblage with both shallow water and slightly deeper water environments being represented. This diverse assemblage is also coincident with the "maximum flooding surface" (see Fig. 3) of this part of the succession and appears to conform to the model proposed by Emery and Myers (1996, fig. 6.14). In the Central Oman Mountains Kennedy and Simmons (1991, fig. 4) record a similarly diverse assemblage from the Natih Formation of mid-Late Cenomanian age (including *Hemicyclammina sigali* and *Praealveolina*).

Bed E is a marly nodular limestone. Lauverjat and Berthou (1973-74, p. 275) record the presence of abundant *Exogyra* in these sediments, while Callapez (1998) records an ammonite fauna that contains *Vascoceras gamai* and *Euomphaloceras septemseriatum* that indicate an equivalence with the Western European zone of *Metoicoceras geslinianum.* This is a different interpretation to that presented in Hardenbol *et al.* (1998, chart 5), who indicate that the Gamai Zone fauna overlies the Geslinianum Zone fauna. This particular lithology is difficult to thin section, being on the boundary between being semi-processable by normal methods and having to be sectioned. The fauna recorded is, therefore, probably reduced because of these difficulties. The fauna includes (Fig. 5) *Thomasinella* (?)*punica, Hemicyclammina sigali, Simplalveolina simplex, Trochammina* sp. cf. *T. kugitangensis* and "*Placopsilina cenomana*". Algal fragments (dominated by *Permocalculus*) are abundant, although the layer of transported *Pseudocyclammina* sp. at the top of the bed that was reported by Lauverjat and Berthou (1973-74) was not located.

Bed F is ~2.5 m of beige-coloured grain supported peloidal packstone with a lime mud matrix. The main allochems are foraminifera (Fig. 6A) and peloids/pisoids. Spines from spatangoids are abundant, although the foraminifera dominate the thin sections. The fauna includes *Hemicyclammina sigali, Trochammina* sp. cf. *T. kugitangensis, Ammobaculites* spp., *Quinqueloculina* sp., *Nautiloculina* sp., *Textularia* sp., (?)*Pseudoglandulina* sp., *Gavelinella* sp. and "*Placopsilina cenomana*". Very small *Hedbergella delrioensis* are also present.

Bed G is a grey compact limestone that is approximately 3 m thick. Bivalves, gastropods, echinoids and branching corals are present but foraminifera are less common. "*Placopsilina cenomana*" , *Heterohelix* sp. and *Hedbergella delrioensis* are recorded, associated with algal debris (including *Permocalculus*).

Bed H is a bioclastic wackestone with echinoid spines, foraminifera, bryozoan fragments and occasional coral fragments (Fig. 6B). The foraminiferal assemblage is much reduced with only rare, indeterminate, agglutinated taxa and very small *Hedbergella* sp. and *Guembelitria* sp.. It is interesting to note the first appearance, up section, of calcispheres (Hart, 1991; Jarvis *et al.*, 1988; Hart *et al.*, 2002, fig.1; and see Fig. 8). Though not as

Fig. 5.– (opposite page) The Cenomanian-Turonian succession of the valley of the Rio Mondego with notes on the lithology of the limestone succession and the ranges of some characteristic foraminifera. Level 1 marks the disappearance of the majority of the Cenomanian microfauna, and this is almost complete by the top of Bed F. Level 2 marks the appearance of *Helvetoglobotruncana praehelvetica.* Note the distribution of calcispheres between Bed H and Bed J. Hiatuses are marked by a wavy line adjacent to the schematic sedimentary log.

Fig. 5.– (página opuesta) Sucesión Cenomaniense-Turoniense del valle del Río Mondego en la que se indica la litología de la sucesión caliza y los rangos de algunos foraminíferos característicos. El Nivel 1 marca la desaparición de la mayoría de la microfauna del Cenomaniense. La desaparición de esta microfauna culmina a techo de la Capa F. El Nivel 2 marca la aparición de *Helvetoglobotruncana praehelvetica.* Adviértase la distribución de calciesferas entre la Capa H y la Capa F. Los hiatos se han marcado mediante una línea ondulada junto a la columna sedimentaria esquemática.

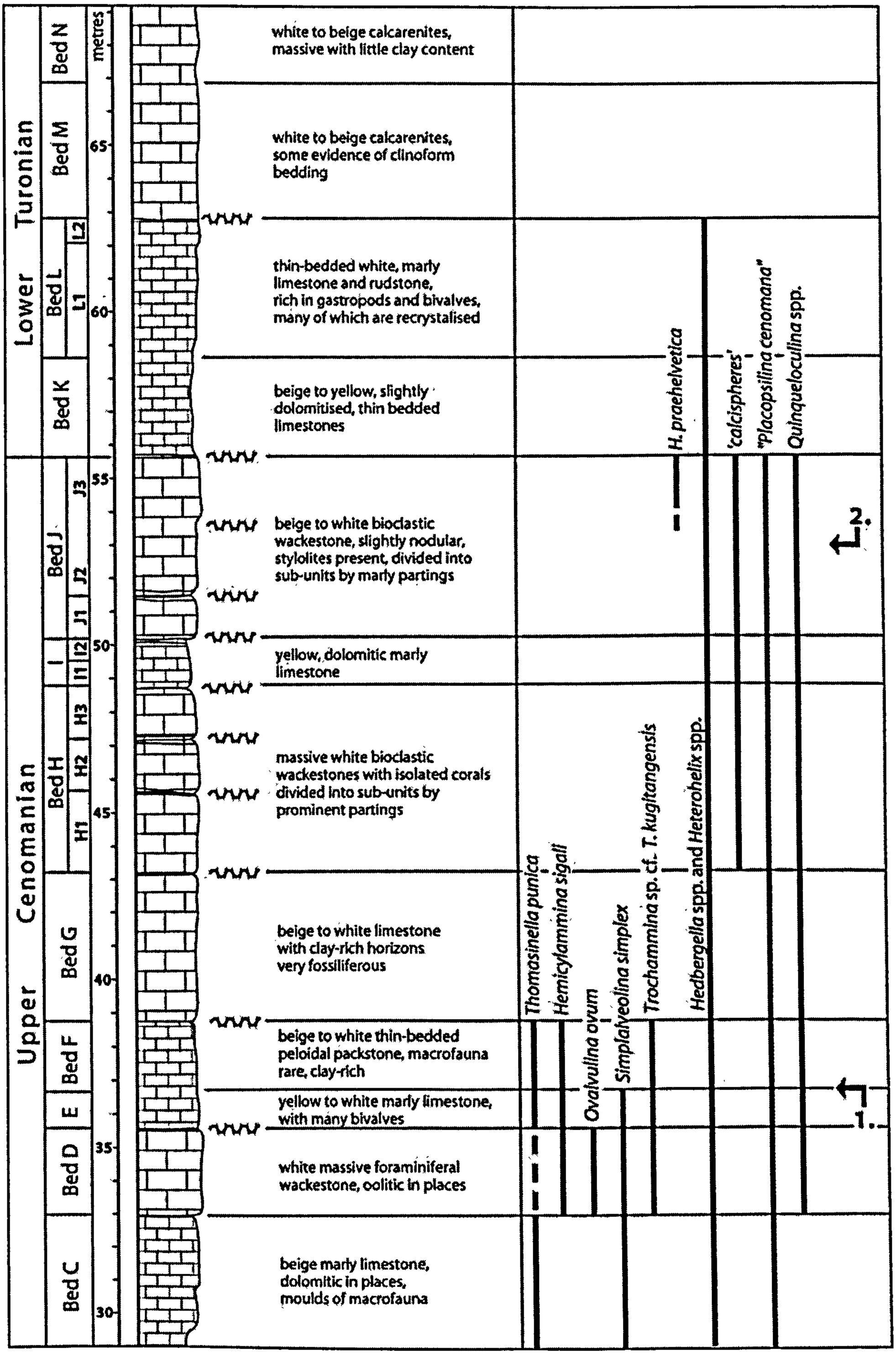
Upper Cenomanian
Lower Turonian
Bed C
Bed D
Bed E
Bed F
Bed G
Bed H
Bed I
Bed J
Bed K
Bed L
Bed M
Bed N
H1
H2
H3
I1
I2
J1
J2
J3
L1
L2
metres
65
60
55
50
45
40
35
30
white to beige calcarenites, massive with little clay content
white to beige calcarenites, some evidence of clinoform bedding
thin-bedded white, marly limestone and rudstone, rich in gastropods and bivalves, many of which are recrystalised
beige to yellow, slightly dolomitised, thin bedded limestones
beige to white bioclastic wackestone, slightly nodular, stylolites present, divided into sub-units by marly partings
yellow, dolomitic marly limestone
massive white bioclastic wackestones with isolated corals divided into sub-units by prominent partings
beige to white limestone with clay-rich horizons very fossiliferous
beige to white thin-bedded peloidal packstone, macrofauna rare, clay-rich
yellow to white marly limestone, with many bivalves
white massive foraminiferal wackestone, oolitic in places
beige marly limestone, dolomitic in places, moulds of macrofauna
H. praehelvetica
'calcispheres'
"Placopsilina cenomana"
Quinqueloculina spp.
Thomasinella punica
Hemicylammina sigali
Ovalvulina ovum
Simplalveolina simplex
Trochammina sp. cf. T. kugltangensis
Hedbergella spp. and Heterohelix spp.
2.
1.

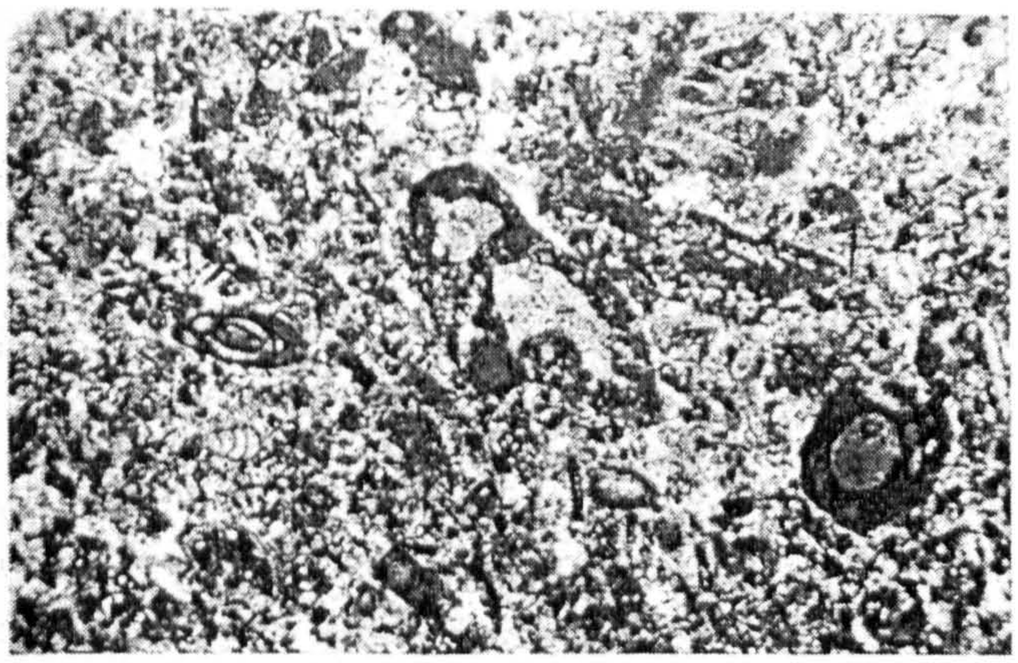

A

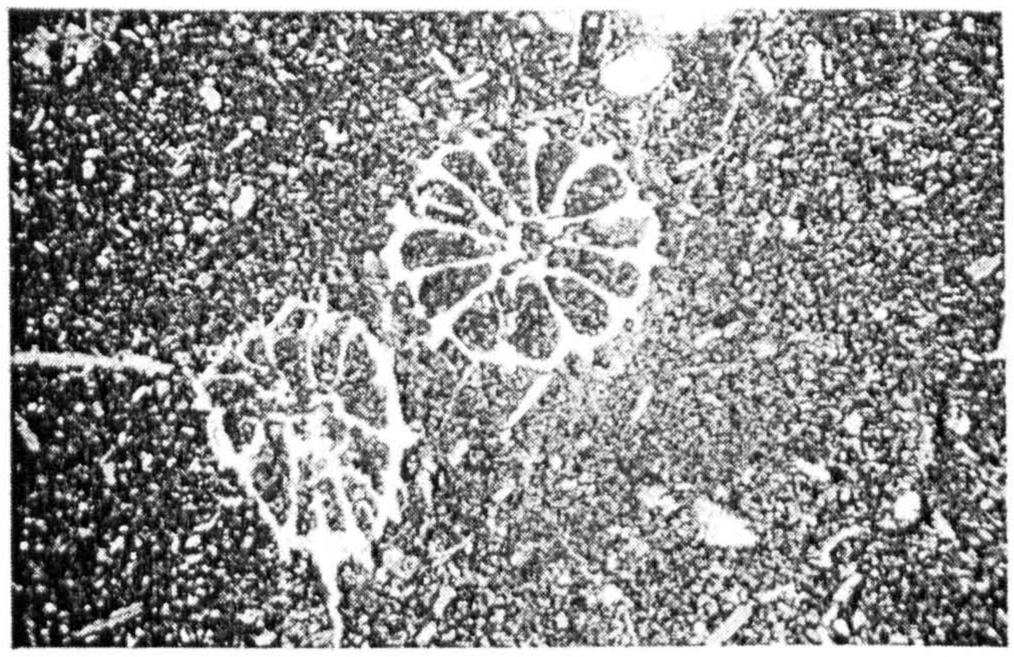

B

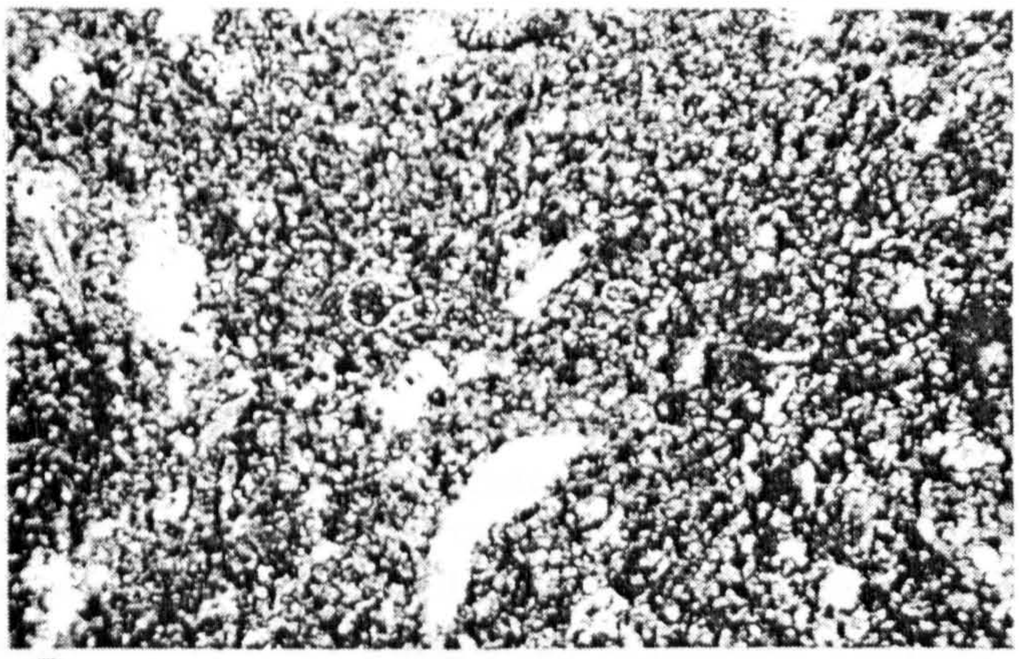

C

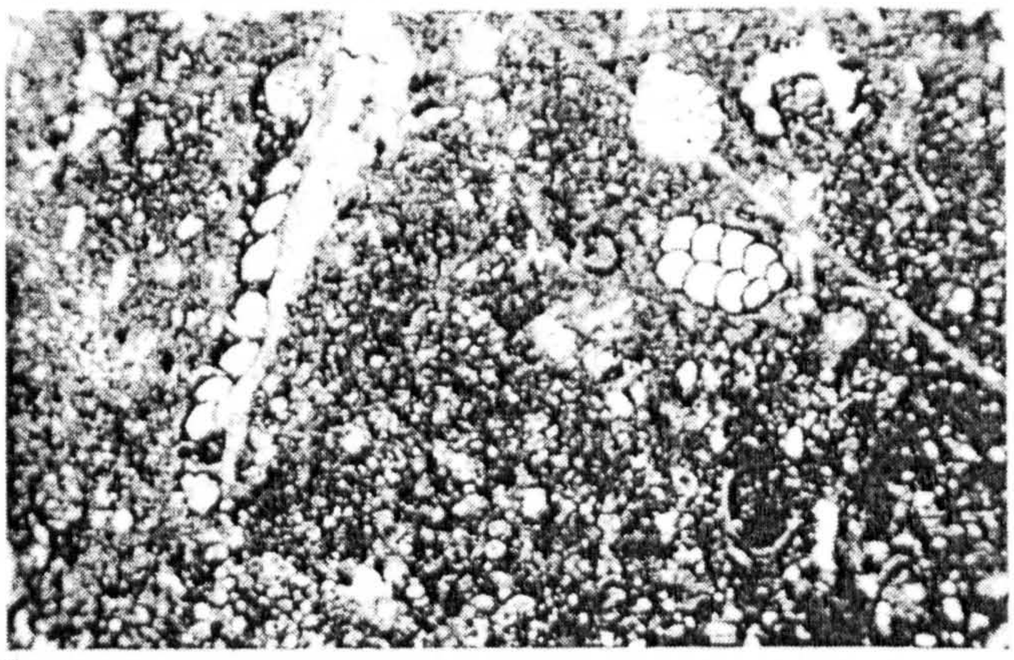

D

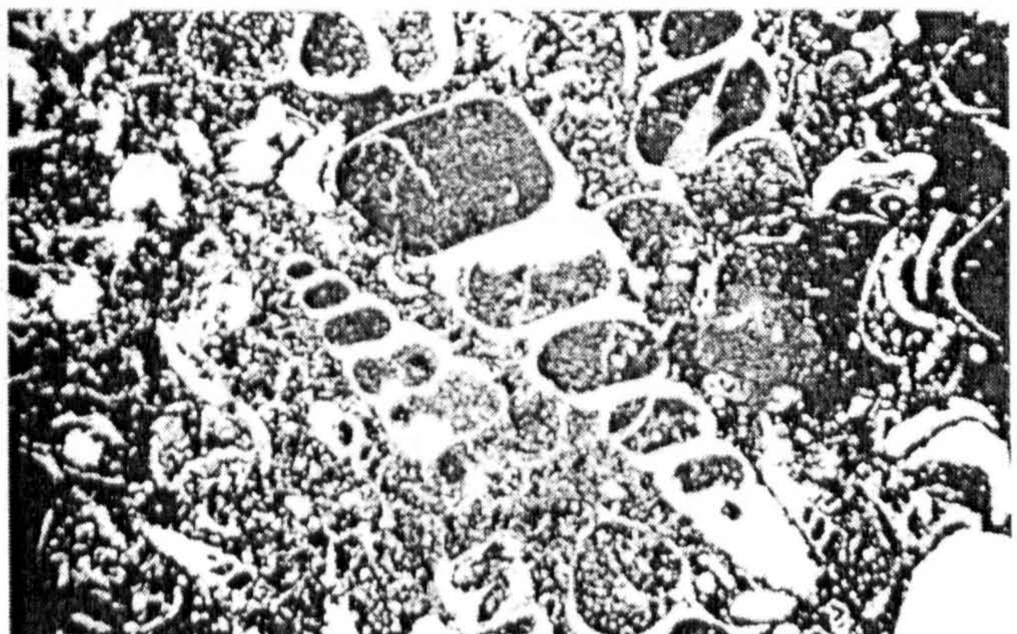

E

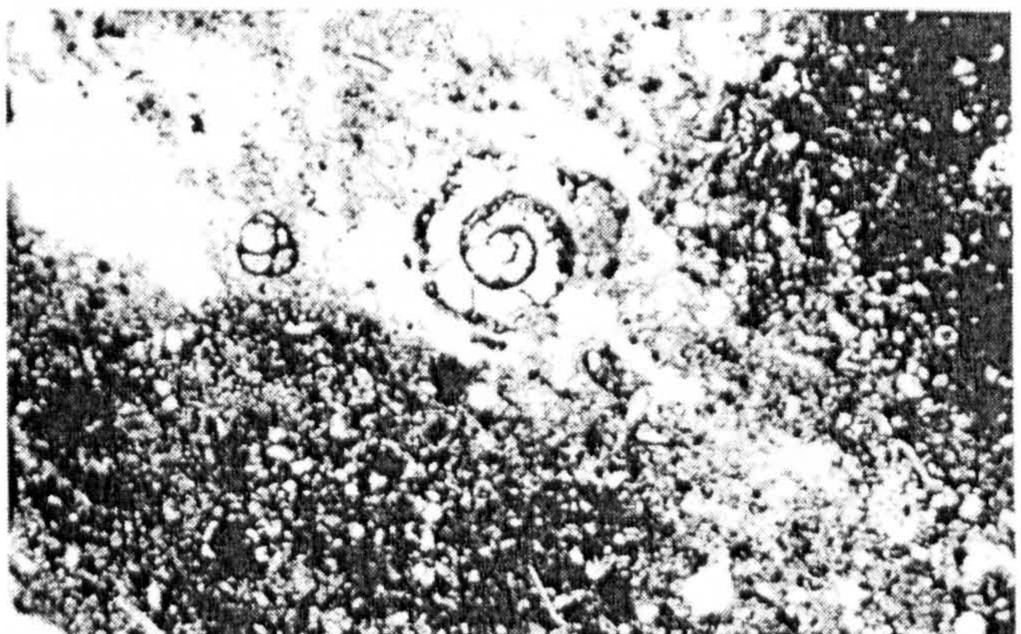

F

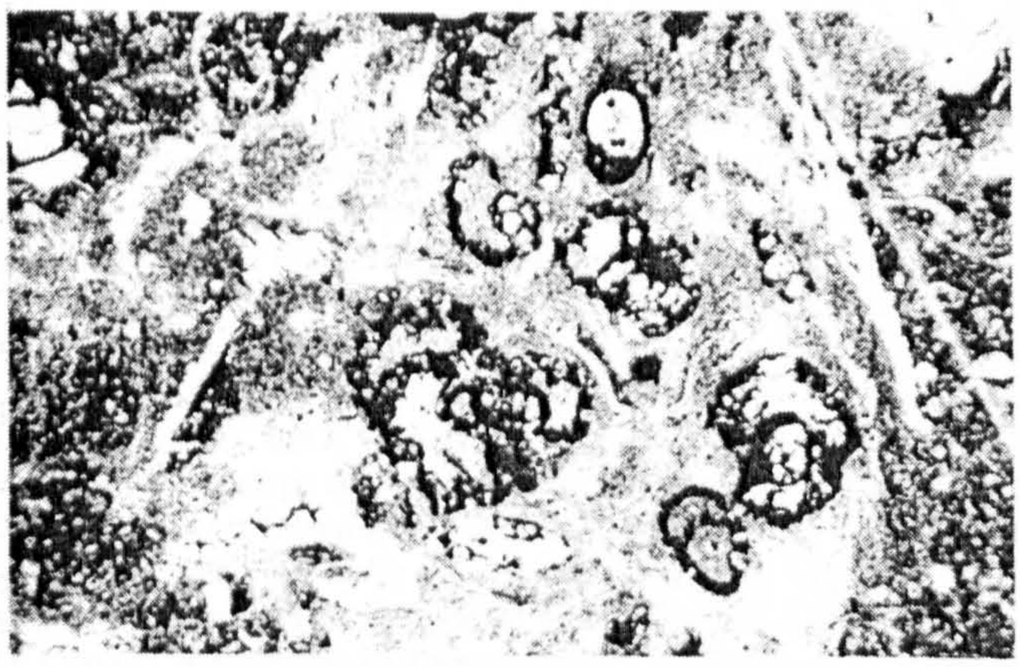

G

H

abundant as illustrated by Hart (1991, fig.1), Jarvis *et al.* (1988, fig. 4(c, d, g, h)) and Caus *et al.* (1997, pl.1, fig. 4) the occurrence of abundant calcispheres has been related to the extinction events in the latest Cenomanian (Fig. 8). Kennedy and Simmons (1991, fig.4) also record an increase in calcispheres at about this level (listed as *Pithonella ovalis* and *Pithonella spherica*). This latest Cenomanian/earliest Turonian flood of calcispheres is exceptionally widespread in Europe, North Africa and the Middle East and is detected, as in Oman, within quite shallow water environments. Bed H, which is within the Juddii Zone (Fig. 4) lies within the interval (Fig. 8) in which calcispheres would be expected (see also Bed J).

Bed I is a bed of gray marl (Callapez, 1999; Lauverjat and Berthou, 1973-74, p.277) or marl limestone with abundant *Hemiaster scutiger*. This lithology was neither processable for microfossils nor lithified enough for thin sectioning.

Bed J is a white/beige bioclastic wackestone that is quite characteristic in appearance (Figs. 6C and 7D/E/F). The macrofauna includes rare ammonites and bivalves (including *Mytiloides*). In thin section there are abundant echinoid spines and fragmentary bryozoans. Foraminifera are quite rare, including *Marssonella oxycona, Quinqueloculina* sp., *Gyroidinoides* sp., "*Placopsilina cenomana*" and calcispheres. Small specimens of (?)*Helvetoglobotruncana praehelvetica* are also recorded and the association of this species with the occurrence of the calcispheres (see also Kennedy and Simmons, 1991, fig. 4, pl. 7, figs B, E, F) is quite characteristic of the Juddii Zone in many areas (e.g., Eastbourne, Fig. 8). The top surface of Bed J is an important unconformity and is marked by a palaeo-karst. Callapez (1998, 1999, fig. 5) indicates a hiatus between Bed J and Bed K, although Berthou (1984a, fig. 5) only shows this boundary as a gap in the succession.

Bed K is a yellow, marly dolomitic limestone with rare inoceramids (*Mytiloides*) that has not been thin sectioned. Field inspection indicated that the identification of a microfauna would be unlikely, if not impossible.

Bed L is a series of "platy" white rudstones with marl intercalations and an ammonite fauna with *Kamerunoceras* and *Fagesia* which appears to be correlative to the North American Rollandi Zone. In the field, concentrations of *Turritella* form the most obvious feature (Fig. 6E). Other bioclasts include echinoderm spines, rare calcispheres and infrequent ostracods. Foraminifera are also rare, including *Marssonella oxycona, Heterohelix globosa, Heterohelix moremani* and *Hedbergella/Whiteinella* sp. indet.. Benthic foraminifera are generally rare in Lower Turonian successions in NW - Europe (Hart and Bailey, 1979) and Bed L contains a typical assemblage for this stratigraphical level. In Southern England (Hart, 1982) this level in the Turonian would be characterised by the presence of *Helvetoglobotruncana helvetica, Dicarinella imbricata, D. marginata, Praeglobotruncana stephani, P. turbinata,* etc. (see also Caus *et al.*, 1997, fig. 5).

Beds M, N, and O consist of calcarenites with fragmentary corals, radiolitids and acteonellids. Foraminifera are rare and generally indeterminate in thin section. Mica increases in abundance up section and the succession terminates with off-white micaceous sandstones.

At other locations (Montemor-o-Velho, Costa d'Arnes, Tentúgal, Carrasqueira) in this area (Callapez, 1998, 1999) different facies can be studied. At Carrasqueira, for example, Beds 'K' and 'L' are dolomitic and while they contain quite amazing biostromes of *Radiolites peroni* they contain few, if any, stratigraphically useful foraminifera.

Fig. 6.– (opposite page) Thin section micro-photographs of representative lithologies and foraminifera. A. Bed F, peloidal packstone with *Ammobaculites* sp., *Quinqueloculina* sp., *Textularia* sp. and other species of smaller foraminifera. Field of view 6 mm; B. Bed H, bioclastic wackestone with scleractinian corals, echinoid spines and rare small planktic foraminifera. Field of view 6 mm; C. Bed 'J', bioclastic wackestone containing very small planktic foraminifera (*Hedbergella delrioensis* visible in the middle of the slide). Field of view 1.5 mm; D. Bed C, foraminiferal wackestone with "*Placopsilina cenomana*" encrusting a shell fragment. *Dorothia* sp., echinoid spines and small planktic foraminifera are also present. Field of view 1.5 mm; E. Bed L, rudstone with complete and fragmentary *Turritella*. Associated with the turritellids are echinoid spines and small planktic foraminifera. Field of view 6 mm; F. Bed C, foraminiferal wackestone with *Hemicyclammina sigali.* Field of view 6 mm ; G. Bed C, foraminiferal wackestone with *Ammobaculites* sp. and *Hemicyclammina sigali.* Field of view 6 mm ; H. Bed C, foraminiferal wackestone with *Thomasinella* (?)*punica* associated with small planktic foraminifera. Field of view 6 mm.

Fig. 6.– (página opuesta) Fotografías a partir de láminas delgadas de las litologías y foraminíferos más representativos. A. Capa F, *packstone* peloidal con *Ammobaculites* sp., *Quinqueloculina* sp., *Textularia* sp. y otras especies de foraminíferos de menor tamaño. Campo de visión 6 mm; B. Capa H, *wackestone* bioclástico con corales escleractinios, espinas de equinoideos y escasos foraminíferos planctónicos pequeños. Campo de visión 6 mm; C. Capa J, *wackestone* bioclástico con foraminíferos planctónicos de muy pequeño tamaño (*Hedbergella delrioensis* en el medio de la imagen). Campo de visión 1,5 mm; D. Capa C, *wackestone* de foraminíferos con "*Placopsilina cenomana*" incrustando un fragmento de concha, junto con *Dorothia* sp., espinas de equinoideos y pequeños foraminíferos planctónicos. Campo de visión 1,5 mm; E. Capa L, *rudstone* con ejemplares de *Turritella* enteros y fragmentados. Junto con los turritélidos se han observado también espinas de equinoideos y pequeños foraminíferos planctónicos. Campo de visión 6 mm; F. Capa C, *wackestone* de foraminíferos con *Hemicyclammina sigali.* Campo de visión 6 mm ; G. Capa C, *wackestone* de foraminíferos con *Ammobaculites* sp. y *Hemicyclammina sigali.* Campo de visión 6 mm ; H. Capa C, *wackestone* de foraminíferos con *Thomasinella* (?) *punica* junto con pequeños foraminíferos planctónicos. Campo de visión 6 mm.

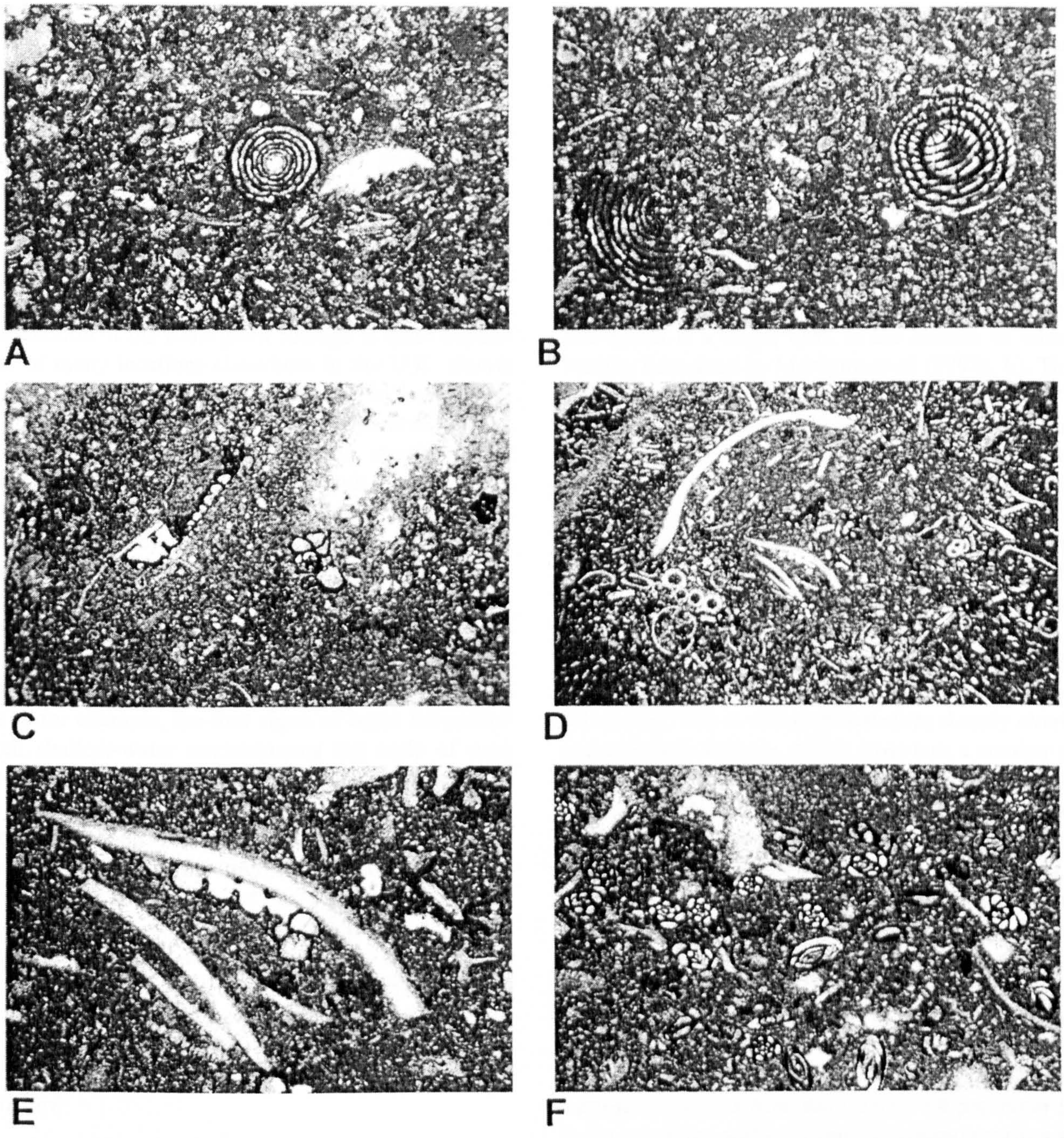

Fig. 7.– Thin section micro-photographs of representative lithologies and foraminifera. A. Bed C, foraminiferal wackestone with *Simplalveolina simplex*. Field of view 6 mm; B. Bed C, foraminiferal wackestone with *Simplalveolina simplex* and *Ovalvulina ovum*. Field of view 6 mm; C. Bed C foraminiferal wackestone with "*Placopsilina cenomana*" overhanging a very small shell fragment. Field of view 6 mm; D. Bed J at Tentúgal. Foraminiferal wackestone with bivalve fragments, serpulids and "*Placopsilina cenomana*". Field of view 6 mm; E. Bed J at Tentúgal. Foraminiferal wackestone with a close-up of the "*Placopsilina cenomana*" visible on the shell fragment in Fig.7E and showing the agglutinated wall structure. Field of view 1.5 mm; F. Bed J at Nazaré. Foraminiferal wackestone with abundant *Quinqueloculina* spp. and *Nautiloculina* spp.. Field of view 1.5 mm.

Fig. 7.– Fotografías a partir de láminas delgadas de las litologías y foraminíferos más representativos. A. Capa C, *wackestone* de foraminíferos con *Simplalveolina simplex*. Campo de visión 6 mm; B. Capa C, *wackestone* de foraminíferos con *Simplalveolina simplex* y *Ovalvulina ovum*. Campo de visión 6 mm; C. Capa C, *wackestone* de foraminíferos con "*Placopsilina cenomana*" que resalta sobre un fragmento muy pequeño de concha. Campo de visión 6 mm; D. Capa J en Tentúgal. *Wackestone* de foraminíferos con fragmentos de bivalvo, serpúlidos y "*Placopsilina cenomana*". Campo de visión 6 mm; E. Capa J en Tentúgal. *Wackestone* de foraminíferos en el que se ve un primer plano de "*Placopsilina cenomana*" sobre el fragmento de concha de la Fig.7E en el que se puede apreciar la estructura de su pared aglutinada. Campo de visión 1.5 mm; F. Capa J en Nazaré. *Wackestone* de foraminíferos con abundantes ejemplares de *Quinqueloculina* spp. y *Nautiloculina* spp.. Campo de visión 1.5 mm.

4. The Late Cenomanian Event

4.1. Rio Mondego

As indicated above, the co-occurrence of abundant calcispheres and *Helvetoglobotruncana praehelvetica* stratigraphically above the disappearance of typically Cenomanian foraminifera clearly points to the presence of the latest Cenomanian extinction event. Figure 8 shows the characteristic features of the Upper Cenomanian – Turonian succession at Eastbourne (Sussex, U.K.). The extinction of the *Rotalipora* lineage is quite characteristic of many locations elsewhere in the U.K. (Jarvis *et al.*, 1988) and this has been confirmed by subsequent work (Morel, 1998; Paul *et al.*, 1999; Keller *et al.*, 2001). In the Rio Mondego succession such stratigraphical markers are missing and it is quite difficult to make direct comparisons. *Helvetoglobotruncana helvetica*, which appears just above the base of the Turonian (drawn at the base of the Devonense Zone), is a deep water taxon and would not be expected in such shallow water environments. The main extinction event(s) would be expected to occur at the level of Beds H, I and J. If this is the case, then what is the cause of the hiatus between Beds J and K? Is it, for example, the first signs of basin inversion? In such shallow-water environments the scale of such an event would have been extremely small; creating no more than a hiatus in the sedimentation during the overall global highstand. This event was probably associated with movements along the main diapiric axes, including those of Caldas da Raihna and São Pedro de Muel. The brecciated limestones of the Praia da Vitória succession (see below and Fig. 9) are probably related to movement of the São Pedro de Muel diapir. The uplift across the hiatus (Beds J – K) is more evident in the south, closer to the "Nazaré Fault" (see Fig. 2).

4.2. Nazaré

To the south of Figueira da Foz is the fishing village and holiday centre of Nazaré (Fig. 2). To the immediate north of the main beach and town centre is a major cliff of Cenomanian limestones (Callapez, 1999, fig. 24). Much of this section is quite difficult to access but the uppermost Cenomanian and lowermost Turonian are exposed immediately north of the lighthouse and fort on the headland of Pedro do Guilhim. The upper part of Bed J (Fig. 7D) is exposed at beach level near two small caves. The top surface of Bed J is again represented by an important unconformity/palaeokarst which is, in turn, overlain by Beds L – O, which at this locality are represented by micaceous limestones and yellow cross-bedded sandstones. These are overlain by grey to white coarse, fluvial/alluvial sandstones of (?) Turonian-Santonian-Campanian age. Though complicated, the Pedra do Guilhim succession provides little new evidence of the Bed J – K hiatus, or the latest Cenomanian extinction event.

4.3. Praia da Vitória

Approximately 10 km north of Nazaré is Praia da Vitória, a long beach backed by a small group of houses and holiday accommodation. One kilometre south along this beach is a major cliff, at the bottom of which is a locality described by Monteiro *et al.* (1998a, b). This succession includes what has been suggested as an "ejecta layer", an iridium anomaly, spherules and a wide range of basement exotics. Of particular note are rounded blocks of fresh basalt up to 85 cm in diameter. The critical horizons are intermittently exposed beneath the active beach sands and the whole area can change in appearance during one tidal cycle. Figure 9 shows a measured section of the key part of the succession. The *in-situ* inner shelfal carbonates are of mid-Late Cenomanian age (Callapez, 1998) on the basis of the macrofauna. The microfauna though not stratigraphically diagnostic by itself, would confirm this dating. The *in-situ* carbonates are sharply overlain by a monomictic breccia, which cross cuts a number of beds in a distinctive manner. The blocks in this monomictic breccia are all local limestones and several contain macrofossils (including some large fragments of Cenomanian *Caprinula*). Within the top metre of this breccia (Fig. 9) is the "ejecta horizon", a complex bed of Lower Jurassic and Cretaceous limestone fragments, cherts, sandstones, assorted metamorphic rocks, iron oxide clasts, diaplectic glass and large (80-85 cm diameter) rounded blocks of fresh olivine basalt. Monteiro *et al.* (1998a, b) have described the glass and other spherules in some detail and have presented a number of geochemical analyses from samples collected from the locality. Of particular interest is the overlying soft grey clay/silt which records a slightly enhanced level of iridium. This clay/silt is overlain by a massive succession of coarse grey sandstones that appear to represent a series of major distributary channel sands. In the base of this sandstone unit is a level of reworked clasts of clay and siltstone. Neither the bed of clay/silt, the reworked sediment clasts nor the sandstones have yielded any microfauna or significant microflora.

No horizon comparable to the "ejecta horizon" is seen at any other locality in the area and this fact, coupled with the nature of the contained blocks, glasses, spherules and the geochemistry led Monteiro *et al.* (1998a, b) to conclude that this could be a potential cause of the latest Cenomanian extinction event; the result of an impact

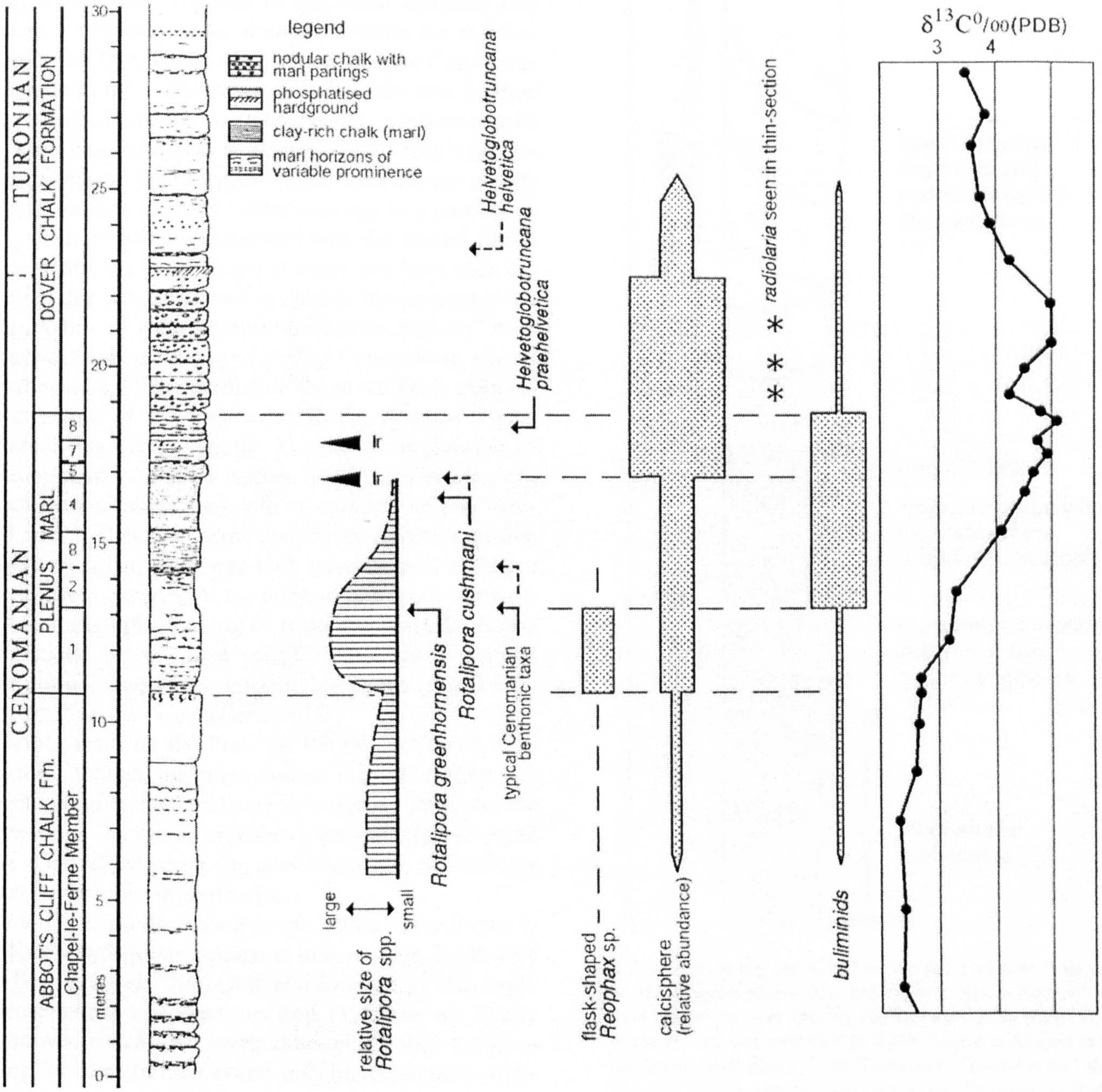

Fig. 8.– Lithostratigraphy, micropalaeontological data and carbon isotope data for the Cenomanian-Turonian boundary succession at Eastbourne, United Kingdom. Figure modified after Hart *et al.* (2002).

Fig. 8.– Litoestratigrafía, datos micropalentológicos y de los isótopos de carbono de la sucesión que incluye el límite Cenomaniense-Turoniense en Eastbourne, Reino Unido. Figura modificada de Hart *et al.* (2002).

in the vicinity of the Tore Sea Mount (Laughton *et al.*, 1975). The *in-situ* carbonates are dipping towards the SE with the strike direction SW/NE. It was this direction – pointing almost directly towards the Tore Sea Mount – that led Monteiro *et al.* (1998a, b) to propose that location as the potential impact site.

Immediately to the north of the succession shown in Figure 9 is a complex outcrop of evaporites, yellow to grey limestones and dark shales. The limestones and shales are reminiscent of the local Hettangian succession and we have interpreted this anomalous outcrop as being the edge of a salt diapir (see Fig. 2). Intra-Cenomanian movements of a salt diapir might explain the disturbance of the strata seen in the monomictic breccia but could not fully explain the "ejecta horizon". The basalt boulders and other exotics are all rounded and appear to have been

water transported. The size of the basalt boulders also implies a relatively close source (certainly not the distance to the Tore Sea Mount). There are Late Cretaceous volcanics in the Lisbon area and there are two isolated outcrops of olivine-rich basalt at Nazaré. As these basalts cut Turonian sediments (Callapez, 1999) they must be younger in age. There are, however, other olivine basalts of Late Jurassic or Early Cretaceous age in a number of areas onshore that are associated with the second rifting phase within the basin. Some of these may have been exposed at this time as a result of diapiric movements in the basin. While of great interest, the "ejecta horizon" does not appear to be evidence of a latest Cenomanian impact and the cause of the extinction event. In their work on the structure of the Lusitanian Basin, Proença Cunha and Pena dos Reis (1995, fig. 3) indicate the presence of salt diapirism in the mid-Aptian, mid-Turonian and early Maastrichtian (associated with movements on the "Nazaré Fault"). They also show that, in the Late Campanian to Maastrichtian, there was both intrusive and extrusive volcanism in the area. At the present time we do not have the biostratigraphic control to relate the Praia da Vitória monomictic breccia to a specific diapirism event and have no radiometric age information on the basalts contained within the "ejecta horizon".

Further work on the Praia da Vitória succession is in progress, though the microfaunas recovered from the limestones give little evidence for a precise dating for the succession. The sandstones above the grey clay/silt layer have also yielded very poor, non-diagnostic, palynofloras and no calcareous microfossils.

How the Praia da Vitória events relate to the hiatus in the Rio Mondego succession is also unclear. Is the Bed J – Bed K hiatus the result of diapirism in that area? Proença Cunha and Pena dos Reis (1995) do not record any movements at that level, although the mid-Turonian dating for some of their events may be within their stratigraphical resolution. If one compares the Rio Mondego succession to that in the Western Interior Seaway of North America the problem is even more challenging. In a detailed analysis, West *et al.* (1998, figs 2 and 8) indicate that the Devonense Zone was a 3rd–Order highstand. One would, therefore, have expected either deposition of some sediments during that interval or the presence of an erosive surface indicative of a transgressive event. The Rio Mondego succession, with an eroded surface and palaeo-karst is suggestive of a regressive event. The Bed J – K hiatus appears, therefore, to be a local event, even though the overall Upper Aptian to Lower Campanian "megasequence" implies a response to global sea level change.

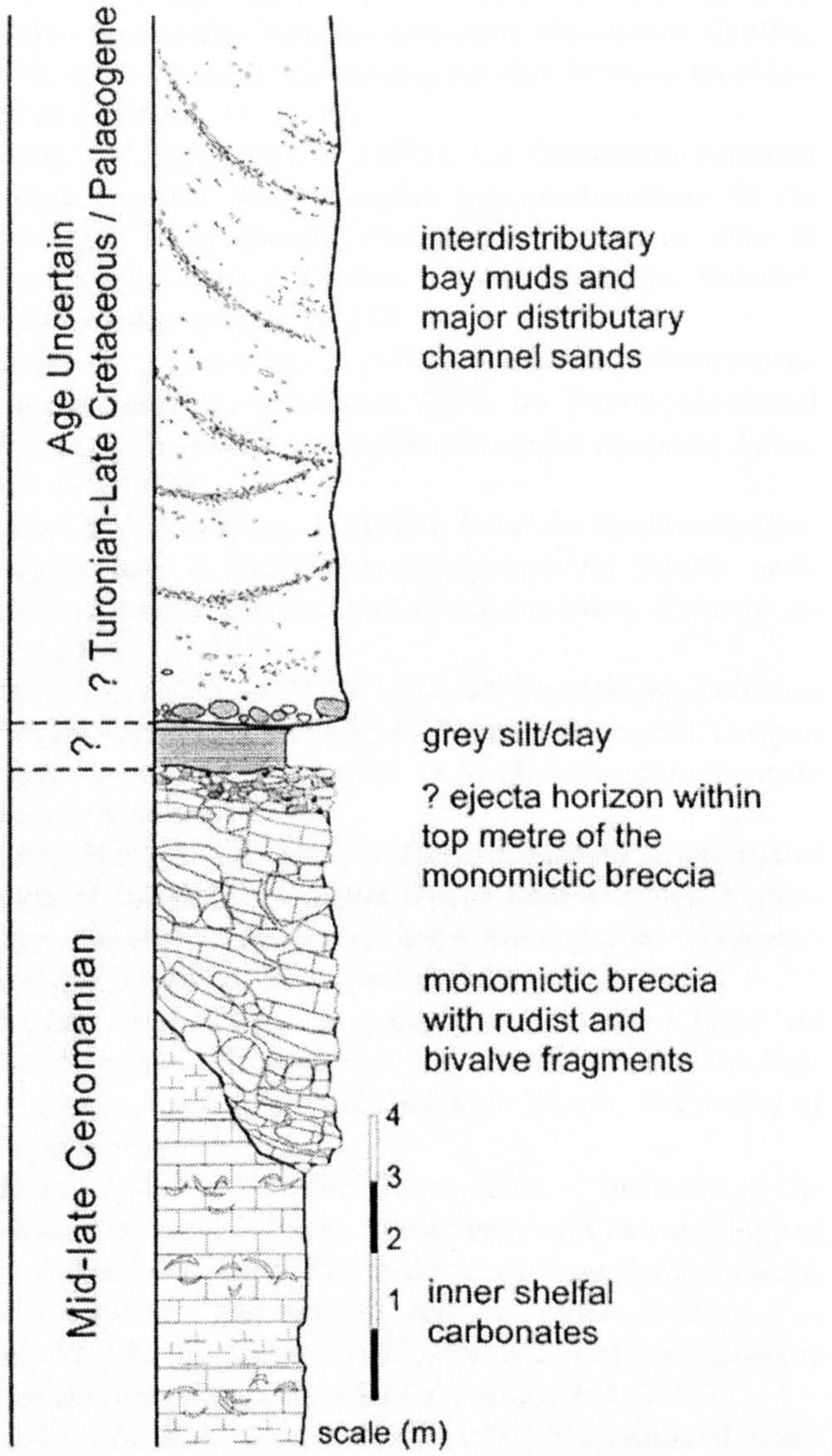

Fig. 9.– Sedimentary log of part of the succession at Praia da Vitória showing the monomictic breccia, the "ejecta horizon" and the overlying bed of grey silt/clay and the coarse sandstones. The sands above the clay layer are most probably a local equivalent of the Oiã Sandstone Formation (of Late Turonian to Coniacian age) shown in Figure 3. The monomictic breccia contains fragments of Beds B, C, D, G and H (see Figure 5).

Fig. 9.– Corte de parte de la sucesión en Praia da Vitória que muestra la brecha monomíctica, el "horizonte de ejecta" y la capa suprayacente de limos/arcillas grises y areniscas gruesas. Las arenas por encima de la capa de arcillas son probablemente un equivalente local de la Formación de Arenas de Oiã (Turoniense superior – Coniaciense) mostrada en la Figura 3. La brecha monomíctica contiene fragmentos de las Capas B, C, D, G y H (ver Figura 5).

5. Conclusions

The Cenomanian-Turonian carbonate succession of the Western Portuguese Margin preserves a shallow water record of the latest Cenomanian extinction event. Few descriptions are available of such a succession through this

interval as most workers on this event have concentrated on localities with open shelf to open oceanic sequences that are rich in planktic microfaunas and microfloras, and which often contain organic rich sediments. In the Rio Mondego succession, none of the normal foraminiferal marker species are present and, instead, there is a record of a wide range of benthic taxa. The 'calcisphere' event appears to be present, but the neobuliminids and gavelinellids used by other authors at this level (West *et al.*, 1998) are not recorded. How the microfaunal events described from the Rio Mondego succession relate to the unusual succession at Praia da Vitória remains to be determined.

Acknowledgements

MBH, GDP, JFM and MPW acknowledge financial support from the British Council (Treaty of Windsor) for fieldwork in Portugal. JKF acknowledges receipt of a University of Plymouth research studentship (2001-2003). Mr John Abraham is thanked for his assistance with the production of the figures.

References

Amédro, F., Berthou, P.Y., Lauverjat, J. (1980): Nouvelles preuves de l'apparition au Cénomanien supérieur des premiers *Vascoceras* dans la série type de la basse vallée du Rio Mondego (Beira Litoral, Portugal). *Boletim da Sociedade Geológica de Portugal,* 22:153-161.

Arnaud-Vanneau, A., Prestat, B. (1984): *Thomasinella* and Co. In: H.J. Oertli (ed.): *Benthos '83; 2nd International Symposium on Benthic Foraminifera (Pau, April 1983),* 19-26, Elf Aquitaine, Esso REP and Total CFP, Pau and Bordeaux.

Berthou, P.Y. (1973): Le Cénomanien de l'Estrémadure portugaise. *Memórias dos Serviços Geológicos, Portugal,* n.s. 23: 1-168.

Berthou, P.Y. (1978): La transgression cénomanienne dans le Bassin Occidental Portugais. *Géologie Mediterranéenne,* 5: 31-38.

Berthou, P.Y. (1984a): Albian-Turonian stage boundaries and subdivisions in the western Portuguese Basin, with special emphasis on the Cenomanian-Turonian boundary in the ammonite facies and rudist facies. *Bulletin of the Geological Society of Denmark,* 33: 41-55.

Berthou, P.Y. (1984b): Répartition stratigraphique actualise des principaux Foraminifères benthiques du Crétacé moyen et supérieur du Bassin Occidental Portugais. In: H.J. Oertli (ed.): *Benthos '83; 2nd International Symposium on Benthic Foraminifera (Pau, April 1983)*, 45-54, Elf Aquitaine, Esso REP and Total CFP, Pau and Bordeaux.

Berthou, P.Y., Brower, J., Reyment, R. (1975): Morphometrical study of Choffat's Vascoceratids from Portugal. *Bulletin of the Geological Institution of the University of Upsala,* 6: 73-83.

Berthou, P.Y., Chancellor, G., Lauverjat, J. (1985): Revision of the Cenomanian-Turonian ammonite *Vascoceras* Choffat, 1898, from Portugal. *Comunicações dos Serviços Geológicos de Portugal,* 71: 55-79.

Berthou, P.Y., Lauverjat, J. (1975): Le Cénomano-Turonien à Vascocératides dans sa région type (embouchure du rio Mondego, Beira littorale, Portugal). Corrélations avec le stratotype du Mans et d'autres séries téthysiennes. *Newsletters in Stratigraphy,* 4: 96-118.

Berthou, P.Y., Lauverjat, J. (1976): La limite Cénomanien-Turonien dans les principaux faciès du Bassin occidental portugais. *Compte Rendu* de l'*Académie des Sciences, Paris,* 282: 2143-2146.

Berthou, P.Y., Lauverjat, J. (1979): Essai de Synthèse paléogéographique et Paléobiostratigraphique du Bassin occidental portugais au cours du Crétacé supérieur. *Ciências da Terra,* 5: 121-144.

Berthou P.Y., Philip, J. (1972): La limite Cénomanien-Turonien dans les Formations récifales du domaine mésogéen. *Compte rendu sommaire des Séances de la Société géologique de France,* 6: 238-239.

Bykova, N.K. (1947): Study of the Cenomanian foraminiferal fauna of the Bukhara region. *Trudy Vsesoyuznogo Neftyanogo Nauchno-issledovatel'skogo Geologorazvedochnogo Instituta (VNIGRI),* 230p. [In Russian].

Callapez, P.M. (1998): *Estratigrafia e Paleobiologia do Cenomaniano – Turoniano O significado do eixo da Nazaré-Leiria-Pombal.* Unpublished PhD Thesis, University of Coimbra, 1-479.

Callapez, P.M. (1999): The Cenomanian - Turonian of the Western Portuguese Basin: Stratigraphy and Paleobiology of the Central and Northern Sectors. *European Palaeontological Workshop, Field Guide B, July 25th, 1999.*

Caron, M., Homewood, P. (1983): Evolution of early planktic foraminifers. *Marine Micropaleontology,* 7: 453-462.

Caus, E., Teixell, A., Bernaus, J.M. (1997): Depositional model of a Cenomanian-Turonian extensional basin (Sopeira Basin, NE Spain): interplay between tectonics, eustasy and biological productivity. *Palaeogeography, Palaeoclimatology, Palaeoecology,* 129: 23-36.

Choffat, P. (1885): *Recueil de monographies stratigraphiques sur le Système Crétacique du Portugal – première etude – Contrée de Cintra, de Bellas et de Lisbonne; Section des Travaux Géologiques du Portugal,* Lisbonne, 1-68.

Choffat, P. (1886): Recueil d'études paléontologiques sur la faune crétacique du Portugal. Vol. 1, Espèces nouvelles ou peu connues, 1ère série. *Memórias dos Serviços Geológicos de Portugal,* 1-40.

Choffat, P. (1896): Coup d'oeil sur les mers mésozoiques du Portugal. *Vierteljahresschrift der naturforschenden Gesellschaft in Zürich,* 41: 294-317.

Choffat, P. (1897a): Faciès ammonitique et faciès récifal du Turonien portugais. *Bulletin de la Société géologique de France,* (3), 25: 470-478.

Choffat, P. (1897b): Sur le Crétacique de la région du Mondego. *Compte Rendu de l'Académie des Sciences, Paris,* 124: 422-424.

Choffat, P. (1898): Recueil d'études paléontologiques sur la faune crétacique du Portugal, 2ème série: Les Ammonées du Bellasien, des couches à *Neolobites vibrayeanus*, du Turonien et du Sénonien. *Memórias dos Serviços Geológicos, Portugal*, 31: 1-46.

Choffat. P. (1900): Recueil de monographies stratigraphiques sur le système crétacique, 2ème étude: Le Crétacique supérieur au Nord du Tage. *Memórias Serviços Geológicos, Portugal*, 32: 1-297.

Cunha, P. (1992): *Estratigrafia e sedimentologia dos depósitos do Cretácico Superior e Terciário de Portugal Central, a Leste de Coimbra.* Unpublished PhD Thesis, University of Coimbra, 1-262.

Emery, D., Myers, K.J. (1996): *Sequence Stratigraphy*, 297 p., Blackwell Science, Oxford.

Hancock, J.M. (1989): Sea-level changes in the British region during the Late Cretaceous. *Proceedings of the Geologists' Association*, 100: 565-594.

Hardenbol, J., Thierry, J., Farley, M.B., Jacquin, T., Graciansky, P.C. de, Vail, P.R. (1998): Mesozoic and Cenozoic Chronostratigraphic Framework of European Basins. In: P.C. de Graciansky, J. Hardenbol, T. Jacquin, P.R. Vail (eds.): *Mesozoic and Cenozoic Sequence Stratigraphy of European Basins.* SEPM, special publication, 60: 3-13 and charts, Tulsa.

Hart, M.B. (1980): A water depth model for the evolution of the planktonic Foraminiferida. *Nature*, 286: 252-254.

Hart, M.B. (1982): Turonian foraminiferal biostratigraphy of Southern England. *Mémoires du Muséum National d'Histoire naturelle, Paris, série nov.*, 49: 203-207.

Hart, M.B. (1991): The Late Cenomanian calcisphere global bioevent. *Proceedings of the Ussher Society*, 7: 413-417.

Hart, M.B. (1999): The evolution and biodiversity of Cretaceous planktonic Foraminiferida. *Géobios*, 32: 247-255.

Hart, M.B., Bailey, H.W. (1979): The distribution of planktonic Foraminiferida in the mid-Cretaceous of N.W.Europe. In: J. Wiedmann (ed.): *Aspekte der Kreide Europas*. IUGS Series A, 6: 527-542, Schweizerbart, Stuttgart.

Hart, M.B., Monteiro, J.F., Watkinson, M.P., Price, G.D. (2002): Correlation of events at the Cenomanian/Turonian boundary: Evidence from southern England and Colorado. In: M. Wagreich (ed.): *Aspects of Cretaceous Stratigraphy and Palaeobiogeography.* Schriftenreihe der erdwissenschaftlichen Kommission der Österreichische Akademie der Wissenschaften, Wien, 15: 35-46, Verlag der Österreichische Akademie der Wissenschaften, Wien

Hodgkinson, R.L. (1992): *'Placopsilina' cenomana* d'Orbigny from France and England and the type species of *Placopsilina* d.Orbigny, 1850 (Foraminiferida). *Bulletin of the British Museum, Natural History (Geology)*, 48: 1-8.

Jarvis, I., Carson, G.A., Cooper, M.K.E., Hart, M.B., Leary, P.N., Tocher, B.A., Horne, D., Rosenfeld, A. (1988): Microfossil assemblages and the Cenomanian-Turonian (late Cretaceous) oceanic anoxic event. *Cretaceous Research*, 9: 3-103.

Kassab, A.S., Obaidalla, N.A. (2001): Integrated biostratigraphy and inter-regional correlation of the Cenomanian-Turonian deposits of Wadi Feiran, Sinai, Egypt. *Cretaceous Research*, 22: 105-114.

Keller, G., Han, Q., Adatte, T., Burns, S.J. (2001): Palaeoenvironment of the Cenomanian-Turonian transition at Eastbourne, England. *Cretaceous Research*, 22: 391-422.

Kennedy, W.J. (1984): Ammonite faunas and the "standard zones" of the Cenomanian to the Maastrichtian stages in their type areas, with some proposals for the definition of stage boundaries by ammonites. *Bulletin of the Geological Society of Denmark*, 33: 147-161.

Kennedy, W.J. (1988): Late Cenomanian and Turonian Ammonite faunas from North-East and central Texas. *Special paper in Palaeontology*, 39: 1-131.

Kennedy, W.J., Cobban, W. (1991): Stratigraphy and interregional correlation of the Cenomanian–Turonian transition in the Western Interior of the United States near Pueblo, Colorado, a potential boundary stratotype for the base of the Turonian stage. *Newsletters in Stratigraphy*, 24: 1-33.

Kennedy, W.J., Cobban, W., Hancock, J.M., Hook, S. (1989): Biostratigraphy of the Chipsa Summit Formation at its type locality: a Cenomanian through Turonian reference section for Trans-Pecos Texas. *Bulletin of the Geological Institution of the University of Upsala*, 15: 39-119.

Kennedy, W. J., Juignet, P. (1994): A revision of the ammonite faunas of the type Cenomanian 6. Acanthoceratinae (*Calycoceras (Proeucalycoceras), Eucalycoceras, Pseudocalycoceras, Neocardioceras*), Euomphaloceratinae, Mammitinae and Vascoceratidae. *Cretaceous Research*, 15: 469-501.

Kennedy, W.J., Simmons, M.D. (1991): Mid-Cretaceous ammonites and associated microfossils from the Central Oman Mountains. *Newsletters in Stratigraphy*, 25: 127-154.

Laughton, A.S., Roberts, D.G., Graves, R. (1975): Bathymetry of the northeast Atlantic. Sheet 3: Mid-Atlantic Ridge to southwest Europe. *Deep-Sea Research*, 22: 792-810.

Lauverjat, J. (1978): Le Cénomanien de la Valée du Mondego (Portugal). Limite avec le Turonien. Evolution Ouest-Est et implications paléogéographiques. *Géologie Méditerranéenne*, 5: 109-114.

Lauverjat, J. (1982): *Le Crétacé Supérieur dans le Nord du Bassin Occidental Portugais.* Unpublished PhD Thesis, Université Pierre et Marie Curie, Paris, 1-716.

Lauverjat, J., Berthou, P.Y. (1973-74): Le Cénomano-Turonien de l'embouchure du Rio Mondego Beira Litoral, Portugal. *Comunicações dos Serviços Geológicos de Portugal*, 57, 263-301, pls 1-8.

Lee, J.J., Anderson, O.R. (1991): Symbiosis in foraminifera. In: J.J. Lee, O.R. Anderson (eds.), *Biology of Foraminifera*, 157-220, Academic Press, London.

Maync, W. (1953): *Hemicyclammina sigali* n.gen. n.sp. from the Cenomanian of Algeria. *Contributions from the Cushman Foundation for Foraminiferal Research, Washington D.C.*, 4: 148-150.

Meister, C., Alzuma, K., Lang, J., Mathey, B. (1992): Les ammonites du Niger (Afrique Occidentale) et la transgression transsaharienne au cours du Cénomanien-Turonien. *Géobios*, 25: 55-100.

Monteiro, J.F., Munha, J., Ribeiro, A. (1998a): Impact ejecta horizon near the Cenomanian-Turonian boundary, north of Nazaré, Portugal. *Comunicações V Congresso Nacional de Geologia, Novembro 1998*, 4pp. [no pagination].

Monteiro, J.F., Munha, J., Ribeiro, A. (1998b): Impact ejecta horizon near the Cenomanian-Turonian boundary, north of Nazaré, Portugal. *Meteoritics and Planetary Sciences,* 33: A112-A113.

Morel, L. (1998): *Stratigraphie à Haute Résolution du Passage Cénomanien-Turonien.* Unpublished PhD Thesis, Université Piere et Marie Curie, Paris, 1-223.

Paul, C.R.C., Lamolda, M.A., Mitchell, S.F., Vaziri, M.R., Gorostidi, A., Marshall, J.D. (1999): The Cenomanian-Turonian boundary at Eastbourne (Sussex, UK): a proposed reference section. *Palaeogeography, Palaeoclimatology, Palaeoecology,* 150: 83-121.

Pena dos Reis, R. (1998): Late Cretaceous sedimentation and controls in Nazaré region (W Portugal). *Geologos,* 2, 117-120 [4ª Conferência Anual GGET. Universidade do Porto].

Pinheiro, L.H., Wilson, R.C.L., Pena dos Reis, R., Whitmarsh, R.B., Ribeiro, A. (1996): The Western Iberia Margin: A Geophysical and Geological Overview. In: R.B. Whitmarsh, D.S. Sawyer, A. Klaus, D.G. Masson (eds.): *Proceedings of the Ocean Drilling Program, Scientific Results,* Vol. 149: 3 – 23, Ocean Drilling Program, College Station, TX.

Proença Cunha, P., Pena dos Reis, R. (1995): Cretaceous sedimentary and tectonic evolution of the northern sector of the Lusitanian Basin (Portugal). *Cretaceous Research,* 16: 155-170.

Raup, D.M., Sepkoski, J.J. (1982): Periodicity of extinctions in the geological past. *Proceedings of the National Academy of Science, USA,* 81: 801-805.

Ribeiro, A., Antunes, M.T., Ferreira, M.P., Rocha, R.B., Soares, A.F.,

Zbyszewski, G., Moitinho de Almeida, F., Carvalho, D., Monteiro, J.H. (1979): *Introduction à la Géologie du Portugal.* Serviços Geológicos de Portugal, Lisboa, 1-114.

Sartorio, D., Venturini, S. (1988): *Southern Tethys Biofacies,* 235p., Agip S.p.A., S. Donato Milanese.

Soares, A. (1966): Estudo das formações pós-jurássicas das regiões de entre Sargento-Mor e Montemor-o-Velho (margem direita do Rio Mondego). *Memórias e Notícias, Universidade de Coimbra,* 62: 1-343.

Soares, A. (1972): Contribuição para o estudo do Cretácico em Portugal (o Cretácico superior da Costa de Arnes). *Memórias e Notícias, Universidade de Coimbra,* 74: 1-56.

Soares, A. (1980): A "Formação Carbonatada" na região do Baixo-Mondego.

Comunicações dos Serviços Geológicos de Portugal, 66: 99-109.

Stelck, C.R., Wall, J.H. (1954): Foraminifera of the Cenomanian *Dunveganoceras* zone from Peace River area of Western Canada. *Alberta Research Council, Report, Edmonton, Alberta,* 70: 1-59.

Tappan, H. (1957): New Cretaceous index foraminifera from northern Alaska. In: Studies in foraminifera; Part 2 – Benthonic foraminifera. *U.S. National Museum, Bulletin, Washington D.C.,* 215: 1-214.

West, O.L.O., Leckie, R.M., Schmidt, M. (1998): Foraminiferal paleoecology and paleoceanography of the Greenhorn Cycle along the southwestern margin of the Western Interior Sea. In: W.E. Dean, M.A. Arthur (eds.): *Stratigraphy and Paleoenvironments of the Cretaceous Western Interior Seaway, USA,* SEPM, Concepts in Sedimentology and Paleontology, 6: 79-99.

Wiedmann, J. (1980): Itineraire Géologique à traverse le Crétacé Moyen ces chaînes vascogotiques et celtibériques (Espagne du Nord). *Cuadernos de Geologia Iberica,* 5: 127-214.

Wiedmann, J., Kauffman, E.G. (1978):Mid-Cretaceous biostratigraphy of northern Spain. *Annales du Muséum d'histoire naturelle, Nice,* 4 [for 1976]: III.1- III.22.

Wilson, R.C.L. (1988): Mesozoic development of the Lusitanian Basin, Portugal. *Revista de la Sociedad Geológica de España, Madrid,* 1: 393-407.